

Reference Series in
Biomedical Engineering

Tissue Engineering and Regeneration
Series Editor: Heinz Redl

SPRINGER
REFERENCE

Aleksandr Ovsianikov · James Yoo
Vladimir Mironov *Editors*

3D Printing and Biofabrication



termis



Springer

Reference Series in Biomedical Engineering

Tissue Engineering and Regeneration

Series Editor

Heinz Redl

Ludwig Boltzmann Institute for Experimental and
Clinical Traumatology/AUVA Research Center
Austrian Cluster for Tissue Regeneration
Vienna, Austria

This series Tissue Engineering and Regeneration consists of comprehensive reference texts encompassing the biological basis of tissue regeneration, basic principles of tissue engineering, and the current state-of-the-art in tissue engineering of specific tissues and organs. Each volume combines established fundamentals and the latest developments, thus forming an invaluable collection for both experienced researchers as well as practitioners from other areas of expertise. The spectrum of topics ranges from the use of cells for tissue regeneration and tissue engineering, growth factors and biological molecules affecting tissue development and regeneration, to the specific roles of biophysical factors in tissue development and regeneration.

Tissue engineering lies at the crossroads of medicine, life sciences, and engineering. The field has developed extensively over the last two decades, addressing the requirements of tissue and organ replacement as well as regeneration in a variety of congenital, traumatic, disease, and aging-related conditions, including some of the most critical unmet challenges in modern medicine. Both our increased understanding of the biological basis of tissue engineering as well as significant technological advances mean that engineering design principles can now be used for the de novo construction of functional tissue replacements that meet the requirements of research and clinical applications.

More information about this series at <http://www.springer.com/series/13441>

Aleksandr Ovsianikov • James Yoo
Vladimir Mironov
Editors

3D Printing and Biofabrication

With 164 Figures and 34 Tables

 Springer

Editors

Aleksandr Ovsianikov
Institute of Materials Science and
Technology
Technische Universität Wien (TU Wien)
Vienna, Austria

James Yoo
Institute for Regenerative Medicine
Wake Forest School of Medicine
Wake Forest Institute for Regenerative
Medicine
Winston-Salem, NC, USA

Vladimir Mironov
3D Bioprinting Solutions (3D Bio)
The Laboratory of Biotechnological
Research
Moscow, Russia
Institute for Regenerative Medicine
Sechenov Medical University
Moscow, Russia

ISBN 978-3-319-45443-6 ISBN 978-3-319-45444-3 (eBook)
ISBN 978-3-319-45445-0 (print and electronic bundle)
<https://doi.org/10.1007/978-3-319-45444-3>

Library of Congress Control Number: 2018940257

© Springer International Publishing AG, part of Springer Nature 2018

This work is subject to copyright. All rights are reserved by the Publisher, whether the whole or part of the material is concerned, specifically the rights of translation, reprinting, reuse of illustrations, recitation, broadcasting, reproduction on microfilms or in any other physical way, and transmission or information storage and retrieval, electronic adaptation, computer software, or by similar or dissimilar methodology now known or hereafter developed.

The use of general descriptive names, registered names, trademarks, service marks, etc. in this publication does not imply, even in the absence of a specific statement, that such names are exempt from the relevant protective laws and regulations and therefore free for general use.

The publisher, the authors and the editors are safe to assume that the advice and information in this book are believed to be true and accurate at the date of publication. Neither the publisher nor the authors or the editors give a warranty, express or implied, with respect to the material contained herein or for any errors or omissions that may have been made. The publisher remains neutral with regard to jurisdictional claims in published maps and institutional affiliations.

Printed on acid-free paper

This Springer imprint is published by the registered company Springer International Publishing AG part of Springer Nature.

The registered company address is: Gewerbestrasse 11, 6330 Cham, Switzerland

Preface

Additive manufacturing, often referred to as simply 3D printing, takes its origins in rapid prototyping and is currently enjoying a skyrocketing market growth across many industrial sectors. 3D bioprinting is an emerging field of biomedical research aimed at additive manufacturing or assembly of living constructs, whereas cells are included in the process. It is an integral part of an ongoing third industrial revolution brought about by digital manufacturing.

3D bioprinting is a truly multidisciplinary field based on cross-fertilization of different disciplines from computer science and mathematical modeling to mechanical engineering and biomaterials science and, of course, biology. Moreover, it has all the characteristics of a novel and rapidly evolving research direction, such as fast growth of the number of related publications, constantly adjusting definitions (computer-aided tissue engineering, 3D bioprinting, organ printing, biofabrication, and so on), and increasing number of workshops, conferences, and congresses, taking place all around the world. There are also certain indications of maturity of this field as a new discipline, such as well-established conceptual framework, new terminology, publication of first books and textbooks, creation of training courses, and establishment of specialized societies and journals.

The potential applications of 3D bioprinting and biofabrication include (i) *in vitro* 3D models of development and human diseases; (ii) new research in *in vitro* 3D tissue models for drug discovery and toxicological and cosmetic research; and (iii) automated robotic biofabrication of 3D human tissues and organs suitable for clinical transplantation.

Many current research projects are still aiming at exploring what can be done with 3D bioprinting instead of focusing on what has to be done. As the field matures, the translational aspects become more pronounced with many recent works already based on preclinical research and moving toward commercialization. Again, as it is typical for new emerging research areas, 3D bioprinting and biofabrication creates excitement, rapidly recruits new especially young researchers from adjacent disciplines, raises great expectations for successful clinical translation, attracts attention not only within the scientific community, but also from the popular media and venture capitalists.

Summarizing all the recent progress and current status of this rapidly emerging research field is not a trivial task. In order to address this challenge, we brought

together a strong multidisciplinary collective of world-famous experts and thought leaders from many countries, which allow us to demonstrate the whole spectrum of research directions, novel approaches, and trends in this exciting field. This challenge is also well-addressed by the novel concept of a living book, enabling the authors to keep the contents of their chapters in pace with new developments and evolve together with the field via regular addition of the new knowledge and findings. Therefore, this idea of a living book per se represents an experiment exploring a new publishing model, kept up to date not as new editions but rather as addition of updated text to already existing chapters and addition of new chapters.

Another unique characteristic of our book is an attempt to make logical bridge and demonstrate how 3D bioprinting and biofabrication historically evolved from 3D printing technology and its biomedical applications. There are also certain novelties in our book, which made it rather different such as special attention to mathematical modeling, clinical translation, intellectual property, business models, and technology commercialization.

We hope that our readers will find this book professionally written, richly illustrated, comprehensive, and, most importantly, exciting. We would be happy and completely satisfied if our collective project will attract more new researchers from different disciplines with their specific expertise in the field of 3D printing and 3D bioprinting and biofabrication. Finally, we hope that this book will be useful for the organization of new courses for training of young generation of researchers and engineers.

Despite the fact that the chapters are peer reviewed, we will be very grateful for any constructive critique, suggestions, and comments regarding separate sections and the book as a whole. We are also looking for new authors for additional possible chapters about ethical, regulatory, economic, and scientometric aspects, as well as clinically relevant therapeutic grade cell sources and organoids in 3D printing and biofabrication.

Acknowledgments

We would like to express our gratitude to all the people who helped us along the way, in particular the authors, the reviewers, the Springer team supporting, and especially Prof. Heinz Redl, who was a trigger and driver of the entire process from the inception of innovative original idea of this “living” books series until final steps of implementation.

List of Reviewers

Aldo Boccaccini, Raphael Devillard, Andy Doraiswamy, Michael Gelinsky, Jürgen Groll, Linxia Gu, Gerald T. Grant, Karin Hofmann, Riccardo Levato, Penny Martens, Narges Shayesteh Moghaddam, Keith Murphy, Makoto Nakamura, Koichi Nakayama, Stefan Scheiner, Will Shu, Ravi Sinha, Ronald Unger, and Ana Raquel Verissimo

Contents

Part I 3D Printing	1
Additive Manufacturing for Tissue Engineering	3
Solaleh Miar, Ashkan Shafiee, Teja Guda, and Roger Narayan	
Characterization of Additive Manufactured Scaffolds	55
Giuseppe Criscenti, Carmelo De Maria, Giovanni Vozzi, and Lorenzo Moroni	
Vascular Networks Within 3D Printed and Engineered Tissues	79
Daniel Sazer and Jordan Miller	
Computational Methods for the Predictive Design of Bone Tissue Engineering Scaffolds	107
Stefan Scheiner, Vladimir S. Komlev, and Christian Hellmich	
Quality Control of 3D Printed Resorbable Implants: The 3D Printed Airway Splint Example	131
Scott J. Hollister, Sarah Jo Crotts, Harsha Ramaraju, Colleen L. Flanagan, David A. Zopf, Robert J. Morrison, Andrea Les, Richard G. Ohye, and Glenn E. Green	
Bioceramics for Musculoskeletal Regenerative Medicine: Materials and Manufacturing Process Compatibility for Synthetic Bone Grafts and Medical Devices	161
Ciro A. Rodriguez, Hernan Lara-Padilla, and David Dean	
Medical Imaging for Three-Dimensional Computer-Aided Models	195
Paulo Henrique Junqueira Amorim, Thiago Franco de Moraes, Rodrigo Alvarenga Rezende, Jorge Vicente Lopes da Silva, and Helio Pedrini	
Mathematical Modeling of 3D Tissue Engineering Constructs	223
Henrique Amorim Almeida and Paulo Jorge da Silva Bártolo	

Part II Biofabrication	253
Extrusion-Based Biofabrication in Tissue Engineering and Regenerative Medicine	255
Monika Hospodiuk, Kazim Kerim Moncal, Madhuri Dey, and Ibrahim T. Ozbolat	
Inkjet Printing for Biofabrication	283
Xinda Li, Jianwei Chen, Boxun Liu, Xiong Wang, Dongni Ren, and Tao Xu	
Laser-Based Cell Printing	303
Lothar Koch, Andrea Deiwick, and Boris Chichkov	
Development of Nanocellulose-Based Bioinks for 3D Bioprinting of Soft Tissue	331
Paul Gatenholm, Hector Martinez, Erdem Karabulut, Matteo Amoroso, Lars Kölby, Kajsa Markstedt, Erik Gatenholm, and Ida Henriksson	
Photopolymerizable Materials for Cell Encapsulation	353
L. Tytgat, Stefan Baudis, H. Ottevaere, R. Liska, H. Thienpont, P. Dubruel, and S. Van Vlierberghe	
Fabrication and Printing of Multi-material Hydrogels	397
Navein Arumugasaamy, Hannah B. Baker, David S. Kaplan, Peter C. W. Kim, and John P. Fisher	
Scaffold-Free Biofabrication	431
Ana Raquel Verissimo and Koichi Nakayama	
Translation and Applications of Biofabrication	451
Ji Hyun Kim, Anthony Atala, and James Yoo	
Bioprinting: The Intellectual Property Landscape	485
Robert W. Esmond and Deborah Sterling	
Emerging Business Models Toward Commercialization of Bioprinting Technology	513
Yakov M. Balakhovsky, Alexander Yu. Ostrovskiy, and Yusef D. Khesuani	
Commercial 3D Bioprinters	535
Frederico David A.S. Pereira, Vladislav Parfenov, Yusef D. Khesuani, Aleksandr Ovsianikov, and Vladimir Mironov	
Index	551

About the Editors

Aleksandr Ovsianikov is currently an Associate Professor at the Vienna University of Technology (TU Wien, Austria) and a member of the Austrian Cluster for Tissue Regeneration. His research is dealing with the use of additive manufacturing technologies for tissue engineering and regeneration. Dr. Ovsianikov has background in laser physics and material processing with femtosecond lasers. A particular focus of his current research is the development of multiphoton processing technologies for engineering of biomimetic 3D cell culture matrices and realization of novel tissue engineering scaffolds. He was awarded a prestigious Starting Grant in 2012 and a Consolidator Grant in 2017 from the European Research Council (ERC) for projects aimed at these topics. His research interests include high-resolution 3D printing, laser-induced photo-chemistry, and development of biomaterials for additive manufacturing and bioprinting.

James Yoo is Professor and Associate Director of the Wake Forest Institute for Regenerative Medicine (WFIRM), with a cross-appointment to the Department of Physiology and Pharmacology, and the Virginia Tech-Wake Forest School of Biomedical Engineering and Sciences. Dr. Yoo's research efforts are directed toward clinical translation of tissue engineering technologies and cell-based therapies. His interest in the bioprinting technology is due to its ability to generate clinically relevant complex tissue and organ constructs with precision and reproducibility for translational applications.

Vladimir Mironov received his MD from the Ivanovo State Medical Institute and Ph.D. from the Second Moscow Pirogov Medical State Institute. He was trained in Max Planck Institute in Martinsried in Germany. Prof. Mironov worked at first as a Director of Bioprinting Research Center and then as a Director of Advanced Tissue Biofabrication Center at the Medical University of South Carolina, Charleston, SC, USA. He is currently Chief Scientific Officer of the company 3D Bioprinting Solutions and Leading Scientist at Institute for Regenerative Medicine, Sechenov Medical University in Moscow, Russia.

Contributors

Henrique Amorim Almeida School of Technology and Management, Polytechnic Institute of Leiria (IPL), Leiria, Portugal

Matteo Amoroso Sahlgrenska University Hospital, Plastic Surgery, Göteborg, Sweden

Navein Arumugasaamy Fischell Department of Bioengineering, University of Maryland, College Park, MD, USA

Sheikh Zayed Institute for Pediatric Surgical Innovation, Children's National Health System, Washington, DC, USA

Anthony Atala Wake Forest Institute for Regenerative Medicine, Wake Forest School of Medicine, Winston-Salem, NC, USA

Hannah B. Baker Fischell Department of Bioengineering, University of Maryland, College Park, MD, USA

Center for Devices and Radiological Health, U.S. Food and Drug Administration, Silver Spring, MD, USA

Yakov M. Balakhovsky Vivax Bio, LLC, New York, NY, USA

Stefan Baudis Institute of Applied Synthetic Chemistry, Technische Universität Wien (TU Wien), Vienna, Austria

Jianwei Chen Department of Precision Medicine and Healthcare, Tsinghua-Berkeley Shenzhen Institute, Shenzhen, People's Republic of China

Boris Chichkov Laser Zentrum Hannover e.V., Hannover, Germany

Giuseppe Criscenti Department of Complex Tissue Regeneration, MERLN Institute for Technology-Inspired Regenerative Medicine, Maastricht University, Maastricht, The Netherlands

Research Center "E. Piaggio", University of Pisa, Pisa, Italy

Sarah Jo Crotts Center for 3D Medical Fabrication and Walter H. Coulter Department of Biomedical Engineering, Georgia Institute of Technology and Emory University, Atlanta, GA, USA

Jorge Vicente Lopes da Silva Division of 3D Technologies, Center for Information Technology Renato Archer, Campinas, SP, Brazil

Paulo Jorge da Silva Bártolo Manchester Biomanufacturing Centre, University of Manchester, Manchester, UK

School of Mechanical, Aerospace and Civil Engineering, University of Manchester, Manchester, UK

Carmelo De Maria Research Center “E. Piaggio”, University of Pisa, Pisa, Italy

Thiago Franco de Moraes Division of 3D Technologies, Center for Information Technology Renato Archer, Campinas, SP, Brazil

David Dean Department of Plastic Surgery, The Ohio State University, Columbus, OH, USA

Andrea Deiwick Laser Zentrum Hannover e.V., Hannover, Germany

Madhuri Dey The Huck Institutes of the Life Sciences, The Pennsylvania State University, University Park, PA, USA

Department of Chemistry, The Pennsylvania State University, University Park PA, USA

P. Dubruel Polymer Chemistry and Biomaterials Group, Ghent University, Ghent, Belgium

Robert W. Esmond Biotechnology/Chemical Group, Sterne, Kessler, Goldstein & Fox P.L.L.C., Washington, DC, USA

John P. Fisher Fischell Department of Bioengineering, University of Maryland, College Park, MD, USA

Sheikh Zayed Institute for Pediatric Surgical Innovation, Children’s National Health System, Washington, DC, USA

Colleen L. Flanagan Department of Biomedical Engineering, The University of Michigan, Ann Arbor, MI, USA

Erik Gatenholm CELLINK AB, Göteborg, Sweden

Paul Gatenholm Chalmers University of Technology, 3D Bioprinting center Väst (BBV), Göteborg, Sweden

Glenn E. Green Department of Otolaryngology Head and Neck Surgery, The University of Michigan, Ann Arbor, MI, USA

Teja Guda Department of Biomedical Engineering, University of Texas at San Antonio, San Antonio, TX, USA

Graduate Program in Biomedical Engineering, University of Texas Health Science Center at San Antonio, San Antonio, TX, USA

Christian Hellmich Institute for Mechanics of Materials and Structures, Technische Universität Wien (TU Wien), Vienna, Austria

Ida Henriksson Chalmers University of Technology, 3D Bioprinting center Väst (BBV), Göteborg, Sweden

Scott J. Hollister Center for 3D Medical Fabrication and Walter H. Coulter Department of Biomedical Engineering, Georgia Institute of Technology and Emory University, Atlanta, GA, USA

Monika Hospodiuk The Huck Institutes of the Life Sciences, The Pennsylvania State University, University Park, PA, USA

Engineering Science and Mechanics Department, The Pennsylvania State University, University Park, PA, USA

Paulo Henrique Junqueira Amorim Division of 3D Technologies, Center for Information Technology Renato Archer, Campinas, SP, Brazil

David S. Kaplan Center for Devices and Radiological Health, U.S. Food and Drug Administration, Silver Spring, MD, USA

Erdem Karabulut Chalmers University of Technology, 3D Bioprinting center Väst (BBV), Göteborg, Sweden

Yusef D. Khesuani Vivax Bio, LLC, New York, NY, USA

The Laboratory of Biotechnological Research, 3D Bioprinting Solutions, Moscow, Russian Federation

Ji Hyun Kim Wake Forest Institute for Regenerative Medicine, Wake Forest School of Medicine, Winston-Salem, NC, USA

Peter C. W. Kim Sheikh Zayed Institute for Pediatric Surgical Innovation, Children's National Health System, Washington, DC, USA

School of Medicine and Health Sciences, The George Washington University, Washington, DC, USA

Lothar Koch Laser Zentrum Hannover e.V., Hannover, Germany

Lars Kölby Sahlgrenska University Hospital, Plastic Surgery, Göteborg, Sweden

Vladimir S. Komlev A.A. Baikov Institute of Metallurgy and Materials Science, Russian Academy of Sciences, Moscow, Russia

Federal Scientific Research Centre "Crystallography and Photonics", Russian Academy of Sciences, Moscow, Russia

Hernan Lara-Padilla Departamento de Ciencias de la Energía y Mecánica, Universidad de las Fuerzas Armadas ESPE, Sangolquí, Ecuador

Andrea Les Department of Otolaryngology Head and Neck Surgery, The University of Michigan, Ann Arbor, MI, USA

Xinda Li Biomanufacturing Center, Department of Mechanical Engineering, Tsinghua University, Beijing, People's Republic of China

R. Liska Institute of Applied Synthetic Chemistry, Technische Universität Wien (TU Wien), Vienna, Austria

Boxun Liu Department of Precision Medicine and Healthcare, Tsinghua-Berkeley Shenzhen Institute, Shenzhen, People's Republic of China

Kajsa Markstedt Chalmers University of Technology, 3D Bioprinting center Väst (BBV), Göteborg, Sweden

Hector Martínez Chalmers University of Technology, 3D Bioprinting center Väst (BBV), Göteborg, Sweden

CELLINK AB, Göteborg, Sweden

Soleah Miar Department of Biomedical Engineering, University of Texas at San Antonio, San Antonio, TX, USA

Graduate Program in Biomedical Engineering, University of Texas Health Science Center at San Antonio, San Antonio, TX, USA

Jordan Miller Department of Bioengineering, Rice University, Houston, TX, USA

Vladimir Mironov 3D Bioprinting Solutions (3D Bio), The Laboratory of Biotechnological Research, Moscow, Russia

Institute for Regenerative Medicine, Sechenov Medical University, Moscow, Russia

Kazim Kerim Moncal The Huck Institutes of the Life Sciences, The Pennsylvania State University, University Park, PA, USA

Engineering Science and Mechanics Department, The Pennsylvania State University, University Park, PA, USA

Lorenzo Moroni Department of Complex Tissue Regeneration, MERLN Institute for Technology-Inspired Regenerative Medicine, Maastricht University, Maastricht, The Netherlands

Robert J. Morrison Department of Otolaryngology Head and Neck Surgery, The University of Michigan, Ann Arbor, MI, USA

Koichi Nakayama Department of Regenerative Medicine and Biomedical Engineering, Faculty of Medicine, Saga University, Saga, Japan

Roger Narayan UNC/NCSU Joint Department of Biomedical Engineering, Raleigh, NC, USA

Diabetes Center for Research, Department of Biomedical Engineering, UNC School of Medicine, Chapel Hill, NC, USA

Richard G. Ohye Department of Cardiac Surgery, The University of Michigan, Ann Arbor, MI, USA

Division of Cardiology, Department of Pediatrics, Ann Arbor, MI, USA

Alexander Yu. Ostrovskiy Independent Laboratory INVITRO, Moscow, Russian Federation

H. Ottevaere Brussels Photonics (B-PHOT), Department of Applied Physics and Photonics, Vrije Universiteit Brussel, Brussels, Belgium

Aleksandr Ovsianikov Institute of Materials Science and Technology, Technische Universität Wien (TU Wien), Vienna, Austria

Ibrahim T. Ozbolat The Huck Institutes of the Life Sciences, The Pennsylvania State University, University Park, PA, USA

Engineering Science and Mechanics Department, The Pennsylvania State University, University Park, PA, USA

Biomedical Engineering Department, The Pennsylvania State University, University Park, PA, USA

Materials Research Institute, The Pennsylvania State University, University Park, PA, USA

Vladislav Parfenov The Laboratory of Biotechnological Research, 3D Bioprinting Solutions, Moscow, Russia

Helio Pedrini Institute of Computing, University of Campinas, Campinas, SP, Brazil

Frederico David A. S. Pereira The Laboratory of Biotechnological Research, 3D Bioprinting Solutions, Moscow, Russia

Harsha Ramaraju Center for 3D Medical Fabrication and Walter H. Coulter Department of Biomedical Engineering, Georgia Institute of Technology and Emory University, Atlanta, GA, USA

Dongni Ren Medprin Regenerative Medical Technologies Co., Ltd., Guangzhou, Guangdong, People's Republic of China

Rodrigo Alvarenga Rezende Division of 3D Technologies, Center for Information Technology Renato Archer, Campinas, SP, Brazil

Ciro A. Rodriguez Escuela de Ingeniería y Ciencias, Tecnológico de Monterrey, Monterrey, Mexico

Daniel Sazer Department of Bioengineering, Rice University, Houston, TX, USA

Stefan Scheiner Institute for Mechanics of Materials and Structures, Technische Universität Wien (TU Wien), Vienna, Austria

Ashkan Shafiee Wake Forest Institute for Regenerative Medicine, Winston-Salem, NC, USA

Deborah Sterling Biotechnology/Chemical Group, Sterne, Kessler, Goldstein & Fox P.L.L.C., Washington, DC, USA

H. Thienpont Polymer Chemistry and Biomaterials Group, Ghent University, Ghent, Belgium

Brussels Photonics (B-PHOT), Department of Applied Physics and Photonics, Vrije Universiteit Brussel, Brussels, Belgium

L. Tytgat Polymer Chemistry and Biomaterials Group, Ghent University, Ghent, Belgium

Brussels Photonics (B-PHOT), Department of Applied Physics and Photonics, Vrije Universiteit Brussel, Brussels, Belgium

Ana Raquel Verissimo Department of Regenerative Medicine and Biomedical Engineering, Faculty of Medicine, Saga University, Saga, Japan

Vascular Surgery Group, Department of Cardiovascular Sciences, University of Leicester, Leicester, UK

S. Van Vlierberghe Polymer Chemistry and Biomaterials Group, Ghent University, Ghent, Belgium

Brussels Photonics (B-PHOT), Department of Applied Physics and Photonics, Vrije Universiteit Brussel, Brussels, Belgium

Giovanni Vozzi Research Center “E. Piaggio”, University of Pisa, Pisa, Italy

Xiong Wang Biomanufacturing Engineering Research Laboratory, Graduate School at Shenzhen Tsinghua University, Shenzhen, People’s Republic of China

Tao Xu Biomanufacturing Center, Department of Mechanical Engineering, Tsinghua University, Beijing, People’s Republic of China

Department of Precision Medicine and Healthcare, Tsinghua-Berkeley Shenzhen Institute, Shenzhen, People’s Republic of China

Biomanufacturing Engineering Research Laboratory, Graduate School at Shenzhen Tsinghua University, Shenzhen, People’s Republic of China

James Yoo Wake Forest Institute for Regenerative Medicine, Wake Forest School of Medicine, Winston-Salem, NC, USA

David A. Zopf Department of Otolaryngology Head and Neck Surgery, The University of Michigan, Ann Arbor, MI, USA

Part I

3D Printing



Additive Manufacturing for Tissue Engineering

Solaleh Miar, Ashkan Shafiee, Teja Guda, and Roger Narayan

Contents

1	Introduction	5
2	Bone	9
3	Cartilage	24
4	Muscle	26
5	Tendons and Ligaments	31
6	Cardiovascular System	37
7	Conclusions	40
	References	41

S. Miar · T. Guda

Department of Biomedical Engineering, University of Texas at San Antonio,
San Antonio, TX, USA

Graduate Program in Biomedical Engineering, University of Texas Health Science Center at San
Antonio, San Antonio, TX, USA

e-mail: solaleh.miar@utsa.edu; teja.guda@utsa.edu

A. Shafiee

Wake Forest Institute for Regenerative Medicine, Winston-Salem, NC, USA

e-mail: asn2@mail.missouri.edu

R. Narayan (✉)

UNC/NCSU Joint Department of Biomedical Engineering, Raleigh, NC, USA

Diabetes Center for Research, Department of Biomedical Engineering, UNC School of Medicine,
Chapel Hill, NC, USA

e-mail: roger_narayan@unc.edu

Abstract

Additive manufacturing is becoming a focus of attention owing to its unique abilities to fabricate different objects using various materials. Perhaps printing technologies are the most popular type of additive manufacturing that is gaining ground in a wide range of industrial and academic utilization. Three- and two-dimensional printing of different materials such as ceramics, plastics, and metals as well as electronic functional materials is considered as the next revolution in science and technology. Importantly, these technologies are being used extensively in medical applications. Tissue engineering, which aims to fabricate human tissues and organs, is benefiting from the reproducible, computer-controlled, and precise procedure that can be obtained by printers. Three-dimensional printings of scaffolds, cell-laden biomaterials, and cellular (scaffold-free) materials hold a great promise to advance the tissue engineering field toward the fabrication of functional tissues and organs. Here, we review the utilization of different printing technologies for various tissue engineering applications. The application of printers in tissue engineering of bones, cartilages, and tendons and ligaments is discussed. Moreover, an overview of the advancements in printing skeletal muscles as well as the cardiovascular system is given. Finally, future directions and challenges will be described.

List of Abbreviations

ATST	Apparent tissue surface tension
AM	Additive manufacturing
ACL	Anterior cruciate ligament
CAD	Computer aided design
CADD	Computer aided design and drafting
DLP	Digital light processing
EBM	Electron beam melting
ECM	Extra cellular matrix
FDM	Fused deposition modeling
FFF	Fused filament fabrication
GAG	Glycosaminoglycan
HA	Hydroxyapatite
hPMSCs	Human placenta-derived mesenchymal stem cells
MHC	Myosin heavy chain
MSCs	Mesenchymal stem cells
PAM	Pressure-assisted microsyringe
PCL	Polycaprolactone
PED	Precision extrusion deposition
PEG	Polyethylene glycol
PEGDMA	Poly (ethylene glycol)dimethacrylate
PEO	Polyethylene oxide
PHBV	Poly (hydroxybutyrate-co-hydroxyvalerate)

PLA	Poly(lactic acid)
PLDLLA	Poly (L-lactide-co-D,L-lactide)
PLGA	Poly-lactic-co-glycolic acid
PLLA	Poly (L-lactide) acid
PPF	Poly (propylene fumarate)
SEM	Scanning electron microscopy
SLA	Stereolithography
SLM	Selective laser melting
SLS	Selective laser sintering
TCP	Tricalcium phosphate
3D	Three-dimensional

1 Introduction

Synthetic scaffold grafts have traditionally been produced using various manufacturing processes, including mold casting; gas foaming; salt leaching; freeze drying; fiber fabrication from polymeric materials; powder metallurgy, forming, and stock machining for metallic biomaterials; and sintering for ceramic biomaterials. Shape, porosity, and interconnectivity are among the most important properties for the success of biomaterials in scaffolds or implants. However, conventional manufacturing processes cannot readily provide independent control over these structural properties. Additive manufacturing (AM) techniques, which were first introduced in 1986 by Charles Hull (Wohlers and Gornet 2014), have been actively embraced for accurate three-dimensional design and development of scaffold materials and implants. Since the first patent published by Hull's group describing stereolithography, various methods have been developed based on similar concepts to prepare highly organized three-dimensional structures. AM is based on the layer-by-layer synthesis of metals, polymers, ceramics, or their composites, with the manufacturing tolerance and resolution based on the thickness of the layer and the method of controlling material deposition within the layer. Various forms of material such as liquids, solids, or powders can be assembled using this approach. The bottom-up approach associated with AM lends itself to the creation of architectures that traditional manufacturing processes are limited in addressing such as internal porosities, lack of residual stress, and interlocking shapes without connections. Figure 1 shows a summary of various AM methods currently in development that are described in the recent literature (Standard 2012; Wong and Hernandez 2012; Thavornmyutikarn et al. 2014). Moreover, AM has recently evolved from the layering of materials to the incorporation of cells during the AM process. This approach, known as bioprinting, has many advantages for tissue regeneration. This method was first reported by Thomas Boland and colleagues at Clemson University in 2003 (Doyle 2014).

Regardless of the different printing approaches, AM involves three main steps (Gibson et al. 2010). First, all designs are precisely prepared through 3D modeling software, which builds spatial image models (CAD, STL, SLI, CADD). The 3D images are corrected or modified. Models are processed by a slicer software to make

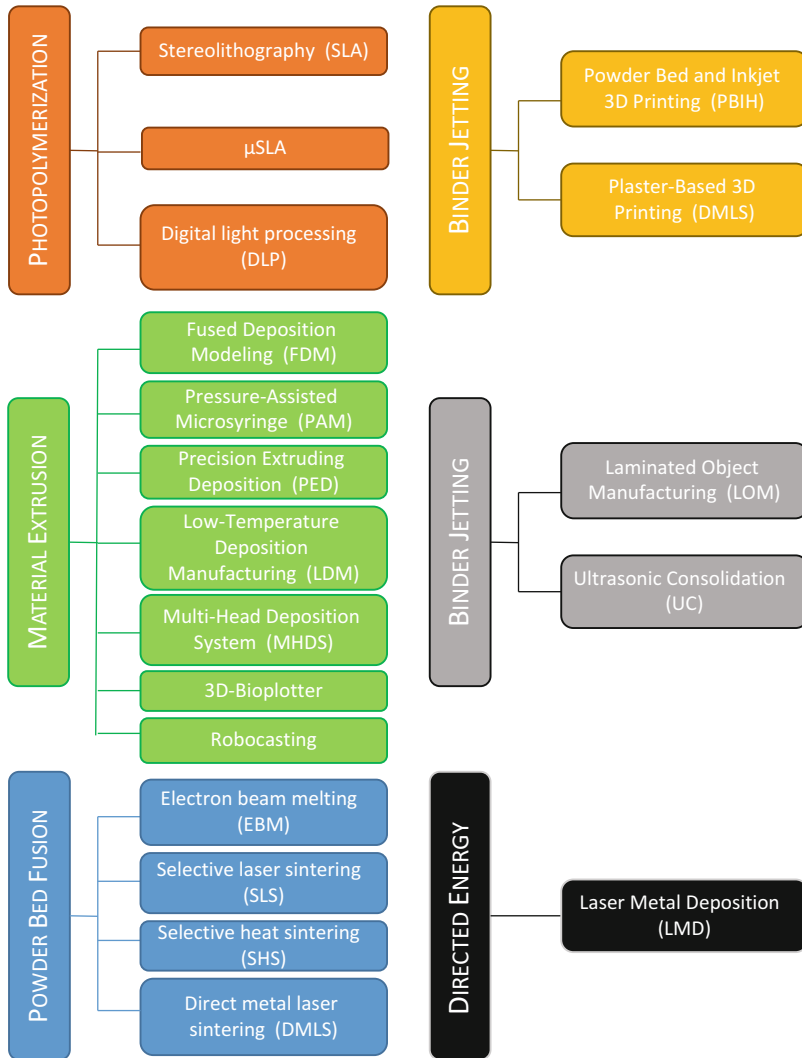


Fig. 1 Techniques utilized for AM of biomaterials

two-dimensional images for the next step (Kruth et al. 1998). The second step includes printing the model in a layer-by-layer manner using different materials or bioinks. The last step is related to curing, sintering, final finishing (Wong and Hernandez 2012), or other post-printing procedures (Kruth 1991). This step is highly dependent on the material. For example, bioprinted structures mostly require a post-printing step to evaluate the stability of the design and availability of sufficient nutrients (Murphy and Atala 2014). Ceramic or polymeric structures may require sintering (Travitzky et al.

2014) or post-polymerization processing (Wang et al. 2017) as well as inspection to validate the geometrical conformity to design tolerances.

The most important advantage of AM is the capability of the approach to produce customized structures, which constitute the prosthesis or scaffold. Modular implant manufacturing specially focuses on femoral (McCarthy et al. 1997; Geetha et al. 2009), wrist (Rahimtoola and Hubach 2004), and other small joint implants (Carignan et al. 1990). Although traditional mold casting and machining methods are time and cost-effective at an industrial scale, they are unable to provide customization tailored to individual patient needs. As a result, patients may face complications such as implant failure. It is anticipated that the next generation of modular implants will be based on accurate patient image data (Rengier et al. 2010; Bhumiratana and Vunjak-Novakovic 2012), in which each part can be customized before fabrication. Figure 2 shows a 3D-printed personalized titanium plate (Ma et al. 2017). Moreover, AM techniques allow for novel surface morphology features that can enhance cellular attachment and tissue infiltration. One such method is electron beam melting (EBM), in which materials are fused together by an electron beam in vacuum environment. EBM can be used for fabrication of

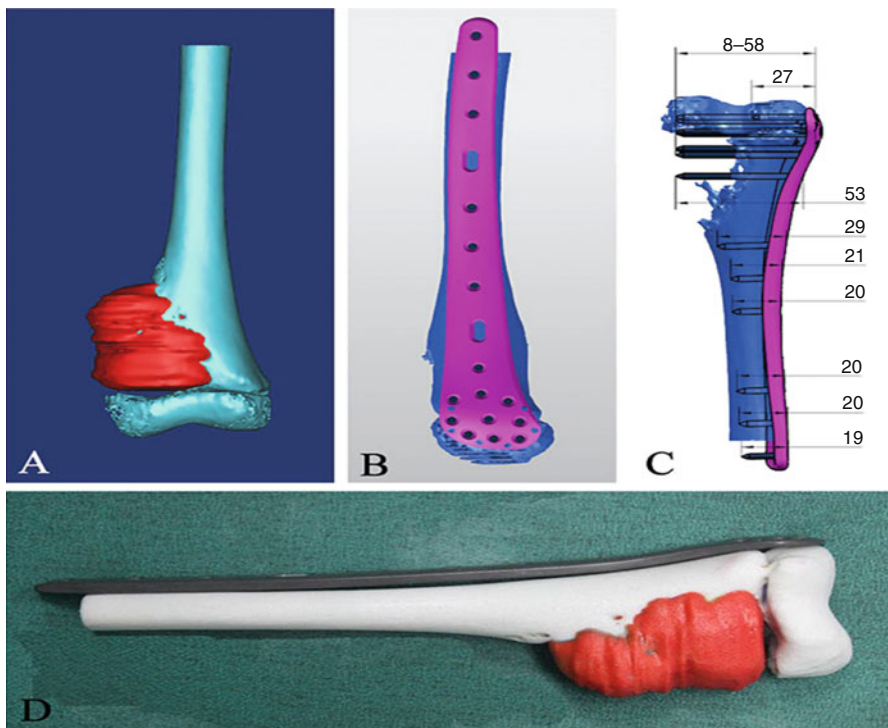


Fig. 2 3D-printed personalized titanium plates (Ma et al. 2017)

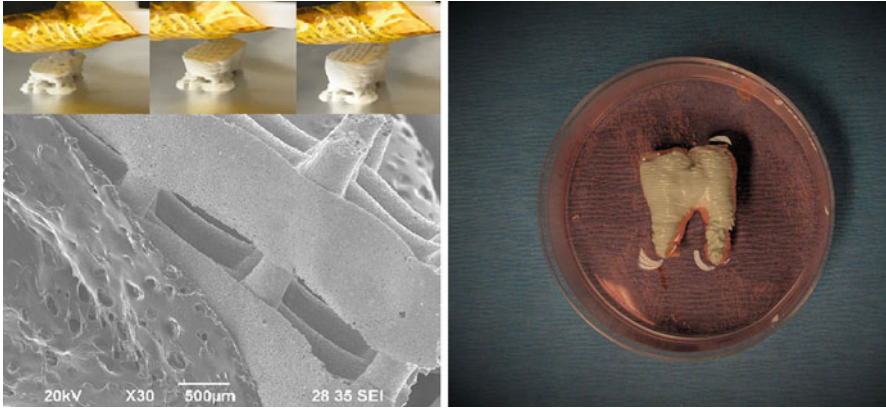


Fig. 3 Hydroxyapatite-based 3D tooth printed by Bioplotter

metallic meshes such as porous Ti6Al4V; the structures can contain surface features (Murr et al. 2010) for bone ingrowth and interfacial integration, enabling cement-free prostheses. Also, internal and external fixation devices including screws and plates have been printed based on patient 3D models (Qiao et al. 2015).

Beside implants, modular tissue engineering (Nichol and Khademhosseini 2009) offers customized fabrication for complex architectures such as the bone. Long bones are made of cancellous and compact bone in addition to the bone marrow and blood vessels (Melchels et al. 2012). However, conventional methods cannot readily produce structures with this complex morphology. AM, being a bottom-up process, has made it possible to produce integrated structures with different porosities, surface contours, and roughness values (Schantz et al. 2003; Naing et al. 2005; Zhang et al. 2008). Figure 3 is a personalized 3D structure of the teeth printed in our lab and an SEM picture of the printed layers.

Cartilage tissue, despite the characteristic low cell density and the absence of vascularization, continues to remain a challenge for tissue engineering. Early studies on the use of AM for cartilage tissue regeneration focused on acellular scaffold fabrication through extrusion-based methods (Hutmacher 2000; Schuurman et al. 2013). More recently, bioprinting methods have been employed to achieve uniform cell seeding and matrix organization through multi-head deposition systems (Kundu et al. 2015). Reports indicate that encapsulated cells, matrix, and proteins can be printed with independent spatial control to mimic the natural structure of the cartilage (Shim et al. 2012; Schuurman et al. 2013).

The skeletal muscle is a complex structure made of microfibers. Muscle contraction depends on actin and myosin filaments, which are stacked to form sarcomeres. As indicated by muscle regeneration studies, electrical (Rangarajan et al. 2014), mechanical (Rangarajan et al. 2014), and chemical (Husmann et al. 1996) factors lead to the differentiation of muscle cells. However, morphology and the scaffold design play prominent roles in the functionality of the muscle fibers. Studies show that aligned fibers facilitate the formation of aligned muscle cells (Avis et al. 2010).

Although electrospun fibers have shown promise for muscle tissue regeneration, this technology is still limited to two-dimensional tissue culture. Bioprinting not only provides more accurate fibrous structures (Ker et al. 2011), but it also produces aligned and reproducible 3D patterns (Cvetkovic et al. 2014; Yeo et al. 2016; Costantini et al. 2017). Bioprinting has been successfully used in interfacial tissue regeneration, including the synthesis of tendon-muscle units (Weiß et al. 2011; Merceron et al. 2015); for example, a combination of two types of polymers (thermoplastic polyurethane and poly (*ε*-caprolactone)) along with C2C12 and 3 T3 cells were printed to form an interface region of a tendon-muscle unit.

One of the advantages of personalized designs is the ability of printing of grafts in situ (Ventola 2014). While in situ bioprinting has been conducted for the treatment of skin lesions (Ozbolat and Yu 2013), it is anticipated that handheld bioprinters for in situ printing will facilitate graft or implant customization (Cui et al. 2012a) and will provide an additional tool for reconstructive surgeons.

Here we overview the application of additive manufacturing in some aspects of tissue engineering such as the bone, cartilage, muscle, tendon, and ligament, as well as cardiovascular research.

2 Bone

Successful new bone formation requires ECM formation, functional vascularization, and proper innervation. Synthetic grafts that meet these criteria are best designed in a modular fashion with an organized spatial design. AM enables the fabrication of structures with tailored microlevel porosity and the design of cell-free scaffolds by precise 3D deposition of metals (Bobbert et al. 2017) and ceramics (Bose et al. 2003; Leukers et al. 2005).

The preferred techniques for manufacturing ceramic-based scaffolds include powder bed fusion, binder jetting, and extrusion-based methods. Powder bed fusion is the method of choice when the stock material is available in powder form and works with both ceramic (Shuai et al. 2013) and polymer powders. Binder jetting, which is a hybrid of powder bed and ink-jet printing approaches, deposits binding agent on specified places of the substrate covered with powder particles. Binder jetting is an ideal technique to fabricate ceramic-based bone grafts made of silica and zinc oxide (Fielding et al. 2012), tricalcium phosphate (TCP) (Gbureck et al. 2007a, b; Tarafder et al. 2013b), and hydroxyapatite (HA) (Seitz et al. 2005; Igawa et al. 2006). Another fabrication technique in this family involves the use of a selective laser sintering (SLS) (Duan et al. 2010) that sinters designed places on a substrate covered with powder. Moreover, a frequently employed extrusion-based technique is robocasting. This method has been used to process HA (Dellinger et al. 2007; Miranda et al. 2008; Fu et al. 2011), TCP (Martínez-Vázquez et al. 2010), Bioglass (Fu et al. 2011), and their composites containing polymers such as polylactic acid (PLA) (Russias et al. 2007) and PCL (Heo et al. 2009).

Systems comprising solely of polymers have also been widely investigated for bone graft fabrication. Among biocompatible polymers, polycaprolactone (PCL) has

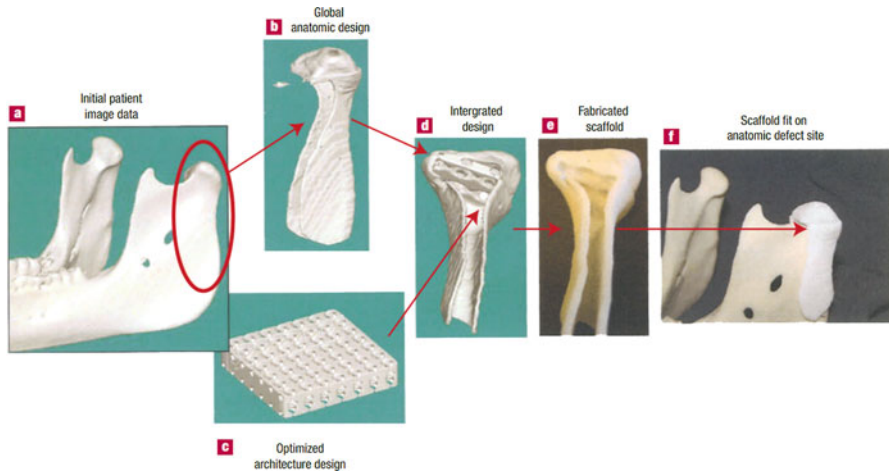


Fig. 4 Customized porous scaffold made through solid free-form fabrication and selective laser sintering. (Hollister 2005)

been used in bone scaffolds due to its mechanical properties, which are similar those of the bone (Oh et al. 2007). Its composites with ceramics, including HA or TCP (Hoque et al. 2012), have been frequently modeled by rapid prototyping and fabricated by extrusion-based printing. Poly-lactic-co-glycolic acid (PLGA) (Ge et al. 2009) and poly (L-lactide-co-D,L-lactide) (PLDLLA) (Lam et al. 2009a) can be processed into bone grafts using extrusion and powder printing. Powder printing is also ideal for ceramics-based scaffolds that require an appropriate binder. Binders affect the mechanical properties of the green (unsintered) part and hence determine the success of the final product. Various categories of binders have been optimized for particulate suspension and print cohesiveness, including water-based (Suwanprateeb and Chumnanklang 2006), organic (Vorndran et al. 2008; Suwanprateeb et al. 2012), and starch-based binders that are suitable for bone scaffold fabrication (Bose et al. 2013). Figure 4 shows a personalized scaffold made of PCL. This scaffold was designed by solid free-form fabrication and printed using SLS (Hollister 2005).

Direct writing is another extrusion-based method to produce polymer scaffolds (Serra et al. 2013). The advantage of this method is that it can be conducted at low temperature; therefore, growth factors and other temperature-sensitive agents can be safely loaded into the ink (Seyednejad et al. 2012). Some natural polymers such as alginate (Luo et al. 2015), gelatin (Zhang et al. 2013), and collagen (Kim and Kim 2013) have been used in bone scaffolds that are produced by this method. This method is based on the same principle as low-temperature deposition (Xiong et al. 2002), namely, direct layer-by-layer assembly of the material. This technique requires solvent compatibility for all of the system components, including one or more polymers, growth factors, or ceramic powders (Kim and Cho 2009; Liu et al. 2009). The other approach in extrusion-based methods is fused filament fabrication

(FFF) based on material melting for extrusion through the printer nozzle (Kalita et al. 2003; Ramanath et al. 2008). The limitation of this method is the high temperature required for melting the polymers, which prevents incorporation of drugs and biologics. Pressure-assisted microsyringe (PAM), precision extruding deposition (PED), and plotting are the other extrusion-based techniques that are used for polymeric bone scaffolds. PAM includes a reservoir with a capillary needle filled with polymer solution. The materials are printed using controlled air pressure. PCL (Vozzi et al. 2002), poly (L-lactide) acid (PLLA) (Vozzi et al. 2002), PLGA (Vozzi et al. 2003), and polyurethane (Tartarisco et al. 2009) are the polymers that are typically processed using the PAM method. PCL (Wang et al. 2004; Khalil et al. 2005; Shor et al. 2005; Shor et al. 2009) scaffolds have also been synthesized using PED. In this technique scaffold materials can be used in a granulated form, and filament preparation is not necessary. In addition to pure PCL, composite inks with alginate (Khalil et al. 2005) and HA (Shor et al. 2005) have also been prepared. Plotters are the other category of extrusion-based AM techniques, with PCL (Sobral et al. 2011) and starch (Oliveira et al. 2009; Oliveira et al. 2012) being the most conducive materials for ink formulation.

Selective laser sintering (SLS) and stereolithography (SLA) are other techniques that require photopolymerization to solidify the scaffold. SLS can involve the use of polymer powder to sinter structures for the preparation of bone scaffolds. One of the most commonly used polymers is poly (hydroxybutyrate-co-hydroxyvalerate) (PHBV) (Pereira et al. 2012) and its composites with other polymers such as PLLA (Duan et al. 2010) and ceramics such as calcium phosphate (Duan and Wang 2010a; Duan et al. 2010). In addition, PCL scaffolds made via SLS were able to incorporate an orthogonally porous structure for load-bearing sites, which optimized porosity and structural strength (Eshraghi and Das 2010; Thavornytikarn et al. 2014). SLA uses photopolymerization to make layer by layer a 3D object. Among SLA methods, both μ SLA and digital light processing (DLP) offer higher resolution and have been used to manufacture scaffolds for bone tissue regeneration (Thavornytikarn et al. 2014). Materials used in these studies include poly (propylene fumarate) (PPF) (Choi et al. 2009) and PCL-infiltrated ceramic scaffolds (Seol et al. 2013), with pore sizes ranging from 100 μ m to 300 μ m; these scaffolds have shown efficacy in supporting both the bone and associated vascular ingrowth.

In addition to accurate morphology and controlled porosity, the mechanical properties of bone scaffolds are the most important parameters that are evaluated for 3D-printed scaffolds. Similar to ceramic scaffold synthesis, the crucial post-printing step is sintering, which is required to reinforce the structure by the reformation of grain domains in the green body; this approach results in significantly greater strength and toughness that are essential parameters to fabricate tissues such as the bones. One of the new methods is microwave sintering, which has gained favor over conventional sintering since it offers lower energy consumption, reduced sintering time, better grain distribution, and improved mechanical properties (Oghbaei and Mirzaee 2010). For example, microwave-sintered TCP scaffolds fabricated by direct 3D printing showed an increase in compressive strength of up to 69% (Tarafder et al. 2013a) in comparison to the conventional sintered material. In

addition, other new methods (Bose et al. 2013) such as bioactive liquid phase sintering have been used to sinter hydroxyapatite/apatite-wollastonite glass composites fabricated by the 3D printing method, which improved the green strength of the composite from 1.27 MPa to 76.82 MPa (Suwanprateeb et al. 2009). A recent method (Khalyfa et al. 2007; Bose et al. 2013) to preform composite green structures has involved the immersion of HA or TCP scaffolds in monomers before sintering. In one report, scaffolds were immersed in copolymers such as PLLA and PCL to improve the mechanical properties via infiltration (Lam et al. 2002). More recently, this approach has also been used to improve the flexural strength of ceramic composites. In these studies, HA scaffolds exhibited an increase in bending modulus and strength by using infiltration after printing (Suwanprateeb et al. 2008).

Post-processing of metallic 3D-printed scaffolds is limited to final finishing; however, finishing may not be necessary due to the accuracy of the printed microstructure (Hedayati et al. 2017). Metallic scaffolds are mostly printed by selective laser melting (SLM) (van Hengel et al. 2017), EBM (Murr et al. 2012; Bsat et al. 2015; Zadpoor and Malda 2017), and SLS (Traini et al. 2008). All of these methods are based on one single sintering source at a powder bed. Recently, a new method called laser engineering net shaping has proposed powder injection in conjunction with the laser source as opposed to powder in bed (Atala and Yoo 2015). Of the methods noted, SLM is not limited to metals alone; polymer-ceramic composites have also been fabricated using this technique (Duan et al. 2010).

While 3D printing has largely been for the synthesis of cell-free scaffolds, bioinks (Ahn et al. 2012) containing various cell types and biomolecules along with polymers or ceramics have been investigated to expand the potential application of AM systems for regenerative medicine. Toxic solvents, high temperatures, and strong UV exposure are incompatible with cells, necessitating a substantive change from traditional 3D printing approaches to enable AM of biologics. Therefore, the selection of materials and systems for bioprinting-based graft fabrication is limited. Ink-jet bioprinting (Samad et al. 2011; Gao et al. 2014), extrusion bioprinting (Poldervaart et al. 2013), and stereolithographic bioprinting (Zhou et al. 2016) are methods that are frequently used for the preparation of cell-laden 3D structures. Cell suspensions containing alginate (Ahn et al. 2013), polyethylene glycol (PEG) (Gao et al. 2015a), and poly (ethylene glycol)dimethacrylate (PEGDMA) with bioactive glass and HA nanoparticles (Gao et al. 2014) have been utilized in bioprinting studies. One of the new techniques, which was first attempted for skin tissue regeneration, is laser printing (Koch et al. 2012); this approach provides a new mechanism for generating multicellular 3D designs with potential use in bone regeneration (Gruene et al. 2010). Moreover, bioprinting methods allow growth factors and other biomolecules to be directly incorporated (potentially in the same locations as the target cells) and locally released. Growth factors such as fibroblast growth factor (Ker et al. 2011), vascular endothelial growth factor (Poldervaart et al. 2014), and bone morphogenetic proteins (Poldervaart et al. 2013) have incorporated within bioprinted scaffolds; localized release from bioprinted scaffolds and release profiles have been reported. Table 1 (I–XI) discusses studies related to the use of AM in bone tissue regeneration.

Table 1 Various AM techniques used in bone tissue regeneration

Publication	Material (s)	Cell type (s)	Porosity (%)	Pore size (μm)	Strength (MPa)
I. Vat photopolymerization – Stereolithography					
(Cooke et al. 2003)	Diethyl fumarate (DEF), poly (propylene fumarate) (PPF)	–	90	150–800	20–70
(Lee et al. 2007b)	Poly (propylene fumarate)	–	61–63	600–1000	11–146
(Padilla et al. 2007)	Bioactive glass	–	–	400, 1400	–
(Bian et al. 2011)	β -TCP and acrylamide, methylenebisacrylamide	–	45	600–800	24
(Tesavibul et al. 2012)	Bioglass	–	50	500	0.33
(Ronca et al. 2013)	Poly (d,l-lactide)/nano-sized hydroxyapatite (PDLLA/nano-hap) composite resin	–	63–66	620–690	50–66
(Barry et al. 2008)	OCM-2	HOBS	40	–	–
(Jansen et al. 2009)	Fumaric acid monoethyl ester-functionalized poly (D, L-lactide)/ N-vinyl-2-pyrrolidone resins	MC3T3	76	260	0.01–2.1
(Melchels et al. 2009)	Poly (d,l-lactide)	MC3T3	83	170–240	–
(Heller et al. 2009)	Vinyl ester	MC3T3-E1	–	–	1.5–1.7
(Lan et al. 2009)	Poly (propylene fumarate) (PPF)	MC3T3-E1 pre-osteoblasts	65	250	68.8 \pm 9.4
(Melchels et al. 2010)	PDLLA	A4–4	70	255	–

(continued)

Table 1 (continued)

Publication	Material (s)	Cell type (s)	Porosity (%)	Pore size (μm)	Strength (MPa)
(Seck et al. 2010)	Poly (ethylene glycol)/poly (d,l,lactide)-based resins	hMSC	52	423	–
(Lee et al. 2011)	PLGA	MC3T3-E1 pre-osteoblasts	69.6	430	–
(Elomaa et al. 2011)	Poly (ϵ -caprolactone)	NIH3T3 fibroblasts	69–71	465	–
(Seol et al. 2013)	HA and TCP powder	hTMSCs	–	300	2.47 ± 0.035
(Elomaa et al. 2013)	Bioactive glass and photocrosslinkable poly (ϵ -caprolactone)	Human gingival fibroblasts	77	476–594	~ 2.5
II. Vat photopolymerization – Two-photon printing					
(Claeys et al. 2009)	Biodegradable triblock copolymer poly (ϵ -caprolactone-co-trimethylenecarbonate)-b-poly (ethylene glycol)-b-poly (ϵ -caprolactone-co-trimethylenecarbonate)	Only cytotoxicity tests: Murine fibroblast cell line NIH-3 T3	–	–	96 ± 2 kPa
(Petrochenko et al. 2015)	Biodegradable urethane and acrylate-based photoelastomer	Human bone marrow stem cells	60	200	–
(Marino et al. 2014)	Hybrid photoresist (Ormocomp [®])	SaOS-2 bone-like cells	–	–	–
III. Vat photopolymerization – Digital light processing					
(Dean et al. 2012)	PPF	–	–	800	–

(Tesavibul et al. 2012)	45S5 Bioglass	–	50	500	–
(Lee et al. 2012)	PCL and PLGA	Mouse osteoblastic cell line MC3T3-E1	57.2	200	6.05–9.81
IV. Vat photopolymerization – uSLA					
(Lu et al. 2006)	PEGDA	Murine OP-9 marrow stromal cells	–	165–650	–
(Kim et al. 2007)	HA	NA	–	250	–
(Lan et al. 2009)	PPF/diethyl fumarate (DEF)	MC3T3-E1 pre-osteoblast	65	250	–
(Lee et al. 2009)	PPF/DEF-HA	MC3T3-E1 pre-osteoblasts	–	430	–
(Lee et al. 2011)	Poly (propylene fumarate)/diethyl fumarate photopolymer loaded PLGA microspheres	MC3T3-E1 pre-osteoblasts	69.6	430	–
(Seol et al. 2013)	Ha-TCP- PCL	Human turbinate mesenchymal stromal cells (hTMSCs)	–	300	–
(Raman et al. 2016)	Poly (ethylene glycol) dimethacrylate (PEG-dma) resin	Murine cells (fibroblasts, myoblasts, endothelial, and bone marrow stromal cells)	–	100	–
(Owen et al. 2016)	Polymerized high internal phase emulsions	Embryonic stem cell-derived mesenchymal progenitor cells (hES-MPs)	–	300 µm (vertically) and 650 µm (laterally)	UTS from 2.03 to 0.11
(Mott et al. 2016)	Poly (propylene fumarate) (PPF)	L929 cell	–	–	7.8–36.5

(continued)

Table 1 (continued)

Publication	Material (s)	Cell type (s)	Porosity (%)	Pore size (μm)	Strength (MPa)
V. Material extrusion – Robocasting					
(Miranda et al. 2006)	β -Tricalcium phosphate	–	45	75	20
(Russias et al. 2007)	HA and bioglass with PLA and PCL as the ink	–	75	200–500	–
(Dellinger et al. 2007)	Hydroxyapatite	–	–	100–600	–
Martínez-Vázquez	β -tricalcium phosphate poly(lactic acid (PLA) and poly (ϵ -caprolactone) (PCL)	–	25	–	20–130
(Fu et al. 2011)	Bioactive glass	–	60	500	136 \pm 22
(Heo et al. 2009)	m-HA/PCL	MG-63 osteoblast-like cells	72–73	500	–
(Serra et al. 2013)	PEG	Rat mesenchymal stem cells	85.7–87.2	375 \pm 25	–
(Keriquel et al. 2010)	Nano-hydroxyapatite (n-HA)	In vivo	–	–	–
VI. Material extrusion – Fused deposition modeling (FDM)					
(Lam et al. 2007)	β -TCP and PCL	–	68	–	–
(Lam et al. 2008)	β -TCP and PCL	–	69	–	–
(lam et al. 2009b)	β -TCP and PCL	–	70	–	–
(Ramanath et al. 2008)	Poly- ϵ -caprolactone	–	–	–	–
(Martins et al. 2009)	Starch and polycaprolactone	–	68.3–79.4	–	–

(Iam et al. 2009a)	PLDLA/TCP	-	-	-	-	23
(Tellis et al. 2008)	Polybutylene terephthalate	-	57-79	-	196-292 and 120-772	-
(Humacher et al. 2001)	PCL	Fibroblast and osteoprogenitor cell	61	-	-	3.1
(Darsell et al. 2003)	Alumina	OPC1	29-44	-	300	130-70
(Kalita et al. 2003)	Polypropylene (PP) polymer and tricalcium phosphate (TCP)	OPC1	36-52	-	160	12.7
(Zhou et al. 2007)	Polycaprolactone and polycaprolactone-tricalcium phosphate	Alveolar bone	43-65	-	-	x-axis, 2.2, 4.4; z-axis, 1.5-3.1
(Shor et al. 2007)	Polycaprolactone/hydroxyapatite	Primary fetal bovine osteoblast	60-70	-	450	-
(Ye et al. 2010)	PCL	MG63 cells	53-76	-	400-500	2.7-7.9
(Korpela et al. 2013)	Poly (ε-caprolactone)/bioactive glass	Fibroblast	30-40	-	400	-
VII. Material extrusion – Precision extruding deposition (PED)						
(Xiong et al. 2001)	PLLA	-	60.3	-	500 × 400	8.32
(Wang et al. 2004)	PCL	-	-	-	200-300	-
(Shor et al. 2005)	Polycaprolactone (PCL)/hydroxyapatite (HA)	Endothelial cells (RHEC)	64	-	400	-
(Khalil et al. 2005)	PCL-alginate	Human endothelial cells	-	-	650	-
(Shor et al. 2009)	Polycaprolactone	Primary fetal bovine osteoblast cells	65	-	350	5.3

(continued)

Table 1 (continued)

Publication	Material (s)	Cell type (s)	Porosity (%)	Pore size (μm)	Strength (MPa)
(Yildirim et al. 2010)	PCL	7F2 mouse osteoblast cells	–	300	–
VIII. Material extrusion – Low-temperature deposition manufacturing (LDM)					
(Xiong et al. 2002)	Poly (l-lactic acid) (PLLA), tricalcium phosphate (TCP)	–	89.6	400	Bend strength, 12.1; compressive yield strength, 4.71
(Liu et al. 2009)	PLGA, collagen, gelatin, chitosan, TCP	–	–	300–500	–
(Li et al. 2011)	PLGA- TCP	HBMSCs	87.4	380	–
(Hsu et al. 2012)	Chitosan	MC3T3-E1	–	From the top view 500 \times 500	–
(Park et al. 2011)	Poly (lactic-co-glycolic acid) grafted hyaluronic acid	In vivo, in vitro release of bmp2	–	250–300	–
IX. Material extrusion – Bioplotter and 3D plotter					
(Oliveira et al. 2009)	Starch/polycaprolactone	–	–	–	–
(Sobral et al. 2011)	Poly (ϵ -caprolactone)	Human osteosarcoma cell line SaOs-2	10–85	100–900	–
(Oliveira et al. 2012)	Starch/poly- ϵ -caprolactone (SPCL)	Bone marrow mesenchymal stem cells	70	–	–
(Lode et al. 2014)	Paste-like CPC	hMSCs	56	–	6.1 \pm 1.8
X. Powder bed fusion – Electron beam melting (EBM)					
(Thomsen et al. 2009)	Ti6Al4V	–	–	–	910–940
(Heiml et al. 2008)	Ti6Al4V	–	59.5–81.1	1230	Diamond structure, 16.1–22 Mpa; hatched structure, 49.6–107.5 Mpa

(Li et al. 2009)	Ti6Al4V	-	66.3	1108	67.7
(Parthasarathy et al. 2010)	Ti6Al4V	-	60.91-74	1000-1230	7.28-163.02
(Murr et al. 2011)	Ti6Al4V	-	-	400	-
(Cheng et al. 2012)	Ti6Al4V	-	62.08-91.65	-	3.8-112.8
(Campoli et al. 2013)	Ti6Al4V	-	10-20	-	-
(Ahmadi et al. 2014)	Ti6Al4V	-	-	-	-
(Zhao et al. 2016)	Ti6Al4V	-	62.1-64.5	30-80	61-196
(lv et al. 2015a)	Ti6Al4V	hMSCs	-	640	-
(lv et al. 2015b)	Ti6Al4V	Rat bone marrow-derived mesenchymal stem cells (rMSCs)	73-81.9	640-1200	-
(Ponader et al. 2010)	Ti6Al4V	In vivo	61.3	450	127.1-148.4
(Palmquist et al. 2013)	Ti6Al4V	In vivo	65-70	500-700	-
(Biemond et al. 2013)	Ti6Al4V	In vivo	49-63	250-800	2.0-3.2
(Wu et al. 2013)	Ti6Al4V	In vivo	68	710	63-120
XI. Powder bed fusion – Selective laser sintering (SLS)					
(Lorrison et al. 2005)	Glass-ceramic and a combination of hydroxyapatite and phosphate glass	-	-	-	-

(continued)

Table 1 (continued)

Publication	Material (s)	Cell type (s)	Porosity (%)	Pore size (μm)	Strength (MPa)
(Simpson et al. 2008)	Poly (L-lactide-co-glycolide)	–	125–250	46.5	12.06 ± 2.53
(Eosoly et al. 2010)	Hydroxyapatite/poly- ϵ -caprolactone	–	–	1200	0.1 and 0.6
(Duan and Wang 2010b)	Ca-P/PHBV	–	$1.0 \times 1.0 \times 1.0 \text{ mm}^3$	–	–
(Kolan et al. 2012)	13–93 bioactive glass	–	50	300–800	41–157
(Pereira et al. 2012)	Poly (3-hydroxybutyrate) (PHB)	–	–	–	–
(Shuai et al. 2013)	β -tricalcium phosphate	–	–	600	–
Dadbakhsh et al. 2014)	NiTi	–	–	–	–
(Wiria et al. 2007)	PCL/HA biocomposite	105	–	–	2.53–11.54
(Zhang et al. 2009)	HA-PE and HA-filled PA	HOB cells	10–100	46–47	–
(Kanezler et al. 2009)	PLA	Human fetal femur-derived cells	–	–	–
(Duan and Wang 2010a)	Ca-P/PHBV	Human osteoblast-like	800	64.6 ± 2.0 – 62.6 ± 1.2	–
(Duan et al. 2010)	Calcium phosphate (ca-P)/poly (hydroxybutyrate-co-hydroxyvalerate) (PHBV) and carbonated hydroxyapatite (CHAp)/poly (l-lactic acid) (PLLA) nanocomposite microspheres	Human osteoblast-like cell line (SaOS-2)	62–70	800	0.47–0.63

(Sudarmadji et al. 2011)	PCL	Osteoblasts	–	40–80	0.17–5.03 MPa
(Eosoly et al. 2012)	Polycaprolactone-hydroxyapatite	MC 3 T3	–	1200	0.15–0.41
(Van Bael et al. 2013)	PCL	hPDC	1500–2000	–	0.97 ± 0.03
(Williams et al. 2005)	Polycaprolactone	Primary human gingival fibroblasts	1750–2500	17.8–55	2.0–3.2 Mpa
(Goodridge et al. 2007)	A–M glass-ceramic and 45S5	In vivo	–	–	–
(Lohfeld et al. 2012)	Polycaprolactone/tricalcium phosphate	In vivo	51–77	Up to 1000	–
XII. Powder bed fusion – Selective heat sintering (SHS)					
(Tosun et al. 2009)	NiTi	–	–	50.7–59.7	–
(Tosun and Tosun 2012)	NiTi	–	–	50.3–57.4	–
(Tosun et al. 2012)	NiTi	–	205.98–741.35	–	–
(Resnina et al. 2013)	NiTi	–	Preheating temperature of 613 for Ti, 48.0 at.% Ni; Ti, 50.0 at.% Ni mixture; 653 K for Ti, 45.0 at.% Ni; Ti, 52.0 at.% Ni mixture, 180–349; preheating temperature of 723 for Ti, 45.0 at.% Ni; Ti, 52.0 at.% Ni mixture; 773 K for Ti, 48.0 at.% Ni; Ti, 50.0 at.% Ni mixture, 220–363	54–66	–

(continued)

Table 1 (continued)

Publication (Shishkovsky et al. 2010)	Material (s)	Cell type (s)	Porosity (%)	Pore size (μm)	Strength (MPa)
	NiTi	In vivo	–	40–50	–
XIII. Powder bed fusion – Direct metal laser sintering (DMLS)					
(Bertol et al. 2010)	Ti6Al4V	–	–	–	–
(Iardini et al. 2011)	Ti6Al4V	–	–	–	–
(Barucca et al. 2015)	Co–Cr–Mo	–	–	–	–
(Ciocca et al. 2011)	Titanium	In vivo	–	–	–
(Stübinger et al. 2013)	Titanium	In vivo	–	500	–
XIV. Binder jetting – Powder bed and ink-jet 3D printing (PBIF)					
(Gbureck et al. 2007)	Calcium phosphate and PLA/PGA polymer solutions	–	HA, 12 μm ; dicalcium phosphate dihydrate, 13 μm	Brushite ceramics, 29–45 and hydroxyapatite ceramics, 55–60	DCPD, 22.3; HA, 5.8
(Klammert et al. 2010)	TCP	–	–	28–35	Bending strength: 3.9–5.2
(Winkel et al. 2012)	Bioactive glass and hydroxyapatite	–	900–2000	–	70
(Suwanprateeb et al. 2012)	HDPE	–	132.6–136.2	22.3–49.7	4
(Seitz et al. 2005)	Hydroxyapatite	Bone patient's cells	565	–	22
(Khalyfa et al. 2007)	TCP	MC3T3-E1	–	38	0.59–0.7

(Ge et al. 2009)	Poly-lactic-co-glycolic acid	Human fetal osteoblasts	1000	50	7.8
(Cooper et al. 2010)	DermaMatrix	C2C12	–	–	–
(Wiria et al. 2010)	Titanium powder	L-929 fibroblast cells	–	–	167–455
(Fielding et al. 2012)	Silicon dioxide and zinc oxide and synthetic β -tricalcium phosphate	Human fetal osteoblast	343.7–698	–	4.34–10.21
(Taraïder et al. 2013a)	β -TCP	Human fetal osteoblast cells (hFOB)	500–1000	42–63	10.95–6.6
(Santos et al. 2012)	TCP	Human osteoblast cell culture	30	46.07–54.44	2.36–8.66
(Xu et al. 2013b)	Alginate	dSMCs-bECs-hAFSCs	–	–	2.2
(Gao et al. 2014)	PEGDMA and ha	hMSCs and mesenchymal stem cell	–	–	–
(Gao et al. 2015a)	PEG-GelMA	hMSCs	–	–	30–63 Kpa
(Igawa et al. 2006)	HA and TCP powder	In vivo	–	55	Bending strength, 9; compressive strength, 20
(Gbureck et al. 2007)	TTCP	In vivo	HA, 12 μ m; dicalcium phosphate dihydrate, 13 μ m	Brushite ceramics, 29–45 and hydroxyapatite ceramics, 55–60	DCPD, 22.3; HA, 5.8
(Saijo et al. 2009)	TCP	In vivo	–	–	–
(Taraïder et al. 2013b)	β -TCP SrO and MgO	In vivo	245–311	27–35	12

3 Cartilage

Restoration of osteochondral tissue damaged due to age, degeneration, or injury is a significant concern in orthopedic health care. When therapies such as autologous chondrocyte transplantation and microfracture surgery are not feasible, cartilage tissue engineering is one of the potential options for articular surface regeneration (Hutmacher 2000; Temenoff and Mikos 2000). Different methods have been developed to design a non-vascularized structure for cartilages with similar mechanical properties to native tissue and an appropriate interface with bone tissue for functional load transfer and shear resistance. Various methods such as solution casting (Freed et al. 1993), freeze drying (Tan et al. 2009), phase separation (Mikos and Temenoff 2000), and fiber fabrication (Hutmacher 2000) have been previously examined; however, there is an absence of precise control over porosity and interconnectivity, which is necessary for successful bone growth at the interface. AM is a promising alternative for cartilage regeneration since it enables precise control over pore morphology as well as bulk structure. It also provides an opportunity to include different cell types (Sharma and Elisseff 2004) during the manufacturing process, which was hitherto impossible using conventional methods due to the harsh environment associated with scaffold fabrication (e.g., high temperature or the presence of harmful solvents).

Additive manufacturing techniques such as stereolithography and methods combining techniques such as ink-jet printing, extrusion-based methods, and powder bed fusion have been successfully employed for cartilage scaffold processing (Santos et al. 2013; Vaezi et al. 2013). Due to the high cellularity of the tissue as well as given the lack of tissue vasculature, AM techniques for cartilage scaffold fabrication have focused to a greater extent on cell printing (Cui et al. 2012b; Di Bella et al. 2015) to enhance cellular delivery to the scaffold interior than methods for bone graft manufacturing.

The use of stereolithography for chondrogenic applications has been reported with a variety of polymers, including poly (trimethylene carbonate)-based resins (Schüller-Ravoo et al. 2013), Fumaric acid monoethyl ester (Jansen et al. 2009), PCL (Elomaa et al. 2011), (PDLA-PEG)/hyaluronic acid (Sun et al. 2015), and polyacrylamide (Linzhong et al. 2010). Modified SLA techniques such as two-photon polymerization (Weiß et al. 2009), μ SLA (Lee et al. 2007a, 2008; Weiß et al. 2011), and digital light processing (Sun et al. 2015) have been utilized to enhance the accuracy of scaffold fabrication for articular cartilage applications. Studies using SLA have so far been limited to biocompatibility and cell proliferation testing. A greater focus on tissue morphogenesis in long-term bioreactor culture or testing in appropriate translational preclinical models is necessary for further therapeutic advances in this area (Santos et al. 2013).

Ink-jet printing technology (Boland et al. 2006; Samad et al. 2010a, b, c) is a method based on the deposition of the polymeric ink in a drop-by-drop manner (Shafiee et al. 2008); this approach is able to form a line similar to those formed by filament extrusion-based systems. Using this technique, the researchers can deposit sub-microliter of materials on precise location of a substrate that reduces the

deposition cost dramatically by minimizing of material waste (Shafiee et al. 2009). An additive pattern containing such lines can be used to construct a 3D structure. This method has been used to create osteochondral scaffolds with different polymers and hydrogels; for example, PLGA-PLA is used in the cartilaginous zone, and PLGA-TCP is used at the transition associated with the cartilage-bone interface (Sherwood et al. 2002). In a study by Sherwood et al., the structural porosity and materials are designed to trigger chondrocyte proliferation and hypertrophy in the PLGA-PLA portion and simultaneously stimulate bone growth in the PLGA-TCP zone. There have also been studies related to the use of this approach for bioprinting. In one study, human chondrocytes were suspended in PEGDA and polymerized photochemically (Cui et al. 2014) to create a bioprinted cartilage gel. A modified version of the polymer (PEGDMA) has been reported for use in chondrocyte bioprinting. The design showed firm attachment of the printed structure to the surrounding tissue and greater proteoglycan deposition at the interface of the scaffold and the native cartilage (Cui et al. 2012b; Gao et al. 2015b), indicating local biocompatibility and cellular migration. In a similar study, it was demonstrated that bioprinted samples treated with growth factors showed chondrogenic properties due to the synergistic action of basic fibroblast growth factor and transforming growth factor beta-1 (Cui et al. 2012c). Other approaches have combined electrospinning with ink-jet printing to fabricate 3D hybrid structures containing electrospun PCL fibers and chondrocytes suspended in a fibrin-collagen hydrogel; this approach has provided an improvement in biological and mechanical properties (Xu et al. 2012).

The use of extrusion techniques and fused deposition modeling (FDM)-based methods to process polymers such as PCL alongside cells and growth factors is limited due to the high temperature (Cao et al. 2003; Hsu et al. 2007) required for polymer extrusion. FDM uses a continuous filament of material that can be melted using a high-temperature heater – the melted filaments fuse and solidify once it is dispensed from the nozzle. Poly (ethylene glycol)-terephthalate-poly (butylene terephthalate) (PEGT/PBT) block copolymer scaffolds have been developed using a modified FDM method that involves a fiber deposition technique (Woodfield et al. 2004). In another study, poly (ethylene oxide-terephthalate)-co-poly (butylene terephthalate) (PEOT/PBT) hollow fibers were extruded to form 3D scaffolds with the potential for controlled growth factor release (Moroni et al. 2006). Using the FDM method, 3D scaffolds were produced using PLGA and were modified post-printing with type II collagen for enhanced chondrocyte compatibility (Yen et al. 2009). It was found that increased fiber spacing in FDM scaffolds led to improved transport of degradation by-products, which limited the influence of the local acidic milieu on tissue regeneration. Liquid-frozen deposition manufacturing (LFDM) is another extrusion-based method that has been used to fabricate PLGA scaffolds. A direct head-to-head comparison between PLGA scaffolds manufactured by FDM and those manufactured by LFDM showed that LFDM scaffolds supported better chondrocyte proliferation and secreted extracellular matrix; FDM scaffolds showed lower cell numbers and matrix production because of heavy swelling (Yen et al. 2008). The LFDM method has been utilized to generate PLGA scaffolds that were loaded with

human placenta-derived mesenchymal stem cells (hPMSCs), which promoted the secretion of glycosaminoglycan (GAG) at twice the rate of mesenchymal stem cells (MSCs) (Hsu et al. 2011) and indicated an ability to support cartilage regeneration. Biodegradable polyurethane elastomers were also synthesized using LFD in the form of nanoparticles, which were combined with polyethylene oxide (PEO); PEO served as a viscosity enhancer. This material was prepared as a scaffold and compared to PLGA using an *in vitro* chondrocyte cell seeding study, which demonstrated that cell proliferation and GAG secretion were higher in the PU scaffold than in the PLGA scaffold (Hung et al. 2014). These studies indicate that significant biomaterials optimization research needs to be conducted to identify the chemical and structural parameters that influence the promotion of a pro-chondrogenic niche. Such studies are essential for the further translation of LFD-processed 3D structures for cartilage tissue engineering.

Cell-laden scaffolds have also been prepared using PLGA/alginate and PLGA-HA containing human fetal-derived stem cells and cartilage-derived ECM, which showed successful cartilage and subchondral layer fabrication up to a height of 5 mm (Yang et al. 2015). Fluorescently labeled human chondrocytes and osteogenic progenitors suspended in alginate have also been used for constructing 3D grafts (Fedorovich et al. 2011). p (HPMAm-lac)-PEG-p (HPMAm-lac)-based hydrogel fibers were generated that showed thermosensitivity as well as photopolymerizability; 3D cell-laden scaffolds were prepared, which demonstrated good mechanical properties and tunable degradation (Censi et al. 2011). Beside the aforementioned methods, use of other techniques such as SLS has been reported. In addition, combinatorial methods have been investigated using materials such as PCL (Chen et al. 2014a) as the fabrication substrate in SLS and modification with polymers such as gelatin (Chen et al. 2011) and collagen (Chen et al. 2014b). Table 2 lists the various additive manufacturing techniques used to generate scaffolds for cartilage regeneration highlighting studies that have investigated bioprinting applications.

4 Muscle

In studies related to skeletal muscle regeneration, structures are mostly bioprinted. Structures have remained essentially two dimensional (in the form of cell sheets) rather than solid volumetric scaffolds. The two primary uses of additive manufacturing in the case of skeletal muscle have been to generate aligned cell growth for improved tissue morphogenesis and to obtain spatial control of growth factors for supporting directed tissue growth. Scaffolds made of directional parallel fibers stimulate muscle cells to grow in an aligned manner and support further myoblast growth, fusion, and myotube formation (Liang et al. 2007; Wang et al. 2012; Ostrovidov et al. 2014). Various approaches have been developed to support the fabrication of aligned fibers, including electrospinning (San Choi et al. 2008) and wet spinning (Razal et al. 2009). AM technologies such as ink-jet bioprinting (Seol et al. 2014) have also been employed to pattern various growth factors on material surfaces (Jose et al. 2016). This approach has been used to pattern fibroblast growth factor-2 (Campbell et al.

Table 2 Various AM techniques used in cartilage tissue regeneration

Category	Method	Publication	Cell density (cell/ml)	Porosity	Cell viability	Modulus (KPA)	Material	Cell type	Bioprinting
Binder jetting	Ink-jet printing	(Cui et al. 2012b)	–	–	89	395.73 – 80.40	PEGDMA	Human articular chondrocytes	Yes
		(Cui et al. 2014)	5×10^6	–	90	–	PEGDA	Chondrocyte	Yes
		(Gao et al. 2015b)	6×10^6	–	$87.9 \pm 5.3\%$	33–67	Acrylated poly (ethylene glycol) (PEG)	Human mesenchymal stem cells (hMSCs)	Yes
		(Cui et al. 2012c)	8×10^6 and 20×10^6	–	$84.9 \pm 2.2\%$	36.90 ± 3.41 and 29.88 ± 2.33	PEGDMA	Human articular chondrocyte	Yes
		(Xu et al. 2012)	$3-4 \times 10^6$	–	$81.58 \pm 3.46\%$	0.41–1.76	PCL-collagen	Articular chondrocytes	Yes
		(Sherwood et al. 2002)	–	25–55	–	Tensile, 83–233; compressive, 54–450 Mpa	d,L-PLGA/l-PLA and l-PLGA/TCP	Chondrocytes	No
Vat photopolymerization	SLA	(Schüller-Ravoo et al. 2013)	–	$54.0 \pm 2.2\%$	–	100	Poly (trimethylene carbonate)	Bovine chondrocytes	No
		(Melchels et al. 2009)	–	73	–	56 ± 2 Mpa	PDLLA	Mouse pre-osteoblasts (MC3T3 cell line)	No
		(Elomaa et al. 2011)	–	$70.5 \pm 0.8\%$	–	$6.7-15.4$ Mpa	PCL	NIH3T3 fibroblasts	No
		(Sun et al. 2015)	4×10^6	–	84	780	Poly-d,l-lactic acid/polyethylene glycol/poly-d,l-lactic acid (PDLLA-PEG)/hyaluronic acid (HA)	Human adipose-derived stem cell	Yes

(continued)

Table 2 (continued)

Category	Method	Publication	Cell density (cell/ml)	Porosity	Cell viability	Modulus (KPA)	Material	Cell type	Bioprinting
		(Linzhong et al. 2010)	–	–	–	4.54 MPa	Acrylamide	–	No
	Two-photon printing	(Weiß et al. 2009)	–	–	–	–	?	Bovine chondrocytes	No
		(Weiß et al. 2011)	–	–	–	–	Poly (ethylene glycol diacrylate) (PEGDA) and acrylamide	Bovine chondrocytes	No
	uSLA	(Lee et al. 2007a)	–	–	–	8.72–519.1 Mpa	PPF/DEF	Fibroblast	No
		(Lee et al. 2008)	–	–	–	–	TMC/TMP	–	No
Material extrusion	Fused deposition modeling (FDM)	(Cao et al. 2003)	–	–	–	–	PCL	Chondrocytes	No
		(Hsu et al. 2007)	–	52–97	–	–	PLA-PCL	Chondrocytes	No
		(Woodfield et al. 2004)	–	55–87	–	0.05–2.5	Poly (ethylene glycol)-terephthalate-poly (butylene terephthalate) (PEGT/PBT)	–	No
		(Yen et al. 2009)	–	47–97	–	Storage moduli: 2.5–8 MPa	PLGA collagen	Chondrocytes	No

	Liquid-frozen deposition	(Yen et al. 2008) (Hsu et al. 2011)	— —	45–78 49.46–5.48%	— —	Storage modulus: 0.26–5.68 MPa	PLGA PLGA/alginate	Chondrocytes Human placenta-derived mesenchymal stem cells (hPMSCs)	No Yes
		(Hung et al. 2014)	—	—	—	1.66 ± 0.06 MPa	Polyurethane (PU)-polyethylene oxide (PEO)-poly(lactic-co-glycolic acid (PLGA))	Chondrocytes	No
	Material extrusion	(Moroni et al. 2006)	—	—	—	—	Poly (ethylene oxide-terephthalate)-co-poly (butylene terephthalate) (PEOT/PBT)	Chondrocytes	No
		(Fedorovich et al. 2011)	MSCs and Chs: 5 · 10 ⁶ and 3 · 10 ⁶ cells/mL	89	35–66	4.5–7.6	Alginate	Human chondrocytes	Yes
		(Censi et al. 2011)	5.0 × 10 ⁶	—	94 ± 3	119	Poly (N-(2-hydroxypropyl) methacrylamide lactate) A-block	Chondrocyte	Yes
	Powder bed fusion	(Chen et al. 2014a)	—	74–77	—	—	PCL	Chondrocyte	No
		(Chen et al. 2011)	—	76.2	—	7.22 ± 0.18 MPa	Gelatin-PCL	Chondrocyte	No
		(Chen et al. 2014b)	—	70–82	—	2–3.8 MPa	PCL-collagen	Chondrocytes	No

2005) or bone morphogenetic protein-2 onto submicrometer polystyrene fibers (Ker et al. 2011). In another study, the same method has been reported for growth factor patterning, which enabled spatial control of stem cell fate on fibrin films (Phillippi et al. 2008). Mesenchymal stem cells are sensitive to the topography of the scaffolds (Patz et al. 2005); it should be noted that the aforementioned designs are limited to two-dimensional structures. 3D scaffolds have been developed by combining electrospinning methods with other techniques to make 3D structures such as nanofiber yarn/hydrogel core-shell scaffolds (Wang et al. 2015). Other techniques, including UV-embossed microchannels, have shown the potential for highly structured skeletal muscle tissue morphogenesis (Ramón-Azcón et al. 2013).

Extrusion-based manufacturing is the most commonly used method for muscle scaffold fabrication. Synthetic polymers such as PCL and PEO have been modified with natural polymers such as alginate for use in muscle regeneration. Scaffold fabrication is performed by extrusion to form a sheet, which is then rolled into a 3D tube to prepare volumetric constructs containing evenly distributed C2C12 cells (Yeo et al. 2016). In vivo results indicate that the myoblasts proliferate within the constructs and that myosin heavy chain (MHC, a marker of myogenic differentiation) expression were influenced by the alignment of extruded fibers (Yeo et al. 2016). Alginate and gelatin have also been printed on 3D scaffolds for muscle regeneration using extrusion-based techniques. These studies demonstrated that the ink formulation was a major factor that determined the mechanical properties, fluid transport, and cell viability for the constructs. The extrusion pressure associated with scaffold synthesis did not have a significant influence on myoblast viability within the investigated range (between 4 and 9.5 psi) (Chung et al. 2013b).

Skeletal muscle regeneration in volumetric defects requires mechanical properties comparable to native tissue, high cell density, and high viability for transplantation. The local cell density affects myoblast fusion and fiber formation; the transport properties of the scaffold are essential for maintenance of tissue viability while vascular infiltration occurs. In an attempt to focus on improving cell seeding efficiency, alginate and cells have been used as a bioink in scaffolds that were reinforced with PCL fibers (Yeo et al. 2016). It was observed that PCL/alginate scaffolds laden with cells within alginate fibers showed the highest cell density homogeneity and better cellular behavior; other samples, including cell-coated PCL/alginate scaffolds and cell-free PCL/alginate scaffolds, exhibited better mechanical properties (Yeo et al. 2016). Co-deposition of fibers remains a crucial strategy in 3D scaffold manufacturing (Malda et al. 2013); synthetic polymers such as PCL provide the mechanical backbone within constructs and hydrogels such as alginate serve as “sacrificial” temporary carriers for cells, growth factors, and biologics. This strategy allows for independently tuning the microenvironment and mechanical properties for optimal cell density and viability. Additionally, extrusion-based methods have been used in fused deposition modeling to fabricate PCL and composite hydrogels made of gelatin, fibrinogen, hyaluronic acid, and glycerol (Kang et al. 2016). Gelatin exhibits a thermosensitive response in gels below 25 °C, while fibrinogen has been used to provide matrix stability for enhancing

cell growth (Kang et al. 2016). Hyaluronic acid and glycerol were introduced as dispenser agents to prevent nozzle clogging. In vivo results show that cell-laden scaffolds have the potential to be directly used for production (Kang et al. 2016) of the skeletal muscle. A variant of this approach has the potential to be used for restoration of bone and cartilage defects. Figure 5 shows data from the bioprinted muscle (Kang et al. 2016).

Additive manufacturing lends itself well to recreating the challenging transition at various orthopedic interfaces, where multiple orders of magnitude of mechanical properties are traversed within small length scales. Integrated tendon-muscle units have been previously fabricated using multichannel nozzles. The material used was a thermoplastic polyurethane, which was co-printed with a bioink containing muscle cells. The muscle component was transitioned to a tendon site graft, which was fabricated using PCL and NIH/3 T3 cell hydrogel-based bioink. The bioink contained hyaluronic acid in addition to gelatin and fibrinogen (Merceron et al. 2015). Results show that the printed complex structure simulates vastly different mechanical properties on the muscle and tendon sides while achieving homogenous cell distribution and maintaining good cell viability (Merceron et al. 2015). AM has great promise for muscle graft fabrication; however, it has not been evaluated as much as additive manufactured bone and cartilage grafts due to the need for high cell density over large volumes and the need for pre-vascularization. A summary of the current state of the art in skeletal muscle bioprinting is shown in Table 3.

5 Tendons and Ligaments

Tendon reconstruction with biologically active scaffolds is hampered by many issues, including the restoration of a highly organized matrix architecture, low cellularity, the need for high cell viability, zones of differential mechanical properties within the matrix, a transition from a stiff tissue to a soft tissue at the interfaces, and a functional need for force transmission. Simulating the collagen fibril orientation and organization to match native tendon tissue has been the most challenging requirement. Different techniques, such as electrospinning (Verdiyeva et al. 2015), wet spinning (Kew et al. 2012), and melt spinning (Webb et al. 2013), have been utilized to produce micro- or nanofibers that resemble the native tissue (Regeneration 2015). Natural polymers such as silk (Sahoo et al. 2010; Shen et al. 2012; Qiu et al. 2013) and collagen type I have been used in tendon tissue regeneration (Kew et al. 2012; Oryan et al. 2013; Xu et al. 2013b); however, the lack of fiber formation and poor mechanical properties have been the drawbacks associated with the use of these materials. Synthetic polymers such as PLLA (Barber et al. 2011), PCL (Kazimoğlu et al. 2003), polydioxanone (Oryan et al. 2013), PLA (Sato et al. 2000), PGA (Chen et al. 2012), and PLGA (Sahoo et al. 2010) have also been used to generate organized fiber scaffolds; among these materials, PLGA is the most commonly used material (Ouyang et al. 2003; Sahoo et al. 2006).

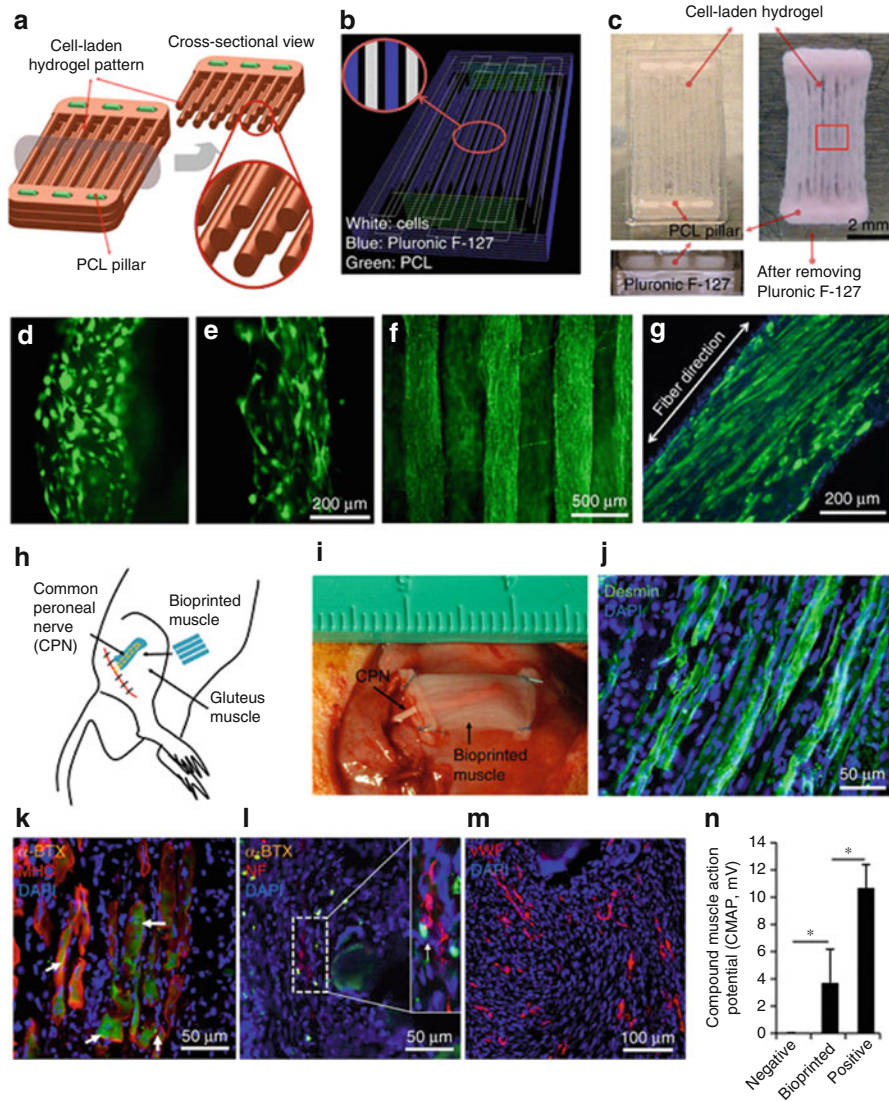


Fig. 5 In vitro bioprinted muscle. (a) Designed fiber bundle structure for muscle organization. (b) Visualized motion program for 3D printing muscle construct. Lines of green, white, and blue indicate the dispensing paths of PCL, cell-laden hydrogel and sacrificial material, respectively. (c) 3D patterning outcome of designed muscle organization (left) before and (after) removing the sacrificial material (Pluronic F127). (d, e) The PCL pillar structure is essential to stabilize the 3D-printed muscle organization and to induce a compaction phenomenon of the patterns of the cell-laden hydrogel that causes cell alignment in a longitudinal direction of the printed constructs, without PCL pillar (d) and with PCL pillar (e). The cells with PCL pillar showed unidirectionally organized cellular morphologies that are consistently aligned along the longitudinal axis of the printed construct, which is in contrast to the randomly oriented cellular morphologies without PCL

Additive manufacturing has been leveraged to simulate fibers with appropriate tensile properties similar to those of the tendon and ligaments (Kim et al. 2016). Among available AM technologies, Bioplotters, in particular, have been utilized for tendon scaffold fabrication (Chung et al. 2013a). This method is based on the extrusion of bioink through different channels to deposit cells and other materials to form a 3D structure. One example is of cells suspended in hyaluronic acid and later printed in a collagen solution using a Bioplotter. Authors suggest that this approach is applicable to other scaffolds as a self-assembling coating. For example, PLLA scaffolds prepared using a Bioplotter have been coated with the collagen-hyaluronic acid membrane. The results demonstrated improvement of implant bioactivity, indicating that this coating may serve as a tissue binder (Chung et al. 2013a).

In another study, a custom-developed electrodynamic jet printing system has been used to fabricate a PCL mat (Wu et al. 2015). The printed mat was made of two types of fibers with different thicknesses and then rolled to form a 3D structure. Mechanical testing indicated that an increase in fiber diameter (20–75 μm) led to improved mechanical properties. Moreover, the design exhibited the ability to support the attachment and growth of human tenocytes. Cell alignment and morphology indicated the formation of a tendon-like architecture and upregulation of collagen type I expression, indicating the suitability of the construct for tendon restoration.

Ligament injuries are the other crucial concerns in orthopedic health care. AM offers a different approach to develop new treatments for ligament injuries, which are more focused on improving the transitions at bone-ligament interfaces; these interfaces are often observed to be the sites of failures in synthetic graft restorations. In addition to the tensile and other mechanical properties of the graft, properties such as osteogenicity matter as well. In one approach, customized cages for anterior cruciate ligament (ACL) treatments were developed using AM technologies. A low-temperature 3D printing method was used to manufacture ligament implants from TCP for cranial cruciate ligament treatment (Castilho et al. 2014). In this study, TCP powder was sintered before printing; the milled powder was later mixed with phosphoric acid. The graft was air-dried at room temperature, and the residual powders were removed. The *in vivo* results indicated that an optimized cage performance resulted in mechanical properties similar to those of the trabecular bone and that limb function was restored without any complication (Castilho et al. 2014). Treatment of cruciate ligament rupture through 3D-printed biodegradable cages was optimized computationally for survival in a preclinical canine model.



Fig. 5 (continued) pillar. **(f)** The live/dead staining of the encapsulated cells in the fiber structure indicates high cell viability after the printing process (green, live cells; red, dead cells). **(g)** Immunofluorescent staining for myosin heavy chain of the 3D-printed muscle organization after 7-day differentiation. **(h–m)** Structural maintenance and host nerve integration of the bioprinted muscle construct in *in vivo* study. **(h)** Schematic diagram of ectopic implantation of bioprinted muscle construct *in vivo*. **(i–k)** The bioprinted muscle construct was subcutaneously implanted with the dissected common peroneal nerve. (Kang et al. 2016)

Table 3 Studies reported the synthesis of muscle scaffolds based on different AM techniques

Category	Method	Publication	Material	Cell type	Cell density (cell/ml)	Porosity %	Cell viability%	Modulus (KPA)	Bioprinting
Material extrusion	Material extrusion	(Yeo et al. 2016)	PCL-alginate-PEO	C2C12 myoblast cells	1×10^7	–	95.2 ± 2.8	43–48	Yes
		(Ahn et al. 2012)	Alginate	(MC3T3-E1)	$(1.7-2.3) \times 10^6$	–	84	–	Yes
		(Chung et al. 2013b)	Alginate	BL6 primary myoblast	5×10^5	–	92–98	1.5–12	Yes
		(Lee et al. 2013)	PCL-alginate	MC3T3-E1	1×10^5	62–68	62–83	4.1–5.1 MPa	Yes
		Kang (Kang et al. 2016)	PCL-gelatin-fibrinogen-ha-glycerol	C2C12 myoblast cells	5×10^6	70	95	–	Yes
		(Merceron et al. 2015)	PCL-gelatin-fibrinogen-ha-glycerol	NIH/3 T3	40×10^6	–	c2c12, 94; NIH/3 T3, 83	Muscle side, 0.39 ± 0.05 Mpa; tendon side, 46.67 ± 2.67 Mpa; interface region, 1.03 ± 0.14 Mpa	Yes

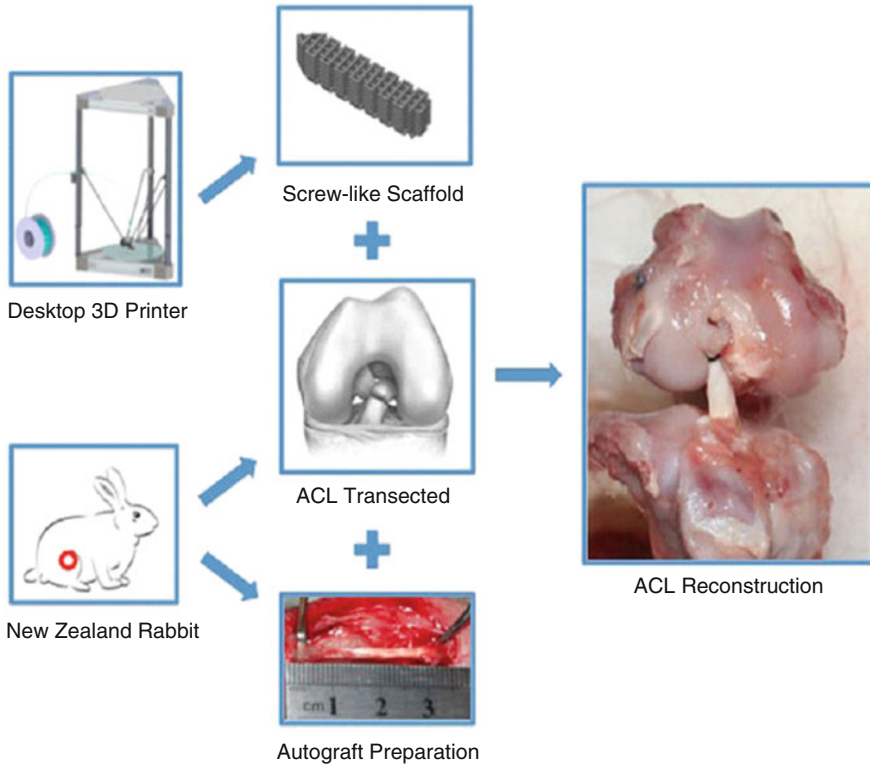


Fig. 6 Porous PLA screwlike scaffold with hydroxyapatite coating as a ligament surgical implant. (Liu et al. 2016)

A low-temperature 3D printing method was developed to synthesize TCP scaffolds with varying porosity in an attempt to optimize mechanical properties that maximized both the porosity to promote bone infiltration and the strength to survive in physiological environments. It was found that the printing direction affected the porosity and overall structural properties (Castilho et al. 2013).

ACL reconstruction has also been performed using a 3D-printed PLA screwlike implant (Liu et al. 2016). The scaffold has been evaluated in a rabbit model using a PLA scaffold that was coated with hyaluronic acid in order to improve its osteoconductivity. Both *in vitro* and *in vivo* studies were conducted to evaluate cell proliferation, osteogenicity, and bone regeneration on the graft surface. This 3D printing technology was based on FDM; PLA was extruded into the porous scaffold through a heated nozzle. The results of this study demonstrated that the seeded scaffolds had improved *in vivo* outcomes compared to cell-free scaffolds; in addition, they offered the ability of “fabricating surgical implants at the clinic” (fab@clinic) as a cost-effective and practical technique (Liu et al. 2016). Figure 6 shows a 3D-printed anterior cruciate ligament surgical implant (Liu et al. 2016). Table 4 shows the studies conducted on ligament regeneration using various AM techniques.

Table 4 Studies reported the synthesis of ligaments and tendon scaffolds based on different AM techniques

Category	Method	Publication	Material	Cell type	Porosity	Pore size (μM)	Elastic modulus (MPa)	Bioprinting
Binder jetting	Powder bed and ink-jet 3D printing (PB/J)	(Castilho et al. 2014)	TCP-DCP	In vivo	59	1000	7.27–19.8	No
Material extrusion	Fused deposition modeling (FDM)	(Liu et al. 2016)	PLA/HA	In vivo	42 ± 5	220	–	No
	Low-temperature deposition manufacturing (LDM)	(Castilho et al. 2013)	TCP	–	38–41	500–1000	–	–

6 Cardiovascular System

Bioprinters are used in various cardiovascular research applications (Moldovan et al. 2017). Cardiovascular diseases are the leading causes of death worldwide (Mosadegh et al. 2015); perhaps the most critical long-term goal in cardiovascular research is to create a human heart for transplantation. As the population is aging, the number of patients requiring organ replacement is increasing (Atala 2009). In addition, the number of new cases of organ failure is growing. On the other hand, the number of organ donors is not sufficient to accommodate patients on waiting lists for organ transplantation, thus creating an organ shortage crisis (Shafiee and Atala 2017). The second important challenge in cardiovascular system research (and in tissue engineering in general) is to manufacture vascularized tissue (Forgacs 2012). Creating thick tissues requires their vascularization, which is indispensable for providing nutrition and removing waste from cells located in tissues thicker than 200 μm (Shafiee and Atala 2017). Large vascular grafts are also required for patients with certain diseases (Pashneh-Tala et al. 2016). Engineering tubular biological structures with particular cell types (including endothelial, smooth muscle, and fibroblast cell types) with properties that are appropriate for creating blood vessels such as suture retention strength and burst pressure resistance is essential. Another unmet need for patients with cardiovascular disease is cardiac patches that replace damaged tissues of an infarcted heart (Weinberger et al. 2017). The engineered heart valve is also a remedy for patients with diseases like pulmonary valve stenosis and bicuspid aortic valve disease (Cheung et al. 2015). The engineering and fabrication of such complex biological structures require advanced technologies and techniques. Bioprinters, with their unique capabilities to create complex tissue structure precisely, automatically, and reproducibly hold promise to advance cardiovascular research (Shafiee and Atala 2016).

In tissue engineering, organs are categorized into four different levels of complexity (Shafiee and Atala 2017). Flat tissues and organs such as the skin are the least complex level. The clinical feasibility of engineering flat tissue fabrication has previously been shown (Centanni et al. 2011). Tubular organ structures such as the tracheas are the next level of complexity, followed by hollow non-tubular organ structures. The latter structures, which include organs such as the bladder, have been engineered *in vitro* and successfully transplanted into the patients (Atala et al. 2006). However, the most complex organs to fabricate are solid organs such as the liver, kidney, and heart. Therefore, bioprinting the heart with current state-of-the-art technology remains a challenge.

Tissue vascularization is another challenge in the field of tissue engineering in general and cardiovascular research in particular. Bioprinting has been used extensively as an effective biofabrication technique for vascularization. In one study, bioprinters were used to print a mixture of sucrose/glucose/dextran as a self-supporting and interconnected lattice (Miller et al. 2012). The lattice was then used as the sacrificial component of a 3D vascular design. The network of adjacent living cells provided appropriate mechanical stiffness and biocompatibility. The

lattice was encapsulated in the ECM; the lattice was then dissolved in a culture medium to leave its imprint. The lattice imprint was subsequently perfused with endothelial cells to be used as the capillary network throughout the tissue. In another study, 3D biomimetic microvascular networks were printed using an omnidirectional printing system (Wu et al. 2011). The network was printed in a hydrogel matrix using a fugitive organic ink patterned in a thermal or photocurable gel reservoir. After photopolymerization of the gel, the fugitive ink was removed under a modest vacuum, leaving a uniform microchannel interconnected network. The technique is able to create complex vascular networks by printing inside the gel reservoir. In another seminal work, 1 cm-thick 3D cell-laden, vascularized tissues were printed (Kolesky et al. 2014; Kolesky et al. 2016). The printed tissues were perfused on a chip for more than 6 weeks; the thickness and the durability accomplished in this method were the highest record achieved in the field to date. A fugitive ink was made of Pluronic F127, thrombin, and transglutaminase, which was used to make the imprint of empty channels as the vascular network. The structure was made by integration of the parenchyma, stroma, and endothelium using bioinks of human mesenchymal stem cells (hMSCs) and human neonatal dermal fibroblast cells. The ECM was customized with embedded vasculature, which was lined with human umbilical vein endothelial cells (HUVECs). The 3D vascularized tissues were perfused with growth factors and demonstrated differentiation of the hMSCs to an osteogenic lineage *in situ*.

Fabrication of blood vessels using various biofabrication techniques, particularly bioprinting, has been a recent focus of attention. Spherical and cylindrical bioink particles composed of different cell types (e.g., human umbilical vein smooth muscle cells and human skin fibroblasts) were printed using extrusion printers; agarose rods were used as support (Norotte et al. 2009) (Fig. 7a–d). Tubular 3D structures underwent self-assembly, and the bioink particles fused to each other (Fig. 7e and f). The fusion of these discrete multicellular systems rendered the structure physically strong, facilitating its transfer to the bioreactor and subsequent maturation. Each cell type relocated to the physiologically appropriate location in the structure through another self-assembly procedure called cell sorting. Predictive modeling to study the shape evolution of multicellular systems was used to predict the fusion time and transfer of the 3D-printed tissue to the bioreactor at the optimal time (when the fusion was complete) (McCune et al. 2014) (Fig. 7g and h). The model successfully predicted the characteristic fusion time for cellular bioink particles with different geometries such as spherical and cylindrical cellular inks (Shafiee et al. 2015). Finally, a biophysical parameter of the bioink particles was introduced to accelerate the tissue maturation process (Shafiee et al. 2017). It was shown that the apparent tissue surface tension (ATST), a viscoelastic characteristic of cellular bioinks, was tunable by various preparation techniques. More importantly, it was demonstrated that cellular bioinks with higher ATST values fused faster than cellular bioinks comprising the same cell types but with lower ATST values. This acceleration translated to a higher adhesion strength of cells on those cellular bioinks with higher surface tension values. The effect of ATST on faster fusion may eventually accelerate the tissue maturation time post-bioprinting.

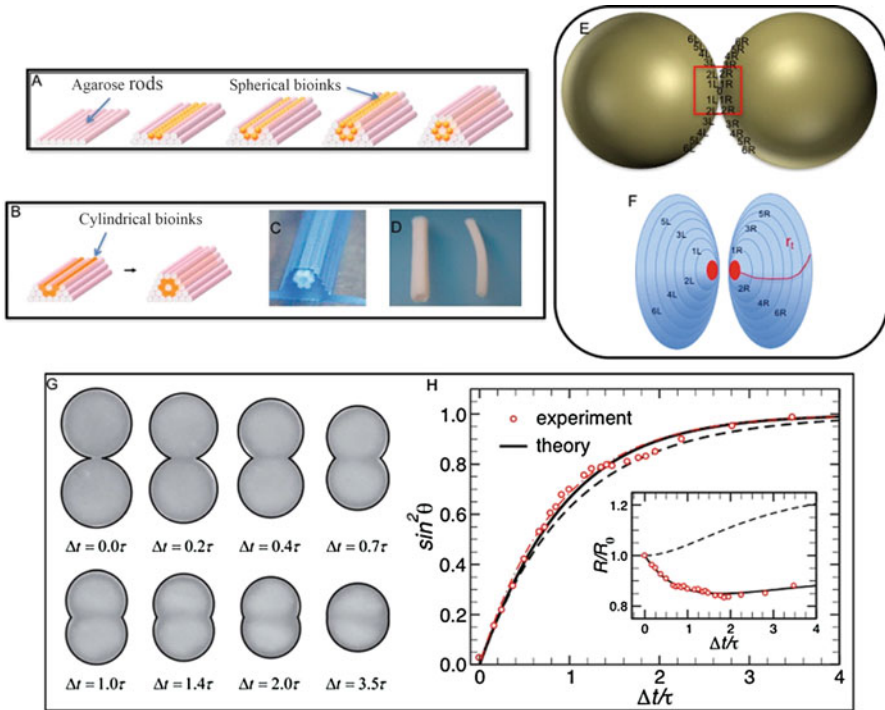


Fig. 7 (a) Bioprinting of tubular organ structures using spherical cellular bioinks. Agarose rods were used as support to build 3D structures. (b) Cylindrical cellular bioink was also used to make tubular bioprinted structures. (c) Bioprinted blood vessels right after the printing procedure. (d) The biological structures after fusion of cellular bioink particles. (a–d) are adapted from Norotte et al. 2009 with permission from Elsevier). (e) Schematic demonstration of fusion of two spherical cellular bioinks. To commence the fusion, the aggregates are placed close to each other. The fusion starts by the development of bonds among adhesion molecules of first initial cells from each aggregate. (f) The fusion process continues by attachment of imaginary strips of cells (1, 2, 3, . . . , n) from the right (R) and left (L) aggregate. (e and f are adapted from Shafiee et al. 2017 with permission from Elsevier). (g) Snapshots of two fusing cellular bioink particles (initial radius $274 \mu\text{m}$) made out of human skin fibroblast (HSF) cells. Over the period of fusion, two aggregates evolve to a single one while the volume decreases. (h) The fusion process can be predicted quantitatively. The red circles are showing the experimental results of fusing HSF aggregates. Theoretical Ashkan with consideration of a change in volume (solid curve). The dashed curve represents the theoretical fit without consideration of the change in volume. Inset: shows the change in radius of the aggregates. (g and h are adapted from McCune et al. 2014 with permission from the Royal Society of Chemistry)

Myocardial infarction causes serious damage to the heart muscle and is associated with a high mortality rate. The heart has limited capability for tissue regeneration and repair (Chiong et al. 2011). It has been shown that transplantation of cardiac patches may significantly enhance functional recovery (Gaebel et al. 2011). Bioprinted cardiac patches have been tested in vitro and in vivo with promising outcomes (Gao et al. 2017). In one study, hMSCs and HUVECs were printed on polyester

urethane urea. These cells were patterned using laser bioprinters; the patches were used for cardiac regeneration in rats with induced myocardial infarctions. This resulted in vessel formation, enhancement of angiogenesis, and eventually improved heart function. Using multiphoton-excited 3D printing, native-like ECM scaffolds were generated. The system created a scaffold with submicrometer resolution, which was seeded with human-induced pluripotent stem cell-derived cardiomyocytes, smooth muscle, and endothelial cells. The generated human-induced pluripotent stem cell-derived cardiac muscle patches (hCMPs) were then evaluated in a murine model. The hCMPs, which were generated with bioprinted ECM-based scaffolds, showed significantly improved recovery from ischemic myocardial injury. High levels of cell engraftment and enhancement of cardiac function were observed. In another study, bioink particles prepared with decellularized ECM were used to print cell-laden constructs of heart tissues (Pati et al. 2013). These bioinks can provide an appropriate microenvironment for the cells similar to that of natural ECM. The printed structures showed stability and produced essential cues for proliferation and engraftment.

Patients may need replacement of their heart valves. The current options are either biological heart valve prostheses or mechanical prostheses (Bloomfield 2002). For biological heart valve prostheses, autologous samples are the most desirable. However, the complex heterogeneous structure of the heart valve makes it difficult to fabricate prostheses from autologous tissue. As such, 3D-printing technologies are being used to create biological heart valve prostheses for patients.

In a series of studies, appropriate heart valve geometries with root walls and tri-leaflets were created using 3D printing. Anatomical heterogeneous valve conduits were fabricated by 3D hydrogel printing with controlled photocrosslinking (Hockaday et al. 2012); polyethylene glycol-diacrylate hydrogels in addition to alginate were used in this study. The scaffolds were seeded with porcine aortic valve interstitial cells and were cultured for 21 days; over this time, the cells maintained viability. Aortic root sinus smooth muscle cells and aortic valve leaflet interstitial cells were encapsulated in alginate/gelatin hydrogel to bioprint valve conduits. The structures showed viability over 7 days in culture (Duan et al. 2013). The production of anatomically accurate living valve scaffolds using bioprinting demonstrated the unique possibilities of bioprinting in valve prosthesis fabrication (Duan et al. 2014). Valvular interstitial cells were encapsulated in hybrid hydrogels composed of methacrylated hyaluronic acid and methacrylated gelatin. The encapsulated cells maintained high viability (>90%) in depths exceeding 700 μm below the surface. The hybrid hydrogel composition could regulate the cellular response and support encapsulated cells.

7 Conclusions

Unique capabilities of bottom-up processes, such as additive manufacturing, include the ability to spatially pattern cells within materials. Significant research efforts have been undertaken to accomplish different architectures and designs of additive

manufacturing-produced scaffolds. Currently unachievable scaffold designs with transitions at tissue interfaces (e.g., bone-ligament or muscle-tendon or bone-cartilage interfaces) or constructs with integrated tissue regions (e.g., blood vessels within the bone or nerves and blood vessels within the skeletal muscle) can be tackled with appropriate advances in bioprinting. Moreover, the application of bioprinters in cardiovascular research has brought much hope to patients in need of heart valves or cardiac patches. Moreover, by fabricating vascularized tissues, the tissue engineering field has benefited immensely from bioprinting technology. However, more sophisticated applications and whole human organ fabrication are still far from coming to fruition using current technology. Therefore, fabrication of solid organs such as the heart, liver, and kidney using bioprinters remains a long-term challenge to overcome. Current challenges in the field include the maintenance of cell viability and graft patency not only during the process of deposition but over the duration of the volumetric print. The translation of these grafts from the benchtop to preclinical animal models is essential to begin envisaging future clinical trials for restorative human surgery. Advances in 3D printing and bioprinting technology have outpaced the available bioinks and scaffold morphologies as well as the specific understanding of precise cell density and distribution required for graft success. While additive manufacturing already offers significant advantages in the manufacture of custom metallic and ceramic implants for orthopedic stabilization, the amalgamation of cellular and material research in bioprinting promises to offer advanced biosynthetic grafts for regeneration and restoration of tissue deficits instead of mere stabilization.

References

- Ahmadi S et al (2014) Mechanical behavior of regular open-cell porous biomaterials made of diamond lattice unit cells. *J Mech Behav Biomed Mater* 34:106–115
- Ahn S et al (2012) Cells (MC3T3-E1)-laden alginate scaffolds fabricated by a modified solid-freeform fabrication process supplemented with an aerosol spraying. *Biomacromolecules* 13(9): 2997–3003
- Ahn S et al (2013) Functional cell-laden alginate scaffolds consisting of core/shell struts for tissue regeneration. *Carbohydr Polym* 98(1):936–942
- Atala A (2009) Engineering organs. *Curr Opin Biotechnol* 20:575–592
- Atala A, Yoo JJ (2015) *Essentials of 3D biofabrication and translation*. Academic Press, Cambridge, MA
- Atala A, Bauer B, Soker S, Yoo J, Retik A (2006) Tissue-engineering autologous bladders for patients needing cystoplasty. *Lancet* 367:1241–1246
- Awiss K et al (2010) Aligned electrospun polymer fibres for skeletal muscle regeneration. *Eur Cell Mater* 19:193–204
- Barber JG et al (2011) Braided nanofibrous scaffold for tendon and ligament tissue engineering. *Tissue Eng A* 19(11-12):1265–1274
- Barry JJ et al (2008) In vitro study of hydroxyapatite-based photocurable polymer composites prepared by laser stereolithography and supercritical fluid extraction. *Acta Biomater* 4(6): 1603–1610
- Barucca G et al (2015) Structural characterization of biomedical co-Cr-Mo components produced by direct metal laser sintering. *Mater Sci Eng C* 48:263–269

- Bertol LS et al (2010) Medical design: direct metal laser sintering of Ti–6Al–4V. *Mater Des* 31(8): 3982–3988
- Bhumiratana S, Vunjak-Novakovic G (2012) Concise review: personalized human bone grafts for reconstructing head and face. *Stem Cells Transl Med* 1(1):64–69
- Bian W et al (2011) Design and fabrication of a novel porous implant with pre-set channels based on ceramic stereolithography for vascular implantation. *Biofabrication* 3(3):034103
- Biamond J et al (2013) Bone ingrowth potential of electron beam and selective laser melting produced trabecular-like implant surfaces with and without a biomimetic coating. *J Mater Sci Mater Med* 24(3):745–753
- Bloomfield P (2002) Choice of heart valve prosthesis. *Heart* 87:583–589
- Bobbert F et al (2017) Additively manufactured metallic porous biomaterials based on minimal surfaces: a unique combination of topological, mechanical, and mass transport properties. *Acta Biomater* 53:572–584
- Boland T et al (2006) Application of inkjet printing to tissue engineering. *Biotechnol J* 1(9): 910–917
- Bose S et al (2003) Pore size and pore volume effects on alumina and TCP ceramic scaffolds. *Mater Sci Eng C* 23(4):479–486
- Bose S et al (2013) Bone tissue engineering using 3D printing. *Mater Today* 16(12):496–504
- Bsat S et al (2015) Effect of alkali-acid-heat chemical surface treatment on electron beam melted porous titanium and its apatite forming ability. *Materials* 8(4):1612–1625
- Campbell PG et al (2005) Engineered spatial patterns of FGF-2 immobilized on fibrin direct cell organization. *Biomaterials* 26(33):6762–6770
- Campoli G et al (2013) Mechanical properties of open-cell metallic biomaterials manufactured using additive manufacturing. *Mater Des* 49:957–965
- Cao T et al (2003) Scaffold design and in vitro study of osteochondral coculture in a three-dimensional porous polycaprolactone scaffold fabricated by fused deposition modeling. *Tissue Eng* 9(4, supplement 1):103–112
- Carignan RG, et al (1990) Thumb joint prosthesis, Google Patents
- Castilho M et al (2013) Fabrication of computationally designed scaffolds by low temperature 3D printing. *Biofabrication* 5(3):035012
- Castilho M et al (2014) Application of a 3D printed customized implant for canine cruciate ligament treatment by tibial tuberosity advancement. *Biofabrication* 6(2):025005
- Censi R et al (2011) A printable Photopolymerizable thermosensitive p (HPMAm-lactate)-PEG hydrogel for tissue engineering. *Adv Funct Mater* 21(10):1833–1842
- Centanni J, Straseski J, Wicks A, Hank J, Rasmussen C, Lokota M, Schurr M, Foster K, Faucher L, Caruso D, Comer A, Allen-Hoffmann B (2011) StrataGraft skin substitute is well-tolerated and is not acutely immunogenic in patients with traumatic wounds: results from a prospective, randomized, controlled dose escalation trial. *Ann Surg* 253(4):672–683
- Chen C-H et al (2011) Effects of gelatin modification on rapid prototyping PCL scaffolds for cartilage engineering. *J Mech Med Biol* 11(05):993–1002
- Chen B et al (2012) In vivo tendon engineering with skeletal muscle derived cells in a mouse model. *Biomaterials* 33(26):6086–6097
- Chen C-H et al (2014a) Surface modification of polycaprolactone scaffolds fabricated via selective laser sintering for cartilage tissue engineering. *Mater Sci Eng C* 40:389–397
- Chen C-H et al (2014b) Selective laser sintered poly-ε-caprolactone scaffold hybridized with collagen hydrogel for cartilage tissue engineering. *Biofabrication* 6(1):015004
- Cheng X et al (2012) Compression deformation behavior of Ti–6Al–4V alloy with cellular structures fabricated by electron beam melting. *J Mech Behav Biomed Mater* 16:153–162
- Cheung D, Duan B, Butcher J (2015) Current progress in tissue engineering of heart valves: multiscale problems, multiscale solutions. *Expert Opin Biol Ther* 15(8):1155–1172
- Chiong M, Wang Z, Pedrozo Z, Cao D, Troncoso R, Ibacache M, Criollo A, Nemchenko A, Hill J, Lavadero S (2011) Cardiomyocyte death: mechanisms and translational implications. *Cell Death Disease* 2:e244

- Choi J-W et al (2009) Fabrication of 3D biocompatible/biodegradable micro-scaffolds using dynamic mask projection microstereolithography. *J Mater Process Technol* 209(15):5494–5503
- Chung EJ et al (2013a) In situ forming collagen–hyaluronic acid membrane structures: mechanism of self-assembly and applications in regenerative medicine. *Acta Biomater* 9(2):5153–5161
- Chung JH et al (2013b) Bio-ink properties and printability for extrusion printing living cells. *Biomater Sci* 1(7):763–773
- Ciocca L et al (2011) Direct metal laser sintering (DMLS) of a customized titanium mesh for prosthetically guided bone regeneration of atrophic maxillary arches. *Med Biol Eng Comput* 49(11):1347–1352
- Claeysens F et al (2009) Three-dimensional biodegradable structures fabricated by two-photon polymerization. *Langmuir* 25(5):3219–3223
- Cooke MN et al (2003) Use of stereolithography to manufacture critical-sized 3D biodegradable scaffolds for bone ingrowth. *J Biomed Mater Res B Appl Biomater* 64(2):65–69
- Cooper GM et al (2010) Inkjet-based biopatterning of bone morphogenetic protein-2 to spatially control calvarial bone formation. *Tissue Eng A* 16(5):1749–1759
- Costantini M et al (2017) Microfluidic-enhanced 3D bioprinting of aligned myoblast-laden hydrogels leads to functionally organized myofibers in vitro and in vivo. *Biomaterials* 131:98–110
- Cui X et al (2012a) Thermal inkjet printing in tissue engineering and regenerative medicine. *Recent Pat Drug Deliv Formul* 6(2):149–155
- Cui X et al (2012b) Direct human cartilage repair using three-dimensional bioprinting technology. *Tissue Eng A* 18(11–12):1304–1312
- Cui X et al (2012c) Synergistic action of fibroblast growth factor-2 and transforming growth factor-beta1 enhances bioprinted human neocartilage formation. *Biotechnol Bioeng* 109(9):2357–2368
- Cui X, Gao G, Yonezawa T, Dai G (2014) Human Cartilage Tissue Fabrication Using Three-dimensional Inkjet Printing Technology. *J. Vis. Exp* (88), e51294, <https://doi.org/10.3791/51294>
- Cvetkovic C et al (2014) Three-dimensionally printed biological machines powered by skeletal muscle. *Proc Natl Acad Sci* 111(28):10125–10130
- Dadbakhsh S et al (2014) Effect of SLM parameters on transformation temperatures of shape memory nickel titanium parts. *Adv Eng Mater* 16(9):1140–1146
- Darsell J et al (2003) From CT scan to ceramic bone graft. *J Am Ceram Soc* 86(7):1076–1080
- Dean D et al (2012) Continuous digital light processing (cDLP): highly accurate additive manufacturing of tissue engineered bone scaffolds: this paper highlights the main issues regarding the application of continuous digital light processing (cDLP) for the production of highly accurate PPF scaffolds with layers as thin as 60 μm for bone tissue engineering. *Virt Phy Prototyp* 7(1):13–24
- Dellinger JG et al (2007) Robotic deposition of model hydroxyapatite scaffolds with multiple architectures and multiscale porosity for bone tissue engineering. *J Biomed Mater Res A* 82(2):383–394
- Di Bella C et al (2015) 3D bioprinting of cartilage for orthopedic surgeons: reading between the lines. *Front Surg* 2:39
- Doyle K (2014) Bioprinting: from patches to parts. *Genetic Engineering and Biotechnology Mary Ann Liebert, Inc. News* 34(10) pp. 1, 34–35 <https://doi.org/10.1089/gen.34.10.02>
- Duan B, Wang M (2010a) Customized Ca–P/PHBV nanocomposite scaffolds for bone tissue engineering: design, fabrication, surface modification and sustained release of growth factor Bin Duan, Min Wang J. R. Soc. Interface, <https://doi.org/10.1098/rsif.2010.0127.focus>. Published 26 May 2010
- Duan B, Wang M (2010b) Encapsulation and release of biomolecules from ca–P/PHBV nanocomposite microspheres and three-dimensional scaffolds fabricated by selective laser sintering. *Polym Degrad Stab* 95(9):1655–1664
- Duan B et al (2010) Three-dimensional nanocomposite scaffolds fabricated via selective laser sintering for bone tissue engineering. *Acta Biomater* 6(12):4495–4505

- Duan B, Hockaday L, Kang K, Butcher J (2013) 3D Bioprinting of heterogeneous aortic valve conduits with alginate/gelatin hydrogels. *J Biomed Mater Res* 101(5):1255–1264
- Duan B, Kapetanovic E, Hockaday L, Butcher J (2014) 3D printed trileaflet valve conduits using biological hydrogels and human valve interstitial cells. *Acta Biomater* 10(5):1836–1846
- Elomaa L et al (2011) Preparation of poly (ϵ -caprolactone)-based tissue engineering scaffolds by stereolithography. *Acta Biomater* 7(11):3850–3856
- Elomaa L et al (2013) Porous 3D modeled scaffolds of bioactive glass and photocrosslinkable poly (ϵ -caprolactone) by stereolithography. *Compos Sci Technol* 74:99–106
- Eosoly S et al (2010) Selective laser sintering of hydroxyapatite/poly- ϵ -caprolactone scaffolds. *Acta Biomater* 6(7):2511–2517
- Eosoly S et al (2012) Interaction of cell culture with composition effects on the mechanical properties of polycaprolactone-hydroxyapatite scaffolds fabricated via selective laser sintering (SLS). *Mater Sci Eng C* 32(8):2250–2257
- Eshraghi S, Das S (2010) Mechanical and microstructural properties of polycaprolactone scaffolds with one-dimensional, two-dimensional, and three-dimensional orthogonally oriented porous architectures produced by selective laser sintering. *Acta Biomater* 6(7):2467–2476
- Fedorovich NE et al (2011) Biofabrication of osteochondral tissue equivalents by printing topologically defined, cell-laden hydrogel scaffolds. *Tissue Eng Part C Methods* 18(1):33–44
- Fielding GA et al (2012) Effects of silica and zinc oxide doping on mechanical and biological properties of 3D printed tricalcium phosphate tissue engineering scaffolds. *Dent Mater* 28(2):113–122
- Forgacs G (2012) Perfusable vascular networks. *Nat Mater* 11:746–747
- Freed LE et al (1993) Neocartilage formation in vitro and in vivo using cells cultured on synthetic biodegradable polymers. *J Biomed Mater Res* 27(1):11–23
- Fu Q et al (2011) Direct ink writing of highly porous and strong glass scaffolds for load-bearing bone defects repair and regeneration. *Acta Biomater* 7(10):3547–3554
- Gaebel R, Ma N, Liu J, Guan J, Koch L, Klopsch C, Gruene M, Toelk A, Wang W, Mark P, Wang F, Chichkov B, Li W, Steinhoff G (2011) Patterning human stem cells and endothelial cells with laser printing for cardiac regeneration. *Biomaterials* 32:9218–9230
- Gao G et al (2014) Bioactive nanoparticles stimulate bone tissue formation in bioprinted three-dimensional scaffold and human mesenchymal stem cells. *Biotechnol J* 9(10):1304–1311
- Gao G et al (2015a) Improved properties of bone and cartilage tissue from 3D inkjet-bioprinted human mesenchymal stem cells by simultaneous deposition and photocrosslinking in PEG-GelMA. *Biotechnol Lett* 37(11):2349–2355
- Gao G et al (2015b) Inkjet-bioprinted acrylated peptides and PEG hydrogel with human mesenchymal stem cells promote robust bone and cartilage formation with minimal printhead clogging. *Biotechnol J* 10(10):1568–1577
- Gao L, Kupfer M, Jung J, Yang L, Zhang P, Da Sie Y, Tran Q, Ajeti V, Freeman B, Fast V, Campagnola P, Ogle B, Zhang J (2017) Myocardial tissue engineering with cells derived from human-induced pluripotent stem cells and native-like high-resolution, 3-dimensionally printed scaffold. *Circ Res* 120:1318–1325
- Gbureck U et al (2007a) Direct printing of bioceramic implants with spatially localized angiogenic factors. *Adv Mater* 19(6):795–800
- Gbureck U et al (2007b) Low temperature direct 3D printed bioceramics and biocomposites as drug release matrices. *J Control Release* 122(2):173–180
- Ge Z et al (2009) Proliferation and differentiation of human osteoblasts within 3D printed polylactic-co-glycolic acid scaffolds. *J Biomater Appl* 23(6):533–547
- Geetha M et al (2009) Ti based biomaterials, the ultimate choice for orthopaedic implants—a review. *Prog Mater Sci* 54(3):397–425
- Gibson I et al (2010) Additive manufacturing technologies. Springer, New York
- Goodridge RD et al (2007) Biological evaluation of an apatite–mullite glass-ceramic produced via selective laser sintering. *Acta Biomater* 3(2):221–231

- Gruene M et al (2010) Laser printing of stem cells for biofabrication of scaffold-free autologous grafts. *Tissue Eng Part C Methods* 17(1):79–87
- Hedayati R et al (2017) How does tissue regeneration influence the mechanical behavior of additively manufactured porous biomaterials? *J Mech Behav Biomed Mater* 65:831–841
- Heinl P et al (2008) Cellular Ti–6Al–4V structures with interconnected macro porosity for bone implants fabricated by selective electron beam melting. *Acta Biomater* 4(5):1536–1544
- Heller C et al (2009) Vinyl esters: low cytotoxicity monomers for the fabrication of biocompatible 3D scaffolds by lithography based additive manufacturing. *J Polym Sci A Polym Chem* 47(24): 6941–6954
- Heo SJ et al (2009) Fabrication and characterization of novel nano-and micro-HA/PCL composite scaffolds using a modified rapid prototyping process. *J Biomed Mater Res A* 89(1):108–116
- Hockaday L, Kang K, Colangelo N, Cheung P, Duan B, Malone E, Wu J, Giradi L, Bonassar L, Lipson H, Chu C, Butcher J (2012) Rapid 3D printing of anatomically accurate and mechanically heterogeneous aortic valve hydrogel scaffolds. *Biofabrication* 4(3):035005
- Hollister SJ (2005) Porous scaffold design for tissue engineering. *Nat Mater* 4(7):518–524
- Hoque ME et al (2012) Extrusion based rapid prototyping technique: an advanced platform for tissue engineering scaffold fabrication. *Biopolymers* 97(2):83–93
- Hsu S-h et al (2007) Evaluation of the growth of chondrocytes and osteoblasts seeded into precision scaffolds fabricated by fused deposition manufacturing. *J Biomed Mater Res B Appl Biomater* 80(2):519–527
- Hsu S-h et al (2011) Chondrogenesis from human placenta-derived mesenchymal stem cells in three-dimensional scaffolds for cartilage tissue engineering. *Tissue Eng A* 17(11-12): 1549–1560
- Hsu S-h et al (2012) Air plasma treated chitosan fibers-stacked scaffolds. *Biofabrication* 4(1): 015002
- Hung KC et al (2014) Synthesis and 3D printing of biodegradable polyurethane elastomer by a water-based process for cartilage tissue engineering applications. *Adv Healthc Mater* 3(10): 1578–1587
- Husmann I et al (1996) Growth factors in skeletal muscle regeneration. *Cytokine Growth Factor Rev* 7(3):249–258
- Hutmacher DW (2000) Scaffolds in tissue engineering bone and cartilage. *Biomaterials* 21(24): 2529–2543
- Hutmacher DW et al (2001) Mechanical properties and cell cultural response of polycaprolactone scaffolds designed and fabricated via fused deposition modeling. *J Biomed Mater Res A* 55(2): 203–216
- Igawa K et al (2006) Tailor-made tricalcium phosphate bone implant directly fabricated by a three-dimensional ink-jet printer. *J Artif Organs* 9(4):234–240
- Jansen J et al (2009) Fumaric acid monoethyl ester-functionalized poly (D, L-lactide)/N-vinyl-2-pyrrolidone resins for the preparation of tissue engineering scaffolds by stereolithography. *Biomacromolecules* 10(2):214–220
- Jardini A et al (2011) Application of direct metal laser sintering in titanium alloy for cranioplasty. Brazilian conference on manufacturing engineering
- Jose RR et al (2016) Evolution of bioinks and additive manufacturing technologies for 3D bioprinting. *ACS Biomater Sci Eng* 2(10):1662–1678
- Kalita SJ et al (2003) Development of controlled porosity polymer-ceramic composite scaffolds via fused deposition modeling. *Mater Sci Eng C* 23(5):611–620
- Kanczler JM et al (2009) Biocompatibility and osteogenic potential of human fetal femur-derived cells on surface selective laser sintered scaffolds. *Acta Biomater* 5(6):2063–2071
- Kang H-W et al (2016) A 3D bioprinting system to produce human-scale tissue constructs with structural integrity. *Nat Biotechnol* 34(3):312–319
- Kazimoğlu C et al (2003) A novel biodegradable PCL film for tendon reconstruction: Achilles tendon defect model in rats. *Int J Artif Organs* 26(9):804–812

- Ker ED et al (2011) Bioprinting of growth factors onto aligned sub-micron fibrous scaffolds for simultaneous control of cell differentiation and alignment. *Biomaterials* 32(32):8097–8107
- Keriquel V et al (2010) In vivo bioprinting for computer-and robotic-assisted medical intervention: preliminary study in mice. *Biofabrication* 2(1):014101
- Kew S et al (2012) Synthetic collagen fascicles for the regeneration of tendon tissue. *Acta Biomater* 8(10):3723–3731
- Khalil S et al (2005) Multi-nozzle deposition for construction of 3D biopolymer tissue scaffolds. *Rapid Prototyp J* 11(1):9–17
- Khalifa A et al (2007) Development of a new calcium phosphate powder-binder system for the 3D printing of patient specific implants. *J Mater Sci Mater Med* 18(5):909–916
- Kim JY, Cho D-W (2009) The optimization of hybrid scaffold fabrication process in precision deposition system using design of experiments. *Microsyst Technol* 15(6):843–851
- Kim Y, Kim G (2013) Collagen/alginate scaffolds comprising core (PCL)–shell (collagen/alginate) struts for hard tissue regeneration: fabrication, characterisation, and cellular activities. *J Mater Chem B* 1(25):3185–3194
- Kim JY et al (2007) Development of a bone scaffold using HA nanopowder and micro-stereolithography technology. *Microelectron Eng* 84(5):1762–1765
- Kim JH et al (2016) Three-dimensional cell-based bioprinting for soft tissue regeneration. *Tissue Eng Regen Med* 13(6):647–662
- Klammert U et al (2010) 3D powder printed calcium phosphate implants for reconstruction of cranial and maxillofacial defects. *J Cranio-Maxillofac Surg* 38(8):565–570
- Koch L et al (2012) Skin tissue generation by laser cell printing. *Biotechnol Bioeng* 109(7):1855–1863
- Kolan KC et al (2012) Effect of material, process parameters, and simulated body fluids on mechanical properties of 13-93 bioactive glass porous constructs made by selective laser sintering. *J Mech Behav Biomed Mater* 13:14–24
- Kolesky D, Truby R, Gladman A, Busbee T, Homan K, Lewis J (2014) 3D Bioprinting of vascularized, heterogeneous cell-laden tissue constructs. *Adv Mater* 26:3124–3130
- Kolesky D, Homan K, Skylar-Scott M, Lewis J (2016) Three-dimensional bioprinting of thick vascularized tissues. *Proc Natl Acad Sci* 113(12):3179–3184
- Korpela J et al (2013) Biodegradable and bioactive porous scaffold structures prepared using fused deposition modeling. *J Biomed Mater Res B Appl Biomater* 101(4):610–619
- Kruth J-P (1991) Material in-process manufacturing by rapid prototyping techniques. *CIRP Annals Manuf Technol* 40(2):603–614
- Kruth J-P et al (1998) Progress in additive manufacturing and rapid prototyping. *CIRP Annals Manuf Technol* 47(2):525–540
- Kundu J et al (2015) An additive manufacturing-based PCL–alginate–chondrocyte bioprinted scaffold for cartilage tissue engineering. *J Tissue Eng Regen Med* 9(11):1286–1297
- Lam CXF et al (2002) Scaffold development using 3D printing with a starch-based polymer. *Mater Sci Eng C* 20(1):49–56
- Lam CX et al (2007) Comparison of the degradation of polycaprolactone and polycaprolactone–(β -tricalcium phosphate) scaffolds in alkaline medium. *Polym Int* 56(6):718–728
- Lam CX et al (2008) Dynamics of in vitro polymer degradation of polycaprolactone-based scaffolds: accelerated versus simulated physiological conditions. *Biomed Mater* 3(3):034108
- Lam C et al (2009a) Composite PLDLLA/TCP scaffolds for bone engineering: mechanical and in vitro evaluations. *13th International Conference on Biomedical Engineering*, Springer
- Lam CX et al (2009b) Evaluation of polycaprolactone scaffold degradation for 6 months in vitro and in vivo. *J Biomed Mater Res A* 90(3):906–919
- Lan PX et al (2009) Development of 3D PPF/DEF scaffolds using micro-stereolithography and surface modification. *J Mater Sci Mater Med* 20(1):271–279
- Lee JW et al (2007a) 3D scaffold fabrication with PPF/DEF using micro-stereolithography. *Microelectron Eng* 84(5):1702–1705

- Lee K-W et al (2007b) Poly (propylene fumarate) bone tissue engineering scaffold fabrication using stereolithography: effects of resin formulations and laser parameters. *Biomacromolecules* 8(4): 1077–1084
- Lee S-J et al (2008) Application of microstereolithography in the development of three-dimensional cartilage regeneration scaffolds. *Biomed Microdevices* 10(2):233–241
- Lee JW et al (2009) Development of nano-and microscale composite 3D scaffolds using PPF/DEF-HA and micro-stereolithography. *Microelectron Eng* 86(4):1465–1467
- Lee JW et al (2011) Bone regeneration using a microstereolithography-produced customized poly (propylene fumarate)/diethyl fumarate photopolymer 3D scaffold incorporating BMP-2 loaded PLGA microspheres. *Biomaterials* 32(3):744–752
- Lee JS et al (2012) Effect of pore architecture and stacking direction on mechanical properties of solid freeform fabrication-based scaffold for bone tissue engineering. *J Biomed Mater Res A* 100(7):1846–1853
- Lee H et al (2013) Cell-laden poly (ϵ -caprolactone)/alginate hybrid scaffolds fabricated by an aerosol cross-linking process for obtaining homogeneous cell distribution: fabrication, seeding efficiency, and cell proliferation and distribution. *Tissue Eng Part C Methods* 19(10):784–793
- Leukers B et al (2005) Hydroxyapatite scaffolds for bone tissue engineering made by 3D printing. *J Mater Sci Mater Med* 16(12):1121–1124
- Li X et al (2009) Fabrication and characterization of porous Ti6Al4V parts for biomedical applications using electron beam melting process. *Mater Lett* 63(3):403–405
- Li J et al (2011) Fabrication of individual scaffolds based on a patient-specific alveolar bone defect model. *J Biotechnol* 151(1):87–93
- Liang D et al (2007) Functional electrospun nanofibrous scaffolds for biomedical applications. *Adv Drug Deliv Rev* 59(14):1392–1412
- Linzhong Z et al (2010) The research of technique on fabricating hydrogel scaffolds for cartilage tissue engineering based on stereo-lithography. *Digital Manufacturing and Automation (ICDMA)*, 2010 International Conference on, IEEE
- Liu L et al (2009) Multinozzle low-temperature deposition system for construction of gradient tissue engineering scaffolds. *J Biomed Mater Res B Appl Biomater* 88(1):254–263
- Liu A et al (2016) 3D Printing Surgical Implants at the clinic: A Experimental Study on Anterior Cruciate Ligament Reconstruction. *Sci Rep* 6:21704; <https://doi.org/10.1038/srep21704>
- Lode A et al (2014) Fabrication of porous scaffolds by three-dimensional plotting of a pasty calcium phosphate bone cement under mild conditions. *J Tissue Eng Regen Med* 8(9):682–693
- Lohfeld S et al (2012) Fabrication, mechanical and in vivo performance of polycaprolactone/tricalcium phosphate composite scaffolds. *Acta Biomater* 8(9):3446–3456
- Lorrison J et al (2005) Processing of an apatite-mullite glass-ceramic and an hydroxyapatite/phosphate glass composite by selective laser sintering. *J Mater Sci Mater Med* 16(8):775–781
- Lu Y et al (2006) A digital micro-mirror device-based system for the microfabrication of complex, spatially patterned tissue engineering scaffolds. *J Biomed Mater Res A* 77(2):396–405
- Luo Y et al (2015) Alginate/nanohydroxyapatite scaffolds with designed core/shell structures fabricated by 3D plotting and in situ mineralization for bone tissue engineering. *ACS Appl Mater Interfaces* 7(12):6541–6549
- Lv J et al (2015a) Electron beam melting fabrication of porous Ti6Al4V scaffolds: cytocompatibility and osteogenesis. *Adv Eng Mater* 17(9):1391–1398
- Lv J et al (2015b) Enhanced angiogenesis and osteogenesis in critical bone defects by the controlled release of BMP-2 and VEGF: implantation of electron beam melting-fabricated porous Ti6Al4V scaffolds incorporating growth factor-doped fibrin glue. *Biomed Mater* 10(3):035013
- Ma L et al (2017) 3D printed personalized titanium plates improve clinical outcome in microwave ablation of bone tumors around the knee. *Sci Rep* 7, 7626; <https://doi.org/10.1038/s41598-017-07243-3>
- Malda J et al (2013) 25th anniversary article: engineering hydrogels for biofabrication. *Adv Mater* 25(36):5011–5028

- Marino A et al (2014) The Osteoprint: a bioinspired two-photon polymerized 3-D structure for the enhancement of bone-like cell differentiation. *Acta Biomater* 10(10):4304–4313
- Martínez-Vázquez FJ et al (2010) Improving the compressive strength of bioceramic robocast scaffolds by polymer infiltration. *Acta Biomater* 6(11):4361–4368
- Martins A et al (2009) Hierarchical starch-based fibrous scaffold for bone tissue engineering applications. *J Tissue Eng Regen Med* 3(1):37–42
- McCarthy JC et al (1997) Custom and modular components in primary total hip replacement. *Clin Orthop Relat Res* 344:162–171
- McCune M, Shafiee A, Forgacs G, Kosztin I (2014) Predictive modeling of post bioprinting structure formation. *Soft Matter* 10:1790–1800
- Melchels FP et al (2009) A poly (D, L-lactide) resin for the preparation of tissue engineering scaffolds by stereolithography. *Biomaterials* 30(23):3801–3809
- Melchels FP et al (2010) Effects of the architecture of tissue engineering scaffolds on cell seeding and culturing. *Acta Biomater* 6(11):4208–4217
- Melchels FP et al (2012) Additive manufacturing of tissues and organs. *Prog Polym Sci* 37(8):1079–1104
- Merceron TK et al (2015) A 3D bioprinted complex structure for engineering the muscle–tendon unit. *Biofabrication* 7(3):035003
- Mikos AG, Temenoff JS (2000) Formation of highly porous biodegradable scaffolds for tissue engineering. *Electron J Biotechnol* 3(2):23–24
- Miller J, Stevens K, Yang M, Baker B, Nguyen D, Cohen D, Toro E, Chen A, Galie P, Yu X, Chaturvedi R, Bhatia S, Chen C (2012) Rapid casting of patterned vascular networks for perfusable engineered three-dimensional tissues. *Nat Mater* 11:768–774
- Miranda P et al (2006) Sintering and robocasting of β -tricalcium phosphate scaffolds for orthopaedic applications. *Acta Biomater* 2(4):457–466
- Miranda P et al (2008) Finite element modeling as a tool for predicting the fracture behavior of robocast scaffolds. *Acta Biomater* 4(6):1715–1724
- Moldovan L, Babbey C, Murphy M, Moldovan N (2017) Comparison of Biomateria-dependent and -independent bioprinting methods for cardiovascular medicine. *Curr Opin Biomed Eng* 2:124–131
- Moroni L et al (2006) Polymer hollow fiber three-dimensional matrices with controllable cavity and shell thickness. *Biomaterials* 27(35):5918–5926
- Mosadegh B, Xiong G, Dunham S, Min J (2015) Current progress in 3D printing for cardiovascular tissue engineering. *Biomed Mater* 10:034002
- Mott EJ et al (2016) Digital micromirror device (DMD)-based 3D printing of poly (propylene fumarate) scaffolds. *Mater Sci Eng C* 61:301–311
- Murphy SV, Atala A (2014) 3D bioprinting of tissues and organs. *Nat Biotechnol* 32(8):773–785
- Murr L et al (2010) Next-generation biomedical implants using additive manufacturing of complex, cellular and functional mesh arrays. *Philos Trans Royal Soc London A Math Phys Eng Sci* 368 (1917):1999–2032
- Murr L et al (2011) Microstructure and mechanical properties of open-cellular biomaterials prototypes for total knee replacement implants fabricated by electron beam melting. *J Mech Behav Biomed Mater* 4(7):1396–1411
- Murr LE et al (2012) Next generation orthopaedic implants by additive manufacturing using electron beam melting. *Int J Biomat* 2012:14
- Naing M et al (2005) Fabrication of customised scaffolds using computer-aided design and rapid prototyping techniques. *Rapid Prototyp J* 11(4):249–259
- Nichol JW, Khademhosseini A (2009) Modular tissue engineering: engineering biological tissues from the bottom up. *Soft Matter* 5(7):1312–1319
- Norotte C, Marga F, Niklason L, Forgacs G (2009) Scaffold-free vascular tissue engineering using bioprinting. *Biomaterials* 30(30):5910–5917
- Oghbaei M, Mirzaee O (2010) Microwave versus conventional sintering: a review of fundamentals, advantages and applications. *J Alloys Compd* 494(1):175–189

- Oh SH et al (2007) In vitro and in vivo characteristics of PCL scaffolds with pore size gradient fabricated by a centrifugation method. *Biomaterials* 28(9):1664–1671
- Oliveira A et al (2009) Nucleation and growth of biomimetic apatite layers on 3D plotted biodegradable polymeric scaffolds: effect of static and dynamic coating conditions. *Acta Biomater* 5(5):1626–1638
- Oliveira A et al (2012) Peripheral mineralization of a 3D biodegradable tubular construct as a way to enhance guidance stabilization in spinal cord injury regeneration. *J Mater Sci Mater Med* 23(11):2821–2830
- Oryan A et al (2013) A long-term in vivo investigation on the effects of xenogenous based, electrospun, collagen implants on the healing of experimentally-induced large tendon defects. *J Musculoskelet Neuronal Interact* 13(3):353–367
- Ostrovidov S et al (2014) Skeletal muscle tissue engineering: methods to form skeletal myotubes and their applications. *Tissue Eng Part B Rev* 20(5):403–436
- Ouyang HW et al (2003) Knitted poly-lactide-co-glycolide scaffold loaded with bone marrow stromal cells in repair and regeneration of rabbit Achilles tendon. *Tissue Eng* 9(3):431–439
- Owen R et al (2016) Emulsion templated scaffolds with tunable mechanical properties for bone tissue engineering. *J Mech Behav Biomed Mater* 54:159–172
- Ozolat IT, Yu Y (2013) Bioprinting toward organ fabrication: challenges and future trends. *IEEE Trans Biomed Eng* 60(3):691–699
- Padilla S et al (2007) Bioactive glass as precursor of designed-architecture scaffolds for tissue engineering. *J Biomed Mater Res A* 81(1):224–232
- Palmquist A et al (2013) Long-term biocompatibility and osseointegration of electron beam melted, free-form-fabricated solid and porous titanium alloy: experimental studies in sheep. *J Biomater Appl* 27(8):1003–1016
- Park JK et al (2011) Solid free-form fabrication of tissue-engineering scaffolds with a poly (lactic-co-glycolic acid) grafted hyaluronic acid conjugate encapsulating an intact bone morphogenetic protein-2/poly (ethylene glycol) complex. *Adv Funct Mater* 21(15):2906–2912
- Parthasarathy J et al (2010) Mechanical evaluation of porous titanium (Ti6Al4V) structures with electron beam melting (EBM). *J Mech Behav Biomed Mater* 3(3):249–259
- Pashneh-Tala S, McNeil S, Claeysens F (2016) The tissue-engineered vascular graft- past, present, and future. *Tissue Eng Part B* 22(1):68–100
- Pati F, Jang J, Ha D, Won K, Rhie J, Shim J, Kim D, Cho D (2013) Printing three-dimensional tissue analogues with decellularized extracellular matrix bioink. *Nat Commun* 5:3935
- Patz T et al (2005) Two-dimensional differential adherence and alignment of C2C12 myoblasts. *Mater Sci Eng B* 123(3):242–247
- Pereira TF et al (2012) 3D printing of poly (3-hydroxybutyrate) porous structures using selective laser sintering. *Macromolecular Symposia*, Wiley Online Library
- Petrochenko PE et al (2015) Laser 3D printing with sub-microscale resolution of porous elastomeric scaffolds for supporting human bone stem cells. *Adv Healthc Mater* 4(5):739–747
- Phillippi JA et al (2008) Microenvironments engineered by inkjet Bioprinting spatially direct adult stem cells toward muscle-and bone-like subpopulations. *Stem Cells* 26(1):127–134
- Poldervaart MT et al (2013) Sustained release of BMP-2 in bioprinted alginate for osteogenicity in mice and rats. *PLoS One* 8(8):e72610
- Poldervaart MT et al (2014) Prolonged presence of VEGF promotes vascularization in 3D bioprinted scaffolds with defined architecture. *J Control Release* 184:58–66
- Ponader S et al (2010) In vivo performance of selective electron beam-melted Ti-6Al-4V structures. *J Biomed Mater Res A* 92(1):56–62
- Qiao F et al (2015) Application of 3D printed customized external fixator in fracture reduction. *Injury* 46(6):1150–1155
- Qiu Y et al (2013) In vitro two-dimensional and three-dimensional tenocyte culture for tendon tissue engineering. *J Tissue Eng Regen Med* 10(3):E216–E226
- Rahimtoola ZO, Hubach P (2004) Total modular wrist prosthesis: a new design. *Scand J Plast Reconstr Surg Hand Surg* 38(3):160–165

- Raman R et al (2016) High-resolution projection Microstereolithography for patterning of Neo-vasculature. *Adv Healthc Mater* 5(5):610–619
- Ramanath H et al (2008) Melt flow behaviour of poly- ϵ -caprolactone in fused deposition modelling. *J Mater Sci Mater Med* 19(7):2541–2550
- Ramón-Azcón J et al (2013) Dielectrophoretically aligned carbon nanotubes to control electrical and mechanical properties of hydrogels to fabricate contractile muscle myofibers. *Adv Mater* 25(29):4028–4034
- Rangarajan S et al (2014) Use of flow, electrical, and mechanical stimulation to promote engineering of striated muscles. *Ann Biomed Eng* 42(7):1391–1405
- Razal JM et al (2009) Wet-spun biodegradable fibers on conducting platforms: novel architectures for muscle regeneration. *Adv Funct Mater* 19(21):3381–3388
- Regeneration T (2015) Understanding tissue physiology and development to engineer functional substitutes. Academic Press, Cambridge, MA
- Rengier F et al (2010) 3D printing based on imaging data: review of medical applications. *Int J Comput Assist Radiol Surg* 5(4):335–341
- Resnina N et al (2013) Influence of chemical composition and pre-heating temperature on the structure and martensitic transformation in porous TiNi-based shape memory alloys, produced by self-propagating high-temperature synthesis. *Intermetallics* 32:81–89
- Ronca A et al (2013) Preparation of designed poly (D, L-lactide)/nanosized hydroxyapatite composite structures by stereolithography. *Acta Biomater* 9(4):5989–5996
- Russias J et al (2007) Fabrication and in vitro characterization of three-dimensional organic/inorganic scaffolds by robocasting. *J Biomed Mater Res A* 83(2):434–445
- Sahoo S et al (2006) Characterization of a novel polymeric scaffold for potential application in tendon/ligament tissue engineering. *Tissue Eng* 12(1):91–99
- Sahoo S et al (2010) A bFGF-releasing silk/PLGA-based biohybrid scaffold for ligament/tendon tissue engineering using mesenchymal progenitor cells. *Biomaterials* 31(11):2990–2998
- Saijo H et al (2009) Maxillofacial reconstruction using custom-made artificial bones fabricated by inkjet printing technology. *J Artif Organs* 12(3):200–205
- Samad WZ, Salleh MM, Shafiee A, Yarmo MA (2010a) Transparent conducting thin films of fluoro doped tin oxide (FTO) deposited using inkjet printing technique. *IEEE Int Conf Semicond Elec* 52–55
- Samad WZ, Salleh MM, Shafiee A, Yarmo MA (2010b) Preparation nanostructure thin films of fluorine doped tin oxide by inkjet printing technique. *AIP Conf Proc* 1284:83–86
- Samad WZ, Salleh MM, Shafiee A, Yarmo MA (2010c) Transparent conductive electrode of fluorine doped tin oxide prepared by inkjet printing technique. *Material Science Forum* 663(665):694–697
- Samad WZ, Salleh MM, Shafiee A, Yarmo MA (2011) Structural, optical and electrical properties of fluorine doped tin oxide thin films deposited using inkjet printing technique. *Sains Malaysiana* 40(3):251–257
- San Choi J et al (2008) The influence of electrospun aligned poly (ϵ -caprolactone)/collagen nanofiber meshes on the formation of self-aligned skeletal muscle myotubes. *Biomaterials* 29(19):2899–2906
- Santos CF et al (2012) Design and production of sintered β -tricalcium phosphate 3D scaffolds for bone tissue regeneration. *Mater Sci Eng C* 32(5):1293–1298
- Santos ARC et al (2013) Additive manufacturing techniques for scaffold-based cartilage tissue engineering: a review on various additive manufacturing technologies in generating scaffolds for cartilage tissue engineering. *Virtual Phy Prototyp* 8(3):175–186
- Sato M et al (2000) Reconstruction of rabbit Achilles tendon with three bioabsorbable materials: histological and biomechanical studies. *J Orthop Sci* 5(3):256–267
- Schantz J-T et al (2003) Repair of calvarial defects with customised tissue-engineered bone grafts II. Evaluation of cellular efficiency and efficacy in vivo. *Tissue Eng* 9(4, Supplement 1):127–139
- Schüller-Ravoo S et al (2013) Flexible and elastic scaffolds for cartilage tissue engineering prepared by Stereolithography using poly (trimethylene carbonate)-based resins. *Macromol Biosci* 13(12):1711–1719

- Schuurman W et al (2013) Gelatin-methacrylamide hydrogels as potential biomaterials for fabrication of tissue-engineered cartilage constructs. *Macromol Biosci* 13(5):551–561
- Seck TM et al (2010) Designed biodegradable hydrogel structures prepared by stereolithography using poly (ethylene glycol)/poly (D, L-lactide)-based resins. *J Control Release* 148(1):34–41
- Seitz H et al (2005) Three-dimensional printing of porous ceramic scaffolds for bone tissue engineering. *J Biomed Mater Res B Appl Biomater* 74(2):782–788
- Seol YJ et al (2013) A new method of fabricating robust freeform 3D ceramic scaffolds for bone tissue regeneration. *Biotechnol Bioeng* 110(5):1444–1455
- Seol Y-J et al (2014) Bioprinting technology and its applications. In: *European journal of cardiothoracic surgery* 46(3):342–348, <https://doi.org/10.1093/ejcts/ezu148>
- Serra T et al (2013) High-resolution PLA-based composite scaffolds via 3-D printing technology. *Acta Biomater* 9(3):5521–5530
- Seyednejad H et al (2012) In vivo biocompatibility and biodegradation of 3D-printed porous scaffolds based on a hydroxyl-functionalized poly (ϵ -caprolactone). *Biomaterials* 33(17): 4309–4318
- Shafiee A, Atala A (2016) Printing technologies for medical applications. *Trends Mol Med* 22:245–265
- Shafiee A, Atala A (2017) Tissue engineering: toward a new era of medicine. *Annu Rev Med* 68:29–40
- Shafiee A, Salleh MM, Yahaya M (2008) Fabrication of organic solar cells based on a blend of donor-acceptor molecules by inkjet printing technique. *IEEE Int Conf Semicond Elect* 2008:319–322
- Shafiee A, Mat Salleh M, Yahaya M (2009) Fabrication of organic solar cells based on a blend of poly (3-octylthiophene-2, 5-diyl) and fullerene derivative using inkjet printing technique. *Proc SPIE* 7493:74932D
- Shafiee A, McCune M, Forgacs G, Kosztin I (2015) Post-deposition bioink self-assembly: a quantitative study. *Biofabrication* 7:045005
- Shafiee A, Norotte C, Ghadiri E (2017) Cellular bioink surface tension: a tunable biophysical parameter for faster bioprinted-tissue maturation. *Bioprinting* 8(C):13–21
- Sharma B, Elisseeff JH (2004) Engineering structurally organized cartilage and bone tissues. *Ann Biomed Eng* 32(1):148–159
- Shen W et al (2012) Allogeneous tendon stem/progenitor cells in silk scaffold for functional shoulder repair. *Cell Transplant* 21(5):943–958
- Sherwood JK et al (2002) A three-dimensional osteochondral composite scaffold for articular cartilage repair. *Biomaterials* 23(24):4739–4751
- Shim J-H et al (2012) Bioprinting of a mechanically enhanced three-dimensional dual cell-laden construct for osteochondral tissue engineering using a multi-head tissue/organ building system. *J Micromech Microeng* 22(8):085014
- Shishkovsky I et al (2010) Porous titanium and nitinol implants synthesized by SHS/SLS: microstructural and histomorphological analyses of tissue reactions. *Int J Self Propag High Temp Synth* 19(2):157–167
- Shor L et al (2005) Precision extruding deposition of composite polycaprolactone/hydroxyapatite scaffolds for bone tissue engineering. *Bioengineering conference, 2005. Proceedings of the IEEE 31st annual northeast*. In: *IEEE*
- Shor L et al (2007) Fabrication of three-dimensional polycaprolactone/hydroxyapatite tissue scaffolds and osteoblast-scaffold interactions in vitro. *Biomaterials* 28(35):5291–5297
- Shor L et al (2009) Precision extruding deposition (PED) fabrication of polycaprolactone (PCL) scaffolds for bone tissue engineering. *Biofabrication* 1(1):015003
- Shuai C et al (2013) In vitro bioactivity and degradability of β -tricalcium phosphate porous scaffold fabricated via selective laser sintering. *Biotechnol Appl Biochem* 60(2):266–273
- Simpson RL et al (2008) Development of a 95/5 poly (L-lactide-co-glycolide)/hydroxyapatite and β -tricalcium phosphate scaffold as bone replacement material via selective laser sintering. *J Biomed Mater Res B Appl Biomater* 84(1):17–25
- Sobral JM et al (2011) Three-dimensional plotted scaffolds with controlled pore size gradients: effect of scaffold geometry on mechanical performance and cell seeding efficiency. *Acta Biomater* 7(3):1009–1018

- Standard A (2012) F2792. 2012. Standard terminology for additive manufacturing technologies. ASTM International. See www.astm.org, West Conshohocken. <https://doi.org/10.1520/F2792-12>
- Stübinger S et al (2013) Histological and biomechanical analysis of porous additive manufactured implants made by direct metal laser sintering: a pilot study in sheep. *J Biomed Mater Res B Appl Biomater* 101(7):1154–1163
- Sudarmadji N et al (2011) Investigation of the mechanical properties and porosity relationships in selective laser-sintered polyhedral for functionally graded scaffolds. *Acta Biomater* 7(2): 530–537
- Sun AX et al (2015) Projection stereolithographic fabrication of human adipose stem cell-incorporated biodegradable scaffolds for cartilage tissue engineering. *Front Bioeng Biotechnol* 3:115
- Suwanprateeb J, Chumnanklang R (2006) Three-dimensional printing of porous polyethylene structure using water-based binders. *J Biomed Mater Res B Appl Biomater* 78(1):138–145
- Suwanprateeb J et al (2008) Fabrication of bioactive hydroxyapatite/bis-GMA based composite via three dimensional printing. *J Mater Sci Mater Med* 19(7):2637–2645
- Suwanprateeb J et al (2009) Mechanical and in vitro performance of apatite–wollastonite glass ceramic reinforced hydroxyapatite composite fabricated by 3D-printing. *J Mater Sci Mater Med* 20(6):1281
- Suwanprateeb J et al (2012) Development of porous powder printed high density polyethylene for personalized bone implants. *J Porous Mater* 19(5):623–632
- Tan H et al (2009) Injectable in situ forming biodegradable chitosan–hyaluronic acid based hydrogels for cartilage tissue engineering. *Biomaterials* 30(13):2499–2506
- Tarafder S et al (2013a) Microwave-sintered 3D printed tricalcium phosphate scaffolds for bone tissue engineering. *J Tissue Eng Regen Med* 7(8):631–641
- Tarafder S et al (2013b) 3D printed tricalcium phosphate bone tissue engineering scaffolds: effect of SrO and MgO doping on in vivo osteogenesis in a rat distal femoral defect model. *Biomater Sci I*(12):1250–1259
- Tartarisco G et al (2009) Polyurethane unimorph bender microfabricated with pressure assisted Microsyringe (PAM) for biomedical applications. *Mater Sci Eng C* 29(6):1835–1841
- Tellis B et al (2008) Trabecular scaffolds created using micro CT guided fused deposition modeling. *Mater Sci Eng C* 28(1):171–178
- Temenoff JS, Mikos AG (2000) Review: tissue engineering for regeneration of articular cartilage. *Biomaterials* 21(5):431–440
- Tesavibul P et al (2012) Processing of 45S5 Bioglass[®] by lithography-based additive manufacturing. *Mater Lett* 74:81–84
- Thavorniyutikarn B et al (2014) Bone tissue engineering scaffolding: computer-aided scaffolding techniques. *Progress Biomat* 3(2–4):61–102
- Thomsen P et al (2009) Electron beam-melted, free-form-fabricated titanium alloy implants: material surface characterization and early bone response in rabbits. *J Biomed Mater Res B Appl Biomater* 90(1):35–44
- Tosun G, Tosun N (2012) Analysis of process parameters for porosity in porous NiTi implants. *Mater Manuf Process* 27(11):1184–1188
- Tosun G et al (2009) A study on microstructure and porosity of NiTi alloy implants produced by SHS. *J Alloys Compd* 487(1):605–611
- Tosun G et al (2012) Investigation of combustion channel in fabrication of porous NiTi alloy implants by SHS. *Mater Lett* 66(1):138–140
- Traini T et al (2008) Direct laser metal sintering as a new approach to fabrication of an isoelastic functionally graded material for manufacture of porous titanium dental implants. *Dent Mater* 24(11):1525–1533
- Travitzky N et al (2014) Additive manufacturing of ceramic-based materials. *Adv Eng Mater* 16(6): 729–754
- Vaezi M et al (2013) A review on 3D micro-additive manufacturing technologies. *Int J Adv Manuf Technol* 67(5–8):1721–1754

- Van Bael S et al (2013) In vitro cell-biological performance and structural characterization of selective laser sintered and plasma surface functionalized polycaprolactone scaffolds for bone regeneration. *Mater Sci Eng C* 33(6):3404–3412
- van Hengel IA et al (2017) Selective laser melting porous metallic implants with immobilized silver nanoparticles kill and prevent biofilm formation by methicillin-resistant *Staphylococcus aureus*. *Biomaterials* 140:1–15
- Ventola CL (2014) Medical applications for 3D printing: current and projected uses. *PT* 39(10):704–711
- Verdiyeva G et al (2015) Tendon reconstruction with tissue engineering approach – a review. *J Biomed Nanotechnol* 11(9):1495–1523
- Vorndran E et al (2008) 3D powder printing of β -tricalcium phosphate ceramics using different strategies. *Adv Eng Mater* 10(12):B67–B71
- Vozzi G et al (2002) Microsyringe-based deposition of two-dimensional and three-dimensional polymer scaffolds with a well-defined geometry for application to tissue engineering. *Tissue Eng* 8(6):1089–1098
- Vozzi G et al (2003) Fabrication of PLGA scaffolds using soft lithography and microsyringe deposition. *Biomaterials* 24(14):2533–2540
- Wang F et al (2004) Precision extruding deposition and characterization of cellular poly- ϵ -caprolactone tissue scaffolds. *Rapid Prototyp J* 10(1):42–49
- Wang PY et al (2012) The roles of RGD and grooved topography in the adhesion, morphology, and differentiation of C2C12 skeletal myoblasts. *Biotechnol Bioeng* 109(8):2104–2115
- Wang L et al (2015) Nanofiber yarn/hydrogel core-shell scaffolds mimicking native skeletal muscle tissue for guiding 3D myoblast alignment, elongation, and differentiation. *ACS Nano* 9(9):9167–9179
- Wang X et al (2017) 3D printing of polymer matrix composites: a review and prospective. *Compos Part B* 110:442–458
- Webb WR et al (2013) The application of poly (3-hydroxybutyrate-co-3-hydroxyhexanoate) scaffolds for tendon repair in the rat model. *Biomaterials* 34(28):6683–6694
- Weinberger F, Mannhardt I, Eschenhagen T (2017) Engineering cardiac muscle tissue- a maturing field of research. *Circ Res* 120:1487–1500
- Weiß T et al (2009) Two-photon polymerization for microfabrication of three-dimensional scaffolds for tissue engineering application. *Eng Life Sci* 9(5):384–390
- Weiß T et al (2011) Two-photon polymerization of biocompatible photopolymers for Microstructured 3D Biointerfaces. *Adv Eng Mater* 13(9):B264–B273
- Williams JM et al (2005) Bone tissue engineering using polycaprolactone scaffolds fabricated via selective laser sintering. *Biomaterials* 26(23):4817–4827
- Winkel A et al (2012) Sintering of 3D-printed glass/HAP composites. *J Am Ceram Soc* 95(11):3387–3393
- Wiria F et al (2007) Poly- ϵ -caprolactone/hydroxyapatite for tissue engineering scaffold fabrication via selective laser sintering. *Acta Biomater* 3(1):1–12
- Wiria FE et al (2010) Printing of titanium implant prototype. *Mater Des* 31:S101–S105
- Wohlers T, Gornet T (2014) History of additive manufacturing. *Wohlers Report* 24:2014
- Wong KV, Hernandez A (2012) International Scholarly Research Network. ISRN Mechanical Engineering 2012:10, <https://doi.org/10.5402/2012/208760>
- Woodfield TB et al (2004) Design of porous scaffolds for cartilage tissue engineering using a three-dimensional fiber-deposition technique. *Biomaterials* 25(18):4149–4161
- Wu W, DeConinck A, Lewis J (2011) Omnidirectional printing of 3D microvascular networks. *Adv Health Mat* 23:178–183
- Wu SH et al (2013) Porous Titanium-6 Aluminum-4 vanadium cage has better Osseointegration and less Micromotion than a poly-ether-ether-ketone cage in sheep vertebral fusion. *Artif Organs* 37(12):E191–E201
- Wu Y et al (2015) Direct E-jet printing of three-dimensional fibrous scaffold for tendon tissue engineering. *J Biomed Mater Res B Appl Biomater* 105(3):616–627

- Xiong Z et al (2001) Fabrication of porous poly (L-lactic acid) scaffolds for bone tissue engineering via precise extrusion. *Scr Mater* 45(7):773–779
- Xiong Z et al (2002) Fabrication of porous scaffolds for bone tissue engineering via low-temperature deposition. *Scr Mater* 46(11):771–776
- Xu T et al (2012) Hybrid printing of mechanically and biologically improved constructs for cartilage tissue engineering applications. *Biofabrication* 5(1):015001
- Xu T et al (2013a) Complex heterogeneous tissue constructs containing multiple cell types prepared by inkjet printing technology. *Biomaterials* 34(1):130–139
- Xu Y et al (2013b) Fabrication of electrospun poly (L-Lactide-co- ϵ -Caprolactone)/collagen Nanoyarn network as a novel, three-dimensional, Macroporous, aligned scaffold for tendon tissue engineering. *Tissue Eng Part C Methods* 19(12):925–936
- Yang SS et al (2015) Fabrication of an osteochondral graft with using a solid freeform fabrication system. *Tissue Eng Regen Med* 12(4):239–248
- Ye L et al (2010) Fabrication and biocompatibility of nano non-stoichiometric apatite and poly (ϵ -caprolactone) composite scaffold by using prototyping controlled process. *J Mater Sci Mater Med* 21(2):753–760
- Yen H-J et al (2008) Fabrication of precision scaffolds using liquid-frozen deposition manufacturing for cartilage tissue engineering. *Tissue Eng A* 15(5):965–975
- Yen H-J et al (2009) Evaluation of chondrocyte growth in the highly porous scaffolds made by fused deposition manufacturing (FDM) filled with type II collagen. *Biomed Microdevices* 11(3): 615–624
- Yeo M et al (2016) Combining a micro/nano-hierarchical scaffold with cell-printing of myoblasts induces cell alignment and differentiation favorable to skeletal muscle tissue regeneration. *Biofabrication* 8(3):035021
- Yildirim ED et al (2010) Accelerated differentiation of osteoblast cells on polycaprolactone scaffolds driven by a combined effect of protein coating and plasma modification. *Biofabrication* 2(1):014109
- Zadpoor AA, Malda J (2017) *Ann Biomed Eng* 45:1, <https://doi.org/10.1007/s10439-016-1719-y>
- Zhang H et al (2008) Microassembly fabrication of tissue engineering scaffolds with customized design. *IEEE Trans Autom Sci Eng* 5(3):446–456
- Zhang Y et al (2009) In vitro biocompatibility of hydroxyapatite-reinforced polymeric composites manufactured by selective laser sintering. *J Biomed Mater Res A* 91(4):1018–1027
- Zhang Q et al (2013) In situ controlled release of rhBMP-2 in gelatin-coated 3D porous poly (ϵ -caprolactone) scaffolds for homogeneous bone tissue formation. *Biomacromolecules* 15(1): 84–94
- Zhao S et al (2016) The influence of cell morphology on the compressive fatigue behavior of Ti-6Al-4V meshes fabricated by electron beam melting. *J Mech Behav Biomed Mater* 59:251–264
- Zhou Y et al (2007) In vitro bone engineering based on polycaprolactone and polycaprolactone-tricalcium phosphate composites. *Polym Int* 56(3):333–342
- Zhou X et al (2016) Improved human bone marrow mesenchymal stem cell osteogenesis in 3D Bioprinted tissue scaffolds with low intensity pulsed ultrasound stimulation. *Sci Rep* 6:12



Characterization of Additive Manufactured Scaffolds

Giuseppe Criscenti, Carmelo De Maria, Giovanni Vozzi, and Lorenzo Moroni

Contents

1	Introduction	56
2	Geometrical Properties Characterization	57
2.1	Porosity and Pore Characterization	58
2.2	Imaging-Based Characterization	59
2.3	Influence of Geometry on Degradation Kinetics	62
3	Mechanical Properties Characterization	62
3.1	Tensile/Compressive Test	63
3.2	Creep and Stress Relaxation Tests	65
3.3	Dynamic Mechanical Analysis	65
3.4	Finite Element Modeling for Scaffold Characterization	66
4	Surface Properties Characterization	66
4.1	Surface Functionalization	68
5	Permeability	68
5.1	Wettability	69
5.2	Permeability Measurement	70
6	Electrical Properties Characterization	72
7	Biological Properties Characterization	72
8	Future Perspectives	74
	References	75

G. Criscenti (✉)

Department of Complex Tissue Regeneration, MERLN Institute for Technology-Inspired Regenerative Medicine, Maastricht University, Maastricht, The Netherlands

Research Center “E. Piaggio”, University of Pisa, Pisa, Italy

e-mail: giu.criscenti@gmail.com

C. De Maria · G. Vozzi

Research Center “E. Piaggio”, University of Pisa, Pisa, Italy

e-mail: carmelo.demaria@centropiaggio.unipi.it; g.vozzi@centropiaggio.unipi.it

L. Moroni

Department of Complex Tissue Regeneration, MERLN Institute for Technology-Inspired Regenerative Medicine, Maastricht University, Maastricht, The Netherlands

e-mail: l.moroni@maastrichtuniversity.nl

Abstract

At the increasing pace with which additive manufacturing technologies are advancing, it is possible nowadays to fabricate a variety of three-dimensional (3D) scaffolds with controlled structural and architectural properties. Examples span from metal cellular solids, which find application as prosthetic devices, to bioprinted constructs holding the promise to regenerate tissues and organs. These 3D porous constructs can display a variety of physicochemical and mechanical properties depending on the used material and on the design of the pore network to be created. To determine how these properties change with changing the scaffold's design criteria, a plethora of characterization methods are applied in the biofabrication field. In this chapter, we review the most common techniques used to characterize such fabricated scaffolds by additive manufacturing technologies.

G. Criscenti and C. De Maria contributed equally to this work.

1 Introduction

Biofabrication for tissue engineering (TE) and regenerative medicine (RM) has been defined as “the automated generation of biologically functional products with structural organization from living cells, bioactive molecules, biomaterials, cell aggregates such as micro-tissues, or hybrid cell-material constructs, through Bioprinting or Bioassembly and subsequent tissue maturation processes” (Groll et al. 2016). Bioprinting, one of the two main strategies for building three-dimensional (3D) scaffolds, encompasses the use of “additive manufacturing technologies for patterning and assembling living and nonliving materials with a prescribed 2D or 3D organization” (Guillemot et al. 2010). Additive manufacturing technologies, commonly known also with the name of 3D printing, have given new degrees of freedom in the design of the scaffolds for TE and RM, due to the possibility to control, layer-by-layer, both the material composition and the internal geometry.

Scaffolds are porous structures with a suitable geometry, which provide mechanical support and biochemical stimuli to the tissue construct in the short term and guides the 3D organization of cells until tissue regeneration is completed; as the tissue grows up, the material should be degraded and replaced by extracellular matrix (ECM).

The cell fate into the scaffold 3D domain depends both on intrinsic variability related with the properties of the cell itself and an extrinsic variability related to the microenvironmental properties (De Maria et al. 2015). If the intrinsic variability cannot be controlled during the culture, the reproducibility, guaranteed by additive manufacturing (with an emphasis on the implicit “mass production” of repeatable objects), helps in minimizing the extrinsic variability by strictly controlling the microenvironmental properties that depend on the scaffold features.

Characterization procedures are essential to ensure that scaffolds present reproducible properties, providing at the same time an opportunity to optimize the final product (Tomlins 2015). Furthermore, regardless of the manufacturing process and the type of

material, scaffolds characterization is fundamental to pave the way toward their clinical application and commercialization (European Commission 2007). In this perspective, the characterization needs to be customized for:

- Off-the-shelf available scaffolds, which don't have to present batch to batch variation and require long term stability
- Just in-time produced scaffolds (in a future vision in the surgery room or directly in the human body), whose features should be assessed during the fabrication

An effective characterization should be fast, accurate, and nondestructive, while giving reliable measurements (Ho and Hutmacher 2006). At the same time, physically-based predictive mathematical models are indicated as fundamental for scaffolds design and estimation nondirectly measurable local properties, such as shear stresses induced on cells when the scaffold is perfused (Zhang et al. 2013). Obviously, the scaffold efficacy, which ultimately can be identified with an optimal biological response (Castilho et al. 2014), depends also on the used biomaterials, whose characterization is beyond the scope of this chapter and can be found elsewhere (Ratner et al. 2013). A robust material specification will help to ensure reproducible results, also using material batches from different sources and from different producers (Tomlins 2015). Woven textile meshes (Masaeli et al. 2013) and foams (Nadeem et al. 2013) represent alternative to AM scaffolds, which are characterized by a limited shape versatility (meshes) and poor control on internal geometry (foams).

This chapter highlights different methodologies to characterize the structural properties of 3D scaffolds, which depend on the peculiar spatial arrangement (geometry) given by the additive manufacturing technologies (Table 1). We will discuss the characterization of geometrical, mechanical, electrical, and surface properties of scaffolds that can be controlled during scaffold design and fabrication. Some material properties should be influenced during the manufacturing process (e.g., polymer crystallinity in melt extrusion process), with limited possibility to control these variations: these are not related to the 3D geometry and are not investigated in this chapter. Furthermore, we have focused to polymers, although most of the methodologies here described are applicable to ceramics and metals as well. Because living and nonliving materials can be printed together (Tirella et al. 2011), a section is also dedicated to the biological tests necessary to assess the functionality of the printed constructs.

2 Geometrical Properties Characterization

The geometrical properties of an AM scaffold inherently depend on the material with which the scaffold is made, by its arrangement in the 3D structure, include porosity, pore size, surface area to volume ratio, interconnectivity, strut thickness, and cross-sectional area (Ho and Hutmacher 2006). They have influence on mechanical, chemical-physical (e.g., degradation), and biological properties (Loh and Choong 2013).

Table 1 Characterization of a scaffold (not including static and dynamic in vitro and in vivo tests for biological validation)

Properties	Techniques	Direct control by AM processes
Molecular weight	Gel permeation chromatography	No
Chemical composition/structure	Nuclear magnetic resonance, X-ray diffraction, Fourier transform infrared, Fourier transform-Raman spectroscopy	No
Thermal properties	Differential scanning calorimetry	No
Porosity	Mercury intrusion porosimetry, gas pycnometry	Yes
Morphology	Optical microscopy, scanning electron microscopy, microcomputed tomography	Yes
Mechanical properties	Mechanical testing, finite element modeling (FEM)	Yes
Degradation properties	In vitro and in vivo degradation tests	No
Permeability	Permeability test, computational fluid dynamics	Yes
Electrical properties	Four point probe $I-V$, cyclic voltammetry	Yes
Surface functionalization	Confocal microscopy, two photon microscopy	Yes
Surface physical properties (texture, wettability)	Atomic force microscopy, contact angle measurement	Yes
Surface chemistry	Time-of-flight secondary ion mass spectrometry, X-ray photoelectron spectroscopy	No

2.1 Porosity and Pore Characterization

Porosity is a fundamental feature to promote nutrient supply and distribution. A pore is defined as a void space within a scaffold, whereas porosity can be considered as a collection of pores (Fig. 1) (Hutmacher et al. 2008).

According to the dimensions, it is possible to classify pores in:

- Macropores (i.e., above 50 μm), which can improve nutrient distribution, catabolites removal, and promote tissue ingrowth
- Micropores (i.e., below 50 μm), at the same scale length of mammalian cells, which play a role on cell activities such as cell attachment
- Pores from 1 nm to 1 μm , generally indicated as nanoporosity, which include also surface textures

Porosity is defined as the ratio of the volume of pores to the apparent volume of the scaffold (including pores). High porosity (e.g., 90%) provides a larger space for cell infiltration and ECM formation, but can determine a decrease in mechanical properties (Zein et al. 2002). The possibility, given by AM technologies, to design the pore shape allows, however, to independently modulate mechanical properties and porosity in a given range, for specific biomaterials (Mattioli-Belmonte et al. 2015). Furthermore, a controlled graded porosity can be achieved (Sudarmadji et al. 2011).

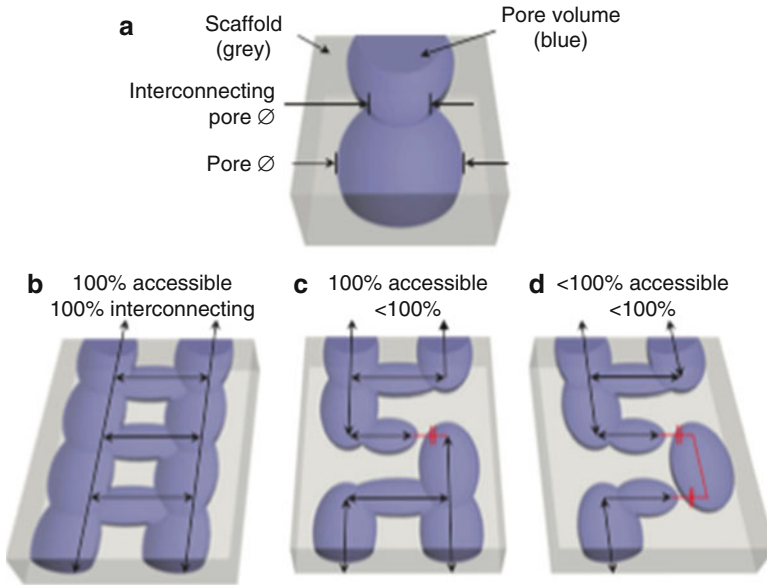


Fig. 1 (a) Section of a porous scaffold (*gray*) and pore geometry (*blue*); (b) pore volume 100% accessible and 100% interconnecting; (c) pore volume 100% accessible but not 100% interconnecting; (d) pore volume neither 100% accessible or 100% interconnecting (from Hutmacher et al. 2008)

Pore interconnectivity (Fig. 1) is fundamental for cell infiltration and exchange of nutrients (e.g., oxygen, glucose) throughout the entire scaffold pore volume (Loh and Choong 2013): for this reason, the accessible pore volume has been defined as the total volume of pores which can be infiltrated from all peripheral borders (Malda et al. 2005).

Apart from imaging-based techniques, described in the next section, fluid-based approach has been used to evaluate pore volume, porosity, and pore size distribution. This approach includes Archimedes methods, liquid displacement, mercury porosimetry, gas pycnometry. These techniques are not always applicable. As example, mercury porosimetry is based on the principle that the pressure required to force mercury (a nonwetting liquid), against the resistance of liquid surface tension, gives information on the pore size. However, the assumption of cylindrical pore shape and the necessity of high pressure, incompatible with soft scaffolds, limit the use of this technique (Ho and Hutmacher 2006).

2.2 Imaging-Based Characterization

Microscopy techniques are fundamental for evaluating pore size distributions, overall scaffold homogeneity, surface properties, and thickness of layers in scaffolds. According to the dimension of the final information, we can classify microscopy techniques in:

- Two-dimensional (2D) techniques, which give a reconstruction of the exposed surface, such as optical microscopy, scanning electron microscope (SEM), atomic force microscope (AFM), and fluorescence microscopy (FM)
- 3D or tomographic methods, which return a 3D matrix in which each element (voxel) represents a specific property of a small volume, such as confocal microscope (CM), microcomputed tomography (μ CT), and magnetic resonance imaging (MRI)

2.2.1 Source of 2D Data

Optical microscopic techniques are the traditional methods employed for visualization of scaffold geometry. However, they are limited to visualize the scaffold surface for high-resolution images because at greater depths light scattering blurs the images (Clarke 2002). For this reason, electron microscopy has gained importance for imaging, probing, and manipulating scaffolds on the micro- and nanoscale levels.

Scanning Electron Microscopy

SEM is based on a focused beam of high-energy electrons which interacts with the surface of a solid specimen, generating a variety of signals: (a) secondary electrons, (b) backscattered electrons (BSE), (c) diffracted backscattered electrons (EBSD), (d) photons, (e) visible light, and (f) heat. Secondary electrons (a) are used to produce SEM images and evaluate the sample characteristics such as the external morphology.

Energy dispersive X-ray spectroscopy (EDS or EDX) is concurrently used with SEM to characterize the elemental composition of a specific volume of the AM scaffold. The electron vacancies, derived from the bombardment of the electron beam, are filled by electrons from a higher state, with the X-ray emission, which is characteristic of the element from which it is emitted. SEM analysis is commonly used to evaluate not only the geometrical properties of AM scaffolds but also cell morphology, attachment, and distribution. The main limitations of SEM analysis are that the sample must be solid and completely dry, and living cells require chemical fixation in a solution of a buffered chemical fixative (glutaraldehyde) to preserve and stabilize their structure (Goldstein 2003; Egerton 2005).

Environmental scanning electron microscopy (ESEM) is an SEM that allows studying wet and uncoated samples, by operating in less than high vacuum thanks to a different suite of detectors. In this case, a gas into the chamber is introduced eliminating the pretreatment and coating of the samples in order to have an electrically conductive surface.

The digital images from SEM can be analyzed to estimate a scaffold's porosity (referred to the entire 3D volume) starting from the surface porosity. Although different software tools, also open source such as ImageJ, are available and easy to use, this porosity extrapolation can be affected by:

- Projection errors
- Deformation during the sectioning of the sample (Ho and Hutmacher 2006)

Other important information such as strut dimensions can be characterized using SEM images. As example, the ImageJ plugin BoneJ (Doubé et al. 2010), developed

for trabecular bone analysis, can provide useful information also for AM scaffolds, such as struts thickness and separation.

2.2.2 Source of 3D Data

Microcomputed Tomography

The μ CT imaging can be used for generating computer 3D model of materials, including AM scaffold and biological materials such as bone, from which porosity and structural details from the micron to the millimeter scale can be measured (Ho and Hutmacher 2006).

The sample is scanned, layer by layer, by X-rays: the emerging X-rays will be captured by a detector array that calculates the X-ray path and attenuation coefficients (Ho and Hutmacher 2006). The resulting radiodensity coefficient 2D map shows the various material phases within the scaffold. A stack of 2D slices can be transformed into a 3D model by the segmentation process, which divides the 3D volume into homogeneous regions. Image histogram thresholding is the easiest methods to identify homogeneous regions; it is widely used, although more accurate algorithms, which takes into account also the morphology of the region other than its radiodensity (e.g., region growing, level-set methods), are available (Ibáñez et al. 2003).

Several papers have highlighted the advantages of μ CT, which is noninvasive and nondestructive (no sectioning or use of chemicals), and is independent from the complexity of the interior structure of the scaffold. However, scaffolds that contain metals cannot be analyzed due to beam hardening (Ho and Hutmacher 2006). Furthermore, μ CT will not discriminate between different hydrogels in a single-generated tissue blueprint (Malda et al. 2013). When a 3D accurate virtual reconstruction of a scaffold is available, the visualization of the difference between a computer design and a μ CT reconstruction of a scaffold is a valuable method to evaluate scaffold accuracy (Malda et al. 2013).

Nuclear Magnetic Resonance Imaging

Magnetic resonance imaging (MRI) is based on strong magnetic fields, radio waves, and field gradients to form a volumetric map of a body. MRI is based on the ability of nuclei in a magnetic field to absorb and re-emit electromagnetic radiation at a specific resonance frequency, which depends on the intensity of the magnetic field and on the magnetic properties of the atoms. The analysis of relaxation times after perturbations (due to field gradients) allows to discriminate the different parts of a sample, thus enabling 3D reconstruction. The dataset is usually represented by a stack of 2D images, as for the μ CT, and the procedure for segmentation is similar.

However, the technology is still scarcely used, likely because of the limited spatial resolution of clinical scanners and their temporally limited availability for many researchers. Benchtop-MRI (BT-MRI) are available, and permitted to analyze diffusion processes and the morphology within the three-dimensional matrices made of hydroxyapatite (HA), collagen, and chitosan wrapped in a polyglycolic acid mesh.

Even if this example is not focused on AM scaffolds, this is a demonstration that BT-MRI is a powerful analytic method for the noninvasive evaluation of tissue engineering constructs (Nitzsche et al. 2009).

2.3 Influence of Geometry on Degradation Kinetics

Scaffold degradation is one of the basic features usually required to scaffolds, in order to be replaced by the neo-formed ECM. Biomaterials can undergo enzymatic degradation, due to cell activity, oxidation, or hydrolysis. The diffusivity of water inside the matrix, the degradation rate of the polymer's functional groups, and the matrix dimensions determine if the biomaterial will present surface or bulk erosion (von Burkersroda et al. 2002). Whereas the degradation rate of the polymer's functional groups is specific to the selected polymer of choice, the other features are also applicable to other biomaterials such as ceramics and composites. Even if an erosion index has been defined for biomaterials, this is not immediately extensible to the whole scaffold, due to the high surface-to-volume ratio, given by the structural porosity. For this reason, scaffold degradation should be tested *in vitro* under conditions that best simulate the real native physiological environment: because degradation kinetics can be affected by fatigue loading or mechanical stress, as well as by the local pH, which may accelerate their degradation. Therefore, degradation tests should be performed in bioreactors under mechanical stimulation at 37 °C with a controlled pH environment. The degradation rate can be monitored using changes in mass and molecular weight of the biomaterials (Shirazi et al. 2016).

3 Mechanical Properties Characterization

A biomimetic scaffold should possess the adequate mechanical properties that mimic those of the native tissues. Especially for soft tissues, comparable mechanical properties between the native tissue and the synthetic substitute can promote adequate mechanical stimuli that, together with other factors, can influence cell growth and differentiation (Gilbert et al. 2010; Urciuolo et al. 2013). Furthermore, scaffold should possess adequate resistance during surgical procedure, and maintain its properties after implantation for the required period. The latter requirement should be critical for load bearing application, because degradation can deeply influence mechanical properties. The mechanical behavior of AM scaffolds depends on:

- The material used to fabricate the scaffold
- Type of applied stress
- Scaffold geometry (shape and sizes, and especially porosity/internal morphology)
- Physical and chemical conditions (temperature, which is defined and constant *in vivo*, environment, strain rate)

Mechanical tests can be classified as:

- Conventional tests that do not reproduce the real working conditions of the scaffold but provide a series of parameters to extrapolate the role of the geometry with respect to the material in reaction to the structural behavior
- Simulated or “under operating conditions” tests that mimic as closely as possible the working conditions of the scaffold

Considering the force application method with respect to time or the experiment, conventional mechanical tests can be classified as:

- Under constant load: creep/stress relaxation (SR) and mechanical wear
- Quasi static: tension, compression, bending
- Cyclic/periodic tests: fatigue
- Dynamic tests: resilience, dynamic mechanical analysis (DMA)

Static, dynamic, periodic, or constant loads can also be classified according to the load direction with respect to the geometric axis of the test sample. Following this classification, four different stresses can be identified: tension/compression, bending, torsion, and shear.

3.1 Tensile/Compressive Test

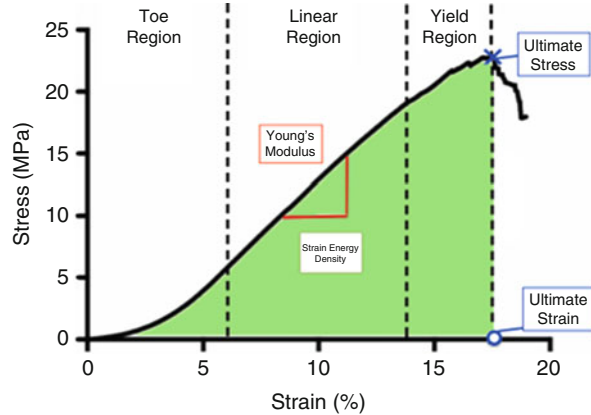
In tensile/compressive testing, a controlled uniaxial displacement is applied until failure on an AM scaffold. The test is performed using a universal testing machine composed of a movable crosshead used to apply the tensile/compressive stress to the specimen and a fixed crosshead. The mobile crosshead is usually actuated by a hydraulic or electromechanical system and equipped with a load cell to measure the applied force.

Specific clamps are used to block the specimen and avoid possible slippage or unexpected movements: especially in tensile tests an anchoring structure to fix the clamps is missing in the scaffold, causing stress concentration or misalignment with the load cell.

AM scaffolds should be mechanically tested under conditions simulating their working state, either *in vitro* or *in vivo*, to confirm their applicability in tissue engineering applications (Boffito et al. 2015). For this reason, tensile/compressive tests can be performed in dry and wet conditions. In the first case, the experiment is performed in a nitrogen atmosphere and standard clamps can be used to secure the sample. In the second one, the experiment is performed in culture medium at 37 °C and a specific experimental setup composed by a watertight container and heater must be used.

The evaluation of the cross-sectional area (CSA) of the specimen defined as the surface that resists to the applied force as well as deformation measurements is critical. Several times the CSA is overestimated using the Feret length of a porous structure, while the strain measurements can be evaluated using the crosshead moving control system, or with an extensometer or a 2D/3D optical system.

Fig. 2 Generic stress-strain plot, which highlights the main mechanical parameters that can be derived



Digital image correlation (DIC) is an optical method that employs tracking and image registration techniques for accurate 2D and 3D measurements of changes in images (Sutton et al. 2009). It tracks the changes in gray value pattern in small subsets during deformation and it is used to measure deformation, displacement, strain, and optical flow. DIC relies on finding the maximum of the correlation array between pixel intensity array subsets on two or more corresponding images, which gives the translational shift between them.

Digital volume correlation (DVC) is an optical analysis similar to DIC and able to evaluate 3D deformations capturing planar images of the surface of a body. In this case, full-field displacement information is evaluated as voxels and an algorithm minimizes a coefficient based on the summed difference of intensity values in a 3D-subset where intensity values correspond to (x,y,z) values (Bay et al. 1999; Huang et al. 2011). This technique is used with MRI imaging, μ CT, confocal microscopy, and two-photon excitation microscopy. With the CSA, the elongation, and force measurements, a stress-strain curve representing the mechanical properties of the AM scaffolds can be obtained (Fig. 2).

In particular, from the stress-strain curves, the following parameters can be evaluated (Fig. 2):

- Young's modulus, that is the elasticity of the AM scaffold in tension or compression expressed as the ratio of stress to strain and calculated as the slope of the stress-strain curve in the linear region
- Ultimate stress, defined as the maximum stress sustained by the specimen before the failure of the material
- Ultimate strain defined as the maximum strain sustained by the specimen before the failure of the material
- Strain energy density at failure defined as the area under the stress-strain curve

The introduction of optical measurements allows evaluating the Poisson's ratio, which describes the strain response in the directions orthogonal to an applied uniaxial stress. For conventional material, the Poisson's ratio is positive, indicating

an enlargement of the sample during compression. With AM technologies, which allow to control the internal geometry, it is possible to design the internal lattice giving to the scaffold a global behavior characterized by a negative Poisson's ratio (Panetta et al. 2015).

3.2 Creep and Stress Relaxation Tests

Polymer-based AM scaffolds are viscoelastic and display time-dependent and load-history-dependent mechanical behavior described by:

- Hysteresis, defined as the energy dissipation with continuous phases of loading and unloading
- Creep, defined as is the increase of length over time under a constant load
- Stress relaxation, defined as the decrease in the load when the material is held at a fixed elongation

Creep and stress relaxation tests are two methods to characterize the viscoelastic response of AM scaffolds to static load. In particular, the viscoelastic behavior of an AM scaffold can be described by Fung's quasilinear viscoelastic (QLV) theory commonly used to characterize soft biological tissues (Fung et al. 1972). In order to determine the five constants of the QLV theory with limited systematic and random experimental noise, the loading phase before the stress relaxation test should be registered and performed with a constant strain rate, instead of an instantaneous displacement, usually not feasible in lab conditions (Abramowitch and Woo 2004).

3.3 Dynamic Mechanical Analysis

Dynamic mechanical analysis (DMA), also called dynamic mechanical spectroscopy or dynamic mechanical thermal analysis (DMTA), is a technique used to evaluate the viscoelasticity of polymers and can be applied to evaluate the viscoelastic behavior of an AM scaffold and its response to stress, temperature, and frequency (Menard 1999; Ge et al. 2006; Moroni et al. 2006). The test is performed applying a sinusoidal (cyclic) stress to a sample of known geometry and recording the resulting strain. During DMA tests, the applied stress and the resulting strain can be described by the following equations:

$$\text{Stress: } \sigma = \sigma_0 \sin(\omega t + \delta) \text{ (Eq. 1)}$$

Strain: $\varepsilon = \varepsilon_0 \sin(\omega t)$ (Eq. 2) where ω is frequency of strain oscillation, t is time, and δ is phase lag between stress and strain.

From a DMA test, the following parameters can be estimated:

$$\text{Storage modulus: } E' = \frac{\sigma_0}{\varepsilon_0} \cos \delta \text{ (Eq. 3) measures the stored energy}$$

$$\text{Loss modulus: } E'' = \frac{\sigma_0}{\varepsilon_0} \sin \delta \text{ (Eq. 4) measures the energy dissipated as heat}$$

$$\text{Phase angle: } \delta = \arctan \frac{E''}{E'} \text{ (Eq. 5)}$$

Complex variables can be used to express the modulus E^* as $E^* = E' + iE''$ (Eq. 6) where $i^2 = -1$. Three different test modes can be used to evaluate the viscoelastic properties of AM scaffold:

- Temperature sweep test; the complex modulus at low constant frequency is evaluated at increasing temperature. The glass transition temperature of the polymer is identified by a peak in $\tan(\delta)$.
- Frequency sweep test; the sample must be held to a fixed temperature and tested at varying frequency. A peaks in $\tan(\delta)$ and in E'' with respect to frequency can be associated with the glass transition.
- Dynamic stress-strain test can be performed increasing the amplitude of oscillations. With this method, the material's linear stress-strain behavior can be determined evaluating the variation of storage and loss moduli with increasing stress.

3.4 Finite Element Modeling for Scaffold Characterization

The investigation of mechanical response of scaffolds can be also performed through numerical simulations, which have been widely used both for design and post hoc analysis (Eshraghi and Das 2010). For scaffold design, a variety of approaches have been proposed in order to optimize, for example, the stress distribution using repetition of elementary unit cells (Cheah et al. 2003) or specific deposition patterns (Hoque et al. 2005). For the post hoc analysis, the characterization of mechanical properties of scaffolds is generally based on finite element modeling (FEM), a numerical technique used for finding approximate solution to problems described by partial differential equations. This numerical technique is based on the discretization of complex geometries into a discrete number of smaller and simpler parts called elements, in which elementary, polynomial functions are defined (shape functions). These equations are assembled in a larger system of equations, and variational methods are applied for minimizing an error function.

The input geometry for the model is represented by a CAD or μ CT of the AM scaffold and it can be used to evaluate structural properties of the whole structure or of the cell grid unit, but can also find applications for evaluating scaffold fluid dynamical properties and its interaction with the surrounding tissue and fluids. The results provided by FEM are highly accurate and often results in the creation of models considered a predictive tool for the design of AM scaffold (Rainer et al. 2012, chapter ► “Mathematical Modeling of 3D Tissue Engineering Constructs”).

4 Surface Properties Characterization

Scaffold surface influences the physicochemical interactions at the interface between biomaterials and cells by affecting adhesion protein and subsequent cytoskeletal arrangement, which in turn has influence on cell differentiation, genetic expression, migration, morphology, orientation, and proliferation. When immersed into the culture

medium containing cells, exposed surfaces are rapidly coated with a protein layer, influenced by the nanoscale surface texture, surface chemistry, and charge (Tomlins 2015).

Several works have shown the possibility to modify the surface texture of AM scaffolds by adding an electrospun layer of a different material, in order to provide bioinspired motifs to unless nonadhesive scaffold surface (Carrabba et al. 2016), or by locally printing adhesion proteins providing binding site (Fujie et al. 2012).

Generally, it is easier to perform these surface characterizations directly on the biomaterial in the raw state and not directly on the scaffold, because of steering impediments. A pragmatic solution is to manufacture a specific sample: a model surface from the same material, which is then exposed to the same treatments (Tomlins 2015).

Chemical surface analysis technique that has a penetration depth of few nanometers is the X-ray photoelectron spectroscopy (XPS), but it requires a footprint around 100 μm , which is larger than most scaffold strut dimension. EDAX instead has a deeper penetration (approximately 2 μm) not suitable for determining the absorbing proteins.

Surface roughness is one of the elements that can directly influence protein attachment, cell adhesion, and growth in an AM scaffold. The surface roughness R_q is defined as (Eq. 7):

$$R_q = \sqrt{\frac{1}{n} \sum_{i=1}^n y_i^2} \quad (7)$$

where n is the number of ordered and equally spaced points along the trace, y_i is the vertical distance from the mean line to the i th data point. This equation assumes that the roughness profile has been filtered from the raw profile data and the mean line has been calculated and assumed horizontal. Therefore, the height is assumed to be positive in the upward direction, moving away from the bulk material.

The most efficient method to evaluate the surface roughness of an AM scaffold is the atomic-force microscopy (AFM) analysis. AFM or scanning-force microscopy (SFM) is a high-resolution type of scanning probe microscopy, with a lateral resolution of ~ 30 nm and a vertical one up to 0.1 nm. The AFM consists of a silicon or silicon nitride cantilever with a sharp tip (probe) used to scan the specimen surface. According to Hooke's law, forces between the tip and the sample deflect the cantilever when the tip is positioned in proximity of a sample surface. Different force typologies can be measured with AFM such as mechanical contact force, van der Waals forces, chemical bonding, electrostatic forces, and magnetic forces (Binnig et al. 1986; Giessibl and Trafas 1994). AFM technology can be used for surface potential measurement (known as Kelvin probe force microscopy (KPFM)) and manipulation at atomic level. In the AFM imaging, the tip is in contact with the sample that is raster scanned along an x - y grid. The surface topography is commonly displayed as a pseudocolor plot in which each pixel represents an x - y position on the sample, and the color represents the recorded signal, which corresponds to the surface roughness of an AM scaffold.

Thus, AFM technology provides a high-resolution 3D surface profile, without any special sample treatments (such as metal/carbon coatings), with the possibility to

work in air or liquid environment. However, the scanning area is usually limited to 150×150 micrometers and a maximum height on the order of 10–20 micrometers, with a very low scan speed. Furthermore, image artifacts, due to steep walls, are possible and overhangs cannot be measured.

4.1 Surface Functionalization

A common technique to enhance imaging capabilities allowing the characterization of surface functionalization is the use of fluorescent stains bound to the biomolecules of interest, which will be deposited on a nonstained AM scaffold (background). Fluorescent molecules absorb excitation light at a certain wavelength and emit light at a longer wavelength: fluorescent microscopy records this emitted light allowing to determine molecular distribution (Kubitscheck 2013). One of the major limitations of 2D imaging method is the inability of visible light to pass through the scaffold over a distance longer than a few microns in opaque samples.

Confocal laser scanning microscopy (CLSM or LSCM), thanks to optical sectioning, allows to acquire in-focus images from selected depths. Images are acquired point-by-point and reconstructed with segmentation algorithms for a 3D representation of topologically complex objects. The penetration depth is limited by opacity of the scaffold (generally around 80 μm): for opaque specimens, confocal microscopy is useful for surface profiling, while for nonopaque specimens, interior structures can be acquired. Multiphoton fluorescence microscopy (MFM) has attractive advantages over confocal microscopy for imaging three-dimensionally resolved fluorescence imaging thanks to two-photon excitation, which occurs only at the focal point of the microscope, minimizes the photobleaching and photodamage (Denk et al. 1990).

The development of PEBBLEs (photonic explorers by biologically localized embedding) has provided a new type of biological imaging method. PEBBLEs are nanoparticle sensors that have been developed for imaging and dynamic monitoring of the molecular or ionic components, constructs, forces, and movement, in real time in live cells and in vivo. With their biocompatible small size and inert matrix, nanoparticle sensors have been successfully applied for noninvasive real-time measurements of analytes concentration in cells, with spatial, temporal, physical, and chemical resolution. It has been demonstrated that ratiometric fluorescent PEBBLE can be incorporated in the scaffold fabrication using inkjet printing, creating pH-sensitive AM scaffolds (Fig. 3) (Orsi et al. 2015).

5 Permeability

Permeability represents a determinant factor to promote cell penetration and nutrient supply and distribution in the AM scaffold. It is a parameter that measures quantitatively the ability of a porous medium to conduct fluid flow and it depends on the combination of porosity, pores size, orientation, tortuosity, and interconnectivity, as well as wettability (Dias et al. 2012).

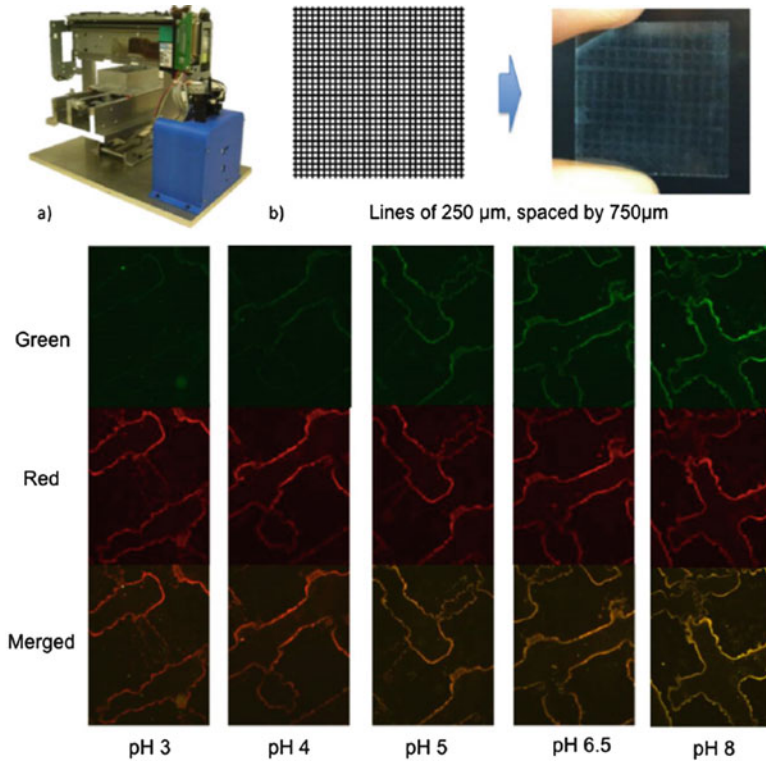


Fig. 3 (a) Thermal Inkjet printer; (b) designed and printed pattern scaffold; and fluorescence response of the structures at different pH (from Orsi et al. 2014)

5.1 Wettability

Wettability is the ability of a liquid to maintain contact with a solid surface thanks to intermolecular interactions. The degree of wetting or wettability is determined by a force balance between adhesive and cohesive forces (de Gennes 1985). Surface wettability can directly influence protein attachment, cell adhesion, and growth in an AM scaffold and can be quantified with a contact angle measurement. Nonwettable pore surfaces require a higher pressure to force the liquid to pass through the scaffold.

The contact angle is the angle, conventionally measured through the liquid, where a liquid–vapor interface meets a solid surface. Assuming a thermodynamic equilibrium between the liquid (L), the solid (S), and the gas or vapor (G) phases (Fig. 4), the equilibrium contact angle θ_c is determined by Young’s equation:

$$\gamma_{SG} - \gamma_{SL} - \gamma_{LG} \cos \theta_c = 0 \tag{8}$$

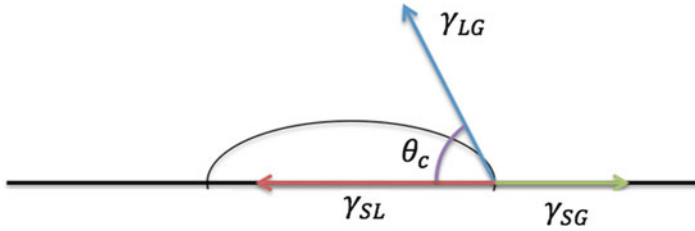


Fig. 4 Schematic of a liquid drop showing the quantities in Young's equation

where,

γ_{SG} is the solid–vapor interfacial energy

γ_{SL} is the solid–liquid interfacial energy

γ_{LG} is the liquid–vapor interfacial energy

Theoretically, a system of solid, liquid, and vapor at a certain temperature and pressure has a unique equilibrium contact angle. However, contact angle hysteresis ranged between (maximal) contact angle to the receding (minimal) contact angle that can be observed, due to surface roughness and chemical inhomogeneity (Della Volpe and Brugnara 2006).

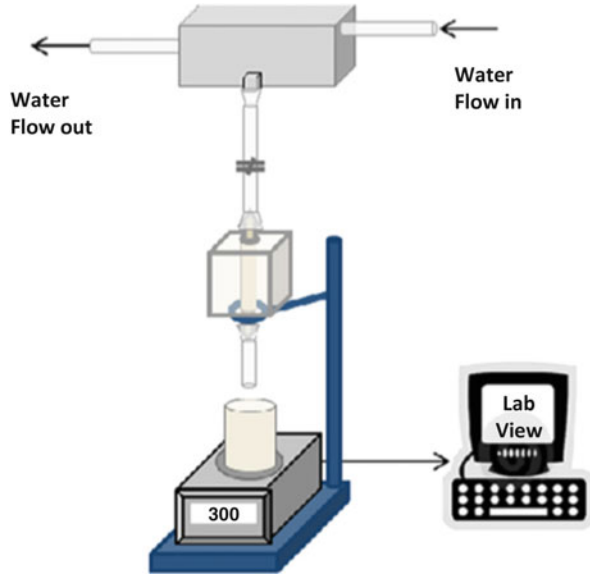
A smaller contact angle means that cohesive forces are weaker than adhesive ones and molecules of the liquid tend to interact more with solid molecules than liquid molecules. A larger contact angle means that cohesive forces are stronger than adhesive one and the molecules of the liquid tend to interact more with each other than with the solid molecules. Different measuring methods have been described in the literature, but only a few of them are applicable to measure the contact angle on an AM scaffold surface, due to the morphology (presence of macropores and/or absence of a flat surface).

- The static sessile drop method: the contact angle is measured by a contact angle goniometer using an optical system to capture the profile a drop deposited on a surface. The angle formed between the liquid–solid interface and the liquid–vapor interface is the contact angle.
- The sessile drop method: it is similar to the static one but the deposited liquid drop volume is dynamically changed without increasing its solid–liquid interface area and this maximum angle is the advancing angle. Volume is then removed to produce the smallest possible angle, which is called the receding angle.

5.2 Permeability Measurement

The permeability of an AM scaffold can be evaluated through experimental and computational methods. Kemppainen (Kemppainen 2008; Kemppainen and Hollister 2010) proposed an experimental method based on a setup composed of a reservoir where the water level is maintained in equilibrium by a continuous water flow in and out (Fig. 5) (Dias et al. 2012).

Fig. 5 Experimental setup for contact angle measurements (from Dias et al. 2012)



The scaffold is placed in an acrylic chamber and the water flows from the reservoir, through the acrylic chamber, to a collector, which in turn is seated on a scale that sends the information to the computer where it is recorded. Consequently, the mass of water can be read at different time points, allowing the calculation of the mass flow. The average of the mass flow is used for the calculation of permeability based on a formulation derived from Bernoulli’s equation and Darcy’s law (Li and Mak 2005; Dias et al. 2012) (Eq. 9):

$$k = \frac{\Delta x}{A M_s} \cdot \frac{2\pi^2 r^4}{(M_0/M_s)^2 - 1} \tag{9}$$

where Δx corresponds to the scaffold’s height, A is the scaffold’s sectional area, r is the outlet radius, and M_s and M_0 are the mass flow rate with the scaffold and without it, respectively.

However, parameters such as shear stress or shear rate and mass transport are difficult to be directly measured, and are generally inferred from biological results. Computational fluid dynamics can gain insight in to these parameters as described by Zhang et al. which demonstrated how AM can be used to tailor scaffold properties by controlling surface roughness and by altering the strut architecture and density (Zhang et al. 2013). In order to evaluate the permeability of selective laser melting (SLM) scaffolds, a computational and experimental approach was applied to samples with structures modified during their fabrication to validate the models. Then, structural modifications were made on the computer design of titanium structures at both microscopic (surface roughness) and macroscopic (strut architecture) levels (Fig. 6).

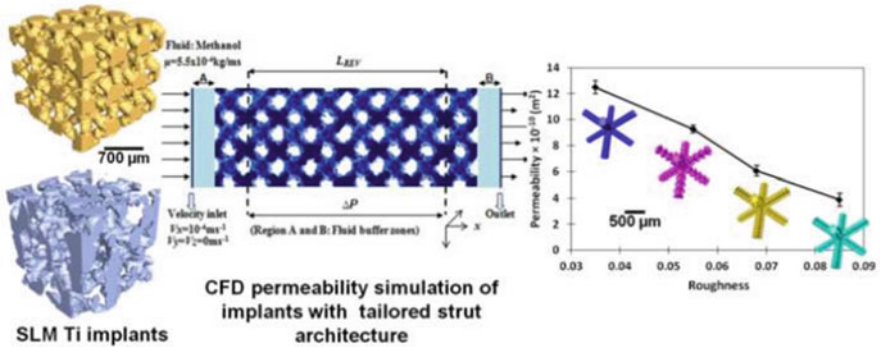


Fig. 6 CFD permeability simulation on structure with tailored architecture (Zhang et al. 2013)

6 Electrical Properties Characterization

There is great interest in designing scaffolds able to monitor local environment and cell function, because, at present, most methods to gain insights on 3D scaffolds are invasive and destructive. Giaever and Keese (1984, 1991) have shown that as the cells attach and spread on a small electrode surface, they alter the effective area available for current flow causing an increase in the impedance of the system. Ehret et al. (1997) used an interdigitated electrode structure to monitor the spreading, attachment, and morphology of fibroblasts in culture.

Consequently, it is possible to monitor cellular activity monitoring electrical properties of the scaffold. As example, to investigate the feasibility of designing biocompatible scaffolds with integrated sensing capabilities, Whulanza et al. (2011, 2013) realized AM scaffolds with embedded carbon nanotubes (CNTs) as a sensor, which presents electroconductive properties. Electrical impedance measurements, including electrochemical impedance spectroscopy (EIS) (Barsoukov 2005), describe the material ability as resistance to electrical current flow and capacity to store electrical charge. In EIS, a specific electrical stimulus (voltage or current) is applied to the electrodes and the response (resulting voltage or current) is registered. By varying the stimulus over a frequency sweep, frequency-dependent information can be obtained. As basic assumption, the system is considered as time invariant during the experimental procedure. EIS data are normally used to validate mathematical distributed model, or serve as starting point for a lumped parameters model of the equivalent circuit.

7 Biological Properties Characterization

Traditionally, biochemical characterization tools have played a major role when studying the maturation or functionality of the tissues. Basic techniques used in this field, together with histology and immunohistochemistry, are immunoblotting,

biochemical spectrometric assays, and reverse transcription polymerase chain reaction (RT-PCR) analysis, which facilitate the quantification of proteins and gene expression, respectively.

Biochemical characterization can be performed to investigate the biochemical “footprint” of a specific cellular population activity on an AM scaffolds. Typical biochemical assays are used to quantify the amount of DNA (DNA assay), glycosaminoglycans (GAGs assay), alkaline phosphatase activity (ALP activity assay), and total collagen, among other proteins that display a specific spectrometric peak or that can be bound to a dye or fluorophore with a specific spectrometric/fluorometric peak.

RT-PCR is a process used to quantify the level of mRNAs, which code the amino acid sequence of the proteins. Because mRNA is used to transmit the genetic information from DNA to ribosomes to produce proteins, the abundance of a specific mRNA sequence gives a quantitative measurement of the expression of that specific coded protein (gene expression). In RT-PCR, the RNA is reverse-transcribed into a more robust DNA molecule (called cDNA), which is copied and amplified in quantitative steps, producing an absolute measurement of the number of copies of original mRNA, typically in units of copies per nanoliter of homogenized tissue or copies per cell. RT-PCR is commonly used to investigate cell differentiation toward a specific lineage. For example, Runt-related transcription factor Runx2 regulates hMSCs differentiation into the osteogenic lineage, triggering the expression of major bone protein genes like collagen type I (Coll1a1), osteopontin, bone sialoprotein, and osteocalcin during the early stages of osteoblast differentiation.

The biological characterization of an AM scaffold is strongly influenced by its sterility. For this reason, AM scaffolds should be fabricated in a sterile and aseptic environment. However, these environmental conditions cannot always be guaranteed and different sterilization procedure can be also used for these scaffolds, as commonly used in many other biomedical applications. The most common methods to sterilize an AM scaffold are: ethylene oxide (EtO) Gas, UV radiation, gamma irradiation, and autoclaving.

Living cells can be printed together with biomaterials in high-resolution patterns to fabricate 3D constructs for tissue engineering, in which case the above-mentioned sterilization methods are not applicable anymore to the scaffold, and sterility has to be guaranteed during manufacturing (chapter ► [“Extrusion-Based Biofabrication in Tissue Engineering and Regenerative Medicine”](#)). This fabrication process can have a strong impact on living cells. Tirella and Ahluwalia (2012) evaluated the impact of processing cells with AM methods and modeled the printing phase of two systems (Biojet, an inkjet-based bioprinter; and Pressure Assisted Microsyringe 2, an extrusion-based bioprinter) that use biomaterial inks containing living cells. They demonstrated that cell damage occurs principally during drop collision on the printing surface and that shear stresses act on cells during extrusion. For these reasons, cell viability analysis represents the standard test to evaluate if the fabrication process is adequate to directly print living cells.

Viability can be measured performing a standard live-dead assay, where cells are stained with fluorescent markers (e.g., calcein AM and ethidium homodimer). Another often used class of viability tests comprise metabolic assays. A cell viability

assay based on a resazurin-based fluorescent compound metabolized by mitochondrial cytosolic and microsomal enzymes to resorufin, which can be detected with a fluorimeter at 590 nm, is an example of such commonly used tests. This test is often used to estimate the total number of cells in a sample because mitochondrial activity is assumed to be proportional to the total cell population. It can also be used to provide a measure of overall cell health between comparative populations.

An intermediate step between classical *in vitro* cell culture on an AM scaffold and *in vivo* tests is often represented by dynamic cultures in bioreactors. A bioreactor is a device or system used to grow cells or tissues as it is engineered to be able to mimic the living tissue environment applying fluid dynamical and/or mechanical stimuli. Due to its characteristics, the bioreactors can be used as checkpoint to evaluate the adequacy of the AM scaffold for a specific targeted application (De Maria et al. 2011).

In vivo experiments in small and large animal models represent an important step toward clinical application and involve the surgical creation of a defect in the tissue of interest for the scaffold implantation. In this scenario, histological analysis plays a key role for the evaluation of the progress in tissue regeneration in presence and in absence of the scaffold (Park et al. 2012). In bone tissue engineering applications, μ CT offers the opportunity to monitor in a noninvasive way the healing process and the tissue-scaffold integration over time (Oest et al. 2007). Where relevant, mechanical properties of the *in vivo* matured engineered constructs are also measured, following the previously mentioned assays.

8 Future Perspectives

In this chapter, we described the characterization methodologies to gain insight in scaffold properties, highlighting how geometrical, surface, and mechanical properties are interdependent.

Many of these tests are destructive (such as several mechanical tests), while others require experimental conditions which do not allow maintaining a living cell culture during the characterization (such as mercury porosimetry). Furthermore, specimen preparation may alter the property under investigation, such as the changes in shape due to cutting or vacuum conditions during SEM. Thus, rarely the analyzed scaffold is the same used for biological tests: although imaging techniques like μ CT and MRI are promising tools to study 3D engineered tissue constructs in a nondestructive manner, they are not applicable to all tissues and organs. A single nondestructive but fully informative characterization technique has yet to be invented.

When thinking of AM constructs characterization toward a commercialization and clinical translation, guidelines have been proposed to characterize both biomaterials and scaffolds, such as ASTM F2027-08 and F2150-13, even if rarely they have been explicitly followed in the scientific literature. The characterization methods here presented are not specific for AM scaffolds, but were adapted from related research field or from test performed on traditional foam scaffolds. As example, a peculiarity of AM technologies is the layer-by-layer approach: this

allows the possibility of an in-line check of integrity and consistency of the scaffold under construction. This feature can be the turning point for the certification of additive manufactured patient-specific implants, proving a 100% identity between computer model and real object as well as error-free fabrication, considered mandatory by clinicians and health insurances (chapter ► [“Translation and Applications of Biofabrication”](#)).

In a future perspective, it is possible to foresee that the so-called 4D printing, that is the 3D printing of complex structures which undergo to a controlled modification of their shape after printing, will be more often used also to fabricate scaffolds. Accurate characterization methods to track these conformational changes are needed.

In conclusion, the passage from prototyping to manufacturing scaffolds and bioprinted constructs relies on the serial production of compliant products, which cannot be separated from a quality control of both printers and manufactured scaffolds.

Acknowledgements This project/research has been made possible with the support of the Dutch Province of Limburg.

References

- Abramowitch SD, Woo SL (2004) An improved method to analyze the stress relaxation of ligaments following a finite ramp time based on the quasi-linear viscoelastic theory. *J Biomech Eng* 126(1):92–97. <https://doi.org/10.1115/1.1645528>
- Barsoukov E (2005) Impedance spectroscopy: theory, experiment, and applications (edited by J Ross Macdonald), 2nd. edn isbn:978-0-471-64749-2.
- Bay BK, Smith TS, Fyhrie DP, Saad M (1999) Digital volume correlation: three-dimensional strain mapping using X-ray tomography. *Exp Mech* 39(3):217–226
- Binnig G, Quate CF, Gerber C (1986) Atomic-Force Microscope. *Phys Rev Lett* 56(9):930–933
- Boffito M, Bernardi E, Sartori S, Ciardelli G, Sassi MP (2015) A mechanical characterization of polymer scaffolds and films at the macroscale and nanoscale. *J Biomed Mater Res A* 103:162–169
- Carrabba M, De Maria C, Oikawa A, Reni C, Rodriguez-Arabaolaza I, Spencer H, Slater S, Avolio E, Dang Z, Spinetti G, Madeddu P, Vozzi G (2016) Design, fabrication and perivascular implantation of bioactive scaffolds engineered with human adventitial progenitor cells for stimulation of arteriogenesis in peripheral ischemia. *Biofabrication* 8(1):015020
- Castilho M, Dias M, Vorndran E, Gbureck U, Fernandes P, Pires I, Gouveia B, Armés H, Pires E, Rodrigues J (2014) Application of a 3D printed customized implant for canine cruciate ligament treatment by tibial tuberosity advancement. *Biofabrication* 6(2):025005
- Cheah CM, Chua CK, Leong KF, Chua SW (2003) Development of a tissue engineering scaffold structure library for rapid prototyping. Part 1: investigation and classification. *Int J Adv Manuf Technol* 21(4):291–301
- Clarke AR (2002) Microscopy techniques for materials science. CRC Press (electronic resource)
- de Gennes PG (1985) Wetting: statics and dynamics. *Rev Mod Phys* 57:827–863
- De Maria C, Giusti S, Mazzei D, Crawford A, Ahluwalia A (2011) Squeeze pressure bioreactor: a hydrodynamic bioreactor for noncontact stimulation of cartilage constructs. *Tissue Eng Part C Methods* 17(7):757–764

- De Maria C, De Acutis A, Vozzi G (2015) Indirect rapid prototyping for tissue engineering. In: *Essential of 3D biofabrication and translation*. Elsevier. isbn:978-0-12-800972-7
- Della Volpe C, Brugnara M (2006) About the possibility of experimentally measuring an equilibrium contact angle and its theoretical and practical consequences. *Contact Angle, Wettability and Adhesion* 4:79–100
- Denk W, Strickler JH, Webb WW (1990) Two-photon laser scanning fluorescence microscopy. *Science* 248(4951):73–76
- Dias MR, Fernandes PR, Guedes JM, Hollister SJ (2012) Permeability analysis of scaffolds for bone tissue engineering. *J Biomech* 45:938–944
- Doube M, Klosowski MM, Arganda-Carreras I, Cordelières F, Dougherty RP, Jackson J, Schmid B, Hutchinson JR, Shefelbine SJ (2010) BoneJ: free and extensible bone image analysis in ImageJ. *Bone* 47:1076–1079. <https://doi.org/10.1016/j.bone.2010.08.023>
- EC Regulation No 1394/2007 on advanced therapy medicinal products and amending Directive 2001/83/EC and Regulation (EC) No 726/2004
- Egerton RF (2005) *Physical principles of electron microscopy: an introduction to TEM, SEM, and AEM*. Springer, New York
- Ehret R, Baumann W, Brischwein M, Schwinde A, Stegbauer K, Wolf B (1997) Monitoring of cellular behaviour by impedance measurements on interdigitated electrode structures. *Biosens Bioelectron* 12(1):29–41
- Eshraghi S, Das S (2010) Mechanical and microstructural properties of polycaprolactone scaffolds with one-dimensional, two-dimensional, and three-dimensional orthogonally oriented porous architectures produced by selective laser sintering. *Acta Biomater* 6(7):2467–2476
- Fujie T, Desii A, Ventrelli L, Mazzolai B, Mattoli V (2012) Inkjet printing of protein microarrays on freestanding polymeric nanofilms for spatio-selective cell culture environment. *Biomed Micro-devices* 14(6):1069–1076
- Fung YC, Perrone N, Anliker M (1972) Stress strain history relations of soft tissues in simple elongation. In: *Biomechanics: its foundations and objectives*. Prentice Hall, Englewood Cliffs, pp 181–207
- Ge Z, Yang F, Goh JCH, Ramakrishna S, Lee EH (2006) Biomaterials and scaffolds for ligament tissue engineering. *J Biomed Mater Res A* 77:639–652
- Giaever I, Keese CR (1984) Monitoring fibroblast behavior in tissue culture with an applied electric field. *Proc Natl Acad Sci USA* 81(12):3761–3764
- Giaever I, Keese CR (1991) Micromotion of mammalian cells measured electrically. *Proc Natl Acad Sci USA* 88(17):7896–7900
- Giessibl FJ, Trafas BM (1994) Piezoresistive cantilevers utilized for scanning tunneling and scanning force microscope in ultrahigh vacuum. *Rev Sci Instrum* 65(6):1923
- Gilbert PM, Havenstrite KL, Magnusson KE, Sacco A, Leonardi NA, Kraft P, Nguyen NK, Thrun S, Lutolf MP, Blau HM (2010) Substrate elasticity regulates skeletal muscle stem cell self-renewal in culture. *Science* 329(5995):1078–1081
- Goldstein J (2003) *Scanning electron microscopy and x-ray microanalysis*. Kluwer Academic/Plenum Publishers, New York
- Groll J, Boland T, Blunk T, Burdick JA, Cho DW, Dalton PD, Derby B, Forgacs G, Li Q, Mironov VA, Moroni L, Nakamura M, Shu W, Takeuchi S, Vozzi G, Woodfield TB, Xu T, Yoo JJ, Malda J (2016) Biofabrication: reappraising the definition of an evolving field. *Biofabrication* 8(1):013001
- Guillemot F, Mironov V, Nakamura M (2010) Bioprinting is coming of age: report from the international conference on bioprinting and biofabrication in Bordeaux (3B'09). *Biofabrication* 2:010201
- Ho ST, Huttmacher DW (2006) A comparison of micro CT with other techniques used in the characterization of scaffolds. *Biomaterials* 27(8):1362–1376
- Hoque ME, Huttmacher DW, Feng W, Li S, Huang MH, Vert M, Wong YS (2005) Fabrication using a rapid prototyping system and in vitro characterization of PEG-PCL-PLA scaffolds for tissue engineering. *J Biomater Sci Polym Ed* 16(12):1595–1610

- Huang J, Pan X, Li S, Peng X, Xiong C, Fang J (2011) A digital volume correlation technique for 3-D deformation measurements of soft gels. *Int J Appl Mech* 3(2):335–354
- Hutmacher D, Woodfield T, Dalton P, Lewis J (2008) Scaffold design and fabrication in tissue engineering. In: *Tissue engineering*, pp 403–454. isbn:978-0-12-370869-4
- Ibáñez L, Schroeder W, Ng L, Cates J, Consortium TIS, Hamming R (2003) *The ITK software guide*. Kitware, Inc., New York
- Kemppainen J (2008) Mechanically stable solid free form fabricated scaffolds with permeability optimized for cartilage tissue engineering. Dissertation, University of Michigan, USA
- Kemppainen J, Hollister S (2010) Differential effects of designed scaffold permeability on chondrogenesis by chondrocytes and bone marrow stromal cells. *Biomaterials* 31:279–287
- Kubitschek U (2013) *Fluorescence microscopy: from principles to biological applications*. Wiley-Blackwell, Weinheim. isbn:978-3-527
- Li J, Mak A (2005) Hydraulic permeability of polyglycolic acid scaffolds as a function of biomaterial degradation. *J Biomater Appl* 19:253–266
- Loh QL, Choong C (2013) Three-dimensional scaffolds for tissue engineering applications: role of porosity and pore size. *Tissue Eng Part B Rev* 19(6):485–502
- Malda J, Woodfield TB, van der Vloodt F, Wilson C, Martens DE, Tramper J, van Blitterswijk CA, Riesle J (2005) The effect of PEGT/PBT scaffold architecture on the composition of tissue engineered cartilage. *Biomaterials* 26(1):63–72
- Malda J, Visser J, Melchels FP, Jüngst T, Hennink WE, Dhert WJ, Groll J, Hutmacher DW (2013) 25th anniversary article: engineering hydrogels for biofabrication. *Adv Mater* 25(36):5011–5028
- Masaeli E, Morshed M, Nasr-Esfahani MH, Sadri S, Hilderink J, van Apeldoorn A, van Blitterswijk CA, Moroni L (2013) Fabrication, characterization and cellular compatibility of poly(hydroxy alkanooate) composite nanofibrous scaffolds for nerve tissue engineering. *PLoS One* 8(2):e57157
- Mattioli-Belmonte M, De Maria C, Vitale-Brovarone C, Baino F, Dicarolo M, Vozzi G (2015) Pressure-activated microsyringe (PAM) fabrication of bioactive glass-poly(lactic-co-glycolic acid) composite scaffolds for bone tissue regeneration. *J Tissue Eng Regen Med*. <https://doi.org/10.1002/term.2095>
- Menard KP (1999) *DMA: introduction to the technique, its applications and theory*. CRC Press, Boca Raton
- Moroni L, de Wijn JR, van Blitterswijk CA (2006) 3D fiber-deposited scaffolds for tissue engineering: influence of pores geometry and architecture on dynamic mechanical properties. *Biomaterials* 27:974–985
- Nadeem D, Kiamehr M, Yang X, Su B (2013) Fabrication and in vitro evaluation of a sponge-like bioactive-glass/gelatin composite scaffold for bone tissue engineering. *Mater Sci Eng C Mater Biol Appl* 33(5):2669–2678
- Nitzsche H, Metz H, Lochmann A, Bernstein A, Hause G, Groth T, Mäder K (2009) Characterization of scaffolds for tissue engineering by benchtop-magnetic resonance imaging. *Tissue Eng Part C Methods* 15(3):513–521. <https://doi.org/10.1089/ten.TEC.2008.0488>
- Oest ME, Dupont KM, Kong HJ, Mooney DJ, Guldborg RE (2007) Quantitative assessment of scaffold and growth factor-mediated repair of critically sized bone defects. *J Orthop Res* 25(7):941–950
- Orsi G, De Maria C, Montemurro F, Chauhan VM, Aylott JW, Vozzi G (2015) Combining inkjet printing and sol-gel chemistry for making pH-sensitive surfaces. *Curr Top Med Chem* 15:271–278
- Panetta J, Zhou Q, Malomo L, Pietroni N, Cignoni P, Zorin D (2015) Elastic textures for additive fabrication. *ACM Trans on Graphics – Siggraph* 34(4):12
- Park CH, Rios HF, Jin Q, Sugai JV, Padiol-Molina M, Taut AD, Flanagan CL, Hollister SJ, Giannobile WV (2012) Tissue engineering bone-ligament complexes using fiber-guiding scaffolds. *Biomaterials* 33(1):137–145
- Rainer A, Giannitelli SM, Accoto D, De Porcellinis S, Guglielmelli E, Trombetta M (2012) Load-adaptive scaffold architecturing: a bioinspired approach to the design of porous additively manufactured scaffolds with optimized mechanical properties. *Ann Biomed Eng* 40(4):966–975

- Ratner BD, Hoffman AS, Schoen FJ, Lemons JE (2013) *Biomaterials science*, 3rd edn. Elsevier Academic Press, San Diego/London. ISBN:978-0-12-374626-9
- Shirazi RN, Ronan W, Rochev Y, McHugh P (2016) Modelling the degradation and elastic properties of poly(lactic-co-glycolic acid) films and regular open-cell tissue engineering scaffolds. *J Mech Behav Biomed Mater* 54:48–59
- Sudarmadji N, Tan JY, Leong KF, Chua CK, Loh YT (2011) Investigation of the mechanical properties and porosity relationships in selective laser-sintered polyhedral for functionally graded scaffolds. *Acta Biomater* 7(2):530–537
- Sutton MA, Orteu JJ, Schreier HW (2009) *Image correlation for shape, motion and deformation measurements*. Springer, New York. isbn:978-0-387-78746-6
- Tirella A, Ahluwalia A (2012) The impact of fabrication parameters and substrate stiffness in direct writing of living constructs. *Biotechnol Prog* 28(5):1315–1320
- Tirella A, Vozzi F, Vozzi G, Ahluwalia A (2011) PAM2 (piston assisted microsyringe): a new rapid prototyping technique for biofabrication of cell incorporated scaffolds. *Tissue Eng Part C Methods* 17(2):229–237
- Tomlins P (2015) *Characterization and design of tissue scaffold*. Woodhead Publishing, Cambridge, UK/Waltham/Kidlington. ISBN:9781782420958
- Urciuolo A, Quarta M, Morbidoni V, Gattazzo F, Molon S, Grumati P, Montemurro F, Tedesco FS, Blaauw B, Cossu G, Vozzi G, Rando TA, Bonaldo P (2013) Collagen VI regulates satellite cell self-renewal and muscle regeneration. *Nat Commun* 4:1964
- von Burkersroda F, Schedl L, Göpferich A (2002) Why degradable polymers undergo surface erosion or bulk erosion. *Biomaterials* 23(21):4221–4231
- Whulanza Y, Ucciferri N, Domenici C, Vozzi G, Ahluwalia A (2011) Sensing scaffolds to monitor cellular activity using impedance measurements. *Biosens Bioelectron* 26(7):3303–3308
- Whulanza Y, Battini E, Vannozzi L, Vomero M, Ahluwalia A, Vozzi G (2013) Electrical and mechanical characterisation of single wall carbon nanotubes based composites for tissue engineering applications. *J Nanosci Nanotechnol* 13(1):188–197
- Zein I, Hutmacher DW, Tan KC, Teoh SH (2002) Fused deposition modeling of novel scaffold architectures for tissue engineering applications. *Biomaterials* 23(4):1169–1185
- Zhang Z, Jones D, Yue S, Lee PD, Jones JR, Sutcliffe CJ, Jones E (2013) Hierarchical tailoring of strut architecture to control permeability of additive manufactured titanium implants. *Mater Sci Eng C Mater Biol Appl* 33(7):4055–4062



Vascular Networks Within 3D Printed and Engineered Tissues

Daniel Sazer and Jordan Miller

Contents

1	Introduction	80
2	Diverse Methods to Produce Macroporous Scaffolds	81
3	Production of Defined 2D Networks Using Replica Molding	83
4	Extrusion of Solid Materials to Define Physical Boundaries of Hollow Vessels	85
5	Coaxial Extrusion Improves the Speed and Ease of Vessel Fabrication	87
6	Extrusion of Sacrificial Filaments Provides Intricate Control Over Vascular Geometry	89
7	Stereolithography as a Single-Step Fabrication Platform for 3D Vessel Networks	92
8	Advanced Fabrication Technologies	95
9	Multiscale Vasculature Produced by Endothelial Matrix Invasion	97
10	Progress Towards Integration In Vivo	99
11	Conclusions	101
	References	101

Abstract

In order to scale benchtop tissue mimics into viable constructs of clinically relevant dimensions, these structures must contain internal vascular networks to support convective mass transport. Without vessels to support perfusion culture, encapsulated cells located farther than 200 μm from the outer surface of a construct will quickly die due to the diffusional limits of oxygen and small molecule nutrients. By endowing artificial tissues with hollow vessels, researchers have made exciting progress towards the longitudinal maintenance of cellular function in large, dense tissues. But the field currently lacks standardized platforms and protocols to fabricate highly vascularized constructs in a rapid and cost-effective manner, which has left the literature base to become crowded

D. Sazer (✉) · J. Miller

Department of Bioengineering, Rice University, Houston, TX, USA

e-mail: dws6@rice.edu; jmil@rice.edu

with custom apparatus and diverse technical schemes. Here we highlight some promising, contemporary strategies for the vascularization of 3D printed and engineered tissues. We discuss the advantages and limitations of various fabrication platforms in the field, making note of desirable properties such as high spatial resolution, freely tunable 3D architecture, and the presence of discrete fluidic ports. With clinical targets in mind, this overview concludes with a brief survey of progress towards fluidic integration with the circulatory system *in vivo*.

1 Introduction

Evidence of human tissue replacement dates back over one thousand years ago. The use of iron dental implants began sometime around 200 AD in Europe, and the Mayans achieved similar success with seashell nacre around 600 AD (Ratner et al. 2004). But the first attempts to create living tissue replacements outside the body were performed in the early 1970s (Vacanti 2006), when an orthopedic surgeon attempted to produce artificial cartilage by seeding chondrocytes onto small pieces of bone. Since then, there has been enormous progress towards developing the cells (Haynesworth et al. 1992; Takahashi and Yamanaka 2006), scaffold materials (Langer and Folkman 1976; Whang et al. 1998), and biochemical factors (Wang et al. 1990; Jaiswal et al. 1997) that support generation of artificial tissues.

Successful demonstrations of synthetic human implants began with thin, flat structures like skin (Yannas et al. 1982; Heimbach et al. 1988) and cornea (Nishida et al. 2004). Building on these early clinical successes, it was soon discovered that planar constructs could be wrapped around mandrels to produce hollow cylindrical tissues for clinical replacement of tubular structures like the trachea (Macchiarini et al. 2008) and urethra (Raya-Rivera et al. 2011). Researchers have also folded these thin tissues into hollow spherical constructs for bladder replacement (Atala et al. 2006). But despite the clinical successes of 2D and hollow tissues, there have been few reports of solid tissue substitutes that can maintain cellular viability and function post implantation. This is because cells within the interior regions of dense, solid tissues will rapidly die in the absence of efficient vasculature, due to the inability of oxygen and nutrients to rapidly diffuse over distances above 100–200 μm (Kang et al. 2016).

Therefore, there is a critical need to fabricate tissue engineered constructs with innate vascular networks. With biomimetic culture conditions, it is possible to induce *de novo* vascular growth by seeding endothelial cells in 3D scaffolds (Wang et al. 2015); but this process is not scalable to constructs of clinically relevant dimensions, as cells on the interior regions will die before they have time to mature into vessels, anastomose, and establish a network of fluidic conduits capable of providing convective nutrient transport. By creating fluidic networks – with or without an endothelial lining – within the bulk of these biomaterial scaffolds as part of the initial fabrication process, it is thus possible to prevascularize artificial tissues. Here, we highlight contemporary strategies for the vascularization of 3D printed and engineered tissues. We discuss the advantages and limitations of various fabrication platforms in the field and explore strategies to achieve fluidic integration with the host circulation.

2 Diverse Methods to Produce Macroporous Scaffolds

At their simplest level, the purpose of vascular networks is to overcome the limits of diffusion by supplying routes for convective mass transport throughout the body. Oxygen, nutrients, and waste products must be dynamically exchanged between native tissues and the circulatory system, so that consumed nutrients can be replenished and so waste does not accumulate. In an engineered tissue, the simplest way to achieve this goal is to incorporate macroscopic porosity into a biomaterial scaffold and subject that construct to perfusion culture. 3D hydrogel scaffolds do in fact have micro- or nanoscopic pores, but the size of these voids translates to immensely high fluidic resistance. With such high resistance to flow, subjecting these scaffolds to perfusion may not elicit physiologically relevant convective transport or hemocompatible flows (McGuigan and Sefton 2007).

One method to produce macroporous polymer scaffolds is gas foaming. In this process, alkaline salt particles are first dissolved in a highly concentrated polymer solution. After solvent evaporation, a solid polymer scaffold remains. A chemical reaction occurs when acidic solution is introduced to the system, causing gas to foam through the polymer scaffold and introducing macroporous architecture to the construct (Fig. 1a). Jun and West examined this technique using polyurethaneurea and demonstrated the ability to control pore size and overall porosity by changing salt size and concentration, respectively (Jun and West 2005).

Similar macroporous scaffolds have also been fabricated with a method known as electrospinning, in which a high voltage is used to draw nanoscopic polymer fibers around the circumference of a rotating mandrel. Pham and colleagues studied the influence of perfusion culture on mesenchymal stem cells (MSCs) when seeded on electrospun polycaprolactone discs (Fig. 1b), which were fit into flow cassettes and subjected to flow rates as large as 1 mL/min (Pham et al. 2006). Successful perfusion at this flow rate indicated the macropores were interconnected, thus providing channels for convective flow that present significant fluidic conductance. Furthermore, this model was also used to show that perfusion enhanced MSC infiltration distance by a factor of 5 when compared to static culture. However, the void space of perfused scaffolds filled with matrix secreted by the cells, eventually blocking perfusion.

Gas foaming and electrospinning offer exceptionally high surface area-to-volume ratios for efficient cell seeding and present a wide variety of materials to work with. But the resultant macroporous architectures are stochastically defined by thermodynamic processes. In comparison, traditional 3D printing by melt extrusion is capable of producing macroporous scaffolds of defined, reproducible, and tunable architectures. By melt extruding thermoplastic polymer onto a receiving build platform, 3D scaffolds can be constructed in a point-by-point fashion with submillimeter resolution. However, this modality is limited to materials that will cool and solidify almost instantaneously after extrusion, which is necessary for the printed features to maintain their geometry before the next layer is printed. Using melt extrusion, Trachtenberg and coworkers fabricated macroporous polycaprolactone scaffolds with uniform or gradient pore sizes (Fig. 1c; Trachtenberg et al. 2014). The study

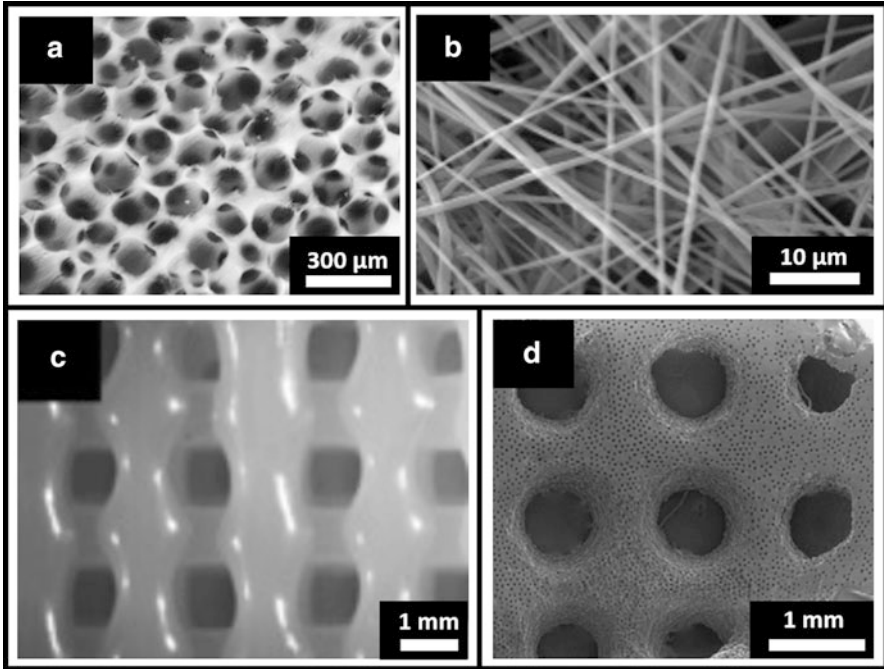


Fig. 1 Macroporous scaffolds to support convective mass transport. Stochastically defined porous architectures generated by (a) gas foaming (Costantini et al. 2016) and (b) electrospinning (Pham et al. 2006). User-defined pore lattices defined by (c) melt extrusion (Trachtenberg et al. 2014) and (d) photolithography (Bryant et al. 2007) (Adapted with permission from Elsevier (a, d), the American Chemical Society (b), and John Wiley and Sons (c))

rigorously explores how pore size and overall porosity can be reproducibly controlled by extrusion pressure, programmed spacing between extruded filaments, and printing speed.

Macroporous scaffolds with defined architectures can also be fabricated by photolithography, in which user-defined light patterns are used to selectively crosslink polymer solutions into rigid hydrogel features. To generate light patterns, a device with patterned holes of arbitrary shape – known as a photomask – is used to transmit light only in predetermined geometries. Liu Tsang and colleagues used this technology to construct hexagonal lattice architectures, whose large void fraction was intended to minimize barriers to nutrient transport during cell culture (Liu Tsang et al. 2007). Hepatocytes were encapsulated within the lattice struts by mixing them into the photosensitive polymer solution prior to crosslinking. The constructs were fit into a customized flow chamber, and it was shown that perfusion culture – supported by the large pores – elicited a higher magnitude of liver-specific albumin secretion and urea synthesis when compared to static controls.

An example of a similar macroporous scaffold built using photolithography can be seen in Fig. 1d. Here, a photomask was used to define circular pores of 500 μm

diameter (Bryant et al. 2007). The material was patterned around removable plastic microspheres of 62 μm , yielding even smaller pores within the lattice struts to complement the macroporous geometry. Pores introduced by microsphere templating were previously demonstrated to improve cell migration (Stachowiak et al. 2005); however, the overall hydraulic conductivity was not examined.

3 Production of Defined 2D Networks Using Replica Molding

Despite the utility of macroporous scaffolds in cellular assays, porosity is different from vascularization. Macropores are not self-contained to a tubular network geometry and do not possess unifying fluidic ports to facilitate controlled perfusion of a vascularized tissue construct. For artificial tissues intended for clinical implantation, discrete access ports must exist so that fluidic connection with the host circulatory system can be made, and so that circulating blood does not leak out into the bodily cavities.

Replica molding is a commonly used technique to fabricate defined vascular networks with unifying fluidic ports. In essence, replica molding of vascular networks involves three distinct stages: fabricating a negative (i.e., complementary) mold of the desired vascular network, casting a biomaterial matrix around the mold, and then removing the mold. Using cylindrical needles as a molding tools, Chrobak and coworkers were able to fabricate single 100 μm channels within collagen matrix (Fig. 2a – left) (Chrobak et al. 2006). Collagen proteins contain cell-binding peptide domains, which enabled endothelial cells to adhere to the vessel walls and spread to form confluent monolayers (Fig. 2a – right). The putative vessels were shown to exhibit strong barrier function and low leukocyte adhesion, which could be reversed by the introduction of inflammatory agonists like histamine. This reversible behavior is characteristic of native vessels, illustrating the physiological relevance of this vascular model.

This needle-molding technique was further developed by Hasan and coworkers, who used three concentric needles as their replica mold to produce a tri-layered structure (Hasan et al. 2015). Here, a single glass capillary of about 1.5 mm diameter was first used as a mold for silicone casting. Two concentric hypodermic needles were then inserted into the resulting channel, with outer diameters chosen so that there was void space between each element. A suspension of fibroblasts in gelatin methacrylate solution was pipetted within the outer void space and was photocrosslinked into a rigid hydrogel by bulk irradiation to form an annular tissue that mimics vascular adventitia. The large needle is removed, and the process is repeated with smooth muscle cell-laden gelatin to form a second annular tissue, mimicking the tunica media. The last needle is removed, and endothelial cells are seeded around the luminal wall. Thus, the three major layers of native vascular tissue were recapitulated in one device while also maintaining a patent lumen for perfusion (Fig. 2b). While these single vessels may likely be useful for studying fundamental vascular biology, it is difficult to imagine scaling this process to build vascularized tissue constructs of clinically relevant dimensions.

A different replica molding technique known as soft lithography is better suited to produce vascular networks of clinical dimension and biomimetic geometry. To make a network of channels using soft lithography, standard photolithography (described earlier) is first used to pattern positive, rigid features on a silicon wafer. A polymer solution of hydrogel or silicone precursor (known as prepolymer) is then cast against these positive features (Fig. 2c – left), leaving negative, trench-like features imprinted on an otherwise solid structure. This trench-containing structure is then bonded to flat slab of similar material, yielding fluidically sealed vascular networks (Fig. 2c – right).

Cabodi and associates used soft lithography to form a rectilinear lattice of perfusable channels with a single pair of fluidic ports and channel diameters as small as 25 μm (Fig. 2d; Cabodi et al. 2005). Importantly, this luminal diameter approaches that of native capillaries, which typically range between 5 and 10 μm .

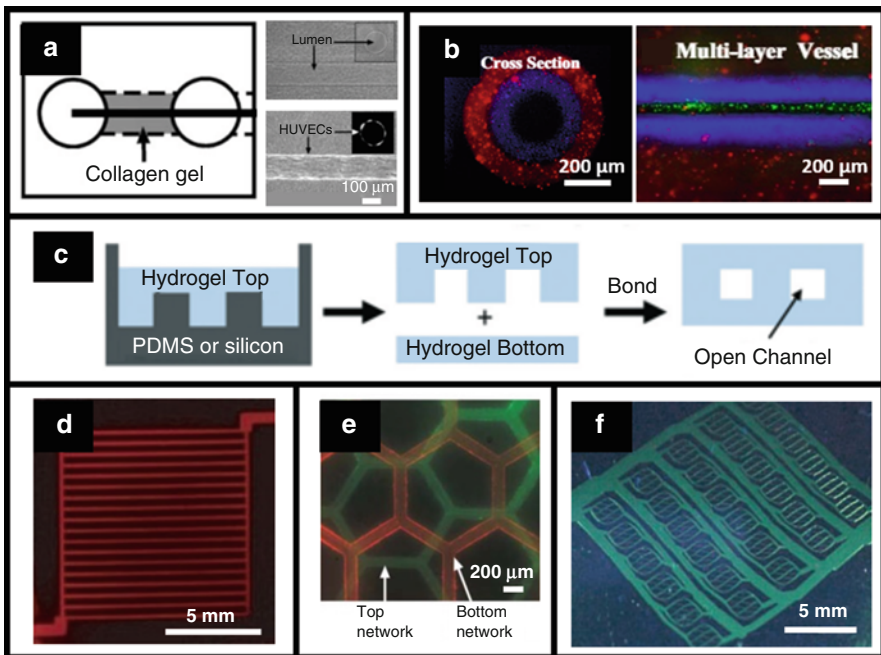


Fig. 2 Replica molding to produce defined fluidic networks. (a) Removal of a metal needle from a collagen hydrogel cast yields a single lumen that supports endothelial cell monolayer formation (Chrobak et al. 2006). (b) Molding over concentric needles provides discrete layer heterogeneity (red cells, blue cells) within a perfusable conduit. Green fluorescent bead perfusion demonstrates vessel patency (Hasan et al. 2015). (c) Simplified schematic of soft lithography (Kinstlinger and Miller 2016). (d) A simple rectilinear lattice, made perfusable by unifying fluidic ports (Cabodi et al. 2005). (e) Two independent networks combined within a single construct (Golden and Tien 2007). (f) Hierarchical branching and diameter reductions within a fluidic network, made perfusable by unifying fluidic ports (King et al. 2004) (Adapted with permission from Elsevier (a), the Royal Society of Chemistry (c, e), the American Chemical Society (d), and John Wiley and Sons (f))

For construct molding, gelation of alginate polymer solution was induced by simple addition of calcium chloride. Importantly, this ionic crosslinking mechanism is amenable to bulk cellular encapsulation. To achieve bonding between the two gel pieces, surface crosslinks were chelated with sodium citrate, pieces were brought into contact, and crosslinks were reestablished by reintroducing calcium chloride solution.

This process has also been extended to produce channel networks within hydrogels in a 3D fashion. By perfusing warm gelatin through a 2D network – formed via soft lithography – and allowing the gelatin to cool into a hydrogel, Golden and colleagues produced thermoreversible filament networks for subsequent hydrogel encapsulation (Golden and Tien 2007). These gelatin networks were stacked, and collagen was cast around them. After warming the entire system to melt the gelatin structures and subsequently flushing them with PBS, the result was a 3D fluidic network contained within a biocompatible, cell-adhesive matrix (Fig. 2e). The authors went further to demonstrate the formation of composite gel networks, in which the fluidic channels were bound by collagen on top and fibrin on bottom. Despite the 3D nature of these fluidic networks, their clinical relevance is limited due to lack of unifying fluidic ports. For each layer of stacked gelatin networks, a new inlet/outlet pair is introduced to the resultant construct. This would make it difficult to manually access the entire fluidic network, limiting the potential of this technique to be utilized for in vitro studies and clinical implantation.

Soft lithography also provides a means to recapitulate the hierarchical nature of vascular branching that is present in native tissues. Avoiding the need for expensive biological gels, King and coworkers fabricated a hierarchical fluidic network by casting melted poly(DL-lactic-co-glycolide) pellets around poly(dimethyl siloxane) (PDMS) molds, and laminating the top and bottom components of the channel via thermal bonding instead of chemical crosslinking as described earlier (King et al. 2004). They were able to demonstrate fluidic networks with fractal-like branching and channel diameter reductions (Fig. 2f), which is a characteristic of native vascular systems that helps blood to quickly reach the entire body, reduce energy loss through viscous dissipation (Razavi et al. 2014), and provide alternate circulatory paths in the event of clotting.

4 Extrusion of Solid Materials to Define Physical Boundaries of Hollow Vessels

Soft lithography, while able to generate near-capillary sized vessel networks, is largely limited to in vitro studies where the resultant chip-like devices can be restrained by microscope stages or mechanical chambers. There have been few – if any – reports of vascularized devices produced by soft lithography that go on to be implanted in animal studies. Thus, there is need to transition from vascular chips to monolithic vascular tissues. The search for prevascularized tissue engineered constructs has recently taken form in extrusion-based methods, where free-standing scaffolds can be fabricated, physically manipulated, and perfused.

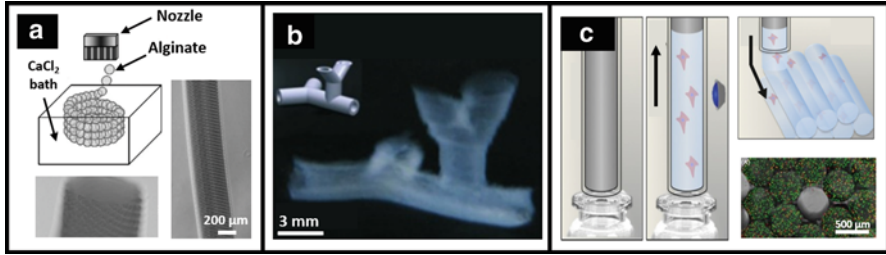


Fig. 3 Extrusion of solid materials to define vascular walls. (a) Hollow conduits fabricated by inkjet printing of alginate into calcium chloride solution (Nakamura et al. 2008). (b) 3D, branching vessels fabricated by alginate inkjet printing (Christensen et al. 2015). (c) Photocrosslinking of cell-laden gelatin filaments. Filaments can be hexagonally stacked to yield a hollow tube (Bertassoni et al. 2014a) (Adapted with permission from the Society for Imaging Science and Technology (a), John Wiley and Sons (b), and the Institute of Physics (c))

The fabrication of monolithic vascular conduits has been repeatedly explored with an extrusion technology known as inkjet printing. These printers use the same extrusion method as their 2D namesake counterparts, where droplets of material are individually released onto a substrate to build a 2D pattern or 3D structure. In 2008, Nakamura and colleagues demonstrated the ability of inkjet printing to construct biocompatible vascular conduits (Nakamura et al. 2008). Droplets of alginate polymer solution were dropped into a bath of aqueous calcium chloride, which induced ionic crosslinking of the droplets into rigid microgel beads with diameters as small as 10 μm . By using microgel beads to plot an annulus pattern, and then superimposing this structure with additional equivalent layers, it was possible to fabricate a hollow tubular construct with 200 μm inner diameter (Fig. 3a). The group went further to show that HeLa cells could be incorporated into the alginate solution prior to gelation, allowing for the fabrication of viable cell-laden tubes (Nishiyama et al. 2009).

A near-identical procedure was outlined by Christensen and associates, but with substantially higher architectural complexity. In this report, inkjet printing of alginate microgels was used to fabricate vascular-like structures with branching in all three dimensions (Fig. 3b), which, as discussed earlier, is a critical component of native vascular systems (Christensen et al. 2015). Furthermore, fibroblasts were incorporated into the alginate solution prior to printing, and 90% viability was observed within the walls of these constructs 24 h after printing.

In an alternative extrusion technique, Jakab and coworkers demonstrated that multicellular aggregates could be used as a bioink for 3D printing (Jakab et al. 2008). To form the aggregates, cells were first centrifuged to a dense pellet and aspirated into a capillary. The compacted cellular filament was then extruded, and a custom device cleaved the material into cylinders of 500 μm height and diameter. A variety of cell types were used to form these bioink aggregates: ovary, smooth muscle, cardiac, and endothelial. Remarkably, it was observed that cellular cylinders could spontaneously round into spherical aggregates, and they were thusly re-aspirated into a capillary for extrusion patterning. Fusion of pellets was observed after printing

in an annular geometry, which allowed for subsequent fabrication of 3D tubes and hollow, branched architectures.

Streamlining this approach in 2014, Bertassoni and coworkers removed the need for point-by-point fabrication by extruding and assembling cell-laden hydrogel filaments into hollow tubes (Bertassoni et al. 2014a). 3T3 fibroblasts were first suspended in a solution of gelatin methacrylate and ultraviolet-absorbing photoinitiator. The mixture was then aspirated into the 500 μm diameter glass capillary of a commercial bioprinter. The entire capillary was irradiated with ultraviolet light, causing free-radical decomposition of the photoinitiator compound, which further reacts by crosslinking gelatin's methacrylate groups to yield a cell-laden hydrogel filament. Mechanical extrusion was used to layer filaments in a hexagonally packed architecture, thus enabling the fabrication of hollow vessels (Fig. 3c).

5 Coaxial Extrusion Improves the Speed and Ease of Vessel Fabrication

While inkjet printing has made great progress towards achieving free-standing vascular mimics, it is difficult to establish fluidic connections with these soft, compliant structures. Unable to be properly manipulated, these constructs are largely incompatible with perfusion culture and *in vivo* integration. Alternatively, researchers have explored coaxial extrusion printing, which directly produces hollow filaments that maintain structural integrity.

This technique has been rigorously described by Zhang and colleagues. First, two syringe tips of different diameters are concentrically fit together to form a single extrusion nozzle with two discrete openings. By simultaneously extruding a jacket of negatively charged alginate solution around an inner solution of calcium chloride, a hollow hydrogel filament is created as divalent calcium ions crosslink the alginate polymer (Zhang et al. 2015). Custom coaxial tips allowed tuning of outer diameter, inner diameter, and wall thickness, achieving patent fluidic channels as small as 700 μm in diameter.

To demonstrate use as a novel bioprinting modality, human smooth muscle cells were incorporated into the alginate solution prior to extrusion and crosslinking. Low post-fabrication viability (33%) was attributed to extrusion shear stress, but the encapsulated cells exhibited substantial proliferation and smooth muscle cell-specific matrix deposition after 6 weeks in static culture. Interestingly, matrix deposition was found most abundantly near the lumen and circumference of the hollow filaments, suggesting higher activity within these regions of greater oxygen and nutrient supply. Although perfusion culture was not explored, it was shown that these conduits could support media perfusion without leakage after connection to a flexible needle was made with the help of surgical clips. With this method, it was possible to achieve arbitrary pattern complexity in 2D, as seen by the branching and zigzag vessels shown in Fig. 4a. It is important to note that the overall construct dimensions presented here would require prohibitively long fabrication times if attempted with inkjet printing.

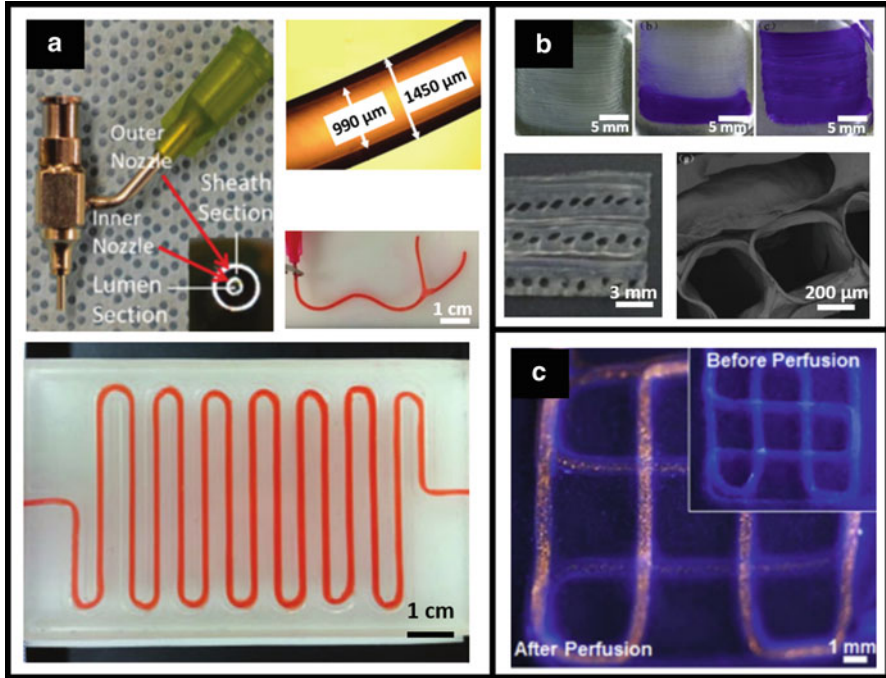


Fig. 4 Coaxial extrusion of hollow vessels. (a) Clockwise from *top left*: photograph of a coaxial extrusion nozzle; micrograph demonstrating the hollow nature of extruded filaments; a branched filament; a large (>1 cm) vessel printed with complex 2D geometry (Zhang et al. 2015). (b) Fusion of hollow filaments into complex structures. *Top panel*: perfusion of a continuous lumen within a 2D sheet. *Bottom panel*: filaments stacked and fused in 3D, but without unifying perfusion ports (Gao et al. 2015). (c) A single hollow filament stacked atop itself in a lattice conformation, which permits continuous 3D perfusion of yellow fluorescent beads (Jia et al. 2016) (Adapted with permission from the Royal Society of Chemistry (a) and Elsevier (b, c))

Using the same coaxial extrusion technique described above, Gao and coworkers explored the capacity for 3D stacking afforded by hollow alginate filaments (Gao et al. 2015). In this report, it was first noted that the inner core of calcium chloride solution was unable to fully crosslink the outer alginate jacket during printing, as rapid gelation prevented complete radial diffusion of the calcium ions. But leveraging this phenomenon provided a means of 2D and 3D filament fusion, as filaments extruded side-by-side could be crosslinked together by immersion in a calcium chloride bath. Single hollow filaments were first fused into 2D sheets of square and spiral geometries, and perfusion of colored dye was used to demonstrate persistence of a continuous $900\ \mu\text{m}$ lumen throughout the sheets (Fig. 4b – top panel). Multiple hollow filaments were then used to build 3D structures in a layer-by-layer process (Fig. 4b – bottom panel); however, perfusion of the entire structure was not possible due to the lack of unifying fluidic ports. In actuality, these 3D structures more closely resemble macroporous scaffolds than vascularized constructs, as the multitude of constituent vessels is not fluidically connected.

In a study by Jia and colleagues, multiple improvements to coaxial extrusion printing were explored (Jia et al. 2016). While previous studies used pure alginate to form hollow hydrogel filaments, here the bioink was formulated as a blend of alginate, gelatin methacrylate, 4-arm poly(ethylene glycol)-tetra-acrylate (PEGTA), and ultraviolet-absorbing photoinitiator. During coaxial extrusion, the rapid ionic crosslinking between alginate and calcium chloride provided temporary structural integrity. The filament networks were then bulk irradiated with ultraviolet light to crosslink the gelatin and PEGTA and immersed in chelating agent to remove the alginate's ionic crosslinks. The incorporation of gelatin provided cell-adhesive peptide domains for cell encapsulation studies, and the presence of PEGTA helped maintain structural integrity after removing alginate. PEGTA forms covalent crosslinks, which were chosen in favor of alginate's ionic crosslinks due to their more permanent nature. While the presence of alginate contributed to enhanced mechanical stability during printing, alginate is bioinert and was thusly chosen to be removed so that cells could more easily spread and proliferate in their artificial matrix (Tamayol et al. 2015)

By utilizing this bioactive hydrogel formulation, it was possible to examine the behavior and function of encapsulated cells beyond simple viability assays. Initially, encapsulated endothelial cells and MSCs were sparsely distributed within the walls of the printed hollow filaments. It was shown that after 21 days in culture these cells were not only able to spread, migrate, and proliferate within this bioactive matrix, but the two cell types had also colocalized. Heterotypic interactions between endothelial cells and MSC support endothelial function (Jeon et al. 2014), and these results thusly demonstrate the potential of the described bioink blend to yield biologically relevant vessels. It was also shown that a single hollow filament could be extruded atop itself in a stacked lattice architecture (Fig. 4c), allowing perfusion of fluorescent beads through a continuous, 3D vessel.

6 Extrusion of Sacrificial Filaments Provides Intricate Control Over Vascular Geometry

At this point, each of the fabrication modalities discussed herein have sought to fabricate vascular networks by focusing on the construction of physical boundaries to define hollow lumen. Recently, an alternative approach known as sacrificial templating has emerged. In this family of techniques, materials are patterned as self-supporting structures that mimic the desired vascular geometry. A bulk material is then cast around this template, and the template is removed to yield a 3D construct with internal fluidic networks (Fig. 5a). By patterning geometries that reflect a vascular network instead of the physical boundaries that define one, researchers have been able to construct vascular networks with intricate curvature and hierarchical branching that are otherwise difficult to produce.

Hydrogels are perhaps the most well-studied sacrificial materials, as their chemistries can be tuned to contain reversible, noncovalent crosslinks that facilitate liquefaction and elution. Bertassoni and colleagues have demonstrated sacrificial templating of agarose (Bertassoni et al. 2014b), which gels via reversible

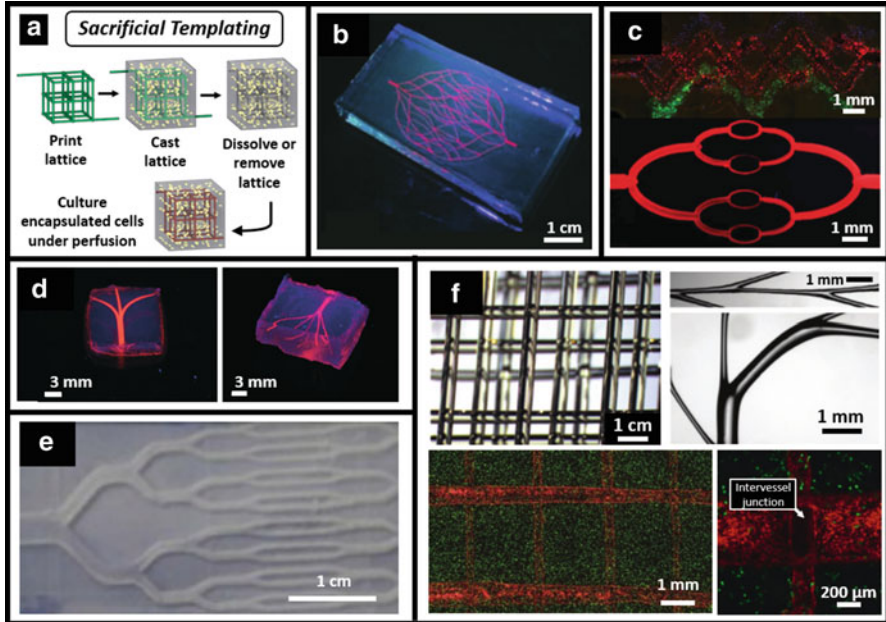


Fig. 5 Sacrificial templating permits fabrication of vascular networks with highly tunable architectures. (a) Schematized process of sacrificial templating (Miller et al. 2012). (b) Sacrificial templating of Pluronic (Wu et al. 2011). (c) Another example of sacrificial templating of Pluronic (Kolesky et al. 2014). (d) Sacrificial templating of agarose (Bertassoni et al. 2014b) and (e) poly (vinyl) alcohol (Jeffries et al. 2014). (f) Clockwise from *top left*: a 3D lattice template made from carbohydrate glass; branching and curvature within a template lattice; endothelial cell (red) monolayer formation within a fibroblast-laden gel (green) after template removal; a patent, 3D inter vessel junction (Miller et al. 2012) (Adapted with permission from John Wiley and Sons (b, c, e) and the Royal Society of Chemistry (d))

temperature-dependent chain entanglement (Horinaka et al. 2014). In this study, a piston was first used to aspirate molten agarose into a capillary, where the temperature was cooled below 32 °C to permit gelation. The rigid filaments were then extruded into branching and 3D lattice architectures, with individual diameters as small as 250 μm. Hydrogels of various chemical nature were cast around these templates, and the template filaments were then removed via manual pulling or light vacuum. This report highlights the chemical versatility of sacrificial templating, as four unique photocrosslinkable polymers – of synthetic and natural origin – were shown to support template casting. With the help of discrete fluidic ports, network perfusion with red fluorescent microbeads was clearly demonstrated (Fig. 5d). Furthermore, it was shown that the presence of microchannels enhanced not only the viability of bulk-encapsulated 3T3 fibroblasts but also osteogenic differentiation.

Pluronic® polymer has also been studied as a sacrificial template for the fabrication of vascularized tissues. Pluronic is a water-soluble polymer that undergoes a thermally reversible gelation process when dissolved in preparations above its

critical micelle concentration (Bohorquez et al. 1999). Transition temperatures range between 4 °C and 10 °C and are a function of polymer concentration. At temperatures slightly above this transition point, Pluronic behaves as a hydrogel with shear-thinning behavior. This unique property enables it to not only be extruded via pressure-driven mechanisms but to also retain structural rigidity after extrusion from a printer nozzle. These printed network patterns can be subsequently casted in an acellular or cell-laden hydrogel. By lowering the temperature below Pluronic's transition point, the printed filaments can be flushed with water or cell culture media leaving behind a perfusable fluidic network. Hence, sacrificial filaments are often referred to as fugitive ink.

In a fabrication scheme realized by Wu and colleagues, fugitive Pluronic ink is extruded directly into a reservoir of photosensitive matrix, providing a physical support for the printed filament network (Wu et al. 2011). As the extrusion nozzle physically translates through the reservoir matrix, it tears a path which is filled in by a photosensitive filler liquid residing atop the support matrix. When the desired geometry is fully printed, the entire system is exposed to ultraviolet light. This crosslinks the support and filler materials together, fully encasing the Pluronic ink. Lowering the system temperature below Pluronic's transition point facilitates liquefaction and flushing of the printed template, yielding 2D vascular networks. Near-capillary sized channels of 18 μm diameter were able to be fabricated, and a network of highly intricate curves and branches was successfully perfused through unifying fluidic ports (Fig. 5b).

This method of sacrificial Pluronic templating was further expanded by the same group to generate 3D fluidic networks within a monolithic cell-laden hydrogel (Kolesky et al. 2014). In a layer-by-layer process, fugitive Pluronic ink was templated concurrently with fibroblast-laden gelatin filaments (Fig. 5c). The entire system was cast with acellular GelMA hydrogel, and the Pluronic template was flushed by lowering the ambient temperature to yield microchannels with diameters down to 150 μm . This printing method was shown to be compatible with immortalized 10T1/2 fibroblasts and primary human neonatal dermal fibroblasts, as demonstrated by post-fabrication viability and proliferation. By simultaneously patterning cells and vasculature within a bulk acellular environment, it was possible to maintain cellular proximity to nutrient supply conduits within a large, monolithic tissue construct. It is important to note that this method enabled fabrication of 3D vascular networks with unifying fluidic ports, facilitating easy template removal and network perfusion.

In a subsequent report by this group, sacrificial templating of Pluronic was used to study longitudinal perfusion culture of a thick ($>1\text{ cm}^3$), vascularized tissue construct (Kolesky et al. 2016). Here, lattice networks of MSC-laden gelatin and acellular Pluronic were first printed in an interpenetrating fashion. The system was cast with fibroblast-laden gelatin, the fugitive template was flushed, and endothelial cells were seeded within the resulting fluidic network. This process enabled successful integration of parenchyma, stroma, and endothelium, which represents a near-complete anatomical unit cell (excluding nerves and lymphatics). Not only did encapsulated cells maintain viability over 6 weeks in perfusion culture, but osteogenic differentiation of the parenchyma was observed after 30 days when supplemented with bone morphogenetic protein 2. It was found that osteogenic expression was inversely

proportional to nearest vessel distance, indicating that perfusion culture provided this thick tissue with enhanced oxygen and nutrient supplies.

Beyond hydrogels, extrusion of carbohydrate glass has also been used to pattern sacrificial templates for tissue vascularization. Using sucrose, glucose, and dextran, Miller and colleagues were able to find an optimal stoichiometric ratio that simultaneously supported aqueous melt extrusion and rapid vitrification (Miller et al. 2012). The resulting filaments were sufficiently rigid to support overhanging features when patterned in a 3D lattice, permitting the fabrication of curves and branches of continuously tunable diameters between 150 and 750 μm (Fig. 5f). To tune filament diameters during printing, nozzle translation speed was modulated. Aside from providing architectural tunability, the templates were also shown to support hydrogel casting through a wide variety of gelation mechanisms: agarose – chain entanglement; alginate – ionic interactions; PEGDA – photopolymerization; fibrin – enzyme activity; Matrigel – protein precipitation.

The sacrificial template geometry was designed to provide unifying fluidic access ports, enabling various perfusion studies after template dissolution in aqueous medium. Importantly, the templated networks supported pulsatile human blood flow, with each microchannel and 3D intervessel junction receiving a visible fraction of the perfusate. It is critical to note that an arbitrarily designed network geometry may produce redundant branches with no pressure drop across their length, resulting in low flow rates or none at all. Remarkably, endothelial cells seeded within the lumens of casted fibrin gels were observed to adhere, form confluent monolayers, and undergo angiogenic sprouting into the bulk after 9 days in perfusion culture. Furthermore, encapsulated fibroblasts were found to exhibit a characteristic radius of viability around each channel, which demonstrates the need for angiogenic sprouting and multiscale anastomosis in tissues of clinically relevant dimensions.

As noted previously, one advantage of sacrificial templating is that it supports casting of a wide variety of materials. In a study by Jeffries and associates, melt extruded poly(vinyl alcohol) (PVA) (Jeffries et al. 2014) templates were used as a vascular mold for electrospun polydioxanone (PDO). PVA is extremely water soluble, which enabled quick dissolution from the PDO cast to yield a hollow fluidic network (Fig. 5e). Due to the fibrous nature of electrospun scaffolds, suturing of vascular constructs was explored. Suture strength was measured by inserting a suture and pulling both ends of the thread away from the construct until rupture. Strengths comparable to commonly sutured polycaprolactone were observed, and anastomosis between channels was demonstrated by directly suturing two PDO conduits. This strategy offers potential for *in vivo* integration of artificial fluidic networks, but the electrospinning process does not currently allow for cellular seeding within the bulk.

7 Stereolithography as a Single-Step Fabrication Platform for 3D Vessel Networks

Empowered by replica molding, direct extrusion, and sacrificial templating, tissue engineers have fabricated perfusable constructs of intricate geometry that support endothelial cell seeding and bulk cell encapsulation. But these fabrication schemes

are time-consuming and often require several intermediate processing steps, limiting their throughput to single construct experiments. Stereolithography (SLA) is a 3D printing technology that promises to dramatically increase the production rates of vascularized tissues, while also maintaining high spatial resolution and a relatively unrestricted design space.

Like extrusion-based methods, SLA builds 3D structures in a layer-by-layer process. However, instead of directly extruding material onto a build platform, SLA uses emitted light patterns to selectively crosslink photosensitive polymer solutions into hydrogel structures of user-defined geometries. The patterned light layers can either be rasterized by a laser spot using mirror galvanometers, or generated using a digital micromirror device (DMD) in a process known as projection stereolithography. DMDs use an array of microscopic mirrors – each able to toggle between an on or off state – to reflect user-defined patterns towards a substrate (Fig. 6a). DMDs are often referred to as dynamic photomasks, because they achieve the same light-patterning function as physical photomasks but can dynamically change their spatial configurations.

In one early demonstration of SLA, Arcaute and coworkers used an ultraviolet laser to photocrosslink PEG-based polymer solutions into 3D hydrogel conduits (Arcaute et al. 2006). Structures with multiple parallel lumens were fabricated, as were constructs of clinically relevant dimensions ($1 \times 1 \times 5$ cm) containing a single inlet that bifurcates twice in different planes to generate four unique outlets (Fig. 6d). Despite this unique ability to achieve truly unrestricted 3D geometry, channel diameters were limited to 500 μm . This limitation is largely governed by the laser

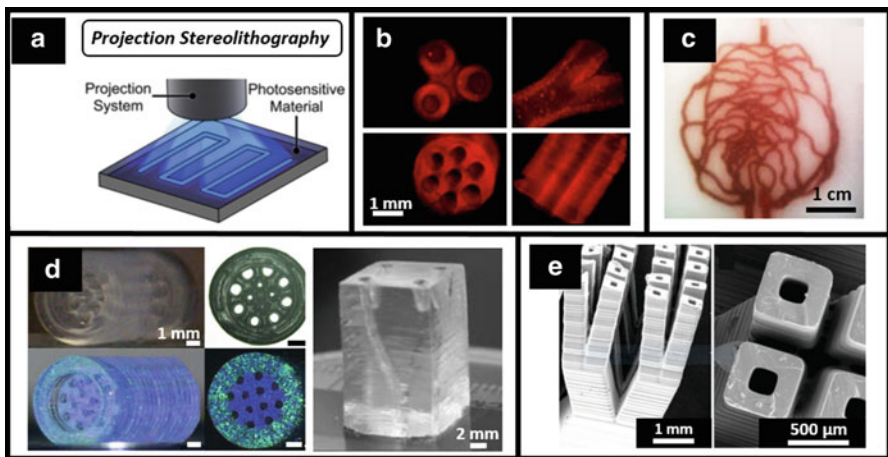


Fig. 6 Single-step fabrication of intricate fluidic networks using SLA. (a) Schematic of projection SLA (Miller and Burdick 2016). (b) Two different vessel architectures printed using projection SLA (Suri et al. 2011). (c) Perfusion of hemoglobin through a laser SLA-printed replica of human retinal vasculature (Ghassemi et al. 2015). (d) Multilumen conduits and a branched 3D network printed with laser SLA (Arcaute et al. 2006). (e) Hierarchical branching of 224 μm diameter channels, fabricated by a commercially available projection SLA printer (Schüller-Ravoo et al. 2014) (Adapted with permission from SPIE (c) and John Wiley and Sons (e))

spot size, which was 250 μm in this particular study. Perfusion through the resultant fluidic networks was not performed; however, it was clear from visual inspection that the channels remained patent. Human dermal fibroblasts were then incorporated into the initial polymer solution to investigate cytotoxic effects of the SLA process. The cells were found to maintain >87% viability 24 h after fabrication, indicating that their SLA process could provide vascular networks within cell-laden tissue constructs.

Similar vascular geometries were fabricated by Suri and colleagues, choosing to use projection SLA in lieu of the laser-based method (Suri et al. 2011). Here, acrylated hyaluronic acid was used as the photosensitive polymer. By incorporating a free radical quenching agent into the initial polymer solution, it was possible to reduce off-target crosslinking and fabricate single-layer channels (i.e., wells) with diameters as small as 150 μm . However, the observed resolution improvement did not translate during multilayer 3D printing, where the minimum printable diameter of multilumen and branched geometries was 500 μm (Fig. 6b).

In the past decade, the SLA process has been formalized into commercial 3D printers for hobbyists, industry, and research. In work by Ghassemi and colleagues, a commercial laser SLA printer was used to build fluidic network geometries derived from optical micrographs of human retinal vasculature (Ghassemi et al. 2015). Hemoglobin solutions were perfused through the networks, and every branch successfully filled (Fig. 6c). These results suggest a possible solution to an open question in vascular tissue engineering: what is the ideal vascular architecture? In its simplest form, an ideal vascular network is one in which each branch receives enough convective mass transport to support proximal cell metabolism. Native vascular systems are capable of pruning redundant, nonflowing branches (Lenard et al. 2015), and thus future designs of artificial fluidic networks may benefit from mimicking geometries derived from *in vivo* imaging. Although the authors eliminated branches with diameters less than 450 μm from the final 3D design – due to resolution constraints – complete perfusion was still observed. Unfortunately, the commercial SLA printer required use of a proprietary, nonbiocompatible polymer, so it would not be feasible to encapsulate cells within the bulk of these constructs to study perfusion culture.

In other studies, commercial SLA printers have been used to fabricate vascularized structures within biocompatible materials. Using a novel polycarbonate derivative with an industrial, projection SLA printer, Schüller-Ravoo and colleagues demonstrated production of channels with internal diameters of 224 μm (Schüller-Ravoo et al. 2014). These microchannels were hierarchically designed to reflect an idealized capillary network, where a single outlet undergoes sequential branching generations to obtain a large number of daughter vessels (Fig. 6e). These vessels anastomose into one outlet, yielding a high-density, perfusable network of microvessels that was shown to support systolic-mimicking fluid pressure of 120 mmHg. Endothelial cells could adhere to and proliferate on the printed material; however, viable cell encapsulation would need to be demonstrated in future work in order to indicate utility as a vascular tissue scaffold.

8 Advanced Fabrication Technologies

Between replica molding, extrusion, and light-based printing technologies, tissue engineers have a wide variety of platforms to choose from when building vascularized constructs. But researchers are still searching for new ways to improve these methods and devise new technologies, *as there is currently no unifying platform that can fabricate vessels with unrestricted 3D geometric control and with lumen dimensions that mirror the multiscale nature of native vasculature.*

In work by Meyer and colleagues, a variation of SLA known as multiphoton polymerization was used to generate branching vessels of near-capillary-sized diameter (Fig. 7a; Meyer et al. 2012). Multiphoton polymerization produces 3D structures by crosslinking photosensitive polymer solutions with a laser, much like laser SLA. But in this technique, the exciting photons have approximately twice the wavelength of the photoinitiator's maximum absorption peak. The nature of this absorption phenomenon confines the free-radical crosslinking reaction to a small 3D volume at the focal plane of the laser beam (Oheim et al. 2006), yielding comparatively higher resolution than traditional SLA. Remarkably, 18 μm lumen diameters and 5 μm wall thicknesses were achieved in this report. But multiphoton polymerization is hindered by comparatively slow fabrication speeds, limiting its dimensional scalability.

With respect to the goal of unrestricted geometric complexity, researchers have turned to some very nontraditional methods to build structures that curve and branch in multiple planes. In one report, Bhattacharjee and colleagues used a novel extrusion method to fabricate multiscale vessel networks with hierarchical branching in numerous planes (Bhattacharjee et al. 2015). To support these branching, overhanging features in 3D space, crosslinkable polymers were directly extruded into a slurry of 7 μm hydrogel particles. This support material fluidizes from a solid state at a threshold shear stress, providing physical support to the extruded material while concurrently allowing the extrusion nozzle to travel to various 3D coordinates. After crosslinking the printed material into a monolithic construct, the structure could be retrieved by water immersion, which disperses the granular slurry. This technique can be used to print PDMS and collagen, which crosslink through chemical reactions, and polymers like PVA, which can be modified to be photosensitive. Impressively small lumen diameters of about 200 μm were printed; however, it can be seen from Fig. 7b that branching junctions are not fluidically sealed and would certainly leak under perfusion.

Choosing a different supporting slurry of 50 μm gelatin particles, Hinton and colleagues fabricated similar branching structures (Fig. 7c – left) and achieved perfusion without leakage (Fig. 7c – right) (Hinton et al. 2015). The supporting gelatin medium was removed by simply raising the ambient temperature above gelatin's melting temperature, yielding overhanging vessel walls that supported convective flow. Despite the merit of nonleaking geometry, vessel diameters were on the order of millimeters; refining the technique to yield higher spatial resolution would be needed to improve its utility in the field.

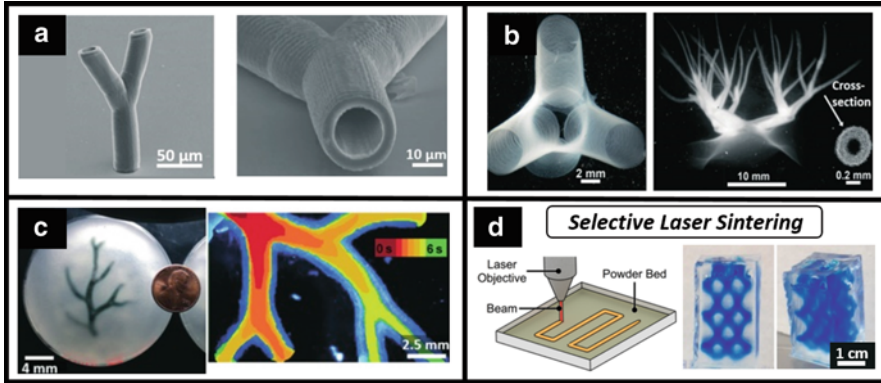


Fig. 7 Advanced technologies to support unrestricted geometric control in 3D space. (a) Multi-photon polymerization of a branched, capillary-scale vessel (Meyer et al. 2012). (b) Hierarchical branching of hollow vessels by extrusion of solid material into granular slurry (Bhattacharjee et al. 2015). (c) *Left*: a branched fluidic network formed by reversible embedding in granular support. *Right*: successful perfusion of the resulting vessels (Hinton et al. 2015). (d) *Left*: schematized printing process of SLS (Miller and Burdick 2016). *Right*: a branching 3D network fabricated by SLS, made perfusable by unifying fluidic ports (Kinstlinger and Miller 2016) (Adapted with permission from MDPI (a), American Association for the Advancement of Science (b, c), and Public Library of Science (d))

An alternative support-based printing method known as selective laser sintering (SLS) can also be used to fabricate branching vessel networks with unrestricted 3D geometry. In SLS, 3D parts are built in a layer-by-layer fashion as a focused laser beam traces 2D patterns into a thin layer of powder (Fig. 7d – left). The powder absorbs the electromagnetic radiation, melts, and fuses into a solid, connected structure. The key advantage of SLS is its ability to build overhanging 3D features that would otherwise collapse if printed in air using traditional extrusion methods. Overhanging features can be sintered atop the unfused powder of previous layers, which acts as a support material much like the microparticle slurries discussed above.

In a study by Kinstlinger and associates, polycaprolactone powder was sintered into a 3D lattice that served as a water-soluble, sacrificial template for hydrogel casting (Kinstlinger et al. 2016). The resulting hydrogel constructs contained fluidic network with overhanging bifurcations in 3D space, and perfusion of blue dye was made possible by a unifying inlet and outlet (Fig. 7d – right). Although not explicitly outlined in this report, this technique would likely be compatible with cell encapsulation for tissue engineering: cells could simply be incorporated into the hydrogel prepolymer solution prior to crosslinking around the SLS-printed template. Furthermore, the ability to fabricate multiple templates at once – each of arbitrary dimensions – enables SLS to function in a high-throughput, geometrically scalable fashion.

9 Multiscale Vasculature Produced by Endothelial Matrix Invasion

The techniques discussed so far have clearly demonstrated achievement of cell-laden tissue constructs that contain intricate, 3D vascular geometries. But the lumens of native capillaries range between 5 and 10 μm in diameter and building fluidic networks of this scale still remains elusive. Instead of further refining 3D printing technologies to achieve capillary-sized vessels, researchers are increasingly relying on the innate developmental abilities of endothelial cells to achieve this task.

In work by Zheng and colleagues, tubular endothelial monolayers were shown to produce angiogenic sprouts into a surrounding collagen matrix in the presence of perfused vascular endothelial growth factor (VEGF) (Zheng et al. 2012). While the diameters of these sprouts were not directly characterized, it was clear from visual inspection that they were smaller than 50 μm . This ability to induce angiogenic sprouting from microfabricated channels may serve as a multiscale link between capillary- and arteriole-sized vessels. However, perfusion of angiogenic factors concurrently led to disorganization of intercellular junctions and diminished barrier function as observed by perfusion of high-molecular weight fluorescent molecules. Interestingly, encapsulation of human brain vascular pericytes, which are known to synthesize VEGF (Dore-Duffy et al. 2006), within the collagen bulk enabled simultaneous maintenance of barrier function and angiogenic sprouting (Fig. 8a) without the presence of exogenous growth factors.

Nugyen and coworkers further explored the use of chemokine gradients and found that robust angiogenic sprouting of ~ 50 μm diameter vessels could support anastomosis between two prefabricated channels (Nguyen et al. 2013). In this study, needle molding of collagen was used to initially form two parallel channels of 400 μm diameter (Fig. 8d – left). One channel was seeded with endothelial cells to achieve a confluent monolayer, while the other channel remained acellular and supported axial perfusion of an angiogenic cocktail that included VEGF. By diffusing across the collagen matrix, the resulting chemotactic gradient induced directional angiogenesis towards the perfusion channel in the form of fully lumenized, multicellular sprouts that exhibited clear apical-basal polarity. Remarkably, the growing sprouts breached the chemokine source channel after 1 week, forming continuous, near-capillary-sized lumens between the two prefabricated channels. 3 μm red fluorescent beads were perfused through the parent channel to visualize flow path, and the beads were indeed able to travel to the factor source channel with no interstitial leakage (Fig. 8d – right).

In addition to exogenous growth factors and pericyte interactions, the effects of fluidic stress on angiogenic sprouting have also been explored. In native vascular systems, circulation exerts shear stress on the endothelium via two mechanisms: luminal flow, which shears the cells across their flat, apical surfaces, and transmural flow, which shears the membrane at intercellular junctions as fluid exists the vessel wall into the interstitium. By seeding endothelial monolayers within needle-molded

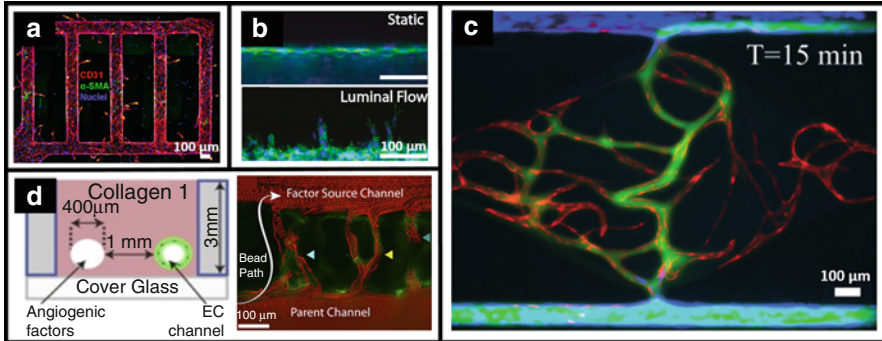


Fig. 8 In vitro models demonstrate the utility of angiogenesis and vasculogenesis in the production of multiscale vasculature. (a) Angiogenic sprouting into a bulk collagen gel, induced by pericyte co-culture. Staining for CD31 – a prominent endothelial marker – provides visualization of sprouts within the otherwise dark collagen bulk (Zheng et al. 2012). (b) Angiogenic sprouting induced by the shear stress associated with luminal perfusion (Galie et al. 2014). (c) Multiscale anastomosis between two patterned microvessels (blue) and a capillary network formed through vasculogenesis of encapsulated endothelial cells (red). Minimal leakage is confirmed by perfusion of 70 kDa fluorophore (green) (Wang et al. 2015). (d) Multiscale anastomosis between an endothelial cell-seeded vessel and a channel perfused with chemotactic factors. Absence of leakage confirmed by red fluorescent bead perfusion (Nguyen et al. 2013) (Adapted with permission from the National Academy of Sciences (a, b, d) and the Royal Society of Chemistry (c))

collagen channels, Galie and colleagues clearly demonstrated that a threshold shear stress exists, above which cells will sprout regardless of whether the shear is presented by luminal flow (Fig. 8b) or transmural flow (Galie et al. 2014). Thus, integration of chemotaxis and mechanotransduction may prove useful in future efforts to fabricate multiscale vasculature within tissue engineered constructs.

As opposed to angiogenesis, vasculogenesis has also been leveraged to establish multiscale vessel networks. Whereas angiogenesis is the process by which new vessels sprout from preexisting ones, vasculogenesis occurs as lumenized tubules (i.e., capillaries) develop de novo from individual endothelial cells (Risau 1997). In work by Wang and coworkers, this process of vasculogenesis was realized by exposing an endothelial cell-laden fibrin gel to chemotactic gradients from two flanking microchannels (Wang et al. 2015). The containing device was made from dense, hydrophobic silicone so diffusive transport of the chemokines from the patterned microchannels into the gel region was made possible by two 50 μm pores. Developing tubules were observable by day 3, at which point the prepatterned microchannels were seeded with endothelial cells to investigate the system's potential for anastomosis through the tunnel. A mature capillary network had formed within the gel region by day 12, and minimal leakage of perfused 70 kDa fluorophore confirmed anastomosis between the lumenized capillaries and patterned microchannels (Fig. 8c).

Using angiogenic and vasculogenic platforms, researchers have established multiscale vascular networks that may support the mass transport needs of artificial tissues. However, these demonstrations of multiscale anastomosis were performed in lab-on-a-chip platforms, which have limited potential for in vivo integration.

10 Progress Towards Integration In Vivo

By fabricating vascular networks within engineered tissues, we ultimately hope to provide cells with vessels for exchange of oxygen, nutrients, and waste after implantation. This requires not only the presence of internal fluidic networks but also a mechanism by which these vessels can integrate with the host circulatory system. So far, host integration has been demonstrated by two primary mechanisms: spontaneous, cell-driven anastomosis, and surgical anastomosis.

Cell-driven anastomosis between implanted vascular networks and the host circulatory system has been demonstrated by Kim and colleagues (2016). In this study, endothelial cells were first encapsulated within a dual-layered hydrogel of chitosan-lactide copolymer. The cell-containing layer was chemically crosslinked using an inorganic reagent, yielding a relatively soft gel that provided a suitable environment for vasculogenesis and construct remodeling. To provide physical support during surgical implantation, the cell-laden hydrogel was laminated to a chemically identical, acellular hydrogel that was instead crosslinked using ultraviolet light to provide a relatively stiff environment. The engineered tissue constructs were cultured for 5 days prior to implantation, giving time for tubule networks to develop through vasculogenesis.

To assess potential for anastomosis in mice, the vascularized gels were physically placed between termini of ligated and transected femoral arteries without direct suturing. Laser Doppler imaging was then used to observe hind limb circulation over time. It was found that circulation rates were significantly higher in animals that received gel implants with microvascular networks (Fig. 9a), thus indicating that the implanted vessels had spontaneously anastomosed with femoral collateral vessels to reestablish hind limb circulation. However, these fluidic networks had no discrete inlets and outlets, and so it is possible that circulating blood was also concurrently leaking into the body cavities.

As we and others have previously demonstrated, fluidically tight connections between artificial and host vascular systems can be achieved by surgical methods as opposed to spontaneous, cell-driven events. In this report, an artificial vascular network was first fabricated by casting PDMS around a sacrificial template of carbohydrate glass (Sooppan et al. 2016). The sacrificial template was designed to have unifying fluidic ports, providing the resultant PDMS construct with discrete connections for surgical anastomosis. This procedure was relatively simple: rat femoral arteries were ligated, transected, and manually inserted – without suturing – into the inlet and outlet ports of the artificial vascular network. After unclamping the femoral artery to introduce circulatory perfusion (Fig. 9b), laser Doppler imaging confirmed network patency and pulsatile flow. It is also important to note that no signs of leakage were observed. The dimensional tolerance between the PDMS channel and femoral artery was apparently small enough to ensure tight fluidic connection, which is a critical finding because many hydrogels used by researchers today would fracture under the stress of suture threading.

While Sooppan and colleagues used acellular PDMS constructs to study circulatory perfusion over 3 h, a different group has used cell-laden, biodegradable gels to study

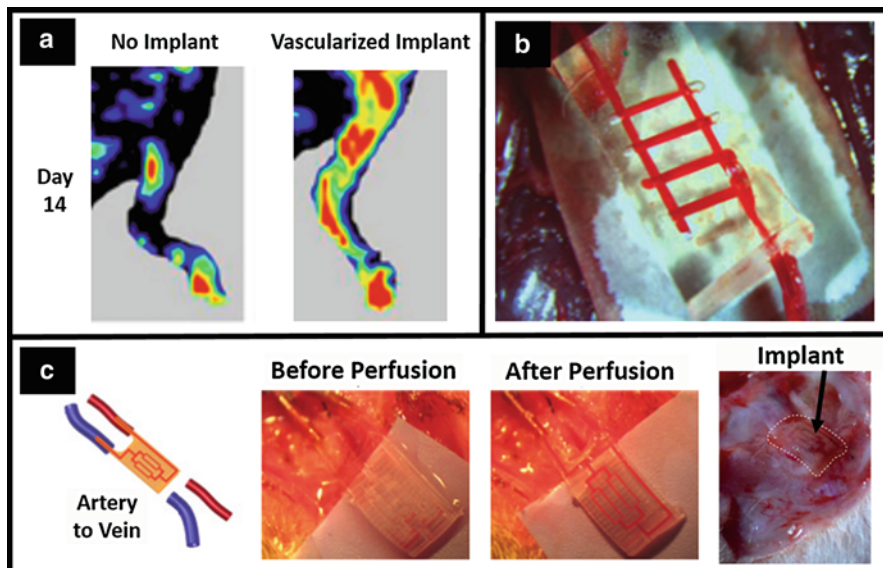


Fig. 9 Spontaneous and surgical anastomosis between artificial fluidic networks and host vasculature. (a) Spontaneous anastomosis between implanted endothelial tubule networks and femoral collateral vessels supported mouse hind limb recirculation (as seen here by laser Doppler imaging) after femoral artery transection (Kim et al. 2016). (b) After severing a rat femoral artery, circulation was reestablished through a fluidic network formed from sacrificial templating of carbohydrate glass (Sooppan et al. 2016). (c) A rat model arteriovenous shunt was established using a fluidic network fabricated via sequential layering of molds, each fabricated in a single soft lithography process (Zhang et al. 2016). Note the immediately successful perfusion and the lack of visible inflammation after 1 week in vivo. Due to the nature of in vivo imaging, scale bars were difficult to obtain (Adapted with permission from the American Chemical Society (a))

the biological behavior of exogenous tissues after surgical anastomosis. In a report by Zhang and coworkers, vascular networks were first fabricated within a rigid scaffold of citric acid-based polymer (Zhang et al. 2016). Cardiomyocytes were then suspended in fibrin or Matrigel prepolymer solution and encapsulated around the fluidic network so that the parenchymal response to in vivo integration could be assessed. The geometry of the bulk construct was cleverly designed to have protruding inlet and outlet regions to facilitate direct cannulation within the femoral artery and vein, respectively (Fig. 9c – left). Fluidic connections were secured with cyanoacrylate tissue glue, in contrast to the manual press fit technique described earlier.

Circulatory perfusion through the vascular construct (Fig. 9c – middle) persisted for 1 week without visible signs of leakage, and with 85% of lumen remaining clot-free. This finding is consistent with previous literature, which suggest that some citric acid-based polymers exhibit antithrombotic properties (Kibbe et al. 2010). In vascular networks preseeded with endothelial cells, angiogenic sprouting into the hydrogel bulk was also observed after 1 week of circulatory perfusion. Furthermore, not only were encapsulated cardiomyocytes able to maintain their physiologic

phenotype – as evidenced by troponin T expression – but they could survive without eliciting visible signs of inflammation (Fig. 9c – right).

11 Conclusions

Presently, researchers seeking to endow their artificial tissues with vascular networks have a wide variety of fabrication platforms to choose from. These methods are well-suited to provide simple *in vitro* platforms and *in vivo* grafts, but there currently exists no unifying technology that can fabricate perfusable networks with unrestricted geometric control that contain vessels spanning from capillary- to artery-sized diameters. Looking forward, it may be possible to merge several methods to achieve this goal. One could imagine angiogenic sprouting between laser-sintered vessels in hydrogel, simultaneously yielding vasculature of intricate, scalable geometries, that is multiscale in nature. But as vascularized tissue constructs evolve, it is important to reconsider the primary goal of vascular tissue engineering: enhanced mass transport within 3D volumes. We can borrow vessel designs from clinical imaging data, but perhaps there exists some ideal network geometry – unrealized by nature – that could provide nutrient and waste exchange at supra-physiological rates. Bioinspired approaches have certainly led to enormous medical achievements in recent years, but we must also aim to transcend what is possible within the confines of human biology.

References

- Arcaute K, Mann BK, Wicker RB (2006) Stereolithography of three-dimensional bioactive poly (ethylene glycol) constructs with encapsulated cells. *Ann Biomed Eng* 34:1429–1441. <https://doi.org/10.1007/s10439-006-9156-y>
- Atala A, Bauer SB, Soker S, Yoo JJ, Retik AB (2006) Tissue-engineered autologous bladders for patients needing cystoplasty. *Lancet* 367:1241–1246. [https://doi.org/10.1016/S0140-6736\(06\)68438-9](https://doi.org/10.1016/S0140-6736(06)68438-9)
- Bertassoni L, Cardoso JC, Manoharan V, Cristino AL, Bhise NS, Araujo WA, Zorlutuna P, Vrana NE, Ghaemmaghami AM, Dokmeci MR, Khademhosseini A (2014a) Direct-write bioprinting of cell-laden methacrylated gelatin hydrogels. *Biofabrication* 6:24105. <https://doi.org/10.1088/1758-5082/6/2/024105>
- Bertassoni L, Cecconi M, Manoharan V, Nikkha M, Hjortnaes J, Cristino AL, Barabaschi G, Demarchi D, Dokmeci MR, Yang Y, Khademhosseini A (2014b) Hydrogel bioprinted micro-channel networks for vascularization of tissue engineering constructs. *Lab Chip* 14:2202–2211. <https://doi.org/10.1039/c4lc00030g>
- Bhattacharjee T, Zehnder SM, Rowe KG, Jain S, Nixon RM, Sawyer WG, Angelini TE (2015) Writing in the granular gel medium. *Sci Adv* 1:e1500655. <https://doi.org/10.1126/sciadv.1500655>
- Bohorquez M, Koch C, Trygstad T, Pandit N (1999) A study of the temperature-dependent micellization of Pluronic F127. *J Colloid Interface Sci* 216:34–40. <https://doi.org/10.1006/jcis.1999.6273>
- Bryant SJ, Cuy JL, Hauch KD, Ratner BD (2007) Photo-patterning of porous hydrogels for tissue engineering. *Biomaterials* 28:2978–2986. <https://doi.org/10.1016/j.biomaterials.2006.11.033>

- Cabodi M, Choi NW, Gleghorn JP, Lee CSD, Bonassar LJ, Stroock AD (2005) A microfluidic biomaterial. *J Am Chem Soc* 127:13788–13789. <https://doi.org/10.1021/ja054820t>
- Christensen K, Xu C, Chai W, Zhang Z, Fu J, Huang Y (2015) Freeform inkjet printing of cellular structures with bifurcations. *Biotechnol Bioeng* 112:1047–1055. <https://doi.org/10.1002/bit.25501>
- Chrobak KM, Potter DR, Tien J (2006) Formation of perfused, functional microvascular tubes in vitro. *Microvasc Res* 71:185–196. <https://doi.org/10.1016/j.mvr.2006.02.005>
- Costantini M, Colosi C, Mozetic P, Jaroszewicz J, Tosato A, Rainer A, Trombetta M, Wojciech Ś, Dentini M, Barbetta A (2016) Correlation between porous texture and cell seeding efficiency of gas foaming and microfluidic foaming scaffolds. *Mater Sci Eng C* 62:668–677. <https://doi.org/10.1016/j.msec.2016.02.010>
- Dore-Duffy P, Katychew A, Wang X, Van Buren E (2006) CNS microvascular pericytes exhibit multipotential stem cell activity. *J Cereb Blood Flow Metab* 26:613–624. <https://doi.org/10.1038/sj.jcbfm.9600272>
- Galie PA, Nguyen D-HT, Choi CK, Cohen DM, Janmey PA, Chen CS (2014) Fluid shear stress threshold regulates angiogenic sprouting. *Proc Natl Acad Sci U S A* 111:7968–7973. <https://doi.org/10.1073/pnas.1310842111>
- Gao Q, He Y, Fu J, Liu A, Ma L (2015) Coaxial nozzle-assisted 3D bioprinting with built-in microchannels for nutrients delivery. *Biomaterials* 61:203–215. <https://doi.org/10.1016/j.biomaterials.2015.05.031>
- Ghassemi P, Wang J, Melchiorri AJ, Ramella-Roman JC, Mathews SA, Coburn JC, Sorg BS, Chen Y, Pfefer TJ (2015) Rapid prototyping of biomimetic vascular phantoms for hyperspectral reflectance imaging. *J Biomed Opt* 20:121312. <https://doi.org/10.1117/1.JBO.20.12.121312>
- Golden AP, Tien J (2007) Fabrication of microfluidic hydrogels using molded gelatin as a sacrificial element. *Lab Chip* 7:720–725. <https://doi.org/10.1039/b618409j>
- Hasan A, Paul A, Memic A, Khademhosseini A (2015) A multilayered microfluidic blood vessel-like structure. *Biomed Microdevices* 17:9993. <https://doi.org/10.1007/s10544-015-9993-2>
- Haynesworth SE, Goshima J, Goldberg VM, Caplan AI (1992) Characterization of cells with osteogenic potential from human marrow. *Bone* 13:81–88. [https://doi.org/10.1016/8756-3282\(92\)90364-3](https://doi.org/10.1016/8756-3282(92)90364-3)
- Heimbach D, Luterman A, Burke J, Cram A, Herndon D, Hunt J, Jordan M, McManus W, Solem L, Warden G (1988) Artificial dermis for major burns. A multi-center randomized clinical trial. *Ann Surg* 208:313–320. <https://doi.org/10.1097/0000658-198809000-00008>
- Hinton TJ, Jallerat Q, Palchesko RN, Park JH, Grodzicki MS, Shue H, Ramadan MH, Hudson AR, Feinberg AW (2015) Three-dimensional printing of complex biological structures by freeform reversible embedding of suspended hydrogels. *Sci Adv* 1:1–10. <https://doi.org/10.1126/sciadv.1500758>
- Horinaka J, Urabayashi Y, Wang X, Takigawa T (2014) Molecular weight between entanglements for κ - and λ -carrageenans in an ionic liquid. *Int J Biol Macromol* 69:416–419. <https://doi.org/10.1016/j.ijbiomac.2014.05.076>
- Jaiswal N, Haynesworth SE, Caplan AI, Bruder SP (1997) Osteogenic differentiation of purified, culture-expanded human mesenchymal stem cells in vitro. *J Cell Biochem* 64:295–312. [https://doi.org/10.1002/\(sici\)1097-4644\(199702\)64:2<295::aid-jcb12>3.0.co;2-i](https://doi.org/10.1002/(sici)1097-4644(199702)64:2<295::aid-jcb12>3.0.co;2-i)
- Jakab K, Norotte C, Damon B, Marga F, Neagu A, Besch-Williford CL, Kachurin A, Church KH, Park H, Mironov V, Markwald R, Vunjak-Novakovic G, Forgacs G (2008) Tissue engineering by self-assembly of cells printed into topologically defined structures. *Tissue Eng Part A* 14:413–421. <https://doi.org/10.1089/ten.2007.0173>
- Jeffries EM, Nakamura S, Lee K-W, Clamppfer J, Ijima H, Wang Y (2014) Micropatterning electrospun scaffolds to create intrinsic vascular networks. *Macromol Biosci* 14:1514–1520. <https://doi.org/10.1002/mabi.201400306>
- Jeon JS, Bersini S, Whisler JA, Chen MB, Dubini G, Charest JL, Moretti M, Kamm RD (2014) Generation of 3D functional microvascular networks with human mesenchymal stem cells in microfluidic systems. *Integr Biol* 6:555–563. <https://doi.org/10.1039/C3IB40267C>

- Jia W, Gungor-Ozkerim PS, Zhang YS, Yue K, Zhu K, Liu W, Pi Q, Byambaa B, Dokmeci MR, Shin SR, Khademhosseini A (2016) Direct 3D bioprinting of perfusable vascular constructs using a blend bioink. *Biomaterials* 106:58–68. <https://doi.org/10.1016/j.biomaterials.2016.07.038>
- Jun H-W, West JL (2005) Endothelialization of microporous YIGSR/PEG-modified polyurethaneurea. *Tissue Eng* 11:1133–1140. <https://doi.org/10.1089/ten.2005.11.1133>
- Kang H-W, Lee SJ, Ko IK, Kengla C, Yoo JJ, Atala A (2016) A 3D bioprinting system to produce human-scale tissue constructs with structural integrity. *Nat Biotechnol*. <https://doi.org/10.1038/nbt.3413>
- Kibbe MR, Martinez J, Popowich DA, Kapadia MR, Ahanchi SS, Aalami OO, Jiang Q, Webb AR, Yang J, Carroll T, Ameer GA (2010) Citric acid-based elastomers provide a biocompatible interface for vascular grafts. *J Biomed Mater Res A* 93:314–324. <https://doi.org/10.1002/jbm.a.32537>
- Kim S, Kawai T, Wang D, Yang Y (2016) Engineering a dual-layer chitosan-lactide hydrogel to create endothelial cell aggregate-induced microvascular networks in vitro and increase blood perfusion in vivo. *ACS Appl Mater Interfaces* 8:19245–19255. <https://doi.org/10.1021/acsami.6b04431>
- King KR, Wang CCJ, Kaazempur-Mofrad MR, Vacanti JP, Borenstein JT (2004) Biodegradable microfluids. *Adv Mater* 16:2007–2012. <https://doi.org/10.1002/adma.200306522>
- Kinstlinger IS, Miller J (2016) 3D-printed fluidic networks as vasculature for engineered tissue. *Lab Chip* 16:2025–2043. <https://doi.org/10.1039/C6LC00193A>
- Kinstlinger IS, Bastian A, Paulsen SJ, Hwang DH, Ta AH, Yalacki DR, Schmidt T, Miller JS (2016) Open-Source Selective Laser Sintering (OpenSLS) of nylon and biocompatible polycaprolactone. *PLoS One* 11:1–25. <https://doi.org/10.1371/journal.pone.0147399>
- Kolesky DB, Truby RL, Gladman AS, Busbee TA, Homan KA, Lewis JA (2014) 3D bioprinting of vascularized, heterogeneous cell-laden tissue constructs. *Adv Mater* 26:3124–3130. <https://doi.org/10.1002/adma.201305506>
- Kolesky DB, Homan KA, Skylar-Scott MA, Lewis JA (2016) Three-dimensional bioprinting of thick vascularized tissues. *Proc Natl Acad Sci U S A* 201521342. <https://doi.org/10.1073/pnas.1521342113>
- Langer R, Folkman J (1976) Polymers for the sustained release of proteins and other macromolecules. *Nature* 263:797–800
- Lenard A, Daetwyler S, Betz C, Ellertsdotter E, Belting HG, Huisken J, Affolter M (2015) Endothelial cell self-fusion during vascular pruning. *PLoS Biol* 13:1–25. <https://doi.org/10.1371/journal.pbio.1002126>
- Liu Tsang V, Chen AA, Cho LM, Jadin KD, Sah RL, DeLong S, West JL, Bhatia SN (2007) Fabrication of 3D hepatic tissues by additive photopatterning of cellular hydrogels. *FASEB J* 21:790–801. <https://doi.org/10.1096/fj.06-7117com>
- Macchiarelli P, Jungebluth P, Go T, Asnaghi MA, Rees LE, Cogan TA, Dodson A, Martorell J, Bellini S, Parnigotto PP, Dickinson SC, Hollander AP, Mantero S, Conconi MT, Birchall MA (2008) Clinical transplantation of a tissue-engineered airway. *Lancet* 372:2023–2030. [https://doi.org/10.1016/S0140-6736\(08\)61598-6](https://doi.org/10.1016/S0140-6736(08)61598-6)
- McGuigan AP, Sefton MV (2007) The influence of biomaterials on endothelial cell thrombogenicity. *Biomaterials* 28:2547–2571. <https://doi.org/10.1016/j.biomaterials.2007.01.039>
- Meyer W, Engelhardt S, Novosel E, Elling B, Wegener M, Krüger H (2012) Soft polymers for building up small and smallest blood supplying systems by stereolithography. *J Funct Biomater* 3:257–268. <https://doi.org/10.3390/jfb3020257>
- Miller JS, Burdick JA (2016) Editorial: special issue on 3D printing of biomaterials. *ACS Biomater Sci Eng* 2:1658–1661. <https://doi.org/10.1021/acsbiomaterials.6b00566>
- Miller JS, Stevens KR, Yang MT, Baker BM, Nguyen D-HT, Cohen DM, Toro E, Chen AA, Galie PA, Yu X, Chaturvedi R, Bhatia SN, Chen CS (2012) Rapid casting of patterned vascular networks for perfusable engineered three-dimensional tissues. *Nat Mater* 11:768–774. <https://doi.org/10.1038/nmat3357>

- Nakamura M, Nishiyama Y, Henmi C, Iwanaga S, Nakagawa H, Yamaguchi K, Akita K, Mochizuki S, Takiura K (2008) Ink jet three-dimensional digital fabrication for biological tissue manufacturing: analysis of alginate microgel beads produced by ink jet droplets for three dimensional tissue fabrication. *J Imaging Sci Technol* 52:1–15. <https://doi.org/10.2352/J.ImagingSci.Technol>
- Nguyen D-HT, Stapleton SC, Yang MT, Cha SS, Choi CK, Galie PA, Chen CS (2013) Biomimetic model to reconstitute angiogenic sprouting morphogenesis in vitro. *Proc Natl Acad Sci U S A* 110:6712–6717. <https://doi.org/10.1073/pnas.1221526110>
- Nishida K, Yamato M, Hayashida Y, Watanabe K, Yamamoto K, Adachi E, Nagai S, Kikuchi A, Maeda N, Watanabe H, Okano T, Tano Y (2004) Corneal reconstruction with tissue-engineered cell sheets composed of autologous oral mucosal epithelium. *N Engl J Med* 351:1187–1196. <https://doi.org/10.1056/NEJMoa040455>
- Nishiyama Y, Nakamura M, Henmi C, Yamaguchi K, Mochizuki S, Nakagawa H, Takiura K (2009) Development of a three-dimensional bioprinter: construction of cell supporting structures using hydrogel and state-of-the-art inkjet technology. *J Biomech Eng* 131:35001. <https://doi.org/10.1115/1.3002759>
- Oheim M, Michael DJ, Geisbauer M, Madsen D, Chow RH (2006) Principles of two-photon excitation fluorescence microscopy and other nonlinear imaging approaches. *Adv Drug Deliv Rev* 58:788–808. <https://doi.org/10.1016/j.addr.2006.07.005>
- Pham QP, Sharma U, Mikos AG (2006) Electrospun poly (ϵ -caprolactone) microfiber and multi-layer nanofiber/microfiber scaffolds: characterization of scaffolds and measurement of cellular infiltration. *Biomacromolecules* 7:2796–2805. <https://doi.org/10.1021/bm060680j>
- Ratner B, Hoffman A, Schoen F, Lemons J (2004) *Biomaterials science: an introduction to materials in medicine*, 2nd edn. Academic, Cambridge
- Raya-Rivera A, Esquiliano DR, Yoo JJ, Lopez-Bayghen E, Soker S, Atala A (2011) Tissue-engineered autologous urethras for patients who need reconstruction: an observational study. *Lancet* 377:1175–1182. [https://doi.org/10.1016/S0140-6736\(10\)62354-9](https://doi.org/10.1016/S0140-6736(10)62354-9)
- Razavi MS, Shirani E, Salimpour MR, Kassab GS (2014) Constructal law of vascular trees for facilitation of flow. *PLoS One* 9:e116260. <https://doi.org/10.1371/journal.pone.0116260>
- Risau W (1997) Mechanisms of angiogenesis. *Nature* 386:671–684
- Schüller-Ravoo S, Zant E, Feijen J, Grijpma DW (2014) Preparation of a designed poly(trimethylene carbonate) microvascular network by stereolithography. *Adv Healthc Mater* 3:2004–2011. <https://doi.org/10.1002/adhm.201400363>
- Sooppan R, Paulsen SJ, Han J, Ta AH, Dinh P, Gaffey AC, Venkataraman C, Trubelja A, Hung G, Miller JS, Atluri P (2016) In vivo anastomosis and perfusion of a three-dimensionally-printed construct containing microchannel networks. *Tissue Eng Part C Methods* 22. <https://doi.org/10.1089/ten.tec.2015.0239>
- Stachowiak AN, Bershteyn A, Tzatzalos E, Irvine DJ (2005) Bioactive hydrogels with an ordered cellular structure combine interconnected macroporosity and robust mechanical properties. *Adv Mater* 17:399–403. <https://doi.org/10.1002/adma.200400507>
- Suri S, Han L-H, Zhang W, Singh A, Chen S, Schmidt CE (2011) Solid freeform fabrication of designer scaffolds of hyaluronic acid for nerve tissue engineering. *Biomed Microdevices* 13:983–993. <https://doi.org/10.1007/s10544-011-9568-9>
- Takahashi K, Yamanaka S (2006) Induction of pluripotent stem cells from mouse embryonic and adult fibroblast cultures by defined factors. *Cell* 126:663–676. <https://doi.org/10.1016/j.cell.2006.07.024>
- Tamayol A, Najafabadi AH, Aliakbarian B, Arab-Tehrany E, Akbari M, Annabi N, Juncker D, Khademhosseini A (2015) Hydrogel templates for rapid manufacturing of bioactive fibers and 3D constructs. *Adv Healthc Mater*. <https://doi.org/10.1002/adhm.201500492>
- Trachtenberg JE, Mountziaris PM, Miller JS, Wettergreen M, Kasper FK, Mikos AG (2014) Open-source three-dimensional printing of biodegradable polymer scaffolds for tissue engineering. *J Biomed Mater Res A* 4326–4335. <https://doi.org/10.1002/jbm.a.35108>

- Vacanti CA (2006) The history of tissue engineering. *J Cell Mol Med* 10:569–576. <https://doi.org/10.1111/j.1582-4934.2006.tb00421.x>
- Wang EA, Rosen V, D'Alessandro JS, Bauduy M, Cordes P, Harada T, Israel DI, Hewick RM, Kerns KM, LaPan P et al (1990) Recombinant human bone morphogenetic protein induces bone formation. *Proc Natl Acad Sci U S A* 87:2220–2224. <https://doi.org/10.1073/pnas.87.6.2220>
- Wang X, Phan DTT, George SC, Hughes CCW, Lee AP (2015) Engineering anastomosis between living capillary networks and endothelial cell-lined microfluidic channels. *Lab Chip* 16:282–290. <https://doi.org/10.1039/C5LC01050K>
- Whang K, Tsai DC, Nam EK, Aitken M, Sprague SM, Patel PK, Healy KE (1998) Ectopic bone formation via rhBMP-2 delivery from porous bioabsorbable polymer scaffolds. *J Biomed Mater Res* 42:491–499. [https://doi.org/10.1002/\(SICI\)1097-4636\(19981215\)42:4<491::AID-JBM3>3.0.CO;2-F](https://doi.org/10.1002/(SICI)1097-4636(19981215)42:4<491::AID-JBM3>3.0.CO;2-F)
- Wu W, Deconinck A, Lewis JA (2011) Omnidirectional printing of 3D microvascular networks. *Adv Mater* 23:178–183. <https://doi.org/10.1002/adma.201004625>
- Yannas V, Burke JF, Orgill DP, Skrabut EM (1982) Wound tissue can utilize a polymeric template to synthesize a functional extension of skin. *Science* 215:174–176. <https://doi.org/10.1126/science.7031899>
- Zhang Y, Yu Y, Akkouch A, Dababneh A, Dolati F, Ozbolat IT (2015) In vitro study of directly bioprinted perfusable vasculature conduits. *Biomater Sci* 3:134–143. <https://doi.org/10.1039/C4BM00234B>
- Zhang B, Montgomery M, Chamberlain MD, Ogawa S, Korolj A, Pahnke A, Wells LA, Massé S, Kim J, Reis L, Momen A, Nunes SS, Wheeler AR, Nanthakumar K, Keller G, Sefton MV, Radisic M (2016) Biodegradable scaffold with built-in vasculature for organ-on-a-chip engineering and direct surgical anastomosis. *Nat Mater*. <https://doi.org/10.1038/nmat4570>
- Zheng Y, Chen J, Craven M, Choi NW, Totorica S, Diaz-Santana A, Kermani P, Hempstead B, Fischbach-Teschl C, López JA, Stroock AD (2012) In vitro microvessels for the study of angiogenesis and thrombosis. *Proc Natl Acad Sci U S A* 109:9342–9347. <https://doi.org/10.1073/pnas.1201240109>



Computational Methods for the Predictive Design of Bone Tissue Engineering Scaffolds

Stefan Scheiner, Vladimir S. Komlev, and Christian Hellmich

Contents

1	Introduction	108
2	Numerical Modeling Approaches	110
3	Rigorous Multiscale Modeling	112
3.1	Motivation	112
3.2	Overview	112
3.3	Example: Granular, Hydroxyapatite-Based Biomaterial	114
4	Concluding Remarks and Outlook	121
	References	126

Abstract

The design of bone tissue engineering materials and scaffold structures made thereof is a delicate task, owing to the various, sometimes contradicting requirements that must be fulfilled. The traditional approach is based on a trial-and-error strategy, which may result in a lengthy and inefficient process. Aiming at improvement of this unsatisfactory situation, computer simulations, based on sound mathematical modeling of the involved processes, have been identified as promising complement to experimental testing. After giving a brief overview of available modeling and simulation concepts, the core of this chapter is

S. Scheiner (✉) · C. Hellmich

Institute for Mechanics of Materials and Structures, Technische Universität Wien (TU Wien), Vienna, Austria

e-mail: stefan.scheiner@tuwien.ac.at; christian.hellmich@tuwien.ac.at

V. S. Komlev

A.A. Baikov Institute of Metallurgy and Materials Science, Russian Academy of Sciences, Moscow, Russia

Federal Scientific Research Centre “Crystallography and Photonics”, Russian Academy of Sciences, Moscow, Russia

presented, namely recent examples of multiscale, continuum micromechanics-based homogenization approaches developed in relation to bone tissue engineering. First, the fundamentals of continuum micromechanics are introduced, in order to lay the groundwork for the subsequently elaborated stiffness and strength homogenization approach related to a hydroxyapatite-based granular bone tissue engineering material. For the latter, the derivation of an upscaling scheme allowing for estimating the macroscopic stiffness and the macroscopic strength is demonstrated. Finally, avenues to utilization of this method in the design process of such materials are pointed out.

1 Introduction

Today's possibilities concerning the manufacturing and processing of materials suitable for being put together in form of scaffold structures are almost unlimited (or at least very diverse). Hence, such structures are nowadays a popular option in bone tissue engineering (Hutmacher 2000; Langer and Tirrell 2004; Hollister 2005; Porter et al. 2009; Amini et al. 2012). The requirements to such materials and structures are well known, see, e.g., (Rezwan et al. 2006; Williams 2008). Nevertheless, these requirements are briefly summarized in the following, given that their fulfilment is paramount so as to ensure successful application in bone tissue engineering.

First of all, the material a tissue engineering scaffold is composed of must be *biocompatible*, meaning that it must not adversely affect the physiological environment into which it is supposed to be implanted. Secondly, the very purpose of bone tissue engineering scaffolds is to act as temporary “filling” of bone defects and to provide the substrate for the ingrowth of newly forming bone tissue. Thus, on the one hand, the applied material must attract and be able to host bone growth-promoting cells and other biological factors (such as growth factors and hormones); then, such materials are considered to be *osteoconductive*. On the other hand, scaffold structures must exhibit a reasonably high porosity (of typically 50–90%), in order to let the involved cells and factors access the sites where new bone tissue should be formed, and to provide physical space for bone ingrowth. As soon as significant amounts of bone tissue have formed in the pore space of the scaffold structure, such that the mechanical support of the scaffold is not required any more, it becomes redundant. For this reason, it is desirable that the scaffold material slowly degrades once it is in contact with the targeted physiological environment, and, in the long run, even disappears. This behavior, standardly called *biodegradation*, makes sure that the respective bone defect may eventually fully regenerate. The desired time period in the course of which degradation should be completed depends on the application – e.g., in craniomaxillofacial applications, degradation should take between 3 and 6 months (Bose et al. 2012). Importantly, one of the main features of bone tissue is its load-bearing capacity. Thus, if tissue engineering scaffolds are temporarily taking the place of bone tissue, the former should match the latter as well as possible. This concerns in particular the material stiffness, besides other

mechanical properties (such as the material strength). Clearly, scaffold structures must not be too soft, in order to avoid structural failure. However, they must not be too stiff either. The latter requirement stems from the fact that the ingrowth of bone tissue, and activities of biological cells in general, are significantly influenced by the mechanical loading they are subjected to (Simmons et al. 2001; Robling et al. 2006; Jacobs et al. 2010). Too stiff scaffolds would inhibit the mechanobiological stimulation of bone ingrowth, potentially leading to very adverse effects, such as stress shielding, in further consequence causing bone degeneration in the immediate vicinity of the implanted tissue engineering scaffold (Engl et al. 1987).

Extensive experimental material testing, based on a trial-and-error approach, is still the gold standard as to study the suitability of a new scaffold material and structure, i.e., to test whether the aforementioned requirements are adequately met. While biocompatibility, osteoconductivity, and biodegradability of the material can be studied reasonably well under laboratory conditions, assessing the mechanical behavior, which may change dynamically due to ongoing bone regeneration and scaffold degradation, is an extremely delicate task. Namely, considering that bone regeneration causes new bone tissue to be added and scaffold material to be resorbed at the same time, “guessing” adequate mechanical properties of the scaffold material appears to be left to pure chance. It seems thus promising to utilize the predictive capabilities of mathematical models, for simulating the development of bone tissue engineering scaffolds under various, physiologically relevant conditions, to gain valuable insights for scaffold design (Geris 2013).

This chapter is devoted to giving an overview on computer simulation-based methods utilizable for supporting the design of bone tissue engineering scaffolds. For this purpose, it is recalled that tissue engineering scaffolds are complicated constructs, highly porous, and often exhibiting different types of pore spaces, separated from each other by orders of magnitude (Li et al. 2013; Bose et al. 2013). Furthermore, while a scaffold itself can be considered as a somewhat inert material, it is conditioned such that it starts to change in terms of composition and possibly also morphology once placed in its targeted physiological environment. When aiming for development of computational tools featuring predictive capabilities that can be utilized in the design of such materials as well as of structures made thereof, taking all these parameters into account is an ambitious challenge (van Gaalen et al. 2008), and calls for a careful choice of underlying theoretical concepts. The variety of tissue engineering-related computational modeling approaches that has been developed over the years can be divided into several categories, introduced next. When aiming at simulation of spatially resolved domains within bone tissue engineering materials, application of numerical methods is usually inevitable, see Sect. 2. Furthermore, when dealing with hierarchically organized materials, so-called multiscale modeling methods gained more and more attention in the past two decades or so. Related modeling frameworks consider the most important features of such materials on all relevant observation scales and take into account mathematical relations for bridging the observation scales. Some examples for such models are presented in Sect. 3. A brief summary and outlook to foreseeable future developments in the field concludes this chapter, see Sect. 4.

2 Numerical Modeling Approaches

When the physical behavior of bone tissue engineering scaffolds across a specific spatial domain is of interest, the related mathematical framework usually comprises partial differential equations. For such equations, analytical solutions are scarce because of which numerical solution methods are standardly applied. In the following, a (nonexhaustive) overview of numerical modeling strategies in the field of bone tissue engineering is presented.

First, the focus is on modeling approaches where the studied domain is considered in a more or less homogeneous fashion, i.e., microstructural features are not taken into account in detail. This way, Botchway et al. (2004) developed a model for performing microcarrier motion analysis within a 3D domain representing a bone tissue engineering construct, based on solving the well-known Darcy equation by means of a Runge–Kutta method, allowing to furthermore estimate the occurring shear forces using a Stokes approximation, and to eventually assess the flow conditions. Also aiming at studying the flow conditions within a tissue engineering material, Chung et al. (2007) simulated the nutrient flow through a cellular construct, as it is relevant for perfusion reactors. For that purpose, a wide range of theoretical concepts were combined, including classical transport equations (such as the diffusion-convection equation, Navier–Stokes equation, and Brinkmann equation), volume averaging of the transport properties, the Maxwell equation for estimation of the diffusion coefficient, cell balance laws, the Carman–Kozeny equation for estimation of the permeability, and non-dimensionalization. Employing the finite element (FE) method, the resulting set of equations was solved and cell growth within the simulated construct was assessed.

In many cases, it is of particular importance how the microstructure, e.g., the shape and distribution of pore spaces, influences the overall behavior of scaffold materials. Then, application of large-scale numerical models is inevitable. Depending on the morphology of the scaffold materials, numerical models exhibiting corresponding complexities have to be generated. For materials which exhibit a regular morphology, probably involving some kind of periodicity, see, e.g., (Adachi et al. 2006; Lacroix et al. 2009; Melchels et al. 2010; Olivares et al. 2009; Sturm et al. 2010; Truscello et al. 2012; Dias et al. 2012; Hutmacher and Singh 2008), numerical models can be easily generated, probably based on so-called unit cells, see, e.g., Fig. 1a. If the morphology is however more intricate, micro-computed tomography (micro-CT) is a popular imaging method for acquiring the three-dimensionally distributed microstructure of a material. The underlying image data can be straightforwardly utilized for generating a corresponding numerical model, see, e.g., (Lacroix et al. 2006, 2009; Jaecques et al. 2004; Milan et al. 2009; Porter et al. 2005; Sandino et al. 2008; Sandino and Lacroix 2011; Voronov et al. 2010; Williams et al. 2005). One main disadvantage of such numerical models is the substantial computational costs related to model evaluation, which limits numerical modeling to somewhat narrow ranges of observation scales. Coupling numerical modeling with other types of models for integrating, e.g., information obtained from observation scales which are too low to be directly considered in the respective numerical model is one way to circumvent this limitation. This strategy was followed in (Sanz-Herrera

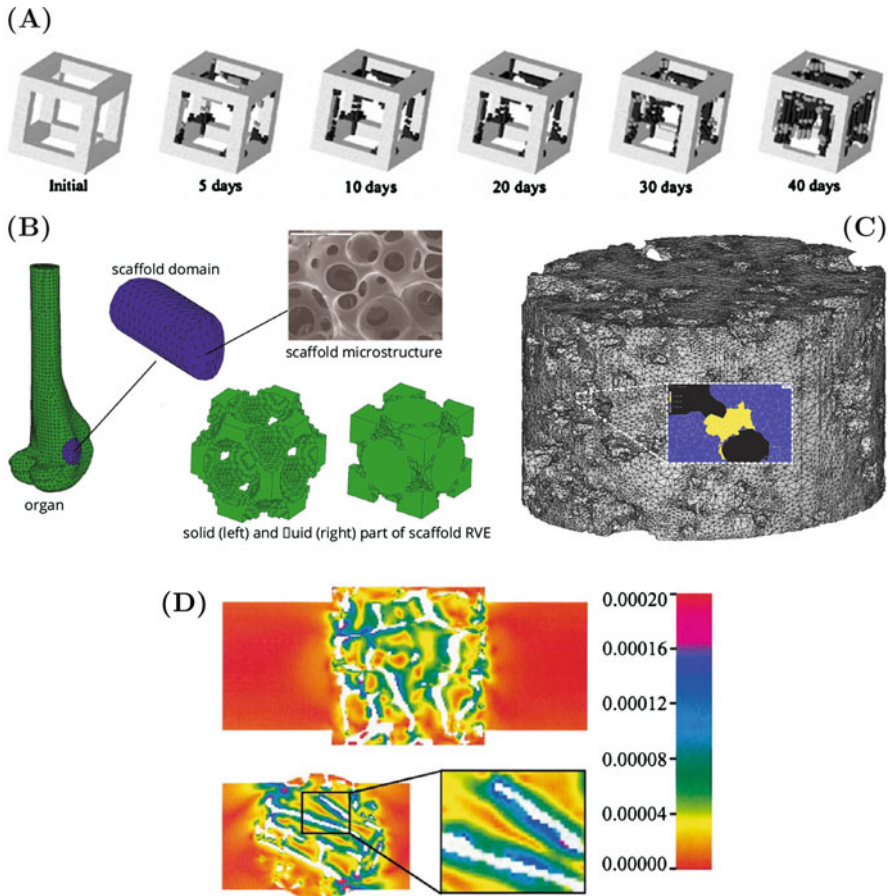


Fig. 1 Exemplary results of numerical simulations showing the performances of different bone tissue engineering materials; (a) Sequence of bone regeneration over 40 days, based on discretization of the scaffold by means of unit cells, reprinted from (Adachi et al. 2006), with permission from Elsevier; (b) Numerical multiscale model, with a representative volume element (RVE) of the scaffold embedded in an organ model of rabbit distal femur, reprinted from (Sanz-Herrera et al. 2008), with permission from Elsevier; (c) Three-dimensional discretization of a small cylinder made up by a calcium phosphate-based tissue engineering material, with the zoom-out showing the distribution of tensile and compressive stresses upon simulation of a uniaxial compression test, reprinted from (Lacroix et al. 2006), with permission from Elsevier; and (d) The distribution of shear stresses arising due to the fluid flow distribution within the pores of a scaffold sample, resulting from simulation of a perfusion test, reprinted from (Porter et al. 2005), with permission from Elsevier

et al. 2008, 2009a, b), who implemented the results of a local analysis of bone regeneration within a porous scaffold structure, by means of a unit cell-type representation of this scaffold structure, in organ-scale bone models, thereby pursuing a numerical multiscale modeling strategy, see, e.g., Fig. 1b. The application range of large-scale numerical modeling is extremely wide, comprising mechanical analyses

for studying local effects due to specific, physiologically relevant loading conditions, see, e.g., Fig. 1c, simulation of the fluid flow conditions as they occur in perfusion tests, see, e.g., Fig. 1d, and, the bone regeneration performance related to specific scaffold morphologies, see, e.g., Fig. 1a and b.

3 Rigorous Multiscale Modeling

3.1 Motivation

While the numerical modeling approaches summarized exemplarily in the previous section impressively show the capacities of numerical modeling, it is also evident that large-scale numerical models are, despite the powerful computer systems that are available nowadays, limited in terms of the considered resolution. This implies that in numerical models microstructural features cannot be taken properly into account, at least not if these features exhibit characteristic lengths which are much smaller than the dimensions of the studied structure. In bone tissue engineering, this concerns, e.g., the change of the pore structure in biodegradable scaffold materials, or in the scaffold-surrounding bone tissue the microstructural changes due to bone metabolism.

In the past decade or so, multiscale modeling approaches for quantifying the mechanical properties of bone tissue engineering scaffolds have been introduced, which allow to eliminate the aforementioned deficit of large-scale numerical modeling approaches. These approaches, all based on the concept of continuum micromechanics, are first briefly reviewed in the following, and one particular, recent example is presented in more detail.

3.2 Overview

Continuum micromechanical modeling (Hill 1963; Zaoui 1997, 2002; Dormieux et al. 2006) aims at consideration of the effects of microstructural features of a material on a macroscopic observation scale. To that end, the material under investigation must fulfil certain requirements concerning the characteristic lengths of the microstructural features and of the macroscopic material. Namely, in continuum micromechanics, a material is, while appearing to be macroscopically homogeneous, considered to be microscopically heterogeneous. If the characteristic length of these microheterogeneities, d , is considerably smaller than the characteristic length of a volume element containing such material, ℓ , this volume element is referred to as representative volume element (RVE). In order to ensure satisfying fulfilment of the requirement $d \ll \ell$, ℓ must be at least two to three times larger than d (Drugan and Willis 1996). In turn, ℓ must be considerably smaller than the characteristic length of the geometry of a structure composed of the material defined on the RVE, \mathcal{L} , as well as of the loading acting onto such structure, \mathcal{P} . In order to ensure satisfying fulfilment of the requirement $\ell \ll \{\mathcal{L}, \mathcal{P}\}$, \mathcal{L} and \mathcal{P} , respectively, must be at least five to ten times larger than ℓ (Kohlhauser and Hellmich 2013).

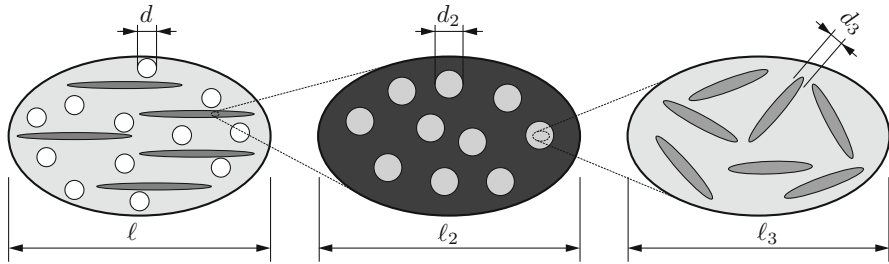


Fig. 2 Separation of scales exemplified for a material comprising three hierarchical levels, $l \gg d \geq l_2 \gg d_2 \geq l_3 \gg d_3$

Usually, the microstructure of the material contained in an RVE is much too complex to be described in minute detail. Instead, so-called material phases, which are assumed to be homogeneous, are introduced. These material phases exhibit known physical properties, such as volume fractions or mechanical properties, and a variety of different phase morphologies can be established, thereby allowing for different phase shapes or interactions between the considered material phases. Continuum micromechanics allows for deriving mathematical relations reconciling this information, for the eventual estimation of macroscopic (mechanical) properties valid on the level of the RVE, based on the phase properties. This upscaling process is often referred to as homogenization. Such homogenization can be carried out in sequential fashion, namely if a material phase itself exhibits a heterogeneous microstructure. Then, an RVE can be introduced within this phase (Fritsch and Hellmich 2007); the characteristic length of this new RVE, l_2 , must fulfil the requirement $l_2 \leq d$, while the principle of scale separation demands that the characteristic length of the heterogeneities within the new RVE, d_2 , are considerably smaller than l_2 , $d_2 \ll l_2$. This leads to a multistep homogenization scheme, see Fig. 2.

The concept of continuum micromechanics has been successfully applied for several different biomaterials. For example, the strength of a hydroxyapatite-based biomaterial was estimated by introducing a Coulomb-type failure criterion describing the brittle failure of the interfaces between the hydroxyapatite crystals and the surrounding material (Fritsch et al. 2007). A similar approach has been chosen in (Fritsch et al. 2009a; Morin et al. 2017), where failure of hydroxyapatite crystals is governed by a Mohr-Coulomb-type criterion. Clearly, while other classical failure criteria (e.g., according to Tresca or von Mises) as well as more elaborate failure criteria (e.g., according to Tsai-Wu) could be also used, it has turned out that in the context of hydroxyapatite failure in bone tissue or in biomaterials, Mohr-Coulomb-type criteria are the most reasonable ones. One of the main advantages of micro-mechanical homogenization is that influences of the RVE morphology can be easily and efficiently studied, as demonstrated in (Fritsch et al. 2010). Continuum micromechanics of biomaterials can be even extended to the theory of poromechanics, allowing to make strength predictions dependent on the respectively relevant poromechanical configuration (Fritsch et al. 2013).

Remarkably, continuum micromechanics can be straightforwardly employed to analyze micro-CT data of bone tissue engineering scaffolds in terms of the exact distribution of mechanical properties. As shown in (Scheiner et al. 2009; Luczynski et al. 2012; Czenek et al. 2014), the three-dimensional distribution of grey values can be converted, based on X-ray physics basics and volume averaging, into a corresponding distribution of the volume fractions defining the microstructural composition of the biomaterial, which, in turn, can be fed into a micromechanical upscaling scheme for estimation of the distribution of elastic constants. Such distribution can be used as input for numerical simulations concerning the mechanical behavior of the biomaterial on a structural scale, even increasing the range of how micromechanical homogenization can be applied for the sake of gaining insights into the mechanical behavior of biomaterials.

3.3 Example: Granular, Hydroxyapatite-Based Biomaterial

In order to demonstrate the potential of multiscale modeling in the field of bone tissue engineering, one particular example is discussed in more detail next.

3.3.1 Definition of the Material

Namely, the focus is on a granular biomaterial composed of carbon-containing hydroxyapatite. The chemical composition of this material is defined as $\text{Ca}_{10}(\text{PO}_4)_6(\text{OH})_{1.9}(\text{CO}_3)_{0.05}$. Furthermore, it contains different kinds of pore spaces and cracks. The granules are produced by means of a method based on the effect of immiscible liquids (Komlev et al. 2002, 2003), allowing for production of granules with diameters ranging from 50 to 2000×10^{-6} m, with the technically relevant granule diameter being approximately 1800×10^{-6} m (Dejaco et al. 2012). Assemblies of such granules have been shown to be adequate in terms of supporting bone regeneration in regions of bone defects, particularly in the human mandible. Exposing these granules to an environment which resembles the targeted physiological solution entails two effects: firstly, new bone tissue is formed on the granule surface(s); and secondly, hydroxyapatite needles continuously dissolve. Figure 3 illustrates the hierarchical organization of this bone tissue engineering material, from the macroscopic scale of granule assemblies to the microscopic scale of hydroxyapatite crystals.

3.3.2 Micromechanical Model Representation

Following the principle of scale separation allows to translate the hierarchical organization of the granular hydroxyapatite-based bone tissue engineering material, shown in Fig. 3, into a correspondingly hierarchical sequence of three RVEs, see Fig. 4. RVE I comprises micropores, being of approximately spherical shape, which interact mutually with hydroxyapatite crystals, being of approximately cylindrical (or needle-) shape, oriented arbitrarily in space. Together, these two phases form a microporous, polycrystalline hydroxyapatite matrix. RVE II includes this matrix, with penny-shaped cracks and mesopores, which are also of approximately spherical

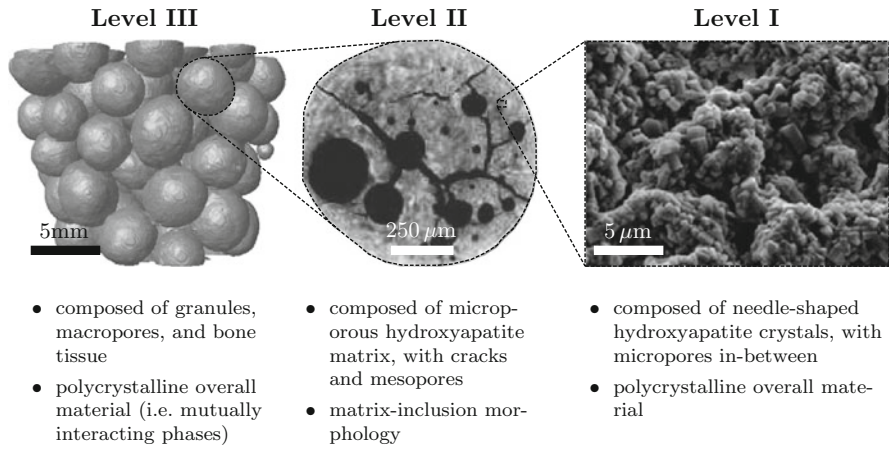


Fig. 3 Morphological features discernible on the three hierarchical levels of the studied biomaterial, based on scanning electron microscopy (level I) and micro-computed tomography (levels II and III)

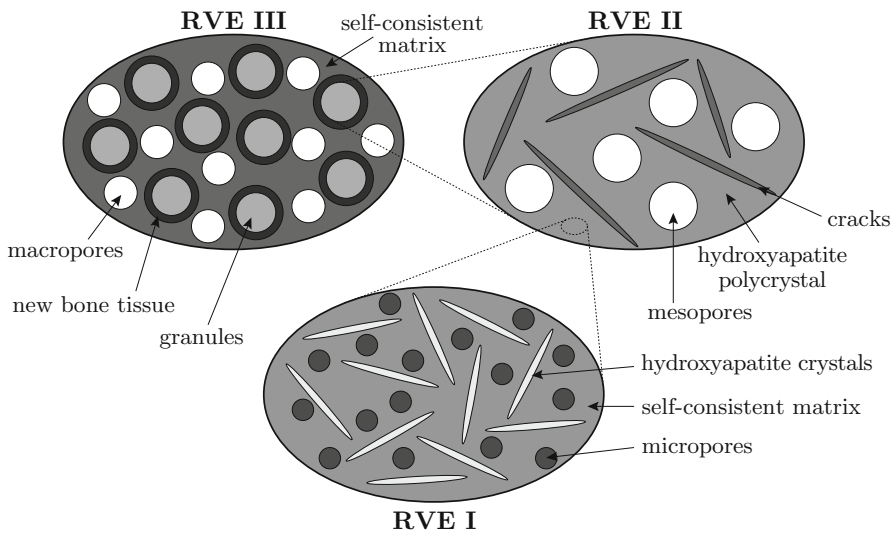


Fig. 4 Micromechanical representation following from the hierarchical organization of the studied biomaterial shown in Fig. 3; RVE I, with a characteristic length of $\ell_{RVEI} \approx 10 \mu\text{m}$, defines the hydroxyapatite polycrystal; RVE II, with a characteristic length of $\ell_{RVEII} \approx 1 \text{mm}$, defines the granules; and RVE III, with a characteristic length of $\ell_{RVEIII} \approx 5 \text{mm}$, defines the macroscopic conglomerate

shape. The resulting matrix-inclusion-type morphology defines the material on the observation scale of single granules. RVE III comprises an assembly of the granules defined on RVE II, with transversally isotropic extracellular bone tissue growing on

the surfaces of the granules, leading to a shell-like arrangement of bone tissue. Bone formation leads to reduction of the macroscopic pore space – in RVE III, the macropores are considered to be of spherical shape.

3.3.3 Micromechanical Stiffness Estimation

In the following, the cornerstones of the micromechanical model allowing to estimate the stiffness of the macroscopic conglomerate material are briefly outlined, based on the experimentally accessible elastic constants of the material's basic constituents, i.e., of hydroxyapatite and extracellular bone tissue.

Homogenization of Hydroxyapatite Matrix Stiffness

On hierarchical level I, a previously developed homogenization scheme (Fritsch et al. 2006) (which could be experimentally validated for a wide range of porous material systems) can be straightforwardly adopted, yielding the following self-consistent, implicit scheme for estimating the stiffness of the microporous hydroxyapatite polycrystal:

$$\begin{aligned}
 \mathbb{C}_{\text{polyHA}} = & \left\{ f_{\text{HA}}^{\text{polyHA}} \mathbb{C}_{\text{HA}} : \left[\int_{\varphi=0}^{2\pi} \int_{\vartheta=0}^{\pi} [\mathbb{I} + \mathbb{P}_{\text{cyl}}^{\text{polyHA}}(\vartheta, \varphi) : \right. \right. \\
 & \left. \left. (\mathbb{C}_{\text{HA}} - \mathbb{C}_{\text{polyHA}})]^{-1} \frac{\sin \vartheta \, d\vartheta \, d\varphi}{4\pi} \right] + \phi_{\text{micro}}^{\text{polyHA}} \mathbb{C}_{\text{micro}\phi} : \right. \\
 & \left. [\mathbb{I} - \mathbb{P}_{\text{sph}}^{\text{polyHA}} : (\mathbb{C}_{\text{micro}\phi} - \mathbb{C}_{\text{polyHA}})]^{-1} \right\} : \left\{ f_{\text{HA}}^{\text{polyHA}} \times \right. \\
 & \left. \left[\int_{\varphi=0}^{2\pi} \int_{\vartheta=0}^{\pi} [\mathbb{I} + \mathbb{P}_{\text{cyl}}^{\text{polyHA}}(\vartheta, \varphi) : (\mathbb{C}_{\text{HA}} - \mathbb{C}_{\text{polyHA}})]^{-1} \frac{\sin \vartheta \, d\vartheta \, d\varphi}{4\pi} \right] + \right. \\
 & \left. \phi_{\text{micro}}^{\text{polyHA}} [\mathbb{I} - \mathbb{P}_{\text{cyl}}^{\text{polyHA}} : (\mathbb{C}_{\text{micro}\phi} - \mathbb{C}_{\text{polyHA}})]^{-1} \right\}^{-1}. \tag{1}
 \end{aligned}$$

In Eq. 1, $\phi_{\text{micro}}^{\text{polyHA}}$ and $f_{\text{HA}}^{\text{polyHA}}$ are the volume fractions of the micropores and the hydroxyapatite needles; \mathbb{C}_{HA} and $\mathbb{C}_{\text{micro}\phi}$ are the stiffness tensors of the hydroxyapatite crystals and of the micropores; ϑ and φ are the Euler angles quantifying the orientations of the hydroxyapatite crystals; $\mathbb{P}_{\text{cyl}}^{\text{polyHA}}(\vartheta, \varphi)$ and $\mathbb{P}_{\text{sph}}^{\text{polyHA}}$ are the Hill (or morphology) tensors related to cylindrical and spherical inclusions, embedded in a matrix made up of the microporous hydroxyapatite polycrystal; and \mathbb{I} is the fourth-order unit tensor, the components of which are defined via the Kronecker delta δ_{ij} ($\delta_{ij} = 1$ if $i = j$ and $\delta_{ij} = 0$ if $i \neq j$), namely $I_{ijkl} = 1/2(\delta_{ik}\delta_{jl} + \delta_{il}\delta_{jk})$. Details regarding the computation of the Hill tensors $\mathbb{P}_{\text{cyl}}^{\text{polyHA}}(\vartheta, \varphi)$ and $\mathbb{P}_{\text{sph}}^{\text{polyHA}}$ can be found elsewhere

(Scheiner et al. 2016a). Stiffness tensor \mathbb{C}_{HA} can be defined based on experimental tests (Katz and Ukraincik 1971; Gilmore and Katz 1982), revealing the Young's modulus of the isotropic hydroxyapatite, $E_{\text{HA}} = 114$ GPa, as well as the respective Poisson's ratio, $\nu_{\text{HA}} = 0.27$, see also (Hellmich and Ulm 2002; Hellmich et al. 2004). Considering that all considered pore spaces are undrained implies $\mathbb{C}_{\text{micro}\phi} = 0$ (Thompson and Willis 1991).

Homogenization of Granule Stiffness

On hierarchical level II, again classical results available in literature (Deudé et al. 2002; Dormieux et al. 2004) can be readily utilized for estimating the stiffness tensor of the granules:

$$\begin{aligned} \mathbb{C}_{\text{gran}} &= \left\{ f_{\text{polyHA}}^{\text{gran}} \mathbb{C}_{\text{polyHA}} + \phi_{\text{meso}}^{\text{gran}} \mathbb{C}_{\text{meso}\phi} : \right. \\ &\quad \left. \left[\mathbb{I} - \mathbb{P}_{\text{sph}}^{\text{polyHA}} : (\mathbb{C}_{\text{meso}\phi} - \mathbb{C}_{\text{polyHA}}) \right]^{-1} \right\} : \\ &\quad \left[f_{\text{polyHA}}^{\text{gran}} \mathbb{I} + \phi_{\text{meso}}^{\text{gran}} \left[\mathbb{I} - \mathbb{P}_{\text{sph}}^{\text{polyHA}} : (\mathbb{C}_{\text{meso}\phi} - \mathbb{C}_{\text{polyHA}}) \right]^{-1} + \right. \\ &\quad \left. \epsilon \left(\frac{16}{9} \frac{1 - (\nu_{\text{polyHA}})^2}{2\nu_{\text{polyHA}}} \mathbb{K} + \frac{32}{45} \frac{(1 - \nu_{\text{polyHA}})(5 - \nu_{\text{polyHA}})}{2 - \nu_{\text{polyHA}}} \mathbb{J} \right) \right]^{-1}, \end{aligned} \quad (2)$$

with $f_{\text{polyHA}}^{\text{gran}}$ and $\phi_{\text{meso}}^{\text{gran}}$ being the volume fractions of the matrix made up of the microporous hydroxyapatite polycrystal and of the mesopores; $\mathbb{C}_{\text{polyHA}}$ is the stiffness tensor of the microporous hydroxyapatite polycrystal matrix (defined on RVE I); $\mathbb{C}_{\text{meso}\phi}$ is the stiffness tensor of the mesopores, being zero due to the assumed drained conditions; and $\mathbb{P}_{\text{sph}}^{\text{polyHA}}$ is the Hill tensor for spherical inclusions embedded in the isotropic microporous hydroxyapatite polycrystal matrix, see (Scheiner et al. 2016a) for details. Furthermore, ϵ is the so-called crack density parameter, defined as $\epsilon = \mathcal{N} r_{\text{cr}}^3$ (Budiansky and O'Connell 1976), where \mathcal{N} is the number of cracks per considered volume and r_{cr} their radius. \mathbb{K} and \mathbb{J} are the volumetric and deviatoric parts of the fourth-order unit tensor, $\mathbb{K} + \mathbb{J} = \mathbb{I}$.

Homogenization of Conglomerate Stiffness

On hierarchical level III, the situation is somewhat different, due to the shell-like morphology resulting from the growth of bone tissue on the granule surfaces. This intricacy can be resolved by considering the work of Hervé and Zaoui (1993). In particular, a spherical granule is considered, with the center of the granule being the origin of a Cartesian coordinate system, with a bone shell surrounding the granule, and with the granule-bone compound embedded in an infinite matrix. The stiffness of the latter is actually the stiffness of the overall conglomerate material (comprising granules, bone tissue, and macropores). Then, some fundamental boundary and field conditions are considered. First, the strain boundary condition reads as

$$r \rightarrow \infty : \boldsymbol{\xi} \rightarrow \mathbf{E}_0 \cdot \mathbf{x} \quad (3)$$

with r being the radial distance from the origin pointing towards a location being infinitely far away from the center of the inclusion, \mathbf{x} is the position vector, $\boldsymbol{\xi}$ is the displacement field, and \mathbf{E}_0 is the strain tensor relating to the uniform displacements on the boundary of the infinite domain. Furthermore, the equilibrium conditions,

$$0 \leq r < \infty : \operatorname{div} \boldsymbol{\sigma} = 0, \quad (4)$$

where $\boldsymbol{\sigma}$ is the stress tensor, and div represents the divergence operator, needs to be fulfilled. Displacements and strains are related through the kinematic relation:

$$0 \leq r < \infty : \boldsymbol{\varepsilon} = \nabla^S \boldsymbol{\xi}, \quad (5)$$

with ∇^S denoting the symmetric gradient operator. Additionally, domain-specific constitutive relations complement the set of the needed fundamental equations:

$$\boldsymbol{\sigma}(r) = \mathbb{C}(r) : \boldsymbol{\varepsilon}(r), \quad (6)$$

with

$$\mathbb{C}(r) = \begin{cases} \mathbb{C}_{\text{gran}} & \text{if } r \leq r_{\text{gran}} \\ \mathbb{C}_{\text{bone}} & \text{if } r_{\text{gran}} \leq r \leq r_{\text{bone}} \\ \mathbb{C}_{\text{congl}} & \text{if } r \geq r_{\text{bone}}, \end{cases} \quad (7)$$

where r_{gran} and r_{bone} are the radii of the individual granule and of the outer surface of the bone coating. \mathbb{C}_{bone} is the stiffness tensor of extracellular bone, see (Scheiner et al. 2016a; Bertrand and Hellmich 2009) for details, while $\mathbb{C}_{\text{congl}}$ is the sought-after stiffness of the overall macroporous scaffold-bone compound defined on hierarchical level III.

For the sake of stiffness homogenization, it is then considered that the overall stiffness of the macroscopic conglomerate is isotropic, thus the respective stiffness tensor is defined through:

$$\mathbb{C}_{\text{congl}} = 3k_{\text{congl}}\mathbb{K} = 2\mu_{\text{congl}}\mathbb{J}. \quad (8)$$

Hence, the stiffness tensor is fully defined by the bulk and shear moduli. For estimation of these two elastic constants, two displacement boundary value problems, which are due to the polycrystal-type morphology of RVE III interrelated with each other, are considered. On the one hand, hydrostatic displacements are considered, giving access, via respective evaluation of the above listed fundamental relations and solution of the resulting differential equation, to the conglomerate bulk modulus, as function of the volume fractions and elastic constants of all constituents, as well as of the shear modulus of the conglomerate material. On the other hand, imposition of a simple shear displacement boundary condition gives likewise access to the conglomerate shear modulus, again as function of the volume

fractions and elastic constants of all constituents but now also of the bulk modulus of the conglomerate material. Eventually, incremental solution of the resulting set of two equations yields the sought-after estimates of the two elastic constants (i.e., k_{congl} and μ_{congl}).

3.3.4 Micromechanical Strength Estimation

The micromechanical model sketched in Sect. 3.3.3 cannot only be used to upscale the stiffness from the micro- to the macroscopic scale but also for downscaling stresses and strains from the macro- to the microscopic scale, see (Scheiner et al. 2016b) for details. This feature is particularly beneficial when aiming at estimation of the macroscopic strength. It is known from previous studies (Fritsch et al. 2009a, b) that hydroxyapatite-based biomaterials fail due to the failure of the most unfavorably loaded hydroxyapatite crystals. Tying in with the aforementioned works, failure of the hydroxyapatite needles is associated to a failure surface mathematically defined by:

$$\begin{aligned} f_{\text{HA}}\left(\sigma_{\text{HA}}^{\text{polyHA}}\right) &= \max_{\vartheta, \varphi} \left(\frac{\sigma_{\text{HA}}^{\text{ult},t}}{\sigma_{\text{HA}}^{\text{ult},s}} \max_{\psi} \left| \sigma_{\text{HA},rn}^{\text{polyHA}}(\vartheta, \varphi, \psi) \right| \right. \\ &\quad \left. + \sigma_{\text{HA},rr}^{\text{polyHA}}(\vartheta, \varphi) \right) - \sigma_{\text{HA}}^{\text{ult},t} = 0. \end{aligned} \quad (9)$$

The tensile strength $\sigma_{\text{HA}}^{\text{ult},t}$ and the shear strength $\sigma_{\text{HA}}^{\text{ult},s}$ are available from experiments (Akao et al. 1981; Shareef et al. 1993), $\sigma_{\text{HA}}^{\text{ult},t} = 52.2$ MPa and $\sigma_{\text{HA}}^{\text{ult},s} = 80.3$ MPa, see also (Fritsch et al. 2009a). Furthermore, the normal stress in longitudinal direction of the hydroxyapatite crystals, $\sigma_{\text{HA},rr}^{\text{polyHA}}(\vartheta, \varphi)$, is defined by:

$$\sigma_{\text{HA},rr}(\vartheta, \varphi) = \mathbf{e}_r(\vartheta, \varphi) \cdot \sigma_{\text{HA}}^{\text{polyHA}}(\vartheta, \varphi) \cdot \mathbf{e}_r(\vartheta, \varphi), \quad (10)$$

while the shear stress to which the hydroxyapatite crystals are subjected to, $\sigma_{\text{HA},rn}^{\text{polyHA}}(\vartheta, \varphi, \psi)$, is defined as:

$$\sigma_{\text{HA},rn}(\vartheta, \varphi, \psi) = \mathbf{e}_r(\vartheta, \varphi) \cdot \sigma_{\text{HA}}^{\text{polyHA}}(\vartheta, \varphi) \cdot \mathbf{n}(\vartheta, \varphi, \psi), \quad (11)$$

where \mathbf{e}_r is the unit base vector in longitudinal direction, depending on Euler angles ϑ and φ , while for calculating the shear stress also, angle ψ , rotating around the longitudinal axis, is required, see (Scheiner et al. 2016b) for details. Considering that the stress tensor on the scale of a single hydroxyapatite crystal, $\sigma_{\text{HA}}^{\text{polyHA}}(\vartheta, \varphi)$ is actually a function of the macroscopic loading Σ_{congl} , according to the aforementioned downscaling scheme, the macroscopic stress tensor causing microscopic failure can be estimated. This macroscopic stress tensor is then consequently the elastic limit-type, macroscopic strength. For uniaxial compressive loading, only one stress component, denoted here as ultimate stress $\Sigma_{\text{congl}}^{\text{ult}}$, fully defines the macroscopic stress tensor leading to failure $f_{\text{HA}}=0$, see (Scheiner et al. 2016b) for further details.

3.3.5 Bone Regeneration Kinetics

Immersing the here discussed bone tissue engineering scaffold in a solution which sufficiently resembles the physiological one leads to (i) dissolution of the hydroxyapatite crystals and (ii) deposition of bone tissue on the granule surfaces. In order to take into account these effects in the model, two types of experimental studies are considered. On the one hand, histological studies allow for deducing a simple equation describing the increase of the bone tissue volume fraction over time, based on growth rate k_{grow} , thereby assuming linear increase of the bone shell radius. On the other hand, dissolution tests give access to a linear dissolution law, based on dissolution rate k_{diss} , thereby assuming constant dissolution. Details on these studies can be found in (Scheiner et al. 2016a).

3.3.6 Numerical Studies

Section 3.3 is concluded by numerical simulations showing how the micro-mechanical model can be utilized for assessing the mechanical performance of the bone tissue engineering scaffold material presented in Sect. 3.3.1. For this purpose, various model parameters must be defined; Table 1 summarizes these parameters, related to standard constituent configurations, standard physiological conditions, and standard processing conditions. Additionally, a crack density parameter of $\epsilon = 10$ is considered to represent a moderately cracked granule, and two initial macroporosities are assessed, namely $\phi_{\text{macro}}^{\text{congl}} = \{0.35, 0.45\}$. Corresponding evaluation of the model shows how the macroscopic porosities affect the developments of the macroscopic bulk modulus k_{congl} , the macroscopic shear modulus μ_{congl} , and the macroscopic ultimate stress for uniaxial loading $\Sigma_{\text{congl}}^{\text{ult}}$ over time, see Fig. 5. Apparently, bone regeneration leads to significantly changing mechanical properties. A higher initial value of the macroscopic porosities leads to lower initial mechanical properties, allows however for a higher regeneration capacity, as more bone tissue (which stiffer and stronger than the granules) can be formed until all pore space is filled by bone tissue – in Fig. 5, the kinks in the graphs representing $\phi_{\text{macro}}^{\text{congl}}$ related to completely filled macropores.

In order to highlight the effects of parameter variations, the results of four further sets of numerical simulations are included in this chapter, each of which is based on varying one specific parameter (in terms of physiologically and technologically reasonable lower and upper limit values), namely k_{grow} , k_{diss} , ϵ , $\phi_{\text{meso}}^{\text{gran}}$, while all other parameters are set as defined above. The considered parameter ranges are $k_{\text{grow}} = [4, 10] \mu\text{m}/\text{week}$, $k_{\text{diss}} = [0, 0.016] \text{w}^{-1}$, $\epsilon = [2, 10]$, and $\phi_{\text{meso}}^{\text{gran}} = [0.05, 0.3]$. The resulting, model-predicted temporal developments of k_{congl} , see Fig. 6, of μ_{congl} , see Fig. 7, and of $\Sigma_{\text{congl}}^{\text{ult}}$, see Fig. 8, underpin the benefits of rigorous multiscale modeling in the field of bone tissue engineering; variations of the considered parameters have significant effects on the mechanical properties, and the presented micromechanical model allows to quantitatively estimate their respective influence. For example, it turns out that the influence of the mesoporosity on the mechanical properties is negligible, whereas the crack density has a very pronounced impact.

Table 1 Summary of the model parameters needed for evaluation of the micromechanical model presented in Sect. 3.3

Parameter	Symbol, value, and unit	Reference
Microporosity	$\phi_{\text{micro}}^{\text{polyHA}} = 0.445$	(Dejaco et al. 2012)
Mesoporosity	$\phi_{\text{meso}}^{\text{gran}} = 0.189$	(Dejaco et al. 2012)
Young's modulus of hydroxyapatite	$E_{\text{HA}} = 114 \text{ GPa}$	(Hellmich and Ulm 2002; Hellmich et al. 2004)
Poisson's ratio of hydroxyapatite	$\nu_{\text{HA}} = 0.27$	(Hellmich and Ulm 2002; Hellmich et al. 2004)
Stiffness tensor of micropores	$\mathbb{C}_{\text{micro}\phi} = 0$	(Thompson and Willis 1991)
Stiffness tensor of mesopores	$\mathbb{C}_{\text{meso}\phi} = 0$	(Thompson and Willis 1991)
Stiffness tensor of macropores	$\mathbb{C}_{\text{macro}\phi} = 0$	(Thompson and Willis 1991)
Components of bone tissue stiffness tensor	$C_{\text{bone},rrrr} = 15.90 \text{ GPa}$	(Scheiner et al. 2016a)
	$C_{\text{bone},\theta\theta\theta\theta} = 21.74 \text{ GPa}$	(Scheiner et al. 2016a)
	$C_{\text{bone},\phi\phi\phi\phi} = 21.74 \text{ GPa}$	(Scheiner et al. 2016a)
	$C_{\text{bone},rr\theta\theta} = 9.00 \text{ GPa}$	(Scheiner et al. 2016a)
	$C_{\text{bone},rr\phi\phi} = 9.00 \text{ GPa}$	(Scheiner et al. 2016a)
	$C_{\text{bone},\theta\theta\phi\phi} = 10.70 \text{ GPa}$	(Scheiner et al. 2016a)
	$C_{\text{bone},\theta\phi\theta\phi} = 5.52 \text{ GPa}$	(Scheiner et al. 2016a)
	$C_{\text{bone},r\phi r\phi} = 3.97 \text{ GPa}$	(Scheiner et al. 2016a)
	$C_{\text{bone},r\theta r\theta} = 3.97 \text{ GPa}$	(Scheiner et al. 2016a)
Shear strength of hydroxapatite	$\sigma_{\text{HA}}^{\text{ult},s} = 80.3 \text{ MPa}$	(Fritsch et al. 2009a)
Tensile strength of hydroxapatite	$\sigma_{\text{HA}}^{\text{ult},t} = 52.2 \text{ MPa}$	(Fritsch et al. 2009a)
Growth rate of bone tissue	$k_{\text{grow}} = 7 \pm 3 \mu\text{m/week}$	(Scheiner et al. 2016a)
Dissolution rate of hydroxapatite	$k_{\text{res}} = 0.008 \text{ w}^{-1}$	(Scheiner et al. 2016a)

The presented homogenization scheme can be used to work out particularly beneficial parameter combinations, leading to, for example, desired stiffness or strength developments over time, see (Scheiner et al. 2016a) for details. This way, computer simulations can provide recommendations for the manufacturing process, for example, in terms of the packing density of granules, the addition of growth factors leading to increasing bone growth rate, the reduction of cracks, or the attainment of specific micro- and mesoporosities.

4 Concluding Remarks and Outlook

Besides giving an overview of different types of mathematical models applicable for estimation of the performance of bone tissue engineering materials and structures, the two major focal points of this chapter were, on the one hand, introducing the concept of continuum micromechanical homogenization techniques, and, on the

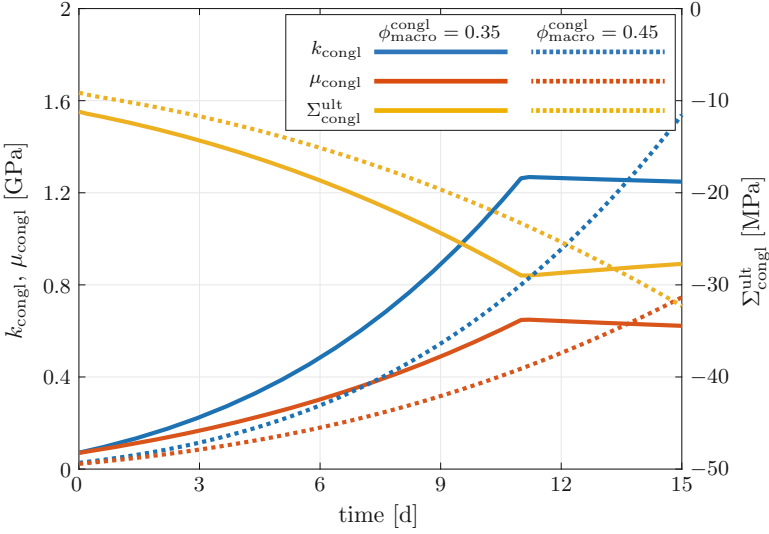


Fig. 5 Model-predicted temporal developments of macroscopic bulk modulus k_{congl} , shear modulus μ_{congl} , and ultimate stress $\Sigma_{\text{congl}}^{\text{ult}}$ for initial macroscopic porosities $\phi_{\text{macro}}^{\text{congl}} = \{0.35, 0.45\}$

other hand, pointing out the benefits of rigorous multiscale modeling (by the example of a hierarchically organized, hydroxyapatite-based granular bone tissue engineering material). On the material level, multiscale modeling is a highly efficient, physically well substantiated, and, in terms of the quality of the model predictions, reliable mathematical tool, as demonstrated in Sect. 3.3. On this basis, a multitude of variations of the material-defining parameters can be studied *in silico*, in order to work out the ideal combination of parameters which can be used as basis for the design of the tissue engineering scaffold. Furthermore, such multiscale model can be easily coupled to structural models, for studying the mechanical behavior (e.g., in terms of material failure) in the context of bone organs with bone defects, with the latter being filled up by a biomaterial.

One major future research direction could be adding another conceptual dimension to the presented modeling strategy, i.e., replacing the empirical equations that are taking into account the effects of bone regeneration by suitable systems biology models. For example, a recently proposed, coupled micromechanics/systems biology approach (Scheiner et al. 2013; Pastrama et al. 2018) allows to predict the progress of bone remodeling driven by both biochemical and biomechanical stimuli.

In conclusion, multiscale modeling can provide otherwise not available information concerning the expected mechanical performance of biomaterials in general and of bone tissue engineering scaffolds in particular. Making use of this information could significantly increase the efficiency of manufacturing by means of 3D printing and biofabrication. Further promoting mathematical modeling as complementing technology in bone tissue engineering is thus a desirable goal for the future.

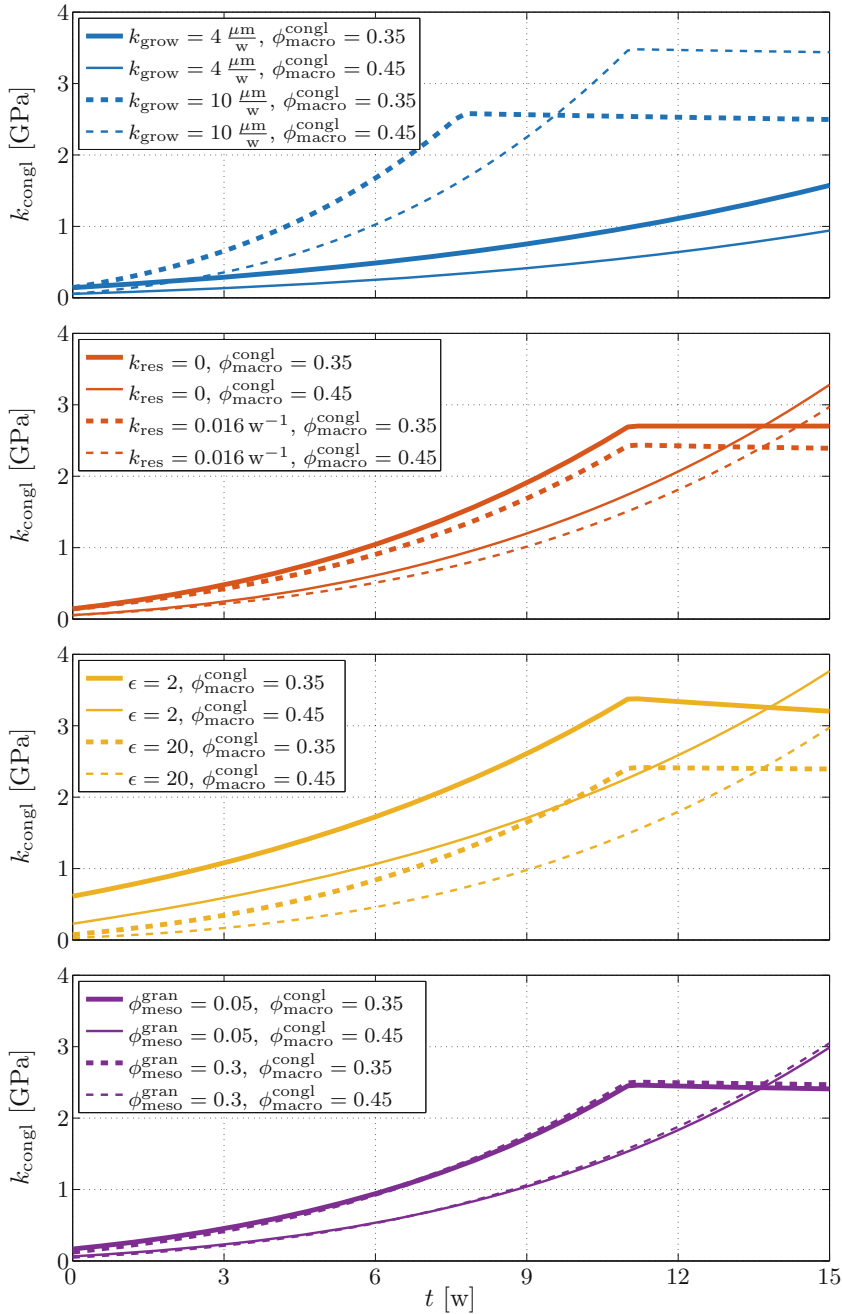


Fig. 6 Numerical studies highlighting the influences the bone growth rate k_{grow} , the hydroxyapatite resorption rate k_{res} , the crack density parameter, and the mesoporosity $\phi_{\text{meso}}^{\text{gran}}$, each for two initial macroporosities, on the model-predicted macroscopic bulk modulus k_{congl}

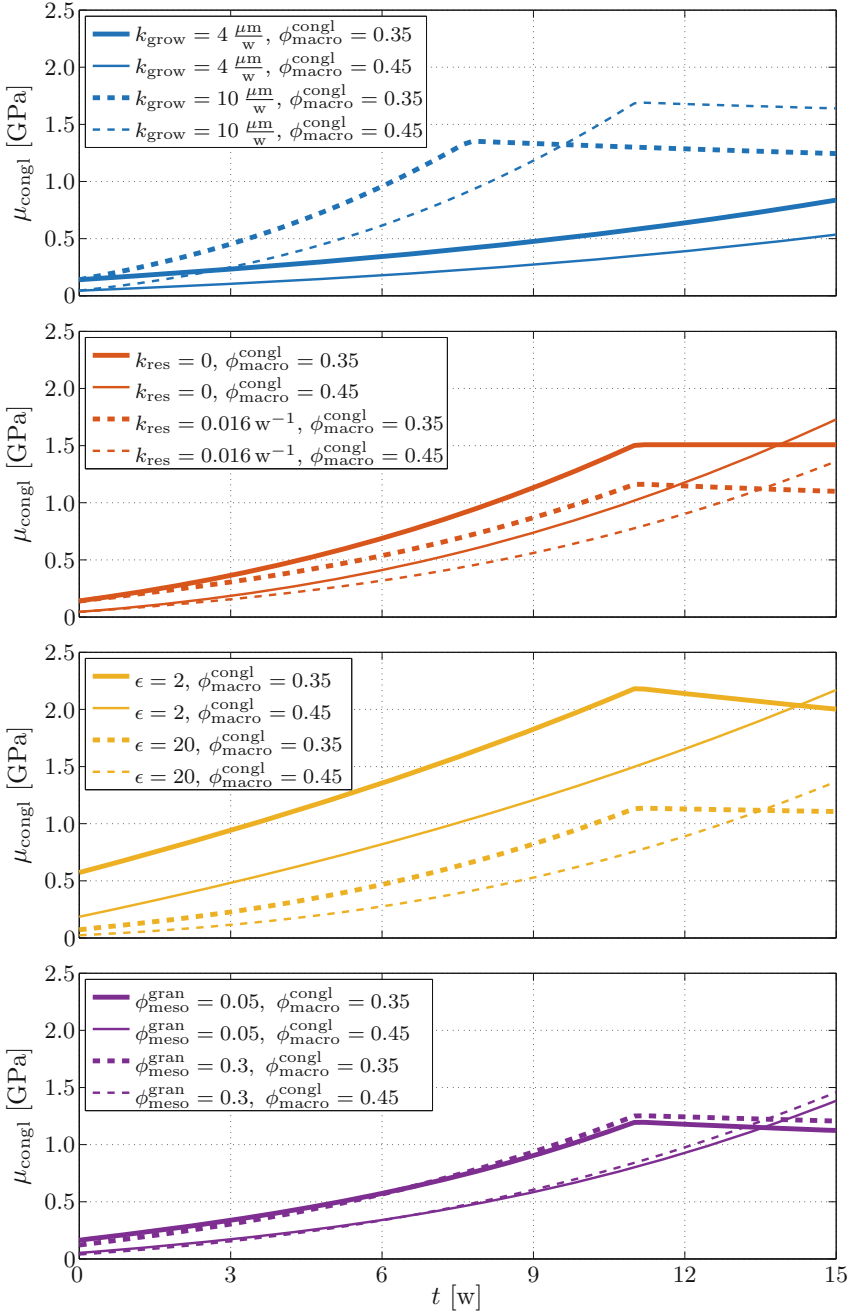


Fig. 7 Numerical studies highlighting the influences the bone growth rate k_{grow} , the hydroxyapatite resorption rate k_{res} , the crack density parameter, and the mesoporosity $\phi_{\text{meso}}^{\text{gran}}$, each for two initial macroporosities, on the model-predicted macroscopic shear modulus μ_{congl}

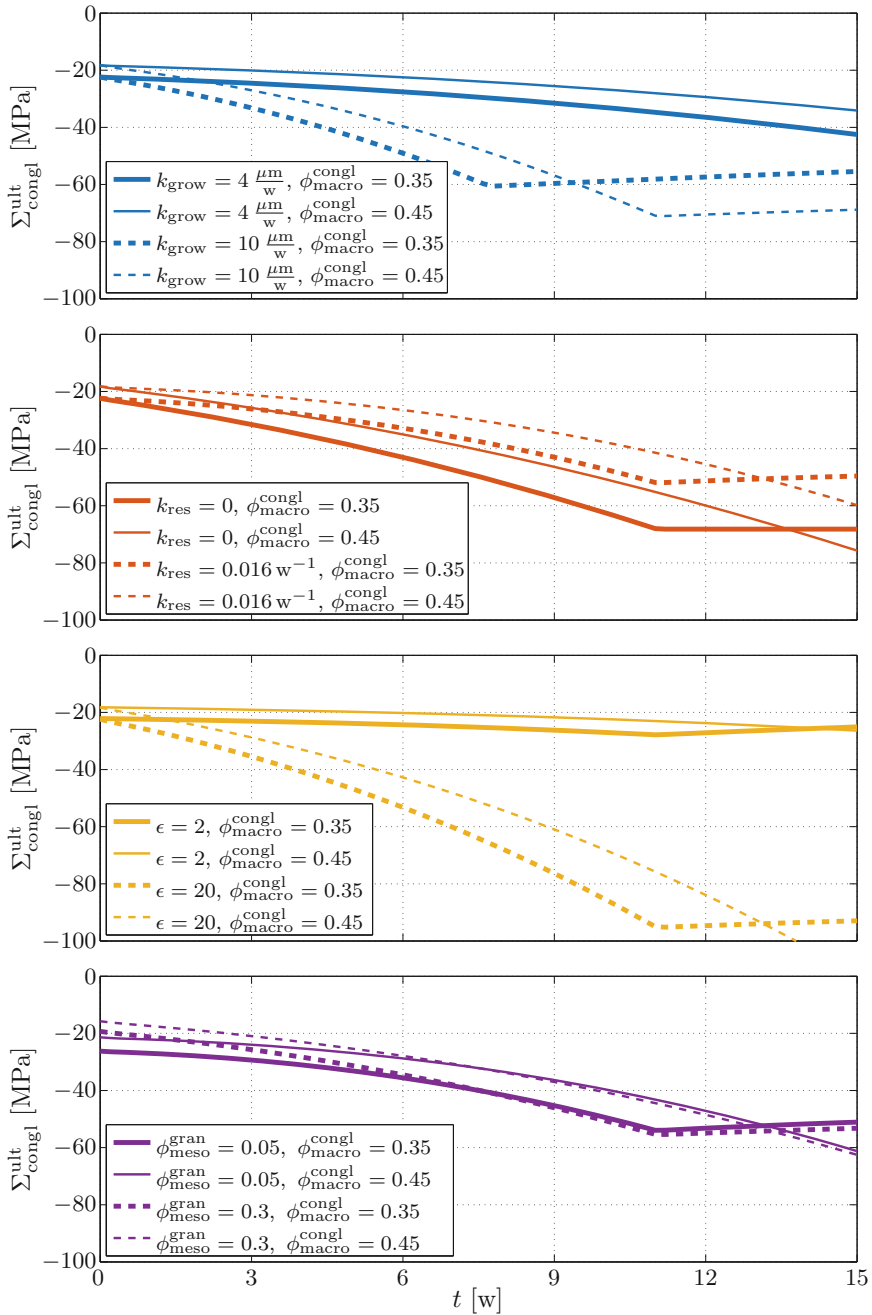


Fig. 8 Numerical studies highlighting the influences the bone growth rate k_{grow} , the hydroxyapatite resorption rate k_{res} , the crack density parameter, and the mesoporosity ϕ_{meso}^{gran} , each for two initial macroporosities, on the model-predicted macroscopic ultimate stress Σ_{congl}^{gran}

Acknowledgments In the context of the research presented in Sect. 3.3 of this chapter, the partial financial support by the European Research Council (ERC), in the framework of the project *Multiscale poromicromechanics of bone materials, with links to biology and medicine* (project number FP7-257023), as well as the partial financial support by the Russian Science Foundation (grant number 15-13-00108), are gratefully acknowledged. Furthermore, COST-action MP1005, *NAMABIO – From nano to macro biomaterials (design, processing, characterization, modeling) and applications to stem cells regenerative orthopedic and dental medicine* has provided means for a sustainable collaboration over several years.

References

- Adachi T, Osako Y, Tanaka M, Hojo M, Hollister SJ (2006) Framework for optimal design of porous scaffold microstructure by computational simulation of bone regeneration. *Biomaterials* 27(21):3964–3972
- Akao M, Aoki H, Kato K (1981) Mechanical properties of sintered hydroxyapatite for prosthetic applications. *J Mater Sci* 16(3):809–812
- Amini AR, Laurencin CT, Nukavarapu SP (2012) Bone tissue engineering: recent advances and challenges. *Crit Rev Biomed Eng* 40(5):363–408
- Bertrand E, Hellmich C (2009) Multiscale elasticity of tissue engineering scaffolds with tissue-engineered bone: a continuum micromechanics approach. *J Eng Mech (ASCE)* 135(5):395–412
- Bose S, Roy M, Bandyopadhyay A (2012) Recent advances in bone tissue engineering scaffolds. *Trends Biotechnol* 30(10):546–554
- Bose S, Vahabzadeh S, Bandyopadhyay A (2013) Bone tissue engineering using 3D printing. *Mater Today* 16(12):496–504
- Botchwey EA, Pollack SR, Levine EM, Johnston ED, Laurencin CT (2004) Quantitative analysis of three-dimensional fluid flow in rotating bioreactors for tissue engineering. *J Biomed Mater Res A* 69A(2):205–215
- Budiansky B, O’Connell RJ (1976) Elastic moduli of a cracked solid. *Int J Solids Struct* 12(2):81–97
- Chung CA, Chen CW, Chen CP, Tseng CS (2007) Enhancement of cell growth in tissue-engineering constructs under direct perfusion: modeling and simulation. *Biotechnol Bioeng* 97(6):1603–1616
- Czenek A, Blanchard R, Dejaco A, Sigurjónsson ÓE, Örylgsson G, Gargiulo P, Hellmich C (2014) Quantitative intravoxel analysis of micro-CT-scanned resorbing ceramic biomaterials – perspectives for computer-aided biomaterial design. *J Mater Res* 29(23):2757–2772
- Dejaco A, Komlev VS, Jaroszewicz J, Swieszkowski W, Hellmich C (2012) Micro CT-based multiscale elasticity of double-porous (pre-cracked) hydroxyapatite granules for regenerative medicine. *J Biomech* 45(6):1068–1075
- Deudé V, Dormieux L, Kondo D, Maghous S (2002) Micromechanical approach to nonlinear poroelasticity: application to cracked rocks. *J Eng Mech (ASCE)* 128(8):848–855
- Dias MR, Fernandes PR, Guedes JM, Hollister SJ (2012) Permeability analysis of scaffolds for bone tissue engineering. *J Biomech* 45(6):938–944
- Dormieux L, Lemarchand E, Kondo D, Fairbairn E (2004) Elements of poromicromechanics applied to concrete. *Mater Struct/Concr Sci Eng* 37(265):31–42
- Dormieux L, Kondo D, Ulm F-J (2006) *Microporomechanics*. Wiley, Chichester
- Drugan WR, Willis JR (1996) A micromechanics-based nonlocal constitutive equation and estimates of representative volume element size for elastic composites. *J Mech Phys Solids* 44(4):497–524
- Engh CA, Bobyn JD, Glassman AH (1987) Porous-coated hip replacement. The factors governing bone ingrowth, stress shielding, and clinical results. *Bone Joint J* 69-B(1):45–55

- Fritsch A, Hellmich C (2007) 'Universal' microstructural patterns in cortical and trabecular, extracellular and extravascular bone materials: micromechanics-based prediction of anisotropic elasticity. *J Theor Biol* 244(4):597–620
- Fritsch A, Dormieux L, Hellmich C (2006) Porous polycrystals built up by uniformly and axisymmetrically oriented needles: homogenization of elastic properties. *C R Méc* 334(3):151–157
- Fritsch A, Dormieux L, Hellmich C, Sanahuja J (2007) Micromechanics of crystal interfaces in polycrystalline solid phases of porous media: fundamentals and application to strength of hydroxyapatite biomaterials. *J Mater Sci* 42(21):8824–8837
- Fritsch A, Dormieux L, Hellmich C, Sanahuja J (2009a) Mechanical behavior of hydroxyapatite biomaterials: an experimentally validated micromechanical model for elasticity and strength. *J Biomed Mater Res – Part A* 88A(1):149–161
- Fritsch A, Hellmich C, Dormieux L (2009b) Ductile sliding between mineral crystals followed by rupture of collagen crosslinks: experimentally supported micromechanical explanation of bone strength. *J Theor Biol* 260(2):230–252
- Fritsch A, Hellmich C, Dormieux L (2010) The role of disc-type crystal shape for micromechanical predictions of elasticity and strength of hydroxyapatite biomaterials. *Philos Trans R Soc Lond A* 368:1913–1935
- Fritsch A, Hellmich C, Young P (2013) Micromechanics-derived scaling relations for poroelasticity and strength of brittle porous polycrystals. *J Appl Mech (ASME)* 80(2):020905
- Geris L (2013) Computational modeling in tissue engineering, *Studies in mechanobiology, tissue engineering and biomaterials*, vol 10. Springer, Berlin/Heidelberg
- Gilmore RS, Katz JL (1982) Elastic properties of apatites. *J Mater Sci* 17(4):1131–1141
- Hellmich C, Ulm F-J (2002) Micromechanical model for ultra-structural stiffness of mineralized tissues. *J Eng Mech (ASCE)* 128(8):898–908
- Hellmich C, Ulm F-J, Dormieux L (2004) Can the diverse elastic properties of trabecular and cortical bone be attributed to only a few tissue-independent phase properties and their interactions? - arguments from a multiscale approach. *Biomech Model Mechanobiol* 2(4):219–238
- Hervé E, Zaoui A (1993) n-Layered inclusion-based micromechanical modelling. *Int J Eng Sci* 31(1):1–10
- Hill R (1963) Elastic properties of reinforced solids: some theoretical principles. *J Mech Phys Solids* 11(5):357–372
- Hollister SJ (2005) Porous scaffold design for tissue engineering. *Nat Mater* 4(7):518–524
- Hutmacher DW (2000) Scaffolds in tissue engineering bone and cartilage. *Biomaterials* 21(24):2529–2543
- Hutmacher DW, Singh H (2008) Computational fluid dynamics for improved bioreactor design and 3D culture. *Trends Biotechnol* 26(4):166–172
- Jacobs CR, Temiyasathit S, Castillo AB (2010) Osteocyte mechanobiology and pericellular mechanics. *Annu Rev Biomed Eng* 12:369–400
- Jacques SVN, Van Oosterwyck H, Muraru L, Van Cleynenbreugel T, De Smet E, Wevers M, Naert I, Vander Sloten J (2004) Individualised, micro CT-based finite element modelling as a tool for biomechanical analysis related to tissue engineering of bone. *Biomaterials* 25(9):1683–1696
- Katz JL, Ukraincik K (1971) On the anisotropic elastic properties of bone. *Calcif Tissue Int* 4(3):221–227
- Kohlhauser C, Hellmich C (2013) Ultrasonic contact pulse transmission for elastic wave velocity and stiffness determination: influence of specimen geometry and porosity. *Eng Struct* 47:115–133
- Komlev VS, Barinov SM, Koplík EV (2002) A method to fabricate porous spherical hydroxyapatite granules intended for time-controlled drug release. *Biomaterials* 23(16):3449–3454
- Komlev VS, Barinov SM, Girardin E, Oscarsson S, Rosengren A, Rustichelli F, Orlovskii VP (2003) Porous spherical hydroxyapatite and fluorhydroxyapatite granules: processing and characterization. *Sci Technol Adv Mater* 4(6):503–508

- Lacroix D, Chateau A, Ginebra M-P, Planell JA (2006) Micro-finite element models of bone tissue-engineering scaffolds. *Biomaterials* 27(30):5326–5334
- Lacroix D, Planell JA, Prendergast PJ (2009) Computer-aided design and finite element modelling of biomaterial scaffolds for bone tissue engineering. *Philos Trans R Soc London, Ser A* 367(1895):1993–2009
- Langer R, Tirrell DA (2004) Designing materials for biology and medicine. *Nature* 428(6982):487–492
- Li X, Wang L, Fan Y, Feng Q, Cui F-Z, Watari F (2013) Nanostructured scaffolds for bone tissue engineering. *J Biomed Mater Res A* 101A(8):2424–2435
- Luczynski K, Dejaco A, Lahayne O, Jaroszewicz J, Swieszkowski W, Hellmich C (2012) MicroCT/micromechanics-based finite element models and quasi-static unloading tests deliver consistent values for Young's modulus of rapid-prototyped polymer-ceramic tissue engineering scaffold. *CMES – Comput Model Eng Sci* 87(6):505–529
- Melchels FPW, Bertoldi K, Gabbriellini R, Velders AH, Feijen J, Grijpma DW (2010) Mathematically defined tissue engineering scaffold architectures prepared by stereolithography. *Biomaterials* 31(27):6909–6916
- Milan J-L, Planell JA, Lacroix D (2009) Computational modelling of the mechanical environment of osteogenesis within a polylactic acid–calcium phosphate glass scaffold. *Biomaterials* 30(25):4219–4226
- Morin C, Vass V, Hellmich C (2017) Micromechanics of elastoplastic porous polycrystals: theory, algorithm, and application to osteonal bone. *Int J Plast* 91:238–267
- Olivares AL, Marsal É, Planell JA, Lacroix D (2009) Finite element study of scaffold architecture design and culture conditions for tissue engineering. *Biomaterials* 30(30):6142–6149
- Pastrama MI, Scheiner S, Pivonka P, Hellmich C (2018) A mathematical multiscale model of bone remodeling, accounting for pore space-specific mechanosensation. *Bone* 107: 208–221
- Porter B, Zauel R, Stockman H, Guldberg R, Fyhrie D (2005) 3-D computational modeling of media flow through scaffolds in a perfusion bioreactor. *J Biomech* 38(3):543–549
- Porter JR, Ruckh TT, Popat KC (2009) Bone tissue engineering: a review in bone biomimetics and drug delivery strategies. *Biotechnol Prog* 25(6):1539–1560
- Rezwan K, Chen QZ, Blaker JJ, Boccaccini AR (2006) Biodegradable and bioactive porous polymer/inorganic composite scaffolds for bone tissue engineering. *Biomaterials* 27(18):3413–3431
- Robling AG, Castillo A, Turner CH (2006) Biomechanical and molecular regulation of bone remodeling. *Annu Rev Biomed Eng* 8:455–498
- Sandino C, Lacroix D (2011) A dynamical study of the mechanical stimuli and tissue differentiation within a cap scaffold based on micro-ct finite element models. *Biomech Model Mechanobiol* 10(4):565–576
- Sandino C, Planell JA, Lacroix D (2008) A finite element study of mechanical stimuli in scaffolds for bone tissue engineering. *J Biomech* 41(5):1005–1014
- Sanz-Herrera JA, García-Aznar JM, Doblaré M, Micro-macro M (2008) Numerical modelling of bone regeneration in tissue engineering. *Comput Methods Appl Mech Eng* 197(33–40):3092–3107
- Sanz-Herrera JA, García-Aznar JM, Doblaré M (2009a) On scaffold designing for bone regeneration: a computational multiscale approach. *Acta Biomater* 5(1):219–229
- Sanz-Herrera JA, García-Aznar JM, Doblaré M (2009b) A mathematical approach to bone tissue engineering. *Philos Trans R Soc London, Ser A* 367(1895):2055–2078
- Scheiner S, Sinibaldi R, Pichler B, Komlev V, Renghini C, Vitale-Brovarone C, Rustichelli F, Hellmich C (2009) Micromechanics of bone tissue-engineering scaffolds, based on resolution error-cleared computer tomography. *Biomaterials* 30(12):2411–2419
- Scheiner S, Pivonka P, Hellmich C (2013) Coupling systems biology with multi-scale mechanics, for computer simulations of bone remodeling. *Comput Methods Appl Mech Eng* 254:181–196
- Scheiner S, Komlev VS, Gurin AN, Hellmich C (2016a) Multiscale mathematical modeling in dental tissue engineering: towards computer-aided design of a regenerative system based

- on hydroxyapatite granules, focusing on early and mid-term stiffness recovery. *Front Physiol* 7 (383):1–18
- Scheiner S, Komlev VS, Hellmich C (2016b) Strength increase during ceramic biomaterial-induced bone regeneration: a micromechanical study. *Int J Fract* 202(2):217–235
- Shareef MY, Messer PF, van Noort R (1993) Fabrication, characterization and fracture study of a machinable hydroxyapatite ceramic. *Biomaterials* 14(1):69–75
- Simmons CA, Meguid SA, Pilliar RM (2001) Differences in osseointegration rate due to implant surface geometry can be explained by local tissue strains. *J Orthop Res* 19(2):187–194
- Sturm S, Zhou S, Mai Y-W, Li Q (2010) On stiffness of scaffolds for bone tissue engineering – a numerical study. *J Biomech* 43(9):1738–1744
- Thompson M, Willis JR (1991) A reformation of the equations anisotropic elasticity. *J Appl Mech* 58(3):612–616
- Truscello S, Kerckhofs G, Van Bael S, Pyka G, Schrooten J, Van Oosterwyck H (2012) Prediction of permeability of regular scaffolds for skeletal tissue engineering: a combined computational and experimental study. *Acta Biomater* 8(4):1648–1658
- van Gaalen S, Kruyt M, Meijer G, Mistry A, Mikos A, van den Beucken J, Jansen J, de Groot K, Cancedda R, Olivo C, Yaszemski M, Dhert W (2008) Chapter 19. Tissue engineering of bone. In: Van Blitterswijk C, Thomsen P, Lindahl A, Hubbell J, Williams DF, Cancedda R, de Bruijn JD, Sohier J (eds) *Tissue Engineering*. Academic, Burlington, pp 559–610
- Voronov R, VanGordon S, Sikavitsas VI, Papavassiliou DV (2010) Computational modeling of flow-induced shear stresses within 3D salt-leached porous scaffolds imaged via micro-ct. *J Biomech* 43(7):1279–1286
- Williams DF (2008) On the mechanisms of biocompatibility. *Biomaterials* 29(20):2941–2953
- Williams JM, Adewunmi A, Schek RM, Flanagan CL, Krebsbach PH, Feinberg SE, Hollister SJ, Das S (2005) Bone tissue engineering using polycaprolactone scaffolds fabricated via selective laser sintering. *Biomaterials* 26(23):4817–4827
- Zaoui A (1997) Chapter 6. Structural morphology and constitutive behavior of microheterogeneous materials. In: Suquet PM (ed) *Continuum micromechanics, CISM courses and lectures*, vol 377. Springer, Wien/New York, pp 291–347
- Zaoui A (2002) Continuum micromechanics: survey. *J Eng Mech (ASCE)* 128(8):808–816



Quality Control of 3D Printed Resorbable Implants: The 3D Printed Airway Splint Example

Scott J. Hollister, Sarah Jo Crotts, Harsha Ramaraju,
Colleen L. Flanagan, David A. Zopf, Robert J. Morrison, Andrea Les,
Richard G. Ohye, and Glenn E. Green

Contents

1	Introduction	132
2	Interpreting Design Control for 3D Printed Patient-Specific Devices	133
3	Phase I: Design Inputs and Development Planning	134
3.1	Phase IA: User Needs, Clinical Objectives, and Clinical Design Hypothesis	135
3.2	Phase IB: Design Inputs and Risk Analysis	137
3.3	Phase IC: Development Planning	147
4	Phase II: Design and Manufacturing Processes	147
4.1	Phase IIA: Design Model Process	147
4.2	Phase IIB: Design Model Output (DMO)	148
4.3	Phase IIC: 3D Printing (Laser Sintering) Splints	149

S. J. Hollister (✉) · S. J. Crotts · H. Ramaraju
Center for 3D Medical Fabrication and Walter H. Coulter Department of Biomedical Engineering,
Georgia Institute of Technology and Emory University, Atlanta, GA, USA
e-mail: scott.hollister@bme.gatech.edu; scottho@umich.edu; sarah.crotts@bme.gatech.edu;
harsha.ramaraju@gatech.edu

C. L. Flanagan
Department of Biomedical Engineering, The University of Michigan, Ann Arbor, MI, USA
e-mail: flanagan@umich.edu

D. A. Zopf · R. J. Morrison · A. Les · G. E. Green
Department of Otolaryngology Head and Neck Surgery, The University of Michigan, Ann Arbor,
MI, USA
e-mail: davidzop@med.umich.edu; robert.j.morrison@vanderbilt.edu; asles@med.umich.edu;
gegreen@med.umich.edu

R. G. Ohye
Department of Cardiac Surgery, The University of Michigan, Ann Arbor, MI, USA
Division of Cardiology, Department of Pediatrics, Ann Arbor, MI, USA
e-mail: ohye@med.umich.edu

5	Phase III: Testing, Design Verification, and Design Validation	151
5.1	Phase IIIA: Design Device Outputs and Design Verification	153
5.2	Phase IIIB: Design Validation	155
6	Conclusions and Future Directions	157
	References	159

Abstract

3D printing combined with design using patient image data has enabled the development of patient-specific devices. This is especially true for smaller commercial entities and academic groups due to the lower barriers for 3D printing as a manufacturing method. Such patient-specific devices can significantly advance patient care but also face significant hurdles to ensure quality since (1) the devices are built in small lots for specific niche patient markets, (2) there is inherent variability in design parameters to match specific patient anatomy and function, and (3) nontraditional groups now have the capability to readily manufacture medical devices. Following the design control paradigm with specific attention to 3D printing idiosyncrasies is one path to address quality issues in patient-specific design. We present in this chapter an example of a design control approach for quality control of 3D patient-specific devices using a recently developed airway splint as a paradigmatic example for small lot 3D printed patient-specific devices.

1 Introduction

3D printing has enabled new implantable biomaterial and combination (i.e., biomaterial plus biologic) devices tailored to individual patient needs, denoted as *patient-specific* devices. 3D printed patient-specific devices may revolutionize medical devices by matching patient anatomic and functional needs at economically feasible manufacturing costs. Most importantly, 3D printing allows production of patient-specific devices at similar prices for one to thousands of devices, making it possible to address the needs of limited patient populations that occur in so-called orphan conditions. However, ensuring device quality, device efficacy, and patient safety in a device that can change for every patient is challenging.

Regulatory agencies around the world are trying to balance the enormous innovative potential of 3D printed patient-specific devices with these quality, safety, and efficacy challenges. The US Food and Drug Administration (FDA) has recently issued specific guidance on Additive Manufacturing of Medical Devices (<https://www.fda.gov/downloads/MedicalDevices/DeviceRegulationandGuidance/GuidanceDocuments/UCM499809.pdf>). This guidance document provides a general overview of issues to consider in the quality control for 3D printing of patient-specific medical devices (note: this document uses “patient-specific” as synonymous with “patient-matched” nomenclature from the FDA. However, it is critical to note that neither term is synonymous with a customized device. Custom device has a specific approval pathway and criteria, including a limitation of five devices per year).

Although the Additive Manufacturing guidance gives some insights, it must be combined with the more general FDA design control process (<https://www.fda.gov/RegulatoryInformation/Guidances/ucm070627.htm>) to better address 3D printed patient-specific device quality issues. The FDA design control process was developed to improve medical device quality by specifying design, verification, and validation steps to prove as much as possible that a medical device fulfills its design requirements and by fulfilling these requirements mitigates the target clinical condition. The FDA only specifies that steps of the design process must be followed and documented; it does not dictate how the manufacturer should implement each step for its specific device.

While the open-ended design control process provides significant flexibility, it can also be daunting in terms of developing the proper implementation to achieve regulatory approval. Furthermore, the nature of 3D printing makes it possible for academic groups to develop and manufacture implantable devices without the significant infrastructure that is the domain of large medical device companies. Such academic groups typically operate under research paradigms that differ significantly from the design control processes necessary for quality control, although there is increasing recognition that academic research processes must incorporate design and quality control if translation from academic environments is to be more successful (Duda et al. 2014; Volk et al. 2015).

While medical device companies naturally hold their design control processes proprietary, given the open nature of academic translation and the new paradigm of 3D printed patient-specific devices, more open design control processes for these devices will need to be published, reviewed, and debated. Such open examples of 3D printed patient-specific design control will become increasingly critical as non-traditional point-of-care (POC) manufacturers including academic medical centers, regional hospitals, and even maker space foundations and crowd source movements like the Enable Foundation (<http://enablingthefuture.org/>) develop and 3D print patient-specific medical devices and implants. The goal of this chapter is to provide an example of design and quality control for a 3D printed, patient-specific implant, an airway splint successfully used to treat nine patients with life-threatening tracheobronchial malacia (Zopf et al. 2013; Morrison et al. 2015; Hollister et al. 2015, 2017a). This chapter presents implementation of portions of splint design control process, as well as those that are underway and proposed for implementation. It will also discuss open questions to address to improve the design control process for 3D printed patient-specific devices. For full disclosure, it is important to note that while the authors have had discussions with the FDA, many of the proposed implementations for 3D printed patient-specific design control are the authors' own thoughts and do not represent the opinions of nor have been vetted by the FDA.

2 Interpreting Design Control for 3D Printed Patient-Specific Devices

Design control is a process required by the FDA for medical device approval and implemented to reduce device recalls and adverse effects on patients due to design and/or manufacturing flaws. Design control proceeds from definition of device

design inputs to final testing of the device in preclinical and clinical environments. Depending on the device approval pathway, a 510 K approval may require only preclinical testing, while a Humanitarian Device Exemption (HDE) or Pre-Market Approval (PMA) pathway for a class III device would require both preclinical and clinical testing. Critical components of the design control process are definition of *design inputs* (i.e., design requirements), proving that the device as manufactured meets the design inputs through a variety of tests and measurements (the measurements are termed *design outputs*; the process of matching design outputs is termed *design verification*) and showing the device mitigates the clinical condition as hypothesized through preclinical and clinical testing (termed *design validation*). The well-known “waterfall” schematic represents entire design control process (<https://www.fda.gov/RegulatoryInformation/Guidances/ucm070627.htm>).

A critical component of design control is the design and manufacturing processes that will convert design inputs into a final device. This is in reality the heart of the matter, as how well a device will fulfill its desired purpose depends on the design and subsequently how well that design can be created in material. The classic design control waterfall schematic (<https://www.fda.gov/RegulatoryInformation/Guidances/ucm070627.htm>) represents the entire design and manufacturing process as a generic “design process,” because of course the document is applied to a plethora of design and manufacturing techniques. However, our implementation will specifically concern image-based patient-specific design and 3D printing (PCL laser sintering), so we have modified the waterfall schematic to include these specific design and manufacturing processes in addition to related design input definition, processes, and validation testing (Fig. 1).

This modified Design Control waterfall consists of three major phases: Phase (1) design inputs/planning (i.e., device definition and concept), Phase (2) design/manufacturing processes (i.e., conversion of the device idea into an actual device), and Phase (3) device testing/verification/validation (i.e., confirmation that the device meets design requirements and mitigates the clinical/disease state). We will demonstrate the implementation of each step using the 3D printed resorbable PCL airway splint as a paradigm.

3 Phase I: Design Inputs and Development Planning

The first part of any medical device development is defining the user needs and then hypothesizing how a device may meet those user needs. This clinical design hypothesis is translated into testable design inputs that define the device. Design inputs must also account for risk to the patient should the device as conceived fail, and additional considerations must be designed to mitigate perceived risks. Rigorously defining design inputs is critical for creating a quality device and efficient engineering process, as design inputs are directly determine the Phase II design/manufacturing processes and the Phase III testing/verification/validation.

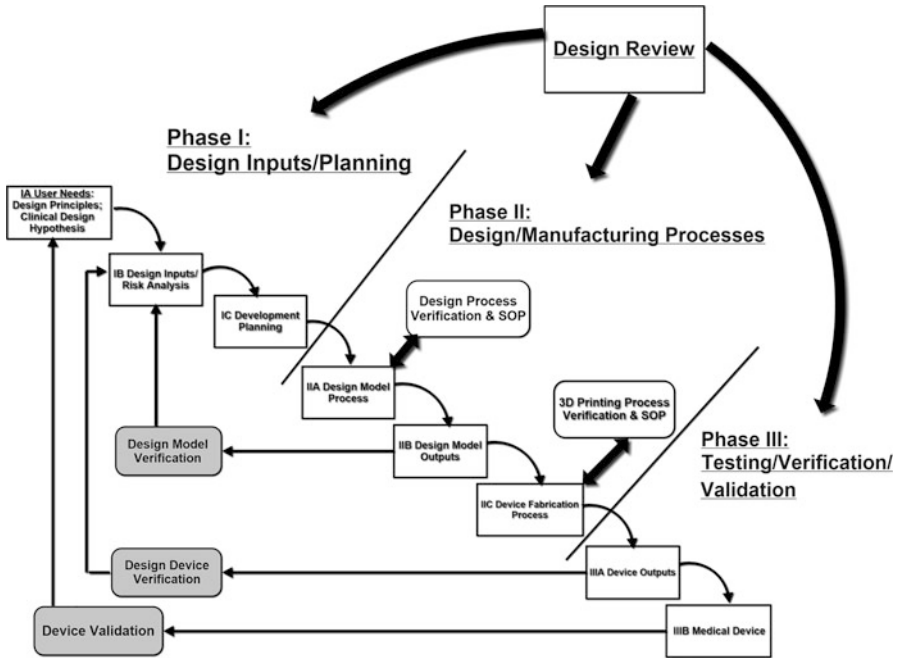


Fig. 1 The modified design control waterfall schematic for 3D printed patient-specific devices. The schematic consists of three major parts: (1) design inputs/planning (device conception), (2) design/manufacturing processes (conversion of device concept to actual device through image-based design and 3D printing), and (3) testing, verification, and validation to ensure the created device meets design inputs and mitigates the clinical condition in preclinical and clinical testing. Design review in the upper right-hand corner indicates that every step of the process must be reviewed in formal meetings and this review must be documented

3.1 Phase IA: User Needs, Clinical Objectives, and Clinical Design Hypothesis

Any medical device starts out as a problem to be solved. This problem arises from user needs, primarily the patient who has a clinical condition to be treated. The problem also is defined by the physician or other healthcare provider who must have a tool that can be used efficiently and easily to address the patients’ clinical condition. Therefore, it is critical to start by defining as thoroughly as possible the clinical condition, the etiology behind the clinical condition, and the impact of the clinical condition on the patient. A thorough definition of the clinical condition will suggest idealized clinical objectives to mitigate the clinical condition. These clinical objectives must be distilled into quantitative design inputs and associated risks.

The bioresorbable airway splint is designed to mitigate tracheobronchomalacia (TBM). TBM is defined as a condition in which tracheal and/or bronchial segment cross-sectional areas are reduced by more than 50% during exhalation. TBM may occur independently or be associated with external vascular compression (such as innominate

artery compression, aortic compression, vascular rings, or pulmonary slings), esophageal atresia, or tracheal surgery. It leads to a wide array of respiratory symptoms which can range from a chronic cough and/or wheezing with vigorous activity to life-threatening apnea. The estimated incidence of congenital tracheomalacia is 1 in 2,600 children (Boogaard et al. 2005) although life-threatening cases are rarer.

It is widely believed that vascular compression, tracheal surgery, and other etiologies cause TBM by inhibiting cartilage ring development or damaging developed cartilage rings (Javia and Harris 2016; Kugler and Stanzel 2014; Fraga et al. 2016; Hysinger and Panitch 2016). The consequential reduction in airway tissue nonlinear elastic properties leads to weakened walls that excessively deform under negative pressure during exhalation. Hollister et al. (2017b) performed nonlinear finite element modeling to determine that snap through instability may lead to sudden complete airway collapse seen in life-threatening TBM. Even if the TBM airway can be protected and grows geometrically, if there is no simultaneous remodeling and stiffening of airway properties during growth (Bucher and Reid 1961; Penn et al. 1989; Doras et al. 1991), the computational modeling results (Hollister et al. 2017b) suggest the risk for severe TBM may actually increase. It is critical to note that there is no published experimental data on malacic airway nonlinear elastic properties and very little data on airway nonlinear elastic properties in general. This type of uncertainty (i.e., lack of experimental data on not only airway mechanical properties but also airway growth and remodeling) plagues a significant part of design input generation and is a ripe area for research.

TBM causes are quite varied, and no single device may be appropriate to treat all etiologies. Therefore, as part of defining user needs, it is important to delineate when a device should be used for treatment (indications) and when it should not be used (contraindications). Indications and contraindications for the bioresorbable airway splint are defined for children 15 years of age and younger:

1. All selected patients will have tracheomalacia causing respiratory distress.
2. Malacia must be greater than 50% based upon CT imaging of the chest on inspiration and expiration.
3. The respiratory distress may be associated with external vascular compression, suprastomal/tracheal or subglottic collapse or tracheoesophageal fistulae.
4. All children to be implanted will be reviewed by the thoracic airway team.
5. Splints will be considered for children undergoing open procedures for other procedures (typically to repair the vascular anomaly, fistula, or collapse).
6. An open procedure specifically for splint placement is only to be used for this study in patients presently requiring a tracheostomy for maintaining the airway or with life-threatening apneic episodes.
7. Informed consent will be obtained for all subjects.

Contraindications for use:

1. Untreated severe tracheal stenosis, complete tracheal rings, and external compression due to active malignancy, active infection, or undrained cyst.

2. Tracheomalacia associated with a storage disease (such as a mucopolysaccharidosis).
3. Contraindications to surgery other than airway compromise.
4. Hypersensitivity to polycaprolactone or any of the components of the tracheal splint.
5. Severe distal (segmental or subsegmental) bronchomalacia or pulmonary disease necessitating artificial ventilation.

The definition of the clinical problem, its etiology, and the impact of the clinical condition on the patient forms the basis for the clinical objectives for an implantable device to treat TBM. These clinical objectives, denoted CO, encapsulate what the ideal device would do to solve the clinical problem (Hollister et al. 2017a).

- CO1. The splint should provide radial compressive mechanical support to keep the trachea/bronchus to protect the malacic segment from continued compression and to keep the malacic segment open and patent.
- CO2. The splint should provide this radial mechanical support for a period of 24–30 months to allow tracheal or bronchial remodeling and development.
- CO3. The splint should allow growth and expansion of the tracheobronchial complex during this 24–30-month period.
- CO4. The splint should allow controlled airway mechanical deformation increasing to normal airway deformation under respiration after a 24–30-month period.
- CO5. The splint should not cause adverse tissue reaction or remodeling.
- CO6. The splint should not interfere with the mucociliary architecture of the tracheal or bronchial lumen; it should therefore be placed externally.
- CO7. It is desirable that a second surgical procedure should be avoided to remove the splint; the splint should therefore be bioresorbable.
- CO8. Surgical placement of the splint and attachment of the trachea or bronchus into the splint should be straightforward.

Based on our clinical objectives, our clinical design hypothesis (CDH) states “suturing the malacic airway segment into a bioresorbable open cylindrical splint that provides sufficient radial compressive stiffness to protect the airway and engender patency, sufficient opening compliance to allow airway growth, and transfers mechanical stimulus to the malacic segment over time to stimulate mechanical remodeling will resolve severe TBM.”

The CDH is tested in the design validation phase. Both preclinical and clinical studies are required for either a Humanitarian Device Exemption (HDE) or Pre-Market Approval (PMA) process. A prenotification pathway, 510 k, typically may require only preclinical testing which would include bench testing and likely a preclinical animal model.

3.2 Phase IB: Design Inputs and Risk Analysis

To mitigate TBM, we created a splint that is surgically placed around the malacic airway segment. The splint is an open cylindrical, bellowed structure with periodically

placed suture holes that allow the malacic airway segment to be tied to the splint. The splint design variables (i.e., splint attributes that we choose and directly control) are listed in Table 1.

Clinical objectives frame the general device concept. However, they are not readily testable and therefore cannot be used to prove that a device meets design requirements for design verification. Furthermore they do not translate directly in values for design requirements. The CO must be translated into requirements that can be measured to verify the device. These measurable requirements are termed design inputs (DI).

The difficulty in translating CO into DI is often finding a rationale for choosing a specific measurable quantity. In many cases, this task is defined by an International Standards Organization (ISO) or American Society for Testing Materials (ASTM) standard. A prime example is the ISO 10993 standard used to establish biocompatibility. However, when no standard exists, the device manufacturer must not only establish the DI but also provide a sound rationale for choosing the measurable DI quantity. This requires scouring the literature for data that may be scarce or not completely relevant or perhaps not even exist.

The splint DI encompass geometric, material, mechanical, surgical, and even packaging/sterilization requirements. The malacic airway segment must be placed within the splint, which requires that the splint have an opening and fit around the malacic airway segment. The geometry must also allow attachment of the malacic airway segment into the splint via sutures, keeping the airway open and patent. The splint must be biocompatible, thus it must satisfy the ISO 10993 biocompatibility standard requirements. The combination of geometry and material will determine the mechanical stiffness of the splint, which must be sufficient to protect the airway from continued compression from surrounding tissues, yet compliant enough to allow airway growth and controlled mechanical deformation during respiration to mechanically stimulate airway tissue growth and remodeling. Finally, DI cover not only the device itself but device sterilization and packaging to ensure that the device arrives in the operating room (OR) ready to implant. For design verification, in addition to specifying a target value, we must also specify a variation around the target value that is acceptable. Thus, we will define target and acceptable values for splint geometric, material, mechanical, and packaging/sterilization DI. A complete account of DI target values, acceptable ranges CO that each DI addresses, and in what process phase (design and/or manufacturing) each DI is determined and measured is summarized in Table 2.

Splint ID and L are patient-specific geometric design variables as the malacic segment length and airway diameter differ from patient to patient. Splint WT upper bound of 3 mm was determined by both the need to surgically fit into a small space and to be sufficiently compliant to allow growth (Hollister et al. 2017a). Splint WT lower bound is determined by mechanical stiffness and fatigue characteristics and at this point requires further testing. Splint OA has been set at 90° such that the splint may be placed around the airway but also allow diametric, 180° separated airway suturing to open malacic airways and engender patency. Splint BP is set at 3 mm to

Table 1 List of splint design variables and associated abbreviations

Splint design variable name	Abbreviation
Splint inner diameter	ID
Splint wall thickness	WT
Splint length	L
Splint open angle	OA
Splint suture hole size	HSi
Splint suture hole spacing	HSp
Splint bellow period	BP
Splint bellow height	BH

accommodate suture holes. Splint HSp for the 90° OA is set at 60°, 120°, 180°, 240°, and 300° circumferentially around the splint to allow diametric suturing, and Splint HSi is set at 3 mm to fit bellow periods. Finally, Splint BH is determined primarily by the need to meet mechanical stiffness DI. Geometric DI may be directly determined by patient anatomy and/or surgical handling requirements (ID, L, HSi, HSp) or bounded by surgical handling requirements (WT). There is limited uncertainty in defining these DI target values.

Mechanical DI entail more uncertainty than most of the geometric DI. Mechanical DI are deduced based on suppositions from the literature. One source of mechanical compression on the tracheobronchial complex is arterial pressure from aorta and innominate arteries. The splint must withstand the repetitive blood flow pressure from these arteries without experiencing significant deformation. Maximum arterial pressures in hypertension will reach 240 mm Hg (Khanafar et al. 2011) or 0.03 N/mm² (MPa). This pressure is a maximum in hypertension. We will assume that the splint must withstand two times the maximum pressure for a 4× factor of safety, giving a target of 960 mm Hg or 0.12 MPa as a target pressure with less than 50% deformation. The total load will be 0.12 MPa times the maximum splint area for a given malacic segment. To maintain a patent airway, we would expect that the trachea should deform less than 50% under a 0.12 MPa pressure. These mechanical stiffness targets should maintain air passage through the airway based on the definition of TBM as a 50% reduction in cross.

Another rationale for splint compressive stiffness is that the splint should have at least the same compressive stiffness as normal, non-malacic trachea tissue. Shi et al. (2009) found that adult pig trachea deformed 50% under a maximum applied load of 20 N. Constantino et al. (2004) found that 200 mm Hg or .025 MPa caused complete occlusion of preterm lamb trachea. For a typical larger splint of 6 mm radius and 20 mm length with a 90° opening angle, the estimated surface area is 565 mm². Assuming a maximum 0.12 MPa compressive pressure is applied over the entire splint surface gives a total compressive force of 67 N. Thus, the estimate that a splint must withstand a compressive force of 67 N with 50% deformation is approximately 3× stiffer than normal pig tracheal tissue. These results support the splint compressive stiffness DI of less than 50% deformation under 0.12 MPa compressive pressure applied parallel to the splint opening angle.

Table 2 Testable design inputs for the tracheal splint, characterized by first by the device aspect affected (geometry, mechanical, material, or packaging/sterilization), the testable design input, the clinical objective address, and the process phase in which the design input is created

Design input #	Design input and value/acceptable range	Clinical objective	Process phase component
1 – Geom	Splint ID: $d^a \pm 10\%$ of range	1,2,4,6,7,8	Design, manufacturing
2 – Geom	Splint WT: $2.5 \text{ mm}^b \pm 15\%$ of range	1,2,3,4,8	Design, manufacturing
3 – Geom	Splint OA: $90^\circ \pm 5^\circ$ ^c	3,4,8	Design, manufacturing
4 – Geom	Splint L: Defect length $\pm 10\%$ of length ^d	1,2,3,4,8	Design, manufacturing
5 – Geom	Splint BP: $3 \text{ mm}^e \pm 10\%$ of range	3,4	Design, manufacturing
6 – Geom	Splint BH: 30% reduction ^f of wall thick $\pm 10\%$ of range	3,4	Design, manufacturing
7 – Geom	Suture HSi: $3 \text{ mm} \pm 10\%$ of range	1,2,6,8	Design, manufacturing
8 – Geom	Splint HSA: $60^\circ/120^\circ/180^\circ/240^\circ/300 \pm 3^\circ$	1,2,3,4,6,8	Design, manufacturing
9 – Mech	Compression – Parallel to opening: 50% max diameter displacement under 50 N load	1,2	Design, manufacturing
10 – Mech	Compression – maximum von Mises stress under 50 N load should be less than fatigue limit	1,2	Design, manufacturing
11 – Mech	Opening: >20% of opening wedge circumference under 15 N load	3,4	Design, manufacturing
12 – Mech/Mat	Bioresorbable material that retains sufficient parallel compression over 24 months but provides for a transition in airway mechanical stimulation	2,3,4	Manufacturing
13 – Mat	ISO 10993-3 genotoxicity: gene mutation – pass/fail	5,6,7	Manufacturing
14 – Mat	ISO 10993-3 genotoxicity: in vitro – pass/fail	5,6,7	Manufacturing
15 – Mat	ISO 10993-5 cytotoxicity – pass/fail	5,6,7	Manufacturing
16 – Mat	ISO 10993-6 muscle implantation: 2 weeks – pass/fail	5,6,7	Manufacturing
17 – Mat	ISO 10993-6 muscle implantation: 6 weeks – pass/fail	5,6,7	Manufacturing
18 – Mat	ISO 10993-11 pyrogen study – pass/fail	5,6,7	Manufacturing
19 – Mat	ISO 10993-11 sub-chronic toxicity: 13 weeks – pass/fail	5,6,7	Manufacturing
20 – Mat	ISO 10993-11 chronic toxicity: 26 weeks – pass/fail	5,6,7	Manufacturing
21 – Mat	ISO 10993-13 accelerated polymer degradation – determine degradation mechanisms and by-products	5,6,7	Manufacturing

(continued)

Table 2 (continued)

Design input #	Design input and value/acceptable range	Clinical objective	Process phase component
22 – Mat	ISO 10993-13 real-time polymer degradation – determine degradation mechanisms and by-products	5,6,7	Manufacturing
23 – PS	ISO 11135-1 determine device sterilization – <	5,7	Packaging and sterilization
24 – PS	ISO 10993-7 determine ethylene oxide residuals	5,7	Packaging and sterilization
25 – PS	ASTM D3078 standard test method for determination of leaks in flexible packaging by bubble emission	5,7	Packaging and sterilization
26 – PS	ASTM F1140-07 standard test methods for internal pressurization failure resistance of unrestrained packages	5,7	Packaging and sterilization

^aInternal diameter will be chosen based on patient airway diameter as determined by CT scan and observation in the operating room – ranges 4–20 mm diameter will be provided

^bSplint wall thickness may range from 1 to 3 mm

^cOpening wedge angle may range from 60° to 120°, based on patient need, but nominally will be 90°

^dMaximum splint length is 40 mm

^eBellow period will range from 1 to 3 mm but nominally will be 2 mm

^fReduction in maximum wall thickness may range from 0% to 50% but will nominally be 30%

The other major mechanical requirement of the tracheal splint is that it allows growth and expansion of the trachea during the 2–3-year period it is in place. The best data available on tracheal growth in adolescents was provided by Wright et al. (1981) in patients with both normal tracheas and tracheostomies. They determined a quadratic regression equation for the narrowest tracheal size for both patient groups, shown below:

$$\begin{aligned} \text{Normal Patients : Tracheal Diameter(cm)} \\ = 0.61 \text{ cm} + 0.002(\text{cm/years}^2) * \text{Age}^2 \text{ (years)}^2 \end{aligned}$$

$$\begin{aligned} \text{Tracheostomy Patients : Tracheal Diameter(cm)} \\ = 0.64 \text{ cm} + 0.001(\text{cm/years}^2) * \text{Age}^2 \text{ (years)}^2 \end{aligned}$$

If we apply these equations to the extreme age ranges (3 months (0.25 years) to 15 years) of the potential patients using both the normal and tracheostomy patients, we obtain the changes in trachea diameters shown in Table 3.

Thus, the normal ranges in Table 3 will represent the upper bound on expected tracheal growth, in this case an expansion of 19% in 3 years. The difficulty is that the pressure exerted by the growing trachea is unknown. It is known that banding of a rat trachea by Kida and Thurlbeck (1981) with an unspecified plastic led to a trachea with a cross-sectional area 26% that of normal or in other words restricted radial expansion by approximately 50%. Thus, we would expect that the splint should be

Table 3 Predicted changes in tracheal diameter for normal and tracheostomy patients for the narrowest tracheal diameter

Patient	Normal – begin	Normal – after 3 years	Percent change	Tracheostomy – begin	Tracheostomy – after 3 years	Percent change
Beginning age – 3 months	0.61 cm	0.62 cm	+1.6%	0.64 cm	0.65 cm	+1.6%
Beginning age – 15 years	1.06 cm	1.26 cm	+18.9%	0.87 cm	0.97 cm	+10.3%

able to allow a 20% expansion of the tracheal diameter under minimal expansion pressure, equal to the pressure exerted by the aorta. In other words, if the expansion pressure of tracheal growth does not at least equal the compression pressure of the aorta, we would not expect radial growth. Given that the maximum aorta pressure of 250 mm Hg or 0.03 MPa, and given a splint surface area of 565 mm², we would expect that any pressure over 17 N should allow 20% expansion of the splint. As a conservative estimate, we will require a 20% expansion of the splint opening under a 15 N load.

The splint is intended to be implanted in the neck around the trachea and/or in the chest around the bronchus. As such, the splint will come in contact with tissue, specifically smooth muscle and cartilage components of the trachea and bronchus, surrounding vascular and thoracic structures, as well as tissue fluid, as defined in ISO 10993-1. Furthermore, although the splint will resorb, its contact with tissue will be considered permanent (contact with tissue greater than 30 days). To ensure tracheal splint biocompatibility, the final 3D printed and sterilized splint structure will be tested under ISO 10993 biocompatibility standards. The appropriate tests to establish biocompatibility are outlined in Table 4.

Splint geometric, mechanical, and material/biocompatibility DI are now defined. However, it is critical to note that there is significant uncertainty in defining many DI, especially mechanical DI. First, the properties of normal airway tissue are not well known (let alone malacic airway tissue). Literature review turns up few papers on airway tissue nonlinear elastic or nonlinear viscoelastic properties, and these papers describe adult human or young animal airway properties, which is not the target patient population for the splint. Given that a major clinical objective is to transition increasing mechanical stimulus to the malacic airway segment, the only design option is a computational model simulating how degrading splint properties affect airway deformation. Lack of airway mechanical property data presents significant uncertainty to understanding this clinical objective.

Second, there is a dearth of data on degradation and coupled fatigue-degradation behavior of most degradable polymers. This again affects CO4 as the ability to transition mechanical load bearing from the splint to malacic airway to mechanically stimulate airway remodeling depends on change in stiffness over time due to degradation. More data on long-term in vivo degradation is needed especially in

Table 4 Relevant ISO 10993 biocompatibility tests for tracheobronchial splint

Nature of contact	Contact duration	Relevant test	ISO 10993 reference
Tissue/bone	Permanent >30 days	Genotoxicity	ISO 10993-3
Tissue/bone	Permanent >30 days	Cytotoxicity	ISO 10993-5
Tissue/bone	Permanent >30 days	Implantation	ISO 10993-6
Tissue/bone	Permanent >30 days	Biodegradation	ISO 10993-9
Tissue/bone	Permanent >30 days	Sensitization	ISO 10993-10
Tissue/bone	Permanent >30 days	Irritation	ISO 10993-10
Tissue/bone	Permanent >30 days	Systemic toxicity	ISO 10993-11
Tissue/bone	Permanent >30 days	Chronic toxicity	ISO 10993-11

relation to in vitro degradation and whether in vitro degradation can be used to predict in vivo degradation.

Third, there is little data on airway growth and what level of mechanical pressure a growing airway would exert on the splint. Effects of medical devices on growth is a significant topic for design control of pediatric devices, as multiple surgeries with multiple devices may be required to allow tissue growth. Various methods including tailoring initial device stiffness to accommodate growth forces, degradable materials where stiffness is reduced over time, and mechanism-based devices that allow large displacements for small increases in force are all methods used in medical devices to accommodate growth over time (Hollister 2017). Again, more data and computational modeling must be applied to address growth design requirements for pediatric medical devices.

Beyond defining DI that enable the device to mitigate the clinical condition, we must also assess risks associated with device failure or improper device use that may endanger the patient. FDA requires risk analysis including assessment and mitigation as part of the design control process. Among the most widely used risk analysis/mitigation procedures is Failure Mode Effects Analysis (FMEA). In FMEA, a failure mode is identified, failure cause is postulated, potential impact on the patient is assessed, and then the potential failure frequency (1 rarely to 10 frequent), failure severity (1 low to 10 high), and ability to detect the failure (1 always to 10 never) are ranked. The total risk to the patient is determined by frequency*severity*detection, with a higher score (i.e., higher frequency combined with high severity and low detection rates) representing a higher risk. Finally, a remedy and test methods to validate the remedy are proposed. Table 5 presents a splint FMEA.

Combining DI and FMEA provides a road map of how to engineer the airway splint. Indeed, the next step in design control is to map out the steps to completing and testing the splint. It is clear that the more rigorously DI and FMEA are defined, the more controlled the development proceeds. This is not to say that changes in design or processes cannot be made in the design control process. In fact, the design control process is set up to expect design and/or processing changes and to make these changes in a controlled and documented manner. All user needs, clinical objectives, clinical design hypothesis, design inputs, and FMEA must be documented in a design history file (DHF).

Table 5 Splint FMEA describing risks to patient from splint. Risks due to implantation are mitigated by proper training for implantation and labeling of splint. Risks due to mechanical failure are mitigated by splint design and mechanical testing. Risks due to degradation characteristics are mitigated by more rigorous splint in vivo and in vitro degradation testing in vitro and in vivo

Failure mode	Cause(s)	Impact	Potential frequency (1 rarely to 10 frequently)	Severity (1 low to 10 high)	Possible detection (1 always to 10 never)	Total risk (G*L*O)	Remedy	Test method to validate
Splint loosens from trachea/bronchus	Splint insufficiently sutured to trachea/bronchus	Loose splint causes damage to surrounding arterial structures Trachea/bronchus collapses	3	5	5	75	Ensure proper suturing of trachea/bronchus to splint	Assess fit via measurements on 3D digital model Build physical airway model to make sure splint fits physically Simulate suturing on trachea/bronchus physical phantom
Splint is nidus for postoperative infection	Trachea/bronchus is perforated during surgery Splint is not adequately sterilized PCL material is not biocompatible		3	6	4	72	Sterilize splint with ethylene oxide Provide antibiotic surgical area Ensure splint biocompatibility	Verify validation with bioburden test Validate sterilization procedure Biocompatibility: splint implantation in animal model and patients Prior 510K approval of PCL

Splint is attached incorrectly to trachea or bronchus causing "kinking" of airway	Incorrect splint attachment	Kinking of airway	4	6	3	72	Draft clear labeling Provide brochure with diagram & video of splint implantation Size splint properly to airway	Test brochure & labeling with peer surgeon group Measure splint fit on digital model & physical prototype
Adverse tissue reaction to splint material or degradation products resulting in excessive scarring sufficient to be symptomatic	PCL material in splint is not biocompatible Degradation products are overly acidic	Formation of fistulas in trachea/bronchi Scarring and granuloma formation	3	5	4	60	Use PCL materials that has been shown to be biocompatible in preclinical and clinical tests PCL also passed ISO 10993 in other devices	Preclinical pig model Human implantation PCL material pass ISO 10993
Splint fracture or tearing	Splint strength is not sufficient for chest loading conditions Splint fatigue strength is not sufficient for cyclic loading	Tracheal collapses because splint does not have mechanical integrity Splint pieces perforate lumen	2	8	3	48	Design splint to withstand 50 N compress load	Finite element analysis Mechanical compression test Fatigue compression test

(continued)

Table 5 (continued)

Failure mode	Cause(s)	Impact	Potential frequency (1 rarely to 10 frequently)	Severity (1 low to 10 high)	Possible detection (1 always to 10 never)	Total risk (G*L*O)	Remedy	Test method to validate
Splint erodes into lumen	Excessive motion between splint & trachea/bronchi	Tracheal perforation, fistula	2	9	4	36	Size splint correctly to trachea/bronchus size based on patient images Properly suture trachea/bronchus into splint	Assess fit via measurements on 3D digital model Build physical airway model to make sure splint fits physically Simulate suturing on trachea/bronchus physical phantom
Perforation of lumen during surgery	Labeling on splint implantation not clear Surgeon does not suture only through outer tracheal bronchial wall	Allows bacteria to migrate from lumen into chest cavity	2	8	2	32	Draft clear labeling Provide brochure with diagram & video of splint implantation	Test brochure & labeling with peer surgeon group
Splint degrades too quickly allowing malacic segment to collapse	Splint geometry effects on degradation not known	Collapse due to loss of splint mechanical properties could risk respiratory arrest	3	5	2	30	Perform in vivo splint degradation testing to determine splint degradation kinetics for 2–3 years	Perform mechanical and GPC testing of in vivo and in vitro tested splints

3.3 Phase IC: Development Planning

CDH, DI, and FMEA provide the road map for developing the medical device. The remaining steps are to develop the design and manufacturing processes that translate idea into device, along with the design outputs that confirm the created device meets the DI and mitigates risks defined in the FMEA. To ensure appropriate timing and resources are available for device development, both should be mapped out using tools such as a Gantt chart, which describes the task to be done, the time to complete the task, and the resources (money and personnel) to complete the task.

4 Phase II: Design and Manufacturing Processes

The next step in design control is determining the design and manufacturing processes that will actually turn the device idea into a reality. For patient-specific devices, design will utilize patient image data, and manufacturing will utilize some form of 3D printing to create the device. Each step of both the design and manufacturing process should have a standard operating procedure (SOP). The SOP describes step by step how to perform the design and manufacturing processes to a level that someone unfamiliar with the process but educated in the art would be able to read the SOP and perform the processes. The SOP are kept in a Device Master Record, the “book” on how to make the medical device. Although not possible to describe this level of detail, we give a high-level overview of the design and manufacturing processes for the splint. Finally, it is important to note that we separate processes into design and manufacturing. Also, we have added a step of design output for the design process separate from the device design output. We believe that such a step helps elucidate whether deviation in the device occurs in the design phase versus the manufacturing phase.

4.1 Phase IIA: Design Model Process

The splint design model process phase begins, as does any patient-specific device, with patient image data. It is important to obtain imaging data that provides information pertinent to device design, properly dimensioned, and as easy as possible to segment relevant anatomic structures. Computed tomography scans are obtained at the height of exhalation to determine malacic segment length and at the height of inhalation to determine malacic segment maximum diameter. It is important to have a phantom of known size in the scan to calibrate scan dimensions.

The next step is image data segmentation to obtain relevant anatomic structures of interest. This may be done using a variety of commercially available software like Simpleware ScanIP™ (Synopsys, <https://www.synopsys.com/simpleware.html>), Mimics™ (Materialise, <http://www.materialise.com/en/medical/software/mimics>), or shareware like 3DSlicer (www.slicer.org). We have used both Simpleware and Mimics to segment anatomic data. However, for implant design it will be important for software to have to meet criteria set by the FDA.

The segmentation procedure consists of thresholding air to isolate the airway and lungs. Subsequently the data is edited on a slice-by-slice basis to remove the airway from the airway/lung model, and a Boolean operation is performed to create the final airway model for both the inhalation and exhalation CT scans. The malacic segment length is determined by measuring the distance between points at which the airway cross-sectional area decreases by 50%. To accommodate the airway wall and allow growth, we assume the wall thickness is 1 mm and allow a 1 mm gap between the outer airway wall and the splint interior. Thus, the inner splint diameter is the lumen diameter plus 4 mm: $ID = 2 * (\text{lumen radius} + 1 \text{ mm wall} + 1 \text{ mm gap}) \rightarrow ID = \text{lumen diameter} + 2 \text{ mm wall} + 2 \text{ mm gap}$.

Malacic segment length (L) and diameter (ID) in addition to the remaining splint design variables (Table 1) are entered into an Excel sheet and may vary along the splint length. This excel sheet is read by a custom MATLAB program that automatically generates the bellowed splint design as a slice-by-slice image representation (Hollister et al. 2015, 2017a). This image representation can be read into ScanIP, Mimics, or 3DSlicer to directly generate a .STL splint surface representation.

4.2 Phase IIB: Design Model Output (DMO)

The immediate question following design is whether the design itself meets the DI. DI measurements are known as design outputs (DO), and the process of measuring DO and comparing the DO to DI is called design verification. To indicate that these DO were determined from the design model, we term these DO as Design Model Output (DMO). Separating DO for the design and manufacturing phase differs from the traditional FDA design control process (<https://www.fda.gov/downloads/MedicalDevices/DeviceRegulationandGuidance/GuidanceDocuments/UCM499809.pdf>). However, it is important to determine if the device design meets DI before manufacturing (3D printing) as discrepancies between DI and DO could occur either in the design or manufacturing phase. There are two important points to note regarding Design Model Output. First, DMO can obviously only address geometric and mechanical DI, not material or sterilization DI. Second, the Design Model Output represents the best case scenario for geometric and mechanical DI, as any manufacturing technique, including 3D printing, may introduce voids or shape imperfections into the biomaterial device. These voids/imperfections will impact both geometric and mechanical DI, and if the Design Model Output is verified, any DI-DO discrepancies can definitively be attributed to manufacturing.

Geometric DO are measured directly on the design image data. Figure 2 shows example measurements for splint ID, L , WT, and OA shown on the 3D model in Simpleware ScanIP. The DI for these splint design variables were $ID = 14 \text{ mm}$, $L = 20 \text{ mm}$, $WT = 2.0 \text{ mm}$, and $OA = 90^\circ$. The resulting measured DMO were $ID = 13.9 \text{ mm}$, $L = 19.9 \text{ mm}$, $WT = 1.99 \text{ mm}$, and $OA = 86.5^\circ$. By Table 2, all measured DI (DI #1–8 Table 2) fit within the target value \pm variation, and we consider the geometric DI verified.

Mechanical DI design verification is performed by finite element (FE) modeling under both mechanical test conditions in addition to simulating idealized malacic

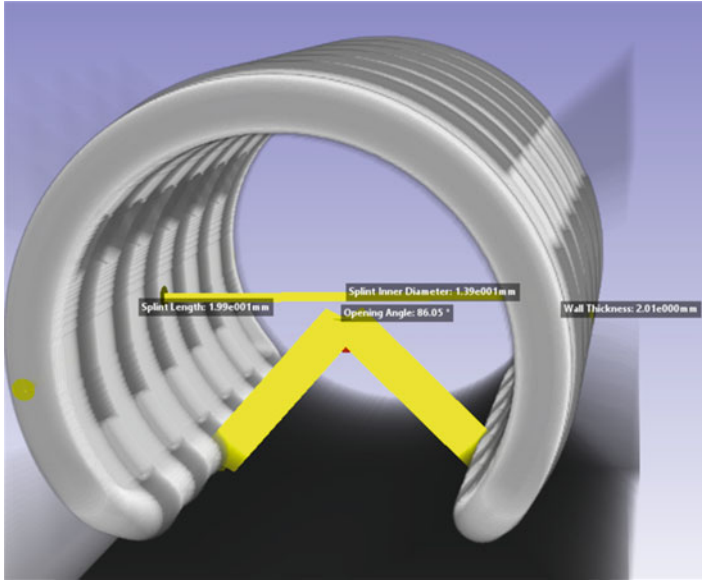


Fig. 2 Example measurements for DMO on design model used for design model verification

airway (idealized to match patient airway diameter and length) within the splint. Splint material, polycaprolactone (PCL), is modeled as an isotropic linear elastic material based on an effective modulus determined by compression testing of cylindrical coupons with different diameter to length ratios. FE models simulate compression parallel to the opening angle and opening/compress perpendicular to the splint opening (Fig. 3). The loading platens are modeled as rigid, and contact is modeled between the platens and splint.

The Device Model Output process runs from patient data through mechanical simulation (Fig. 4).

Although DMO cannot assess all device design inputs, geometric and mechanical DI can be assessed as a best-case scenario without manufacturing flaws. The actual manufactured device can then be compared to the DMO to determine variability in splint performance due to manufacturing.

4.3 Phase IIC: 3D Printing (Laser Sintering) Splints

Once the design is verified for geometric and mechanical DI, the next step following is manufacturing, for patient-specific devices, via 3D printing. The splint is manufactured by laser sintering of a PCL with 4% hydroxyapatite mixture. An SOP is written for all stages of the laser sintering process, from receiving and expecting material to loading powder in the EOS P110 machine with appropriate laser parameters to removing and inspecting the builds. The complete laser sintering process is outlined in Fig. 5.

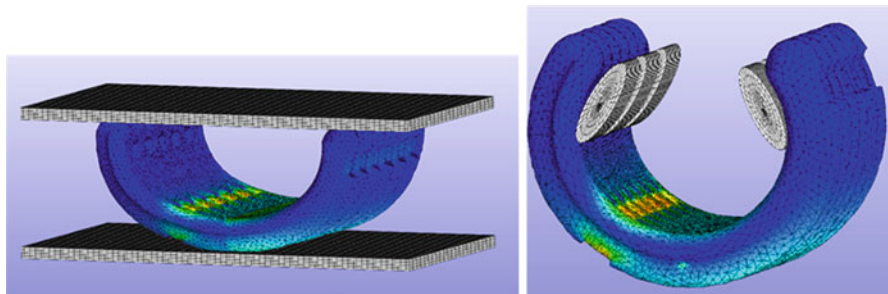


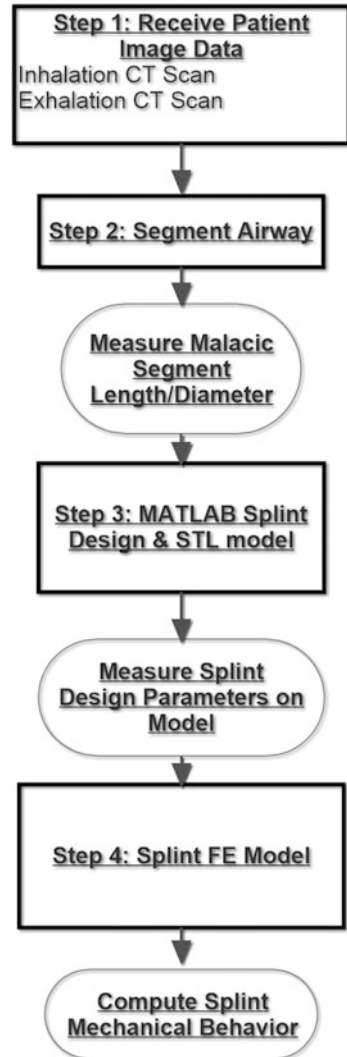
Fig. 3 Example finite element simulations of splint mechanical tests. **(a)** Splint compression under rigid platens. **(b)** Splint opening pulled by rigid platens. Such simulations determine if splints under idealized design conditions (i.e., not manufacturing flaws) can meet mechanical DI

Running a process with predictable results is a critical component of quality control. Such processes may either be validated (process validation) or verified (process verification). Process validation entails running a statistically powered sample size of samples that will have the same design parameters and use the same processes every time. Appropriate tests are performed to determine the samples are the same within an accepted variation for each process run, in this case, each 3D print build. The given process parameters to produce such samples are determined, and the process is always run using those parameters.

Process validation may not be appropriate for 3D printing of patient-specific devices for two reasons: (1) the design parameters by definition change for each patient and device, and (2) there is inherent variability in 3D printing exacerbated by producing parts with varying design parameters. Thus, process verification is more appropriate for 3D printing patient-specific devices, due to variability from design and processing as well as the inherent ability to produce both device replicates and coupons (specimens with simple geometry like cylinders reproducibly tested across multiple device builds for ready comparison and interpretation). Figure 6 shows a micro-CT scan of a 3D airway splint printed on the University of Michigan P100 laser sintering system, which has been used for all patient cases to date (Zopf et al. 2013; Morrison et al. 2015; Hollister et al. 2015). Results show that the actual 3D printed splints with 2 mm wall thickness have a smaller volume envelope by 30% than the designed STL file plus approximately 6% internal void volume. Actual 3D printed splints with 3 mm wall thickness had a smaller volume envelope by 13% compared to the designed STL file plus approximately 8% internal void volume. These results suggest that discrepancies between actual 3D printed splints and design STL files depend on wall thickness and therefore design parameters. Thus, micro-CT scanning offers a thorough evaluation of external 3D printed device shape and internal material flaws. *For splint (or any patient-specific device) process verification, we recommend building both cylindrical coupons and devices in every build for micro-CT scanning and mechanical testing.*

There is a 16% discrepancy between designed and manufactured wall thickness for the 2 mm WT design and a 5% discrepancy between designed and manufactured

Fig. 4 Splint design processes beginning from patient image through simulation of splint mechanical behavior. Oval boxes represent DMO to match against geometric and mechanical DI

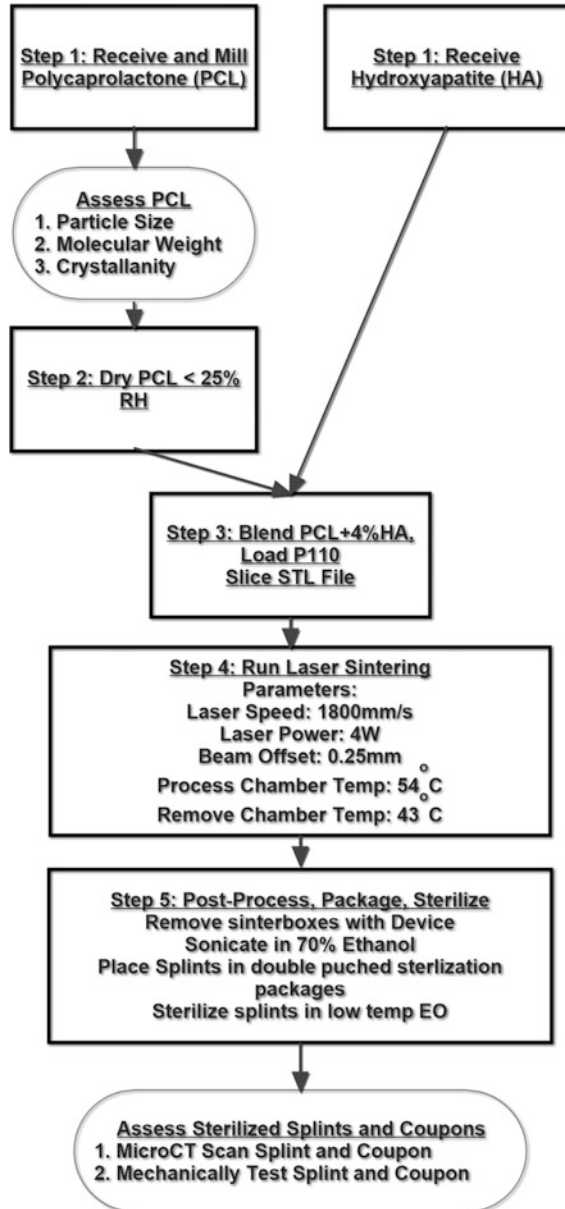


wall thickness for the 3 mm WT design. Micro-CT also revealed a 6–8% void volume in each design.

5 Phase III: Testing, Design Verification, and Design Validation

Once a device is manufactured, there are two basic questions concerning its use. First, is the manufactured device actually the proposed and designed device? Second, does the manufactured device mitigate the clinical condition by meeting the CO

Fig. 5 Simplified schematic of PCL laser sintering process from receipt of raw material to final device. Operations in circle are tests used for process verification



and satisfying the CDH? The process of answering the first question (Does the manufactured device meet all DI and mitigate potential risks from FMEA?) is termed *design verification*. The process of answering the second question (Does the manufactured device mitigate the clinical condition?) is termed *design validation*. Design verification must be performed before design validation. If a non-verified

design were to fail design validation, it would be unclear if the failure was due to the device not meeting DI or the original CDH being rejected and a correctly made device not mitigating the clinical condition.

5.1 Phase IIIA: Design Device Outputs and Design Verification

Device outputs are measurements made on the final manufactured and *sterilized* device. We denote design outputs from the manufactured device as device design outputs (DDO). In most cases as per many ASTM standards, a sample size of six is used for each measurement. The mean \pm standard deviation for each measurement for each DDO should be greater or less than a one-sided DDO or within the target plus accepted variation for a bounded DDO.

Geometric DI (Table 2 DI 1–8) are measured on $n = 6$ splint samples. Measurements are made either by direct caliper measures or from micro-computed tomography (micro-CT) splint scans. Three measures are made along each splint and averaged. The mean \pm standard deviation of these average splint measurements are then used to determine if the manufactured/sterilized splints meet geometric DI. Micro-CT offers a significant advantage by showing the splint interior and the void fracture produced by the 3D printing process. As seen in Fig. 6, micro-CT can provide information not only on external geometric DI but also on internal void distributions, a measure of 3D printing quality. Thus, *micro-CT provides a quality control measure and should be done for every patient-specific splint (or any device) manufacturing batch since design parameters change for every manufacturing round.*

DDO for mechanical DI (Table 2 DI 9–12) are measured by mechanical testing $n = 6$ splint samples. DI 9 and 10 are measured by compressing the splint with open side face down. The splint should not displace more than 50% of the ID nor yield under a 50 N load. DDO for DI 11 is measured by either compressing the splint on its side or opening the splint with hooks. DDO for DI 9–11 are static mechanical

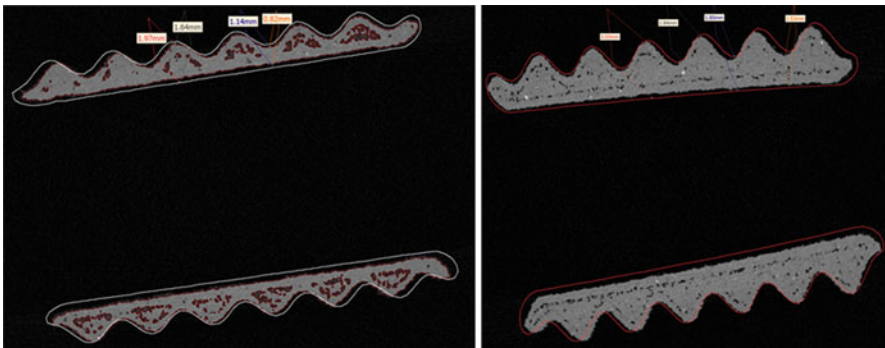


Fig. 6 Comparison of micro-CT scan of 3D printed splint (greyscale) to actual STL design file (red outline) for (a) 2 mm wall thickness splint and (b) 3 mm wall thickness splint

measures that can be made as quality control for each manufacturing lot. In previous mechanical testing for splint implantation in patients, we demonstrated that PCL laser sintered splints met DI 9–11 (Hollister et al. 2015).

DDO for DI 12 is much more involved and difficult to characterize. Material degradation depends primarily on material composition but may be influenced by both geometry and mechanical stress. Material degradation will change mechanical properties and therefore change airway deformation within the splint over time. In vitro degradation tests can be performed accelerated or real time. It is unclear how either in vitro tests relate to in vivo degradation, both because of the different chemical and mechanical environments of the device. In vitro testing may be done under more controlled testing and are less expensive, while in vivo tests are more expensive but of course allow the device to be placed in the proper chemical and mechanical environments.

There is a dearth of results from all three tests for PCL degradation. Lam and colleagues (2007, 2008a) suggested that in vitro accelerated PCL degradation occurred via surface erosion, while real-time in vitro degradation occurred via bulk hydrolysis. They also found that mechanical stiffness decreased by approximately 33% over a period of 50 months, while molecular weight decreased by 50% over a period of 30 months under real-time degradation. Lam et al. (2008a) also found that PCL yield stress decreased by over 80% between 10 and 25 months, potentially raising failure risk. Therefore we propose to perform all three tests (accelerated in vitro, real-time in vitro, and in vivo fatigue/degradation) and determine if and how well in vitro degradation/fatigue tests relate to in vivo results. Lam et al. (2008b) also followed PCL calvarial scaffolds for 2 years in one rabbit. They found a 63% molecular weight loss and significant scaffold geometric changes. Finally, Rasperini et al. (2015) found a 21% molecular weight loss in a retrieved periodontal PCL scaffold retrieved 14 months after implantation in a patient. Real-time in vitro degradation data at 14 and 24 months was 33% and 50%, respectively (Lam et al. 2008a), in the range of in vivo results. Although all these studies represent a significant effort, there is simply not enough data or understanding of PCL degradation to rationally incorporate degradation data into the splint design. *Thus, more in vitro and in vivo studies of the coupled fatigue/degradation behavior of the PCL splint are needed, including taking studies out past 2 years.* The same can likely be said for any device 3D printed from resorbable material.

Device material biocompatibility is a significant requirement for any implantable device. Unlike geometric and mechanical DI for which the manufacturer may have to define DI, biocompatibility is defined by the ISO 10993 standard. DI 13–22 (Table 2) track the pertinent parts of ISO 10093 for assessing biocompatibility. DI 13–15 are cell-based tests, DI 16–20 are small animal (typically mice and rats) tests, and DI 21–22 are in vitro degradation studies. DI 13–20 are performed on small discs on which cells are cultured or that can readily be implanted subcutaneously or in muscle beds of mice and rats. As such, they do not take on the actual device geometry. However, these samples should be processed the same way as the actual device, using the same raw material source and processing, using the same 3D printing process, and

using the same sterilization process for the actual device. DI 21–22 are carried out using the actual device geometry performing in vitro degradation tests. All tests should be performed under good laboratory practices (GLP) (<https://www.accessdata.fda.gov/scripts/cdrh/cfdocs/cfcfr/CFRSearch.cfm?CFRPart=58>; <https://www.fda.gov/downloads/ICECI/EnforcementActions/BioresearchMonitoring/UCM133748.pdf>).

The final device must be sterilized, transported, and stored for application. Design verification also entails determining that the device can be sterilized and packaged. Sterilization is verified by testing DI 23 and 24 in the final packaging. Since the splint is made from PCL, it is sterilized in a special low-temperature ethylene oxide (EO) cycle run below 50 °C. Splint sterilization DI are defined by ISO 10993-7 for EO residuals, and ISO 11135-1 to verify the device is sterile. Packaging for the splint entails double Tyvek pouches that are torn open at time of implantation. Packaging verification is done real time for the entire duration that the device is expected to be available on the shelf. ASTM D3078 and ASTM F1140-07 are standards defining DI 25 and 25 to test packaging.

5.2 Phase IIIB: Design Validation

Completion of design verification (including packaging and sterilization) gives us confidence that the fabricated device is the device we intended to create. The final step in design control is to test if the device actually mitigates the clinical condition. In other words, design validation determines if the clinical design hypothesis is rejected. As in testing general scientific hypotheses, we can never truly accept the CDH since design (and thus Design Inputs) is always based on incomplete knowledge. Long-term clinical use may reveal failures and/or design flaws due to information that was overlooked or that was not known during device development.

Design validation is performed using multiple tests, not just a single test. The type of tests depends on device classification. Class II devices are devices having a clinical history, and in most cases design validation will consist of bench and preclinical animal tests, although limited testing in humans could be requested. The approval pathway for class II devices is prenotification, more commonly known as 510 k. Class III devices are higher-risk devices whose failure could lead to patient disability or death. These devices will require human clinical trials in addition to bench and preclinical animal models for design validation. Class III devices are generally approved through the Pre-Market Approval (PMA) pathway. PMA approval requires Phase I clinical trials with limited patients to prove device *safety* (largely addressing issues in the FMEA) followed by a Phase II clinical trial with larger numbers of patients to prove device *efficacy* by comparing clinical results with the device to clinical results with the currently accepted “gold standard” clinical treatment. The Phase II trial is the final test in humans to test the CDH and show the clinical objectives are satisfied by showing the device performs better than current clinical treatments. A secondary approval path for class III devices is Humanitarian Device Exemption (HDE) for conditions affecting 4,000 or less patients per year in the United States. HDE applies when no device is currently considered the accepted

clinical treatment for a condition. In this case, only a Phase I trial is required since there is no standard against which to test efficacy. Clinical trials are carried out under investigational device exemption (IDE), since an exemption must be issued to allow the device to be used in humans. Obtaining an IDE requires evidence that the device is safe for human use based on bench and preclinical animal model testing.

The airway splint is a class III device since it is considered high risk, but approval is through the HDE pathway since the expected number of US patients is less than 4,000 (current estimates are 1,000–1,500 patients per year). The major safety concerns for the splint are whether it causes adverse tissue reaction, if it withstands respiration and thoracic tissue loads without failing, and whether it allows airway growth. The major efficacy questions are whether the splint protects the airway from thoracic compressive loads, engenders airway patency, and allows long-term airway remodeling and mechanical stiffening.

5.2.1 Design Validation: Preclinical Animal Results

Due to the large number of unknowns in splint design (e.g., nonlinear elastic properties of malacic and even normal airway tissue; magnitude of loads applied by malformed vascular tissue on the malacic airway; magnitude of forces generated on the splint by airway growth), it is difficult to validate clinical objectives by bench testing. Thus, to proceed to clinical use, it is important to answer as many questions as possible in an appropriate preclinical animal model. For the splint we created TBM surgically by resecting trachea cartilages leading to airway collapse in 1-month-old domestic Yorkshire pigs (Zopf et al. 2014) a model also proposed by other research groups (Vinograd et al. 1987; Nalwa et al. 2001). The resulting malacia was significantly severe that left untreated pigs would lose consciousness and have to be euthanized within 24 h. Pigs treated with the splint survived significantly longer. This provided supporting evidence for design validation that verified splints could engender immediate patency in malacic airways.

The difficulty with surgically created malacia was that it is difficult to avoid rents in the tracheal mucosa when resecting cartilage rings, which lead to infection. Thus, to test long-term safety issues like growth, we decided to suture splints to intact trachea in 1-month-old domestic pigs. We varied splint opening stiffness from the upper bound of DI 11 (20% opening displacement under 15 N load) to less than 10% opening displacement (Hollister et al. 2017a). Pigs were followed up for 8 months after splint implantation. Results demonstrated that the stiffest scaffolds restricted growth and led to stenosis. Splints meeting DI 11 allowed 8-month tracheal growth in pigs similar to native tracheal growth.

Preclinical large animal models demonstrated that splints meeting DI 1–11 could engender patency in surgically created TBM while allowing growth over 8 months (Hollister et al. 2017a). However, there are still important questions regarding long-term splint biocompatibility as well as coupled degradation and fatigue that must be addressed using a large preclinical animal model. These specifically include how PCL degradation products affect airway tissue, the changes in splint mechanical behavior over time, and whether *in vitro* fatigue/degradation experiments (real time and accelerated) can predict *in vivo* results. We are currently running a 3-year

combined large preclinical animal study with in vitro fatigue and degradation testing to answer these questions. We believe that these experiments and even longer 4-year preclinical animal model experiments run until the PCL splint is completely degraded which will be necessary to determine the long-term splint effects on airway development and remodeling.

5.2.2 Design Validation: Clinical Results

The general progression for design validation is to utilize preclinical animal results to support an IDE submission and then run a Phase I clinical trial followed by a Phase II clinical trial. However, the splint is an example of exceptions for patients that may need an experimental treatment when no other treatment is available. In these cases, no IDE generally exists, but the physician may utilize the device for implantation if no other satisfactory treatments exist. This clinical utilization is through expanded access (<https://www.fda.gov/downloads/Training/CDRHLearn/UCM180888.pdf>; <https://www.fda.gov/NewsEvents/PublicHealthFocus/ExpandedAccessCompassionateUse/default.htm>).

The airway splint was initially used in patients under emergency clearance (Zopf et al. 2013; Morrison et al. 2015; Les et al. 2018) but in later patients has been utilized under expanded access, also known as compassionate use. To date, nine patients have received the PCL splint, with follow-up ranging from 9 to 67 months (median follow-up 26 months). One patient died from a ventricular cardiac defect unrelated to the splint. Based on CT scans and measures of airway area on exhalation and inhalation, airway patency (defined as >50% area on exhalation related to inhalation) was maintained for all patients (Morrison et al. 2015; Les et al. 2018). Detailed results on three patients (Morrison et al. 2015) demonstrated airway growth in splinted bronchi similar to untreated normal bronchi up to 30 months postoperatively. These clinical results suggest that splints meeting DI 1–11 do meet clinical objectives 1–3 and 6–8. Early evidence indicates that the CDH is not rejected.

Although early clinical evidence supports the CDH concerning the splint mitigating severe TBM, the final supporting design validation for the airway splint is through clinical trials. Based on the splint being used for less than 4,000 patients per year in the United States, it has received designation as a Humanitarian Use Device (HUD) and can be approved through a Humanitarian Device Exemption (HDE) pathway. This will require a Phase I clinical trial to show that the splint is safe in patients.

6 Conclusions and Future Directions

The goal of this chapter was to propose a path for design control and quality control for 3D printed patient-specific devices using the 3D printed resorbable airway splint as an example. The entire design control process was presented from developing design inputs to specifying design and manufacturing processes to design verification and design validation. On one level, the design control process proceeds along the same path regardless of the manufacturing process or number of devices

produced. However, on another level, patient-specific design and 3D printing do introduce special considerations as the design parameters for the same indication change which can alter achievable manufacturing quality for similar devices. For patient-specific devices using the splint as a paradigm, we would make the following observations and recommendations:

1. Airway tissue properties and remodeling

Little information is available on normal airway and malacic airway nonlinear elastic properties nor about mechanically stimulated airway remodeling. Such information is critical for developing accurate design inputs. In general, as devices are increasingly tailored to patients, better understanding and more information on individual tissue mechanical properties will be critical.

2. Splint computational simulation for each patient-specific device

The splint length and inner diameter change for each patient. To determine the best wall thickness, bellow height, and other design parameters that best meet mechanical requirements, finite element analyses for each patient are recommended. Due to varying design parameters for each patient, computational simulation (FEA, CFD) would be useful to assess variations in each design. Most patient-specific devices will have design parameter changes for patient to patient, so computational simulation of each design with parameter changes should be performed.

3. Micro-CT scanning and mechanical testing for each 3D printing lot for quality monitoring of 3D printing processes

Changing design parameters, especially wall thickness, may change 3D printing quality. Therefore, micro-CT scans and mechanical testing should be performed for each patient manufacturing lot to assess manufacturing quality, specifically determining differences between 3D printed device and design STL file.

4. Long-term preclinical animal testing for bioresorbable materials

There is a dearth of information on the long-term behavior of bioresorbable materials, especially changes in material mechanics and tissue response. Long-term (up to 4 years for PCL) in vivo studies should be performed on 3D printed bioresorbable devices. In vivo studies should be compared to in vitro studies.

5. Post-market surveillance monitoring of in vivo 3D printed resorbable device changes

There is significant uncertainty in developing design input for patient-specific pediatric resorbable devices. This translates into uncertainty in design validation that may mean pre-market safety approval may not be sufficient. Post-market surveillance may be required, especially using means like ultrasonic elastography (Kim et al. 2008) to assess changes in bioresorbable mass device and mechanical properties due to bioresorption.

Acknowledgments Studies reported in the chapter on the airway splint were supported by the National Institutes of Health through NIH/NIHCD R21HD076370, NIH/NIHCD R01HD086201, and NIH T32DC005356. The content is solely the responsibility of the authors and does not necessarily represent the official views of the National Institutes of Health.

References

- Boogaard R, Huijsmans SH, Pijnenburg MW et al (2005) Tracheomalacia and bronchomalacia in children: incidence and patient characteristics. *Chest* 128(5):3391–3397
- Bucher U, Reid L (1961) Development of the intrasegmental bronchial tree: the pattern of branching and development of cartilage at various stages of intra-uterine life. *Thorax* 16:207–218
- Constantino ML, Bagnoli P, Dini G, Fiore GB, Soncini M, Como C, Acocella F, Colombi R (2004) A numerical and experimental study of compliance and collapsibility of preterm lamb tracheae. *J Biomech* 37:1837–1847
- Doras KS, Wolfson MR, Searls RL, Hilfer SR, Shaffer TH (1991) Developmental changes in tracheal structure. *Pediatr Res* 30:170–175
- Duda GN, Grainger DW, Frisk ML, Bruckner-Tuderman L, Carr A, Dirnagl U, Einhaupl KM, Gottschalk S, Gruskin E, Huber C, June CH, Mooney DJ, Rietschel ET, Schutte G, Seeger W, Stevens MM, Urban R, Veldman A, Wess G, Volk HD (2014) Changing the mindset in life sciences toward translation: a consensus. *Sci Transl Med* 6:264cm12
- Fraga JC, Jennings RW, Kim PC (2016) Pediatric tracheomalacia. *Semin Pediatr Surg* 25:156–164
- Hollister SJ (2017) Paediatric devices that grow up. *Nat Biomed Eng* 1:777–778
- Hollister SJ, Flanagan CL, Zopf DA, Morrison RJ, Nasser H, Patel JJ, Ebramzadeh E, Sangiorgio SN, Wheeler MB, Green GE (2015) Design control for clinical translation of 3D printed modular scaffolds. *Ann Biomed Eng* 43:774–786
- Hollister SJ, Flanagan CL, Morrison RJ, Patel JJ, Wheeler MB, Edwards SP, Green GE (2017a) Integrating image-based design and 3D biomaterial printing to create patient specific devices within a design control framework for clinical translation. *ACS Biomater Sci Eng* 2:1827–1836
- Hollister SJ, Hollister MP, Hollister SK (2017b) Computational modeling of airway instability and collapse in tracheomalacia. *Respir Res* 18:62–69
- Hysinger EB, Panitch HB (2016) Paediatric tracheomalacia. *Paediatr Respir Rev* 17:9–15
- Javia L, Harris MA (2016) Fuller 5. Rings, slings, and other tracheal disorders in the neonate. *Semin Fetal Neonatal Med* 21:277–284
- Khanafar K, Duprey A, Zainal M, Schlicht M et al (2011) Determination of the elastic modulus of ascending thoracic aortic aneurysm at different ranges of pressure using uniaxial tensile testing. *J Thorac Cardiovasc Surg* 142:682–686
- Kida K, Thurlbeck WM (1981) Tracheal banding in weanling rats diminishes lung growth and alters lung architecture. *Pediatr Res* 15:269–277
- Kim K, Jeong CG, Hollister SJ (2008) Non-invasive monitoring of tissue scaffold degradation using ultrasound elasticity imaging. *Acta Biomater* 4:783–790
- Kugler C, Stanzel F (2014) Tracheomalacia. *Thorac Surg Clin* 24:51–58
- Lam CXF, Teoh SH, Hutmacher DW (2007) Comparison of the degradation of polycaprolactone and polycaprolactone-(b-tricalcium phosphate) scaffolds in alkaline medium. *Polym Int* 56:718–728
- Lam CXF, Savalani MM, Teoh SH, Hutmacher DW (2008a) Dynamics of in vitro polymer degradation of polycaprolactone-based scaffolds: accelerated versus simulated physiological conditions. *Biomed Mater* 3:034108
- Lam CXF, Hutmacher DW, Schantz J-T, Woodruff MA, Teoh SH (2008b) Evaluation of polycaprolactone scaffold degradation for 6 months in vitro and in vivo. *J Biomed Mater Res Part A* 90:906–919
- Les AS, Flanagan CL, Premanathan A, Hollister SJ, Ohye RG, Green GE (2018) A novel, patient-specific, 3D printed, bioresorbable external airway splint for the treatment of life-threatening tracheobronchomalacia, American Academy of Thoracic Surgeons 98th Annual Meeting, San Diego, 28 Apr–1 May
- Morrison RJ, Hollister SJ, Niedner MF, Ghadimi Mahani G, Park AH, Mehta DK, Ohye RG, Green GE (2015) Mitigation of tracheobronchomalacia with 3D-printed personalized medical devices in pediatric patients. *Sci Transl Med* 7:285–296

- Nalwa SS, Hartig GK, Connor NP, Warner T, Thielman MJ (2001) Evaluation of poly-l-lactic acid and polyglycolic acid resorbable stents for repair of tracheomalacia in a porcine model. *Ann Otol Rhinol Laryngology* 110:993–999
- Penn RB, Wolfson MR, Shaffer TH (1989) Developmental differences in tracheal cartilage mechanics. *Pediatr Res* 26:429–433
- Rasperini G, Filipchuk SP, Flanagan CL, Park CH, Pagni G, Hollister SJ, Gainnobile WV (2015) 3D-printed bioresorbable scaffold for periodontal repair. *J Dent Res* 94:153S–157S
- Shi HC, Deng WJ, Pei C et al (2009) Biomechanical properties of adult-excised porcine trachea for tracheal xenotransplantation. *Xenotransplantation* 16:181–186
- Vinograd I, Filler RM, England SJ, Smith C, Poenaru D, Bahoric A, Kent G (1987) Tracheomalacia: an experimental animal model for a new surgical approach. *J Surg Res* 42:597–604
- Volk HD, Stevens MM, Mooney DJ, Grainger DW, Duda GN (2015) Key elements for nourishing the translational research environment. *Sci Transl Med* 8:282cm2
- Wright A, Ardran GM, Stell PM (1981) Does tracheostomy in children retard the growth of trachea or larynx? *Clin Otolaryngol* 6:91–96
- Zopf DA, Hollister SJ, Nelson ME, Ohye RG, Green GE (2013) Bioresorbable three-dimensional printed airway splint. *New Engl J Med* 368:2043–2045
- Zopf DA, Flanagan CL, Wheeler M, Hollister SJ, Green GE (2014) Treatment of severe porcine tracheomalacia with a 3-dimensionally printed, bioresorbable, external airway splint. *JAMA Otolaryngol Head Neck Surg* 140:66–71



Bioceramics for Musculoskeletal Regenerative Medicine: Materials and Manufacturing Process Compatibility for Synthetic Bone Grafts and Medical Devices

Ciro A. Rodriguez, Hernan Lara-Padilla, and David Dean

Contents

1	Introduction	162
1.1	Historic Perspective	163
1.2	Markets	164
2	Bioceramics and Manufacturing Process Compatibility	164
2.1	Load-Bearing Implants	166
2.2	Bone Substitutes for Void Filling	167
2.3	Synthetic Bone Grafts	167
3	Synthetic Bone Grafts	168
3.1	Morphology and Mechanical Properties of Scaffolds	170
3.2	Bioceramics and Manufacturing Process Compatibility	173
4	Conclusions	178
4.1	High Resolution Manufacturing Processes and Composites	178
4.2	Graded Materials	178
4.3	Standardized In Vivo Testing	179
	Glossary	180
	Appendix	180
	References	189

C. A. Rodriguez

Escuela de Ingeniería y Ciencias, Tecnológico de Monterrey, Monterrey, Mexico

e-mail: ciro.rodriguez@itesm.mx

H. Lara-Padilla

Departamento de Ciencias de la Energía y Mecánica, Universidad de las Fuerzas Armadas ESPE, Sangolquí, Ecuador

e-mail: hvlara@espe.edu.ec

D. Dean (✉)

Department of Plastic Surgery, The Ohio State University, Columbus, OH, USA

e-mail: David.Dean@osumc.edu

Abstract

This chapter is focused on bioceramics for musculoskeletal regenerative medicine, with emphasis on material and manufacturing compatibility in the development of synthetic bone grafts. Bioceramics are classified into families depending on their relative bioactivity: passive, bioactive, and bioresorbable. Passive bioceramics, such as alumina and zirconia, are mainly used for load-bearing implants. Bioactive ceramics, such as bioactive glass, are useful to generate a strong bond between metallic surfaces and bone. Bioresorbable ceramics are applied to bone void filling and scaffolds for synthetic grafts. A description of bioceramics and their use in manufacturing processes is given, with major emphasis on techniques that may be useful in the fabrication of regenerative devices such as synthetic bone grafts. The manufacturing processes of interest are classified into molding, additive manufacturing, and coating techniques. The use of bioceramic-based scaffolds in bone repair animal models and clinical studies is reviewed. Finally, this chapter provides an outlook of future research directions for improved bioceramic use in synthetic bone grafts or regenerative skeletal devices.

1 Introduction

Ceramics are nonmetallic and inorganic solids (Kingery et al. 1976). The majority of ceramics are compounds of metals, metalloids, or nonmetals. Most frequently they are oxides, nitrides, and/or carbides. However, diamond and graphite are also classified as ceramics. Glass, not a solid in strict terms, is therefore considered a special type of ceramic. Semiconductors are also ceramics, although sometimes they are considered a separate family of materials (Carter and Norton 2007).

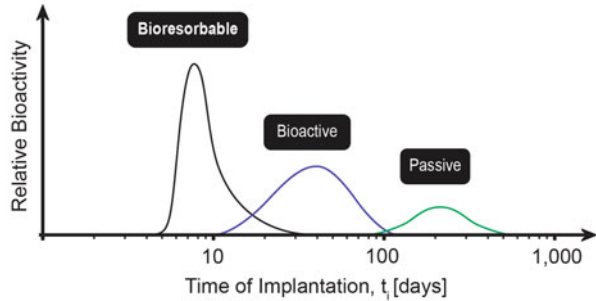
An alternative definition for ceramics is given by McCollm: “Any of a class of inorganic, nonmetallic products which are subjected to a temperature of 540 °C or above during manufacture or use, including metallic oxides, borides, carbides, or nitrides, and mixtures or compounds of such materials” (McCollm 2013). Thus, the study of ceramics encompasses a wide range of materials.

When used in biomedical applications, especially when placed inside the human body, ceramics are referred to as bioceramics. The relative bioactivity of a given type of bioceramic allows its classification into one of the three following broad families: passive, bioactive, and bioresorbable ceramics (see Fig. 1).

Passive or nearly inert bioceramics show minor interaction with human tissues. The most widely used passive ceramics are formulations of alumina and zirconia.

In contact with human tissue, bioactive materials generate a specific biological response at the interface, often resulting in the formation of a bond between the tissue and the material. Bioactive ceramics may also be resorbable. If the resorption byproducts are safe, they are referred to as bioresorbable ceramics. Examples of bioactive ceramics include glasses such as Bioglass[®], glass-ceramics such as apatite-wollastonite (A/W), dense synthetic hydroxyapatite (HAP), and a variety of bioceramic composites. When implanted bioactive ceramics form a layer of hydroxy-carbonate

Fig. 1 Classification of bioceramics based on their relative bioactivity. Adapted from (Hench and Wilson 2013)



apatite (HCA), where collagen fibrils are incorporated, therefore binding the inorganic surface to the organic constituents of tissues (Hench and Wilson 2013). Bioresorbable ceramics include several calcium phosphates such as tricalcium phosphate (TCP) that degrades into calcium and phosphate salts (Hench and Wilson 2013).

1.1 Historic Perspective

In orthopedics, although the total hip replacement operation was first conducted in 1938, it was not until 1961 that much improved designs and materials made this procedure a clinical success (Learmonth et al. 2007). The use of alumina as a coating for the joint surface in hip implants was first attempted in the 1970s. Indeed, the current use of bioceramics as implant components is mostly limited to coatings, particularly for hip and knee implants. These coatings are an improvement over previous metal-on-metal joints and metal-bone interfaces (Semlitsch et al. 1977; Chevalier and Gremillard 2009). In the case of alumina coatings, it has been observed that they significantly reduce the generation of wear particles over previous metal-on-metal solutions (Hannouche et al. 2005). In order to improve the mechanical properties and reliability of hip implants, zirconia was also introduced as a candidate joint surface coating in the 1980s (Piconi and Maccauro 1999).

In its early use, approximately one of every six alumina- or zirconia-containing hip implants failed. With continuous improvement of alumina and zirconia, these materials today deliver much better ceramic coating-related failure rates in hip implant applications (i.e., less than 0.01%). The clinical success associated with the use of these advanced bioceramics has led to the implantation of millions of hip and knee total joint replacement devices worldwide (Chevalier and Gremillard 2009).

Feldspathic porcelain teeth and dentures were first introduced in the late 1700s in France. However, widespread use of porcelain in dentistry did not begin until the 1950s with new porcelain formulations that provided improved mechanical properties and affordable manufacturing procedures (Kelly et al. 1996). In addition to porcelain, alumina and zirconia are now widely used in dental applications.

In the 1960s, the development of bioactive ceramics began with the formulation of bioactive glass, commonly referred to as Bioglass[®] (Hench 2006). Systematic study of various bioresorbable synthetic calcium phosphates, such as hydroxyapatite

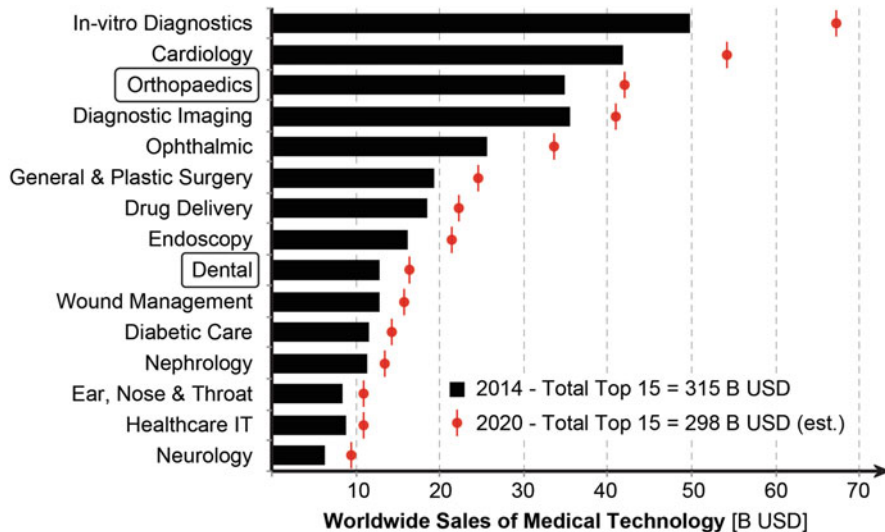


Fig. 2 Trends in worldwide sales of medical technology, considering the top 15 product categories (Evaluate 2015). The circled clinical fields indicate the best opportunities for bioceramics. Please note that many surgical fields other than orthopedics contribute to skeletal repair and regeneration. To that extent those therapies are equally good opportunities for bioceramic applications

and tricalcium phosphate, dates back to the 1980s (Best et al. 2008; Metsger et al. 1982). Today, industry provides a wide range of bone substitute products for use in non-weight-bearing defects. Most of these materials are composites that combine various calcium phosphates (Liu et al. 2013).

1.2 Markets

In regards to medical technology, bioceramics have a significant clinical and economic relevance (see Fig. 2). Orthopedics and dental applications are the mayor drivers in this field, with combined sales of \$47.7 billion USD worldwide and significant projected growth in the next few years (Evaluate 2015).

2 Bioceramics and Manufacturing Process Compatibility

The complete scope of medical bioceramic uses includes a large number of material compositions and manufacturing processes. In order to provide a comprehensive map, Fig. 3 shows a general representation of material vs. manufacturing process compatibility.

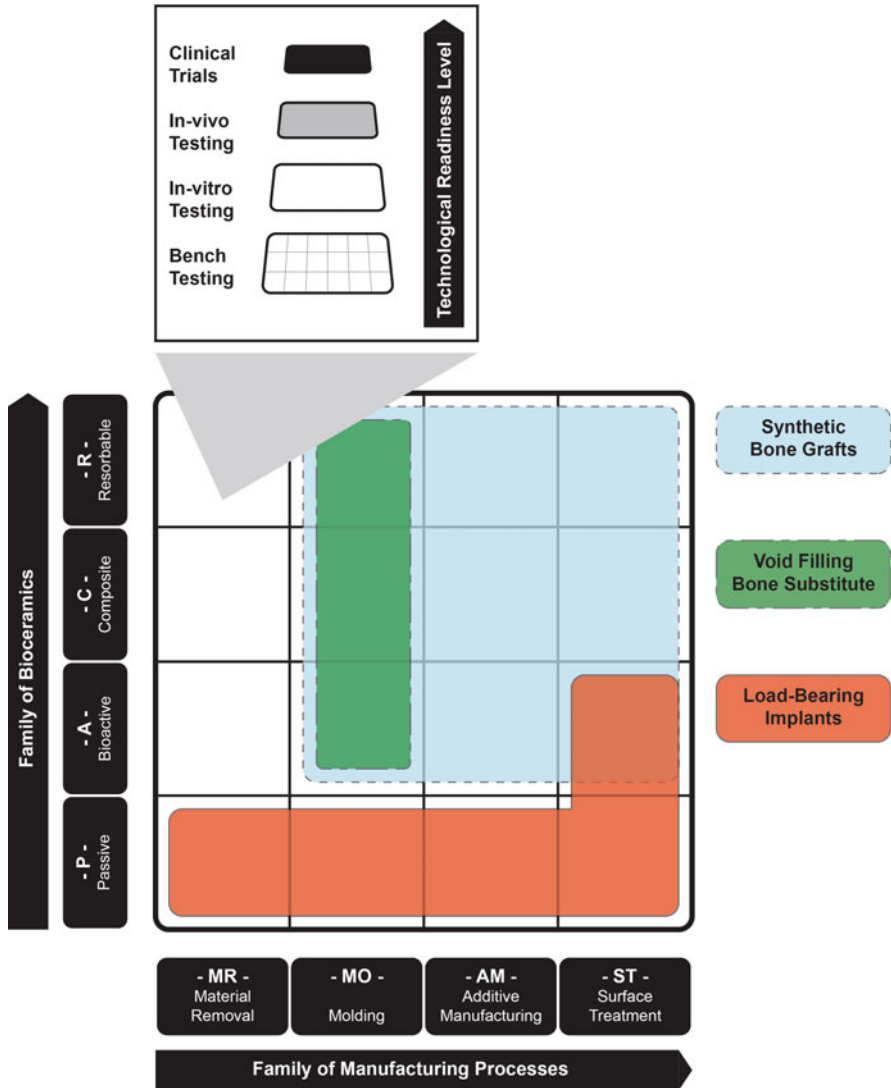


Fig. 3 Material vs. manufacturing process compatibility for bioceramics in musculoskeletal regenerative medicine

The forming of bioceramics involves manufacturing processes that utilize material removal (cutting and machining), molding, additive manufacturing, and surface treatments. In addition to the compatibility and process capability issues, there is also interest in mapping technology readiness levels of devices and current manufactur-

ing processes. This places each device in the continuum between proof-of-concept ideas and use in the clinic (i.e., bench to clinic progression) (Woodruff et al. 2012).

2.1 Load-Bearing Implants

Figure 4 shows the major application categories for bioceramics in musculoskeletal regenerative medicine. Load-bearing implants include components made mainly with passive bioceramics through material removal and molding processes. Bioactive ceramics are used as coatings or metallic components such as the stem or joint of

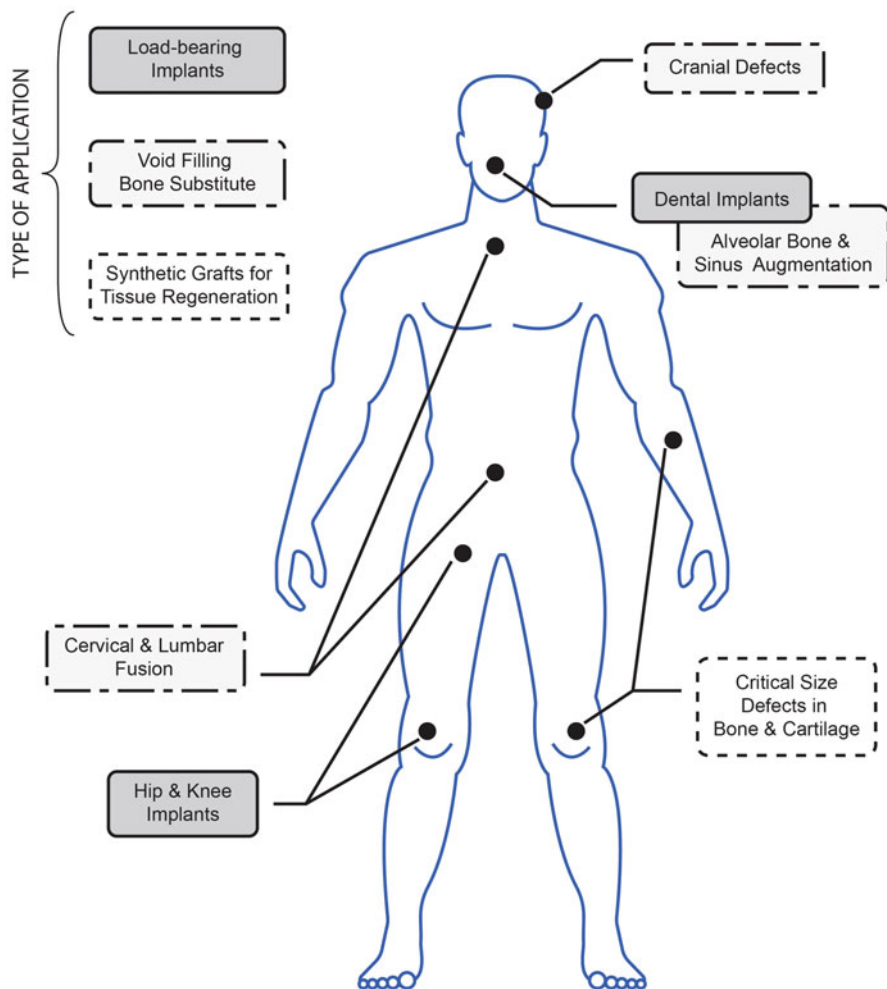


Fig. 4 Application of bioceramics in musculoskeletal regenerative medicine (Agarwal et al. 2009; Bartolo et al. 2012; Bonda et al. 2015; Obregon et al. 2015)

hip implants or the post, literally a bone screw, of a dental implant. Passive bioceramics can be processed via additive manufacturing processes but are more commonly used for product prototyping purposes than for the fabrication of clinical devices. Functional components require the close tolerance and surface finish capability of machining and grinding processes in order to minimize micro cracks and potential catastrophic failure.

2.2 Bone Substitutes for Void Filling

Bone substitutes for void filling may be manufactured with molding processes, using materials such as hydroxyapatite, tricalcium phosphate, or combinations of different bioceramics (see Fig. 3). These bone substitutes are available in the form of chips, granules, putties, or blocks that can be cut to fit a bone defect (Crowley et al. 2013). Some products are formulated with a matrix of collagen that contains a bioceramic phase (Pilipchuk et al. 2015).

When spinal fusion is indicated, the procedure involves: (a) removal of the disc, which in turn creates a void between adjacent vertebrae; (b) implantation of a spinal cage (a kind of spacer usually made from titanium alloy or high strength polymer such as PEEK); (c) stabilization with titanium screws and rods; and, finally, (d) filling the spinal cage with a bioceramic bone substitute. There are a number of products on the market, each with a specific formulation for spinal fusion and repair of fracture vertebrae (i.e., balloon kyphoplasty) procedures (Liu et al. 2013). Another major application of bone substitutes for void filling is related to dental extraction or periodontal diseases where teeth or jaw bone mass has been lost to the point that the deficient region cannot support dental implants. This bone supports the roots of the teeth and is therefore referred to as alveolar (i.e., tooth socket) bone. Repair and/or reconstruction of alveolar bone and or associated facial sinus augmentation procedures can involve the use of bioceramic bone fillers (Pilipchuk et al. 2015). Bone substitutes are also used to regenerate cavity defects left by tumors (Crowley et al. 2013) and repair small cranial defects (Bonda et al. 2015).

2.3 Synthetic Bone Grafts

Synthetic grafts are porous constructs, often shaped in the operating room, to a specific bone or cartilage defect. These synthetic grafts may include resorbable bioceramics that may act as a scaffold for cells and growth factors (Bonda et al. 2015). The synthetic bone graft category is a demanding application for bioceramics in musculoskeletal regenerative medicine. These materials have found limited clinical application in the repair of load-bearing defects.

The use of bioceramics in scaffolds as synthetic grafts can also be prepared as bioactive and bioresorbable ceramic composites. These composites can be fabricated with processes such as molding, additive manufacturing, or coating. The composite materials used for this type of scaffold may also be combined with polymers and

metals. Biphasic calcium phosphates are a widely studied composite that combine the properties of hydroxyapatite (HA; bioactive) and beta-tricalcium phosphate (β -TCP; bioresorbable) (Baradararan et al. 2012). The following sections will focus on synthetic bone graft materials and constructs, detailing the currently available bioceramics and manufacturing processes.

3 Synthetic Bone Grafts

Bone is a key component of the musculoskeletal system, providing structure for ambulatory and environmental manipulating functions, storing nutrients, protecting vital organs, and playing a key role in hematopoietic and immunological functions. Although bone possesses an extraordinary regenerative capacity, it can fail to heal under unstable and large deficit conditions. Defects in bone can be caused by trauma, cancer, congenital and developmental deformities, arthritis, aging, and infection (Larsen et al. 2015). In the trauma category alone, there is an estimate of 15 million fracture cases per year worldwide, with up to 10% of repairs subsequently having complications due to nonunion of large defects (Liu et al. 2013).

The standard of care treatment for nonreducible bone fractures (i.e., “reduction” of the gap caused by the break) and resections is an autologous bone graft, also referred to as autograft. Autografts are harvested from a donor site and implanted elsewhere in the same patient (Shrivats et al. 2014). Grafted bone has excellent osteogenic, osteoinductive, and osteoconductive properties. However, this approach also brings some important disadvantages: potential complications at the donor site (e.g., pain and morbidity), possibly a limited or insufficient blood supply, and often there is difficulty shaping the autograft to fit the bone defect (Crowley et al. 2013).

Another option is to seek bone via allogeneic graft (also referred to as allograft). Allografts are tissues harvested from human donors (i.e., people other than the patient), with subsequent graft processing for implantation in the patient. The main disadvantages of this approach are the risk of adverse immunological response (i.e., immunological rejection), potential disease transmission, and reduced osteogenic capacity due to devascularization, decellularization, demineralization, and/or sterilization processing. Xenografts are donor tissues derived from nonhuman species. Similar to allografts, these tissues are processed for sterility and biocompatibility. The risk of immunological response, disease transmission, and ethical issues associated with the use of animal tissues has limited the clinical use of xenografts (Shrivats et al. 2014).

The common clinical problem of bone defects and the limitations of current solutions (i.e., autografts, allografts, and xenografts) motivate an enthusiastic, worldwide search by the scientific community for alternatives to autologous or allogeneic bone grafts such as entirely synthetic bone graft strategies. Advances in bioceramics and manufacturing processes have opened a number of new paths for research and development into an artificial approach.

Early clinical applications of synthetic bone graft materials included scaffolds shaped from blocks of coral (primarily CaCO_3) (Pountos and Giannoudis 2016).

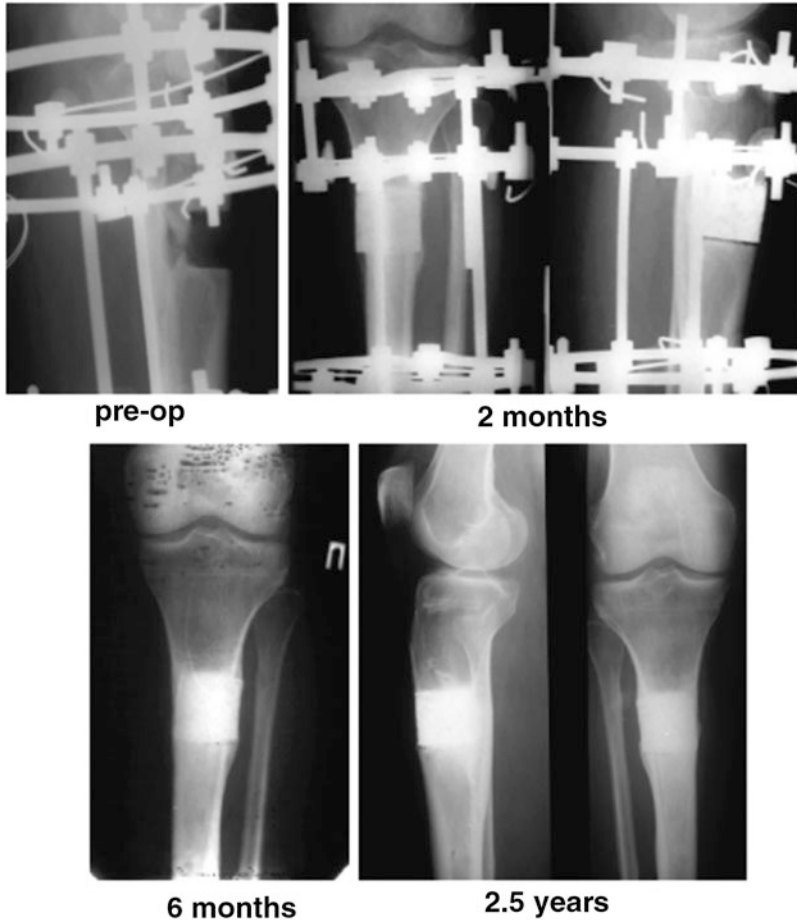


Fig. 5 Implantation of a porous bioceramic scaffold seeded with autologous BM-MSCs for clinical treatment of critical size segmental tibial defect (Marcacci et al. 2007)

Similarly, porous hydroxyapatite blocks with 60% interconnected porosity and an apparent density of 1.26 g/cm^3 have been studied. Autologous bone marrow-derived mesenchymal stem cells (BM-MSC) were expanded *in vitro* and seeded by capillarity into the scaffold. A pre-operative radiograph shows a 40 mm gap in the bone (see Fig. 5). After 2.5 years, much of the synthetic HAP was evident indicating an extremely slow resorption rate (Quarto et al. 2001; Marcacci et al. 2007).

The tissue engineering approach to bone repair studied by Marcacci et al. still has had limited clinical application due to a number of challenges (Cancedda et al. 2007). However, that clinical experience, together with numerous studies with animal models, can lead to a more systematic approach to the development of synthetic bone grafts (Crowley et al. 2013; Li et al. 2015).

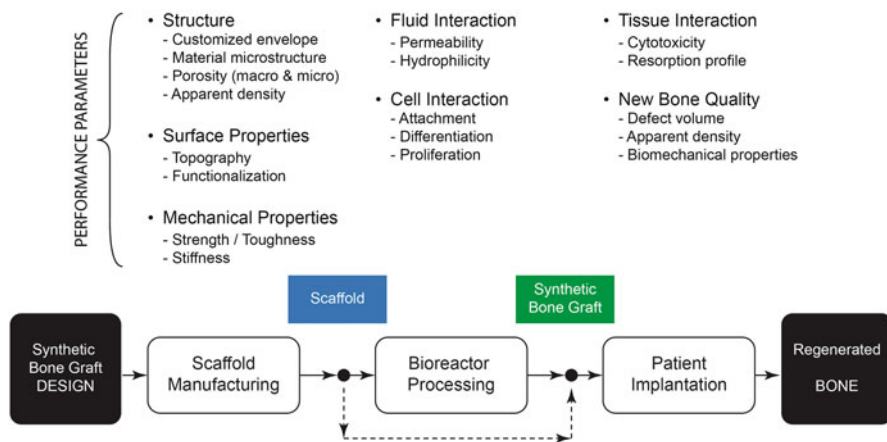


Fig. 6 Tissue engineering process for bone repair based on synthetic bone grafts

Another potentially promising process for the generation of a synthetic bone graft is outlined in Fig. 6. Studies have attempted to capture key performance parameters of the process at each stage. Based on the type of bone defect repaired, the starting point will be synthetic bone graft design. At the next stage, a scaffold is manufactured. The following stage involves combining cells with the scaffold to constitute a synthetic bone graft. Growth factors (bioactive molecules) may be added at this stage. For some cases, the scaffold alone (i.e., cell-free) is used as the graft. Finally, the synthetic bone graft is implanted into the bone defect to help regenerate new tissue.

Ultimately, we are interested in the quality of the newly regenerated bone. Neobone quality is measured in terms of the regenerated volume compared to the original bone defect size, the new bone's apparent density and its biomechanical properties. The final bone quality will depend on a complex interaction between the defect's wound healing and remodeling response and the synthetic bone graft material over time. Remodeling is necessary for the production/regeneration of strong bone. Nonresorbing material that does not degrade within 4–12 months may block this process.

It is clear that much research is still needed to understand and model the bone repair process (Larsen et al. 2015). However, a systematic approach to this challenge calls for defining and controlling key performance parameters at the different stages of graft fabrication and the healing response.

3.1 Morphology and Mechanical Properties of Scaffolds

In the context of synthetic bone grafts, the morphology and quality of scaffolds requires standard and comparable parameters. Figure 7 shows examples of this type of scaffold.

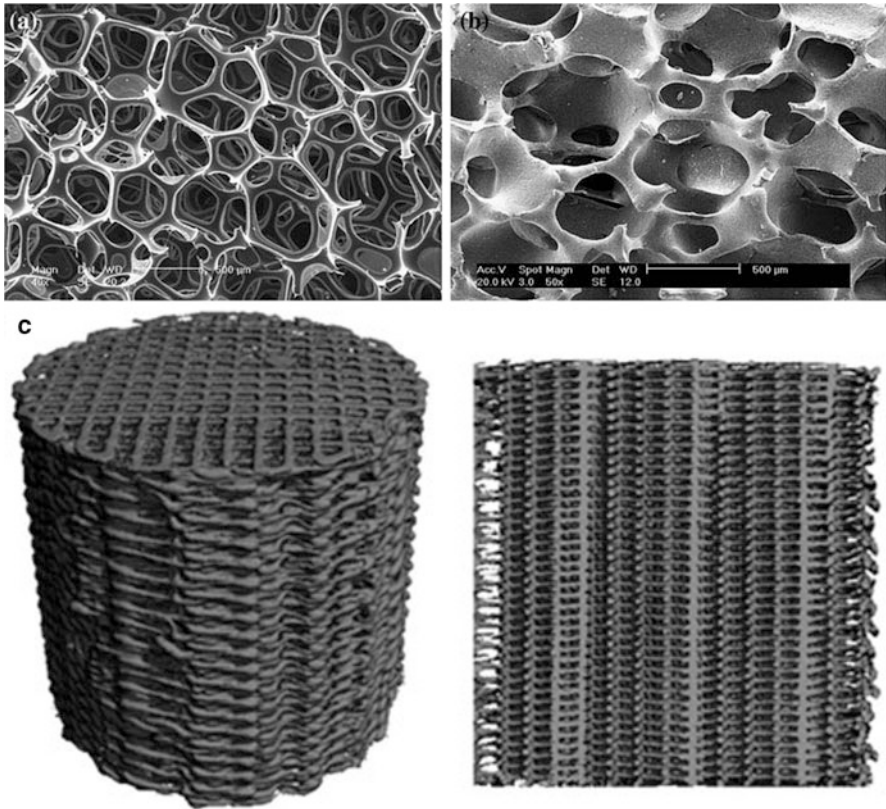


Fig. 7 Examples of scaffolds generated via molds and additive manufacturing (3D printing): (a) polyurethane foam (Cai et al. 2009), (b) scaffold from β -TCP/BG with 75% porosity (after sponge impregnation using the polyurethane foam as template and sintering), (c) micro tomography reconstruction of scaffold from composite of PCL and TCP, using fused deposition modeling (FDM) for processing (Reichert et al. 2011)

Total scaffold porosity (Π_{total}) is defined as a combination of the open or macroporosity (Π_{macro}) and the internal or microporosity (Π_{micro}) of the base material, as follows:

$$\Pi_{total} = \Pi_{macro} + \Pi_{micro} \tag{1}$$

When designing a scaffold, macroporosity (with dimensions over 100 microns) should be interconnected to allow flow (e.g., influx of nutrients and chemical signals and removal of waste products) during the osteogenic process. Porosity, tortuosity, hydrophilicity, and microporosity will all have an effect on scaffold permeability and its ability to guide new tissue formation. Some of the manufacturing processes for bioceramics produce an inherent microporosity (i.e., dimensions between

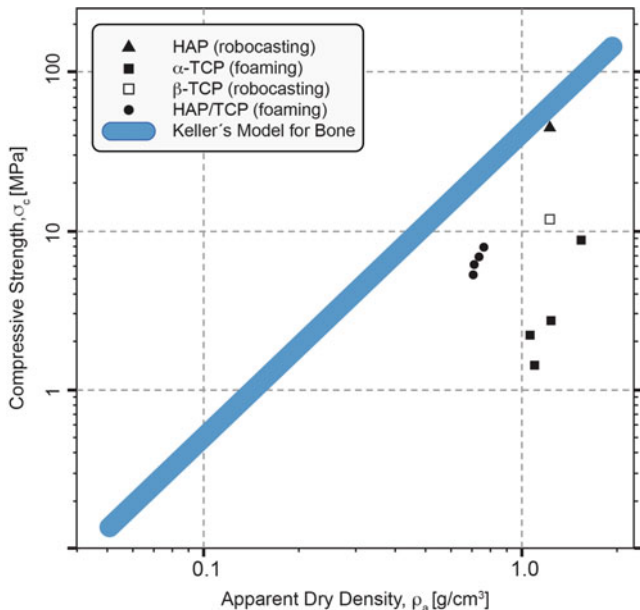


Fig. 8 Compressive strength vs. apparent dry density for bone and bioceramics-based scaffolds (Almirall et al. 2004; Baradararan et al. 2012; Keller 1994; Miranda et al. 2008)

100 nanometers and a few microns). Microporosity is not interconnected in these constructs. Some authors refer to the base material microporosity as “strut porosity” (Hing et al. 2005).

Total scaffold porosity (Π_{total}) is related to the apparent dry density (ρ_a) as follows:

$$\Pi_{\text{total}} = (1 - \rho_a/\rho_m) * 100\% \quad (2)$$

where the base material theoretical density is represented by ρ_m .

The apparent dry density of bone has been closely correlated to its mechanical properties, such as compressive strength and elastic modulus (see Fig. 8) (Keller 1994). Similarly, any comparison of bioceramic scaffolds and a manufacturing process should consider the mechanical properties as a function of apparent dry density.

A synthetic bone graft is intended to facilitate the regeneration and remodeling of bone. While performing this function, the graft should gradually resorb in response to bone formation. For many critical size defects, the adjacent bone segments would require stabilization with metallic plates or a rod during this process. Therefore, in this context, the ideal mechanical properties of the scaffold are not necessarily those of the healthy bone, but rather what is needed for bone regeneration. However, in terms of standardized parameters, it is useful to rate mechanical performance of scaffolds relative to each other and relative to Keller’s Model for resilient bone (see Fig. 8).

3.2 Bioceramics and Manufacturing Process Compatibility

3.2.1 Bioceramic Devices Produced in Molds

Scaffolds for bone regeneration with interconnected porous structure can be produced in molds using a variety of methods, such as sponge impregnation, freeze drying, phase inversion, sol-gel foaming, particulate leaching, injection molding, and direct casting.

In the sponge impregnation method, a polyurethane foam template is impregnated with bioceramic slurry. The objective is to generate a thick coating of bioceramic slurry around the struts of the template. After drying the impregnated sponge, a sintering process is used to remove the polymer leaving behind the intended interconnected porous structure (Dai et al. 2015; Zreiqat et al. 2010).

Freeze drying, thermally induced phase inversion, and sol-gel foaming involve chemical reactions that produce a porous structure (Guo et al. 2012; Midha et al. 2013; Tamjid and Simchi 2015; Wang et al. 2007). Particulate leaching is based on a mixture of bioceramic material and a salt that is either compacted within a mold or poured into a mold. In a second step, the salt particulates are leached with water to form a porous structure (Zhang et al. 2016). The size, shape, concentration, and distribution of the particulate can be important. However, the resulting pore geometry cannot insure interconnectivity.

Injection molding requires a special mold with multiple cores and slides (i.e., moving components of the mold) that generate an interconnected geometry (Vivanco et al. 2012). In direct casting, a core (sometimes referred to as a “negative mold”) is used to form the complete interconnected network of macropores. Then, a ceramic slurry is cast around the core (Li et al. 2013). Only injection molding and direct casting can use a mold to produce a designed structure that includes macroporosity. All other molding techniques tend to deliver a random distribution of interconnected macropore diameters, in a foam-like structure (see Fig. 7).

When the material for the scaffold is only bioceramic, a sintering process can be used to achieve a microstructure with good mechanical properties. The sintering step is itself a complex process that involves a number of parameters and requires optimization (Champion 2013). In general, an increased sintering temperature reduces microporosity and the resorption rate of the bioceramic scaffold (Yuan et al. 2010).

In terms of materials, some of the most promising advances involve processing composites that combine bioceramics and polymers through molding processes. In vivo testing with rats and rabbits were recently reported with this approach: freeze drying (Park et al. 2016; Chiba et al. 2016), compression molding, and particle leaching (Zhang et al. 2016), followed by phase inversion (Guo et al. 2012). More details about these studies can be found in the appendix.

The work reported by Chiba et al. uses octacalcium phosphate with gelatin. The scaffolds were tested on Japanese white rabbits with cavity tibial defect. Biomechanical testing of neobone was conducted with an indentation test, reaching near 100% of the compressive load compared to control cortical bone (Chiba et al. 2016).

The composite used by Zhang et al. combines HAP and PLLA/PLGA. They tested this material in a Sprague-Dawley rat calvarial defect (i.e., 6 mm round defect) model. After 12 weeks of implantation, an indentation test shows that new bone has obtained 85% of the hardness and 78% of the elastic modulus, compared to natural rat cranial bone. In this case, the scaffold had 80% macro porosity, with average pore size of 145 μm and compressive strength of 0.1 MPa.

Recently, the use of bioactive glass has been studied as a scaffold in *in vivo* studies utilizing rabbit, goat, dog, and sheep models (El-Rashidy et al. 2017). Selected animal studies with emphasis on biomechanical properties include rabbits (Tang et al. 2016) and goats (Ghosh et al. 2008). Tang et al. shows excellent biomechanical properties of new bone in rabbit radius segmental defect (16 mm), utilizing bioactive glass scaffolds manufactured by the sponge impregnation technique and BMP-2 (Bone Morphogenetic Protein).

A summary of selected *in vivo* studies using molding processes for scaffolds is shown in Table A.1. The studies are classified based on the bioceramic family and manufacturing process.

3.2.2 Additive Manufacturing Methods

Additive manufacturing (3D printing) technologies provide a wide range of possibilities for the fabrication of bioceramic scaffolds that may then be useful as synthetic bone graft scaffolds, particularly with bioceramics as a printable material or component of a printable material. Table 1 shows the most common suitable additive manufacturing methods for bioceramic materials. Other references provide extensive and detailed description of additive manufacturing (Larsen et al. 2015; Pati et al. 2015; Raman and Bashir 2015). Here, we provide only brief descriptions of these technologies.

In addition to those additive manufacturing processes used to produce bioceramic scaffolds, there are significant advances in recent years in developing powder bed additive manufacturing for load-bearing passive bioceramics. Partial melting (SLS) and full melting (SLM) approaches use bioceramics in the form of powder or slurry to produce parts in a single step or multiple steps (i.e., postprocessing after additive manufacturing). In this field, the main challenges are the bioceramic powder's flowability during the 3D printing process and the final material's microstructure (Deckers et al. 2014; Sing et al. 2017; Zocca et al. 2015).

The most advanced applications of bioceramic scaffolds produced via additive manufacturing are summarized here through *in vivo* animal model studies. Scaffolds based on inkjet printing of tricalcium phosphate scaffolds have been tested with rat, mouse, goat, and dog models. These studies have tested the viability of these bone regeneration strategies (Tarafder et al. 2013; Inzana et al. 2014; Habibovic et al. 2008; Igawa et al. 2006, respectively). High concentrations of ceramic have been suspended and 3D printed in polycaprolactone (PCL) or poly(lactic-co-glycolic-acid) (PLGA) for extrusion 3D printing as a flexible material referred to as "hyper-elastic bone". This material presented promising results in a rat spine model (Jakus et al. 2016, 2017). More details about these studies can be found in the appendix.

Table 1 Additive manufacturing processes suitable for bioceramics, as discussed in ISO/ASTM 52900 (2015). Please see glossary for process column acronyms

ASTM category		Process	Description
Material extrusion	Material melting	FDM: Fused deposition modeling	Extrusion of thermoplastic material through a heated nozzle. Variations of FDM are LDM (low-temperature deposition modeling) and PED (precision extruding deposition)
		MES: Melt electrospinning	In this process, the extruded FDM filament is further stretched by an electrical field
	Pressure dispensing	PAD: Pressure assisted dispensing	Dispensing of hydrogels with pressure assistance (sometimes used for cell bioprinting)
		DIW: Direct ink writing/robocasting	Dispensing of ceramic paste with pressure assistance
		ELS: Electrospinning	Stretching of polymer fibers through electrical field, after a polymer/solvent solution is injected through a needle
Powder bed fusion	SLS: Selective laser sintering	Sintering or partial melting of powder via laser without controlled atmosphere (i.e., variable humidity)	
	SLM: Selective laser melting	Full melting of powder e-beam or via laser with controlled atmosphere	
Binder jetting	3DP: Inkjet printing	Consolidation of powder material through binder jet	
Vat photopolymerization	SLA: Stereolithography	Curing of photopolymer through UV laser	
	DMD: Direct micromirror device	Curing of photopolymer through UV lamp and DLP mask	

Recently, bioactive glass (processed by SLS) was used as a BMP-2 carrier and tested in rats with a femur segmental defect (5 mm) and stabilization with an internal rod (Liu et al. 2014). Biomechanical performance of the resulting neobone was assessed via a three point bending test.

Ceramic/metal composites have also shown promise as viable scaffold biomaterials for bone regeneration. Sun et al. report the use of direct ink writing of a paste made of Wollastonite (CSi) and magnesium for the fabrication of bone scaffolds. Rabbits with round calvarial defects (8 mm) were used in an in vivo model to test the viability of these scaffolds. The regenerated bone showed compressive strengths up to 45 MPa (Sun et al. 2016).

The use of larger animal models with critical size cranial, radial, femoral, or tibial segmental defects is common (e.g., rabbits, dogs, sheep, goats, pig, or horse models) once small mammal work, often with a mouse, guinea pig, or rat model, has shown biocompatibility and other aspects of safety and effectiveness. These larger mammal models are a more challenging test due to slower metabolism and wound healing as well as load-bearing, all of which are more like what is seen in a human patient. Recent studies with a sheep tibial segmental defect show some

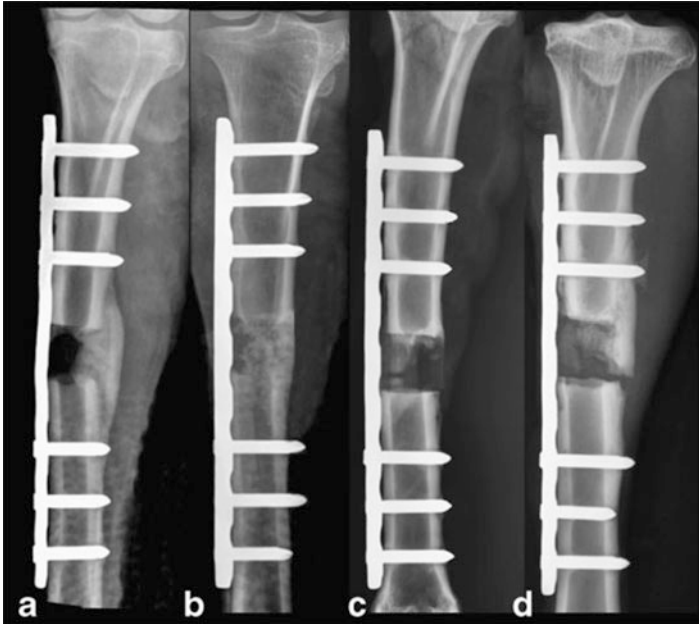


Fig. 9 Tibial segmental defect (20 mm) in sheep: (a) untreated defect, (b) autologous bone graft, (c) synthetic bone graft with mPCL-TCP scaffold, (d) synthetic bone graft with PDLLA-TCP-PCL scaffold (Reichert et al. 2011)

preliminary results with bioceramic bone scaffolds (Lohfeld et al. 2012; Reichert et al. 2011). Lohfeld et al. tested a composite scaffold composed of β -TCP + PCL (polycaprolactone) powder (fabricated via SLS). Reichert et al. tested FDM 3D printed scaffolds composed of a composite of TCP and a resorbable polymer. By comparison with the mechanical properties of a (control) healthy tibia, the combination of medical grade PCL with TCP achieved 15% of the torsional moment, while the autologous bone graft showed 19% (sacrifice at 12 weeks post-implantation) (see Fig. 9). Abbah et al. tested an FDM-based scaffold for intervertebral fusion in a pig model with scaffolds combining β -TCP and PCL. They observed that the biomechanical properties of the fused vertebrae with a scaffold were similar to those of the autograft treatment (Abbah et al. 2009).

Other promising fabrication processes include electrospinning, which can be used to generate fine fibers with diameters in the micron and submicron range (Bartolo et al. 2012). Jaiswal et al. showed the viability of this process in bone regeneration by combining PLLA fibers and a coating of HAP and testing these composite scaffolds in vivo (Jaiswal et al. 2013). It is also possible to use electrospun fibers for drug delivery (Ji et al. 2011).

Electrospun fibers can also be woven into defined or undefined meshes. The orientation of electrospun fibers is determined by the orientation of the fiber source and the cylindrical mandrel onto which those fibers are spun. Melt electrospinning

has been used to deposit polymer fibers with a diameter of about 30 μm , with embedded bioceramics, in a controlled manner. Therefore, a scaffold with controlled macroporosity, ceramic constituents, and/or a roughened texture can be fabricated with this process (Ren et al. 2014).

A summary of selected *in vivo* studies using additive manufacturing for scaffolds is shown in Table A.2. The studies are classified based on the bioceramic family and manufacturing process.

3.2.3 Surface Treatment Methods

The bioceramic-based surface treatment methods discussed here are limited to bioceramic coatings for scaffolds. In this case, a scaffold or another type of medical device is first generated through molding, CNC, or an additive manufacturing process. Then, a coating is applied to improve functional properties of the device.

Recently, Li et al. report a baghdadite ($\text{Ca}_3\text{ZrSi}_2\text{O}_9$) scaffold (initially processed by sponge impregnation) with a coating of nano bioactive glass/PCL (coating processing by immersion). This scaffold was tested in a sheep tibial segmental defect (30 mm) model. A plate and a cast provided stabilization for the first 3 weeks of healing. After 3 weeks, only the cast is removed. Baghdadite scaffolds with and without the coating were tested. Normalized torsional test of the tibial diaphysis was conducted after 26 weeks of implantation, resulting in 5–10% torsional strength and 10–25% torsional stiffness compared with reference healthy tissue (Li et al. 2016).

In a different study, a PPF scaffold (3D printed by SLA [stereolithography, i.e., polymer photocrosslinking]) was coated with biphasic calcium phosphate (BCP), HAP only, or β -TCP only (by immersion). Different BMP-2 doses were used with each type of scaffold in a round rabbit calvarial defect (15 mm) model. After a 6-week implantation period, push-out testing was conducted (i.e., with a flat round indenter). There was no significant difference in volume of new bone among the different coatings (Dadsetan et al. 2015).

Nie et al. showed compressive strength of bioceramic scaffolds (sponge impregnation of BCP, with 94–97% macroporosity) coated with a composite of nanoHAP/PLLA cited as reaching the range of spongy bone in a rabbit femoral head defect (5×15 mm) (Nie et al. 2015). Qui et al. report on the use of a coated bioceramic scaffold for drug delivery in a rat calvarial defect model (6 mm) (Qiu et al. 2016).

Recently a different approach to delivering bioactive molecules involving ceramic coatings has been tried. Instead of infusing whole bioactive cytokines such as BMP-2 into the microporous spaces of a ceramic coating, a bioactive peptide, often the active site, or ligand, of a naturally occurring cytokine, is attached to a ceramic coating. The Becker laboratory has shown methods utilizing a catechol strategy for polymer (Policastro et al. 2015) and metal (Tang et al. 2014; Xu et al. 2017) substrates. More details about these studies can be found in the appendix.

A summary of selected *in vivo* studies using coating processes for medical device, is shown in Table A.3. These studies are classified based on the bioceramic material and manufacturing process.

4 Conclusions

The development of bioceramics has shown promise for contributing to musculoskeletal regenerative medicine. Bioceramic solutions have been found to reduce friction at joint surfaces in hip and knee joint replacement devices, which are recognized as standard-of-care practice. The use of bone substitutes for non-load-bearing skeletal void filling has spurred much research, but, to date, few clinical applications reliably use regenerative bioceramic materials for use in load-bearing skeletal segments with or without the assistance of metallic hardware (Kurien et al. 2013).

Thus, when it comes to taking advantage of the inherent properties of bioceramics for the construction of synthetic bone grafts to regenerate cortical bone, clinical translation has been more limited. The tissue engineering approach that combines scaffolds, cells, and signals (mainly in the form of growth factors) involves complex sets of interactions between synthetic materials and bone-wound healing and bone biology. Therefore, it is not surprising that the development of load-bearing synthetic bone graft strategies remains a technology gap area.

Next, we summarize some of the trends observed in our review of the study and use of bioceramic synthetic bone grafts materials.

4.1 High Resolution Manufacturing Processes and Composites

While bioceramic coatings have become very sophisticated, there remain tremendous challenges in improving bioceramic materials for use in traditional (e.g., grinding and molding) and advanced (e.g., electrospinning, additive manufacturing) fabrication processes. Early scaffold tested in animal models had relatively simple sources for porous spaces (i.e., uncontrolled, naturally formed, with imprecise porosity and permeability) macroporosity (Habibovic et al. 2008). As new additive manufacturing technologies were developed for ceramic powders, higher resolution and therefore more design flexibility can be achieved with processes like SLA (Elomaa et al. 2013; Zanchetta et al. 2016) and DMD (Digital Micromirror Device which houses a Digital Light Processing [DLP] chip; Felzmann et al. 2012; Tesavibul et al. 2012) photocrosslinking of polymer/ceramic resins. For example, the use of nano size particles and doping of ceramic material formulations with 3D printable polymer resins or metallic powders is being explored (Bose et al. 2013; Shao et al. 2016) for use in regenerative medical devices.

4.2 Graded Materials

Of the research and clinical cases reviewed here, all utilize uniform levels of macroporosity and microporosity throughout (Paderni et al. 2009; Li et al. 2016). Moreover, the relationship of geometry, material properties, and functions such as walking, manipulating the environment, or chewing are rarely considered in the

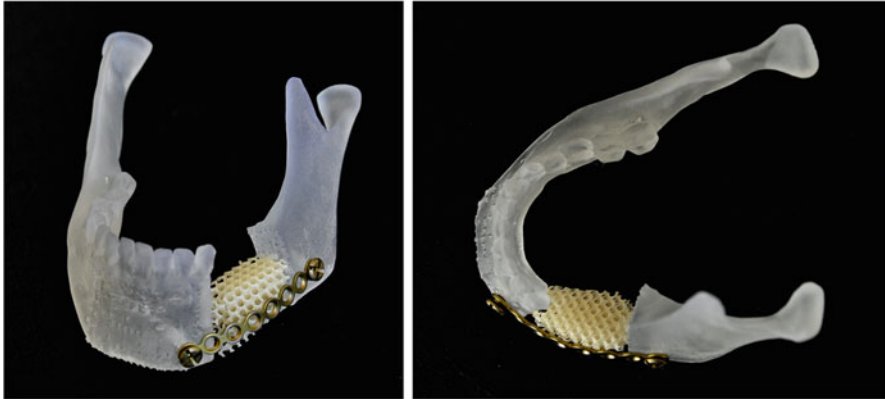


Fig. 10 Model simulating the regeneration of mandibular segmental with a synthetic bone graft and a stabilization plate that will be needed during the bone regeneration process

design of regenerative medical devices (an exception: Moghaddam et al. 2016a). The graded nature of natural bone structure suggests that graded material properties may better mimic the original structure and/or promote regeneration (Jahadakbar et al. 2016; Muller et al. 2015; Zhou et al. 2014). It may be useful to place more effort on the study of simultaneous restoration of shape and function as part of healthy tissue capable of maintaining both (see Fig. 10) (Moghaddam et al. 2016b).

4.3 Standardized In Vivo Testing

Currently, the research literature shows a wide range of animal models and testing methods. There is little discussion about the relationship of the model used to the intended therapy. It is likely that a generalized, load-bearing, bone substitute will have success in both small rodents and large mammal models. However, a large animal model will likely be more comparable to humans as critical size, cortical bone defects, of the size seen in humans are only available in mammals the size of rabbits and larger (Schmitz and Hollinger 1986). Rabbits are easy to handle but do not present any bone that is directly comparable to one that will be treated in human patients. Dogs are considered an appropriate model for some bones. Sheep, goats, horses, and pigs also provide some bones that are similar to the structures found in the human skeleton (Zoetis et al. 2003; Pearce et al. 2007). While nothing will replace the need for human clinical trials to accurately assess safety and efficacy, it is essential that these studies demonstrate the regeneration of biomechanically competent, critical size, fractures or segmental bone defects relevant to the intended human therapy.

Acknowledgments The authors acknowledge partial support from the Army, Navy, NIH, Air Force, VA, and Health Affairs to support the AFIRM II effort under award No. W81XWH-14-2-

0004. The US Army Medical Research Acquisition Activity is the awarding and administering acquisition office for award No. W81XWH-14-2-0004. Partial support was also provided by a Third Frontier (State of Ohio) Technology Validation and Startup Fund (TVSF) grant #15-791 grant, CONACyT grant #DCI from the Government of Mexico to Hernan Lara Padilla, and CONACyT #grant #274867 from the Mexican Government to Ciro A. Rodriguez.

Glossary

- 3DP** Inkjet printing (type of additive manufacturing process)
BCP Biphasic calcium phosphate
BG Bioactive glass
CaP Calcium phosphate
CSF Calcium sulfate (CaSO_4)
DCS Dicalcium silicate (Ca_2SiO_4)
DIW Direct ink writing/robocasting (type of additive manufacturing process)
DLP Digital light processing (type of additive manufacturing process)
DMD Direct micromirror device (type of additive manufacturing process)
ELS Electrospinning (type of additive manufacturing process)
FDM Fused deposition modeling (type of additive manufacturing process)
HAP Hydroxyapatite
LDM Low-temperature deposition modeling (type of additive manufacturing process)
MES Melt electrospinning (type of additive manufacturing process)
nHA Nano-hydroxyapatite
OCP Octacalcium phosphate ($\text{Ca}_8\text{H}_2(\text{PO}_4)_6 \cdot 5\text{H}_2\text{O}$)
PA Polyamide
PAD Pressure assisted dispensing (type of additive manufacturing process)
PCL Polycaprolactone
PED Precision extruding deposition (type of additive manufacturing process)
PLA Polylactide acid
PLDLLA Poly(L-lactide-co-D,L-lactide)
PPF Poly(propylene fumarate)
SLA Stereolithography (type of additive manufacturing process)
SLM Selective laser melting (type of additive manufacturing process)
SLS Selective laser sintering (type of additive manufacturing process)
Slide In the design of injection molds, slides are moving components
Sr-HT Sr-hardystonite ($\text{Sr-Ca}_2\text{ZnSi}_2\text{O}_7$)
TCP Tricalcium phosphate
TTCP Tetracalcium phosphate ($\text{Ca}_4(\text{PO}_4)_2\text{O}$)

Appendix

See Tables [A.1](#) to [A.3](#).

Table A.1 Molding processes for bio ceramic-based scaffolds (selected studies with in vivo testing)

Bioceramic family	Scaffold					In vivo testing		Reference
	Mfg. process	Type of bioactive bio ceramic	Macro porosity, Π_{macro} [%]	Pore diameter, D_p [μm]	Compressive strength, σ_c [MPa]	Type of animal model	New bone evaluation	
Bioresorbable	Phase inversion (solvent: polyvinyl alcohol)	β -TCP	37.0	8–150	24.5* *Flexural strength	Bengal goat with cavity radius defect ($10 \times 5 \text{ mm}^2$)	Histology Biomechanical testing: push out (no natural tissue control)	Ghosh et al. 2008
Composite	Freeze drying	Silk fibroin + β -TCP	–	50	0.7	Sprague-Dawley rats with round calvarial defect (4 mm) Implantation period: 8 weeks	Histology Qualitative microCT	Park et al. 2016
		Gelatin + OCP	–	10–500	–	Japanese white rabbits with cavity tibial defect (6 mm in diameter) Implantation period: 8 weeks	Histology Biomechanical testing: push-out test (control with normal tissue)	Chiba et al. 2016
	Compression molding (NaCl particles 100–200 μm in diameter and distilled water leaching)	PLLA/ PLGA + hap	80	145	0.9	Sprague-Dawley rats with round calvarial defect (6 mm) Implantation period: 6 & 12 weeks	Bone density Biomechanical testing: indentation hardness (control with normal tissue)	Zhang et al. 2016

(continued)

Table A.1 (continued)

	Scaffold				In vivo testing		Reference	
	Mfg. process	Type of bioactive bioceramic	Macro porosity, Π_{macro} [%]	Pore diameter, D_p [μm]	Compressive strength, σ_c [MPa]	Type of animal model		New bone evaluation
	Phase inversion (solvent: ethanol)	PA + HAP	81	100–500	4.4	New Zealand white rabbits with rectangular mandibular angle and body defect (15×8 mm). 2, 4, & 12 weeks	Histology MicroCT for new bone volume	Guo et al. 2012
		PA + nHA	52–70	50–500	13.2–33.9	New Zealand white rabbits with rectangular mandibular defect (8×12 mm) Implantation period: 2, 4, 8 & 12 weeks	Histology (new bone volume estimation)	Wang et al. 2007
Bioactive	Sol-gel foaming	BG	93	100–500	–	Wistar male rats with cavity tibial defect (3 mm) Implantation period: 11 weeks	MicroCT for new bone volume	Midha et al. 2013
	Phase inversion (solver: polyvinyl alcohol)	HAP BG	35.2 38.6	6–164 14–160	42.20* 6.70* *Flexural strength	Bengal goat with cavity radius defect (10×5 mm ²)	Histology Biomechanical testing: push out (no natural tissue control)	Ghosh et al. 2008

	BG	38.6	14–160	–	Bengal goat with cavity radius defect ($12 \times 5 \times 3 \text{ mm}^3$)	Histology Radiological examination	Nandi et al. 2009
Sponge impregnation (template: Polyurethane foam)	β -DCS	53–71	300	10.4–28.1	Mice as incubators in subcutaneous scaffold implantation Implantation period: 9 weeks	Histology	Dai et al. 2015
	Sr-HT	78	–	2.2	Wistar female rats with cavity tibial defect ($3 \times 3 \text{ mm}$) Implantation period: 3 & 6 weeks	Histology Histomorphometry	Zreiqat et al. 2010
	BG	60–90	–	0.64–4.28 MPa	New Zealand rabbit with radius segmental defect (16 mm) Implantation period: 2 & 4 weeks	MicroCT: new bone volume Biomechanical testing: three point bending (normal tissue as control).	Tang et al. 2016

BG bioactive glass, DCS dicalcium silicate (Ca_2SiO_4), HAP hydroxyapatite, nHA nano-hydroxyapatite, OCP octacalcium phosphate ($\text{Ca}_8\text{H}_2(\text{PO}_4)_6\cdot 5\text{H}_2\text{O}$), PA polyamide, PCL polycaprolactone, Sr-HT Sr-Hardystonite ($\text{Sr-Ca}_2\text{ZnSi}_2\text{O}_7$), TCP tricalcium phosphate

Table A.2 Additive manufacturing processes for bioceramic-based scaffolds (selected studies with in vivo testing)

	Scaffold				In vivo testing				Reference
	Mfg. process	Bioceramic	Macro porosity, Π_{macro} [%]	Pore diameter, D_p [μm]	Compressive strength, σ_c [MPa]	Type of animal model	New bone evaluation		
Bioceramic family	Bioresorbable	β -TCP	32–43/ 28–40/ 24–35	500/750/ 1000	5–11/5–6/ 4–5	Sprague-Dawley rats with femur cavity defect (3 mm) Implantation period: 2 weeks	Histology	Tarafder et al. 2013	
		TCP	–	1300	8.3–21.7	Dutch milk goats with decorticated transverse processes of the vertebrae Implantation period: 12 weeks	Histology	Habibovic et al. 2008	
		α -TCP	61	2000	18.6	Beagle dogs with square calvarial defect Implantation period: 24 weeks	Histology	Igawa et al. 2006	
	Composite	HAP + α -TCP	22–45	30–150	–	Female BALB/cJ mice with femoral segmental defect (2 mm). Stabilization: PEEK plate Implantation period: 9 weeks	MicroCT Biomechanical testing: torsional strength (treatment with allograft as control)	Inzana et al. 2014	

					40.0–65.0	Rabbit with round calvarial defect (8 mm) Implantation period: 12 weeks	Histology (new bone area estimation) Biomechanical testing: compressive strength (no natural tissue as control)	Sun et al. 2016
DIW	CSi + Mg	60–63	–	–	–	Female mountain sheep with segmental tibial defect (20 mm). Stabilization: plate and cast for implantation duration. Implantation period: 14 weeks	Histology Peripheral quantitative computed tomography scanner for bone density Biomechanical testing: three-point bending stiffness (natural tissue as control)	Lohfeld et al. 2012
SLS	β -TCP + PCL	68	–	–	–	Merino sheep with segmental tibial defect (20 mm). Stabilization: titanium plate Implantation period: 12 weeks	MicroCT for new bone volume Biomechanical testing: torsional strength and stiffness (natural tissue as control)	Reichert et al. 2011
FDM	a: mPCL + TCP b: PLDLLA + TCP + PCL	71 (a) 44 (b)	350–500	–	–			

(continued)

Table A.2 (continued)

	Scaffold				In vivo testing			Reference
	Mfg. process	Bioceramic	Macro porosity, Π_{macro} [%]	Pore diameter, D_p [μm]	Compressive strength, σ_c [MPa]	Type of animal model	New bone evaluation	
	FDM	β -TCP + PCL	70	350–500	–	SPF Yorkshire pig with removal of intervertebral disk Implantation period: 6 months	Histology hismorphometry. MicoCT: new bone volume Biomechanical testing: lateral bending and axial rotation (intact disk as control)	Abbah et al. 2009
Bioactive	SLS	BG	Cylinder with four side through holes	40	Long-Evans male rats with femur segmental defect (5 mm) Stabilization: Internal rod (1.6 mm diameter) Implantation period: 15 weeks	Radiology scoring Biomechanical testing: three-point bending (no natural tissue as control)	Liu et al. 2014	

BG bioactive glass, CaP calcium phosphate, CSF calcium sulfate (CaSO_4), HAP hydroxyapatite, PCL polycaprolactone, PLA polylactide acid, PLDLLA poly (L-lactide-co-D,L-lactide), TCP tricalcium phosphate, TTCP tetracalcium phosphate ($\text{Ca}_4(\text{PO}_4)_2\text{O}$)

Table A.3 Coatings for bioceramic-based for scaffolds (selected studies with in vivo testing)

Bioceramic family	Scaffold						In vivo testing		Reference
	Bioresorbable	Mfg. process	Coating bioceramic	Substrate	Macro porosity, Π_{macro} [%]	Pore diameter, D_p [μm]	Type of animal model	Performance	
		Immersion	BCP	PPF (SLA)	39	429	New Zealand white rabbits with round calvarial defect (15 mm) Implantation period: 6 weeks	MicroCT for new bone volume Biomechanical testing: push-out test (no control with natural tissue)	Dadsetan et al. 2015
	Composite	Immersion	PCL + nBG	Baghdadite (sponge impregnation + sintering)	75–77	–	Merino wethers with segmental tibia defect (30 mm) Stabilization: plate and cast for 3 weeks Implantation period: 6 weeks	MicroCT for new bone volume Biomechanical testing normalized torsional testing (natural tissue as control)	Li et al. 2016
		Immersion	Mg-substituted β -TCP	PPF (SLA)	40	354	New Zealand white rabbits with round calvarial defect (15 mm) Implantation period: 6 weeks	MicroCT for new bone volume Biomechanical testing: push-out test (no control with natural tissue)	Dadsetan et al. 2015

(continued)

Table A.3 (continued)

		Scaffold					In vivo testing			Reference
		Mfg. process	Coating bioceramic	Substrate	Macro porosity, Π_{macro} [%]	Pore diameter, D_p [μm]	Type of animal model	Performance		
Bioactive	Immersion	Immersion	PLLA/nHA	BCP (sponge impregnation + sintering)	94–97	300–600	Japanese rabbits with cavity femur head defect (5×15 mm)	Histology	Nie et al. 2015	
	Eletrophoretic deposition	Mesoporous silica nanoparticles	PLLA/PCL (thermally induced phase separation)	–	–	Sprague-Dawley male rats with round calvarial defect (6 mm)	Qualitative analysis with microCT	Qiu et al. 2016		
	Immersion	Carbonated HAP	PPF (SLA)	39	403	New Zealand white rabbits with round calvarial defect (15 mm) Implantation period: 6 weeks	MicroCT for new bone volume Biomechanical testing: Push-out test (no control with natural tissue)	Dadsetan et al. 2015		

BCP biphasic calcium phosphate, HAP hydroxyapatite, nHA nano-hydroxyapatite, PCL polycaprolactone, PPF poly(propylene fumarate), PLA polylactide acid

References

- Abbah SA, Lam CXL, Hutmacher DW, Goh JCH, Wong H-K (2009) Biological performance of a polycaprolactone-based scaffold used as fusion cage device in a large animal model of spinal reconstructive surgery. *Biomaterials* 30:5086–5093
- Agarwal R, Williams K, Umscheid CA, Welch WC (2009) Osteoinductive bone graft substitutes for lumbar fusion: a systematic review. *J Neurosurg Spine* 11:729–740
- Almirall A, Larrecq G, Delgado J, Martinez S, Planell J, Ginebra M (2004) Fabrication of low temperature macroporous hydroxyapatite scaffolds by foaming and hydrolysis of an α -TCP paste. *Biomaterials* 25:3671–3680
- Baradararan S, Hamdi M, Metselaar IH (2012) Biphasic calcium phosphate (BCP) macroporous scaffold with different ratios of HA/ β -TCP by combination of gel casting and polymer sponge methods. *Adv Appl Ceram* 111:367–373
- Bartolo P, Kruth J-P, Silva J, Levy G, Malshe A, Rajurkar K, Mitsuiishi M, Ciurana J, Leu M (2012) Biomedical production of implants by additive electro-chemical and physical processes. *CIRP Ann Manuf Technol* 61:635–655
- Best SM, Porter AE, Thian ES, Huang J (2008) Bioceramics: past, present and for the future. *J Eur Ceram Soc* 28:1319–1327
- Bonda DJ, Manjila S, Selman WR, Dean D (2015) The recent revolution in the design and manufacture of cranial implants. *Neurosurgery* 77:814–824
- Bose S, Fielding G, Tarafder S, Bandyopadhyay A (2013) Understanding of dopant-induced osteogenesis and angiogenesis in calcium phosphate ceramics. *Trends Biotechnol* 31:594–605
- Cai S, Xu GH, Yu XZ, Zhang WJ, Xiao ZY, Yao KD (2009) Fabrication and biological characteristics of β -tricalcium phosphate porous ceramic scaffolds reinforced with calcium phosphate glass. *J Mater Sci Mater Med* 20:351–358
- Cancedda R, Giannoni P, Mastrogiacomo M (2007) A tissue engineering approach to bone repair in large animal models and in clinical practice. *Biomaterials* 28:4240–4250
- Carter B, Norton G (2007) *Ceramic Materials*. Springer, New York, pp 3–6
- Champion E (2013) Sintering of calcium phosphate bioceramics. *Acta Biomater* 9:5855–5875
- Chevalier J, Gremillard L (2009) Ceramics for medical applications: a picture for the next 20 years. *J Eur Ceram Soc* 29(7):1245–1255
- Chiba S, Anada T, Suzuki K, Saito K, Shiwaku Y, Miyatake N, Baba K, Imaizumi H, Hosaka M, Itoi E, Suzuki O (2016) Effect of resorption rate and osteoconductivity of biodegradable calcium phosphate materials on the acquisition of natural bone strength in the repaired bone. *J Biomed Mater Res A* 104:2833–2842
- Crowley C, Wong JM-L, Fisher DM, Khan WS (2013) A systematic review on preclinical and clinical studies on the use of scaffolds for bone repair in skeletal defects. *Curr Stem Cell Res Ther* 8:243–252
- Dadsetan M, Guda T, Runge MB, Mijares D, Legeros RZ, Legeros JP, Silliman DT, Lu L, Wenke JC, Brown Baer PR, Yaszemski MJ (2015) Effect of calcium phosphate coating and rhBMP-2 on bone regeneration in rabbit calvaria using poly(propylene fumarate) scaffolds. *Acta Biomater* 18:9–20
- Dai Y, Liu H, Liu B, Wang Z, Li Y, Zhou G (2015) Porous β -Ca₂SiO₄ ceramic scaffolds for bone tissue engineering: in vitro and in vivo characterization. *Ceram Int* 41:5894–5902
- Deckers J, Vleugels J, Kruth JP (2014) Additive manufacturing of ceramics: a review. *J Ceram Sci Technol* 5:245–260
- Elomaa L, Kokkari A, Närhi T, Seppälä JV (2013) Porous 3D modeled scaffolds of bioactive glass and photocrosslinkable poly(ϵ -caprolactone) by stereolithography. *Compos Sci Technol* 74:99–106
- El-Rashidy AA, Roether JA, Harhaus L, Kneser U, Boccaccini AR (2017) Regenerating bone with bioactive glass scaffolds: a review of in vivo studies in bone defect models. *Acta Biomater* 62:1–28
- Evaluate (2015) EvaluateMedTech® – world preview 2015, Outlook to 2020. www.evaluategroup.com

- Felzmann R, Gruber S, Mitteramskogler G, Tesavibul P, Boccaccini AR, Liska R, Stampfl J (2012) Lithography-based additive manufacturing of cellular ceramic structures. *Adv Eng Mater* 14:1052–1058
- Ghosh SK, Nandi SK, Kundu B, Datta S, De DK, Roy SK, Basu D (2008) In vivo response of porous hydroxyapatite and β -tricalcium phosphate prepared by aqueous solution combustion method and comparison with bioglass scaffolds. *J Biomed Mater Res B Appl Biomater* 86:217–227
- Guo J, Meng Z, Chen G, Xie D, Chen Y, Wang H, Tang W, Liu L, Jing W, Long J, Guo W, Tian W (2012) Restoration of critical-size defects in the rabbit mandible using porous nanohydroxyapatite-polyamide scaffolds. *Tissue Eng A* 18:1239–1252
- Habibovic P, Gbureck U, Doillon CJ, Bassett DC, van Blitterswijk CA, Barralet JE (2008) Osteoconduction and osteoinduction of low-temperature 3D printed bioceramic implants. *Biomaterials* 29:944–953
- Hannouche D, Hamadouche M, Nizard R, Bizot P, Meunier A, Sedel L (2005) Ceramics in total hip replacement. *Clin Orthop Relat Res*:62–71
- Hench LL (2006) The story of Bioglass[®]. *J Mater Sci Mater Med* 17:967–978
- Hench LL, Wilson J (2013) Introduction. In: Hench LL (ed) *An introduction to bioceramics*, 2nd edn. Imperial College Press, London, pp 1–26
- Hing KA, Annaz B, Saeed S, Revell PA, Buckland T (2005) Microporosity enhances bioactivity of synthetic bone graft substitutes. *J Mater Sci Mater Med* 16:467–475
- Igawa K, Mochizuki M, Sugimori O, Shimizu K, Yamazawa K, Kawaguchi H, Nakamura K, Takato T, Nishimura R, Suzuki S, Anzai M, Chung U II, Sasaki N (2006) Tailor-made tricalcium phosphate bone implant directly fabricated by a three-dimensional ink-jet printer. *J Artif Organs* 9:234–240
- Inzana JA, Olvera D, Fuller SM, Kelly JP, Graeve OA, Schwarz EM, Kates SL, Awad HA (2014) 3D printing of composite calcium phosphate and collagen scaffolds for bone regeneration. *Biomaterials* 35:4026–4034
- ISO/ASTM 52900 (2015) Additive manufacturing – general principles – terminology. ISO Central Secretariat, Geneva
- Jahadakbar A, Shayesteh Moghaddam N, Amerinatanz A, Dean D, Karaca H, Elahinia M (2016) Finite element simulation and additive manufacturing of stiffness-matched NiTi fixation hardware for mandibular reconstruction surgery. *Bioengineering* 3:36
- Jaiswal AK, Dhupal RV, Ghosh S, Chaudhari P, Nemani H, Soni VP, Vanage GR, Bellare JR (2013) Bone healing evaluation of nanofibrous composite scaffolds in rat calvarial defects: a comparative study. *J Biomed Nanotechnol* 9:2073–2085
- Jakus AE, Rutz AL, Jordan SW, Kannan A, Mitchell SM, Yun C, Koube KD, Yoo SC, Whiteley HE, Richter CP, Galiano RD (2016) Hyperelastic bone: A highly versatile, growth factor-free, osteoregenerative, scalable, and surgically friendly biomaterial. *Science translational medicine* 8:358
- Jakus AE, Ramille S (2017) Multi and mixed 3D-printing of graphene-hydroxyapatite hybrid materials for complex tissue engineering. *J Biomed Mater Res A* 105:274–283
- Ji W, Sun Y, Yang F, Van Den Beucken JJJP, Fan M, Chen Z, Jansen JA (2011) Bioactive electrospun scaffolds delivering growth factors and genes for tissue engineering applications. *Pharm Res* 28:1259–1272
- Keller TS (1994) Predicting the compressive mechanical behavior of bone. *J Biomech* 27:1159–1168
- Kelly JR, Nishimura I, Campbell SD (1996) Ceramics in dentistry: historical roots and current perspectives. *J Prosthet Dent* 75:18–32
- Kingery WD, Bowen HK, Uhlmann DR (1976) *Introduction to ceramics*, 2nd edn. Wiley, New York, p 3
- Kurien T, Pearson RG, Scammell BE (2013) Bone graft substitutes currently available in orthopaedic practice: the evidence for their use. *Bone Joint J* 95B:583–597

- Larsen M, Mishra R, Miller M, Dean D (2015) Bioprinting of bone. In: Atala A, Yoo JJ (eds) Essentials of 3D biofabrication and translation. Academic press (Elsevier), Cambridge, MA, pp 293–308
- Learmonth ID, Young C, Rorabeck C (2007) The operation of the century: total hip replacement. *Lancet* 370:1508–1519
- Li Z, Chen X, Zhao N, Dong H, Li Y, Lin C (2013) Stiff macro-porous bioactive glass-ceramic scaffold: fabrication by rapid prototyping template, characterization and in vitro bioactivity. *Mater Chem Phys* 141:76–80
- Li Y, Chen SK, Li L, Qin L, Wang XL, Lai YX (2015) Bone defect animal models for testing efficacy of bone substitute biomaterials. *J Orthop Transl* 3:95–104
- Li JJ, Roohani-Esfahani S-I, Dunstan CR, Quach T, Steck R, Saifzadeh S, Pivonka P, Zreiqat H (2016) Efficacy of novel synthetic bone substitutes in the reconstruction of large segmental bone defects in sheep tibiae. *Biomed Mater* 11:15016
- Liu Y, Lim J, Teoh SH (2013) Review: development of clinically relevant scaffolds for vascularised bone tissue engineering. *Biotechnol Adv* 31:688–705
- Liu W-C, Robu IS, Patel R, Leu MC, Velez M, Gabriel Chu T-M (2014) The effects of 3D bioactive glass scaffolds and BMP-2 on bone formation in rat femoral critical size defects and adjacent bones. *Biomed Mater* 9(45013)
- Lohfeld S, Cahill S, Barron V, McHugh P, Dürselen L, Kreja L, Bausewein C, Ignatius A (2012) Fabrication, mechanical and in vivo performance of polycaprolactone/tricalcium phosphate composite scaffolds. *Acta Biomater* 8:3446–3456
- Marcacci M, Kon E, Moukhachev V, Lavroukov A, Kutepov S, Quarto R, Mastrogiacomo M, Cancedda R (2007) Stem cells associated with macroporous bioceramics for long bone repair: 6- to 7-year outcome of a pilot clinical study. *Tissue Eng* 13:947–955
- McColm IJ (2013) Dictionary of ceramic science and engineering. Springer, New York, pp 83–84
- Metsger DS, Driskell TD, Paulsrud JR (1982) Tricalcium phosphate ceramic – a resorbable bone implant: review and current status. *J Am Dent Assoc* 105:1035–1038
- Midha S, Kim TB, Van Den Bergh W, Lee PD, Jones JR, Mitchell CA (2013) Preconditioned 70S30C bioactive glass foams promote osteogenesis in vivo. *Acta Biomater* 9:9169–9182
- Miranda P, Pajares A, Saiz E, Tomsia AP, Guiberteau F (2008) Mechanical properties of calcium phosphate scaffolds fabricated by robocasting. *J Biomed Mater Res A* 85:218–227
- Moghaddam NS, Skoracki R, Miller M, Elahinia M, Dean D (2016a) Three dimensional printing of stiffness-tuned, nitinol skeletal fixation hardware with an example of mandibular segmental defect repair. *Procedia CIRP* 49:45–50
- Moghaddam N, Jahadakbar A, Amerinatanzi A, Elahinia M, Miller M, Dean D (2016b) Metallic fixation of mandibular segmental defects. *Plast Reconstr Surg Glob Open* 4:e858
- Muller B, Reseland JE, Haugen HJ, Tiainen H (2015) Cell growth on pore-graded biomimetic TiO2 bone scaffolds. *J Biomater Appl* 29:1284–1295
- Nandi SK, Kundu B, Datta S, De DK, Basu D (2009) The repair of segmental bone defects with porous bioglass: an experimental study in goat. *Res Vet Sci* 86:162–173
- Nie L, Chen D, Fu J, Yang S, Hou R, Suo J (2015) Macroporous biphasic calcium phosphate scaffolds reinforced by poly-L-lactic acid/hydroxyapatite nanocomposite coatings for bone regeneration. *Biochem Eng J* 98:29–37
- Obregon F, Vaquette C, Ivanovski S, Huttmacher DW, Bertassoni LE (2015) Three-dimensional bioprinting for regenerative dentistry and craniofacial tissue engineering. *J Dent Res* 94:143S–152S
- Paderni S, Terzi S, Amendola L (2009) Major bone defect treatment with an osteoconductive bone substitute. *Musculoskelet Surg* 93:89–96
- Park HJ, Min KD, Lee MC, Kim SH, Lee OJ, Ju HW, Moon BM, Lee JM, Park YR, Kim DW, Jeong JY, Park CH (2016) Fabrication of 3D porous SF/β-TCP hybrid scaffolds for bone tissue reconstruction. *J Biomed Mater Res A*:1779–1787
- Pati F, Jang J, Lee JW, Cho D-W (2015) Extrusion bioprinting. In: Atala A, Yoo JJ (eds) Essentials of 3D biofabrication and translation. Academic, Boston, pp 123–152

- Pearce AI, Richards RG, Milz S, Schneider E, Pearce SG (2007) Animal models for implant biomaterial research in bone: a review. *Eur Cells Mater* 13:1–10
- Piconi C, Maccauro G (1999) Zirconia as a ceramic biomaterial. *Biomaterials* 20:1–25
- Pilipchuk SP, Plonka AB, Monje A, Taut AD, Lanis A, Kang B, Giannobile WV (2015) Tissue engineering for bone regeneration and osseointegration in the oral cavity. *Dent Mater* 31:317–338
- PolICASTRO GM, Lin F, Smith Callahan LA, Esterle A, Graham M, Stakleff KS, Becker ML (2015) OGP functionalized phenylalanine-based poly(ester urea) for enhancing osteoinductive potential of human mesenchymal stem cells. *Biomacromolecules* 16:1358–1371
- Pountos I, Giannoudis PV (2016) Is there a role of coral bone substitutes in bone repair? *Injury* 47:2606–2613
- Qiu K, Chen B, Nie W, Zhou X, Feng W, Wang W, Chen L, Mo X, Wei Y, He C (2016) Electrophoretic deposition of dexamethasone-loaded mesoporous silica nanoparticles onto poly(l-lactic acid)/poly(ϵ -caprolactone) composite scaffold for bone tissue engineering. *ACS Appl Mater Interfaces* 8:4137–4148
- Quarto R, Mastrogiacomo M, Cancedda R, Kutepov SM, Mukhachev V, Lavroukov A, Kon E, Marcacci M (2001) Repair of large bone defects with the use of autologous bone marrow stromal cells. *N Engl J Med* 344:385–386
- Raman R, Bashir R (2015) Stereolithographic 3D bioprinting for biomedical applications. In: Atala A, Yoo JJ (eds) *Essentials of 3D biofabrication and translation*. Academic press (Elsevier), Cambridge, MA, pp 89–121
- Reichert JC, Wullschlegler ME, Cipitria A, Lienau J, Cheng TK, Schütz MA, Duda GN, Nöth U, Eulert J, Huttmacher DW (2011) Custom-made composite scaffolds for segmental defect repair in long bones. *Int Orthop* 35:1229–1236
- Ren J, Blackwood KA, Doustgani A, Poh PP, Steck R, Stevens MM, Woodruff MA (2014) Melt-electrospun polycaprolactone strontium-substituted bioactive glass scaffolds for bone regeneration. *J Biomed Mater Res A* 102:3140–3153
- Schmitz JP, Hollinger JO (1986) The critical size defect as an experimental model for craniomandibulofacial nonunions. *Clin Orthop Relat Res* 205:299–308
- Semlitsch M, Lehmann M, Weber H, Doerre E, Willert HG (1977) New prospects for a prolonged functional lifespan of artificial hip joints by using the material combination polyethylene/aluminium oxide ceramic/metal. *J Biomed Mater Res* 11:537–552
- Shao H, He Y, Fu J, He D, Yang X, Xie J, Yao C, Ye J, Xu S, Gou Z (2016) 3D printing magnesium-doped wollastonite/ β -TCP bioceramics scaffolds with high strength and adjustable degradation. *J Eur Ceram Soc* 36:1495–1503
- Shrivats AR, Alvarez P, Schutte L, Hollinger JO (2014) Bone regeneration. In: *Principles of tissue engineering*. Elsevier, San Diego, pp 1201–1221
- Sing SL, Yeong WY, Wiria FE, Tay BY, Zhao Z, Zhao L, Tian Z, Yang S (2017) Direct selective laser sintering and melting of ceramics: a review. *Rapid Prototyp J* 23:611–623
- Sun M, Liu A, Shao H, Yang X, Ma C, Yan S, Liu Y, He Y, Gou Z (2016) Systematical evaluation of mechanically strong 3d printed diluted magnesium doping wollastonite scaffolds on osteogenic capacity in rabbit calvarial defects. *Sci Rep* 6:34029
- Tamjid E, Simchi A (2015) Fabrication of a highly ordered hierarchically designed porous nanocomposite via indirect 3D printing: mechanical properties and in vitro cell responses. *Mater Des* 88:924–931
- Tang W, PolICASTRO GM, Hua G, Guo K, Zhou J, Wesdemiotis C, Doll GL, Becker ML (2014) Bioactive surface modification of metal oxides via catechol-bearing modular peptides: multivalent-binding, surface retention, and peptide bioactivity. *J Am Chem Soc* 136:16357–16367
- Tang W, Lin D, Yu Y, Niu H, Guo H, Yuan Y, Liu C (2016) Bioinspired trimodal macro/micro/nanoporous scaffolds loading rhBMP-2 for complete regeneration of critical size bone defect. *Acta Biomater* 32:309–323

- Tarafder S, Balla VK, Davies NM, Bandyopadhyay A, Bose S (2013) Microwave-sintered 3D printed tricalcium phosphate scaffolds for bone tissue engineering. *J Tissue Eng Regen Med* 7:631–641
- Tesavibul P, Felzmann R, Gruber S, Liska R, Thompson I, Boccaccini AR, Stampfl J (2012) Processing of 45S5 Bioglass[®] by lithography-based additive manufacturing. *Mater Lett* 74:81–84
- Vivanco J, Aiyangar A, Araneda A, Ploeg HL (2012) Mechanical characterization of injection-molded macro porous bioceramic bone scaffolds. *J Mech Behav Biomed Mater* 9:137–152
- Wang H, Li Y, Zuo Y, Li J, Ma S, Cheng L (2007) Biocompatibility and osteogenesis of biomimetic nano-hydroxyapatite/polyamide composite scaffolds for bone tissue engineering. *Biomaterials* 28:3338–3348
- Woodruff MA, Lange C, Reichert J, Berner A, Chen F, Fratzl P, Schantz JT, Huttmacher DW (2012) Bone tissue engineering: from bench to bedside. *Mater Today* 15:430–435
- Xu Y, Luong D, Walker JM, Dean D, Becker ML (2017) Modification of poly (propylene fumarate) – bioglass composites with peptide conjugates to enhance bioactivity. *Biomacromolecules* 18:3168–3177
- Yuan H, Fernandes H, Habibovic P, de Boer J, Barradas AMC, de Ruiter A, Walsh WR, van Blitterswijk CA, de Bruijn JD (2010) Osteoinductive ceramics as a synthetic alternative to autologous bone grafting. *Proc Natl Acad Sci USA* 107:13614–13619
- Zanchetta E, Cattaldo M, Franchin G, Schwentenwein M, Homa J, Brusatin G, Colombo P (2016) Stereolithography of SiOC ceramic microcomponents. *Adv Mater* 28:370–376
- Zhang J, Liu H, Ding J-X, Wu J, Zhuang X-L, Chen X-S, Wang J-C, Yin J-B, Li Z-M (2016) High-pressure compression-molded porous resorbable polymer/hydroxyapatite composite scaffold for cranial bone regeneration. *ACS Biomater Sci Eng* 2:1471–1482
- Zhou C, Ye X, Fan Y, Ma L, Tan Y, Qing F, Zhang X (2014) Biomimetic fabrication of a three-level hierarchical calcium phosphate/collagen/hydroxyapatite scaffold for bone tissue engineering. *Biofabrication* 6:35013
- Zocca A, Colombo P, Gomes CM, Günster J (2015) Additive manufacturing of ceramics: issues, potentialities, and opportunities. *J Am Ceram Soc* 98:1983–2001
- Zoetis T, Tassinari MS, Bagi C, Walthall K, Hurtt ME (2003) Species comparison of postnatal bone growth and development. *Birth Defects Res B Dev Reprod Toxicol* 68:86–110
- Zreiqat H, Ramaswamy Y, Wu C, Paschalidis A, Lu Z, James B, Birke O, McDonald M, Little D, Dunstan CR (2010) The incorporation of strontium and zinc into a calcium-silicon ceramic for bone tissue engineering. *Biomaterials* 31:3175–3184



Medical Imaging for Three-Dimensional Computer-Aided Models

Paulo Henrique Junqueira Amorim, Thiago Franco de Moraes, Rodrigo Alvarenga Rezende, Jorge Vicente Lopes da Silva, and Helio Pedrini

Contents

1	Introduction	196
2	Medical Image Acquisition	196
2.1	Imaging Techniques	196
2.2	DICOM Format	199
3	Preprocessing	200
3.1	Noise Filtering	200
3.2	Edge Detection	201
3.3	Contrast Enhancement	203
4	Segmentation	205
4.1	Thresholding	205
4.2	Region Growing	205
4.3	Watershed	206
5	Registration	206
6	Volume Rendering	207
6.1	Isosurface Rendering	207
6.2	Direct Volume Rendering	208
7	3D Printing and Biofabrication	211
8	Conclusions	218
	References	218

P. H. Junqueira Amorim (✉) · T. F. de Moraes · R. A. Rezende · J. V. L. da Silva
Division of 3D Technologies, Center for Information Technology Renato Archer, Campinas, SP,
Brazil
e-mail: paulo.amorim@cti.gov.br; thiago.moraes@cti.gov.br; rodrigo.rezende@cti.gov.br;
jorge.silva@cti.gov.br

H. Pedrini
Institute of Computing, University of Campinas, Campinas, SP, Brazil
e-mail: helio@ic.unicamp.br

Abstract

Technological advances in medical imaging have provided healthcare professionals with powerful resources for storing, analyzing, and visualizing three-dimensional images in a variety of diagnostic tasks. Equipments for acquiring high-quality images and computer-aided tools for image interpretation play an important role in surgical planning, disease assessment, and therapy response monitoring. This chapter presents an overview of relevant aspects related to image processing and computer graphics techniques for the construction of three-dimensional models for visualization and biofabrication.

1 Introduction

Imaging techniques have been extensively used for diagnosis in many medical specialties, whose main purpose is to create visual representations of the interior of human body. Internal anatomic structures of the body can be revealed, providing physicians with valuable clinical information about patient's conditions. Technological advances in medical imaging have aided the comprehension of structures and functions of organs, as well as the detection of abnormalities.

Several medical imaging modalities (Macovski 1983) are currently available for medical diagnosis, such as computed tomography, magnetic resonance imaging, ultrasonography, mammography, photon emission tomography, among others.

Among the various tools available for medical applications, InVesalius (Amorim et al. 2015) is an open-source framework with several functionalities for processing, analysis, visualization, and 3D printing support for medical images.

This chapter focuses on relevant image processing and computer graphics techniques for the generation of three-dimensional (3D) models for visualization and bioprinting.

In the following sections, we will describe some relevant aspects of medical imaging, preprocessing, segmentation, registration, volume rendering, 3D printing, and biofabrication.

2 Medical Image Acquisition

This section briefly describes (i) some medical imaging modalities used for diagnostic purposes and (ii) DICOM standard.

2.1 Imaging Techniques

Medical imaging is one of the most common noninvasive techniques for acquiring and interpreting images for medical diagnosis purpose. Images of internal structures

of the body can be generated and analyzed to provide a visual representation of organs and tissues.

Three-dimensional visualization of anatomic structures allow for more accurate surgical planning, reducing interventions and patient's risk.

Several imaging modalities have been developed to assist clinicians in diagnosis and treatment of patients, making beneficial impacts on healthcare. Imaging technologies currently available include computed tomography, magnetic resonance imaging, ultrasound, positron emission tomography, among others.

Computed tomography (CT) uses X-ray images acquired from different orientation angles to generate cross-sectional images around specific areas of a patient. The attenuation coefficients measured by the CT equipment are organized into a two-dimensional sinogram (Leondes 2005). Image processing and computer graphics techniques are used to produce a three-dimensional image from a sequence of two-dimensional slices (radiographic images), known as reconstruction process (Fig. 1).

Each pixel of the reconstructed image is represented in the Hounsfield unit (HU) scale. The HU value for a voxel with average linear attenuation coefficient μ is given by

$$HU = 1000 \times \frac{\mu - \mu_{\text{water}}}{\mu_{\text{water}} - \mu_{\text{air}}} \quad (1)$$

where μ_{air} and μ_{water} are the linear attenuation coefficients of air and water, respectively. In this scale, water is represented by 0, air by -1000 , and more dense bones are represented by 3000 HU (Hsieh 2003).

Typical applications of CT include the detection of brain tumors, visualization of blood vessel defects, and differentiation of soft tissues, among others. There are some variations of computed tomography such as positron emission tomography (PET-CT) used to diagnose certain tumors (Wahl and Wagner 2009) and cone beam tomography (CBCT) used in dentistry (Kapila 2014).

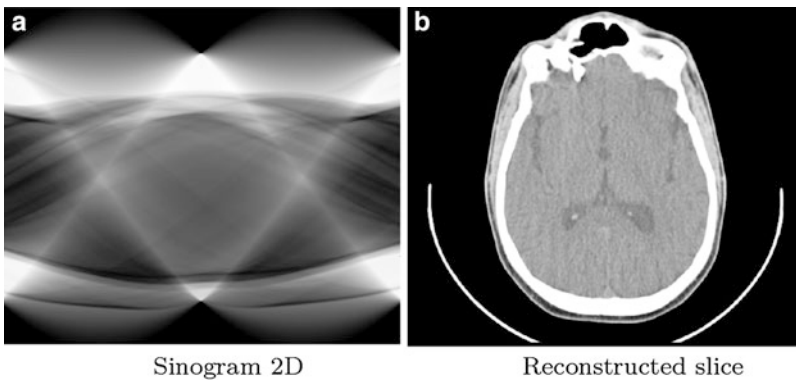


Fig. 1 Example of sinogram 2D and reconstructed image

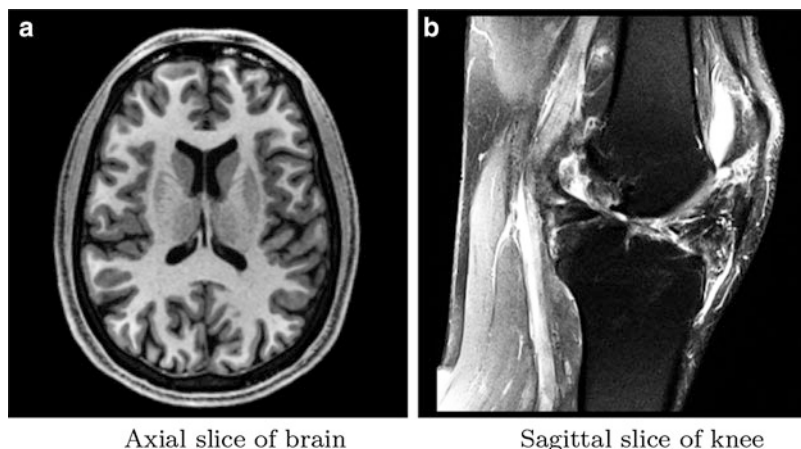


Fig. 2 Examples of MRI images

Magnetic resonance imaging (MRI) is another medical imaging technique used in radiology for diagnosis and treatment purposes.

MRI scanners employ strong magnetic fields to align the nuclei of hydrogen atoms (proton) and apply radio frequency pulses in the region under analysis to create a resonance in the proton atoms (Kelsey et al. 2013). When the radio frequency pulse is turned off, the protons align again to the magnetic field, releasing energy that is recorded by the MRI equipment. Signals at different frequencies are used to reconstruct an image.

Advantages of the MRI include its absence of ionizing radiation and capacity of providing detailed images of soft tissues (for instance, in brain and spine examination). Disadvantages include the cost of equipments compared to other modalities (Sistrom and McKay 2005), as well as counter-indication in patients with metallic devices (pacemakers, orthopedic implants) or who are claustrophobic. Figure 2 shows some examples of MRI images.

Ultrasonography is a diagnostic imaging technique that employs sound waves to form images. This technique allows the visualization of internal structures of the body such as muscles, joints, tendons, blood vessels, liver, and heart. Ultrasonography is also widely used in examination of pregnant women to evaluate the development of the fetus.

As shown in Fig. 3, a transducer converts electrical current into sound waves with frequencies between 3 and 30 MHz (Lutz et al. 2011), which are sent into the body tissues. These frequencies are higher than those audible to humans (>20 KHz). The waves are echoed off the internal structures and reflected back to the transducer, which converts the waves into electrical signals. Then, a computer converts the electrical signal patterns into an image (Dowsett et al. 2006).

Ultrasonography has several advantages compared to other medical imaging techniques. It can provide real-time images, the equipments are portable and lower

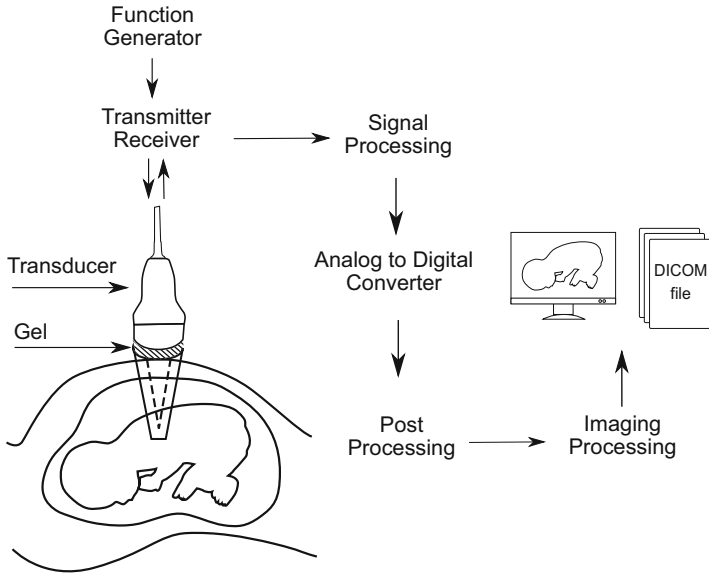


Fig. 3 Main components of an ultrasound system

Fig. 4 Example of a 2D ultrasound image



in cost, and it does not use ionizing radiation. Disadvantages include certain limitations in terms of its field of view, noise, and difficulties in visualizing structures behind air and bones. Figure 4 shows a 2D ultrasound image.

2.2 DICOM Format

Until the early 1980s, the examinations based on medical imaging were printed on X-ray film or paper in the case of ultrasonography. Many practices and specifications

were generated by a variety of manufacturers, causing serious problems in terms of data management and connectivity incompatibilities (Oosterwijk and Gihring 2002). With the development of advanced imaging techniques and availability of computers, manufacturers started storing medical images in digital format, however, in their own proprietary format.

Digital Imaging and Communications in Medicine (DICOM) (Pianykh 2009) is a standard for storing, printing, and transmitting information in medical imaging. The first version of the standard was released by American College of Radiology (ACR) and National Electrical Manufacturers Association (NEMA) in 1985. The second and third versions were released in 1988 and 1993, respectively.

DICOM provides a file format definition and a network communication protocol based on the Transmission Control Protocol/Internet Protocol (TCP/IP) (Stallings 2005). DICOM enables the integration of different equipments, such as scanners, computers, printers, and servers from different manufacturers, such that files can be exchanged among heterogeneous devices capable of recognizing patient images and data in DICOM format. DICOM standard has been widely adopted by hospitals, medical offices, and dental clinics.

3 Preprocessing

The preprocessing step concerns the techniques for enhancing characteristics of the image, before its use in subsequent tasks such as segmentation and recognition. The preprocessing includes noise filtering, contrast enhancement, and edge detection.

3.1 Noise Filtering

Noise is a random variation in color or brightness of the image, but not present in the physical objects of the scene. Noise usually occurs during the image acquisition process, and it is an undesirable artifact and may decrease the efficiency of segmentation, registration, and classification stages. As desirable characteristic, a smoothing filter, should reduce the occurrence of noise while preserving the edges of an image, since they are important visual features.

Several techniques have been proposed to filter images with the purpose of reducing noise effect. Pixel or voxel values are modified by taking into account intensity values over a neighborhood.

Mean filtering (Gonzalez and Woods 2002; Parker 2010; Russ 2015) is a simple method for smoothing images, where each pixel or voxel intensity value of the image is replaced with the average value of its neighbors. Mean filtering can be performed through a convolution operation with a kernel of adequate shape and size.

Median filtering (Gonzalez and Woods 2002; Parker 2010; Russ 2015) replaces the pixel or voxel intensity value of the image with the median of the neighboring values. The median filtering is more robust than the mean filtering since

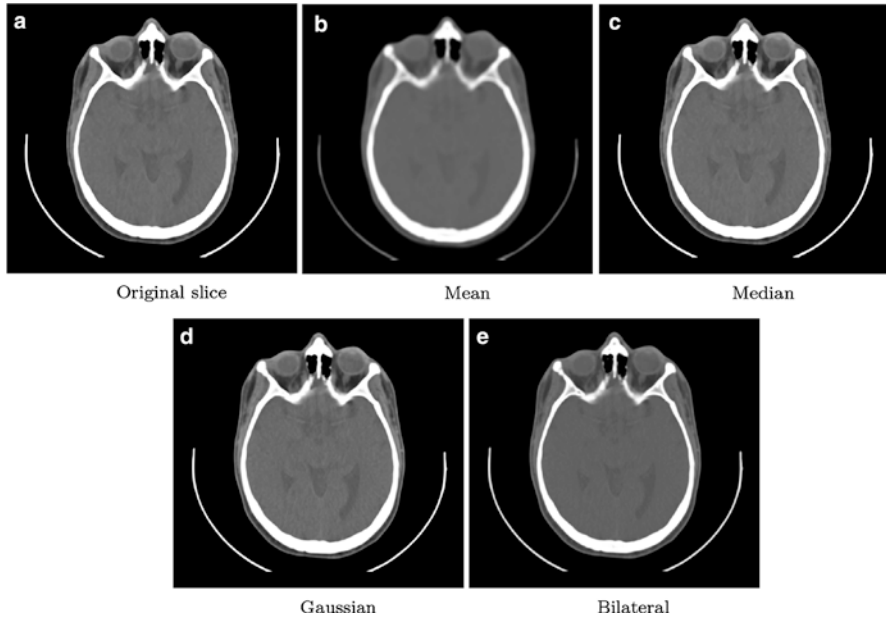


Fig. 5 Different techniques for image noise filtering

nonrepresentative values will have little impact on the median value. Furthermore, it can preserve sharp edges.

Gaussian filtering (Gonzalez and Woods 2002; Parker 2010; Russ 2015) is a smoothing operator that uses a Gaussian shape in the convolution process. In this filtering, the pixel or voxel values are replaced with weighted average of its neighbors following a Gaussian distribution.

Bilateral filtering (Tomasi and Manduchi 1998) is a smoothing technique that preserves image edges. Each pixel or voxel of the image is replaced with the weighted average of its neighbors, such that the weights take into account both spatial distances and intensity differences.

Figure 5 illustrates the application of smoothing filtering with mean, median, Gaussian, and bilateral filters to a given input image. The performance of noise filtering techniques varies according to the image modality. Quantitative and qualitative analysis studies have been reported in the literature (Andria et al. 2012; Manjón et al. 2008; Michailovich and Tannenbaum 2006; Salinas and Fernández 2007).

3.2 Edge Detection

Edge detection techniques (Gonzalez and Woods 2002; Parker 2010; Russ 2015) aim to identify boundaries between regions or objects through radiometric (intensity)

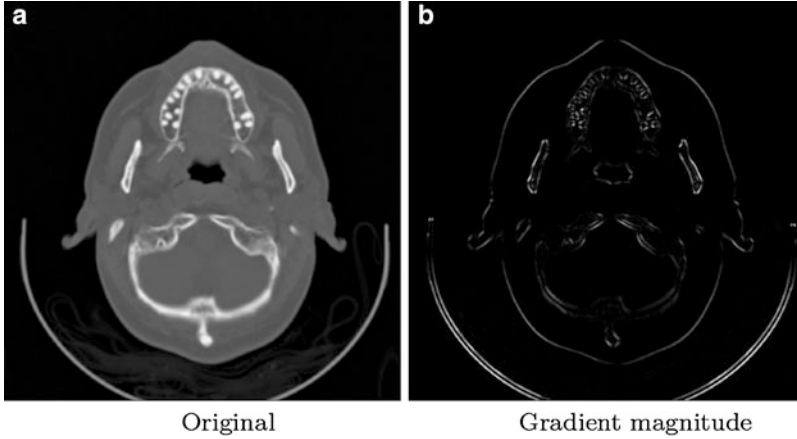


Fig. 6 Example of edge map obtained through gradient magnitude

discontinuities in the image. Pixels or voxels with sharp changes in brightness correspond to the edges of the image.

Most edge detection methods are based on the directional maxima of the gradient magnitude computed in a local neighborhood of each pixel in the image. The gradient direction is used to estimate the local orientation of the edges.

More formally, the gradient ∇f of an image f is expressed as

$$\nabla f = \left[\frac{\partial f}{\partial x}, \frac{\partial f}{\partial y} \right] \quad (2)$$

The edge strength corresponds to the gradient magnitude, given by

$$\|\nabla f\| = \sqrt{\left(\frac{\partial f}{\partial x}\right)^2 + \left(\frac{\partial f}{\partial y}\right)^2} \quad (3)$$

The gradient direction, perpendicular to the edge, is given by

$$\theta = \tan^{-1} \left(\frac{\partial f}{\partial y} / \frac{\partial f}{\partial x} \right) \quad (4)$$

Figure 6 shows an example of edge map calculated as the gradient magnitude in a neighborhood of each pixel in an input image.

The image gradient can be estimated by applying finite-difference approximations by applying first-order and second-order derivatives. Examples of edge detectors based on gradient information are Prewitt and Sobel (Gonzalez and Woods 2002), whose 3×3 kernels are expressed in Eqs. (5) and (6), respectively, expressed as

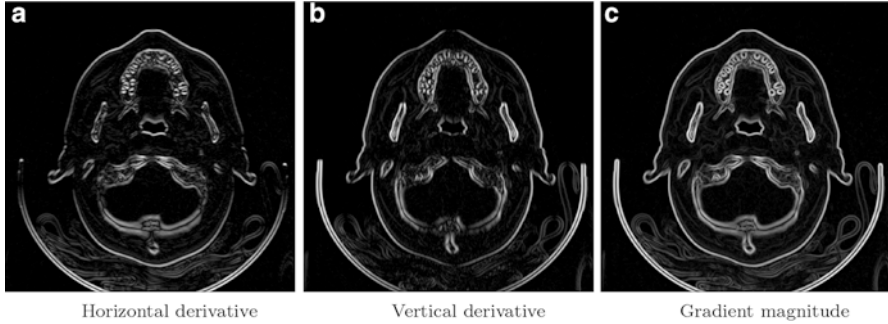


Fig. 7 Illustration of edge map computed through the Sobel operator

$$\frac{\partial f}{\partial x} \approx \begin{bmatrix} -1 & 0 & +1 \\ -1 & 0 & +1 \\ -1 & 0 & +1 \end{bmatrix} \quad \frac{\partial f}{\partial y} \approx \begin{bmatrix} -1 & -1 & -1 \\ 0 & 0 & 0 \\ +1 & +1 & +1 \end{bmatrix} \tag{5}$$

$$\frac{\partial f}{\partial x} \approx \begin{bmatrix} -1 & 0 & +1 \\ -2 & 0 & +2 \\ -1 & 0 & +1 \end{bmatrix} \quad \frac{\partial f}{\partial y} \approx \begin{bmatrix} -1 & -2 & -1 \\ 0 & 0 & 0 \\ +1 & +2 & +1 \end{bmatrix} \tag{6}$$

Figure 7 illustrates the results after applying Sobel operator to the image shown in Fig. 6a. Horizontal and vertical derivative approximations are computed and combined to generate the final edge map.

The Canny edge detector (Canny 1986) uses a Gaussian filter to initially smooth the image and attenuate noise. Then, the gradient is computed through a filtering such as Prewitt or Sobel, as mentioned previously. A nonmaximum suppression stage is used to maintain only the local maximum gradient values. This steps works as an edge thinning technique. Since the resulting edges can still contain pixels caused by noise or intensity variation, a double-threshold strategy is employed to remove spurious responses. Strong edge pixels correspond to those pixels with gradient value higher than the high threshold value, whereas weak edge pixels are those ones whose gradient value is smaller than the high threshold and larger than the low threshold. Pixels whose gradient value is smaller than the low threshold are suppressed. A hysteresis step is applied to keep the strong edge pixels while weak edge pixels can be connected to a strong edge pixel or removed according to its 8-neighborhood. Figure 8 illustrates the result after applying the Canny edge detector to the image shown in Fig. 6a.

3.3 Contrast Enhancement

Image enhancement techniques (Gonzalez and Woods 2002; Parker 2010; Russ 2015) have been developed to improve the quality of images for human interpretation purposes. Contrast is one of the most common aspects involved in the subjective

Fig. 8 Canny edge detector applied to an image

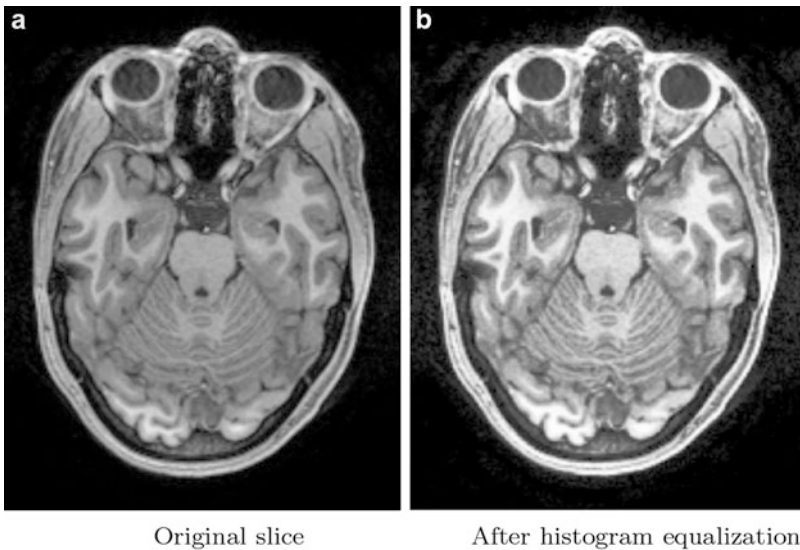


Fig. 9 Histogram equalization technique applied to an image

evaluation of image quality, which is measured as the difference in brightness or color between two adjacent regions.

Several contrast enhancement techniques (Kim et al. 1998; Singh and Bovis 2005; Stark 2000) use the image histogram to adjust its intensity values. An image histogram is a graphical representation of the number of pixels as a function of their intensity.

Examples of contrast enhancement approaches based on histograms include linear and nonlinear transformations. An important nonlinear technique is the histogram equalization, which redistributes the intensity values of pixels in the image such that the resulting image contains a uniform distribution of intensities. Figure 9 illustrates the result after applying histogram equalization to an image.

4 Segmentation

Image segmentation is the process of extracting objects or regions of interest from an image. This procedure is usually performed by applying a certain criterion to a range of intensity values, such as connectivity, similarity among others. An example of medical image segmentation is the selection of bone or a specific organ, such as heart or lung, for analysis and visualization purposes. Several methods have been proposed for image segmentation in the literature (Haralick and Shapiro 1985; Pal and Pal 1993; Zhang 1996). The following subsections present some relevant image segmentation techniques.

4.1 Thresholding

A common segmentation technique is known as thresholding (Sankur and Sezgin 2001), whose purpose is to identify an intensity value (grayscale or color) to separate objects from the background. Thresholding can find a global and unique threshold value for the entire image or a local and adaptive threshold for different regions of the image. For instance, considering an interval of values between t_{\min} and t_{\max} , pixel values outside this range could be set to 0, whereas pixel values within the interval could be assigned to 1. Let $f(x, y)$ and $g(x, y)$ be the input image and the resulting image after the thresholding process, respectively. Then,

$$g(x, y) = \begin{cases} 1 & \text{if } t_{\min} \leq f(x, y) \leq t_{\max} \\ 0 & \text{otherwise} \end{cases} \quad (7)$$

Global thresholding presents some drawbacks since it is sensitive to noise and dependent on the actual image intensity range. For instance, if the patient has a metallic material prosthesis, the global thresholding applied to a computerized tomography can produce artifacts due to the presence of noise with intensity similar to bone structures. In this case, adaptive local thresholding would be more effective.

4.2 Region Growing

The region growing technique (Adams and Bischof 1994) uses a seed located on the object or region of interest, which can be manually specified by the user or automatically assigned. Then, the seed expands gradually in accordance with its neighboring pixels. The expansion process interrupts when neighboring pixels satisfy a stopping criterion. Typical connectivity types for two-dimensional images are 4 and 8 connected neighborhood, whereas for three-dimensional images are 6-, 18-, and 26-connected neighborhood.

Stopping criteria are usually based on the homogeneity of the grayscale values or textural information present in the medical images.

4.3 Watershed

The watershed segmentation technique (Beucher 1994) is based on concepts of topography and hydrography, where an image is considered as a topographic surface, such that catchment basins are formed through a flooding process. The water follows the gradient of the image and flows along a path to reach a local minimum. At the end of the flooding process, the watershed of a relief corresponds to the limits defined by adjacent catchment basins.

An example of watershed segmentation applied to medical images is the separation of normal and abnormal tissues for detecting brain tumor in MR images.

5 Registration

Image registration (Brown 1992; Zitova and Flusser 2003) is the process of integrating two or more images into a common coordinate system. Medical image registration can be usually categorized into single-modality and multimodality approaches. Single-modality methods align images acquired by the same scanner type, whereas multimodality methods align images acquired by different sensor types, such CT and MR.

The registration process is useful for aligning data of a same patient captured at different view points or along different periods of time to monitor a treatment or the progress of a disease, such as a tumor growth.

Substantial research has been conducted on the image registration field over the last decades (Crum et al. 2014; Hill et al. 2001; Lester and Arridge 1999; Maintz and Viergever 1998). Several techniques have been developed to make the task successful with little or no human intervention, more precise, faster, and less sensitive to noise or occlusions.

Two stages are usually involved in the image registration: geometric and radiometric transformations. A geometric transformation maps spatial positions in one image to another, whereas a radiometric transformation maps intensity values in one image to another.

Geometric transformations perform basic operations such as resizing, translation, rotation, and projections. In addition to such rigid transformations, nonrigid or elastic transformation can also be applied to locally align one target image with a reference image. Examples of elastic transformations include the radial basis functions, which can be further categorized into other basis functions (Buhmann 2000), such as thin-plate spline, spline with tension, and multiquadric function.

Geometric transformations in the spatial domain aim to match features or intensity patterns in the images. On the other hand, frequency-domain geometric transformations explore invariance properties to simplify the location of correspondences between a pair of images. Peaks found in phase correlation methods through the fast Fourier transform (FFT) correspond to the relative translation between a pair of images. Differences under scaling and rotation can also be determined using log-polar coordinates and exploring Fourier transform properties.

Salient features, such as corners, edges and regions, can be detected from the images and used to match them. Common metrics used in the matching process include cross-correlation and mutual information.

6 Volume Rendering

Volume rendering can be defined as a set of techniques for displaying bidimensional projections from tridimensional data sets. These techniques can be categorized into two groups: *isosurface rendering* and *direct volume rendering*.

6.1 Isosurface Rendering

Isosurface rendering methods involve the extraction of an intermediary geometric representation from the volume data set. The most commonly used representation is the triangle mesh, which is formed by vertices and triangles that connect its vertices through edges. Figure 10 shows a triangle mesh and a magnified region to allow visualization of more details. Isosurfaces are useful to represent internal organs, bones, or other anatomic structures.

The technique of Marching Cubes (Lorenson and Cline 1987) is one of the most employed methods to generate isosurfaces, where a regular 3D grid, formed by cubes, overlaps the data volume, such that the vertices on the grid match the scalar values of the volume. Each cube edge is verified if it intercepts the surface. These intersections will be part of the isosurface vertices, which will be connected by triangles following one of 256 possibilities to form the surface. The final isosurface is generated by joining the surfaces from all cubes. However, the technique of Marching Cubes presents some ambiguities in some triangle configurations that

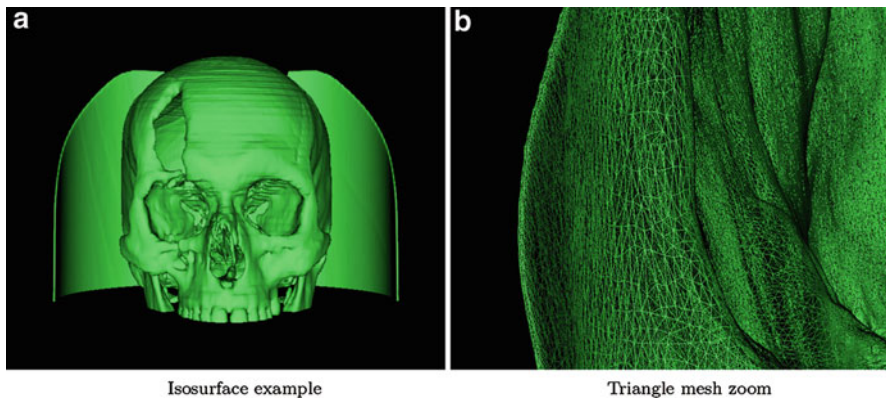


Fig. 10 Illustration of (a) an isosurface extracted from a volumetric medical data and (b) a magnified region of the mesh

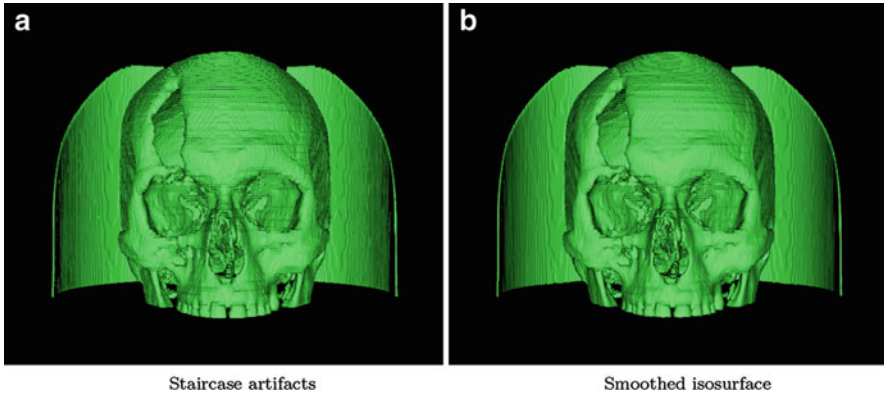


Fig. 11 (a) Isosurface with staircase artifacts and (b) same isosurface after the application of context aware smoothing algorithm to attenuate staircase artifacts

may generate holes in the isosurface. Other methods have been developed to avoid these problems, such as Marching Tetrahedra (Akio and Koide 1991) and Surface Nets (Gibson 1999).

Graphics processing units (GPUs) have been extensively used to process and display triangle meshes, as well as in 3D printing tasks. The triangle meshes can be used and edited in CAD tools to support surgical planning and prosthesis generation.

The quality of the isosurface depends on the methods used to generate it and on the segmentation process. Segmentation can generate a binary volume as result. Isosurfaces generated from binary volume usually present staircase artifacts, such as the ones shown in Fig. 11a. These artifacts are not natural to the patient's anatomy and they emerge mainly in high-curvature regions. Some techniques have been proposed to avoid these artifacts. The method developed by Whitaker (2000) smooths the binary volume toward the gradient direction to find the isosurface with minimum area. The context aware smoothing (Moench et al. 2011) method assigns high weighting coefficients to regions with occurrence of staircase while other regions have low weighting coefficients. The weighting coefficients control the degree of smoothing, such that high weighting coefficient areas are more smoothed. This is accomplished to reduce the loss of fine details in the resulting isosurface. Figure 11b shows the result after applying the context aware smoothing to a volumetric data.

6.2 Direct Volume Rendering

In direct volume rendering (DVR) (Roth 1982), the voxel values are mapped to colors and opacities according to a transfer function. Figure 12 illustrates an example of a transfer function. Color and opacity values are used to compose the final image according to the technique used. Volume ray casting (Levoy 1990) is one of the most common DVR techniques. In this technique, rays are traced from the observer,

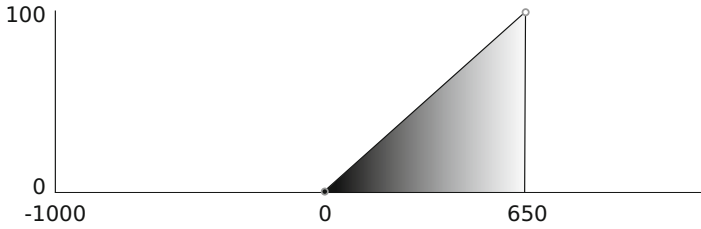


Fig. 12 Example of a linear transfer function, which maps scalar value 0 to black and 0% opacity. The scalar value 650 is mapped to white with 100%, whereas intermediate values are linearly interpolated to obtain color and opacity values

passing through an image plane, toward the object. The rays intercept the object voxels, such that the color and opacity values are accumulated to generate the final image. The emission-absorption (Fernando 2004) is an example of model to accumulate color and opacity values, expressed as

$$\begin{aligned}
 C &= \sum_{i=1}^n C_i \prod_{j=1}^{i-1} (1 - \alpha_j) \\
 \alpha &= 1 - \prod_{j=1}^n (1 - \alpha_j)
 \end{aligned}
 \tag{8}$$

where C and α are the accumulated color and opacity values computed iteratively, whereas C_i and α_i correspond to color and opacity, respectively, obtained from the segment i along the viewing ray.

In volume ray casting, structures of interest may be occluded by other structures. For instance, in a CT data set, soft tissues may occlude bones or regions due to contrast. However, it is possible to modify the transfer function, which can be done through user interaction or automatic methods for generating transfer functions. Figure 13 illustrates examples of volume ray casting applied to a volumetric data.

Maximum intensity projection (MIP) (Bruckner and Gröller 2009) addresses the problem of occlusion by taking into account the regions of interest with high scalar values. In MIP, the projection rays are not accumulated, instead the maximum scalar values are selected. One characteristic of MIP is its lack of visual depth information, which may lead to ambiguities in the visualization. MIP is useful to visualize bone structures, regions with different contrast, and tumors. Figure 14a illustrates an example of MIP rendering.

Minimum intensity projection (MinIP) (Mistelbauer et al. 2013) and average intensity projection (AIP) (Wu et al. 2008) are variations of MIP. In MinIP, the projection rays select the minimum values and can be used to provide information about blood flow deviation. In AIP, the projection rays show the mean value of scalar values obtained along their path. An example of AIP rendering is shown in Fig. 14b.

Maximum intensity difference accumulation (MIDA) (Bruckner and Gröller 2009) ponders the accumulation of color and opacity values along the rays through

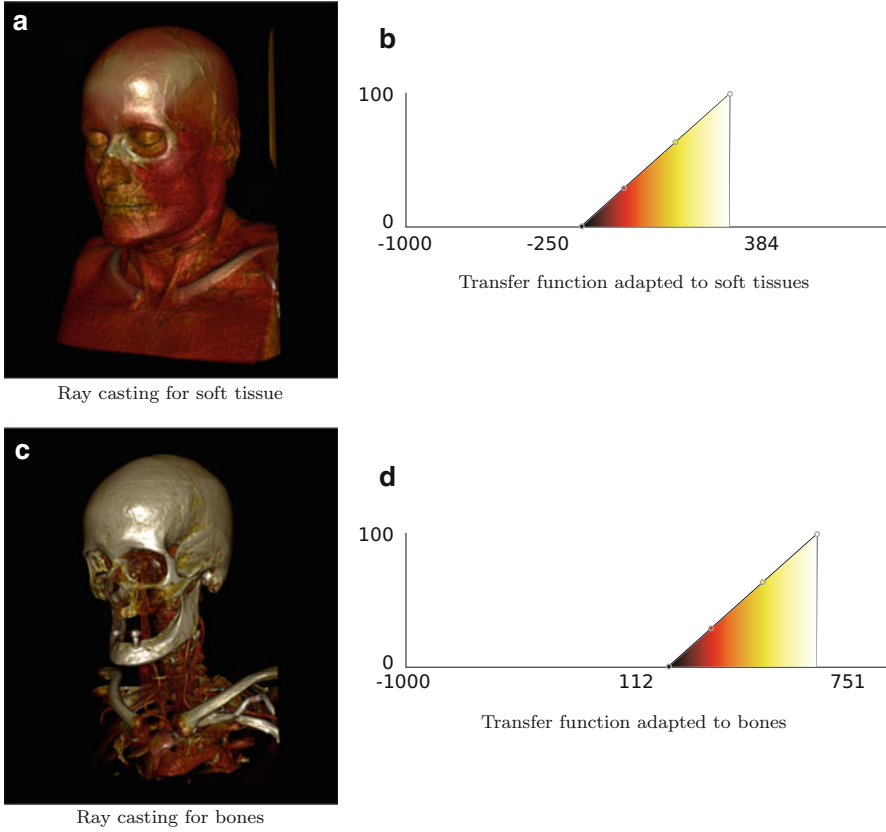


Fig. 13 Different views from ray casting for the same volume data set by modifying the transfer function. **(a)** the transfer function is adapted to reveal soft tissues; **(b)** the transfer function is modified to display bone structures

weights, which are calculated according to the maximum values intercepted along the ray path. The greater the difference between the maximum values, the higher the weights are assigned. Prioritizing the maximum values, MIDA can attenuate the problems associated with occlusion. Since MIDA uses accumulation, such as ray casting, the generated visualization presents depth information, which may reduce artifacts related to visualization ambiguities. Figure 14c shows an example of MIDA. Similar to MIP, MIDA is useful to visualize bone structures, regions with contrast, and tumors.

Contour MIP (Csèbfalvi et al. 2001) takes into account the angle between the viewing direction and the gradient vector from voxels intercepted by the projection rays, described as

$$s(P, V) = (1 - |(P) \cdot V|)^n \quad (9)$$

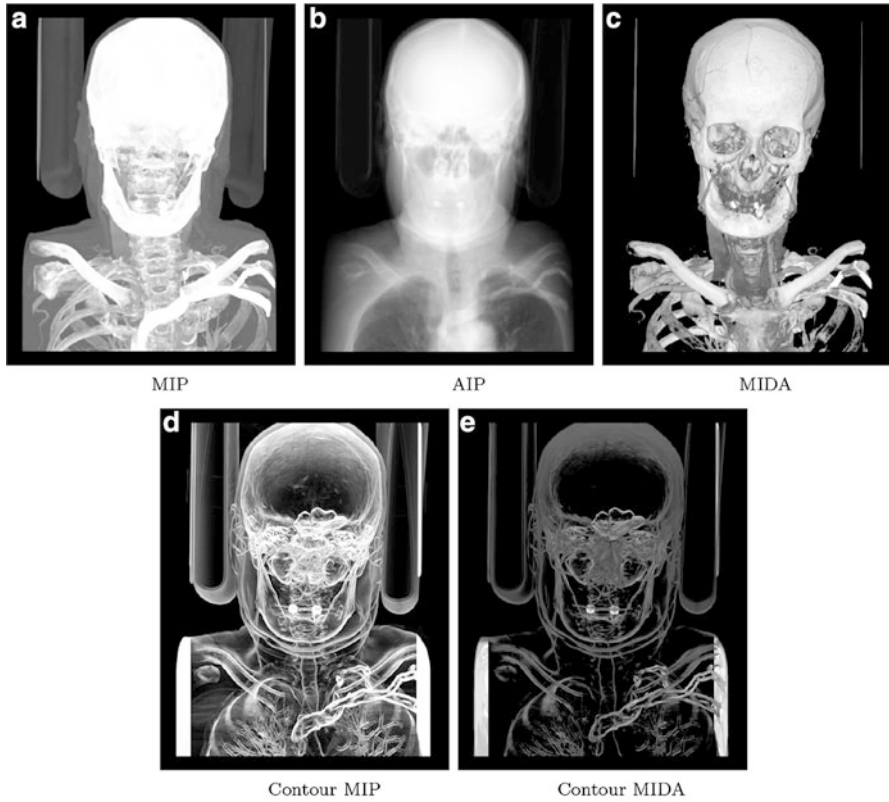


Fig. 14 A volume data set rendered through different volume rendering techniques

where $\nabla(P)$ is the gradient of voxel P , V is the viewing direction, and n is a sharpness coefficient for the contour. To compose the final image, contour MIP uses the MIP technique, since contour MIP may suffer from ambiguities in its visualization. Contour MIDA (de Moraes et al. 2015) follows the same idea as contour MIP; however, it uses MIDA to compose the final image to attenuate problems associated with ambiguities when compared to contour MIP. Both techniques emphasize voxels with higher values of gradient information, highlighting surfaces of different objects. Examples are illustrated in Fig. 14d and e.

7 3D Printing and Biofabrication

Nowadays, imaging is the basis for a series of applications that are already consolidate for a tailored treatment in medicine and odontology. Imaging is a noninvasive technique for human diagnosis and treatment. Therefore, a 3D model of an anatomy, generated from a patient CT or MRI medical scanner, can be integrated with additive

manufacturing (AM) technologies for many medical purposes. This is possible due to the concurrent development of scanning, imaging, and AM technologies. AM, also known as 3D printing or rapid prototyping, is based on the paradigm of a layer-by-layer automatically controlled deposition of materials by means of a myriad of processes. AM can produce directly a physical model from a virtual computational model and is considered a groundbreaking technology due to its flexibility and capacity to produce geometrically accurate complex models. A schematic diagram for 3D printing and additive manufacturing is illustrated in Fig. 15.

Imaging and AM technologies came to the market in the 1980s decade. Since then, a great evolution on both technologies and its integration for healthcare applications is paramount. Among them can be highlighted the production of 3D physical models, called biomodels, for a better and safer treatment, as well as the development of customized prostheses, medical devices, and surgical instruments (Silva et al. 2009; Sannomiya et al. 2008; Kemmoku et al. 2010; Oliveira et al. 2014; Giacomo et al. 2014).

Today's AM technologies use as a reference to print objects in a file format called STL (STereoLithography) created for the first machines in the 1980s decade by Albert Consulting Group under 3D Systems demand. This is a very simple representation of an object using triangle meshes to define all of its surfaces (internal and external). Each triangle is represented by means of three coordinates, one coordinate for each triangle vertex, and a normal vector pointing out of the object material, which allows to define the real boundaries of the object. The advantages of STL representation are mainly due to its easy interpretation from computing systems and cross-platform interoperability. To be used in AM, the STL file is sliced by means of parallel planes corresponding to the minimal layer thickness assured by the AM technology being used. The disadvantage is its redundant data representation composed of planar facets without any topological connectivity information. STL is still de facto standard for AM data exchange. The majority of the medical imaging software generate only STL format after all the steps explained in the previous sections of this chapter.

The AMF (Additive Manufacturing File Format) representation is an initiative of ASTM (American Society for Testing and Materials) since 2013 adopted by ISO (International Standardization Organization) as the international standard ISO/-ASTM 52915 (2013). The main idea of AMF is to overcome deficiencies and challenges of the STL file format, such as the independence among different AM technologies, represent geometry with colors, texture, multimaterials, and other properties, associated with the simplicity to be implemented and interpreted by computer systems. The adaptability to support part complexity and performance in terms of file size and processing is a desirable specification. AMF is also designed for compatibility with legacy systems (e.g., STL) and potential possibilities to be adapted for new demands for future technology evolutions. One important feature is the possibility to use not only flat triangles but also curved and surface triangles. AMF uses the XML (eXtensible Markup Language) as a standard to store and transport data readable for both human and computer.

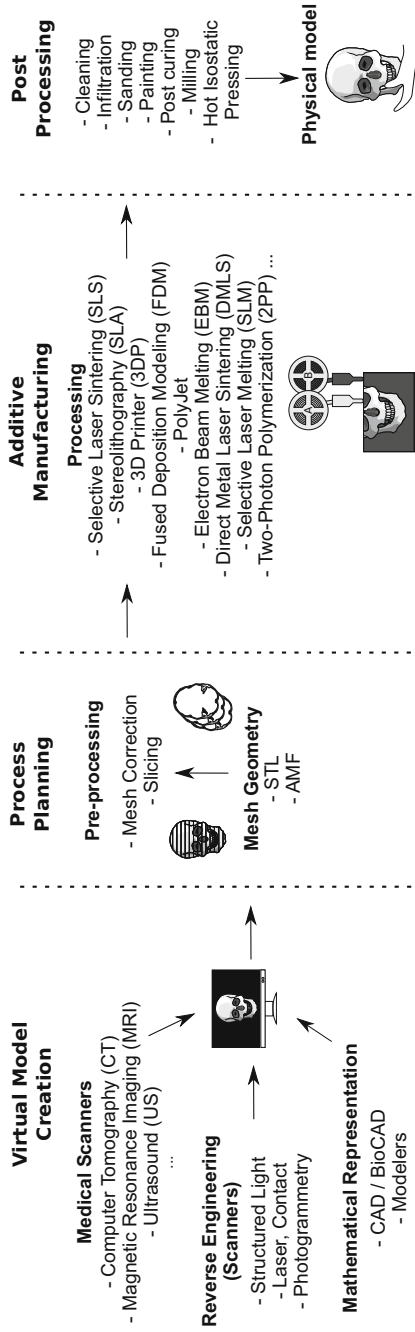


Fig. 15 3D printing and additive manufacturing techniques

Another 3D representation for AM is the 3MF (3D Manufacturing Format) file format. It is being developed by a joint development foundation project for creating the new file standard of AM. This project was originally created by some of the AM, CAD systems and software solutions providers such as Siemens, Dassault Systèmes, 3D Systems, Stratasys, SLM, HP, Materialise, Autodesk, Shapeways, NetFabb, and Microsoft. The 3MF format is developed under the philosophy of open-source. Similarly to STL and AMF, this format is a representation of an object composed of triangle element meshes. The proposal of 3MF is to promote a rich representation of an object in details, including colors, materials, and other characteristics. The 3MF will support extensions and innovations of the AM area, and interoperability among systems (3MF Consortium 2016b, c). It is expected for the consortium members a wide adoption. Its specification and codification can be found and downloaded from GitHub (3MF Consortium 2016a).

Looking toward biological directions of AM, imaging will play a fundamental role as a basis for the reverse engineering of organs and tissues anatomy. More recently, AM started to include biomaterials and biological materials as cells and microtissues as an option for printing. This is a new area called Biofabrication as rapidly growing field of research as a solution for the shortage of tissues and organs donation for restoration and replacement of human functionalities. Then, Biofabrication has appeared and grown in the last decade with many developments, potentials, and trials but also challenges.

Very recently, the term Biofabrication was reappraised by the 2010 created International Society of Biofabrication (ISB). Many novelties and developments obliged ISB to update the meaning of this wide word considering the derivations Bioprinting and Bioassembly. Then, the new ISB definition repositions Biofabrication as “the automated generation of biologically functional products with structural organization from living cells, bioactive molecules, biomaterials, cell aggregates such as micro-tissues, or hybrid cell-material constructs, through Bioprinting or Bioassembly and subsequent tissue maturation processes” (Groll et al. 2016). Three approaches as branches of Biofabrication have evolved: scaffold-based, solid-scaffold-free based on cell and tissue spheroids deposition, and a mix of them named as third strategy or hybrid technology (Rezende et al. 2012; Danilevicius et al. 2015).

The scaffold, as a first approach, consists of a three-dimensional structure as a temporary support for cells growing and maturing of a new tissue. The scaffold must be biodegradable, offering suitable conditions in such way the cells can be seeded and posteriorly adhere, differentiate, and proliferate for new tissue formation. Since AM allows for highly precise construction of 3D complex geometries and controlled porosity, scaffolds have been fabricated in many materials for different applications such as bone, cartilage, coronary, skin, and dental, among others. Reinforcing the role of controlled geometry of scaffolds with interconnectivity and therefore the guidance for the new tissue formation, many imaging techniques have been applied in order to verify the real scaffold's shape and geometry and to validate their applications. Noninvasive imaging techniques using CT and MRI have been researched to be used as a follow-up tool for an accurate assessment of bioresorbable

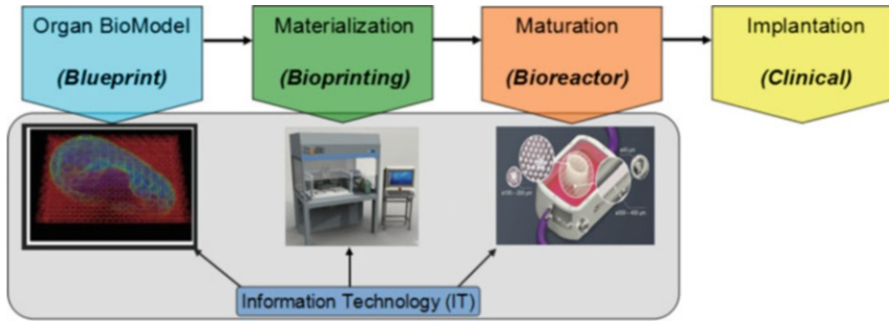


Fig. 16 Stages of bioprinting, from blueprint to clinical (Rezende et al. 2015; Murphy and Atala 2014)

vascular scaffolds (BVSs) after a percutaneous coronary intervention (Hickethier et al. 2016). Other authors have analyzed BVSs implanted in vivo by means of the optical frequency domain imaging (Naganuma et al. 2015). Even for scaffolds produced by conventional methods (non-AM), imaging has benefited the diagnosis of implanted scaffolds allowing for 3D quantification of parameters such as porosity, thickness, and surface area (Kłodowski et al. 2014).

In turn, solid-scaffold-free, based on cell or tissue spheroids controlled deposition, so-called Bioprinting or Organ Printing is defined as a layer-by-layer additive robotic computer-aided biofabrication of functional 3D organ constructs using self-assembling tissue spheroids according to a digital model or blueprint (Derby 2012; Melchels et al. 2012; Mironov et al. 2008; Rezende et al. 2015). On the other hand, Bioprinting is a dynamic strategy of biofabrication and is conceptually split into four stages: blueprint, materialization, maturation, and clinical application (Fig. 16). Each of these Biofabrication steps will, in the future, make use of imaging techniques for anatomical reverse engineering, mimicking and characterizing tissue micro and macro anatomic details, and also for quality control during maturation and clinical applications.

Different processes for bioprinting have been proposed (Atala and Yoo 2015), and they can be summarized as follows:

- **Inkjet Printing:** a noncontact printing technique that takes data from a computer representing an image or character, and reproduces it onto a substrate by ejecting tiny ink drops on a drop-on-demand manner (Mohebi and Evans 2002; Chua and Yeong 2014). Presorted cells are available in a 2D–printer cartridge-like. These cells are disposed drop-by-drop onto an $XY Z$ platform.
- **Scaffold-Free Printing:** this technique makes use of fluidity, where the fusion of the cell aggregates or cell rods are governed by the surface tension among two or more of those structures (Jakab et al. 2008). The live cells are encapsulated by some hydrogel, which assures mechanical protection and stability in order for the whole structure to become stronger. Thus, the cells can fuse to each other, generating the tissue and posteriorly the organ.

- **Extrusion-Based Deposition:** this technique uses a syringe for extrude the material under controlled pressure and temperature onto the platform. The material is normally at semi-melted condition which eases its deposition (Skardal et al. 2010). The materials are normally polymers or hydrogels and must be soft or fluid enough to facilitate extrusion through the small diameter tip or nozzle assuring mechanical strength itself after the deposition (Atala and Yoo 2015).
- **Laser-Induced Forward Transfer:** this technique utilizes a pulsed laser that is used to induce the transfer of material from a source film spread onto an optically transparent quartz support to a substrate in close proximity to or in contact with the film (Guillemot et al. 2010). This film is comprised of a printable material (biopolymer or protein) containing cells inside that are then deposited in a pattern on the substrate to create cellular structures and patterns. LIFT is supported on a transport layer, such as gold or titanium, which absorbs the laser energy and transfers it to the ribbon.

Bioprinting technology has a broad utility in various application areas, such as tissue engineering and regenerative medicine, transplantation and clinics, drug screening and high-throughput assays, and cancer research. Currently, a wide variety of tissues have been successfully bioprinted, such as thin or hollow tissues, for example, blood vessel, and tissues as such as bone, cardiac, cartilage, liver, lung, neural, pancreas, skin, and vascular (Ozbolat et al. 2016).

Image processing and computer graphics techniques for the creation of three-dimensional models or a blueprint for visualization and building of a complex organ are largely required. Therefore, for a bioprinting process the preprocessing includes data acquisition, printing model construction, printing path optimization, and materials preparation. Data acquisition refers to the process of obtaining anatomic geometries of the targeted tissues/organs and is usually implemented via medical imaging techniques, such as MRI and CT (Wu et al. 2017). So far, there is no sufficient knowledge to precisely define in which extent imaging will contribute for the Biofabrication field.

Medical imaging technology is an essential tool used by tissue engineers to provide information on 3D structure and function at the molecular, cellular, tissue, organ, and organism level. Computer-aided design/computer-aided manufacturing (CAD/ CAM) tools are also used to collect and digitize the complex tomographic and architectural information of the tissues. A comprehensive understanding of the composition and organization of the components that make up these tissues is the key requirement for reproducing the complex heterogeneous architectures that exist within functional tissues and organs (Murphy and Atala 2014).

For a complete blueprint, the most critical point is to obtain the best representation of human organs due to their complexity. For instance, replicating details of microvasculature of a 3D structure is hard task either from the anatomical or from mathematical and computational perspectives. Most of complex human organs are highly vascularized and have elaborated intraorgan branched vascular trees which dramatically increase the level of their structural organization and make task of designing corresponding organ blueprint more challenging (Rezende et al. 2015).

Furthermore, so far there is no software or model powerful enough to establish a blueprint.

Additionally, biomimicry and biomimetic are also considerable resources for the making-up of the blueprint, and they can be grouped in two main categories: those based on the use of imaging resources for the digitization of biological structures and those based on the use of mathematical and software resources for the construction of geometries with properties similar to those found in biological materials (Lantada 2016).

During the last decade, increasing attention has been paid for using fractals for promoting modeling, design, and simulation tasks in several areas of Biomedical Engineering, some of them also linked to the development of novel biomedical microdevices for interacting at a cellular and even molecular level. This includes modeling the behavior of microorganisms, complex organisms and their systems, scaffolds for tissue engineering, and the surfaces of organs and tissues (Lantada 2016).

In the conventional production systems, not only a product representation associated with user requirements and applications will not suffice. It is necessary to have available production lines and methods for fast, safe, and lean production of any product. As an analogy with this field, Biofabrication will face the same needs to be competitive when all the intermediate steps and associate challenges are overcome. Hence, a biofabrication line will be necessary with all the processes planning and execution needed.

A smart platform that enables real-time monitoring, informative decision-making, and automated operation will be necessary. Some key components include a data-driven interface, automated biofabrication line, efficient communication, and novel monitoring techniques customized for biomedical applications (Wu et al. 2017).

From an engineering point of view, the successful clinical translation of organ printing technology will depend not only on the development of a single tool or device, such as a robotic bioprinter, but rather on the entire complex of related technologies and their seamless integration, i.e., an Organ Biofabrication Line (OBL). The design and development of a fully integrated OBL, or development of a series of integrated automated robotic tools, is imperative for the future commercial translation of the organ printing technology (Mironov et al. 2011).

An organ biofabrication line will combine design, computer simulation, visual information of machines, devices, human resources and processes, as well as it must include *in silico* assays about tissue spheroids formation, spheroids fusion, cell viability, tissue and organ development in each corresponding stage. A virtual OBL must integrate essential tools such as CAD, CAE, CAM, complex mathematical modeling, and new specific software for biological simulations, special equipment and information technologies in general (Passamai et al. 2016).

Beyond the 3D representation available and in development today for AM, the Biofabrication field will need a complete new way to represent tissues and organs, based on its functionality, multimaterials composition, and micro/macro anatomic details. Imaging will play a fundamental role for this purpose. More comprehensive design systems need to be developed in order to integrate other crucial biological

factors into the process of building successful tissue constructs (Ozbolat and Gudapati 2016). A biofabrication line for organ production will be the next generation of production and, again, imaging will be necessary for characterization and quality control. Finally, new engineering tools associated with strong biological knowledge and translational methods will be necessary to support the biofabrication emerging area.

8 Conclusions

Continuous developments in medical image analysis have aided healthcare professionals in several diagnostic tasks. Technological advances in digital computing, medical imaging, biomaterials, and biofabrication have contributed to a broad range of medical applications. Critical diagnostic decisions have been improved by the integration of powerful computer-aided tools and manufacturing technologies.

In this chapter, we provided an overview of fundamental concepts related to the construction of three-dimensional models for visualization and biofabrication purposes. The understanding of such key topics is challenging due to the diverse and multidisciplinary field of biomedical engineering, however, of paramount importance to the development of innovative solutions to a variety of medical and health problems.

Acknowledgments We are grateful to São Paulo Research Foundation (FAPESP) for the Brazilian Research Institute for Neuroscience and Neurotechnology BRAINN (CEPID process 2013/07559-3) and for the Thematic Projects (Grants 2011/22749-8 and 2014/12236-1). We are thankful to Brazilian Council for Scientific and Technological Development (CNPq) for the Brazilian Institute of Biofabrication (INCT-BIOFABRIS process 2008/57860-3) and for the Regenerative Medicine grant (process 467643/2014-8) for the financial support. We also thank Otávio Henrique Junqueira Amorim for creating some of the illustrations and pictures.

References

- 3MF Consortium (2016a) 3MF materials and properties extension specification and reference guide. <https://github.com/3mfconsortium/>. Accessed May 2016
- 3MF Consortium (2016b) 3MF materials and properties extension specification and reference guide. http://3mf.io/wp-content/uploads/2015/04/3MFmaterialsSpec_1.0.1.pdf. Accessed May 2016
- 3MF Consortium (2016c) 3MF materials and properties extension specification and reference guide. http://3mf.io/wp-content/uploads/2015/04/3MFcoreSpec_1.0.1.pdf. Accessed May 2016
- Adams R, Bischof L (1994) Seeded region growing. *IEEE Trans Pattern Anal Mach Intell* 16 (6):641–647
- Akio D, Koide A (1991) An efficient method of triangulating equi-valued surfaces by using tetrahedral cells. *IEICE Trans Inf Syst* 74(1):214–224
- Amorim P, Moraes T, Silva J, Pedrini H (2015) InVesalius: an interactive rendering framework for health care support. In: Bebis G, Boyle R, Parvin B, Koracin D, Pavlidis I, Feris R, McGraw T, Elendt M, Kopper R, Ragan E, Ye Z, Weber G (eds) *Lecture notes in computer science*, vol 9474. Springer International Publishing, Switzerland, pp 45–54

- Andria G, Attivissimo F, Cavone G, Giaquinto N, Lanzolla A (2012) Linear filtering of 2-D wavelet coefficients for denoising ultrasound medical images. *Measurement* 45(7):1792–1800
- Atala A, Yoo JJ (2015) *Essentials of 3D biofabrication and translation*. Academic, London
- Beucher S (1994) Watershed, hierarchical segmentation and waterfall algorithm. In: *Mathematical morphology and its applications to image processing*. Springer, Dordrecht, Netherlands, pp 69–76
- Brown LG (1992) A survey of image registration techniques. *ACM Comput Surv* 24(4):325–376
- Bruckner S, Gröller ME (2009) Instant volume visualization using maximum intensity difference accumulation. *Comput Graphics Forum* 28(3):775–782
- Buhmann MD (2000) Radial basis functions. *Acta Numerica* 2000(9):1–38
- Canny J (1986) A computational approach to edge detection. *IEEE Trans Pattern Anal Mach Intell* 6:679–698
- Chua CK, Yeong WY (2014) *Bioprinting: principles and applications, vol 1*. World Scientific Publishing Co Inc., Singapore
- Crum WR, Hartkens T, Hill D (2014) Non-rigid image registration: theory and practice. *Br J Radiol* 77:S140–S153
- Csèbfalvi B, Mroz L, Hauser H, König A, Gröller ME (2001) Fast visualization of object contours by non-photorealistic volume rendering. *Comput Graphics Forum* 20:452–460
- Danilevicius P, Rezende RA, Pereira FD, Selimis A, Kasyanov V, Noritomi PY, Silva JV, Chatziniakolaidou M, Farsari M, Mironov V (2015) Burr-like, laser-made 3D microscaffolds for tissue spheroid engagement. *Biointerphases* 10(2):021011
- de Moraes TF, Amorim PH, Silva JV, Pedrini H, Meurer MI (2015) Medical volume rendering based on gradient information. In: *Computational vision and medical image processing V: 5th ECCOMAS thematic conference on computational vision and medical image processing*, p 181, Tenerife, Spain. CRC Press
- Derby B (2012) Printing and prototyping of tissues and scaffolds. *Science* 338(6109):921–926
- Dowsett D, Kenny PA, Johnston RE (2006) *The physics of diagnostic imaging*. A Hodder Arnold Publication. Taylor & Francis
- Fernando R (2004) *GPU gems: programming techniques, tips and tricks for real-time graphics*. Pearson Higher Education, London
- Giacomo G, Silva J, Martines R, Ajzen S (2014) Computer-designed selective laser sintering surgical guide and immediate loading dental implants with definitive prosthesis in edentulous patient: a preliminary method. *European Journal of Dentistry* 8(1):100–106
- Gibson SFF (1999) Constrained elastic surfacenet: generating smooth models from binary segmented data. TR99 24. Mitsubishi Electric Research Laboratories, Inc., Cambridge
- Gonzalez RC, Woods RE (2002) *Digital image processing*. Prentice Hall, Inc., Upper Saddle River
- Groll J, Boland T, Blunk T, Burdick JA, Cho D-W, Dalton PD, Derby B, Forgacs G, Li Q, Mironov VA et al (2016) Biofabrication: reappraising the definition of an evolving field. *Biofabrication* 8(1)
- Guillemot F, Souquet A, Catros S, Guillotin B (2010) Laser-assisted cell printing: principle, physical parameters versus cell fate and perspectives in tissue engineering. *Nanomedicine* 5(3):507–515
- Haralick RM, Shapiro LG (1985) Image segmentation techniques. *Comput Vis Graphics Image Process* 29(1):100–132
- Hickethier T, Kröger JR, Von Spiczak J, Baessler B, Pfister R, Maintz D, Bunck AC, Michels G (2016) Non-invasive imaging of bioresorbable coronary scaffolds using CT and MRI: first in vitro experience. *Int J Cardiol* 206:101–106
- Hill DL, Batchelor PG, Holden M, Hawkes DJ (2001) Medical image registration. *Phys Med Biol* 46(3)
- Hsieh J (2003) *Computed tomography: principles, design, artifacts, and recent advances*. SPIE Press
- ISO/ASTM 52915 (2013) Standard specification for additive manufacturing file format (AMF). ASTM International, West Conshohocken
- Jakab K, Norotte C, Damon B, Marga F, Neagu A, Besch-Williford CL, Kachurin A, Church KH, Park H, Mironov V (2008) Tissue engineering by self-assembly of cells printed into topologically defined structures. *Tissue Eng A* 14(3):413–421
- Kapila S (2014) *Cone beam computed tomography in orthodontics: indications, insights, and innovations*. Wiley, New York

- Kelsey CA, Heintz PH, Chambers GD, Sandoval DJ, Paffett NLAKS (2013) Radiation biology of medical imaging. Wiley, Hoboken
- Kemmoku D, Noritomi P, Toland F, Silva J (2010) Use of BioCAD in the development of a growth compliant prosthetic device for cranioplasty of growing patients. In: Innovative developments in design and manufacturing. Taylor & Francis, London, pp 127–130
- Kim TK, Paik JK, Kang BS (1998) Contrast enhancement system using spatially adaptive histogram equalization with temporal filtering. *IEEE Trans Consum Electron* 44(1):82–87
- Kłodowski K, Nowicka K, Tarasiuk J, Wroński S, Świketek M, B-lazewicz M, Figiel H, Turek K, Szponder T (2014) Micro-imaging of implanted scaffolds using combined MRI and micro-CT. *Comput Med Imaging Graph* 38(6):458–468
- Lantada AD (2016) Microsystems for enhanced control of cell behavior. In: Lantada AD (ed) *Studies in mechanobiology, tissue engineering and biomaterials*, vol 18. Springer International Publishing, Berlin
- Leondes CT (2005) Medical imaging systems technology: modalities, Medical imaging systems technology. World Scientific, Hackensack
- Lester H, Arridge SR (1999) A survey of hierarchical non-linear medical image registration. *Pattern Recogn* 32(1):129–149
- Levoy M (1990) Efficient ray tracing of volume data. *ACM Trans Graph* 9(3):245–261
- Lorensen WE, Cline HE (1987) Marching cubes: a high resolution 3D surface construction algorithm. *Comput Graph* 21(4):163–169
- Lutz H, Buscarini E, W. H. Organization (2011) Manual of diagnostic ultrasound, vol 1. World Health Organization, Geneva
- Macovski A (1983) Medical imaging systems. Prentice Hall, Englewood Cliffs
- Maintz JA, Viergever MA (1998) A survey of medical image registration. *Med Image Anal* 2(1):1–36
- Manjón JV, Carbonell-Caballero J, Lull JJ, García-Martí G, Martí-Bonmatí L, Robles M (2008) MRI denoising using non-local means. *Med Image Anal* 12(4):514–523
- Melchels FP, Domingos MA, Klein TJ, Malda J, Bartolo PJ, Hutmacher DW (2012) Additive manufacturing of tissues and organs. *Prog Polym Sci* 37(8):1079–1104
- Michailovich OV, Tannenbaum A (2006) Despeckling of medical ultrasound images. *IEEE Trans Ultrason Ferroelectr Freq Control* 53(1):64–78
- Mironov V, Kasyanov V, Drake C, Markwald RR (2008) Organ printing: promises and challenges. *Regen Med* 3(1):93–103
- Mironov V, Kasyanov V, Markwald RR (2011) Organ printing: from bioprinter to organ biofabrication line. *Curr Opin Biotechnol* 22(5):667–673
- Mistelbauer G, Morar A, Varchola A, Schernthaner R, Baclija I, Köchl A, Kanitsar A, Bruckner S, Gröller E (2013) Vessel visualization using curvicircular feature aggregation. *Comput Graphics Forum* 32(3):231–240
- Moench T, Gasteiger R, Janiga G, Theisel H, Preim B (2011) Context-aware mesh smoothing for biomedical applications. *Comput Graph* 35(4):755–767
- Mohebi MM, Evans JR (2002) A drop-on-demand ink-jet printer for combinatorial libraries and functionally graded ceramics. *J Comb Chem* 4(4):267–274
- Murphy SV, Atala A (2014) 3D bioprinting of tissues and organs. *Nat Biotechnol* 32(8):773–785
- Naganuma T, Ishiguro H, Takagi K, Fujino Y, Mitomo S, Nakamura S, Nakamura S, Colombo A (2015) Provisional T-stenting with bioresorbable vascular scaffolds in vivo: insights from optical frequency domain imaging. *J Am Coll Cardiol Interv* 8(4):635–637
- Oliveira AT, Camilo AA, Bahia PRV, Carvalho ACP, Santos MF, Silva JVL, Monteiro AA (2014) A novel method for intraoral access to the superior head of the human lateral pterygoid muscle. *Biomed Res Int* 2014:1–8
- Oosterwijk H, Gihring P (2002) *Dicom basics*. OTech Inc, Aubrey
- Ozbolat I, Gudapati H (2016) A review on design for bioprinting. *Bioprinting* 3:1–14
- Ozbolat IT, Peng W, Ozbolat V (2016) Application areas of 3D bioprinting. *Drug Discov Today* 21(8):1257–1271

- Pal NR, Pal SK (1993) A review on image segmentation techniques. *Pattern Recogn* 26(9): 1277–1294
- Parker JR (2010) *Algorithms for image processing and computer vision*. Wiley, Indianapolis
- Passamai V, Dernowsek J, Nogueira J, Lara V, Vilalba F, Mironov V, Rezende R, Silva J (2016) From 3D bioprinters to a fully integrated organ biofabrication line. *J Phys Conf Ser* 705:012010
- Pianykh OS (2009) *Digital imaging and communications in medicine (DICOM): a practical introduction and survival Guide*. Springer, Berlin/Heidelberg
- Rezende RA, Pereira FD, Kasyanov V, Ovsianikov A, Torgensen J, Gruber P, Stampfl J, Brakke K, Nogueira JA, Mironov V, Silva JV (2012) Design, physical prototyping and initial characterization of ‘lockyballs’. *Virtual Phys Prototyping* 7(4):287–301
- Rezende RA, Kasyanov V, Mironov V, Silva JVL (2015) Organ printing as an information technology. *Procedia Eng* 110:151–158
- Roth SD (1982) Ray casting for modeling solids. *Comput Graphics Image Process* 18(2):109–144
- Russ JC (2015) *The image processing handbook*. CRC Press, New York
- Salinas HM, Fernández DC (2007) Comparison of PDE-based nonlinear diffusion approaches for image enhancement and denoising in optical coherence tomography. *IEEE Trans Med Imaging* 26(6):761–771
- Sankur B, Sezgin M (2001) Image thresholding techniques: a Survey over categories. *Pattern Recogn* 34(2):1573–1583
- Sannomiya EK, Silva JVL, Brito AA, Saez DM, Angelieri F, Silva Dalben G (2008) Surgical planning for resection of an ameloblastoma and reconstruction of the mandible using a selective laser sintering 3D biomodel. *Oral Surg Oral Med Oral Pathol Oral Radiol Endod* 106(1):36–40
- Silva J, Almeida A, Raposo do Amaral C, Ferreira D, Hotta L, Raposo do Amaral CA, Guidi M, Buzzo CL (2009) Three-dimensional virtual and physical technologies in the treatment of craniofacial anomalies. In: 11th international congress on cleft lip and palate related craniofacial anomalies, vol 1, pp 5–10, Bologna, Medmond Italy
- Singh S, Bovis K (2005) An evaluation of contrast enhancement techniques for mammographic breast masses. *IEEE Trans Inf Technol Biomed* 9(1):109–119
- Sistrom CL, McKay NL (2005) Costs, charges, and revenues for hospital diagnostic imaging procedures: differences by modality and hospital characteristics. *J Am Coll Radiol* 2(6): 511–519
- Skardal A, Zhang J, McCoard L, Xu X, Ottamasathien S, Prestwich GD (2010) Photocrosslinkable hyaluronan-gelatin hydrogels for two-step bioprinting. *Tissue Eng A* 16(8):2675–2685
- Stallings W (2005) *Data and computer communications*. Prentice Hall, Upper Saddle River
- Stark JA (2000) Adaptive image contrast enhancement using generalizations of histogram equalization. *IEEE Trans Image Process* 9(5):889–896
- Tomasi C, Manduchi R (1998) Bilateral filtering for gray and color images. In: Sixth international conference on computer vision, IEEE, pp 839–846
- Wahl RL, Wagner HN (2009) *Principles and practice of PET and PET/CT*. Lippincott Williams & Wilkins
- Whitaker RT (2000) Reducing aliasing artifacts in iso-surfaces of binary volumes. In: IEEE symposium on volume visualization, IEEE, pp 23–32
- Wu Q, Merchant F, Castleman KR (2008) *Microscope image processing*, 1st edn. Academic, Boston
- Wu C, Wang B, Zhang C, Wysk RA, Chen Y-W (2017) Bioprinting: an assessment based on manufacturing readiness levels. *Crit Rev Biotechnol* 37(3):333–354
- Zhang YJ (1996) A survey on evaluation methods for image segmentation. *Pattern Recogn* 29(8): 1335–1346
- Zitova B, Flusser J (2003) Image registration methods: a Survey. *Image Vis Comput* 21(11): 977–1000



Mathematical Modeling of 3D Tissue Engineering Constructs

Henrique Amorim Almeida and Paulo Jorge da Silva Bártolo

Contents

1	Introduction	224
2	Mathematical-Based Scaffold Modeling	225
3	Triply Periodic Minimal Surfaces	231
3.1	Definition	231
3.2	Periodic Surface Modeling	232
3.3	Schwarz TPMS Primitives	234
3.4	Schoen TPMS Primitives	235
4	Numerical Implementation of the Designed Models	237
4.1	Elastic Modulus Evaluation	238
4.2	Shear Modulus Evaluation	244
5	Design of a Functionally Gradient Scaffold Using TPMS Basic Units	245
6	Conclusions	246
	References	249

Abstract

Tissue engineering represents a new field aiming at developing biological substitutes to restore, maintain, or improve tissue functions. In this approach, scaffolds provide a temporary mechanical and vascular support for tissue regeneration while tissue ingrowth is being formed. The design of optimized scaffolds for tissue engineering applications is a key topic of research, as the complex

H. A. Almeida (✉)

School of Technology and Management, Polytechnic Institute of Leiria (IPL), Leiria, Portugal
e-mail: henrique.almeida@ipleiria.pt

P. J. da Silva Bártolo

Manchester Biomanufacturing Centre, University of Manchester, Manchester, UK

School of Mechanical, Aerospace and Civil Engineering, University of Manchester, Manchester, UK

e-mail: paulojorge.dasilvabartolo@manchester.ac.uk

macro- and micro-architectures required for a scaffold depends on the mechanical and vascular properties and physical and molecular queues of the surrounding tissue at the defect site. One way to achieve such hierarchical designs is to create a library of unit cells, which can be assembled through a computational tool.

Besides presenting an overview scaffold designs based hyperbolic surfaces, this chapter investigates the use of two different types of triply periodic minimal surfaces, Schwarz and Schoen, in order to design better biomimetic scaffolds with high surface-to-volume ratio, high porosity, and good mechanical properties. The effect of two parametric parameters (thickness and surface radius) is also evaluated regarding its porosity and mechanical behavior.

1 Introduction

The loss or failure of an organ or tissue is a frequent, devastating, and costly problem in health care. Currently, this problem is treated either by transplanting organs from one individual to another or performing surgical reconstructions, transferring tissue from one location in the human body into the diseased site. With the aging of the population and higher expectations for a better quality of life, the need for substitutes to replace or repair tissues or organs due to disease, trauma, or congenital problems is overwhelming and increasing on a daily basis. To overcome these limitations, tissue engineering emerged as a rapidly expanding approach to address the organ shortage problem by creating cell-based substitutes of native tissues comprising tissue regeneration, organ substitution, and gene therapy (Melek 2015; Risbud 2001; Langer and Vacanti 1993).

Tissue engineering is a multidisciplinary field focusing on the use of cells and engineered materials, combining the principles of biology, engineering, and medicine to create biological substitutes for lost or defective native tissues (Jiang et al. 2015; Eshraghi and Das 2010; Bártolo et al. 2008, 2009a, b; Gibson 2005; Tan et al. 2005; Vozzi et al. 2003; Risbud 2001). According to Skalak and Fox (1988), tissue engineering is defined as “the application of the principles and methods of engineering and life sciences toward the fundamental understanding of structure–function relationships in normal and pathological mammalian tissues and the development of biological substitutes to restore, maintain, or improve tissue and organ functions” (Jiang et al. 2015; Bártolo et al. 2008).

In tissue engineering applications, a temporary three-dimensional scaffold that mimics the physiological functions of the native extracellular matrix is vital to stimulate and maintain the cells’ ability to express their native differentiated phenotypes. An optimal scaffold design can promote cell proliferation and cell-specific matrix production, which will eventually take over the supporting role of the biodegrading scaffold in situ (Xue et al. 2017; Fallahiarezoudar et al. 2015; Janik and Marzec 2015; Osman et al. 2015; Selimis et al. 2015; Bártolo et al. 2009a, 2009b).

To achieve these goals, an ideal scaffold must satisfy some biological and physical requirements (Tajbakhsh and Hajiali 2017; Law et al. 2016; Brunello et al. 2016; Tollemar et al. 2016; Stratton et al. 2016; Jana and Lerman 2015; Almeida and Bártolo 2012a, b). The biological requirements are biocompatibility (the scaffold material must interact positively with the cells, allowing cell attachment, proliferation, differentiation and with the host environment, without eliciting adverse host/tissue responses), biodegradability (the scaffold material must degrade into nontoxic products), controlled degradation rate (the degradation rate of the scaffold must be adjustable in order to match the rate of tissue regeneration), and bioactivity (promoting and guiding cell proliferation, differentiation, and tissue growth). The physical requirements are appropriate porosity, pore size and pore shape to encourage tissue ingrowth and vascularization, sufficient strength and stiffness to withstand stresses in the host tissue environment, adequate surface finish to ensure a good biomechanical coupling between the scaffold and the tissue, and easily sterilized by either exposure to high temperatures or immersing in a sterilization agent, remaining unaffected by neither of these processes.

Alongside the listed biological and physical requirements, an optimum scaffold should also have functional and anatomical requirements, in other words, a gradient functionality of the organ or tissue, meaning that the external geometry and size of the scaffold should be the same of the natural tissue, in order for the scaffold to fit and anchor onto the defected location. By applying these design concepts, a better fixation can be achieved by the scaffold, while facilitating better stress distribution in the interface between the surrounding tissue and the scaffold (Jazayeri et al. 2017; Giannitelli et al. 2015; Bártolo et al. 2012).

Several research works developed methodologies to control the topological architecture of scaffolds, aiming at obtaining better biological and mechanical properties and scaffold performance (Almeida et al. 2007a, b). As a result, several libraries and computational systems have been developed and applied for optimal scaffold design (Almeida and Bártolo 2008). This chapter gives an overview of mathematical design methodologies that have been applied to optimize scaffold design, namely, periodic-based geometric modeling approaches.

2 Mathematical-Based Scaffold Modeling

Most works on scaffold design for tissue engineering applications are either based on lattice structures with straight edges and sharp corners or in shapes obtained through Boolean operations with geometric primitives. Recently, hyperbolic surfaces, namely, triply periodic minimal surface (TPMS), have received increasing attention, as they enable the design of biomimetic scaffolds allowing the design of scaffolds with very high surface-to-area ratios, enhancing cell proliferation and cell-cell interactions, maximizing both porosity and mechanical performance (Qi and Wang 2009; Jung et al. 2007; Wang 2007; Gandy et al. 2001; Nesper and Leoni 2001; Hyde and Oguey 2000).

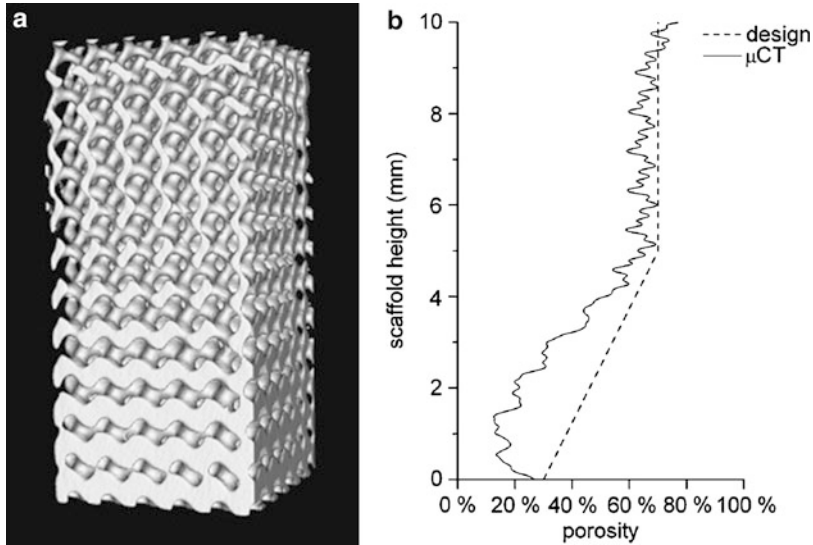


Fig. 1 Built PDLLA scaffold with gyroid architecture showing a gradient in porosity and pore size. (a): μ CT visualization. (b): Change in the average porosity with scaffold height (solid line) in comparison with the designed porosity (dotted line) (Melchels et al. 2010b)

Rajagopalan and Robb (2006) obtained results in the first effort regarding computer-controlled fabrication, modulation, and mechanical characterization of tissue engineering scaffolds based on TPMS. They designed simple cube models of P-scaffolds and manufactured them with a layer-based fabrication device. They also presented novel strategies to realize coterminous seeding-feeding networks, thereby assuring blood/nutrient supply to the proliferating cells at close proximity with the proposed geometries. The work provided insights on the reason behind the natural choice of TPMS forms in biological systems, by performing uniaxial and bulk compressive simulation using the finite element code.

Melchels et al. (2010b) used the K3DSurf software to generate scaffolds based on gyroid (G) and diamond (D) architectures. The gradient in pore size and porosity of the gyroid structure was introduced by adding a linear term to the equation for z-values (Fig. 1). They also demonstrated that, in the gyroid architectures, stress and strain are much more homogeneously distributed throughout the structure than for regular cubic architectures. A tissue engineering scaffold with gyroid architecture will expose adhering cells to a more equal mechanical stimuli throughout the structure. As cells respond to the deformation of the matrix to which they adhere (Bao and Suresh 2003), these structures present optimum mechanobiological stimulation.

Melchels et al. (2010a) assessed the influence of scaffold pore architecture on cell seeding and static culturing, by comparing a computer-designed gyroid architecture fabricated by stereolithography with a random pore architecture resulting from salt leaching. The scaffold structures showed comparable porosity and pore size values,

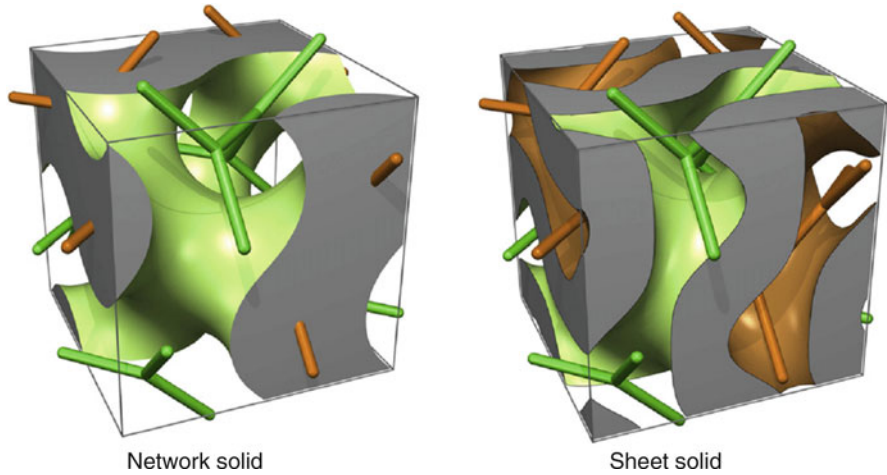


Fig. 2 Scaffold designs of 50% volume fraction derived from the gyroid minimal surface. *Left:* Network solid architecture. The minimal surface partitions space into two interwoven domains. One is filled with an isotropic elastic material, the other is left empty (void domain). *Right:* Sheet solid architecture: The solid domain is given by a sheet of thickness r , folded onto the gyroid minimal surface. The value of r is adjusted to yield a volume fraction of 50% (Kapfer et al. 2011)

but the gyroid type showed a 10-fold higher permeability, due to the absence of size-limiting pore interconnections. The results also demonstrated that it is possible to control the cell seeding upon the scaffold with the geometric gyroid variation within the scaffold.

Yoo (2011a) presented a computer-aided porous scaffold design method based on TPMS. In this work, Yoo proposed a novel method for extracting surface and solid models directly from the approximated implicit surfaces for TPMS, based on the periodic surface model. The TPMS were described with periodic surfaces, composed of simple trigonometric functions, thus enabling easy generation of TPMS for use in various mechanical, chemical, and physical applications. A new control approach for pore size distribution was also presented, based on the pore-making element composed of TPMS, and conformal refinement of all hexahedral mesh, showing the practical applicability of the newly suggested modeling approach. The proposed modeling method was successfully validated through many designs of bone scaffold models.

Kapfer et al. (2011) observed that two types of scaffold architectures can be generated using TPMS-based unit cell libraries (Fig. 2). In this work, two types of solids based on minimal surface network solids and minimal surface sheet solids were designed. They showed that, for the same solid volume fraction, sheet solids have a substantially higher effective bulk modulus and direction-averaged Young's modulus than network solids, for a wide range of volume fractions and material parameters. The sheet solids also present a larger surface area for cell adhesion and proliferation.

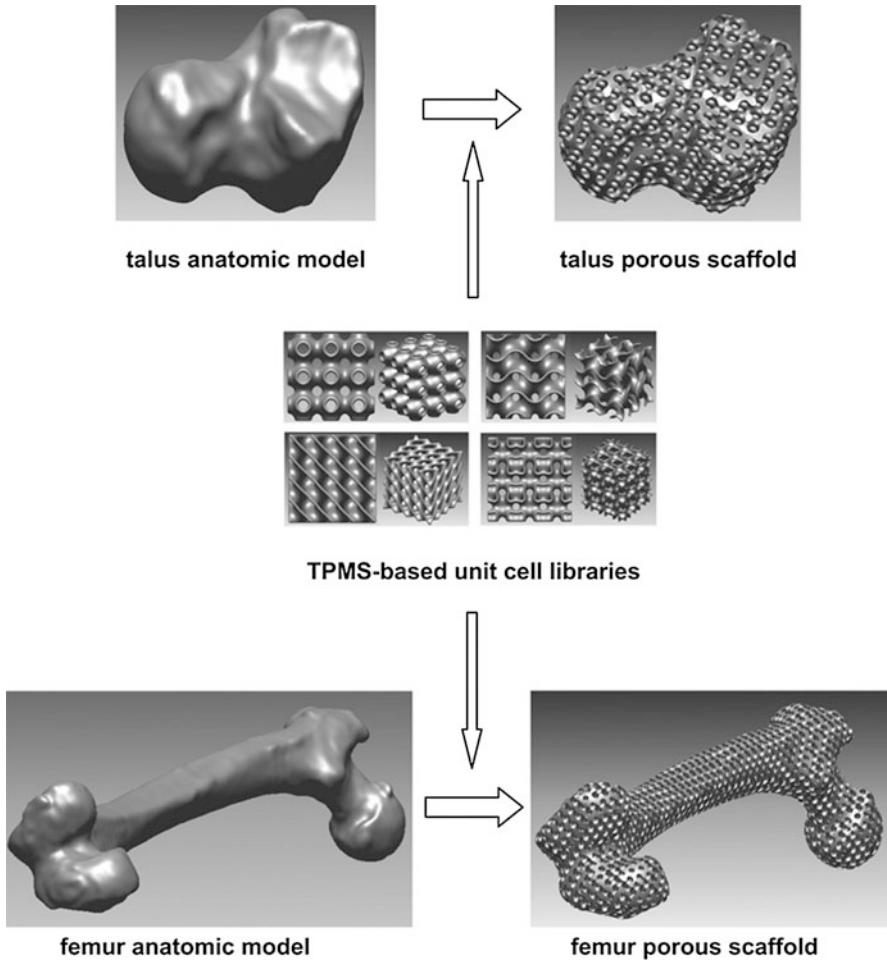


Fig. 3 Porous scaffolds designed with intricate internal architectures and high-quality external surfaces (Yoo 2011b)

Yoo (2011b) proposed an effective method for the design of 3D porous scaffolds, based on a hybrid method of distance field and TPMS. By the creative application of a traditional distance field algorithm into the Boolean operations of the anatomical model and TPMS-based unit cell library, an almost defects' free porous scaffolds with a complicated microstructure and high-quality external surface, faithful to a specific anatomic model, can be easily obtained without difficult and time-consuming trimming and re-meshing processes. Figure 3 illustrates the Boolean operations between the anatomic models and TPMS-based unit cell libraries.

Yoo (2012a) proposed a heterogeneous porous scaffold design scheme, which is a direct extension of the control approach for pore size distribution in a previous work (Yoo 2011a). In this work, he proposes a novel heterogeneous modeling

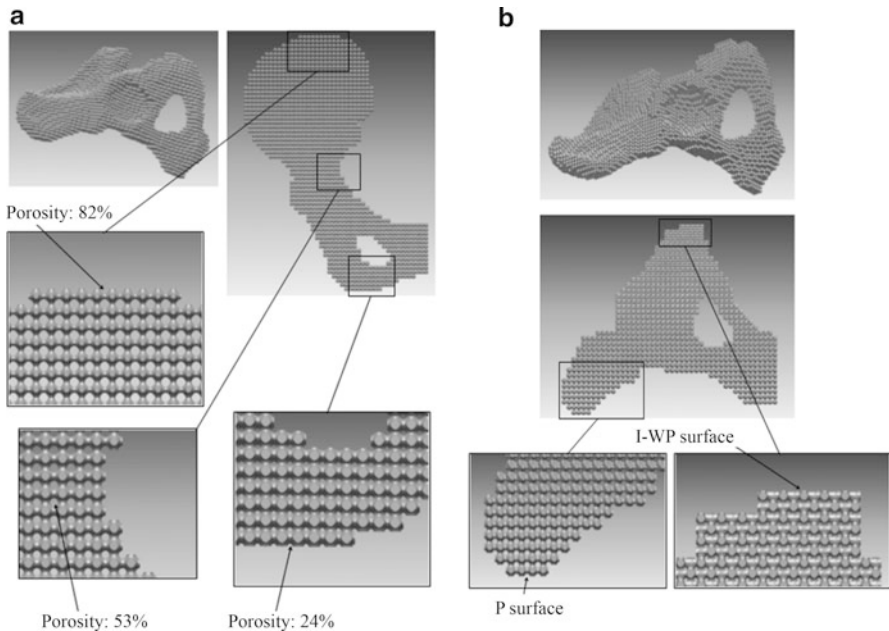


Fig. 4 (a) Heterogeneous iliac scaffold design with controlled porosity. (b) Heterogeneous iliac scaffold design with controlled internal architectures (Yoo 2012a)

methodology for designing tissue engineering scaffolds, with precisely controlled porosity and internal architectures using TPMS. The major contribution of this work was to extend the range of heterogeneity, from the porosity only, to the combination of porosity and internal architecture type. In addition, by introducing a fourth scalar value at the nodes of eight-node hexahedral element related to the porosity and internal architecture type, he could determine the internal architecture type and porosity at the spatial locations, uniquely and continuously within arbitrary and complex 3D anatomical shapes. Another advantage of the proposed method is the possibility to control the pore size distribution without changing the size of hexahedral element, while maintaining perfectly interconnected pore networks. Figure 4 illustrates a heterogeneous iliac scaffold design showing either a controlled porosity or internal architecture.

Yoo (2012b) presented a general design framework for 3D internal scaffold architectures to match desired mechanical properties and porosity simultaneously, by introducing an implicit interpolation algorithm based on the radial basis function (RBF) (Fig. 5). Similarly to his previous work, the work focused on the computational heterogeneous tissue engineering scaffold design. While using all the strategies developed in previous works, such as Boolean operations based on the distance field and internal architecture construction using the TPMS-based unit cell libraries, special emphasis was given to an automated porosity distribution control algorithm based on the RBF. With the developed computer program, he demonstrated that the

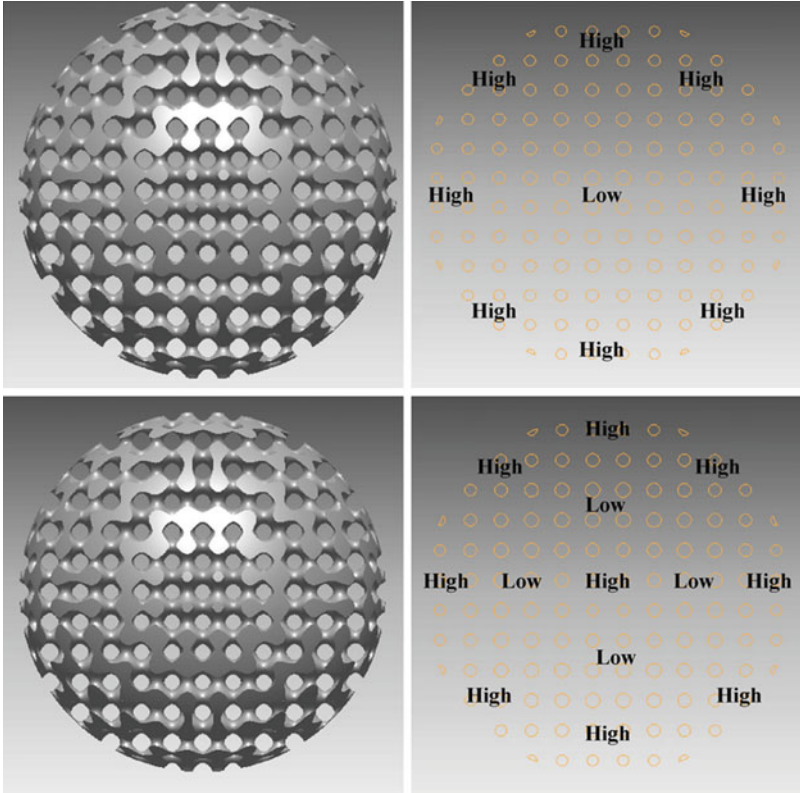


Fig. 5 Heterogeneous sphere-shaped scaffolds having P-surface internal architectures with various gradients in porosity in the radial direction (Adapted from Yoo 2012b)

method can produce highly porous and heterogeneous structures matching the required anisotropic stiffness, using a set of porosity levels defined at some points selected by the user. In a later work, Yoo (2013) developed a hybrid method which combines radial basis functions with the TPMS transformation strategy. Experimental results show that the proposed scaffold design method is capable of controlling the internal pore architectures within an arbitrarily shaped scaffold while preserving the advantages of the distance field and TPMS-based pore architectures as illustrated in Fig. 6.

Yoo (2014) developed another design concept of multi-void TPMS-based scaffolds that increase the surface area to volume ratios of conventional TPMS scaffolds. Yoo suggests that the proposed novel design methodology can be applied to create a variety of design models for biomimetic scaffolds and bioartificial tissues. Figure 7 illustrates the multi-void design algorithm that was implemented for the scaffold design.

Dinis et al. (2014) developed an open source software tool for the design of scaffolds (Fig. 8). With the aid of the developed software and its geometric database

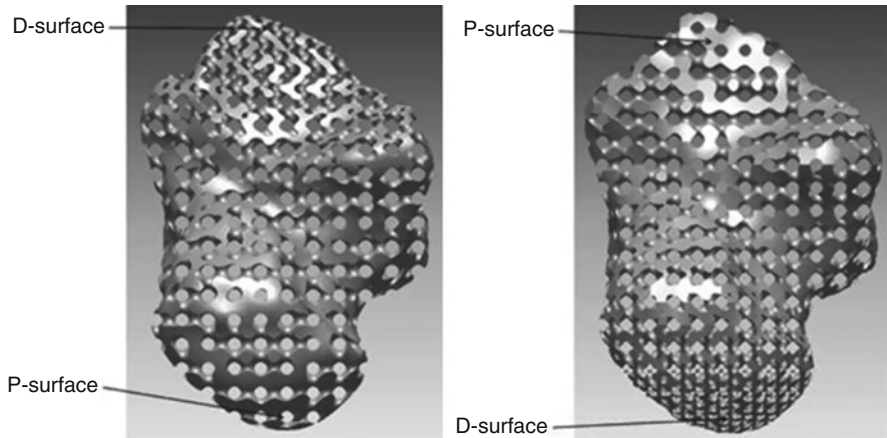


Fig. 6 Heterogeneous talus bone porous scaffolds with continuous gradients in pore architectures between D-surface and P-surface (Adapted from Yoo 2013)

based on TPMS, different highly complex geometric models with different levels of porosity and permeability can be obtained. Based on the results, it is possible to observe that with the same construction parameters, the Neovius present the highest levels of porosity followed by the Gyroid, Schwartz_P, Schwartz_D, and (IWP) respectively.

3 Triply Periodic Minimal Surfaces

3.1 Definition

In the 1880s, Schwarz described the first periodic minimal surface (Dinis et al. 2014). A minimal surface is a surface that is locally area minimizing, in other words, a small piece presents the smallest possible area of a surface spanning the boundary of that same piece. The surfaces were generated using symmetry arguments: given a solution to a Plateau's problem for a polygon, and the reflections of the surface across the boundary lines also produce valid minimal surfaces that can be continuously joined to the original solution (Dinis et al. 2014; Karcher and Polthier 2014). Among the various hyperbolic surfaces, the minimal surfaces are the most studied. If a minimal surface presents a space group symmetry, it is both infinite and periodic in three independent directions; therefore, it is called triply periodic minimal surface (TPMS). Another geometric characteristic of TPMS is that they present a mean curvature of zero. Examples of TPMS are illustrated in Fig. 9 (Kapfer et al. 2011).

Triply periodic minimal surfaces are also considered biomimetic surfaces as they commonly exist in natural structures, such as lyotropic liquid crystals, zeolite sodalite crystal structures, diblock polymers, hyperbolic membranes (prolamellar structure of chloroplasts in plants), echinoderm plates (interface between the

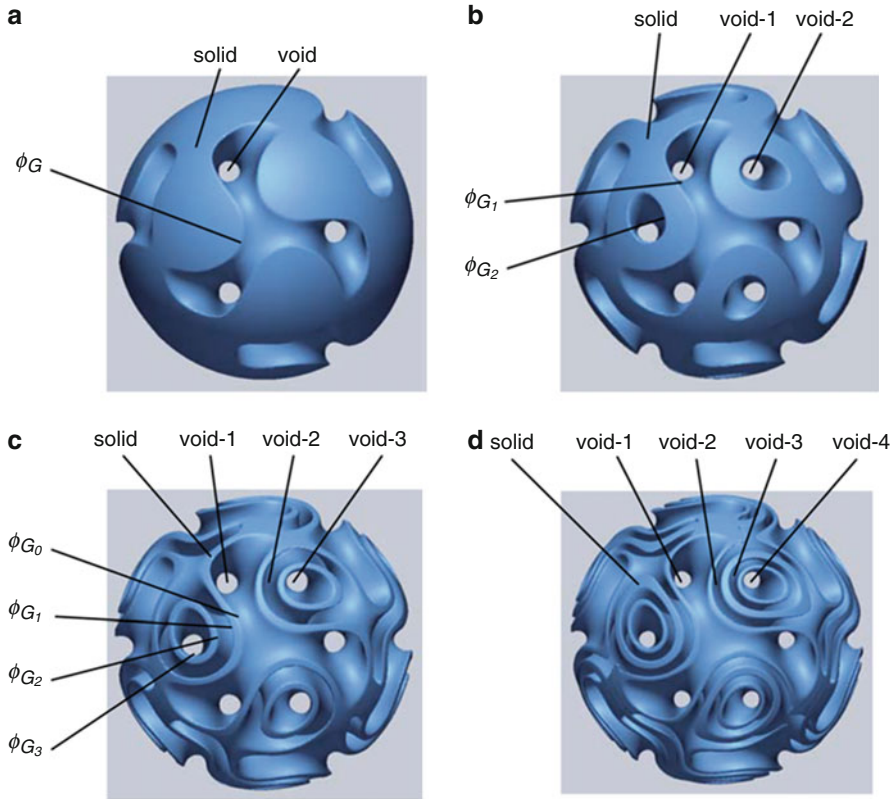


Fig. 7 A sphere-shaped scaffold model with: (a) 1 void, (b) 2 voids, (c) 3 voids, and (d) 4 voids (Yoo 2014)

inorganic crystalline and organic amorphous matter in the skeleton), cubosomes and certain cell membranes (Dinis et al. 2014; Karcher and Polthier 2014; Almeida and Bártolo 2012a, b; Larsson et al. 2003; Sun and Lal 2002; Hyde 1996; Andersson 1983; Scriven 1976).

3.2 Periodic Surface Modeling

A periodic surface can be defined by the following mathematical model (Wang 2007; Rajagopalan and Robb 2006; Lord and Mackay 2003; Andersson et al. 1988):

$$\varphi(r) = \sum_{k=1}^K M_k \cos [2\pi (\mathbf{L}_k \cdot r) / \beta_k + P s_k] = C \quad (1)$$

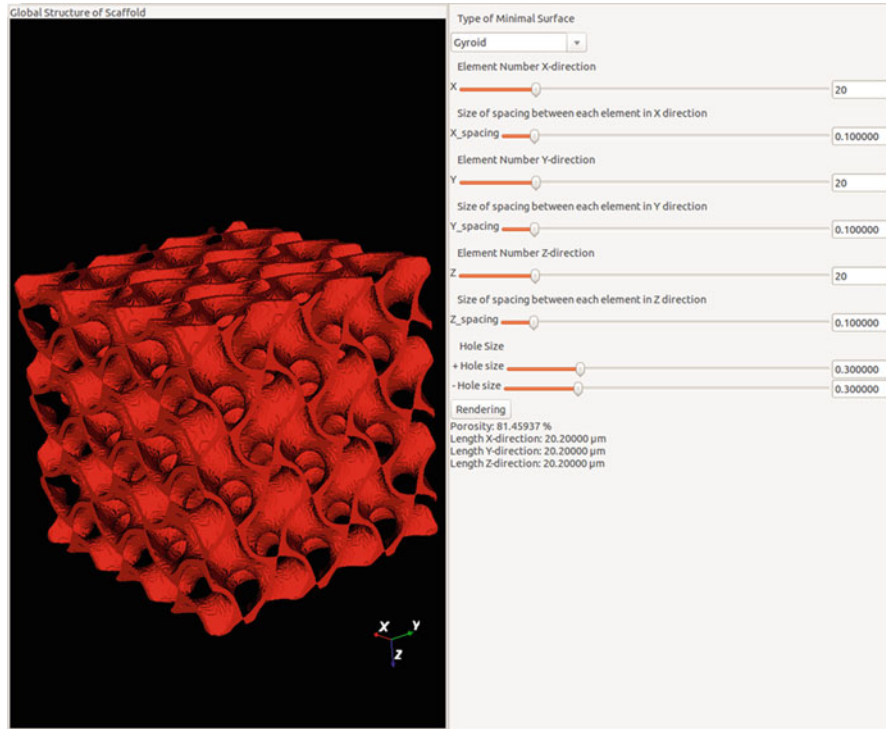


Fig. 8 Example of the “interface scaffold” developed in Python (Dinis et al. 2014)

where r is the location vector in the Euclidean space, L_k is the k lattice vector in the reciprocal space, M_k is the magnitude factor, β_k is the wavelength of periods, Ps_k is the phase shift, and C is a constant (Wang 2007; Rajagopalan and Robb 2006; Lord and Mackay 2003; Andersson et al. 1988).

In the TPM case, the Weierstrass formula can be used to describe these surfaces in a parametric way (Wang 2007; Rajagopalan and Robb 2006; Lord and Mackay 2003; Andersson et al. 1988):

$$\begin{cases} x = \text{Re} \int_{\omega_0}^{\omega^1} e^{i\theta} (1 - \omega^2) R(\omega) d\omega \\ y = \text{Im} \int_{\omega_0}^{\omega^1} e^{i\theta} (1 + \omega^2) R(\omega) d\omega \\ z = -\text{Re} \int_{\omega_0}^{\omega^1} e^{i\theta} (2\omega^2) R(\omega) d\omega \end{cases} \quad (2)$$

where ω is a complex variable, θ is the so-called Bonnet angle, and $R(\omega)$, Re , and Im are geometric functions varying for different surfaces.

Within the several TPMS models, only the Schwarz Primitive and Schoen I-WP surfaces were considered in this research work (Fig. 10).

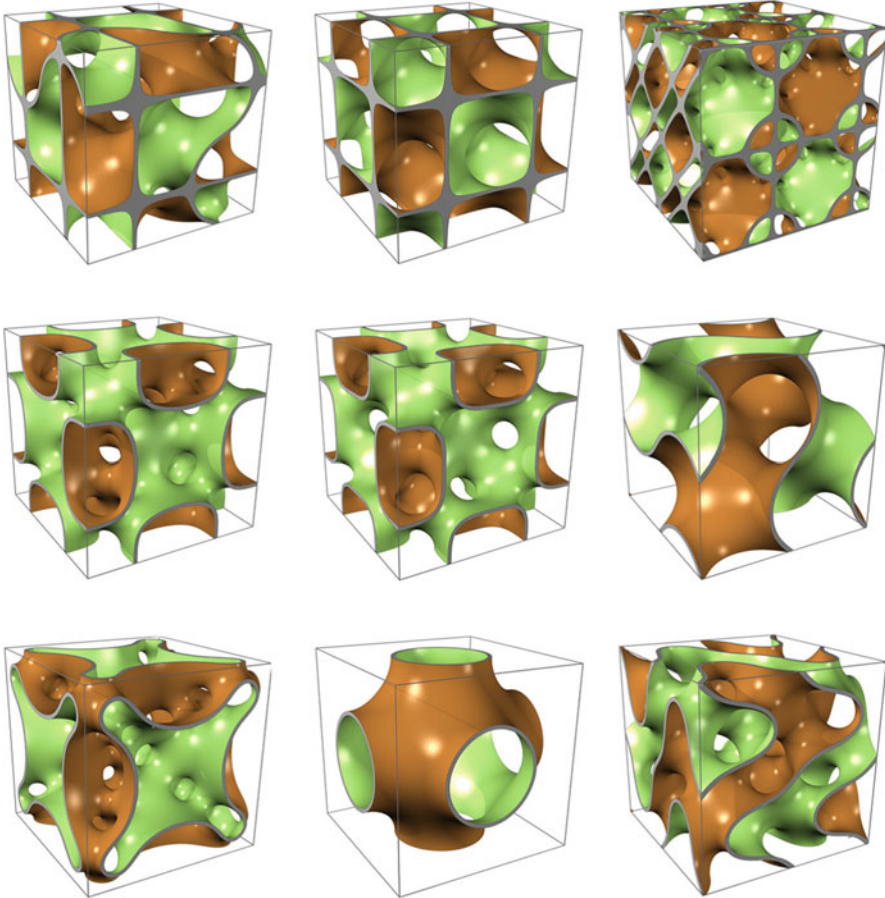


Fig. 9 Various examples of triply periodic minimal surfaces. From *top left* to *bottom right*, translational unit cells of Fischer Koch Y, Diamond, Disphenoid, Batwing, F-RD, Gyroid, Manta, Schwartz, and Fischer Koch S (Kapfer et al. 2011)

3.3 Schwarz TPMS Primitives

A periodic Schwarz Primitive surface can be mathematically described by the following nodal approximation (Wang 2007; Rajagopalan and Robb 2006; Lord and Mackay 2003; Andersson et al. 1988):

$$\phi(r) = M_p \left[\cos(2\pi x/\beta_x) + \cos(2\pi y/\beta_y) + \cos(2\pi z/\beta_z) \right] \quad (3)$$

Since the previous equation only defines the surface model, the solid geometric modeling of the Schwarz units was obtained using a commercially available CAD software (*Solidworks* from *Dassault Systemes*, www.3ds.com) through offset and thickening operations in order to obtain solid models for production and simulation. Through these operations, the solid geometric modeling enabled to define two

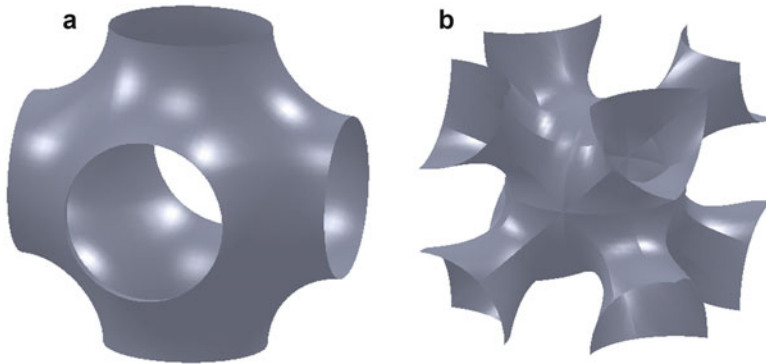


Fig. 10 (a) Schwarz' Primitive and (b) Schoen I-WP surfaces

important geometric modeling constraint parameters, namely, thickness and radius. Based on these two geometric modeling parameters, two sub-models were defined as follows:

- Thickness variations (the obtained models varied their geometric thickness while maintaining the same geometric radius as illustrated in Fig. 11a and similarly in Fig. 12a)
- Radius variations (the obtained models varied their geometric radius while maintaining the same geometric thickness as illustrated in Fig. 11b and similarly in Fig. 12b).

The variation of these geometric parameters enables changes to the architectural topology of each basic unit of a scaffold, varying its porosity and mechanical and vascular behavior (Fig. 11).

3.4 Schoen TPMS Primitives

The mathematical description of a Schoen's I-WP surface is given by the following nodal approximation (Wang 2007; Rajagopalan and Robb 2006; Lord and Mackay 2003; Andersson et al. 1988):

$$\varphi(r) = M_1 \begin{bmatrix} 2 \cos(2\pi x/\beta_x) \cos(2\pi y/\beta_y) + 2 \cos(2\pi y/\beta_y) \cos(2\pi z/\beta_z) \\ 2 \cos(2\pi z/\beta_z) \cos(2\pi x/\beta_x) \\ - \cos(4\pi x/\beta_x) - \cos(4\pi y/\beta_y) + \cos(4\pi z/\beta_z) \end{bmatrix} \quad (4)$$

Similarly to the Schwarz Primitive solid modeling, the solid Schoen units were obtained through the same design offset and thickening operations. By varying the thickness (Fig. 12a) and radius (Fig. 12b) values, different solid geometric models can be obtained as illustrated in Fig. 12.

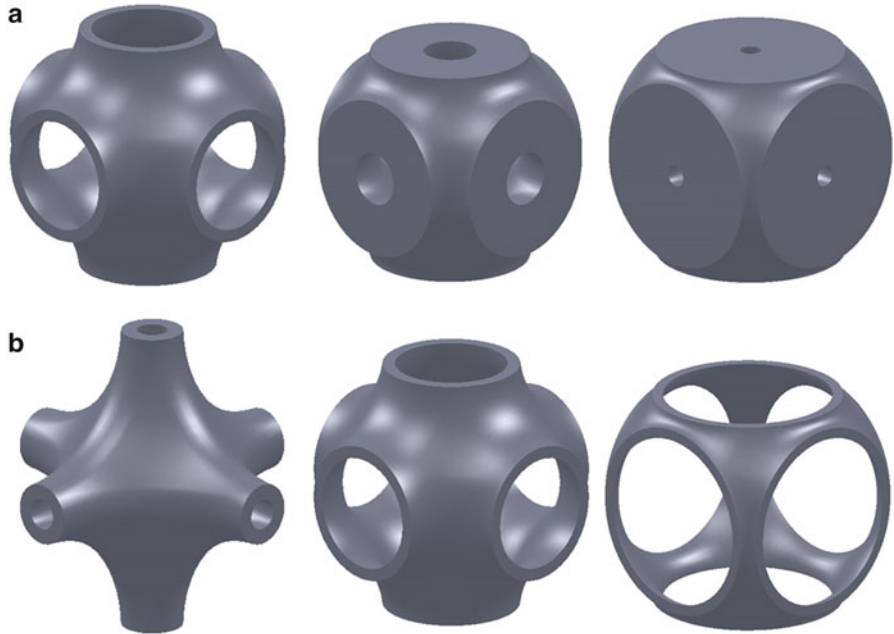


Fig. 11 Schwarz' Primitive surfaces obtained through (a) surface thickness variation with constant radius and (b) surface radius variation with constant thickness

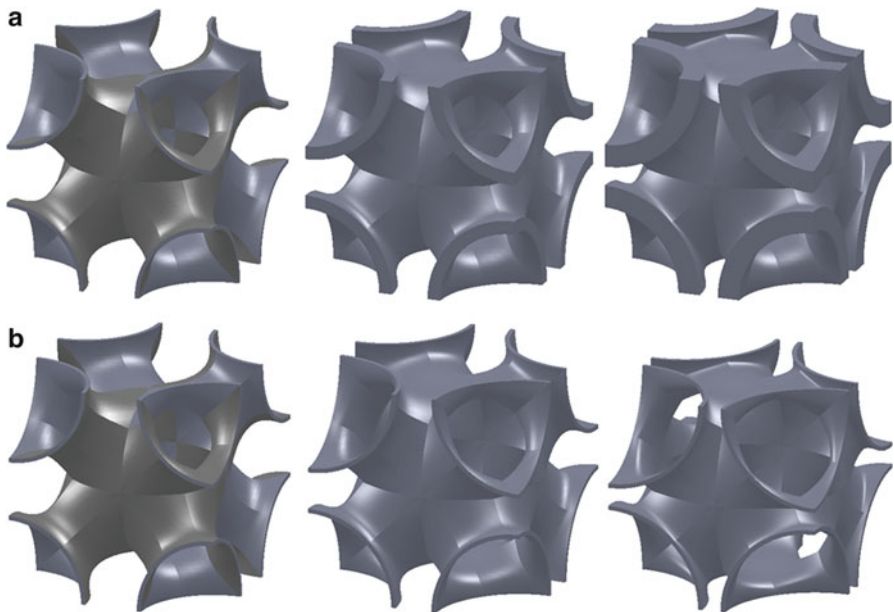


Fig. 12 Schoen's I-WP surfaces obtained through (a) surface thickness variation with constant radius and (b) surface radius variation with constant thickness

4 Numerical Implementation of the Designed Models

The main goal for simulating the scaffold mechanical behavior is to evaluate the porosity dependence on the elastic and shear modulus. The mechanical behavior of these structures is assessed through the finite element method (*Abaqus* from *Dassault Systemes*, www.3ds.com). For a given unit block with a specific open pore architecture, boundary and loading conditions considered for evaluating mechanical properties are shown in Fig. 13:

- For the numerical computation of the elastic modulus (Fig. 13a), a uniform displacement in a single direction is considered (in this case the X direction), which is equivalent to the strain in the same direction (ϵ_x), imposed to a face of the block (Face A). The displacement value is a percentage of displacement (Pd_x) equivalent to 0.1% of the unit's block length (L_x). The opposite face (Face B) of the scaffold unit is constrained and unable to have any displacement. The average reaction forces (Rf_x) produced on Face B of area (A_x) are used to determine the elastic modulus (E) (eq. 5) due to the imposed displacement.
- For the numerical computation of the shear modulus (Fig. 13b), a uniform displacement in a single direction is considered (in this case the Y direction), which is equivalent to the strain in the same direction (γ_{xy}), imposed to a face of the block (Face B). The displacement value is a percentage of displacement (Pd_y) equivalent to 0.1% of the unit's block length (L_y). The opposite face (Face A) of the scaffold unit is constrained and unable to have any displacement. The two lateral faces (Faces C) are also constrained and unable to have any displacement in the X direction. The average reaction forces (Rf_y) produced on Face A of area (A_y) is used to determine the shear modulus (G) (Eq. 6) due to the imposed displacement.

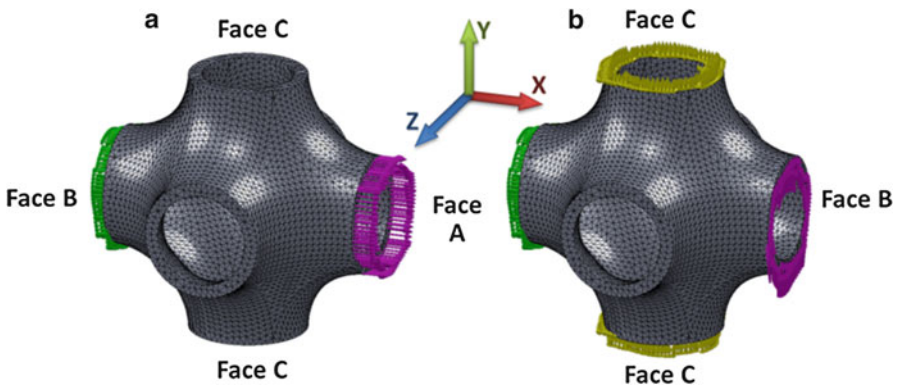


Fig. 13 Loads and constraints for the numerical analysis of scaffolds under a (a) tensile solicitation and (b) shear solicitation

$$E_{xx} = \frac{\sigma_x}{\epsilon_x} = \frac{\frac{Rf_x}{Pd_x \times L_x} \frac{A_x}{L_x}}{\frac{A_x}{Pd_x}} = Rf_x \quad (5)$$

$$G_{xy} = \frac{\tau_{xy}}{\gamma_{xy}} = \frac{\frac{Rf_x}{Pd_x \times L_y} \frac{A_y}{L_y}}{\frac{A_y}{Pd_x}} = \frac{Rf_x}{Pd_x \times A_y} \quad (6)$$

The material considered for simulation purposes is Poly(ϵ -caprolactone) (PCL), a semicrystalline biodegradable polymer with a melting point of $\sim 60^\circ\text{C}$ and a glass transition temperature $\sim -60^\circ\text{C}$. The elastic modulus (E_0), shear modulus (G_0), and Poisson's ratio of the PCL material considered in the numerical simulations were 400 MPa, 150.38 MPa, and 0.33, respectively (Almeida and Bártolo 2013).

The results will be displayed in function of the scaffold's tensile stress ratio (E/E_0) and the scaffold's shear stress ratio (G/G_0). The scaffold's tensile stress ratio (E/E_0) is determined between the scaffold's tensile modulus (E) obtained from the numerical simulations and the material's tensile reference modulus (E_0). Similarly, the scaffold's shear stress ratio (G/G_0) is determined between the scaffold's shear modulus (G) obtained from the numerical simulations and the material's tensile reference modulus (G_0). Figures 14, 15, 16, 18, and 19 contain two charts with two data curves each, whereas each data curve corresponds to either the Schwarz Primitive or the Schoen I-WP surfaces. Accompanying each data curve, there are two figures associated with the type of corresponding TPMS and its geometric variation.

The variation of the scaffold's porosity as a function of surface thickness and surface radius for both Schwarz' Primitives and Schoen's I-WP surfaces are presented in Fig. 14. Results show that the porosity decreases with the increasing of surface thickness (Figs. 14a).

Regarding the surface radius for the Schwarz Primitive surfaces, it is possible to observe its effect on the porosity (Fig. 14b). The porosity tends to decrease with increasing surface radius till a threshold value, from which it starts to increase. In this case, the relationship between porosity and surface radius has a hyperbolic behavior. In the case of the Schoen I-WP surfaces, the effect of changing the surface radius, as illustrated in Fig. 14b, shows that the porosity increases with increasing surface radius.

4.1 Elastic Modulus Evaluation

The variation of the elastic modulus as a function of surface thickness and surface radius for both Schwarz' Primitives and Schoen's I-WP surfaces are presented in Fig. 15. Results show that the elastic modulus tends to increase with the increase of

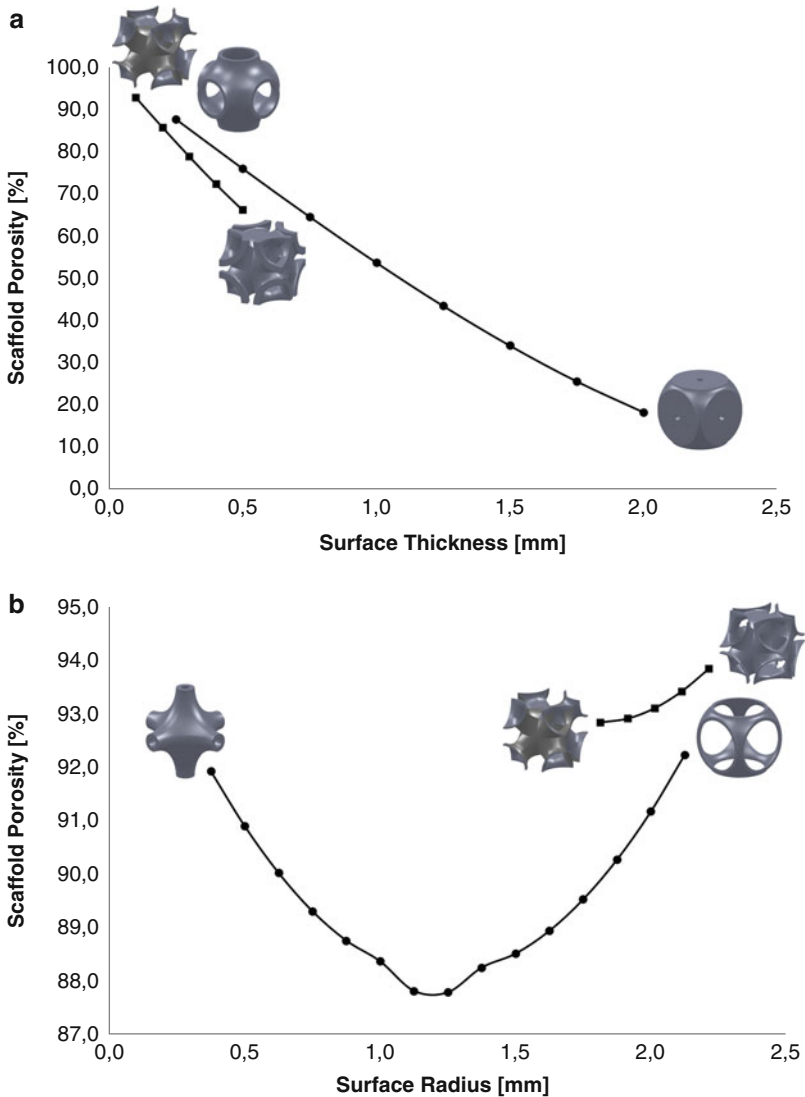


Fig. 14 Variation of the scaffold’s porosity with the (a) surface thickness and (b) surface radius for both geometries

surface thickness, for both geometric surfaces (Fig. 15a). Regarding the influence of the surface radius in both TPMS models, as the surface radius increases, the elastic modulus tends to decrease in a nonlinear way, as illustrated in Fig. 15b).

Figure 16 illustrates the variation of the elastic modulus of both TPMS models based on the variation of the surface thickness (Fig. 16a) and surface radius (Fig. 16b).

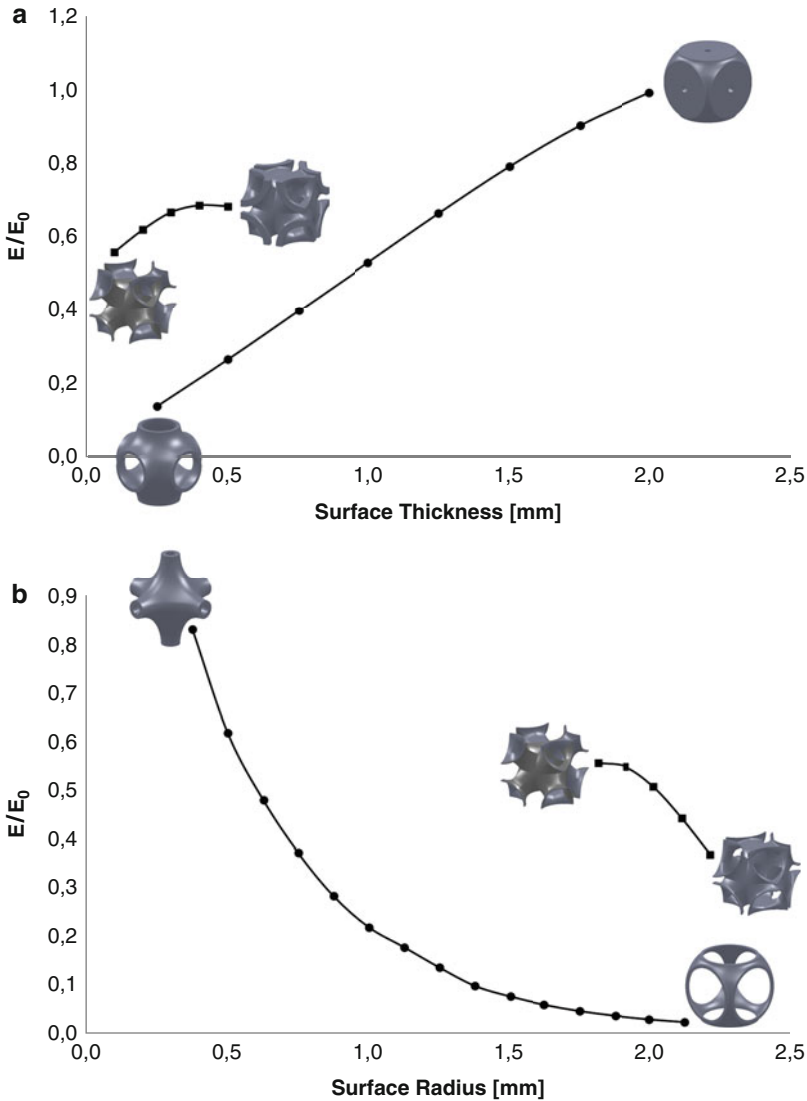


Fig. 15 Variation of the scaffold’s elastic modulus with the (a) surface thickness and (b) surface radius for both geometries

Regarding the thickness variation, both models present an almost linear dependence between the scaffold’s porosity and the elastic modulus. In both TPMS models, the elastic modulus decreases with the increasing surface thickness (Fig. 16a).

Regarding the surface radius, a similar hyperbolic behavior was observed for the Schwarz Primitive surfaces between the elastic modulus and porosity (Fig. 16b), so

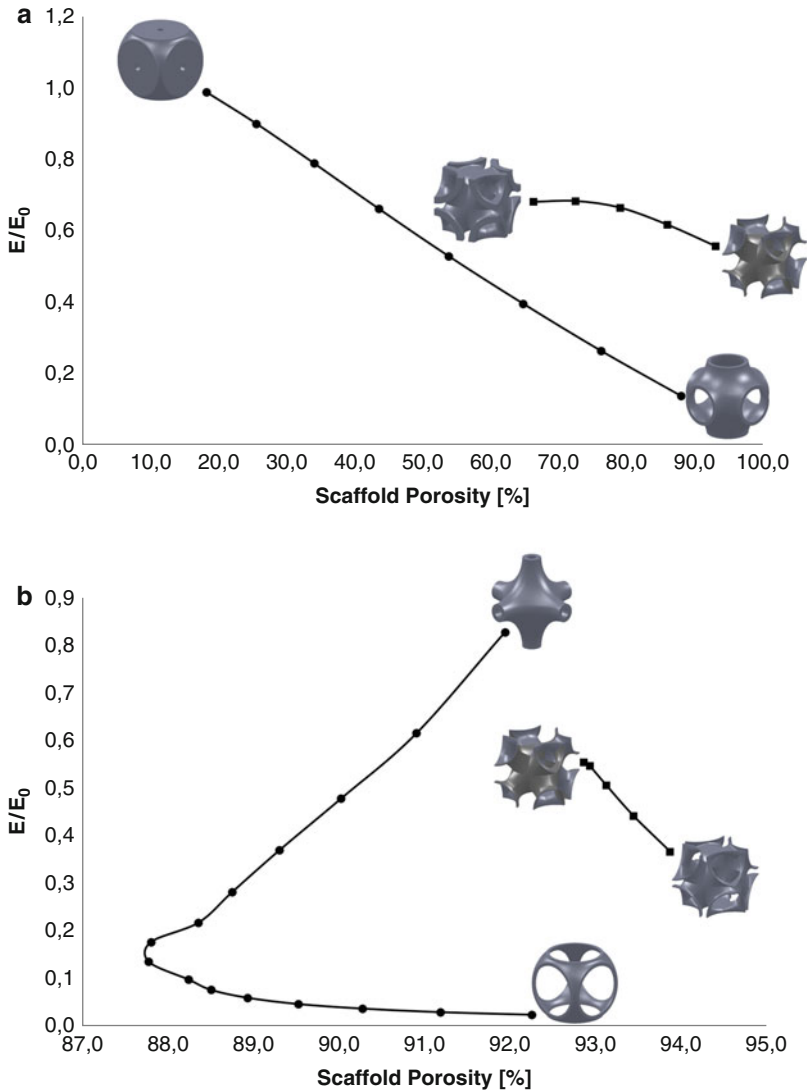


Fig. 16 Variation of the scaffold’s elastic modulus as a function of porosity with the (a) surface thickness and (b) surface radius for both geometries

we may decrease or increase the elastic modulus of the scaffold while maintaining high porosity values, which offers great flexibility regarding scaffold design. High porosity is critical for vascularization and tissue ingrowth. In the case of Schoen’s I-WP surfaces, the elastic modulus tends to increase with the increase of porosity (Fig. 16b).

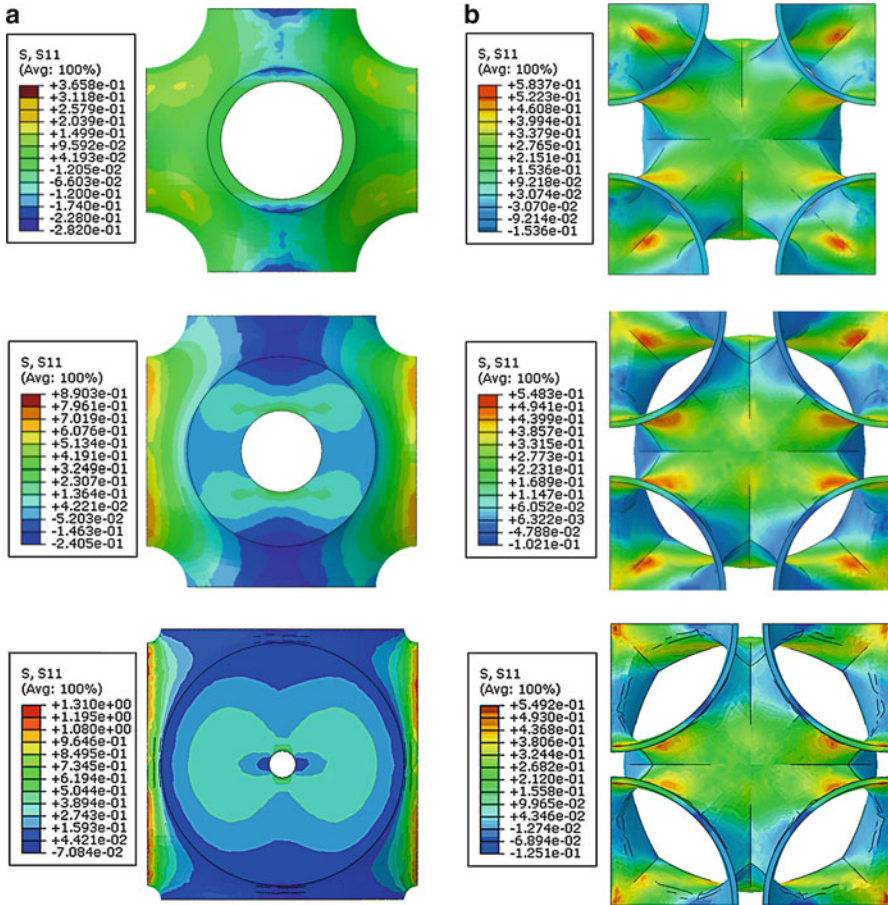


Fig. 17 Variation of the scaffold's tensile stress for (a) Schwarz' Primitive surface with surface thickness and (b) Schoen's I-WP surface with surface radius

Figures 15 and 16 illustrate the scaffold's basic unit mechanical behavior on a macroscale level regarding geometric parameters, such as radius and thickness, for both Schwarz' Primitive and Schoen's I-WP surfaces. Figure 17 illustrates the tensile stress variation of the scaffold on a microscale level, considering the variation of both the thickness (Fig. 17a) for the Schwarz Primitive geometry and the radius for the Schoen I-WP (Fig. 17b)).

Figure 17a shows that by increasing the thickness in the Schwarz Primitive geometries, the tensile stresses tend to assume lower values at the two lateral faces, resulting in an uneven tensile stress distribution. The scaffold presents a more homogenous tensile distribution for lower thickness values. Regarding the radius variation, there is no significant tensile stress variation with the radius increase.

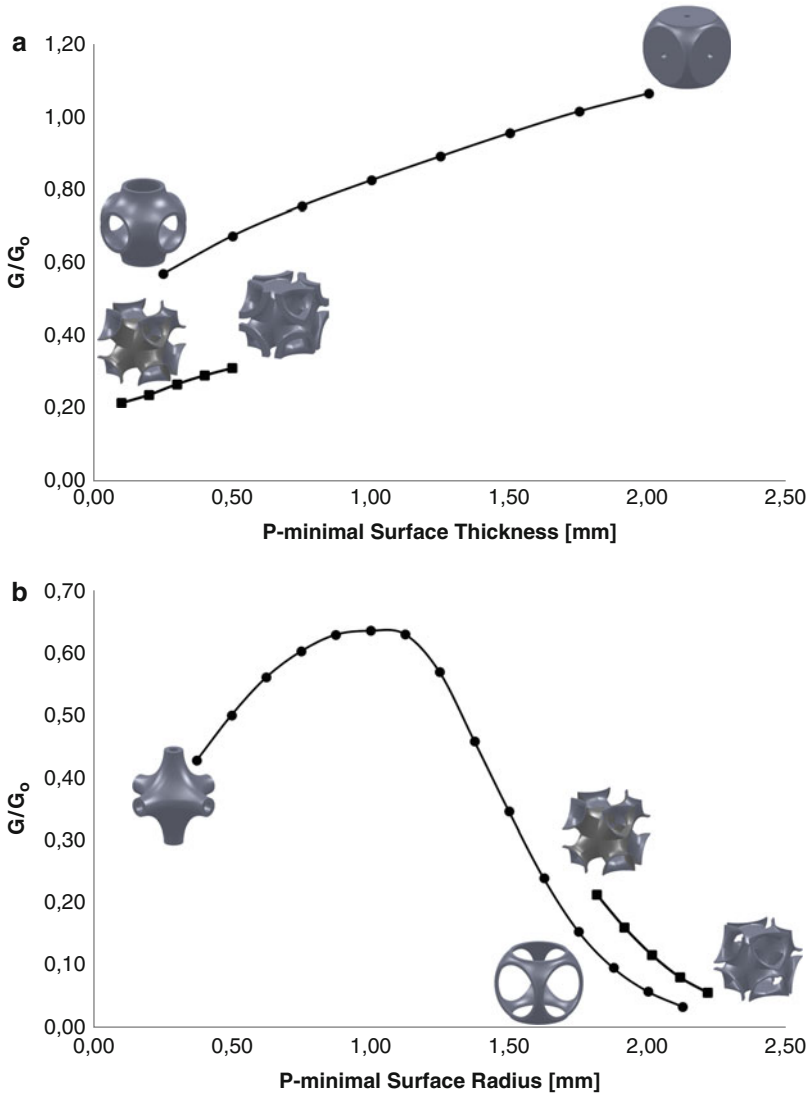


Fig. 18 Variation of the scaffold’s shear modulus with the (a) surface thickness and (b) surface radius for both geometries

A similar behavior is observed for the Schoen I-WP thickness variation. The Schoen geometries present a more homogenous tensile stress for lower thickness values. Regarding the radius variation (Fig. 17b), results show that, as the radius increases, a more differentiated tensile stress distribution is observed, namely, in the central sphere of the Schoen geometry. In this case, Schoen geometries with lower radius values present a more homogenous tensile distribution for cell differentiation and proliferation.

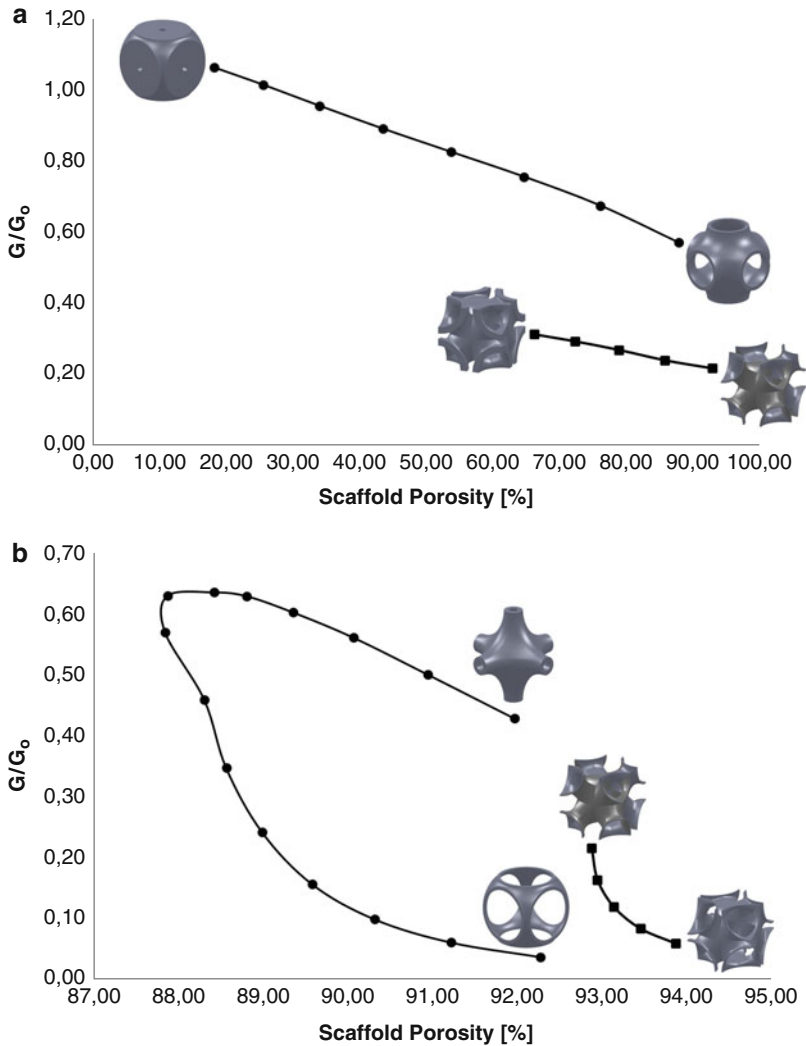


Fig. 19 Variation of the scaffold shear modulus as a function of porosity with the (a) surface thickness and (b) surface radius for both geometries

4.2 Shear Modulus Evaluation

Figure 18a shows that the shear modulus ratio increases with thickness. This figure also demonstrates that the Schwarz Primitive surface presents a higher shear modulus behavior compared to the material's reference shear modulus. In other words, the Schwarz Primitive surface increases the shear performance above reference for high thickness values. For the Schoen I-WP surface, Fig. 18a shows that the shear modulus ratio increases with thickness. Regarding the effect of the Schwarz

Primitive surface radius variations, Fig. 18b shows that the shear modulus ratio increases and then begins to decrease as the Schwarz Primitive surface radius increases. Regarding the Schoen I-WP surface, the shear modulus ratio decreases by increasing the surface radius (Fig. 18b).

A linear dependence between the scaffold porosity and the shear modulus ratio was obtained as observed in Fig. 19a. For the Schoen I-WP surface, Fig. 19a shows that the shear modulus ratio decreases with porosity. In spite of the porosity and the radius having a hyperbolic behavior, the shear modulus ratio with the Schwarz Primitive surface radius has a sinusoidal behavior, while the shear modulus ratio with the porosity has an approximated hyperbolic behavior (Fig. 19b). In this case, we may decrease or increase the shear modulus of the scaffold while maintaining high porosity values. Regarding the Schoen I-WP surface, the shear modulus ratio decreases by increasing the porosity (Fig. 19b).

Figures 18 and 19 illustrate the scaffold's basic unit mechanical behavior on a macroscale level regarding geometric parameters, such as radius and thickness, for both the Schwarz Primitive and Schoen I-WP surfaces. Figure 20 illustrates the shear stress variation of the scaffold on a microscale level, considering the variation of both the thickness (Fig. 20a) for the Schwarz Primitive geometry and the radius for the Schoen I-WP (Fig. 20b).

Figure 20a shows that by increasing the thickness in the Schwarz Primitive geometries, the shear stresses tend to assume lower values at the two lateral faces that present either no constraint or solicitation, resulting in an uneven shear stress distribution. The scaffold presents a more homogenous tensile distribution for lower thickness values. Regarding the radius variation, there is no significant shear stress variation with the radius increase.

A similar behavior is observed for the Schoen I-WP thickness variation. The Schoen I-WP geometries present a more homogenous shear stress for lower thickness values. Regarding the radius variation (Fig. 20b), results show that, as the radius increases, a more differentiated shear stress distribution is observed, namely, in the central sphere of the Schoen geometry. In this case, Schoen's I-WP geometries with higher radius values present a more homogenous shear distribution for cell differentiation and proliferation.

5 Design of a Functionally Gradient Scaffold Using TPMS Basic Units

Figure 21 illustrates the Boolean operations by the addition of the repeating units into an arbitrary unit with thickness variation, resulting in a scaffold with a thickness gradient. Figure 22 illustrates the production of both scaffolds in ABSPlus material through an extrusion-based additive manufacturing system, called the uPrint SE 3D Printer from Stratasys.

Structural simulations were performed on the combined model, including several the Schwarz Primitive and Schoen I-WP elementary scaffold units with a thickness gradient. A displacement solicitation along the direction of the thickness gradient

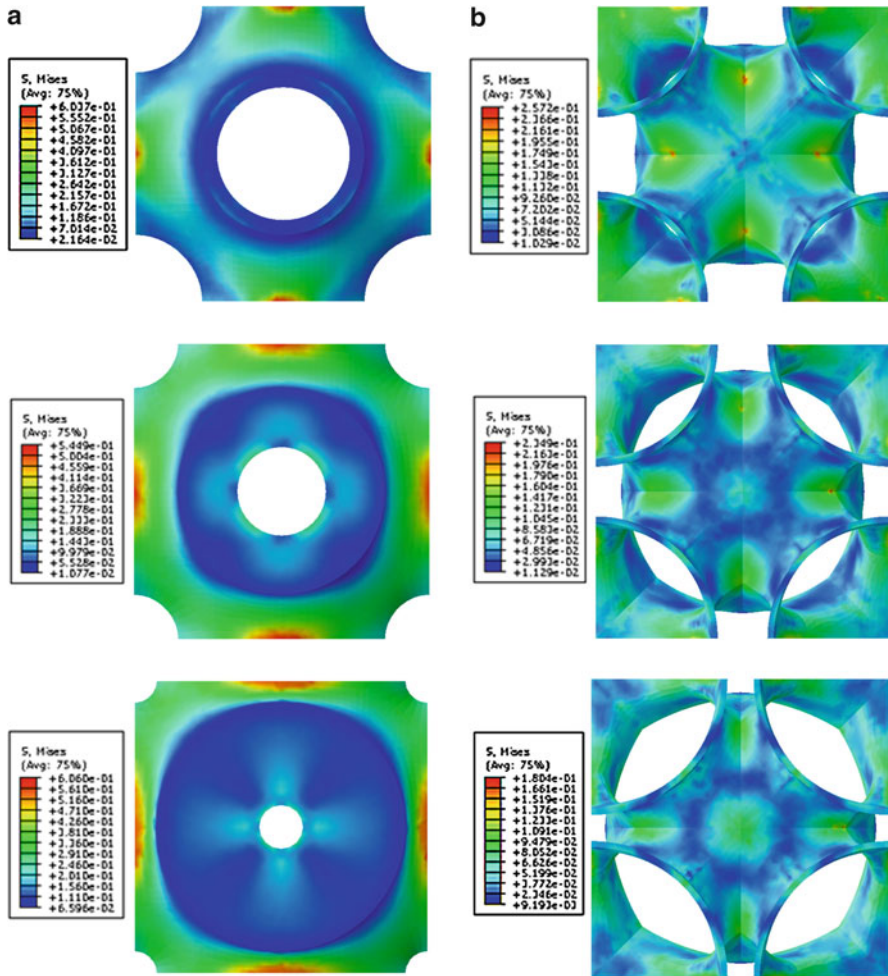


Fig. 20 Variation of the scaffold's shear stress for the (a) Schwarz Primitive surface with surface thickness and (b) Schoen I-WP surface with surface radius

was defined, in order to undergo the simulations. For both scaffold models, results show that as the thickness of the elementary units increase, the tensile variations tend to lower in value and become more homogenous, as illustrated in Fig. 23.

6 Conclusions

The design of optimized scaffolds for tissue engineering applications is a key topic of research, as the complex macro- and micro-architectures required for a scaffold depends on the mechanical and vascular properties and physical and molecular

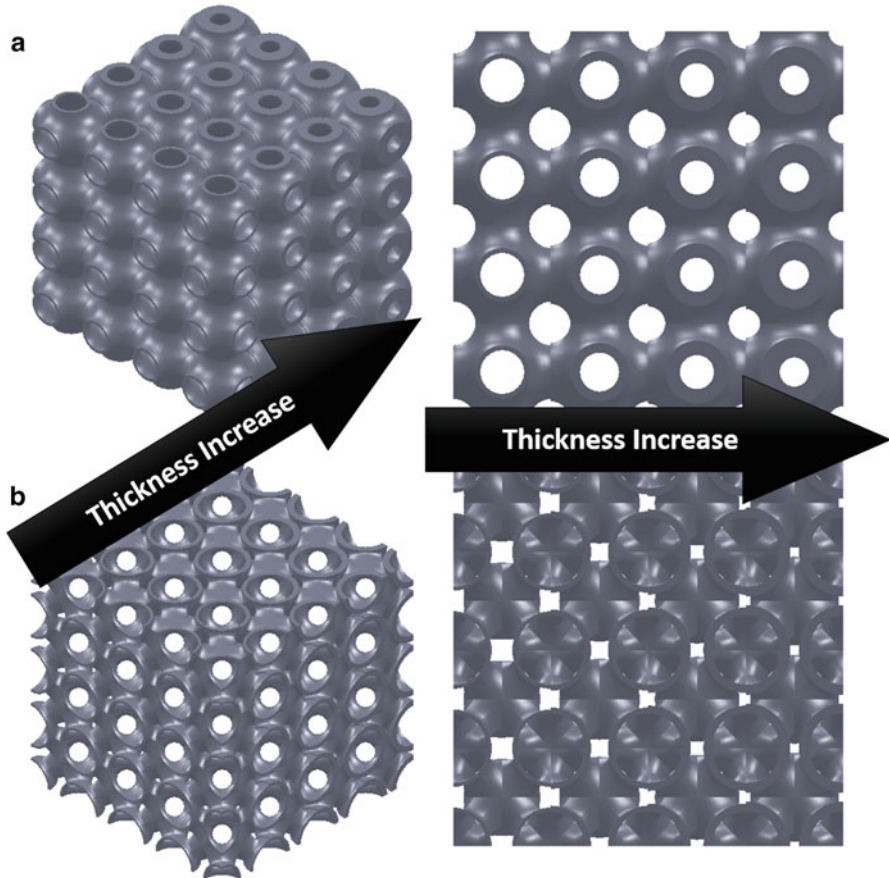


Fig. 21 CAD models illustrating thickness gradient within the scaffold structures for the (a) Schwarz Primitive and (b) Schoen I-WP geometries

queues of the surrounding tissue at the defect site. One way to achieve such hierarchical designs is to create a library of unit cells which can be assembled through a computational tool. Several scaffold design methodologies were presented. The initial designs contemplated regular geometric designs, either based on geometric designs (struts, spheres, beams, rods, etc.), medical images, or homogenization theories. Recently, periodic surface modeling was implemented into the scaffold design process, presenting higher mechanical, vascular, and biological performance in tissue engineering applications.

Understanding the mechanical properties of highly porous scaffolds, from the knowledge of its microstructure, is a topical research area in tissue engineering. In this work, porous scaffolds were designed, and its mechanical behavior was simulated using triply periodic minimal surfaces, namely, Schwarz and Schoen geometries. These geometries allow the design of highly porous structures with optimum mechanical and vascular properties.

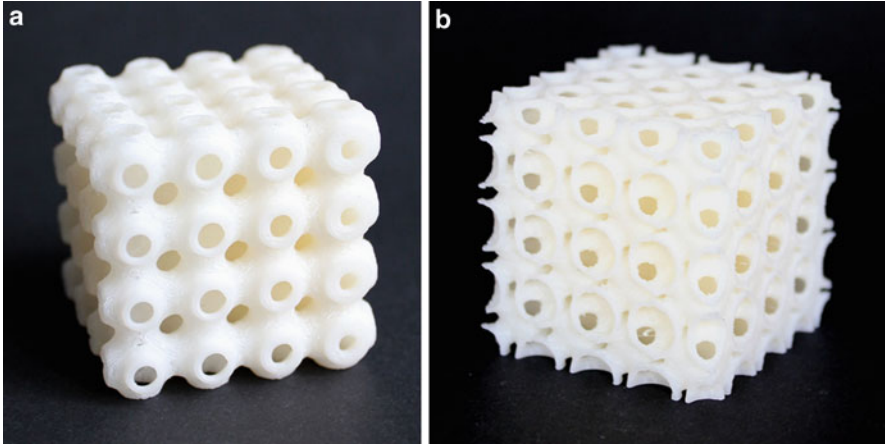


Fig. 22 Physical models of (a) the Schwarz Primitive and (b) Schoen I-WP geometries produced through extrusion-based additive manufacturing

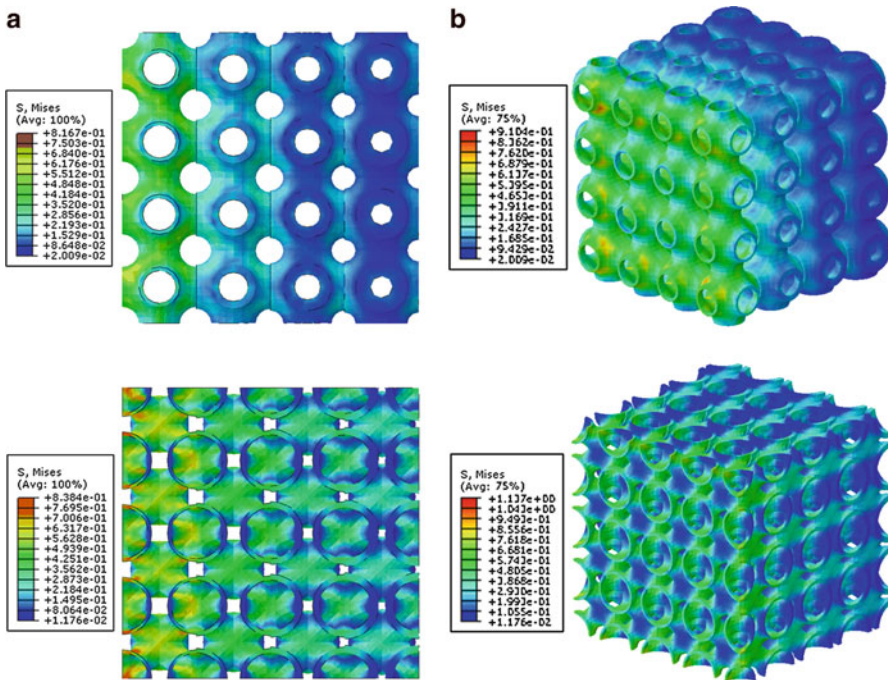


Fig. 23 Variation of the Tensile Stress along the thickness gradient for both scaffold structures for the (a) Schwarz Primitive and (b) Schoen I-WP geometries

Based on the tensile simulations, both geometries, results show that an increase in the surface thickness implies both a decrease in the porosity and improved mechanical performance. Nevertheless, as the thickness increases, and despite an

increase in the mechanical properties, the tensile stress distribution of the geometries becomes less homogenous inside the models.

Results also show that, for Schoen's I-WP surfaces, the increase of the surface radius increases the porosity and decreases the mechanical performance. The Schoen I-WP surfaces also have less optimum mechanical distributions as the radius increases. In the case of the Schwarz geometries, as the radius increases, the porosity tends to decrease until a certain threshold value, after which it starts to increase again (parabolic behavior). The mechanical performance decreases with the radius increase. A parabolic behavior is also observed for the mechanical performance, as a function of the porosity for the Schwarz geometries.

Based on the shear simulations, the Schwarz geometries, the results show that porosity decreases with the P-minimal surface thickness, decreasing also till a threshold value for the P-minimal surface radius. From this threshold value, the porosity then starts to increase. The shear modulus ratio increases with the P-minimal surface thickness and presents an approximated hyperbolic behavior by increasing the P-minimal surface radius.

Regarding the Schoen geometries, the results show that porosity decreases and the shear modulus ratio increases with the P-minimal surface thickness. On the other hand, the porosity increases and the shear modulus decreases with the P-minimal surface radius. In both cases, the shear modulus ratio decreases with the porosity.

When comparing both geometries, concerning the thickness variation, Schoen geometries present both lower values of porosity and lower values of shear modulus ratio. Regarding the radius variations, Schoen geometries present slightly higher porosity levels but still lower values of shear modulus ratio when compared to the Schwarz geometries. Schwarz geometries present a more versatile behavior, for one given porosity, you may have a structure with a lower or higher shear modulus, and they also present a higher range of values for both shear modulus ratio and porosity levels, when compared to Schoen geometries.

Minimal surfaces (surfaces of zero mean curvature or an average negative Gaussian curve) enable the design of smooth biomorphic constructs, providing an optimal biomechanical environment for cell attachment, migration, and proliferation, enabling optimization of the relationship between surface area, porosity, and mechanical properties. By using triply periodic surfaces in scaffold design for tissue engineering applications, it is possible to use highly porous structures with optimum mechanical properties. Several of the previous works performed by Yoo presented design schemes on how to developed bone scaffold implants, but by associating the mechanical behavior, it is possible to optimize the designs and produce bone scaffolds as a function of both geometric design and mechanical performance.

References

- Almeida, H.A. and Bártolo, P.J. (2008) computer simulation and optimisation of tissue engineering scaffolds: mechanical and vascular behaviour", 9th biennial ASME conference on engineering systems design and analysis (ESDA2008), Y. Halevi and A. Fischer (Eds.), ASME conference proceedings, Haifa Isreal.

- Almeida HA, Bártolo PJ (2012a) Chapter 12: Structural and vascular analysis of tissue engineering scaffolds: part 1 – numerical fluid analysis. In: Liebschner M, Kim D (eds) *Computer-aided tissue engineering*. Springer, London
- Almeida HA, Bártolo PJ (2012b) Chapter 13: Structural and vascular analysis of tissue engineering scaffolds: part 2 – topology optimization. In: Liebschner M, Kim D (eds) *computer-aided tissue engineering*. Springer, London
- Almeida HA, Bártolo PJ (2013) Numerical simulations of BioExtruded polymer scaffolds for tissue engineering applications. *Polym Int* 62(11):1544–1552
- Almeida HA, Bártolo PJ, Ferreira J (2007a) Mechanical behaviour and vascularisation analysis of tissue engineering scaffolds. In: Bártolo PJ et al (eds) *Virtual and rapid manufacturing – Advanced research in virtual and rapid prototyping*. Taylor & Francis, London, pp 73–80
- Almeida HA, Bártolo PJ, Ferreira J (2007b) Design of scaffolds assisted by computer. In: Brebbia CA (ed) *Modelling in medicine and biology VII*. Wit Press, pp 157–166
- Andersson S (1983) On the description of complex inorganic crystal structures. *Angew Chem Int Ed* 22(2):69–81
- Andersson S, Hyde ST, Larsson K, Lidin S (1988) Minimal surfaces and structures: from inorganic and metal crystals to cell membranes and biopolymers. *Chem Rev* 88:221–242
- Bao G, Suresh S (2003) Cell and molecular mechanics of biological materials. *Nature Materials* 2:715–725
- Bártolo PJ, Almeida HA, Rezende RA, Laoui T, Bidanda B (2008) Advanced processes to fabricate scaffolds for tissue engineering. In: Bidanda B, Bártolo PJ (eds) *Virtual Prototyping & bio-Manufacturing in medical applications*. Springer, New York, pp 151–174
- Bártolo PJ, Almeida H, Laoui T (2009a) Rapid prototyping & manufacturing for tissue engineering scaffolds. *Int J Comput Appl Technol* 36(1):1–9
- Bártolo PJ, Chua CK, Almeida HA, Chou SM, Lim ASC (2009b) Biomanufacturing for tissue engineering: present and future trends. *Virtual Phys Prototyping* 4(4):203–216
- Bártolo PJ, Kruth JP, Silva J, Levy G, Malshe A, Rajurkar K, Mitsuishi M, Ciurana J, Leu M (2012) Biomedical production of implants by additive electro-chemical and physical processes. *CIRP Ann Manuf Technol* 61(2):635–655
- Brunello G, Sivolella S, Meneghello R, Ferroni L, Gardin C, Piattelli A, Zavan B, Bressan E (2016) Powder-based 3D printing for bone tissue engineering. *Biotechnol Adv* 34:740–753
- Dinis JC, Morais TF, Amorin PHJ, Ruben RB, Almeida HA, Inforçati PN, Bártolo PJ, Silva JVL (2014) Open source software for the automatic Design of Scaffold Structures for tissue engineering applications. *Procedia Technol* 16:1542–1547
- Eshraghi S, Das S (2010) Mechanical and microstructural properties of polycaprolactone scaffolds with one-dimensional, two-dimensional, and three-dimensional orthogonally oriented porous architectures produced by selective laser sintering. *Acta Biomater* 6(7):2467–2476
- Fallahiarezoudar E, Ahmadipourrouposht M, Idris A, Yusof NM (2015) A review of: application of synthetic scaffold in tissue engineering heart valves. *Mater Sci Eng C* 48:556–565
- Gandy PJF, Bardhan S, Mackay AL, Klinowski J (2001) Nodal surface approximations to the P, G, D and I-WP triply periodic minimal surfaces. *Chem Phys Lett* 336(3):187–195
- Giannitelli SM, Mozetic P, Trombetta M, Rainer A (2015) Combined additive manufacturing approaches in tissue engineering. *Acta Biomater* 24:1–11
- Gibson LJ (2005) Biomechanics of cellular solids. *J Biomech* 38:377–399
- Hyde S (1996) Bicontinuous structures in lyotropic liquid crystals and crystalline hyperbolic surfaces. *Curr Opin Solid State Mater Sci* 1:653–662
- Hyde ST, Oguey C (2000) From 2D hyperbolic forests to 3D Euclidean entangled thickets. *Eur Phys J B* 16(4):613–630
- Jana S, Lerman A (2015) Bioprinting a cardiac valve. *Biotechnol Adv* 33:1503–1521
- Janik H, Marzec M (2015) A review: fabrication of porous polyurethane scaffolds. *Mater Sci Eng C* 48:586–591

- Jazayeri HE, Tahriri M, Razavi M, Khoshroo K, Fahimipour F, Dashtimoghadam E, Almeida L, Tayebi L (2017) A current overview of materials and strategies for potential use in maxillofacial tissue regeneration. *Mater Sci Eng C* 70:913–929
- Jiang T, Carbone EJ, Lo KWH, Laurencin CT (2015) Electrospinning of polymer nanofibers for tissue regeneration. *Prog Polym Sci* 46:1–24
- Jung Y, Chu KT, Torquato S (2007) A variational level set approach for surface area minimization of triply-periodic surfaces. *J Comput Phys* 223(2):711–730
- Kapfer SC, Hyde ST, Mecke K, Arns CH, Schroder-Turk GE (2011) Minimal surface scaffold designs for tissue engineering. *Biomaterials* 32(29):6875–6882
- Karcher H, Polthier K (2014) Construction of triply periodic minimal surfaces. *Philos Trans R Soc Lond A* 354(1715):2077–2104
- Langer R, Vacanti JP (1993) Tissue engineering. *Science* 260:920–926
- Larsson M, Terasaki O, Larsson K (2003) A solid state transition in the tetragonal lipid bilayer structure at the lung alveolar surface. *Solid State Sci* 5(1):109–114
- Law JX, Liau LL, Aminuddin BS, Ruszymah BHI (2016) Tissue-engineered trachea: a review. *Int J Pediatr Otorhinolaryngol* 91:55–63
- Lord EA, Mackay AL (2003) Periodic minimal surfaces of cubic symmetry. *Curr Sci* 85(3):346–362
- Melchels FPW, Barradas AMC, Blitterswijk CA, Boer J, Feijen J (2010a) Effects of the architecture of tissue engineering scaffolds on cell seeding and culturing. *Acta Biomater* 6(11):4208–4217
- Melchels FPW, Bertoldi K, Gabblielli R, Velders AH, Feijen J (2010b) Mathematically defined tissue engineering scaffold architectures prepared by stereolithography. *Biomaterials* 31(27):6909–6916
- Melek LN (2015) Tissue engineering in oral and maxillofacial reconstruction. *Tanta Dent J* 12:211–223
- Nesper R, Leoni S (2001) On tilings and patterns on hyperbolic surfaces and their relation to structural chemistry. *ChemPhysChem* 2(7):413–422
- Osman NI, Hillary C, Bullock AJ, MacNeil S, Chapple CR (2015) Tissue engineered buccal mucosa for urethroplasty: progress and future directions. *Adv Drug Deliv Rev* 82–83:69–76
- Qi C, Wang Y (2009) Feature-based crystal construction in computer-aided nano-design. *Comput Aided Des* 41(11):792–800
- Rajagopalan S, Robb RA (2006) Schwarz meets Schwann: design and fabrication of biomorphic and durataxic tissue engineering scaffolds. *Med Image Anal* 10(5):693–712
- Risbud M (2001) Tissue engineering: implications in the treatment of organ and tissue defects. *Biogerontology* 2:117–125
- Scriven LE (1976) Equilibrium bicontinuous structure. *Nature* 263(5573):123–125
- Selimis A, Mironov V, Farsari M (2015) Direct laser writing: principles and materials for scaffold 3D printing. *Microelectron Eng* 132:83–89
- Skalak R, Fox CF (1988) *Tissue Engineering*. Alan R. Liss, New York
- Stratton, S., Shelke, N.B., Hoshino, K., Rudraiah, S. and Kumber S.G. (2016) “Bioactive polymeric scaffolds for tissue engineering”, *Bioact Mater*, 1:93–108.
- Sun W, Lal P (2002) Recent development on computer aided tissue engineering - a review. *Comput Methods Prog Biomed* 67:85–103
- Tajbakhsh S, Hajiali F (2017) A comprehensive study on the fabrication and properties of biocomposites of poly(lactic acid)/ceramics for bone tissue engineering. *Mater Sci Eng C* 70:897–912
- Tan KH, Chua CK, Leong KF, Cheah CM, Gui WS, Tan WS, Wiria FE (2005) Selective laser sintering of biocompatible polymers for applications in tissue engineering. *Biomed Mater Eng* 15:113–124
- Tollema V, Collier ZJ, Mohammed MK, Lee MJ, Ameer GA, Reid RR (2016) Stem cells, growth factors and scaffolds in craniofacial regenerative medicine. *Genes Dis* 3:56–71
- Vozzi G, Flaim C, Ahluwalia A, Bhatia S (2003) Fabrication of PLGA scaffolds using soft lithography and microsyringe deposition. *Biomaterials* 24:2533–2540
- Wang Y (2007) Periodic surface modeling for computer aided nano design. *Comput Aided Des* 39(3):179–189

- Xue Y, Sant V, Phillippi J, Sant S (2017) Biodegradable and biomimetic elastomeric scaffolds for tissue engineered heart valves. *Acta Biomater* 48:2–19
- Yoo DJ (2011a) Computer-aided porous scaffold design for tissue engineering using triply periodic minimal surfaces. *Int J Precis Eng Manuf* 12(1):61–71
- Yoo DJ (2011b) Porous scaffold design using the distance field and triply periodic minimal surface models. *Biomaterials* 32(31):7741–7754
- Yoo DJ (2012a) Heterogeneous porous scaffold design for tissue engineering using triply periodic minimal surfaces. *Int J Precis Eng Manuf* 13(4):527–537
- Yoo, D.J. (2012b) Heterogeneous minimal surface porous scaffold design using the distance field and radial basis functions, *Med Eng Phys* 34(5):625–639
- Yoo DJ (2013) Heterogeneous porous scaffold design using the continuous transformations of triply periodic minimal surface models. *Int J Precis Eng Manuf* 14(10):1743–1753
- Yoo DJ (2014) Advanced porous scaffold design using multi-void triply periodic minimal surface models with high surface area to volume ratios. *Int J Precis Eng Manuf* 15(8):1657–1666

Part II

Biofabrication



Extrusion-Based Biofabrication in Tissue Engineering and Regenerative Medicine

Monika Hospodiuk, Kazim Kerim Moncal, Madhuri Dey, and Ibrahim T. Ozbolat

Contents

1	Introduction	256
2	Extrusion-Based Bioprinting	257
2.1	Principles of Extrusion-Based Bioprinting	257
2.2	Bioink	261
2.3	Limitations	272
2.4	Future Perspectives	273
3	Conclusions	274
	References	274

M. Hospodiuk (✉) · K. K. Moncal
The Huck Institutes of the Life Sciences, The Pennsylvania State University, University Park, PA, USA

Engineering Science and Mechanics Department, The Pennsylvania State University, University Park, PA, USA
e-mail: mxh96@psu.edu; kxm5653@psu.edu

M. Dey
The Huck Institutes of the Life Sciences, The Pennsylvania State University, University Park, PA, USA

Department of Chemistry, The Pennsylvania State University, University Park, PA, USA
e-mail: mxd5491@psu.edu

I. T. Ozbolat
The Huck Institutes of the Life Sciences, The Pennsylvania State University, University Park, PA, USA

Engineering Science and Mechanics Department, The Pennsylvania State University, University Park, PA, USA

Biomedical Engineering Department, The Pennsylvania State University, University Park, PA, USA

Materials Research Institute, The Pennsylvania State University, University Park, PA, USA
e-mail: ito1@psu.edu

Abstract

Extrusion-based bioprinting is a powerful three-dimensional (3D) bioprinting technology that provides unique opportunities for use in organ fabrication. This technology has grown rapidly during the last decade. Extrusion-based bioprinting provides great versatility in printing various biological compounds or devices, including cells, tissues, organoids, and microfluidic devices that can be applied in basic research, pharmaceuticals, drug testing, transplantation, and clinical uses. Extrusion-based bioprinting offers great flexibility in printing wide range of bioinks, including tissue spheroids, cell pellets, microcarriers, decellularized matrix components, and cell-laden hydrogels. Despite these assets, extrusion-based bioprinting has several limitations, such as inadequate control and resolution cell deposition, to create a complex tissue micro-microenvironment, shear stress-induced cell damage, and constraints associated with the current bioink materials.

1 Introduction

The extrusion process has been widely used in the fabrication of plastic and metal parts. The ease of complex structure formation and full process automation of extrusion printing drew the attention of tissue engineering and regenerative medicine scientists more than a decade ago (Vozzi et al. 2002; Yang et al. 2002; Pfister et al. 2004; Smith et al. 2004). Biocompatible hydrogels replaced plastics, and 3D printers were modified to print tissue scaffolds. Subsequent efforts were made to investigate the bioprintability of a wide range of soft materials blended with biological compounds. With the advent of live cell printing and the emergence of other bioprinting technologies, such as laser-based biofabrication (Odde and Renn 2000) and inkjet-based bioprinting (Pardo et al. 2003), the use of extrusion-based bioprinting had begun in earnest (Mironov et al. 2003). Extrusion-based bioprinting can be defined as the dispensing of a biological medium via an automated robotic system. During bioprinting, bioink is dispensed by a computer-controlled system, resulting in precise deposition of cells encapsulated in cylindrical filaments arranged in custom-shaped 3D structures.

Several researchers have demonstrated extrusion-based bioprinting of tissue substitutes (Ozbolat and Hospodiuk 2016). Various cell types have been loaded and deposited in a wide range of biocompatible hydrogels. Recently, artificial liver tissue constructs were engineered by encapsulation of hepatocytes within a gelatin methacrylamide (GelMA) hydrogel; cell viability in the construct was 97% after the bioprinting process (Billiet et al. 2014). In an adipose tissue engineering experiment, human adipose tissue-derived mesenchymal stem cells (hASCs) were loaded in a decellularized matrix. The bioink solution was printed in flexible dome shape in precisely defined patterns. Bioprinted cells showed significantly higher

adipogenic differentiation than hASCs cultured in nonprinted decellularized adipose tissue matrix (Pati et al. 2015a). Moreover, a new GelMA-based bioink containing gellan gum and mannose has been developed, which can be printed in a variety of 3D structures (pyramid, hemisphere, hollow cylinder) without compromising cell viability (Melchels et al. 2014). Kesti et al. showed 3D bioprinting of bovine chondrocytes into a complex 3D scaffold that was designed based on magnetic resonance imaging (MRI) scans (Kesti et al. 2015). Two types of hydrogels (bioink and support) were required in order to bioprint the nose- and ear-shaped patterns.

This chapter presents the principles of extrusion-based bioprinting including the extrusion mechanisms and the physical interactions that occur during extrusion. The bioink materials including hydrogels, decellularized matrix (dECM) components, cell aggregates, and microcarriers are presented along with their strengths and weaknesses. The limitations of extrusion-based bioprinting technology are discussed and future prospects are provided to the reader.

2 Extrusion-Based Bioprinting

2.1 Principles of Extrusion-Based Bioprinting

Extrusion-based bioprinting system relies on dispensing and positioning of a bioink solution through a nozzle on a computer-controlled motion stage. The blueprint design, which can be obtained from medical images, such as computed tomography (CT) and MRI, or freeform design models, is converted into a toolpath plan that is sent to the motion control system (Khoda et al. 2011). To bioprint the tissue construct automatically, an advanced control system that can simultaneously control both the motion of the bioprinter and the dispensing of the bioink solution is required. Here, we classify the dispensing mechanisms of extrusion-based bioprinting systems according to the means of extrusion.

2.1.1 Extrusion-Based Bioprinting Mechanisms

Extrusion-based bioprinting enables dispensing and writing of biomaterials such as cell-laden hydrogels (Khalil and Sun 2009; Chung et al. 2013; Murphy et al. 2013), cell aggregate-based biomaterials (Boland et al. 2003; Mironov et al. 2009; Jakab et al. 2010), and dECM (Pati et al. 2014) through an extrusion printhead driven by a computer-controlled dispensing system. A wide variety of cells can be combined with biomaterials, loaded into syringes and dispensed by pneumatic, mechanical, or solenoid-driven forces onto a printing platform, as shown in Fig. 1.

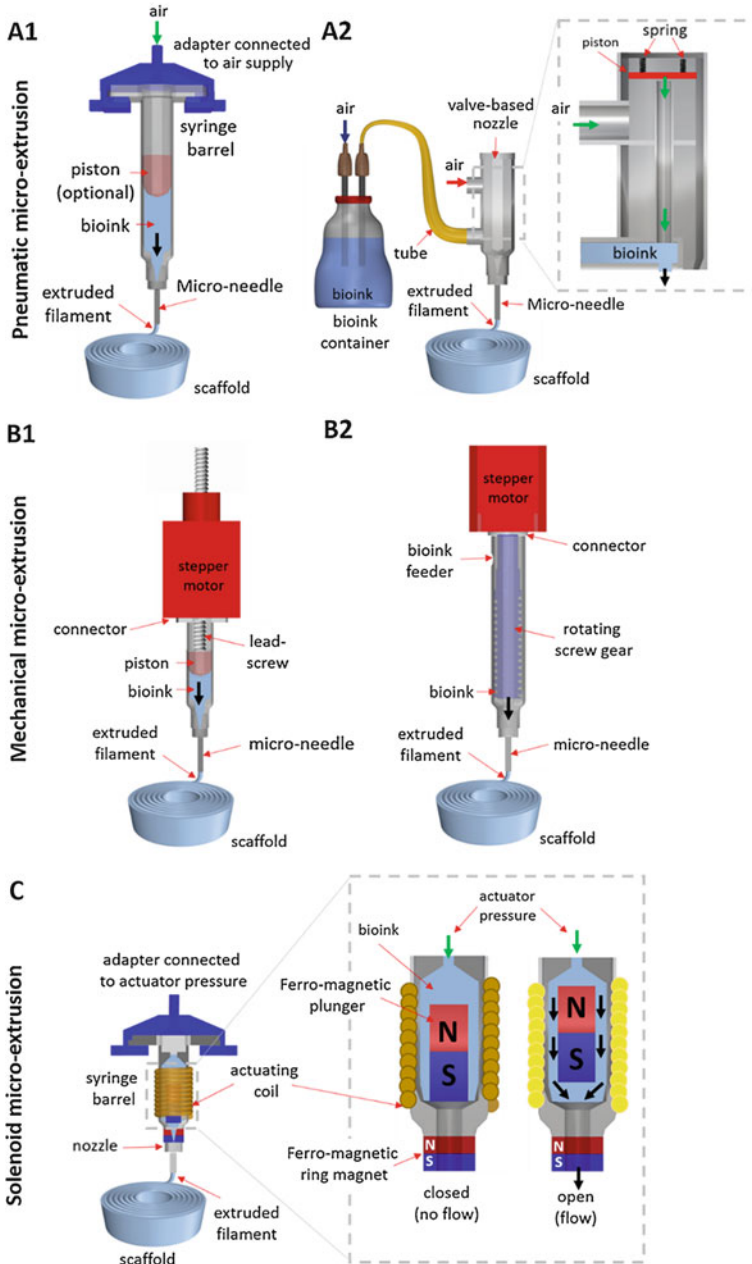


Fig. 1 Extrusion-based bioprinting mechanisms: (A) pneumatic micro-extrusion including (A1) valve-free and (A2) valve-based, (B) mechanical micro-extrusion including (B1) piston- or (B2) screw-driven and (C) solenoid micro-extrusion (Reproduced with permission from Ozbolat and Hospodiuk (2016))

Pneumatic-based extrusion system contains a pneumatic dispenser, which utilizes pressurized air with a valve-free (Fig. 1A1) or a valve-based (Fig. 1A2) configuration. The valve-free extrusion system has a syringe barrel that can be loaded with the bioink solution. An air pressure line is connected on top of the syringe barrel via an adapter to extrude the bioink solution through a micro-needle nozzle. When extrude pneumatically, the bioink solution must undergo certain shear stress. In that respect, hydrogels, which have shear-thinning properties, perform best in pneumatically driven extrusion-based bioprinting as they can maintain the filament shape upon extrusion. The valve-free extrusion system has been widely preferred due to its simplicity. However, for high-precision applications, a valve-based configuration is preferred since it is necessary to maintain a high degree of air pressure control and pulse frequency (Khalil et al. 2005). The valve-based system controls the air channel in the printhead via *on-off* valve switching that activates the air pressure externally when the valve is on and closes the channel when the valve is off. The bioink solution is dispensed from the bioink container through the printhead via air. In general, pneumatically driven systems have a high degree of precision and accuracy; a microdroplet size of 0.5 nL can be generated using a valve-based system. However, the cost of the system increases as the precision of the deposition volume increases. This approach has several disadvantages, as the pneumatic-based system requires sterilization of the air provided by a compressor. Thus, a filter in the airway must be used to minimize contamination of bioprinted structures. In order to extrude bioink solutions smoothly through the nozzle tip, the bioink solutions should be as homogenous as possible. If the bioink is in semisolid or solid form, it may require an additional liquid or gel medium to deliver the bioink solution successfully. Additionally, the bioink can easily attach on the wall of the nozzle. Due to their liquid nature, gel-based bioink solutions can easily transmit the extrusion force equally in all directions without entrapment inside the nozzle.

Mechanical micro-extrusion system is another mechanism which is preferred for the deposition of highly viscous materials such as synthetic and natural polymers. Mechanical extrusion can be designed in piston- (Fig. 1B1) or screw-driven (Fig. 1B2) configurations. The piston-driven mechanical extrusion system utilizes a piston connected to an electric motor. When the motor starts to rotate via electrical pulses, it converts the rotational motion to a linear motion. As a result, the piston advances in the barrel. The screw-driven configuration is useful for extrusion of bioink solutions with higher viscosity (Fielding et al. 2012). Furthermore, the screw-driven configuration can accommodate larger pressure drops along the nozzle. Mechanically driven systems are affordable, easy to program, portable, and do not need an air compressor unit and accessories. Moreover, sterilization of a mechanically driven system is simple as the mechanical dispenser head can be easily autoclaved. A mechanically driven system requires a tighter tolerance selection on the ram and the nozzle unit. An incorrect selection results in an unnecessary power draw on the motor, additional friction forces, leakage of bioink, or failure of the nozzle assembly due to overloading. Mechanically driven systems provide a better bioprinting ability for semisolid or solid bioink materials such as tissue strands.

Lastly, **solenoid micro-extrusion** (Fig. 1C) system mechanism operates via electric pulses. In order to open the valve, the magnetic pull force generated between a floating ferromagnetic plunger and a ferromagnetic ring magnet is canceled when the coil is actuated. Similarly, a piezoelectric-actuated system can be modified to dispense a sub-mL range volume of bioink solution (Bammesberger et al. 2013). Both systems are suitable for extrusion of low viscosity bioink solutions with an ionic- or UV-irradiation-based cross-linking mechanism. Additionally, the accuracy and reproducibility of the bioprinted constructs using this mechanism depend on several factors including the deflection time between actuation time (where the coil is energized) and the time when the valve opens. Highly viscous bioink solutions require a higher actuating pressure in order to extrude the bioink. Also, variations in the temperature and, hence, the viscosity, significantly, affect the valve opening time when the bioink has to be displaced in order to move the plunger. Solenoid-based micro-extrusion systems may not be ideal for thermally controlled nozzle configurations. In addition, re-calibration is required for the valve, especially if long dispensing tips are mounted. With that in mind, tolerance selection of the nozzle could be an important factor for the successful initialization of the bioprinting process.

Extrusion-based bioprinter systems provide a high degree of reproducibility between bioprinted scaffolds when appropriate bioink materials are utilized; in particular, hydrogels with suitable shear-thinning properties and rapid cross-linking capabilities can readily retain their printed shape. In addition, reproducibility of bioprinted constructs depends on several parameters such as dispensing tip diameter, viscosity of the bioink, bioprinter motion speed, extrusion force or pressure, and printing platform surface properties. The resolution of extrusion-based bioprinting is considerably lower than that of droplet- and laser-based systems. However, anatomically correct structures (Gou et al. 2014) and larger 3D constructs are rapidly generated. One of the most important aspects of nozzle selection is the friction coefficient on the wall of the nozzle tip; the friction coefficient mediates shear stress, which can be detrimental to live cells. Thus, a nozzle surface with a small friction coefficient that is easy to sterilize would be ideal for bioprinting cells (Bruzewicz et al. 2012).

2.1.2 Physical Interactions During Extrusion-Based Bioprinting

In order to dispense bioink solutions, the viscosity of the bioink should be able to quickly recover its original rheological state after extrusion. This is particularly important in order to maintain the shape of printed constructs. If the viscosity changes are reversible, the shear-thinning effect is observed (Jungst et al. 2016). Shear thinning is a time-independent property of a material's rheological behavior whereby the viscosity decreases when shear stress is applied and rapidly reverts to its original state as soon as the pressure is released. High-viscosity bioink will not flow through the printhead until pressure is exerted. Once shear stress is applied during extrusion, viscous bioink solutions behave like a liquid under pressure. Thus, bioink materials with shear-thinning properties are preferred as they can be held as a gel in a syringe barrel and extruded only when pressure is applied.

Extrusion-based bioprinting can change the viscosity of the bioink solution over time when mechanical or air pressure is applied. A viscosity change (particularly for non-Newtonian pseudoplastic hydrogels) that occurs in a time-dependent manner after the extrusion-induced disturbance is called thixotropy (Mewis and Wagner 2009). This behavior is similar to shear thinning except the reversion of the material to its original state takes place over time. In order to hasten and enhance reversibility, the bioink concentration can be increased using micro- or nanoparticles, which help decrease the relaxation behavior of the bioink during and after extrusion.

Lastly, in order to deposit the bioink successfully, surface properties of the printing stage should be optimized to stabilize the bioprinted filaments after extrusion. The surface adhesion and roughness of the printing platform is important in order for the filaments to stick and maintain their original shape. The printing surface should not warp or deform; bioprinting failure can result from attempting to print on an uneven surface.

2.2 Bioink

Extrusion-based bioprinting technology (see Fig. 2A) is a universal tool for deposition of a broad spectrum of bioink materials including, but not limited to, hydrogels, tissue spheroids, microcarriers, tissue strands and cell pellets, and dECM components. Material deposition is governed by the bioink type, a wide range of micro-nozzle diameters, and nozzle/tip designs.

2.2.1 Hydrogels: Characteristics and Limitations

A wide variety of hydrogels have been investigated for use in extrusion-based bioprinting. Depending on the cross-linking mechanism, hydrogels in extrusion-based bioprinting can be classified into three groups:

- (i). Physical (temperature (Duarte Campos et al. 2014) or light (Billiet et al. 2014))
- (ii). Enzymatic (Gregor and Hošek 2011)
- (iii). Chemical (pH (Smith et al. 2004) or ionic compound (Cohen et al. 2010))

Several review papers have been published on hydrogels used in tissue engineering (Drury and Mooney 2003); thus, this chapter focuses only on bioprintable hydrogels and their application and performance in extrusion-based bioprinting.

Alginate is an anionic polysaccharide which is present in brown seaweeds. It is made of copolymers of α -L-guluronic and β -D-mannuronic acid. Its biocompatibility, affordability, and fast gelation rate popularized this hydrogel in extrusion-based bioprinting (example shown in Fig. 3A) (Cohen et al. 2011; Jia et al. 2014; Wüst et al. 2014). Several extrusion-based bioprinting techniques have been investigated that exploit the rapid gelation property of alginate in ionic solutions of calcium (Ca^{2+}), such as calcium chloride, calcium carbonate, or calcium sulfate. These automated techniques include (i) bioplotting (Pfister et al. 2004), (ii) bioprinting with a secondary nozzle and with cross-linker deposition over hydrogel or a spraying system (Ahn et al.

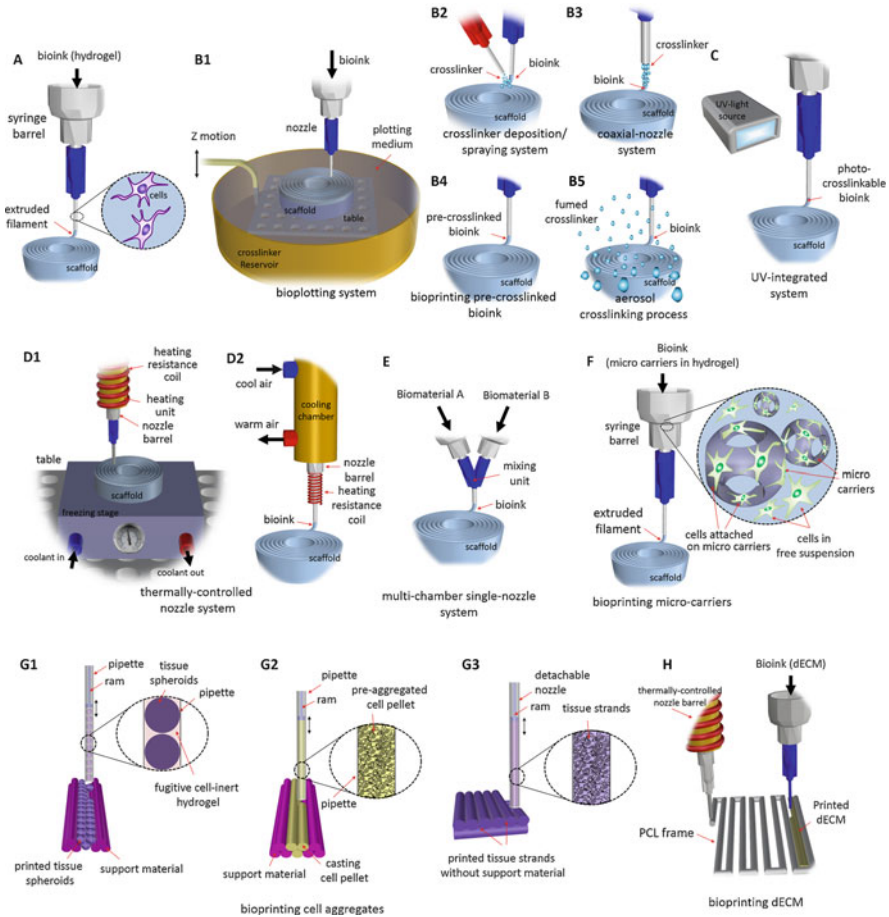


Fig. 2 Processes configurations for various bioink materials: (A) bioprinting cells in hydrogel-based bioink, (B1) bioplotting hydrogel bioink into a cross-linker reservoir, (B2) cross-linker deposition or spraying system, (B3) coaxial-nozzle system, (B4) bioprinting pre-cross-linked bioink, (B5) aerosol cross-linking system, (C) UV-integrated system, (D1) a heating unit-assisted barrel with cooling unit-assisted bioprinting stage, (D2) a cooling unit-assisted barrel with a heating unit-assisted nozzle tip, (E) multi-chamber single-nozzle system, (F) bioprinting microcarriers (preloaded with cells) that can be extruded in hydrogels as a delivery medium, (G1) extrusion of tissue spheroids in a fugitive cell-inert hydrogel into a support mold for fusion and maturation of spheroids, (G2) bioprinting pre-aggregated cell pellet into a support material that is inert to cell adhesion, (G3) bioprinting tissue strands directly without using delivery medium or support mold, and (H) bioprinting dECM within printed PCL frame to mechanically support gelation of dECM (Reproduced with permission from Ozbolat and Hospodiuk (2016))

2012a), (iii) bioprinting with coaxial nozzle-assisted technology (Ozbolat et al. 2014), (iv) bioprinting precross-linked hydrogel followed by full cross-linking after deposition (Chung et al. 2013), and (v) bioprinting hydrogel with an aerosol cross-linking system (Ahn et al. 2012b). Bioplotting is sometimes confused with “bioprinting,” but

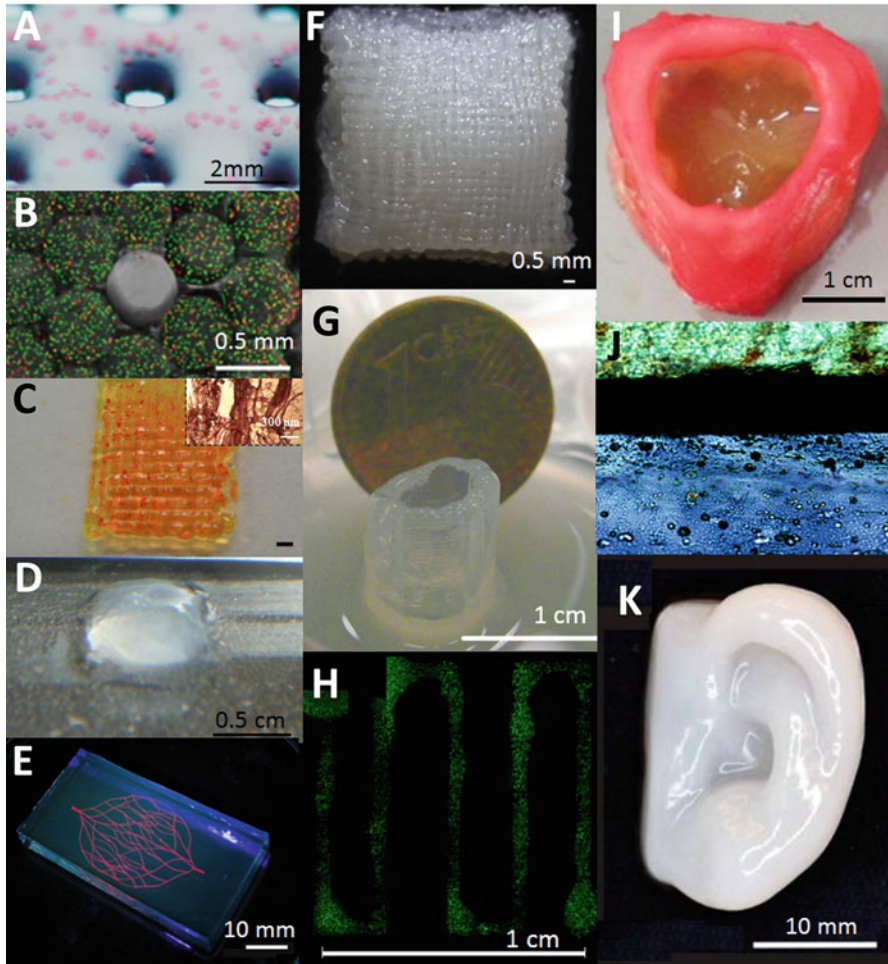


Fig. 3 Extrusion-based bioprinted constructs made of various hydrogels: (A) alginate scaffold with sustained release of proteins (*pink color*) (Reproduced with permission from Poldervaart et al. (2013)), (B) cell-laden GelMA constructs stained for live and dead cells (Reproduced with permission from Bertassoni et al. (2014)), (C) 3D bioprinted Pluronic-collagen scaffolds stained with picosirius red for visualization of collagen type I fibers, (D) 30 layers of fibrin forming a 3D scaffold (Reproduced with permission from Gregor and Hošek (2011)), (E) omnidirectional printing of Pluronic F-127 used for 3D microvascular network fabrication (Reproduced with permission from Wu et al. (2011b)), (F) chitosan scaffold with adipose stem cells extruded in a lattice pattern (Reproduced with permission from Ye et al. (2014)), (G) a cell-laden tubular agarose construct bioprinted into fluorocarbon (Reproduced with permission from Duarte Campos et al. (2013)), (H) live and dead staining of printed cells in Matrigel for a radioprotection study (Reproduced with permission from Snyder et al. (2011)), (I) PEG as aortic valve scaffold (Reproduced with permission from Hockaday et al. (2012)), (J) Alcian blue staining of a hyaluronic acid-based osteochondral-mimetic structure (PCL in black and collagen type I in turquoise color) (Reproduced with permission from Park et al. (2014)), (K) a nanocellulose scaffold in human ear shape for cartilage tissue engineering applications (Reproduced with permission from Markstedt et al. (2015))

they are not the same. In bioplotting (see Fig. 2B1), the hydrogel solution is deposited into a cross-linker pool, and the tissue construct stays within the pool until the process is completed. Therefore, the extrusion of bioink without a bioplotting pool is not considered “bioplotting.” The next technique is shown in Fig. 2B2, where the cross-linker is deposited or sprayed onto the bioprinted hydrogel using a secondary nozzle that can rotate around the primary nozzle (Geng et al. 2005). In the third technique (see Fig. 2B3), alginate is bioprinted through an inner nozzle and the cross-linker is deposited through the outer nozzle. Using a similar approach but an opposite configuration, alginate can be extruded for fabricating core-shell fibers for controlled drug delivery (Zhang et al. 2012; Davoodi et al. 2014); bioprinting microfluidic channels for tissue engineering applications (Zhang et al. 2013), generally blood vessels (Zhang et al. 2015); and immobilizing cell pellets for tissue strand fabrication (Akkouch et al. 2015). In the fourth technique, as shown in Fig. 2B4, precross-linked alginate is bioprinted with a low cross-linker concentration, providing a bioink deposition that endures sufficient structural integrity of the tissue construct. This can be further enhanced by exposing the tissue construct to a second higher concentration cross-linker solution. This method deposits the bioink unevenly, resulting in discontinuities and proportional variation during the extrusion process. In the last approach, the cross-linker is fumed over the bioprinting stage using an ultrasonic humidifier (see Fig. 2B5). This process provides simultaneous cross-linking between layers and develops constructs that are well integrated mechanically and structurally. All these techniques have pros and cons; however, the systems showing promising results (well-integrated interlayers in 3D) are illustrated in Figs. 2B3–B4 (Ozbolat et al. 2014). Despite the advantages, alginate is hydrophilic; thus, cell surface receptors are unable to interact with an alginate matrix. Cells in alginate are immobilized; proliferation and intercellular interactions are limited. Additionally, mechanical properties of alginate are poor if low concentration is used; however, lower concentrations support greater cell viability and an improved proliferation rate. Furthermore, cells do not adhere easily to alginate surface unless modified with a hydrogel. Therefore, researchers attempted to modify alginate by addition of cell adhesion ligands as arginine–glycine–aspartic acid (RGD) peptides (Rowley et al. 1999), which significantly improved cell adhesion, spreading, and proliferation.

Gelatin is a denatured form of collagen (Gómez-Guillén et al. 2011). It is a thermally reversible hydrogel which is solid at low temperatures and characterized by instability under physiological conditions and low mechanical integrity. Gelatin is used in extrusion-based bioprinting with various chemical and physical modifications, i.e., metal ions or glutaraldehyde, to improve its bioprintability and stability (Wang et al. 2006; Xing et al. 2014). One of the common methods to stabilize gelatin at 37 °C is by chemical modification with methacrylamide (MA) side groups which enables photopolymerization of gelatin for cell encapsulation. To cross-link methacrylamide modified gelatin, a water-soluble photoinitiator is required (Van Den Bulcke et al. 2000). The resulting product, which is a GelMA, can be smoothly extruded with a pneumatic dispenser fitted with a UV light source (Billiet et al. 2014; Bertassoni et al. 2014). The reader is referred to Figs. 2C and 3B for a schematic of the process and an example of a bioprinted tissue construct, respectively. The

printability of GelMA relies on the following: the hydrogel concentration, cell density, and duration and intensity of UV curing. The duration of UV exposure affects cell viability, hydrogel density, and final stiffness of the printed tissue construct (Billiet et al. 2014; Bertassoni et al. 2014). In addition, chemically unmodified gelatin can be used as a sacrificial material in fabrication of 3D printed constructs with open fluidic channels (Lee et al. 2010a). After printing, gelatin is liquefied by incubating the construct at 37 °C, creating perfusable channels within the construct. Fluidic networks within the construct enable the flow of nutrition, oxygen, and drugs throughout the construct.

Collagen type I has been broadly used in tissue engineering as a scaffold material (Achilli and Mantovani 2010). Collagen type I possesses the amino acid sequence RGD, which binds to cellular transmembrane receptors known collectively as integrins (Grzesik and Robey 1994). It mediates interactions between the cytoskeleton and ECM and serves as a signal conductor, activating various intracellular signaling pathways and cell functions. Collagen molecules dissolve in acids but cross-link when the pH, temperature, and ionic strength are adjusted close to physiological values. When collagen is neutralized to a pH between 7 and 7.4, collagen cross-links within 30–60 min at 37 °C (Park et al. 2014) making collagen an attractive candidate for in situ bioprinting. This type of bioprinting refers to the direct printing of tissue substitutes into a defect or lesion site in a clinical setting (Ozbolat 2015a). The collagen cross-linking mechanism is also compatible with thermally controlled extrusion-based bioprinting systems. The ideal time for extrusion is the instant polymerization of the collagen begins. Extruded collagen needs to be incubated at 37 °C until fully cross-linked in order to possess sufficient structural integrity, as shown in Fig. 3C. Bioprintability of collagen was first demonstrated by Smith et al. (Smith et al. 2004); collagen type I was blended with bovine aortic endothelial cells (BAECs) and bioprinted by a pneumatic-driven extrusion-based bioprinting system. The configuration presented in Fig. 2D2 is used to bioprint collagen; the bioink is maintained at approximately 4 °C then raised to physiologically relevant temperatures. After deposition, collagen can be fully cross-linked after about 30 min of incubation. Collagen type I has also been 3D printed with different cell types, as well as blended with natural or synthetic biomaterials for chapter ▶ “Fabrication and Printing of Multi-material Hydrogels” that enhance its bioprintability and mechanical properties (Rücker et al. 2006).

Fibrin has superior cell adhesion capabilities and is widely used in tissue engineering (Lee et al. 2010b; Yu et al. 2012; Ehsan et al. 2014). The cross-linking of fibrin is accomplished simply by mixing fibrinogen and thrombin solutions in an enzymatic reaction at room temperature or 37 °C. Based on the desired gel stiffness or cell adhesion properties, cross-linking conditions can be optimized by adjusting thrombin and fibrinogen concentrations. Despite its extensive use in biological applications, fibrin exhibits weak mechanical stiffness and rapid degradation. The rapid and irreversible cross-linking can cause difficulties during bioprinting, generating unstable structures after deposition (Murphy et al. 2013). There are several ways to deposit fibrin in an extrusion-based bioprinting system. One involves the separate deposition of the two fibrin components (fibrinogen and thrombin)

(Xu et al. 2006; Cui and Boland 2009). The second approach combines fibrinogen and thrombin on ice, inducing slow gelation; the material is then extruded using the arrangement illustrated in Fig. 2D2 (Fig. 3D shows an actual printed fibrin construct). The third method uses a multi-chamber single-nozzle approach, where thrombin and fibrinogen solution are blended into one solution at the end of the extrusion process, as shown in Fig. 2E (Gregor and Hošek 2011). In the fourth method, fibrinogen is blended with another hydrogel, bioprinted in a desired pattern, and then cross-linked with thrombin (Wei et al. 2007). Fibrin has great potential for in situ bioprinting applications as bioprinted fibrinogen can rapidly cross-link with naturally occurring thrombin in situ (Li et al. 2015a).

Pluronic[®] is a triblock polymer consisting of a poly(propylene oxide) core flanked by two poly(ethylene oxide) chains (PEO-PPO-PEO). Pluronic is temperature sensitive; the intermolecular assembly of PPO blocks leads to the development of micelle structures above critical temperature. For example, a 20% Pluronic F-127 solution is semi-sol at room temperature and gel above 20 °C. The sol–gel transformation can be modulated by adjusting the solution concentration (Skardal and Atala 2014). The temperature-dependent gelation of Pluronic F-127 makes it a superior bioink material for extrusion-based bioprinting technology (Wu et al. 2011b; Chang et al. 2011); however, it requires a thermally controlled extrusion mechanism. Therefore, a nozzle system with temperature control (shown in Fig. 2D2) is essential to solidify the bioink during the extrusion process. The bioink is loaded into the syringe barrel as a liquid and kept at low temperature in a cooling chamber. A heating unit surrounds the dispensing tip, enabling precise control of the extrusion temperature. This approach allows extrusion of Pluronic in solid form. Another option is a heated plate to prevent melting and deterioration of the structure and shape upon extrusion (see Fig. 4A). Spatially well-defined tissue constructs can be accurately bioprinted using Pluronic bioink (Smith et al. 2004). Although easily bioprinted, Pluronic has weak structural and mechanical properties and dissolves rapidly over time in aqueous solutions (Müller et al. 2015). Recent work, however, demonstrated that Pluronic could be chemically modified to improve its structural and biological properties (Melchels et al. 2016). Pluronic F-127 has been used as a sacrificial material, or fugitive ink (Wu et al. 2011b) as shown in Fig. 3E, or as a support material to create a vascular network (Homenick et al. 2011).

Chitosan is an antibacterial, antifungal, nontoxic, and biodegradable hydrogel produced by deacetylation of chitin; it has been used as wound dressing in regenerative medicine (Ong et al. 2008). It is widely used in the bone, skin, and cartilage tissue engineering, due to hyaluronic acid and glycosaminoglycan content that is similar to native tissue (Ma et al. 2003; Hong et al. 2007; Zhang et al. 2008; Hao et al. 2010). Chitosan is soluble in acid solutions and cross-linked by ionic and covalent agents; however, a water-soluble form at neutral pH ranges was found to facilitate gelation at about 40 °C (Rinaudo 2006). The disadvantage of chitosan in extrusion-based bioprinting is its slow gelation rate and weak mechanical properties. In order to maintain structural integrity of a printed shape for several hours, chitosan must be highly viscous (Hao et al. 2010; Ren et al. 2013). A multilayer printed

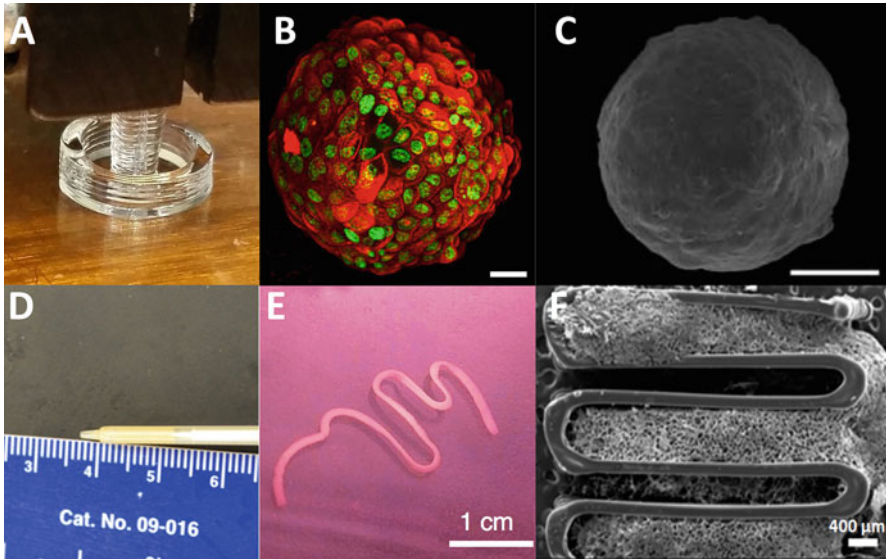


Fig. 4 Bioink types used in extrusion-based bioprinting: (A) Pluronic gel printed in concentric tubes, (B) polymer microcarriers preloaded with cells (scale bar 20 μm) (Reproduced with permission from Jakob et al. (2016)), (C) tissue spheroids made of cells and ECM (scale bar 100 μm) (Reproduced with permission from Norotte et al. (2009)), (D) cell pellet in nozzle tip, (E) tissue strands, and (F) hybrid printing of dECM with PCL framework (Reproduced with permission from Pati et al. (2014))

chitosan structure with embedded adipocytes is shown in Fig. 3F. To optimize strength and polymerization rate, chitosan can be blended with hydrogels with better mechanical properties. Chitosan has been used in extrusion-based bioprinting of various tissue constructs and devices, for example, microfluidic perfusable channels (Zhang et al. 2013), chondrogenic scaffolds encapsulated with adipose stem cells (Ye et al. 2014), and 3D printed scaffolds to study inflammatory responses (Almeida et al. 2014). The bioprinting mechanisms shown in Figs. 2B1–5 can be used in bioprinting of chitosan hydrogel.

Agarose is a polymer extracted from seaweed-based galactose with both thermoreversible and thermosensitive properties. Several types of agarose, with varying melting temperatures depending on the degree of hydroxyethylation, are available (Serwer et al. 1983). For extrusion-based bioprinting, the most suitable agarose is one with low-melting and low-gelling temperatures that is easy to liquefy and can solidify at 26–30 $^{\circ}\text{C}$ (Landers et al. 2002). The system configuration for agarose in extrusion-based bioprinting is presented in Fig. 2D1, where agarose is extruded in liquid state onto a cold stage resulting in rapid solidification. Recently, mesenchymal stem cells were encapsulated in agarose and then bioprinted in a tubular structure with fluorocarbon supporting the entire construct (see Fig. 3G) (Duarte Campos et al. 2013). The deposited cells are maintained in nearly 100% cell viability over 21 days. Agarose is also a suitable hydrogel for developing 3D cell

culture platforms; cells do not adhere to agarose but instead form large cell aggregates (Dean et al. 2007; Norotte et al. 2009; Mironov et al. 2011).

Matrigel, extracted from mouse Engelbreth–Holm–Swarm sarcoma cells and comprised primarily of laminin, collagen type IV, and enactin, forms a gelatinous protein mixture. The major advantage of Matrigel is the ability to support differentiation of many cell types and promote tissue outgrowth (Kleinman and Martin 2005). Another important characteristic of this hydrogel is its thermosensitive behavior (Wu and Ringeisen 2010). Matrigel is liquid at 4 °C but cross-links to form a gel at 24–37 °C. Complete gelation takes approximately 30 min and is a nonreversible process. Similar to collagen type I, in order to extrude Matrigel, the extrusion mechanism must possess a thermally controlled unit (as presented in Fig. 2D2) to hold the hydrogel at 4 °C. Extrusion-based bioprinting of Matrigel yielded high viability of human epithelial cells as shown in a live-dead staining image (see Fig. 3H) (Snyder et al. 2011). Moreover, bone marrow stromal cells bioprinted in Matrigel showed higher survival rates than cells encapsulated in alginate or agarose (Fedorovich et al. 2008). Also, multicellular constructs have been bioprinted and implanted in vivo for bone regeneration. Host tissue vascularization was demonstrated within 2 weeks after implantation (Fedorovich et al. 2011).

Poly(ethylene glycol) (PEG), as well as **poly(ethylene oxide)** (PEO), is widely used in non-pharmaceutical products and medical supplements (Giovagnoli et al. 2010; Mooney et al. 2011; Elbert 2012). The PEG-based hydrogels are biocompatible, are minimally immunogenic, and are approved by the Food and Drug Administration (FDA). One of the advantages of PEG-based hydrogels is their wide selection of cross-linking methods, using covalent, physical, or ionic agents (Veronese and Pasut 2005). Photopolymerization of PEG attracted major attention because of its tunable mechanical properties. A UV-integrated system can be used, as presented in Fig. 2C, to photocross-link polyethylene glycol diacrylate (PEG-DA) for quick 3D bioprinting of mechanically heterogeneous, complex, and clinically accurate scaffolds of aortic valve shapes (see Fig. 3I). Porcine aortic valve interstitial cells were seeded on the scaffold and cultured for up to 21 days (Hockaday et al. 2012). Unfortunately, cells seeded on the scaffold showed limited adhesion and spreading. Although PEG is a plausible option for cell encapsulation, it does not possess the cell adhesion motifs of bioink materials such as collagen. Hence, PEG-based materials need to be functionalized with the addition of cell binding sites growth factors during the bioprinting process to promote cell proliferation, migration, and regeneration of tissues (Zhang et al. 1998; Fedorovich et al. 2007).

Hyaluronic acid (HA) is an ubiquitous glycosaminoglycan present in most connective tissues (Oxlund and Andreassen 1980). During early embryogenesis, a high concentration of HA is present controlling a variety of cell functions and behavior, such as movement, angiogenesis, and proliferation. Hyaluronic acid is an attractive material for extrusion-based bioprinting due to its tunable physical and biological properties. Moreover, HA is the primary ECM component in cartilage tissue. A recent study revealed that 3D bioprinted chondrocyte-laden HA hydrogels (see Fig. 3J, in blue color) exhibited higher cell viability compared to cells loaded in collagen (Park et al. 2014). The disadvantages of HA are its poor mechanical

properties and rapid degradation rates (Jeon et al. 2007) that limit the use of HA in extrusion-based bioprinting; however, chemical modifications make it possible to control the degradation rate. One example is the functionalization of HA with UV-curable methacrylate (MA), where the duration of photopolymerization readily controls the degree of stiffness (Gerecht et al. 2007). Thus, the mechanism presented in Fig. 2C can be applied in the bioprinting of HA hydrogels functionalized with MA (Dana et al. 2004; Skardal et al. 2010b; Malda et al. 2013; Skardal and Atala 2014).

Methylcellulose (MC), a chemical compound obtained from cellulose as a semiflexible linear arrangement of polysaccharides, has the simplest chemical composition (Lott et al. 2013). Similar to gelatin and Pluronic, methylcellulose has thermosensitive and thermoreversible properties. The transition between sol and gel depends on the polymer concentration and molecular weight (Kobayashi et al. 1999). Methylcellulose in aqueous solution is used for cell culture purposes, as gelling occurs below 37 °C (Thirumala et al. 2013). Silanized hydroxypropyl methylcellulose hydrogel, a derivative of MC with pH-sensitive capabilities, has been patented and is used for 3D chondrogenic and osteogenic cultures (Trojani et al. 2005; Vinatier et al. 2005). Extrusion-based bioprinting of MC, as with other thermosensitive and thermoreversible hydrogels, requires an additional system such as a thermally controlled chamber (as presented in Fig. 3D2) and a heating stage. However, MC can be unstable exhibiting partial degradation with exposure to aqueous solutions such as cell culture media; hence, it is not suitable for long-term culturing of cells (Thirumala et al. 2013). Extrusion-based bioprinting of a bioactive glass with MC has shown good mechanical strength, which makes it an excellent candidate for use in bone regeneration (Wu et al. 2011a). Also, nanofibrillated cellulose has been blended with alginate, loaded with chondrocytes, and then bioprinted in the shape of a human ear, which demonstrates the ability of 3D bioprinting complex structures (see Fig. 3K) (Markstedt et al. 2015). Methylcellulose was also used as a scaffold matrix for corneal stromal cell spheroids fabricated under both rotary and static cell culture system, which were later used in a bioprinting procedure (Li et al. 2015b).

For simultaneous bioprinting of multiple hydrogels, a multi-chamber single-nozzle unit configuration has been developed, as shown in Fig. 2E. A major advantage of this approach is the ability to print one or more hydrogels to fabricate a heterogeneous construct with variations along the filament deposition direction (Ozbolat and Koc 2010). Biofabrication of hybrid porous tissue scaffolds have been demonstrated using the nozzle assembly, where various functional properties can be manipulated by modifying the nature and the concentration of the biomaterial used (Ozbolat and Koc 2011). The rate at which a bioink material is dispensed from the nozzle depends on the pressure applied using the pneumatic controller unit. An advanced design with a similar approach is the triple chamber (Mogas-Soldevila et al. 2014), where chitosan, sodium alginate, and chitin powder were blended in a static mixer nozzle, and scaffolds were fabricated using a six-axis robotic printer.

Synthetic as well as some naturally available hydrogels lack the proper constituents, such as native ECM proteins, for sustainable growth and proliferation of cells. Additionally, it is challenging to maintain a cell density similar to that of the native

tissue (Ozbolat 2015b). Hydrogels containing the RGD sequence, such as gelatin and collagen, or those with a fibrous microstructure, readily allow cell adhesion. In absence of such cell binding motifs, cells will not preferentially adhere and proliferate on a biomaterial surface. High concentrations of hydrogels result in a mechanically stronger construct but can be detrimental to cells. Hydrogels, such as Pluronic F-127, preserve the integrity when deposited in bulk but are unable to preserve mechanical and structural integrity when printed in filaments as they rapidly dissolve in culture media. In extrusion-based bioprinting, rheological properties of hydrogel play an important role, where bioink suspension must overcome surface tension-driven droplet formation and be extrudable in straight filaments form. The material can quickly spread over the printing stage if a very low concentration of the bioink is used as opposed to a highly viscous or concentrated bioink, which requires high pressure for continuous extrusion. However, increased pressure might induce cell lysis due to increased shear stress.

Another limitation in hydrogel-based bioinks is the degradation time of hydrogels and the production of potentially detrimental by-products. Generally, hydrogels *in vitro* degrade much slower than *in vivo* and the degradation behavior differs from hydrogel to hydrogel. Encapsulated cells often cannot deposit sufficient amounts of ECM and proliferate within a hydrogel to begin tissue reconstruction before construct degradation takes place *in vivo*. Degradation may also trigger a chronic inflammatory response in the host after implantation. Also, hydrogels should not produce toxic degradation by-products that are harmful to biologics. In summary, the hydrogel utilized in extrusion-based bioprinting should be compatible with the targeted tissue type and support cell growth and function until the tissue regeneration process is completed.

2.2.2 Other Bioink Types

Microcarriers are defined as small spherical carriers with a porous structure that provides an expanded surface area for cell attachment and growth (Fig. 4B). Commercially available microcarriers for bone and cartilage regeneration are made of dextran (Malda et al. 2003; Skardal et al. 2010a), polymers (Bayram et al. 2005; Curran et al. 2005), glass (Malda et al. 2003), gelatin (Liu et al. 2004), and collagen (Overstreet et al. 2003; Shikani et al. 2004). Cells proliferate more rapidly on microcarriers and exhibit improved interaction and aggregation inside microcarriers than the cells loaded in the hydrogel solution alone. Total surface area available for cell expansion is significantly higher than 2D culture (Levato et al. 2014). Extrusion-based bioprinting of microcarriers is similar to printing cell aggregates; however, due to polymer stiffness, printing may be difficult. Microcarriers are blended with a hydrogel solution, loaded into the barrel, and dispensed (see Fig. 2F). The major limitation of polymeric microcarriers is a prolonged degradation time and associated toxic by-products. Degradation of hydrogel-based microcarriers is dependent on concentration and material type. If microcarriers are made of hard polymers, they can clog the nozzle during extrusion process. Deposition of microcarriers is challenging, as precise delivery to ensure contact between microcarriers is essential to 3D development of the construct.

Cell aggregates are scaffold-free bioink materials used in self-assembly directed fabrication of tissues. The greatest advantage of this approach is the short fabrication required compared to scaffold-based approaches. Large numbers of cells are initially seeded resulting in rapid deposition of native ECM biomolecules. Several approaches have been explored for fabrication of cell aggregates, particularly tissue spheroids, including hanging drop, pellet culture, nonadhesive micromold hydrogels, microfluidics by hydrodynamic cell trapping, liquid overlay, spinner flask, and rotating wall vessel techniques (Breslin and O'Driscoll 2013; Mehesz et al. 2011). It should be noted that not all of these techniques have been applied to bioprinting, but any of them can be considered as an alternative approach. Examples of homocellular, as shown in the Fig. 4C, and heterocellular tissue spheroids have been demonstrated in the literature (Hsiao et al. 2009; Torisawa et al. 2009). Despite the numerous advantages, cell aggregates present certain challenges when applied to extrusion-based bioprinting. One of the major difficulties is loading tissue spheroids into the nozzle, as shown in the Fig. 2G1 (Mironov et al. 2009). Moreover, aggregates need to be extruded in a delivery medium of either a fugitive ink or a thermosensitive hydrogel that does not allow cell adhesion. Also, cell aggregates fuse quickly which resulting in accumulation inside the nozzle tip thereby hindering printability. Post bioprinting and discontinuities in the printed tissue are possible if the tissue spheroids have not been deposited in close proximity. Also, permeability of tissue spheroids is lower than that of hydrogels, limiting the diffusion of oxygen and other nutrients. Hence, fabrication of spheroids over 400 μm in diameter induces hypoxia leading to cell death (Achilli et al. 2012). However, resilient cells (such as stromal cells) or cells that can tolerate hypoxia (such as chondrocytes) can overcome this issue. Neocapillarization inside the tissue spheroid is highly desirable for scale-up fabrication of tissues and organs. An example of naturally existing spheroids in the human body is lymph nodes. This tissue is composed of stromal cells such as fibroblasts, endothelial cells, and follicular dendritic cells, which provides physiological function in tissue ranging from a few millimeters to 1–2 cm long (Katakai et al. 2004). For neo vascularization of 3D printed and engineered tissues, cell aggregates need to be printed before becoming fully mature. Otherwise, mature tissue spheroids lose their potential to fuse and vascularize. Another type of dense cell suspension bioink material is a cell pellet, which can be molded into any shape, as shown in Figs. 2G2 and 4D (Ozbolat 2015b). The main limitation of the cell pellet is fabrication of large-scale tissues without using a temporary molding material. Therefore, tissue strands (Akkouch et al. 2015) (Figs. 2G3 and 4E) are considered as an alternative technique. These constructs are produced as elongated filaments using a custom-made nozzle apparatus. The labor-intensive method of preparing cell aggregates is eliminated in this technique. This technique also adds in the advantage of printing tissue strands with vasculature. Thus this method has great potential in generating larger-scale tissues and organ constructs (Yu et al. 2014; Yu and Ozbolat 2014).

Decellularized extracellular matrix has recently been developed as a hydrogel-free technique to transform natural cell matrix into a bioprintable material. This material has also been blended with other hydrogels for bioprinting purposes (Jang

et al. 2016). Native tissue ECM is decellularized and fragmented into small pieces for extrusion bioprinting (Pati et al. 2014). One of the major disadvantages of dECM is the extremely low yield of material after extraction. In addition, dECM loses its mechanical and structural integrity as well as some biochemical properties when it is fragmented. Therefore, polycaprolactone (PCL) can be used as a support structure for bioprinted dECM bioink (see Figs. 2H and 4F) (Pati et al. 2015b).

2.3 Limitations

Extrusion-based bioprinting is the most convenient technique for rapid fabrication of 3D cellular porous structures. This technology holds great promise for future organ fabrication and scale-up tissue engineering. However, it has several limitations that need to be overcome to enhance the potential of extrusion-based bioprinting systems in organ fabrication. The main disadvantage is the low printing resolution due to the large nozzle configurations of extrusion-based systems. The need for rapid gelation to encapsulate cells and form a stable 3D constructs in a shorter span of time limits the choice of bioink materials. The other impediment is the presence of shear stress caused by the extrusion process. Shear stress on the nozzle tip wall results in a lower cell viability in highly concentrated bioinks. Moreover, changes in the nozzle geometry, dispensing pressure, and bioink concentration could collectively induce cell death (Yu et al. 2013). In addition, accumulation of bioink material in the nozzle can result in nozzle clogging over time. Depending on the type of biologics being printed, a number of events might lead to clogging of the nozzle such as diffusion of the cross-linker solution into the nozzle, imprecise control of the temperature, early fusion of spheroids, coagulation of the bioparticles/microcarriers loaded in relatively small diameter nozzles, and heterogeneous bioink solutions.

As the field of bioprinting is rapidly expanding its range of applications, a wide variety of extrusion-based systems have been developed to increase its functionality including motion capability of the robotic arms with high degree of freedom, ease of operation, compact size, full-automation capability, and ease of sterilization (Dababneh and Ozbolat 2014). Despite its versatility and assets, extrusion-based bioprinting has some disadvantages when compared to other technologies. First, the resolution of the technology is quite limited; the minimum feature size is generally over 100 μm (Duan et al. 2013), which is considerably lower than the resolution of other bioprinting techniques (Dababneh and Ozbolat 2014). Therefore, cells cannot be precisely patterned and organized due to limited resolution. In addition, the bioink, in liquid or sol-gel state, requires shear-thinning ability to overcome surface tension-driven droplet formation to be extruded in the form of cylindrical filaments. Furthermore, gelation and solidification requirements for the materials limit the hydrogel options used in extrusion-based systems. Shear stress on the nozzle tip has a substantial effect on cell viability, especially if the bioink solution contains high cell density (Chang et al. 2008).

2.4 Future Perspectives

Extrusion-based bioprinting is a versatile technique owing to its flexibility in incorporating different bioink types, its ability to fabricate perfusable and porous tissue structures, and its capability to rapidly build large tissue constructs with enhanced mechanical and biological properties, which cannot be achieved using laser or droplet-based bioprinting. Although remarkable progress has been made in the field of bioprinting, more efficient and robust end products are needed in order to transition from basic research to pharmaceuticals and clinics (Ozbolat 2015b).

In situ bioprinting is a very promising technology, which involves the bioprinting of porous tissue analogues into defects and lesion sites. These printed constructs can integrate with the endogenous tissue and producing a new vascularized tissue to complete the healing process. Only a few attempts have been made to in situ bioprint materials employing inkjet (Wang et al. 2009; Hussain et al. 2010) and laser-based bioprinting techniques (Lopes et al. 2014). Conversely, extrusion-based bioprinting offers wide flexibility in printing tissue analogues with controlled porous architecture. A pilot study was performed by Cohen et al., in which precross-linked sodium alginate was deposited into a defect on an ex vivo femur model (Cohen et al. 2010). This ex vivo defect model provided a translational step toward clinical in situ bioprinting, bringing the technology from bench to bedside. It is envisaged that in situ bioprinting can be effectively applied to deep dermal injuries, composite tissues and flaps, and calvarial or craniofacial defects during maxillofacial or brain surgeries.

Although considerable progress has been made in developing novel biomaterials, there is a great need for developing new bioinks with enhanced gelation capabilities, higher mechanical and structural integrity, and bioprintability, which will be well suited for extrusion-based bioprinting and adapted for soft tissues. This would usher in a new field of research under biomaterials and biofabrication, “bioprintable biomaterials.” One of the major weaknesses in currently existing hydrogel-based bioinks is the lack of environment for promoting growth and differentiation of stem cells into multiple lineages (Ker et al. 2011). To mimic the native organizational structure of tissues and organs which consists of multiple cell types, it is essential to develop a bioink which would support a similar organization of the heterocellular tissue microstructure (Carrow and Gaharwar 2014). The structural and physical properties of the native tissue can be faithfully recapitulated by integrating chemical, mechanical, and physical stimuli. An ideal hydrogel material should be able to promote cell adhesion, proliferation, and differentiation toward multiple lineages, should possess appropriate mechanical integrity and structural stability to persist even after bioprinting, facilitate engraftment with the endogenous tissue without generating an immune response, possess shear-thinning properties to ease bioprinting and rapid gelation, and be abundant, affordable, and commercially available with appropriate regulatory guidelines for clinical use.

One of the exciting future directions in the field of bioprinting is the bioprinting of new types of organs. These organs can be tuned to perform specific functions such as augment the physiology of the human body beyond its normal capabilities or treat

diseases. The nature of such organs could be entirely biological in perspective or in the form of cyborg organs intertwining biology and electronics. A proof of concept cyborg organ has been recently demonstrated by Zhang et al. (2012) where bionic ears were printed using a hybrid approach. This technique involved bioprinting chondrocytes in alginate along with silver nanoparticles in the form of an inductive coil antenna. This cultured cyborg organ model was evaluated and was found to exhibit enhanced auditory sensing for radio frequency reception.

3 Conclusions

Over the past decade, extrusion-based bioprinting has proven to be a useful technique for tissue fabrication. There is a rapidly growing interest in extrusion-based bioprinting systems among researchers in the tissue engineering community due to the recent advances in bioink materials and new processes for vascularized tissue fabrication. Due to its greater flexibility in bioprinting of various bioink materials including hydrogels, dECM components, cell aggregates, and microcarriers, extrusion-based bioprinting has enabled fabrication of a wide array of tissue constructs, organ modules, and organ-on-a-chip devices. One of the major advances in this field relies on the development of superior bioink materials with fast gelation mechanisms, simplifying the process of extrusion and bioprinting. Overcoming the limitations of extrusion-based bioprinting including the improvement of bioprinting resolution, full automation of the technology, and development of novel bioink compositions would help translate this technique from bench to bedside.

Acknowledgments This work has been supported by National Science Foundation CMMI Awards 1349716 and 1462232. We thank Fisayo Olashore and Donna Sosnoski from the Pennsylvania State University for improving the quality of the paper. The authors are grateful to the support from the Engineering Science and Mechanics Department and the College of Engineering at the Penn State University. *The authors confirm that there are no known conflicts of interest associated with this publication, and there has been no significant financial support for this work that could have influenced its outcome.*

References

- Achilli M, Mantovani D (2010) Tailoring mechanical properties of collagen-based scaffolds for vascular tissue engineering: the effects of pH, temperature and ionic strength on gelation. *Polymers (Basel)* 2:664–680. <https://doi.org/10.3390/polym2040664>
- Achilli T, Meyer J, Morgan JR (2012) Advances in the formation, use and understanding of multicellular spheroids. *Expert Opin Biol Ther* 12:1347–1360. <https://doi.org/10.1517/14712598.2012.707181>. *Advances*
- Ahn S, Lee H, Bonassar LJ, Kim G (2012a) Cells (MC3T3-E1)-laden alginate scaffolds fabricated by a modified solid-freeform fabrication process supplemented with an aerosol spraying. *Biomacromolecules* 13:2997–3003. <https://doi.org/10.1021/bm3011352>

- Ahn S, Lee H, Puetzer J et al (2012b) Fabrication of cell-laden three-dimensional alginate-scaffolds with an aerosol cross-linking process. *J Mater Chem* 22:18735. <https://doi.org/10.1039/c2jm33749e>
- Akkouch A, Yu Y, Ozbolat IT (2015) Microfabrication of scaffold-free tissue strands for three-dimensional tissue engineering. *Biofabrication* 7:31002. <https://doi.org/10.1088/1758-5090/7/3/031002>
- Almeida C, Serra T, Oliveira M et al (2014) Impact of 3-D printed PLA- and chitosan-based scaffolds on human monocyte/macrophage responses: unraveling the effect of 3-D structures on inflammation. *Acta Biomater* 10:613–622. <https://doi.org/10.1016/j.actbio.2013.10.035>
- Bammesberger SB, Kartmann S, Tanguy L et al (2013) A low-cost, normally closed, solenoid valve for non-contact dispensing in the sub- μ l range. *Micromachines* 4:9–21. 10.3390/mi4010009
- Bayram Y, Deveci M, Imirzalioglu N et al (2005) The cell based dressing with living allogenic keratinocytes in the treatment of foot ulcers: a case study. *Br J Plast Surg* 58:988–996. <https://doi.org/10.1016/j.bjps.2005.04.031>
- Bertassoni LE, Cardoso JC, Manoharan V et al (2014) Direct-write bioprinting of cell-laden methacrylated gelatin hydrogels. *Biofabrication* 6:024105. <https://doi.org/10.1088/1758-5082/6/2/024105>
- Billiet T, Gevaert E, De Schryver T et al (2014) The 3D printing of gelatin methacrylamide cell-laden tissue-engineered constructs with high cell viability. *Biomaterials* 35:49–62. <https://doi.org/10.1016/j.biomaterials.2013.09.078>
- Boland T, Mironov V, Gutowska A et al (2003) Cell and organ printing 2: fusion of cell aggregates in three-dimensional gels. *Anat Rec Part A Discov Mol Cell Evol Biol* 272A:497–502. <https://doi.org/10.1002/ar.a.10059>
- Breslin S, O'Driscoll L (2013) Three-dimensional cell culture: the missing link in drug discovery. *Drug Discov Today* 18:240–249. <https://doi.org/10.1016/j.drudis.2012.10.003>
- Bruzewicz DA, Reches M, Whitesides GM (2012) Low-cost printing of PDMS barriers to define microchannels in paper. *Changes* 29:997–1003
- Carrow JK, Gaharwar AK (2014) Bioinspired polymeric nanocomposites for regenerative medicine. *Macromol Chem Phys*. <https://doi.org/10.1002/macp.201400427>
- Chang R, Nam J, Sun W (2008) Effects of dispensing pressure and nozzle diameter on cell survival from solid freeform fabrication-based direct cell writing. *Tissue Eng Part A* 14:41–48. <https://doi.org/10.1089/ten.a.2007.0004>
- Chang CC, Boland ED, Williams SK, Hoying JB (2011) Direct-write bioprinting three-dimensional biohybrid systems for future regenerative therapies. *J Biomed Mater Res B Appl Biomater* 98:160–170. <https://doi.org/10.1002/jbm.b.31831>
- Chung JHY, Naficy S, Yue Z et al (2013) Bio-ink properties and printability for extrusion printing living cells. *Biomater Sci* 1:763. <https://doi.org/10.1039/c3bm00012e>
- Cohen DL, Lipton JI, Bonassar LJ, Lipson H (2010) Additive manufacturing for in situ repair of osteochondral defects. *Biofabrication* 2:035004. <https://doi.org/10.1088/1758-5082/2/3/035004>
- Cohen J, Zaleski KL, Nourissat G et al (2011) Survival of porcine mesenchymal stem cells over the alginate recovered cellular method. *J Biomed Mater Res A* 96:93–99. <https://doi.org/10.1002/jbm.a.32961>
- Cui X, Boland T (2009) Human microvasculature fabrication using thermal inkjet printing technology. *Biomaterials* 30:6221–6227. <https://doi.org/10.1016/j.biomaterials.2009.07.056>
- Curran SJ, Chen R, Curran JM, Hunt J (2005) Expansion of human chondrocytes in an intermittent stirred flow bioreactor, using modified biodegradable microspheres. *Tissue Eng* 11:1312–1322. <https://doi.org/10.1089/ten.2005.11.1312>
- Dababneh AB, Ozbolat IT (2014) Bioprinting technology: a current state-of-the-art review. *J Manuf Sci Eng* 136:061016. <https://doi.org/10.1115/1.4028512>
- Dana N, Parker V, Meredith M et al (2004) Photocrosslinkable hyaluronan as a scaffold for articular cartilage repair. *Ann Biomed Eng* 32:391–397

- Davoodi P, Feng F, Xu Q et al (2014) Coaxial electrohydrodynamic atomization: microparticles for drug delivery applications. *J Control Release*. <https://doi.org/10.1016/j.jconrel.2014.12.004>
- Dean DM, Napolitano AP, Youssef J, Morgan JR (2007) Rods, tori, and honeycombs: the directed self-assembly of microtissues with prescribed microscale geometries. *FASEB J* 21:4005–4012. <https://doi.org/10.1096/fj.07-8710com>
- Drury JL, Mooney DJ (2003) Hydrogels for tissue engineering: scaffold design variables and applications. *Biomaterials* 24:4337–4351. [https://doi.org/10.1016/S0142-9612\(03\)00340-5](https://doi.org/10.1016/S0142-9612(03)00340-5)
- Duan B, Hockaday L, Kang KH, Butcher JT (2013) 3D bioprinting of heterogeneous aortic valve conduits with alginate/gelatin hydrogels. *J Biomed Mater Res Part A* 101 A:1255–1264. <https://doi.org/10.1002/jbm.a.34420>
- Duarte Campos DF, Blaeser A, Weber M et al (2013) Three-dimensional printing of stem cell-laden hydrogels submerged in a hydrophobic high-density fluid. *Biofabrication* 5:015003. <https://doi.org/10.1088/1758-5082/5/1/015003>
- Duarte Campos DF, Blaeser A, Korsten A et al (2014) The stiffness and structure of three-dimensional printed hydrogels direct the differentiation of mesenchymal stromal cells toward adipogenic and osteogenic lineages. *Tissue Eng Part A*:1–17. <https://doi.org/10.1089/ten.TEA.2014.0231>
- Ehsan SM, Welch-Reardon KM, Waterman ML et al (2014) A three-dimensional in vitro model of tumor cell intravasation. *Integr Biol (Camb)* 6:603–610. <https://doi.org/10.1039/c3ib40170g>
- Elbert DL (2012) Liquid-liquid two phase systems for the production of porous hydrogels and hydrogel microspheres for biomedical applications: a tutorial review. *Acta Biomater* 7:31–56. <https://doi.org/10.1016/j.actbio.2010.07.028.Liquid-liquid>
- Fedorovich NE, Alblas J, de Wijn JR et al (2007) Hydrogels as extracellular matrices for skeletal tissue engineering: state-of-the-art and novel application in organ printing. *Tissue Eng* 13:1905–1925. <https://doi.org/10.1089/ten.2006.0175>
- Fedorovich NE, De Wijn JR, Verbout AJ et al (2008) Three-dimensional fiber deposition of cell-laden, viable, patterned constructs for bone tissue printing. *Tissue Eng Part A* 14:127–133. <https://doi.org/10.1089/ten.a.2007.0158>
- Fedorovich NE, Wijnberg HM, Dhert WJ, Alblas J (2011) Distinct tissue formation by heterogeneous printing of osteo- and endothelial progenitor cells. *Tissue Eng Part A* 17:2113–2121. <https://doi.org/10.1089/ten.tea.2011.0019>
- Fielding G, Bandyopadhyay A, Bose S (2012) Effects of silica and zinc oxide doping on mechanical and biological properties of 3D printed tricalcium phosphate tissue engineering scaffolds. *Dent Mater* 28:113–122. <https://doi.org/10.1016/j.dental.2011.09.010>
- Geng L, Feng W, Huttmacher DW et al (2005) Direct writing of chitosan scaffolds using a robotic system. *Rapid Prototyp J* 11:90–97. <https://doi.org/10.1108/13552540510589458>
- Gerecht S, Burdick J, Ferreira LS et al (2007) Hyaluronic acid hydrogel for controlled self-renewal and differentiation of human embryonic stem cells. *Proc Natl Acad Sci U S A* 104:11298–11303. <https://doi.org/10.1073/pnas.0703723104>
- Giovagnoli S, Tsai T, DeLuca PP (2010) Formulation and release behavior of doxycycline-alginate hydrogel microparticles embedded into pluronic F127 thermogels as a potential new vehicle for doxycycline intradermal sustained delivery. *AAPS PharmSciTech* 11:212–220. <https://doi.org/10.1208/s12249-009-9361-8>
- Gómez-Guillén MC, Giménez B, López-Caballero ME, Montero MP (2011) Functional and bioactive properties of collagen and gelatin from alternative sources: a review. *Food Hydrocoll* 25:1813–1827. <https://doi.org/10.1016/j.foodhyd.2011.02.007>
- Gou M, Qu X, Zhu W et al (2014) Bio-inspired detoxification using 3D-printed hydrogel nanocomposites. *Nat Commun* 5:3774. <https://doi.org/10.1038/ncomms4774>
- Gregor A, Hošek J (2011) 3D printing methods of biological scaffolds used in tissue engineering. *Rom Rev Precis Mech Opt Mechatronics* 3:143–148
- Grzesik WJ, Robey PG (1994) Bone matrix RGD glycoproteins: immunolocalization bone cells in vitro. *J Bone Miner Res* 9:487–496

- Hao T, Wen N, Cao JK et al (2010) The support of matrix accumulation and the promotion of sheep articular cartilage defects repair in vivo by chitosan hydrogels. *Osteoarthritis Cartilage* 18:257–265. <https://doi.org/10.1016/j.joca.2009.08.007>
- Hockaday L, Kang KH, Colangelo NW et al (2012) Rapid 3D printing of anatomically accurate and mechanically heterogeneous aortic valve hydrogel scaffolds. *Biofabrication* 4:035005. <https://doi.org/10.1088/1758-5082/4/3/035005>
- Homenick CM, de Silveira G, Sheardown H, Adronov A (2011) Pluronics as crosslinking agents for collagen: novel amphiphilic hydrogels. *Polym Int* 60:458–465. <https://doi.org/10.1002/pi.2969>
- Hong Y, Song H, Gong Y et al (2007) Covalently crosslinked chitosan hydrogel: properties of in vitro degradation and chondrocyte encapsulation. *Acta Biomater* 3:23–31. <https://doi.org/10.1016/j.actbio.2006.06.007>
- Hsiao AY, Torisawa YS, Tung YC et al (2009) Microfluidic system for formation of PC-3 prostate cancer co-culture spheroids. *Biomaterials* 30:3020–3027. <https://doi.org/10.1016/j.biomaterials.2009.02.047>
- Hussain I, Hussain SZ, Habib-ur-Rehman et al (2010) In situ growth of gold nanoparticles on latent fingerprints-from forensic applications to inkjet printed nanoparticle patterns. *Nanoscale* 2:2575–2578. <https://doi.org/10.1039/c0nr00593b>
- Jakab K, Norotte C, Marga F et al (2010) Tissue engineering by self-assembly and bio-printing of living cells. *Biofabrication* 2:22001
- Jakob PH, Kehrler J, Flood P et al (2016) A 3-D cell culture system to study epithelia functions using microcarriers. *Cytotechnology* 1–13. <https://doi.org/10.1007/s10616-015-9935-0>
- Jang J, Kim TG, Kim BS et al (2016) Tailoring mechanical properties of decellularized extracellular matrix bioink by vitamin B2-induced photo-crosslinking. *Acta Biomater* 33:88–95. <https://doi.org/10.1016/j.actbio.2016.01.013>
- Jeon O, Song SJ, Lee K-J et al (2007) Mechanical properties and degradation behaviors of hyaluronic acid hydrogels cross-linked at various cross-linking densities. *Carbohydr Polym* 70:251–257. <https://doi.org/10.1016/j.carbpol.2007.04.002>
- Jia J, Richards DJ, Pollard S et al (2014) Engineering alginate as bioink for bioprinting. *Acta Biomater* 10:4323–4331. <https://doi.org/10.1016/j.actbio.2014.06.034>
- Jungst T, Smolan W, Schacht K et al (2016) Strategies and molecular design criteria for 3D printable hydrogels. *Chem Rev* 116:1496–1539. <https://doi.org/10.1021/acs.chemrev.5b00303>
- Katakai T, Hara T, Lee JH et al (2004) A novel reticular stromal structure in lymph node cortex: an immuno-platform for interactions among dendritic cells, T cells and B cells. *Int Immunol* 16:1133–1142. <https://doi.org/10.1093/intimm/dxh113>
- Ker EDF, Chu B, Phillippi J et al (2011) Engineering spatial control of multiple differentiation fates within a stem cell population. *Biomaterials* 32:3413–3422. <https://doi.org/10.1016/j.biomaterials.2011.01.036>
- Kesti M, Eberhardt C, Pagliccia G et al (2015) Bioprinting complex cartilaginous structures with clinically compliant biomaterials. *Adv Funct Mater* 25:7406–7417. <https://doi.org/10.1002/adfm.201503423>
- Khalil S, Sun W (2009) Bioprinting endothelial cells with alginate for 3D tissue constructs. *J Biomech Eng* 131:111002. <https://doi.org/10.1115/1.3128729>
- Khalil S, Nam J, Sun W (2005) Multi-nozzle deposition for construction of 3-D biopolymer tissue scaffolds. *Rapid Prototyp J* 11:9–17
- Khoda A, Ozbolat IT, Koc B (2011) Engineered tissue scaffolds with variational porous architecture. *J Biomech Eng* 133:011001. <https://doi.org/10.1115/1.4002933>
- Kleinman HK, Martin GR (2005) Matrigel: basement membrane matrix with biological activity. *Semin Cancer Biol* 15:378–386. <https://doi.org/10.1016/j.semcancer.2005.05.004>
- Kobayashi K, Huang C, Lodge TP (1999) Thermoreversible gelation of aqueous methylcellulose solutions. *Macromolecules* 32:7070–7077. <https://doi.org/10.1021/ma990242n>
- Landers R, Hübner U, Schmelzeisen R, Mülhaupt R (2002) Rapid prototyping of scaffolds derived from thermoreversible hydrogels and tailored for applications in tissue engineering. *Biomaterials* 23:4437–4447. [https://doi.org/10.1016/S0142-9612\(02\)00139-4](https://doi.org/10.1016/S0142-9612(02)00139-4)

- Lee W, Lee V, Polio S et al (2010a) On-demand three-dimensional freeform fabrication of multi-layered hydrogel scaffold with fluidic channels. *Biotechnol Bioeng* 105:1178–1186. <https://doi.org/10.1002/bit.22613>
- Lee Y-B, Polio S, Lee W et al (2010b) Bio-printing of collagen and VEGF-releasing fibrin gel scaffolds for neural stem cell culture. *Exp Neurol* 223:645–652. <https://doi.org/10.1016/j.expneurol.2010.02.014>
- Levato R, Visser J, Planell J et al (2014) Biofabrication of tissue constructs by 3D bioprinting of cell-laden microcarriers. *Biofabrication* 6:35020
- Li C, Faulkner-Jones A, Dun AR et al (2015a) Rapid formation of a supramolecular polypeptide-DNA hydrogel for in situ three-dimensional multilayer bioprinting. *Angew Chem Int Ed Engl* 1–6. <https://doi.org/10.1002/anie.201411383>
- Li H, Dai Y, Shu J, et al (2015b) Spheroid cultures promote the stemness of corneal stromal cells. *Tissue Cell* 47:39–48. <https://doi.org/10.1016/j.tice.2014.10.008>
- Liu JY, Hafner J, Dragieva G et al (2004) Autologous cultured keratinocytes on porcine gelatin microbeads effectively heal chronic venous leg ulcers. *Wound Repair Regen* 12:148–156. <https://doi.org/10.1111/j.1067-1927.2004.012205.x>
- Lopes AJ, Lee IH, Macdonald E et al (2014) Laser curing of silver-based conductive inks for in situ 3D structural electronics fabrication in stereolithography. *J Mater Process Technol* 214:1935–1945. <https://doi.org/10.1016/j.jmatprotec.2014.04.009>
- Lott JR, McAllister JW, Arvidson S et al (2013) Fibrillar structure of methylcellulose hydrogels. *Biomacromolecules* 14:2484–2488. <https://doi.org/10.1021/bm400694r>
- Ma L, Gao C, Mao Z et al (2003) Collagen/chitosan porous scaffolds with improved biostability for skin tissue engineering. *Biomaterials* 24:4833–4841. [https://doi.org/10.1016/S0142-9612\(03\)00374-0](https://doi.org/10.1016/S0142-9612(03)00374-0)
- Malda J, van Blitterswijk C, Grojec M et al (2003) Expansion of bovine chondrocytes on microcarriers enhances redifferentiation. *Tissue Eng* 9:939–948. <https://doi.org/10.1089/107632703322495583>
- Malda J, Visser J, Melchels FP et al (2013) 25th anniversary article: engineering hydrogels for biofabrication. *Adv Mater* 25:5011–5028. <https://doi.org/10.1002/adma.201302042>
- Markstedt K, Mantas A, Tournier I et al (2015) 3D bioprinting human chondrocytes with nanocellulose-alginate bioink for cartilage tissue engineering applications. *Biomacromolecules* 150325142328001. <https://doi.org/10.1021/acs.biomac.5b00188>
- Mehesz AN, Brown J, Hajdu Z et al (2011) Scalable robotic biofabrication of tissue spheroids. *Biofabrication* 3:25002
- Melchels FPW, Dhert WJ, Hutmacher DW, Malda J (2014) Development and characterisation of a new bioink for additive tissue manufacturing. *J Mater Chem B* 2:2282. <https://doi.org/10.1039/c3tb21280g>
- Melchels FPW, Blokzijl MM, Levato R et al (2016) Hydrogel-based reinforcement of 3D bioprinted constructs. *Biofabrication* 8:035004. <https://doi.org/10.1088/1758-5090/8/3/035004>
- Mewis J, Wagner NJ (2009) Thixotropy. *Adv Colloid Interface Sci* 147–148:214–227. <https://doi.org/10.1016/j.cis.2008.09.005>
- Mironov V, Boland T, Trusk T et al (2003) Organ printing: computer-aided jet-based 3D tissue engineering. *Trends Biotechnol* 21:157–161. [https://doi.org/10.1016/S0167-7799\(03\)00033-7](https://doi.org/10.1016/S0167-7799(03)00033-7)
- Mironov V, Visconti RP, Kasyanov V et al (2009) Organ printing: tissue spheroids as building blocks. *Biomaterials* 30:2164–2174
- Mironov V, Kasyanov V, Markwald RR (2011) Organ printing: from bioprinter to organ biofabrication line. *Curr Opin Biotechnol* 22:667–673. <https://doi.org/10.1016/j.copbio.2011.02.006>
- Mogas-Soldevila L, Duro-Royo J, Oxman N (2014) Water-based robotic fabrication: large-scale additive manufacturing of functionally graded hydrogel composites via multichamber extrusion. *3D Print Addit Manuf* 1:141–151. <https://doi.org/10.1089/3dp.2014.0014>
- Mooney R, Haeger S, Lawal R et al (2011) Control of neural cell composition in poly(ethylene glycol) hydrogel culture with soluble factors. *Tissue Eng Part A* 17:2805–2815. <https://doi.org/10.1089/ten.tea.2010.0654>

- Müller M, Becher J, Schnabelrauch M, Zenobi-Wong M (2015) Nanostructured pluronic hydrogels as bioinks for 3D bioprinting. *Biofabrication* 7:035006. <https://doi.org/10.1088/1758-5090/7/3/035006>
- Murphy SV, Skardal A, Atala A (2013) Evaluation of hydrogels for bio-printing applications. *J Biomed Mater Res Part A* 101(A):272–284. <https://doi.org/10.1002/jbm.a.34326>
- Norotte C, Marga FS, Niklason LE, Forgacs G (2009) Scaffold-free vascular tissue engineering using bioprinting. *Biomaterials* 30:5910–5917. <https://doi.org/10.1016/j.biomaterials.2009.06.034>
- Odde DJ, Renn MJ (2000) Laser-guided direct writing of living cells. *Biotechnol Bioeng* 67:312
- Ong SY, Wu J, Moochhala SM et al (2008) Development of a chitosan-based wound dressing with improved hemostatic and antimicrobial properties. *Biomaterials* 29:4323–4332. <https://doi.org/10.1016/j.biomaterials.2008.07.034>
- Overstreet M, Sohrabi A, Polotsky A et al (2003) Collagen microcarrier spinner culture promotes osteoblast proliferation and synthesis of matrix proteins. *In Vitro Cell Dev Biol Anim* 39:228–234. [https://doi.org/10.1290/1543-706X\(2003\)039](https://doi.org/10.1290/1543-706X(2003)039)
- Oxlund H, Andreassen TT (1980) The roles of hyaluronic acid, collagen and elastin in the mechanical properties of connective tissues. *J Anat* 131:611–620
- Ozbolat IT (2015a) Bioprinting scale-up tissue and organ constructs for transplantation. *Trends Biotechnol* 33:395–400. <https://doi.org/10.1016/j.tibtech.2015.04.005>
- Ozbolat IT (2015b) Scaffold-based or scaffold-free bioprinting: competing or complementing approaches? *J Nanotechnol Eng Med*. <https://doi.org/10.1115/1.4030414>
- Ozbolat IT, Hospodiuk M (2016) Current advances and future perspectives in extrusion-based bioprinting. *Biomaterials* 76:321–343. <https://doi.org/10.1016/j.biomaterials.2015.10.076>
- Ozbolat IT, Koc B (2010) Modeling of spatially controlled biomolecules in three-dimensional porous alginate structures. *J Med Devices* 4:041003. <https://doi.org/10.1115/1.4002612>
- Ozbolat IT, Koc B (2011) Multi-function based modeling of 3D heterogeneous wound scaffolds for improved wound healing. *Comput Aided Des Applic* 8:43–57. <https://doi.org/10.3722/cadaps.2011.43-57>
- Ozbolat IT, Chen H, Yu Y (2014) Development of “multi-arm bioprinter” for hybrid biofabrication of tissue engineering constructs. *Robot Comput Integr Manuf* 30:295–304. <https://doi.org/10.1016/j.rcim.2013.10.005>
- Pardo L, Wilson WC, Boland T (2003) Characterization of patterned self-assembled monolayers and protein arrays generated by the ink-jet method. *Langimur* 19:1462–1466
- Park JY, Choi J-C, Shim J-H et al (2014) A comparative study on collagen type I and hyaluronic acid dependent cell behavior for osteochondral tissue bioprinting. *Biofabrication* 6:035004. <https://doi.org/10.1088/1758-5082/6/3/035004>
- Pati F, Jang J, Ha D-H et al (2014) Printing three-dimensional tissue analogues with decellularized extracellular matrix bioink. *Nat Commun* 5:3935. <https://doi.org/10.1038/ncomms4935>
- Pati F, Ha D, Jang J et al (2015a) Biomimetic 3D tissue printing for soft tissue regeneration. *Biomaterials* 62:164–175. <https://doi.org/10.1016/j.biomaterials.2015.05.043>
- Pati F, Jang J, Lee JW, Cho DW (2015b) Extrusion bioprinting. *Essentials of 3D biofabrication and translation*. <https://doi.org/10.1016/B978-0-12-800972-7.00007-4>
- Pfister A, Landers R, Laib A et al (2004) Biofunctional rapid prototyping for tissue-engineering applications: 3D bioplotting versus 3D printing. *J Polym Sci Part A Polym Chem* 42:624–638. <https://doi.org/10.1002/pola.10807>
- Poldervaart MT, Wang H, van der Stok J et al (2013) Sustained release of BMP-2 in bioprinted alginate for osteogenicity in mice and rats. *PLoS One* 8:e72610. <https://doi.org/10.1371/journal.pone.0072610>
- Ren X, Kim Y, Zhou J (2013) Design and fabrication of chitosan for application of artificial photosynthesis. *J Mech Eng Automat* 3:739–746
- Rinaudo M (2006) Chitin and chitosan: properties and applications. *Prog Polym Sci* 31:603–632. <https://doi.org/10.1016/j.progpolymsci.2006.06.001>
- Rowley JA, Madlambayan G, Mooney DJ (1999) Alginate hydrogels as synthetic extracellular matrix materials. *Biomaterials* 20:45–53. [https://doi.org/10.1016/S0142-9612\(98\)00107-0](https://doi.org/10.1016/S0142-9612(98)00107-0)

- Rücker M, Laschke MW, Junker D et al (2006) Angiogenic and inflammatory response to biodegradable scaffolds in dorsal skinfold chambers of mice. *Biomaterials* 27:5027–5038. <https://doi.org/10.1016/j.biomaterials.2006.05.033>
- Serwer P, Allen JL, Hayes SJ (1983) Agarose gel electrophoresis of bacteriophages and related particles III. Dependence of gel sieving on the agarose preparation. *Electrophoresis* 4:232–236. <https://doi.org/10.1002/elps.1150040309>
- Shikani AH, Fink DJ, Sohrabi A et al (2004) Propagation of human nasal chondrocytes in microcarrier spinner culture. *Am J Rhinol* 18:105–112
- Skardal A, Atala A (2014) Biomaterials for integration with 3-D bioprinting. *Ann Biomed Eng.* <https://doi.org/10.1007/s10439-014-1207-1>
- Skardal A, Sarker SF, Crabbé A et al (2010a) The generation of 3-D tissue models based on hyaluronan hydrogel-coated microcarriers within a rotating wall vessel bioreactor. *Biomaterials* 31:8426–8435. <https://doi.org/10.1016/j.biomaterials.2010.07.047>
- Skardal A, Zhang J, McCoard L et al (2010b) Photocrosslinkable hyaluronan-gelatin hydrogels for two-step bioprinting. *Tissue Eng Part A* 16:2675–2685. <https://doi.org/10.1089/ten.TEA.2009.0798>
- Smith CM, Stone A, Stewart RL et al (2004) Three-dimensional bioassembly tool for generating viable tissue-engineered constructs. *Tissue Eng* 10:1566–1576
- Snyder JE, Hamid Q, Wang C et al (2011) Bioprinting cell-laden matrigel for radioprotection study of liver by pro-drug conversion in a dual-tissue microfluidic chip. *Biofabrication* 3:034112. <https://doi.org/10.1088/1758-5082/3/3/034112>
- Thirumala S, Gimble J, Devireddy R (2013) Methylcellulose based thermally reversible hydrogel system for tissue engineering applications. *Cells* 2:460–475. <https://doi.org/10.3390/cells2030460>
- Torisawa Y, Mosadegh B, Luker GD et al (2009) Microfluidic hydrodynamic cellular patterning for systematic formation of co-culture spheroids. *Integr Biol (Camb)* 1:649–654. <https://doi.org/10.1039/b915965g>
- Trojani C, Weiss P, Michiels JF et al (2005) Three-dimensional culture and differentiation of human osteogenic cells in an injectable hydroxypropylmethylcellulose hydrogel. *Biomaterials* 26:5509–5517. <https://doi.org/10.1016/j.biomaterials.2005.02.001>
- Van Den Bulcke I, Bogdanov B, De Rooze N et al (2000) Structural and rheological properties of methacrylamide modified gelatin hydrogels. *Biomacromolecules* 1:31–38. <https://doi.org/10.1021/bm990017d>
- Veronese FM, Pasut G (2005) PEGylation, successful approach to drug delivery. *Drug Discov Today* 10:1451–1458. [https://doi.org/10.1016/S1359-6446\(05\)03575-0](https://doi.org/10.1016/S1359-6446(05)03575-0)
- Vinatier C, Magne D, Weiss P et al (2005) A silanized hydroxypropyl methylcellulose hydrogel for the three-dimensional culture of chondrocytes. *Biomaterials* 26:6643–6651. <https://doi.org/10.1016/j.biomaterials.2005.04.057>
- Vozzi G, Previti A, De Rossi D, Ahluwalia A (2002) Microsyringe-based deposition of two-dimensional and three-dimensional polymer scaffolds with a well-defined geometry for application to tissue engineering. *Tissue Eng* 8:1089–1098. <https://doi.org/10.1089/107632702320934182>
- Wang X, Yan Y, Pan Y et al (2006) Generation of three-dimensional hepatocyte/gelatin structures with rapid prototyping system. *Tissue Eng* 12:83–90. <https://doi.org/10.1089/ten.2006.12.ft-16>
- Wang Z, Wu W, Yang Q et al (2009) In-situ fabrication of flexible vertically integrated electronic circuits by inkjet printing. *J Alloys Compd* 486:706–710. <https://doi.org/10.1016/j.jallcom.2009.07.044>
- Wei Xu, Xiaohong Wang, Yongnian Yan, et al (2007) Rapid prototyping three-dimensional cell/gelatin/fibrinogen constructs for medical regeneration. *J Bioact Compat Polym* 22:363–377. <https://doi.org/10.1177/0883911507079451>
- Wu PK, Ringeisen BR (2010) Development of human umbilical vein endothelial cell (HUVEC) and human umbilical vein smooth muscle cell (HUVSMC) branch/stem structures on hydrogel

- layers via biological laser printing (BioLP). *Biofabrication* 2:014111. <https://doi.org/10.1088/1758-5082/2/1/014111>
- Wu C, Luo Y, Cuniberti G et al (2011a) Three-dimensional printing of hierarchical and tough mesoporous bioactive glass scaffolds with a controllable pore architecture, excellent mechanical strength and mineralization ability. *Acta Biomater* 7:2644–2650. <https://doi.org/10.1016/j.actbio.2011.03.009>
- Wu W, DeConinck A, Lewis J (2011b) Omnidirectional printing of 3D microvascular networks. *Adv Mater* 23:H178–H183. <https://doi.org/10.1002/adma.201004625>
- Wüst S, Müller R, Hofmann S (2014) 3D bioprinting of complex channels – effects of material, orientation, geometry and cell embedding. *J Biomed Mater Res A*. <https://doi.org/10.1002/jbm.a.35393>
- Xing Q, Yates K, Vogt C et al (2014) Increasing mechanical strength of gelatin hydrogels by divalent metal ion removal. *Sci Rep* 4:4706. <https://doi.org/10.1038/srep04706>
- Xu T, Gregory C, Molnar P et al (2006) Viability and electrophysiology of neural cell structures generated by the inkjet printing method. *Biomaterials* 27:3580–3588. <https://doi.org/10.1016/j.biomaterials.2006.01.048>
- Yang S, Leong K-F, Du Z, Chua C-K (2002) The design of scaffolds for use in tissue engineering. Part II. Rapid prototyping techniques. *Tissue Eng* 8:1–11. <https://doi.org/10.1089/107632702753503009>
- Ye K, Felimban R, Traianedes K et al (2014) Chondrogenesis of infrapatellar fat pad derived adipose stem cells in 3D printed chitosan scaffold. *PLoS One*. <https://doi.org/10.1371/journal.pone.0099410>
- Yu Y, Ozbolat IT (2014) Tissue strands as “bioink” for scale-up organ printing. *Conf Proc IEEE Eng Med Biol Soc* 2014:1428–1431. <https://doi.org/10.1109/EMBC.2014.6943868>
- Yu Y, Brouillette MJ, Seol D et al (2012) Functional full-thickness articular cartilage repair by rhSDF-1 α loaded fibrin/HA hydrogel network via chondrogenic progenitor cells homing. *Arthritis Rheum* 1–30. <https://doi.org/10.1002/art>
- Yu Y, Zhang Y, Martin J, Ozbolat IT (2013) Evaluation of cell viability and functionality in vessel-like bioprintable cell-laden tubular channels. *J Biomech Eng* 135:91011. <https://doi.org/10.1115/1.4024575>
- Yu Y, Zhang Y, Ozbolat IT (2014) A hybrid bioprinting approach for scale-up tissue fabrication. *J Manuf Sci Eng* 136:061013. <https://doi.org/10.1115/1.4028511>
- Zhang M, Desai T, Ferrari M (1998) Proteins and cells on PEG immobilized silicon surfaces. *Biomaterials* 19:953–960. [https://doi.org/10.1016/S0142-9612\(98\)00026-X](https://doi.org/10.1016/S0142-9612(98)00026-X)
- Zhang Y, Venugopal JR, El-Turki A et al (2008) Electrospun biomimetic nanocomposite nanofibers of hydroxyapatite/chitosan for bone tissue engineering. *Biomaterials* 29:4314–4322. <https://doi.org/10.1016/j.biomaterials.2008.07.038>
- Zhang L, Huang J, Si T, Xu RX (2012) Coaxial electrospray of microparticles and nanoparticles for biomedical applications. *Changes* 29:997–1003
- Zhang Y, Yu Y, Ozbolat IT (2013) Direct bioprinting of vessel-like tubular microfluidic channels. *J Nanotechnol Eng Med* 4:020902. <https://doi.org/10.1115/1.4024398>
- Zhang Y, Yu Y, Akkouch A et al (2015) In vitro study of directly bioprinted perfusable vasculature conduits. *Biomater Sci* 3:134–143. <https://doi.org/10.1039/C4BM00234B>



Inkjet Printing for Biofabrication

Xinda Li, Jianwei Chen, Boxun Liu, Xiong Wang, Dongni Ren, and Tao Xu

Contents

1	Introduction	284
2	Inkjet Cell Printing	288
3	Inkjet-Mediated Gene Transfection and Inkjet Printing Biology Molecule	292
4	Application of Inkjet Bioprinting	295

X. Li

Biomufacturing Center, Department of Mechanical Engineering, Tsinghua University, Beijing, People's Republic of China
e-mail: li-xd15@mails.tsinghua.edu.cn

J. Chen · B. Liu

Department of Precision Medicine and Healthcare, Tsinghua-Berkeley Shenzhen Institute, Shenzhen, People's Republic of China
e-mail: chenjw17@mails.tsinghua.edu.cn; lbx16@mails.tsinghua.edu.cn

X. Wang

Biomufacturing Engineering Research Laboratory, Graduate School at Shenzhen Tsinghua University, Shenzhen, People's Republic of China
e-mail: xiong-wa15@mails.tsinghua.edu.cn

D. Ren

Medprin Regenerative Medical Technologies Co., Ltd., Guangzhou, Guangdong, People's Republic of China
e-mail: dongniren742@yahoo.com

T. Xu (✉)

Biomufacturing Center, Department of Mechanical Engineering, Tsinghua University, Beijing, People's Republic of China

Department of Precision Medicine and Healthcare, Tsinghua-Berkeley Shenzhen Institute, Shenzhen, People's Republic of China

Biomufacturing Engineering Research Laboratory, Graduate School at Shenzhen Tsinghua University, Shenzhen, People's Republic of China
e-mail: taoxu@mail.tsinghua.edu.cn

5 Conclusion	297
References	298

Abstract

Inkjet printing is a noncontact printing technology with high resolution, high throughput, and considerable reproducibility. Instead of printing normal ink, inkjet technology is also applied in the field of biofabrication to print living cells and other biological factors. Cell viability and function were demonstrated to be sustained after printing. Besides two dimensional cell patterns, three-dimensional cell-laden hydrogel structures can also be inkjet printed through cross-linking. Special phenomena such as the temporary permeability change of cell membranes were also observed during printing procedures, thus making it possible to achieve gene transfection through inkjet printing. Inkjet-printed biomolecule patterns with gradient concentration were also used to direct cell fates. Since the diversity of bioink and the capability of fabricating complex structures, inkjet bioprinting behaves as an effective tool in the field of biofabrication. The applications of inkjet printing include but not limit to drug formulation, tissue repair, and cancer research.

1 Introduction

Inkjet printers, based on a noncontact printing technology, are widely used to print computer data onto paper for family users or print information onto cans and bottles for industrial users, which account for major part of printers used for color printing in offices (Le 1998; Svanholm 2007). Figure 1 shows the technology map of inkjet printing (Fig. 1).

In 1878, Lord Rayleigh first described the mechanism of a liquid stream breaking up into droplets, establishing the theoretical foundation for liquid jets (Rayleigh 1878). In 1931, Weber illustrated the formation of droplets from the breakup of viscous liquid jets (Weber 1931). In 1951, Rune Elmqvist of Siemens-Elsa patented the first inkjet device on the basis of the Rayleigh and Weber's breakup inkjet theories (Rune 1951). Henceforth, many researchers paid much attention on controlling the drop break-off mechanism to improve the image quality.

In 1965, Dr. Sweet from Stanford University achieved droplets with uniform size and spacing from the ink steam by applying a pressure wave pattern to the orifice (Sweet 1965). Then, one of the first continuous inkjet (CIJ) printers was produced by Dr. Sweet. The continuous inkjet printer systems can be divided into two categories, including binary deflection system and multiple deflection system. For the multiple deflection system, some droplets are charged to deflect to the media at different levels to form patterns as they pass through an electric field, while uncharged droplets fly straight to a gutter for recirculation (Le 1998). This idea was commercialized by IBM; IBM 4640 inkjet printer was introduced in 1976. Continuous inkjet printing is mainly used for high-speed printing such as textile printing and labeling (De Gans et al. 2004).

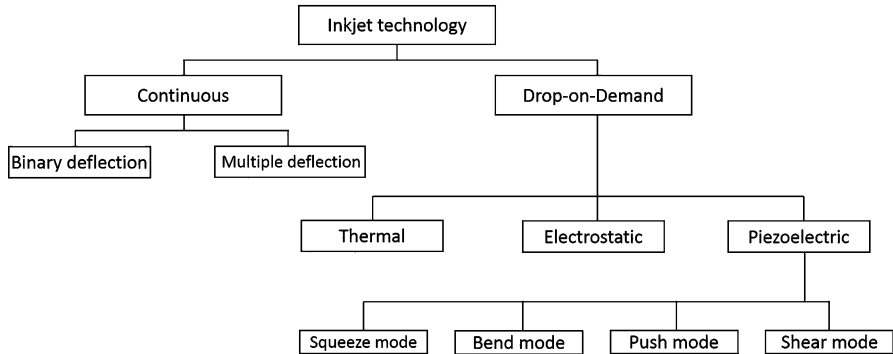


Fig. 1 Inkjet printing technology map

While continuous inkjet technology was commercialized, the development of drop-on-demand inkjet method also emerged. Unlike the continuous inkjet printers, the drop-on-demand inkjet printers eject ink droplets only when they are used for imaging on the media. This new method overcomes the disadvantages of continuous inkjet such as the complexity of drop charging, the deflection hardware, and the unreliability of the ink recirculation system (Le 1998). In addition, drop-on-demand inkjet printers selectively generate droplets, which can lower the cost and are easy to control and user friendly (Gudapati et al. 2016). Zoltan et al. composed the first group to study drop-on-demand inkjet systems (Zoltan 1972; Kyser and Sears 1980). Many drop-on-demand ideas were commercialized in the 1970s and 1980s. It turned out that drop-on-demand inkjet systems were more reliable than continuous inkjet systems.

According to different driving force, drop-on-demand inkjet methods can be divided into three categories, such as thermal inkjet printing, electrostatic inkjet printing, and piezoelectric inkjet (PIJ) printing (Cui et al. 2012a).

The thermal inkjet printer is not the first commercial product but the most successful printer on the market today. The thermal inkjet system consists of an ink chamber, a thermal actuator, and nozzles (Fig. 2a). A short current pulse is applied to the thermal actuator located in the ink chamber near the nozzle to generate ink droplets (Dababneh and Ozbolat 2014). Consequently, the temperature of the ink near the thermal actuator increases to 300 °C, which is higher than the bubble nucleation temperature, and lasts for a few microseconds during printing (Hudson et al. 2000). Then, the bubble emerges and forces the ink out of the nozzle orifice. The droplet formation could be controlled by adjusting the current pulse. The size of droplets varies due to the applied temperature gradient, usually by current pulse and ink viscosity (Hudson et al. 2000; Hock et al. 1996; Canfield et al. 1997).

Electrostatic inkjet printers generate droplets by changing the volume of the fluid chamber (Fig. 2b). The driven force depends on the coulomb force between charges. The charged pressure plate could lead a brief increase in the volume of the fluid chamber so that the ink in reservoir flows into the fluid chamber. When voltage is turned off, the pressure plate restores to the original shape. Consequently, the

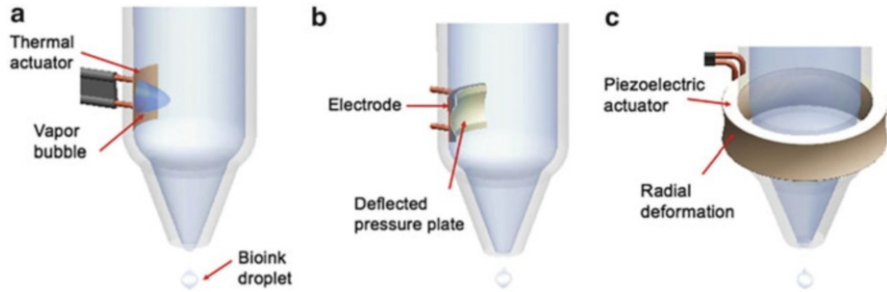


Fig. 2 Mechanisms of droplet-based printing. (a) Thermal inkjet printing, (b) electrostatic inkjet printing, (c) piezoelectric inkjet printing (Reprinted from A comprehensive review on droplet-based bioprinting: Past, present and future, 102, Gudapati et al., Tissue engineering and regeneration. 3d printing and biofabrication, Copyright (2016), with permission from Elsevier)

suddenly increased pressure forces droplets out (Kamisuki et al. 2000). Electrostatic inkjet printing method is also suitable for solid ink. Kamisuki developed static-electricity actuator inkjet in 1998 (Kamisuki et al. 1998). The electric power consumption is quite low due to its electrostatic driven force. Generally, electrostatic inkjet printing is still in its infancy that commercial electrostatic inkjet printers are still rather rare.

Piezoelectric inkjet printing method is similar to thermal inkjet printing method (Fig. 2c). The voltage pulse makes piezoelectric actuator change its shape and then deforms the fluid chamber (Gudapati et al. 2016). The sudden change in the fluid chamber volume leads a pressure variation. Consequently, a droplet is ejected by overcoming the surface tension of the nozzle orifice. Since Zoltan developed the first piezoelectric inkjet printer, there have been four different types of printheads used in piezoelectric inkjet printing. They are squeeze mode, bend mode, push mode, and shear mode printhead, respectively.

It can be concluded from the previous part that the two most dominant drop-on-demand inkjet printing methods are based on thermal and piezoelectric effects. In the initial stage, thermal inkjet printing was more popular due its low cost. However, the application of thermal inkjet printing is limited by the bubble mechanism which is only suitable for part of the ink. Piezoelectric inkjet printing method is more commonly used when printing functional materials, as there is no risk of thermal degradation and damage of the ink or need to use ink only with a specific nucleation temperature.

In recent years, much effort has been invested in expanding the application of inkjet printing via replacing conventional ink with conductive materials, polymers, biomaterials, and cells (Cummins and Desmulliez 2012). As mentioned above, inkjet printing has many advantageous characteristics, such as drop-on-demand printing, precise printing with very small ink droplets, noncontact printing, high-speed printing with multiple nozzles, and completely digitalized printing as an output of computer. On the other hand, scaffold-based tissue engineering was the most major approach in tissue engineering in the 1990s. After Langer and Vacanti

Table 1 Characteristics of inkjet technology and advantages for tissue engineering (Nakamura 2012)

	Characteristics of inkjet technology	Advantages for tissue engineering
1	High resolution Extremely small ink droplets	For manufacturing of microscopic structures with cellular-sized resolution Micro to macro, multiscaled fabrication
2	Drop-on-demand printing	Enabling on-demand direct cell printing
3	Direct printing of ink droplets	For direct arrangement of cells and materials for biofabrication
4	Color printing	For fabrication of composite products with different cells, materials, and growth factors
5	High-speed printing more than 10 kHz Per one nozzle Multi-nozzle system can be integrated	Handling massive amount of individual cells Rapid fabrication Lessens cell damage during fabrication
6	3D fabrication using hydrogels	Enabling 3D construction by layer-by-layer printing Enabling to printing living cells For prevention from drying Enabling 3D fabrication into the liquid
7	Linkage to digital data sources	For digital printing Easy to apply to computer-aided biofabrication For CAD-, CAM-, and CAE-based biofabrication
8	Noncontact printing	Usability of reactive materials Preventive effects for friction or contact damages
9	Printability of several inks; aqueous inks, pigment inks, suspension of several materials, and reactive solution	Printing biological materials; cell proteins, DNAs, biopolymers, humoral factors, drugs, and nanomaterials
10	Printability onto several subjects; papers, solid mass, disc, dishes, gels, and aqueous solution	Printable onto gels, aqueous solution, cell sheets; directly printing onto the tissues, organs, and wounds during surgical operation

proposed the concept of tissue engineering (Langer and Vacanti 1993), some breakthrough were desired to overcome several limitations, which included difficulties in the control of cell position and distribution, composition of multicell types, inner structures of 3D constructs, distribution of growth factors, and induction of blood vessels. Then, the challenging studies using inkjet printing were started in fabrication of 3D scaffolds and indirect printing of cells. In this way, bioprinting was started, which is sometimes called organ printing, jet-based tissue engineering. Nakamura has summarized the characteristics of inkjet technology and its advantages for tissue engineering in Table 1 (Nakamura 2012).

Then, several innovative concepts of bioprinting were proposed, such as the concepts of tissue engineering based on blueprint (bio-CAD), bioink (cells, biomaterials, and bioactive factors), bioprinter (bio-CAM, bio-CAM

machine), biopaper (printing onto some designed scaffolds or bio-substrates), and bio-products (2D and 3D bio-constructs) as final products. This process is just compatible for the concept of computer-aided tissue engineering (Sun and Lal 2002; Mironov et al. 2003). In addition, laminated printing developed 3D bioprinting or digital biofabrication or bottom-up tissue manufacturing, too. Although recently 3D printing procedure is called additive manufacturing, this concept is just same as inkjet 3D bioprinting in tissue engineering. In this way, several concepts and strategies have been proposed and many challenging researches on bioprinting were started.

The increasing studies showed that printed cells retained their growth-promoting properties which provided new approaches in regenerative medicine (Xu et al. 2005, 2006; Cui and Boland 2009).

2 Inkjet Cell Printing

Xu et al. used a modified commercial inkjet printer to deliver viable cells for the first time (Xu et al. 2004). In their study, *Escherichia coli* DH5 α cells were blended with sterilized water at a concentration of 3×10^7 cells/ml to form the bioink and then printed on soy agar substrate by a modified HP DeskJet 550C printer. The printing pattern, a colony array, was edited by Microsoft PowerPoint software, while a single colony had a circular shape with an approximate diameter of 500 μm . Some complex patterns, such as a cartoon tiger paw, were also successfully printed through this method (Fig. 3a). Xu et al. further used this printer to deposit Chinese hamster ovary cells, which showed high viability (>90%) after printing (Xu et al. 2005). This study demonstrated that mammalian cells could be printed with high viability by inkjet method for the first time, which means that inkjet printing has the potential to be utilized in tissue engineering. Based on this, cell function maintenance after inkjet printing was also proved by Xu et al. (2006). In their study, rat embryonic hippocampal and cortical neurons were printed. Immunostaining and patch-clamp analysis were further implemented to test cell function post-printing (Fig. 3b). Their results showed that printed neurons exhibited strong immunoreactivity to specific antibodies, which indicated high cell marker expression. Besides, voltage-gated potassium and sodium channels were detected on cell membrane by patch-clamp. Thus, neuronal phenotypes and electrophysiology were proved to be retained. This series of studies elucidated that living cells can be printed into predefined patterns by inkjet printing, while cell viability and cell function were maintained after passing the hot and narrow nozzle. These findings formed the foundation of inkjet cell printing.

Planar cell patterns were first created by inkjet printing in early studies (Cui and Boland 2009; Nakamura et al. 2005; Saunders et al. 2008). Briefly, cell suspensions, sometimes blended with biocompatible materials, were inkjet printed on pretreated or non-pretreated substrates. Agar, collagen (Xu et al. 2005), albumin (Yamazoe and Tanabe 2009), and fibrinogen (Cui and Boland 2009) were pre-coated on substrates

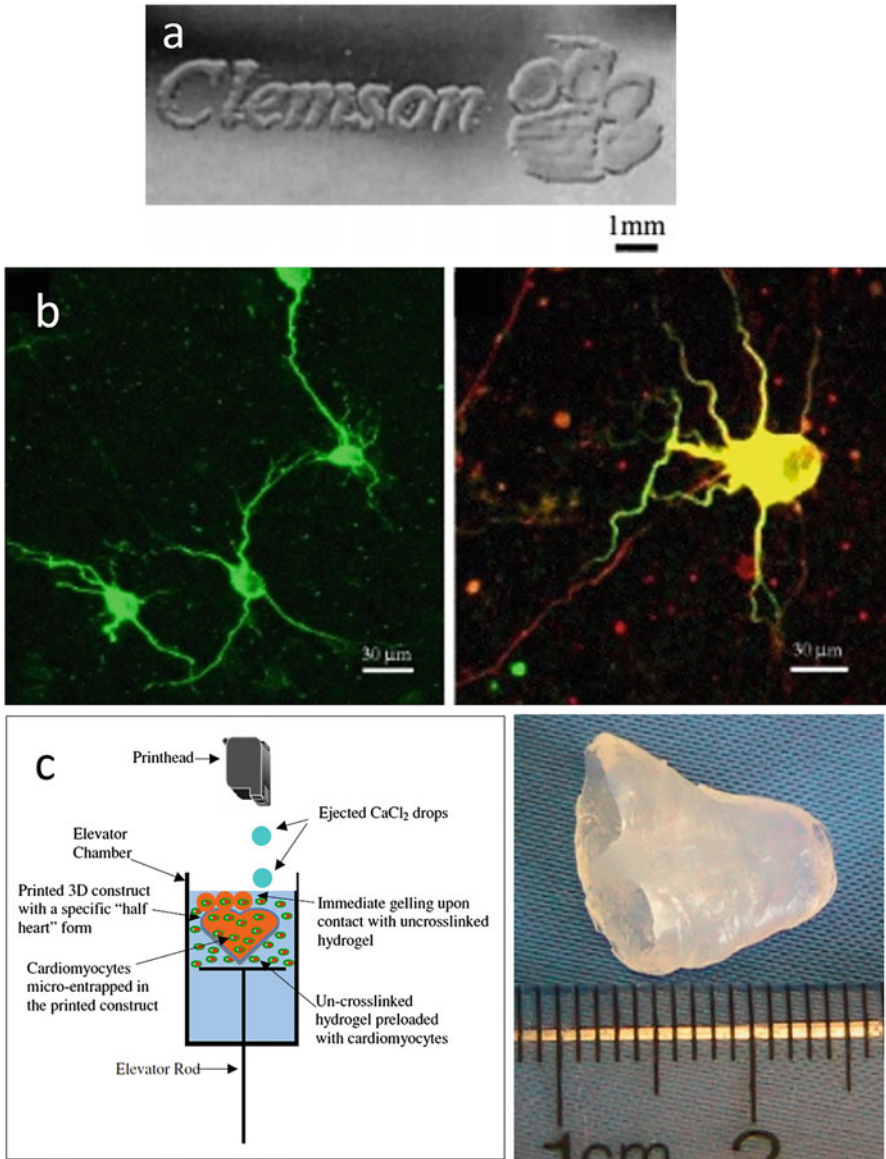


Fig. 3 (a) A 2D cartoon tiger paw printed with *Escherichia coli* DH5α cells (Xu et al. 2004). (b) Printed neurons stained with neuron markers anti-MAP 2 monoclonal antibodies (green) and anti-neurofilament monoclonal antibodies (red) after 15 days of culture (Xu et al. 2006). (c) 3D “half-heart” scaffold printed with cardiac cells (Xu et al. 2009a). Left: a schematic diagram of the printing process. Right: the real printed object

for optimal cell immobilization and modified microenvironment. Cell patterns were deposited on these substrates with droplet ejection from the multi-nozzle printheads. The diameter of a single printed dot was in micrometer magnitude, which is similar to the diameter of single cells (Nakamura et al. 2005). Meanwhile, by controlling the concentration of cell suspension, few cells could be contained in a single droplet. In some extreme conditions, only single cell was ejected within one droplet, which might have the potential to achieve single cell printing (Nakamura et al. 2005). Shuichi et al. realized this one-cell-per-droplet inkjet printing with a push–pull piezoelectric ejection method, and 100% accuracy was achieved (Yamaguchi et al. 2012). Cell viability and cell function post-printing were also evaluated in these researches. Cui et al. deposited bioink composed by human microvascular endothelial cells, thrombin, and calcium ions on a coverslip pre-coated with fibrin channel patterns (Cui and Boland 2009). After 21 days of culture, the printed endothelial cells proliferated and formed tubular structures inside the fibrin channels, which showed high functionality of the printed cells. In this work, to some extent, the printed fibrin channels could be regarded as 3D fibers with micro-diameter. It can be concluded that if these layers with defined patterns accumulated to a certain thickness, a so-called 3D structure is achieved.

3D cell-laden scaffold plays an important role in tissue or organ regeneration. A successfully constructed 3D scaffold must have structural integrity, proper mechanical strength, and cytocompatibility. The cytocompatibility of inkjet printing has been proved as mentioned above. Thus, the main concern turns to fabricate a 3D cell-laden structure with structural integrity while keeping mechanical strength by inkjet printing. However, in inkjet printing, to avoid nozzle clogging and to enable droplet formation, bioink must have low viscosity and low cell density (Murphy and Atala 2014). This restriction leads to proper cross-linking strategies which must be designed. The fibrinogen–thrombin system is one of the feasible cross-linking strategies. In this procedure, high-viscosity fibrinogen is coated on substrates as biopaper while low-viscosity thrombin is mixed with cells as bioink. Gelation occurs immediately after thrombin is ejected onto fibrinogen substrates and cells are trapped in the fibrin gel. There are some related works reported (Xu et al. 2006; Cui and Boland 2009). Another system is alginate–calcium system. Xu et al. printed calcium chloride into an alginate–gelatin–cell mixture to fabricate a “half-heart” with two connected ventricles (Fig. 3c) (Xu et al. 2009a). The alginate–gelatin–cell mixture was filled in an elevator chamber which could move along the z-axis. The chamber was lowered after one layer was printed and cross-link occurred between alginate and calcium ions. Meanwhile, new cell-laden gel was added for the fabrication of a new layer. The printed scaffolds showed adequate moduli and tensile strength. The cardiac cells embedded in the scaffold exhibited contractile properties under mild electrical stimuli *in vitro*. With a same system, collagen can also be used as extracellular matrix. Xu et al. printed an alginate–collagen tissue construct containing multiple cell types (Xu et al. 2013). This study also demonstrated the feasibility to fabricate heterogeneous tissue constructs by inkjet technology. In contrast, low-concentration cell-laden alginate solution could also be printed into calcium ion solution (Pataky et al. 2012; Arai et al. 2011). In this method,

gelation time and droplet deposit position were precisely controlled to obtain fine pattern quality. 3D tissue such as lumen structure was successfully built through this way (Xu et al. 2012; Xu 2014; Christensen et al. 2015). Poly(ethylene glycol) dimethacrylate (PEGDMA) is also inkjet-printable for its water-soluble nature, and it can be further photocross-linked to get more reasonable mechanical strength than that of cross-linked alginate or fibrinogen. Therefore, PEGDMA or similar photocross-linkable synthetic biomaterials may play an important role in bone or cartilage tissue reconstruction (Cui et al. 2012b, 2014). Besides, novel materials such as gellan gum and Pluronic F127 have been successfully used as bioink for inkjet printing (Ferris et al. 2013; Biase et al. 2011). Gellan gum has similar cross-linking mechanism as alginate but can form gels at lower concentrations. This property may allow the content of bioink to be kept at low levels while cell content will be more.

Although cell viability and phenotype have been proved to be retained after inkjet printing process, damage occurred to the cells by thermal heat or stress when passing the nozzles still exists and could not be neglected (Xu et al. 2009b; Cui et al. 2010). Thus, cell viability loss could not be eliminated and varies according to the printing parameters, droplet size, printing velocity, cell concentration, etc. Several studies focused on adjusting the printing parameters to optimize cell viability. Hendriks et al. established a model describing the cell viability as a function of droplet impact parameters (Hendriks et al. 2015). The model will certainly help to modulate the parameters to maximize cell viability. On the other hand, some changes to cells may also be caused by inkjet printing process. Tse et al. presented a study to print Schwann cells using a piezoelectric inkjet printer (Tse et al. 2016). Schwann cell is a kind of neuronal-related cell which exists in peripheral nervous systems. They have neurites elongated which will form sheaths surrounding the neuron axons. In Tse's study, inkjet-printed Schwann cells were found to generate neurites earlier than normal Schwann cells, and the neurites were longer. This result may either due to a piezoelectric effect or a transient high shear stress during ejection. At all events, this finding indicates that inkjet printing may be benefitted to produce fine neuronal networks in neural tissue engineering. Moreover, the precisely aligned cell patterns generated by printing may be more similar to their natural states, which may provide higher stage of biomimicry. Cui et al. presented a study to deposit evenly aligned mouse myoblasts onto micro-sized cantilevers by thermal inkjet printing (Cui et al. 2013). The printed myoblasts formed myotubes – a function unit in muscular system – within a few days, while randomly deposited cells took more than 14 days.

Though inkjet printing has been successfully used in 2D and 3D cell pattern fabrication and some beneficial impacts on cells have been revealed, inkjet printing technology is still not the best choice to fabricate complex 3D cell-laden constructs for several drawbacks. First, the small inkjet orifice is easy clogged, which limits a wide majority of bioinks to be used. Second, the ejected droplet may gel in air before assembling to the substrates, though printing parameters may be well controlled before printing procedures. Third, structures with high mechanical strength and structural integration could probably not be achieved by inkjet printing because of the low bioink viscosity and droplet ejecting mechanism. It is noteworthy that porous structures can hardly be fabricated by inkjet printing, which is vital to the

supply of nutrition and oxygen needed by the cells loaded in a hydrogel scaffold. Take these into account: other printing technologies, such as extrusion printing and laser-assisted printing, may be more suitable to build 3D cell-laden constructs (Gudapati et al. 2016). In our opinion, the future directions of inkjet cell printing should be built on its superiorities, for instance, multichannel, high-throughput, rapid printing speed and noncontact printing style. Multicellular or cell–molecule dot arrays can be easily printed by inkjet printing in a high-throughput and reproducible manner. Researches on cell–cell interactions or cell–drug resistance may be facilitated by this model (Choi et al. 2011; Matsusaki et al. 2013; Rodríguez-Dévora et al. 2012). On the other hand, based on its noncontact style, no strict distance limitations exist between the printing nozzle and substrates. When the surface morphology of the substrate becomes irregular, cells could also be deposited on the preset location by inkjet printing with high accuracy. This may indicate that inkjet technology could achieve *in situ* printing to directly deposit cells onto superficial wounds, thus accelerating wound healing and reducing processing steps. Finally, stem cell functionality after inkjet printing has been proved to be preserved (Xu et al. 2013). Since stem cell bioprinting has attracted significant attention due to its pluripotency and *in vitro* expansion ability, inkjet may also play a part in stem cell array printing and *in situ* stem cell printing.

3 Inkjet-Mediated Gene Transfection and Inkjet Printing Biology Molecule

In addition to print cells, inkjet printing also have capacity to print proteins, cell guidance, and combination biologics. Several reports have demonstrated the interesting side effect of thermal inkjet printing technology and apply it to gene transfection and intracellular delivery (Xu et al. 2009b; Cui et al. 2010; Shattil et al. 1992; Owczarczak et al. 2012). Xu et al. firstly introduced a novel inkjet-mediated technology that gene transfection and cell delivery can be simultaneously achieved (Xu et al. 2009b). In this study, porcine aortic endothelial (PAE) cells and green fluorescent protein-coding (GFP) plasmids were co-printed into fibrin gel substrate. The co-printed plasmids could be transfected into cells and then expressed. They found that the viability of printed cells was over 90% and transfection efficiency was over 10%. The transfected cells could then be precise printed into predefined positions, and GFP could be expressed in *in vitro* and *in vivo* experiments. The author also postulated the mechanism of inkjet-mediated gene transfection. When cells and plasmids pass through the channel of printing head during the co-printing process, the high shear stress and heat may produce transient membrane pores. Plasmids can then get into the pores and expressed in cells (Fig. 4). Combining gene modification and cell delivery can benefit the field of tissue engineering and regenerative medicine, because it is important to facilitate the cell with certain function to form functional tissue and organ. Cui et al. further studied the thermal inkjet printing induced gene transfection (Cui et al. 2010). This study had a more comprehensive understanding on the influence of printing procedure on printed

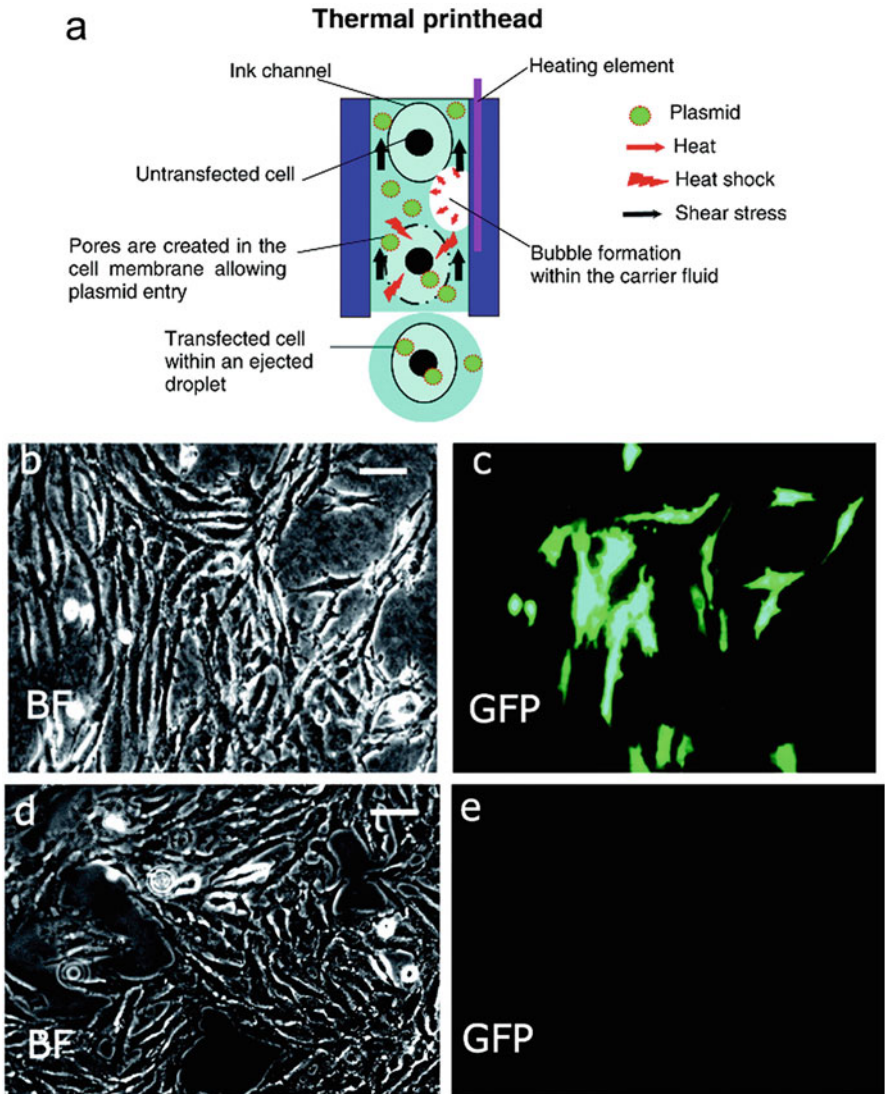


Fig. 4 (a) Schematic drawing of the postulated mechanism for inkjet-induced gene transfection. (b) The co-printed PAE cells after 2 days. (c) The green fluorescence expressed in co-printed cells. (d) The controlled nonprinted cells. (e) No fluorescence showed in the nonprinted cells (Xu et al. 2009b)

cells, such as cell viability and the size of cell membrane pores. Cell concentration was also optimized. Chinese hamster ovary (CHO) cells and fibrillar- or GFP-fused plasmids were co-printed to achieve transfected cells, and it was observed that the transfection efficiency was above 30%, while cell viability was 89%. Furthermore, the study evaluated the membrane pore size and membrane repair time by incubating

and staining the printed cells with dextran molecules (Shattil et al. 1992). Dextran can only penetrate the membrane pores, so the average Stokes diameters of the dextran molecules were used to indicate the size of membrane pores. Finally, it was observed that transient membrane pores can be repaired within 2 h. The study introduced that inkjet cell printing technology creates transient membrane pores during the printing process which holds possibility to be applied in intracellular delivery, such as genes, proteins, and factors' transfection. Owczarczak et al. reported how to use a standard inkjet printer to process cells with fluorescent G-actin transfected (Owczarczak et al. 2012). Other researchers can follow their video instruction to convert a standard HP DeskJet 500 printer to an inkjet bioprinter. The printer has the capability to print cells and defined cellular microenvironments, leading to defined functional tissue structures.

Inkjet-mediated gene transfection (IMGT) may avoid the drawback of normal stem cell induction process, such as low efficiency, low throughput, and teratoma formation during transgene reactivation. Paquian et al. co-printed plasmid with stem cells to test whether IMGT would work in stem cells (Paquian et al. 2016). This study found that stem cells remained viable after printing, and one of them can be transfected by GFP-coding plasmid. However, it was unable to deliver 4-factor encoding plasmids into stem cells, likely due to the large size of the plasmid. Meanwhile, considering that different cells may produce different levels of membrane disruption, the match of vector size and membrane pore size may be well considered before transfection.

In current years, there are some reports focusing on the combination of bioprinting technology and stem cell research. Spatial patterns of biology factors have been printed to guide the fate of stem cells. Campbell et al. initiated the study of using inkjet to print spatially controlled growth factor to affect cell behavior (Campbell et al. 2005). In this study, the number of preosteoblastic cells increased as the concentration of fibroblast growth factor-2 (FGF-2) increased. In another report, the proliferation of MG-63 cells responded to the concentration of FGF-2 (Miller et al. 2006). Ilkhanizadeh et al. modified a thermal inkjet (TIJ) printer to print spatially defined gradients of biology molecules, including FGF-2, ciliary neurotrophic factor (CNTF), and fetal bovine serum (FBS) on a polyacrylamide gel (Ilkhanizadeh et al. 2007). The response of neural stem cells (NSCs) cultured on biological molecule patterns was observed, and it was found that NSCs differentiated into astrocytes when CNTF presented and undifferentiated when FGF-2 presented (Ilkhanizadeh et al. 2007; Hermanson et al. 2002; Johe et al. 1996). When cultured on the adjacent regions of FGF2 and CNTF, stem cell fate was controlled. The number of glial fibrillary acidic protein (GFAP) expressed cells increased correlated with CNTF concentration (Hermanson et al. 2002; Johe et al. 1996; Kazuhiko et al. 2002). Similar phenomenon was seen when NSCs were cultured on the FBS substrate, which led NSCs to differentiate into smooth muscle cells (Kazuhiko et al. 2002). Phillippi et al. observed the differentiation of muscle-derived stem cells (MDSCs) responded to the spatial patterned gradients of bone morphogenic protein-2 (BMP-2) (Phillippi et al. 2008). They used a piezoelectric printing system to print BMP-2 onto fibrin substrates. The same as NSC studies

mentioned above, MDSC fate can be controlled by different spatial gradients' pattern of proteins. However, this report demonstrated that MDSC can differentiate into two different fates as osteogenic and myogenic lineage.

Currently, several biology molecule printings which applied in cell migration (Miller et al. 2011), combination of multiple growth factor gradients (Miller et al. 2009), multilineage stem cell differentiation (Ker et al. 2011a), and control of cell alignment (Ker et al. 2011b) have been reported. All these researches provide us a new way to better understand stem cells. Fabricating spatial gradient of protein pattern would help us better study the role of protein in tissue and organ on influencing tissue repair, regeneration, and even cell fate.

4 Application of Inkjet Bioprinting

Inkjet printing combined with biotechnology has been exploited in various application areas such as high-throughput screening and cancer research, drug formulation, and tissue repair and organ regeneration (Gudapati et al. 2016; Scoutaris et al. 2016).

High-throughput screening and cancer research. Because of the highly controlled accuracy, repeatability, and uniformity of 3D manufactured microarrays, inkjet printing was first applied to high-throughput screening (HTS). HTS usually requires testing and collecting hundreds or more samples and performing subsequent analysis. Due to the need of repeatability and accuracy, HTS requires highly automated and convenient sample preparation, which can be totally featured by inkjet printing (Scoutaris et al. 2016). One of the first works related to inkjet printing in HTS was Silzel's spotted monoclonal antibodies that retain specificity and affinity on specific recognition of four human immunoglobulins and human myeloma proteins (Silzel et al. 1998). In another study, Rodríguez-Dévora et al. presented inkjet printing to assemble a high-throughput miniature drug screening platform (Rodríguez-Dévora et al. 2012). Using a modified Hewlett Packard model 5360 compact disc printer, *Escherichia coli* cells' expression green fluorescent protein, along with alginate gel solution, has been arrayed on a coverslip chip. Different antibiotic droplets were patterned on the cell spots to evaluate the inhibition of bacteria for antibiotic screening. The results revealed that thermal inkjet bioprinting, comparing with micro-pipetted samples, is a powerful method to generate high-throughput arrays of samples for drug screening applications. Matsusaki et al. presented piezoelectric inkjet (PIJ) bioprinting of multilayer liver tissue models for drug screening and high-throughput applications (Matsusaki et al. 2013). Rapid and automatic development of three-dimensional human micro-tissue chips is carried out by droplet printing technology. Xu et al. introduced a high-throughput automated cell printing system to bioprint a 3D co-culture model using cancer cells and normal fibroblasts micropatterned on Matrigel™ (Xu et al. 2011). This approach can support the research on the unknown regulatory feedback mechanisms between tumors and stromal cells and provide a tool for high-throughput drug screening in cancer research.

Drug formulation. Inkjet printing is a new drug formulation method with several reports. Meléndez et al. first reported using thermal inkjet technology to work for the development of solid dosage forms of low water-soluble active pharmaceutical ingredients (Meléndez et al. 2008). After that, many research groups tried to improve the dissolution rates of poorly soluble drugs through inkjet printing, by dispensing nanoparticle complexes of ciprofloxacin–polysaccharide with polyethylene–glycol (Cheow et al. 2015) and naproxen/PEG 3350 (Hsu et al. 2015). With the help of inkjet printing technology, Hauschild et al. obtained drug-loaded polymer microspheres of narrow size distribution and controlled diameter of 50–200 nm which can be used as drug carriers (Hauschild et al. 2005). Totally, as a simple and convenient approach of drug-loaded polymer particles with controlled size and shapes, inkjet printing has its irreplaceable position in drug formulation.

Tissue repair and organ regeneration. Regenerative medicine aims to search for effective therapeutic strategies to promote self-repair and regeneration of tissues and organs, hopefully to restore their function. Regenerative repair includes structural and functional repair (Huang 2011). Great achievements were made in structural repair (bone, cartilage, vessel, etc.) for relatively low technical requirements, and some of the technologies and products have been applied to clinics. On the other hand, the functional repair, mainly the repair and regeneration of solid organs, usually has fewer breakthroughs. Inkjet printing is anticipated to accelerate the development of personalized regenerative medicine.

Structural repair. Cui's group evaluated bioactive ceramic nanoparticles in stimulating osteogenesis of printed bone marrow-derived human mesenchymal stem cells in poly(ethylene glycol) dimethacrylate (PEGDMA) scaffold (Gao et al. 2014). hMSCs suspended in PEGDMA were co-printed by a TIJ bioprinter with nanoparticles of bioglass (BG) and hydroxyapatite (HA) under simultaneous polymerization so the printed substrates were delivered with high accuracy in three-dimensional (3D) locations. This technology demonstrated the capacity for both soft and hard tissue engineering with anatomic structures. Campbell's group engineered stem cell microenvironments, using inkjet bioprinting technology, to create spatially defined patterns of immobilized growth factors (Phillippi et al. 2008). Using this approach, they engineered cell fate toward the osteogenic lineage by printing patterns of BMP-2 within a population of primary muscle-derived stem cells (MDSCs) isolated from adult mice. This patterning approach was conducive to pattern the MDSCs into subpopulations of osteogenic or myogenic cells simultaneously on a same chip. When cells were cultured under myogenic conditions on BMP-2 patterns, those cells on pattern differentiated toward the osteogenic lineage, whereas cells off pattern differentiated toward the myogenic lineage. Boland's group improved wound healing through bioprinted skin grafts (Yanez et al. 2015). A layer of human microvascular endothelial cell-laden thrombin was bioprinted using a TIJ bioprinter onto fibrinogen. A full-thickness wound was created at the top back of athymic nude mice and the area was covered by the graft. As a result, wound contraction improved up to 10% when comparing with the control groups. The grafts supported the formation of new skin with comparable morphological

characteristics of native skin but lacked sebaceous glands, hair follicles, and hair bulbs.

Functional repair. In the study of substantive organs, inkjet printing has a lot of related researches. With the help of modified inkjet printers, Xu et al. fabricated cardiac (heart) tissue with beating response (Xu et al. 2009a). In this study, model cardiac cells remained viable in constructs as 1 cm thickness due to the programmed porosity, which suggested that the inkjet bio-prototyping method can be used for hierarchical design of functional cardiac pseudo-tissues, balanced with porosity for mass transportation and structural support. Akashi's group bioprinted liver tissue through layer-by-layer deposition of hepatocytes, endothelial cells, fibronectin, and gelatin using a PIJ bioprinter (Matsusaki et al. 2013), and the tissue model was used for evaluating drug metabolism of antidiabetic drug troglitazone. Rothen-Rutishauser's group reported about the biofabrication of human air-blood tissue barrier analogue composed of endothelial cell, basement membrane, and epithelial cell layer with a bioprinting technology (Horváth et al. 2015). In contrary to the manual method, this technique enables automatic and reproducible creation of thinner and more homogeneous cell layers, which is required for an optimal air-blood tissue barrier. This bioprinting platform offered a tool to engineer advanced 3D lung model for high-throughput screening for safety assessment and drug efficacy tests.

Although there are more and more researches about inkjet bioprinting, most of these technologies are still kept in lab and away from clinical and commercial use. Although the technology of bioprinting with growth factors and other biologics other than cells, or used in drug testing and HTS and drug formulation, began to be used in clinics, translation of inkjet bioprinting on tissue repair and organ regeneration still remains difficult.

5 Conclusion

Due to the rapidity, high resolution, and reproducibility, inkjet printing plays a unique part in biofabrication to print cells and biomolecules. Two-dimensional and three-dimensional patterns have all been successfully built by inkjet printing. With the sustaining of cell viability and cell expression, functional biomimetic tissue scaffolds have also been achieved by this method. Furthermore, the transient heat and stress may possibly give positive affection to cells, thus facilitating cell function expression. On the other hand, the precise deposition of different biomolecules with different concentrations will direct stem cell fate by zones. Complex heterogeneous structure with different cell types may probably be achieved by this way. Though the current application of inkjet bioprinting has not reached to the clinic, commercial inkjet bioprinters have been developed to serve in the researches of drug screening, tissue and organ repairing, and cancer modeling. It is believed that with the maturation of this technique and the whole field, inkjet bioprinting may serve for clinic and benefit the human beings in the future.

References

- Arai K, Iwanaga S, Toda H, Genci C, Nishiyama Y, Nakamura M (2011) Three-dimensional inkjet biofabrication based on designed images. *Biofabrication* 3(3):034113
- Biase MD, Saunders RE, Tirelli N, Derby B (2011) Inkjet printing and cell seeding thermo-reversible photocurable gel structures. *Soft Matter* 7(6):2639–2646
- Campbell P, Miller EG, Walker L, Weiss L (2005) Engineered spatial patterns of FGF-2 immobilized on fibrin direct cell organization. *Biomaterials* 26(33):6762
- Canfield B, Holstun C, Yeun KWW (1997) Method and apparatus for reducing the size of drops ejected from a thermal ink jet printhead. US, US5673069
- Cheow WS, Kiew TY, Hadinoto K (2015) Combining inkjet printing and amorphous nanonization to prepare personalized dosage forms of poorly-soluble drugs. *Eur J Pharm Biopharm* 96:314–321
- Choi WS, Ha D, Park S, Kim T (2011) Synthetic multicellular cell-to-cell communication in inkjet printed bacterial cell systems. *Biomaterials* 32(10):2500–2507
- Christensen K, Xu C, Chai W, Zhang Z, Fu J, Huang Y (2015) Freeform inkjet printing of cellular structures with bifurcations. *Biotechnol Bioeng* 112(5):1047
- Cui X, Boland T (2009) Human microvasculature fabrication using thermal inkjet printing technology. *Biomaterials* 30(31):6221–6227
- Cui X, Dean D, Ruggeri ZM, Boland T (2010) Cell damage evaluation of thermal inkjet printed chinese hamster ovary cells. *Biotechnol Bioeng* 106(6):963–969
- Cui X, Boland T, D’Lima D, Martin K (2012a) Thermal inkjet printing in tissue engineering and regenerative medicine. *Recent Pat Drug Deliv Formul* 6(2):149–155
- Cui X, Breitenkamp K, Finn MG, Lotz M, D’Lima DD (2012b) Direct human cartilage repair using three-dimensional bioprinting technology. *Tissue Eng A* 18(11–12):1304
- Cui X, Gao G, Qiu Y (2013) Accelerated myotube formation using bioprinting technology for biosensor applications. *Biotechnol Lett* 35(3):315
- Cui X, Gao G, Yonezawa T, Dai G (2014) Human cartilage tissue fabrication using three-dimensional inkjet printing technology. *J Vis Exp* 2014(88):e51294
- Cummins G, Desmulliez MPY (2012) Inkjet printing of conductive materials: a review. *Circuit World* 38(4):193–213
- Dababneh AB, Ozbolat IT (2014) Bioprinting technology: a current state-of-the-art review. *J Manuf Sci Eng* 136(6):061016
- de Gans BJ, Duineveld P, Schubert U (2004) Inkjet printing of polymers: state of the art and future developments. *Adv Mater* 16(3):203–213
- Ferris C, Gilmore K, Beirne S, McCallum D, Wallace G, Inhetpanhuis M (2013) Bio-ink for on-demand printing of living cells. *Biomaterials* 1(2):224–230
- Gao G, Schilling AF, Yonezawa T, Wang J, Dai G, Cui X (2014) Bioactive nanoparticles stimulate bone tissue formation in bioprinted three-dimensional scaffold and human mesenchymal stem cells. *Biotechnol J* 9(10):1304
- Gudapati H, Dey M, Ozbolat I (2016) A comprehensive review on droplet-based bioprinting: past, present and future. *Biomaterials* 102:20
- Hauschild S, Dr UL, Rumpelcker A, Borchert U, Rank A, Schubert R et al (2005) Direct preparation and loading of lipid and polymer vesicles using inkjets. *Small* 1(12):1177–1180
- Hendriks J, Visser CW, Henke S, Leijten J, Saris DBF, Sun C et al (2015) Optimizing cell viability in droplet-based cell deposition. *Sci Rep* 5:11304
- Hermanson O, Jepsen K, Rosenfeld MG (2002) N-cor controls differentiation of neural stem cells into astrocytes. *Nature* 419(6910):934
- Hock SW, Johnson DA, Van Veen MA (1996) Print quality optimization for a color ink-jet printer by using a larger nozzle for the black ink only. US, US 5521622 A
- Horváth L, Umehara Y, Jud C, Blank F, Petrifink A, Rothenrutishauser B (2015) Engineering an in vitro air-blood barrier by 3d bioprinting. *Sci Rep* 5:7974

- Hsu HY, Toth S, Simpson GJ, Harris MT (2015) Drop printing of pharmaceuticals: effect of molecular weight on PEG coated-naproxen/PEG 3350 solid dispersions. *AICHE J* 61(12):4502–4508
- Huang YS (2011) Tissue regeneration is a key tool for burn tissue repair. *Zhonghua Shao Shang Za Zhi* 27(1):6–7
- Hudson KR, Cowan PB, Gondek JS (2000) Ink drop volume variance compensation for inkjet printing. US 6042211 A
- Ilkhanizadeh S, Teixeira AI, Hermanson O (2007) Inkjet printing of macromolecules on hydrogels to steer neural stem cell differentiation. *Biomaterials* 28(27):3936–3943
- Johe KK, Hazel TG, Muller T, Dugich-Djordjevic MM, Mckay RD (1996) Single factors direct the differentiation of stem cells from the fetal and adult central nervous system. *Genes Dev* 10(24):3129–3140
- Kamisuki S, Hagata T, Tezuka C, Nose Y (1998) A low power, small, electrostatically-driven commercial inkjet head. In: Proceedings of the eleventh international workshop on MICRO electro mechanical systems, 1998. Mems 98. IEEE, pp 63–68
- Kamisuki S, Fujii M, Takekoshi T, Tezuka C (2000) A high resolution, electrostatically-driven commercial inkjet head. In: Proceedings of the thirteenth international conference on MICRO electro mechanical systems. IEEE, pp 793–798
- Kazuhiko O, Yasuhiro O, Shuji G, Uchida MK (2002) Contractile responses of smooth muscle cells differentiated from rat neural stem cells. *J Physiol* 540(Pt 1):139
- Ker ED, Chu B, Phillippi JA, Gharaibeh B, Huard J, Weiss LE et al (2011a) Engineering spatial control of multiple differentiation fates within a stem cell population. *Biomaterials* 32(13):3413
- Ker ED, Nain AS, Weiss LE, Wang J, Suhan J, Amon CH et al (2011b) Bioprinting of growth factors onto aligned sub-micron fibrous scaffolds for simultaneous control of cell differentiation and alignment. *Biomaterials* 32(32):8097–8107
- Kyser EL, Sears, SB (1980) Method and apparatus for recording with writing fluids and drop projection means therefor. US, US 4189734 A
- Langer R, Vacanti JP (1993) Tissue engineering. *Science* 260(5110):920–926
- Le HP (1998) Progress and trends in ink-jet printing technology. *J Imaging Sci Technol* 42(1):49–62
- Matsusaki M, Sakaue K, Kadowaki K, Akashi M (2013) Three-dimensional human tissue chips fabricated by rapid and automatic inkjet cell printing. *Adv Healthc Mater* 2(4):534
- Meléndez PA, Kane KM, Ashvar CS et al (2008) Thermal inkjet application in the preparation of oral dosage forms: dispensing of prednisolone solutions and polymorphic characterization by solid-state spectroscopic techniques. *J Pharm Sci* 97(7):2619–2636
- Miller ED, Fisher GW, Weiss LE, Walker LM, Campbell PG (2006) Dose-dependent cell growth in response to concentration modulated patterns of FGF-2 printed on fibrin. *Biomaterials* 27(10):2213
- Miller ED, Phillippi JA, Fisher GW, Campbell PG, Walker LM, Weiss LE (2009) Inkjet printing of growth factor concentration gradients and combinatorial arrays immobilized on biologically-relevant substrates. *Comb Chem High Throughput Screen* 12(6):604–618
- Miller ED, Li K, Kanade T, Weiss LE, Walker LM, Campbell PG (2011) Spatially directed guidance of stem cell population migration by immobilized patterns of growth factors. *Biomaterials* 32(11):2775–2785
- Mironov V, Boland T, Trusk T, Forgacs G, Markwald RR (2003) Organ printing: computer-aided jet-based 3d tissue engineering. *Trends Biotechnol* 21(4):157
- Murphy SV, Atala A (2014) 3D bioprinting of tissues and organs. *Nat Biotechnol* 32(8):773–785
- Nakamura M (2012) Tissue engineering: a case study. In: *Inkjet technology for digital fabrication*, 1st edn. Wiley, Hoboken, pp 307–324
- Nakamura M, Kobayashi A, Takagi F, Watanabe A, Hiruma Y, Ohuchi K et al (2005) Biocompatible inkjet printing technique for designed seeding of individual living cells. *Tissue Eng* 11(11–12):1658
- Owczarczak AB, Shuford SO, Wood ST, Deitch S, Dean D (2012) Creating transient cell membrane pores using a standard inkjet printer. *J Vis Exp* 2012(61):e3681

- Paquian Gi, et al. (2016) Stem cell induction via inkjet-mediated gene transfection. ETD Collection for University of Texas, El Paso. AAI10249984
- Pataky K, Braschler T, Negro A, Renaud P, Lutolf MP, Brugger J (2012) Microdrop printing of hydrogel bioinks into 3d tissue-like geometries. *Adv Mater* 24(3):391
- Phillippi JA, Miller E, Weiss L, Huard J, Waggoner A, Campbell P (2008) Microenvironments engineered by inkjet bioprinting spatially direct adult stem cells toward muscle- and bone-like subpopulations. *Stem Cells* 26(1):127–134
- Rayleigh L (1878) On the instability of jet. *Proc Lond Math Soc* 10(1):4–13
- Rodríguez-Dévora JI, Zhang B, Reyna D, Shi ZD, Xu T (2012) High throughput miniature drug-screening platform using bioprinting technology. *Biofabrication* 4(3):035001
- Rune E (1951) Measuring instrument of the recording type. US, US2566443
- Saunders RE, Gough JE, Derby B (2008) Delivery of human fibroblast cells by piezoelectric drop-on-demand inkjet printing. *Biomaterials* 29(2):193–203
- Scoutaris N, Ross S, Douroumis D (2016) Current trends on medical and pharmaceutical applications of inkjet printing technology. *Pharm Res* 33(8):1799
- Shattil SJ, Cunningham M, Wiedmer T, Zhao J, Sims PJ, Brass LF (1992) Regulation of glycoprotein IIb-IIIa receptor function studied with platelets permeabilized by the pore-forming complement proteins C5b-9. *J Biol Chem* 267(26):18424
- Sizel JW, Cercek B, Dodson C, Tsay T, Obremski RJ (1998) Mass-sensing, multianalyte microarray immunoassay with imaging detection. *Clin Chem* 44(9):2036–2043
- Sun W, Lal P (2002) Recent development on computer aided tissue engineering – a review. *Comput Methods Prog Biomed* 67(2):85–103
- Svanholm E (2007) Printability and ink-coating interactions in inkjet printing. Faculty of Technology & Science, Karlstad
- Sweet RG (1965) High frequency recording with electrostatically deflected ink jets. *Rev Sci Instrum* 36(2):131–136
- Tse C, Whiteley R, Yu T, Stringer J, Macneil S, Haycock JW et al (2016) Inkjet printing schwann cells and neuronal analogue NG108-15 cells. *Biofabrication* 8(1):015017
- Weber C (1931) Zum zerfall eines flüssigkeitsstrahles. *ZAMM* 11(2):136–154
- Xu C (2014) Freeform vertical and horizontal fabrication of alginate-based vascular-like tubular constructs using inkjetting. *J Manuf Sci Eng* 136(6):061020
- Xu T, Petridou S, Lee EH, Roth EA, Vyavahare NR, Hickman JJ et al (2004) Construction of high-density bacterial colony arrays and patterns by the ink-jet method. *Biotechnol Bioeng* 85(1):29–33
- Xu T, Jin J, Gregory C, Hickman JJ, Boland T (2005) Inkjet printing of viable mammalian cells. *Biomaterials* 26(1):93
- Xu T, Gregory CA, Molnar P, Cui X, Jalota S, Bhaduri SB et al (2006) Viability and electrophysiology of neural cell structures generated by the inkjet printing method. *Biomaterials* 27(19):3580–3588
- Xu T, Baicu C, Aho M, Zile M, Boland T (2009a) Fabrication and characterization of bio-engineered cardiac pseudo tissues. *Biofabrication* 1(3):035001
- Xu T, Rohozinski J, Zhao W, Moorefield EC, Atala A, Yoo JJ (2009b) Inkjet-mediated gene transfection into living cells combined with targeted delivery. *Tissue Eng A* 15(1):95
- Xu F, Celli J, Rizvi I, Moon S, Hasan T, Demirci U (2011) A three-dimensional in vitro ovarian cancer coculture model using a high-throughput cell patterning platform. *Biotechnol J* 6(2):204
- Xu C, Chai W, Huang Y, Markwald RR (2012) Scaffold-free inkjet printing of three-dimensional zigzag cellular tubes. *Biotechnol Bioeng* 109(12):3152–3160
- Xu T, Zhao W, Zhu JM, Albanna MZ, Yoo JJ, Atala A (2013) Complex heterogeneous tissue constructs containing multiple cell types prepared by inkjet printing technology. *Biomaterials* 34(1):130–139

- Yamaguchi S, Ueno A, Akiyama Y, Morishima K (2012) Cell patterning through inkjet printing of one cell per droplet. *Biofabrication* 4(4):045005
- Yamazoe H, Tanabe T (2009) Cell micropatterning on an albumin-based substrate using an inkjet printing technique. *J Biomed Mater Res A* 91A(4):1202–1209
- Yanez M, Rincon J, Dones A, Maria CD, Gonzales R, Boland T (2015) In vivo assessment of printed microvasculature in a bilayer skin graft to treat full-thickness wounds. *Tissue Eng A* 21(1–2):224
- Zoltan SI (1972) Pulsed droplet ejecting system. US, US 3683212 A



Laser-Based Cell Printing

Lothar Koch, Andrea Deiwick, and Boris Chichkov

Contents

1	Introduction	304
2	Laser-Based Cell Printing Techniques	305
2.1	Laser-Guided Direct Writing	305
2.2	Laser-Induced Forward Transfer	306
3	Applied Materials and Lasers	308
3.1	Dynamic Release Layer	308
3.2	Bio-ink	309
3.3	Laser Parameters	310
3.4	Controlling the Droplet Volume	311
4	Process Impact on Cells	313
5	Applications	314
5.1	Printed Stem Cell Grafts	315
5.2	Printed Multicellular Arrays for Cell–Cell Interaction Studies	317
5.3	Stackable Biopapers with Printed Cells	319
5.4	Printed Skin Tissue	320
5.5	In Situ Printing	323
6	Discussion	323
7	Conclusions	326
	References	327

Abstract

The development of reproducible well-defined 3D cell models is a key challenge for the future progress in tissue engineering. The structural dimensions in natural tissue are significantly lower than 100 μm . Thus, the ability to precisely position different cells in complex 3D patterns is of essential importance, even if it is not fully determined which precision or resolution is really required.

L. Koch (✉) · A. Deiwick · B. Chichkov
Laser Zentrum Hannover e.V., Hannover, Germany
e-mail: l.koch@lzh.de; a.deiwick@lzh.de; b.chichkov@lzh.de

This chapter discusses laser-based techniques for printing living cells in two- or three-dimensional patterns. One method known as laser-guided direct writing has been used to position individual cells in a cell medium bath by applying the laser optical tweezer technique.

A more common method applies the laser-induced forward transfer (LIFT) for cell printing. For this method, many different designations are used like biological laser printing (BioLP), laser-assisted bioprinting (LAB, LaBP), or matrix-assisted pulsed laser evaporation - direct write (MAPLE-DW). There are also some technical differences in the realization of cell printing with this method that are discussed in this chapter. Applications like printing of multicellular arrays, stem cell grafts, and tissue as well as in situ printing will be presented.

1 Introduction

In principle, the field of bioprinting can be separated in printing of scaffolds and patterns of molecules and biomaterials, randomly seeded with cells after printing if applicable, and printing of cells and microorganisms. Laser-based techniques have been developed for both applications. While laser-based scaffold generation is described in chapter ► [“Additive Manufacturing for Tissue Engineering”](#) this chapter describes laser-based printing of vital cells.

The ultimate goal of bioprinting certainly is the *ex vivo* generation of fully functional organs from cultivated cells and biomaterials. Therefore, complex three-dimensional (3D) patterns of different cell types have to be printed, mimicking tissue structure, often including a perfusable vascular network. The distance between adjacent vessels in some tissue well supplied with blood like liver is partly below 200 μm with the size of microvessels down to 10 μm . Since the size of most human cells is about 10 μm , the printing resolution for tissue printing should be in the lower double-digit micron range.

For printing, cells are mostly embedded in a sol, the non-gelled precursor of a hydrogel, often referred to as bio-ink, and deposited at their designated position in a droplet or strand. For 3D printing, the sol is gelled after printing to achieve an adequate stiffness.

Mainly three different techniques are applied to bioprinting (Ringeisen et al. 2006; Hon et al. 2008): ink-jet printing, extrusion printing (also referred to as robotic dispensing, bioplotting, syringe-based printing), and laser-assisted bioprinting (LaBP, also referred to as laser-induced forward transfer, biological laser printing, laser bioprinting, matrix-assisted pulsed laser evaporation - direct write (MAPLE-DW)). Ink-jet and extrusion printing are nozzle-based techniques, while LaBP is nozzle-free. Inside nozzles, cells undergo mechanical stress due to shear forces which are dependent on velocity and viscosity of the sol as well as nozzle diameter and cell density. To achieve a high resolution, a small nozzle diameter is required. However, if the nozzle diameter is not much bigger than the cell size, viscosity and cell density or velocity needs to be low.

Ink-jet printing requires certain velocity and applies typically nozzle diameters below 100 μm . This allows printing of droplets with very small volumes at high repetition rates

(chapter ► [“Inkjet Printing for Biofabrication”](#)). However, only low cell densities (typically $10^6/\text{ml}$, compared to $10^8/\text{ml}$ for LaBP) and low-viscosity materials (typically lower than $10 \text{ mPa} \cdot \text{s}$, compared to $1 \text{ Pa} \cdot \text{s}$ for LaBP (Lin et al. 2009)) are printable.

With extrusion printing (chapter ► [“Extrusion-Based Biofabrication in Tissue Engineering and Regenerative Medicine”](#)), the biomaterial is pressed (extruded) through a nozzle as a strand. Therefore, nozzles with inner diameters between 50 and 1000 μm are used. To achieve sufficient printing velocity with small nozzles, only low-viscosity materials and low cell densities might be printed, comparable to ink-jet printing. Therefore, usually nozzles with diameters between 500 and 1000 μm are applied, resulting in relatively low printing resolution not sufficient to print complex microvascular networks. With bigger nozzle diameters, sols with high viscosity and embedded high cell density can be printed.

LaBP as a nozzle-free technique is capable of printing small droplets comparable to ink-jet printing and printing highly viscous sols and high cell densities comparable to extrusion technique. The advantage of LaBP is that printing of high cell densities and highly viscous materials can be combined with high resolution. With LaBP, more than 100,000 cells per second can be printed with high cell survival rate. Printed tissue with tens of millions of cells already has been demonstrated. However, each of the aforementioned printing techniques has its individual advantages and drawbacks and may be preferred for specific applications.

2 Laser-Based Cell Printing Techniques

2.1 Laser-Guided Direct Writing

While LaBP is the laser-based technique most commonly applied for cell printing, it is not the only one. A method based on the optical tweezer effect, usually referred to as laser-guided direct writing (LGDW), was used by Odde and Renn (1999), to arrange cells in two- and three-dimensional patterns without a sol or hydrogel.

The peculiarity of LGDW compared to most other cell printing techniques is the absence of a sol as bio-ink and droplet or strand formation. Cells swimming in cell culture media are trapped by a laser beam and moved slowly to their designated position on a surface. Therefore usually coherent wave lasers are applied. Cells get into the laser beam more or less randomly and act like a convex lens due to their spherical shape, translucence for the laser wavelength, and an index of refraction different from water. The laser photons are deflected by this lens, changing their momentum, which implies an opposite change in the momentum of the cell (conservation of momentum). This results in photon-induced movement of the cell (Fig. 1). While the photon is deflected toward the cell's center, the cell is accelerated in the opposite direction. Since many photons interact with the cell at the same time, the cell moves toward the area with the highest cell density; typically this is the center of the laser beam. Additionally, photons reflected or absorbed by the cell transfer a momentum in the direction of the laser beam onto the cell. Therefore, the cell moves along the optical axis of the laser beam. With LGDW, the laser beam is directed onto a surface in the cell medium, and a cell is

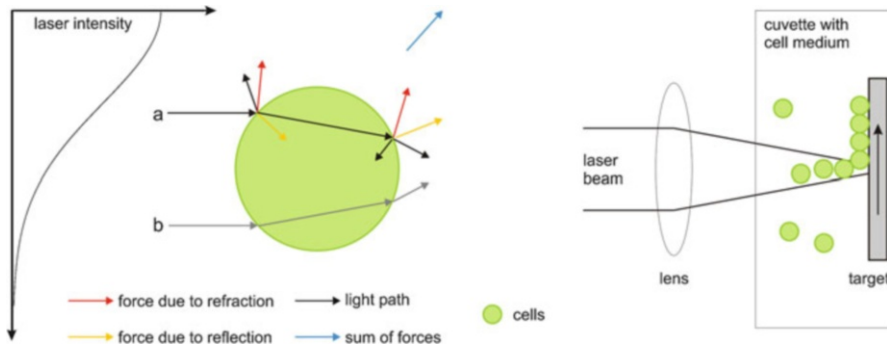


Fig. 1 Schematic of the laser-guided direct writing technique similar to Odde and Renn (1999) (Copyright © 1999 Elsevier Science Ltd. All rights reserved). *Left*: Optical forces of the laser tweezer effect. Laser photons are reflected and refracted at each interface between cells and cell media, resulting in a redirection of the photons. Since photons have momentum, their redirection by interacting with the cell results in a corresponding momentum transfer to the cell. The sum of forces from interactions with a ray pushes the cell toward the (original) optical axis of the ray and along the beam axis. If the laser intensity varies over the cell-beam cross-section, the cell is pushed toward the region with the highest intensity (forces from stronger ray overcome forces from ray b), which is in the beam's center in case of a Gaussian beam. Thus, the cell is pulled radially inward and pushed axially forward in the direction of the laser beam. *Right*: If the laser beam is weakly focused onto a target that is positioned in cell suspension, the cells are propelled to the focal spot and attach to the target's surface. By moving the target relatively to the laser beam, a line of cells can be written

propelled by the photons to this laser spot where it adheres. Now the laser is moved to another position to deposit the next cell on the surface or to cells already present at this position (analog to 3D printing).

LGDW offers an unbeatable resolution since it is a pure single cell printing technique without any surrounding bio-ink, enabling printing of 3D structures consisting of cells only.

However, this technique is extremely slow, since the photons need to push the cell against the fluid resistance of the cell media; Odde and Renn (1999) achieved a cell velocity of $10\ \mu\text{m}$ (a typical cell diameter) per second which implies printing of fewer than one cell per second. Therefore, this technique is suitable for positioning of a few cells in well-defined patterns with precise distances, also in 3D, but not for printing tissue with millions of cells. LGDW is therefore rarely used nowadays and will not be considered in the following.

2.2 Laser-Induced Forward Transfer

More common is LaBP, adapting for cell printing a technique called laser-induced forward transfer that is used for electronic circuits, for example, electrodes on solar panels. The principal setup for LaBP applies a pulsed laser and a substrate transparent for the laser wavelength. Usually, the substrate is a glass slide (e.g., 1 mm thick) or fused silica for UV lasers. Most often, it is coated with a thin layer of material that

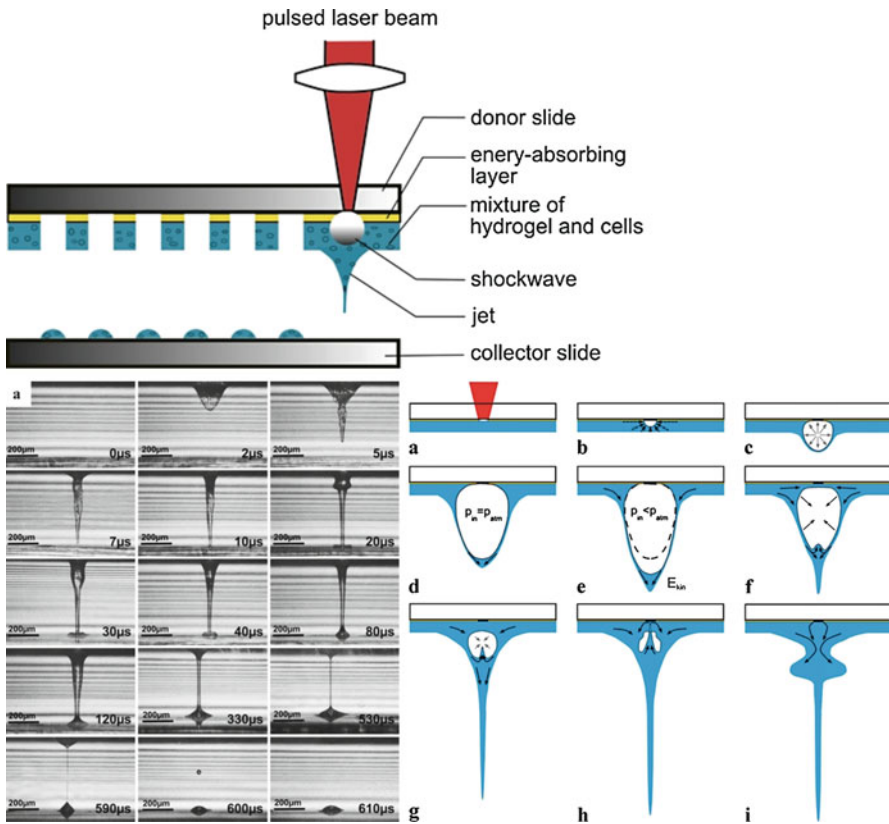


Fig. 2 Schematic LIFT setup for hydrogel printing; time-resolved images of the hydrogel jet formation during LIFT; scheme of the bubble dynamics and jet formation during LIFT. *Gray arrows* indicate expansion or contraction of the vapor, *black arrows* mark flows, and *dashed arrows* resistance of the hydrogel against vapor bubble expansion (Reprinted from Unger et al. (2011) Copyright © 2011 Springer-Verlag)

absorbs the laser radiation. Onto this layer, the bio-ink to be printed is spread, usually a sol with embedded cells.

The substrate is mounted upside down into the printing setup (Fig. 2), and the laser pulses are focused through the transparent substrate into the absorption layer (also referred to as dynamic release layer).

The electrons in this layer absorb the laser photons. Thereby, plasma is generated within tens of picoseconds. This plasma is further heated by laser irradiation. Thereby, the absorption layer is evaporated in the focal spot, and a vapor bubble is generated. Since this bubble was generated at the glass slide surface (Fig. 2), it expands into a half-space. The resistance against bubble expansion is lowest perpendicular to the surface, because in this direction the amount of sol to be pushed aside is small compared to the lateral one. Therefore, the vapor bubble expands in an elongated shape. The stretching of the sol layer initiates a flow inside this layer.

While the vapor bubble expands, the inner pressure decreases below the atmospheric pressure, resulting in a re-collapsing of the bubble within a few microseconds after the laser pulse impact. However, the sol at the forefront of the bubble moves on due to inertia, surface tension, and the bubble collapsing from the sides and forms a sol jet that is fed further by the sol flow lasting for some hundred microseconds (Unger et al. 2011). For printing, the glass slide is positioned in a short distance above an object to print onto. The sol flows via this jet to a spot on the surface of this object. The sol jet disrupts after a few hundred microseconds due to a limitation of the sol “reservoir,” springing from an area on the glass slide with about 200 μm in diameter. The sol remains as a droplet on the object. Each laser pulse is focused on a new spot on the absorption layer. By moving the substrate and repositioning the laser focus, every desired two-dimensional pattern can be printed, and layer by layer also 3D patterns can be generated. Cells have been printed onto different objects like glass slides, sheets of different materials (see below), and heart valve leaflets (Klopsch et al. 2012) and into scaffolds (Ovsianikov et al. 2010).

3 Applied Materials and Lasers

For cell printing, a wide range of absorption materials, bio-inks, and laser parameters are applied. For some absorption materials, certain wavelength ranges are required; polymers, for example, often require applying ultraviolet lasers. Here, an overview of the laser wavelengths and pulse durations, the absorption materials, and bio-inks that have been used by different groups will be given, which, however, does not claim to be exhaustive.

3.1 Dynamic Release Layer

The most widely used group of absorption materials are thin layers (about 10–100 nm thick) of metals like gold (Dinca et al. 2007), silver (Hopp et al. 2005), and titanium (Duocastella et al. 2010a), usually applied by sputter coating. They are combined with a wide range of laser wavelengths. Sputter coating of these metals is well established with high reproducibility and relatively cost efficient. Due to the surface properties of metal absorption layers, sol layers can be applied quite homogeneous and reproducible on them. The disadvantage of metal layers is the generation of debris. Ions, clusters, and micro- and macroscopic particles will be printed together with the bio-ink. This is not necessarily problematic with gold and titanium (oxide) as inert biocompatible materials; the debris is not toxic for the cells (see paragraph on process impact on cells below). Nevertheless, if thicker 3D structures are printed, the debris is clearly visible. If one day complete organs will be printed for implantation, this debris presumably cannot be tolerated.

Alternatively, polymer layers like 90–150 nm triazene (Palla-Papavlu et al. 2011), 7 μm polyimide (Brown et al. 2012), 1.35 μm polyethylene naphthalate foil (Vogel et al.

2007), gelatin layers (Schiele et al. 2011), or a two-layer system (10 μm cyanoacrylate + 25 μm brass foil (Lin et al. 2011)) have been used for different purposes.

Triazene is expected to be transferred completely into gaseous reaction products by ultraviolet laser irradiation. Thus, the debris problem would be avoided. However, there still might be a small amount of debris and maybe some altered chemical substances are generated that are embedded in the printed structure.

To completely eliminate the debris problem, Lin et al. (2011) investigated a two-layer absorption system with an adhesive cyanoacrylate layer on the glass slide and a brass foil on top. The laser pulse evaporates the cyanoacrylate only, and the vapor bubble bulges the brass foil without disrupting it. By using a relatively thick 7 μm layer of polyimide and an ultraviolet laser with 355 nm wavelength, Brown et al. (2012) realized this so-called blister effect with a single layer. The laser pulse vaporized the polyimide layer only partially near the substrate, while the absorption layer surface opposite to the substrate remains intact. The vapor bubble at the substrate polyimide interface only bulges the non-vaporized part of the absorption layer. This bulging or blister effect transferred enough momentum into the bio-ink to induce jet generation and the printing of the bio-ink.

Sometimes, systems without an absorption layer (e.g., Barron et al. 2004) are used. Thereby, the biomaterial to be printed also serves as laser-absorbing material; a small part of it is vaporized thereby. However, the biomaterial not necessarily has good optical properties for absorbing laser radiation. Furthermore, focused laser radiation, especially in the ultraviolet range, potentially harms cells.

3.2 Bio-ink

For printing 3D cell patterns or tissue, mostly the cells are suspended in a bio-ink, which is usually a sol or a mixture with a sol component. To achieve three-dimensionality, a certain stiffness of the bio-ink after printing is required. For the printing process itself, a viscous sol but not a stiff gel has to be used; therefore, the gelling should occur after printing. For printing of 2D cell patterns, stiffness is not required, and even printing of cells suspended in pure culture media is possible. Furthermore, the bio-ink needs to support cell survival. Therefore, nontoxicity, a neutral pH value near 7.4, a suitable temperature, and permeability for oxygen and nutrients are prerequisites, but some cell types have further demands like peptides to adhere to. Furthermore, bio-inks might induce stimuli to the cells, which are not always desirable. Typically, these different aspects are addressed by different components of a sol mixture.

In general, the mixture consists of four components. One component offers a suitable environment with nutrients for the cells; a second component is added for optimized viscosity. Depending on the application, stimuli like growth factors or agents are added. This sol mixture is printed with embedded cells and gelled with a cross-linker. The cross-linker may be printed in a second step or can be sprayed onto the printed sol. Alternatively, the sol can be printed directly into a cross-linker reservoir (Yan et al. 2013).

For LaBP, sols and hydrogels with a wide range of rheological properties (Lin et al. 2009; Gruene et al. 2011a) have been applied. As one example, alginate (1–6% w/v) provides a suitable viscosity for printing and gels by adding calcium ions. For cell-friendly environment, blood plasma might be added. After printing alginate mixed with plasma and cells, calcium chloride solution is sprayed on the printed pattern for gelation.

A second example is fibrin gel, which is generated by the human body to close wounds. The gelation is started by mixing fibrinogen with thrombin. Both provide a cell-friendly environment, but their viscosity is below the optimum for printing. Therefore, fibrinogen is printed mixed with cells and hyaluronic acid, which has a higher viscosity and can also be found in the human body. As the next layer, thrombin is also printed mixed with hyaluronic acid and cells. Thereby, fibrinogen and thrombin from succeeding layers gel and stiffen the printed structure. By the way, fibrin is also an example of undesired stimuli. It stimulates keratinocyte cells to migrate. If printed within fibrin, keratinocytes reorganize in the printed structure and can be found later in completely different formations than the printed one.

Collagen is a further gel of interest, since it is the most abundant protein in the human body. However, the collagen sol is acidic, and therefore, cells inside would die quickly. Thus, it does not allow a post-print gelling. For neutralization, collagen needs to be mixed with a base to yield a physiological pH value of 7.4 and a buffer, before adding cells. Thereby, collagen starts to gel. Depending on temperature and concentration, the gelling process takes some minutes. The gelling process is typically inhomogeneous, with a viscosity changing over time and varying locally by differently advanced gelling. Thus, printing is possible with reduced resolution only, if the neutralized collagen is printed during the gelling process. For printing 3D constructs mainly from gels like collagen, where the gelling occurs by a change of the pH value, the ability of printing high viscosity gels is required.

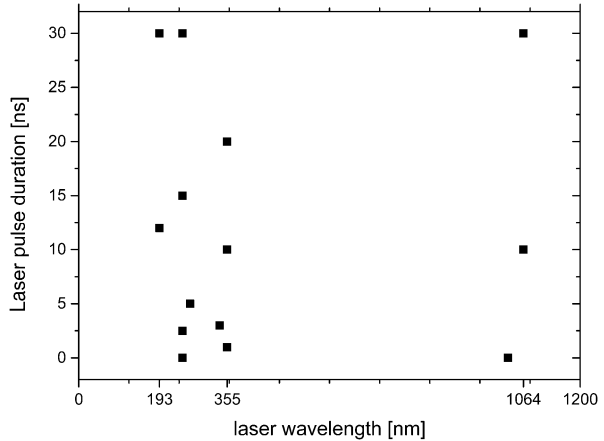
It is the dynamic viscosity that is important and which may differ significantly from the static viscosity. The viscosity dependence on the shear velocity is material specific. Since shear forces can destroy cells, shear-thinning sols are advantageous. Their viscosity decreases when propelled forward by the vapor bubble and in the sol jet, inducing lower shear forces to the cells. Shear-thickening sols would be problematic. Alginate and hyaluronic acid are shear thinning.

3.3 Laser Parameters

In addition to diverse laser absorption materials, also lasers with different parameters have been applied for LaBP. The wavelengths range from 193 to 1064 nm, and the pulse durations are mostly in the nanosecond domain (see Fig. 3). Furthermore, focusing optics with different focal length and spot sizes and different laser pulse energies are applied.

Most groups printing cells by LaBP use ultraviolet lasers with pulse durations from 3 to 30 ns and 193 nm (Palla-Papavlu et al. 2011; Lin et al. 2011), 248 nm (Pirlo et al. 2011; Dinca et al. 2008), 266 nm (Othon et al. 2008), 337 nm (Vogel et al. 2007), or

Fig. 3 Pulsed lasers with a wide range of parameters are used for laser-assisted bioprinting. Typically, the pulse duration is in the range from 1 to 30 ns, while the wavelength is in the ultraviolet (from 193 to 355 nm) or in the infrared (1027 or 1064 nm) range



355 nm (Duocastella et al. 2010a; Brown et al. 2010) wavelength. UV lasers are used in combination with all mentioned laser-absorbing materials. They are advantageous for polymeric absorption materials, since single UV photons have enough energy to induce chemical reactions. Thus, they break up solid polymers and convert them into gaseous substances – ideally completely. On the other hand, UV radiation with wavelengths below 300 nm is also used for sterilization and may be harmful to cells.

As an alternative, near-infrared (NIR) lasers with 10 or 30 ns pulse duration and 1064 nm (Catros et al. 2012; Koch et al. 2010) wavelength have been used in combination with metallic absorption layers (gold, titanium). Duocastella et al. (2010b) printed a glycerol-water blend with 1027 nm wavelength and 450 femtosecond pulse duration.

Mostly, near-infrared lasers are combined with metal (gold, titanium) absorption layers, causing debris deposition in the printed structure. However, metal absorption layers are advantageous for most evenly spreading biomaterials on the absorption layer surface.

In spite of these wide ranges of applied laser parameters, so far their impact on the transfer process has hardly been analyzed in direct comparison with the exception of laser pulse energy. There is one publication, in which Dinca et al. (2008) laser-printed proteins and DNA but not cells with 500 fs pulse duration at 248 nm wavelength and compared the results with those achieved with 15 ns pulse duration. As a result, applying ultrashort laser pulses with 500 fs pulse duration allowed printing of significantly smaller droplets.

3.4 Controlling the Droplet Volume

Several parameters determine the volume of droplets printed by LaBP. Obviously, the achievable droplet volume depends on laser pulse energy and focal spot size, but it also depends on the bio-ink's viscosity and surface tension and on the thickness of the laser absorption layer and the bio-ink layer.

Sometimes it is aspired to print droplets as small as possible to achieve high resolution. However, going to the limit increases the risk that inhomogeneity of the bio-ink layer on the donor may lead to missing droplets, which are not printed from positions where the bio-ink layer is a bit thicker. Therefore, the intended droplet size needs to be a bit above the limit, and the homogeneity of the bio-ink layer is very important for a good printing result. Besides layer thickness homogeneity, also homogeneity of the bio-ink composition and viscosity is important.

In general, there are three laser pulse energy domains. Below a certain threshold (lower limit), there is no material transfer; though a vapor bubble is generated and there might be a jet formation as well, the bio-ink will remain at or return to (if a sol jet is formed) the donor slide due to the surface tension. Above an upper limit, the vapor bubble will not re-collapse but burst, causing strong splashing with the deposition of several droplets in an irregular pattern on the acceptor.

In the energy domain of interest between these limits, a jet dynamic occurs leading to the deposition of a single droplet at a predefined position. In this energy domain, the droplet volume increases with the laser pulse energy in a nearly linear correlation. Of course, besides the laser pulse energy, also the laser focus area is of importance for the printed droplet volume.

The dependence of the printed droplet volume on viscosity and thickness of the bio-ink layer is more complex. A thicker layer usually results in bigger droplet volume at the same laser pulse energy, if there are printed droplets at all. In contrast, there is no systematic dependence of droplet volume on the viscosity at different laser pulse energies. The droplet volume increases with rising viscosity until a maximum value is reached and decreases with further rising of the sol's viscosity (Gruene et al. 2011a). With an increased sol layer thickness, this effect is even more pronounced. The specific viscosity, at which the printed droplet volume reaches its maximum, reduces with a lower thickness of the sol layer. Depending on the printed material, the volume of a printed droplet can be in the range of sub-picoliter (Baum et al. 2013) to several nanoliters and more.

Examples of laser-printed cell patterns with different droplet volumes are shown in Fig. 4. The quantity of cells per droplet is usually dependent on the cell density in the sol layer and the droplet volume and is subject to statistical variations.

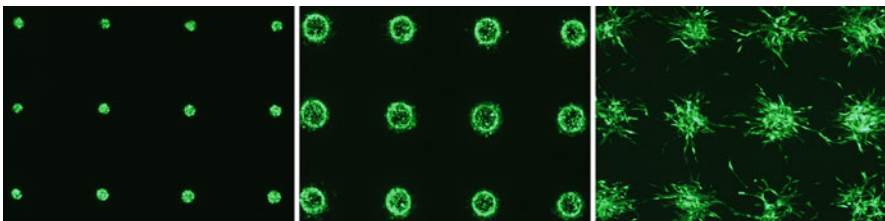


Fig. 4 Dependence of the droplet volume on laser pulse energy (*left*, 20 μJ ; *middle*, *right*, 30 μJ): Printed droplets with transduced fibroblasts (GFP labeled NIH3T3) embedded in a 3:2 mixture of fibrinogen and hyaluronic acid and printed onto a layer of fibrin, imaged directly after printing (*left*, *middle*) and after 2 days (*right*). Distance between adjacent droplets is 500 μm

Alternatively, droplets containing single cells might be printed, but this requires a low cell density and is time consuming, since each cell needs to be targeted separately.

4 Process Impact on Cells

Successful cell printing was reported by several groups with various kinds of cell types and different laser printing setups. For applying bioprinting techniques, it is crucial that cells are not affected by the printing process. This implies that the printed cells maintain their vitality and behavior and their phenotype and genotype and that stem cells retain their differentiation potential. Therefore, the impact of the printing process on cells and especially stem cells was extensively investigated.

Directly after printing the cell vitality was determined. Several groups (Barron et al. 2005b; Hopp et al. 2005; Koch et al. 2010) reported near 100% post-printing cell viability with different lasers, absorption layers, and cell types.

It was further investigated if the mechanical forces during printing might induce DNA strand breaks, which potentially could induce a medium-term degradation of the cell not directly visible after printing. This genotoxicity was investigated via a single cell gel electrophoresis (comet assay), and it was demonstrated that the printing process does not induce DNA strand breaks (Ringeisen et al. 2004; Koch et al. 2010). Thus, the genotype of printed cells is not affected.

Since high temperatures are generated locally in the plasma and the vapor bubble, cells potentially may be damaged by heat. Theoretically, the laser pulse's energy of a few ten micro-joules is sufficient to heat up a hundred picoliter (a typical droplet volume) from room temperature to a temperature above 42 °C in which cells may be harmed. Therefore, it was analyzed via immunocytochemical studies (Barron et al. 2005a, b; Gruene et al. 2011b), if the printed cells express a so-called heat shock protein; no increased expression was observed.

As a further parameter of possible cell death in the aftermath of LaBP, Koch et al. (2010) assessed apoptosis by measuring the activity of caspases 3/7 up to 48 h after printing of cell lines and human mesenchymal stem cells (hMSC). No increase in apoptosis was detected, neither compared to nonprinted control cells nor compared at different test intervals.

Additionally, the effect of the printing process on cell proliferation was studied by cell counting up to 6 days after printing. In accordance with experiments of other groups on other cell types (Barron et al. 2005b; Hopp et al. 2005), no difference in the proliferation behavior of cell lines and stem cells compared to nonprinted control cells was observed (Koch et al. 2010).

Since stem cell differentiation can be induced by mechanical forces, it is important for the printing of stem cells that the printing does not affect their differentiation potential and behavior. In a flow cytometric analysis of the immunophenotype of human mesenchymal stem cells (hMSC) 4 days after printing, Koch et al. (2010) observed no significant difference in the ratio of expression of typical MSC-marker

proteins on the printed cells versus control cells; the immunophenotype was not influenced. The influence of laser printing on the differentiation behavior of MSCs was studied by Gruene et al. (2011b, c). No difference was observed between the printed and nonprinted stem cells in their differentiation behavior toward different lineages.

Summing up, so far all studies consistently stated that the laser printing procedure with suitable parameters does not affect the cells; they are vital and fully functional.

5 Applications

Besides studying fundamental aspects of LaBP, like the effect of laser parameters, absorption layer material and thickness, or bio-ink material mixtures, viscosity, layer thickness, and cell density, also different applications were tested. Such application studies have two aims. Of course, the printing technique itself needs to be tested, but it is also necessary to investigate the principal requirements for printing biological systems like tissue.

So far, it can only roughly be estimated, which printing resolution is actually needed for generation of complex tissue, since it is not well known, how to make the cells establish the desired structures like vascular networks or nerves, for example. Since the cells are spherically shaped when printed with the bio-ink between them, there is always some self-organization of the cells required for tissue generation. During some time after printing, there is a cellular migration and arrangement due to stimuli from surrounding cells and the chemical and mechanical cues from the bio-ink, maybe as a cross-linked hydrogel. These stimuli and cues need to be considered or – better – harnessed for generating a specific cell construct or tissue. Thus, the printing pattern does not necessarily need to be (or even should not be) exactly like the tissue to be generated. This is sometimes referred to as “4D printing” with time and cell organization as the fourth dimension. To understand how exact cells need to be printed in a specific position, to make them fulfill the intended function, requires further extensive studies. This is true not only for LaBP but for all cell printing techniques. However, LaBP is particularly suitable for such studies due to its versatility.

Many different studies on applications of LaBP have been published so far, of which an overview will be given in the following. Really complex tissue, especially with an integrated perfusable vascular network, has not been printed so far. Nevertheless, first steps in this direction have already been taken. Different laser-printed 3D cell constructs are presented below, defined 3D spot arrays for microscopically observation of cell–cell interactions, a monocellular 3D stem cell graft, a multicellular 3D skin equivalent, stackable biopapers with printed cells, and in situ printing of cells into mice.

5.1 Printed Stem Cell Grafts

Stem cells are very interesting for regenerative medicine due to their self-renewal and differentiation ability. These abilities are regulated by cell density, cell–cell contacts, cell–matrix adhesion, and the exchange of growth factors and oxygen in the cell’s 3D microenvironment (Discher et al. 2009), also referred to as stem cell niche. Therefore, one important application for cell printing technologies would be fabricating 3D *in vitro* models mimicking such cell niches for studying cell behavior under predefined conditions more complex than conventional 2D cell cultures but more controllable than *in vivo* models.

The ability of LaBP for generating such 3D environments was demonstrated by Gruene et al. (2011b, c). They printed 3D patterns of mesenchymal stem cells (MSCs), approximately 300 μm high, for studying, if the differentiation potential toward different lineages of these stem cells (porcine bone marrow-derived (pMSCs) and human adipose-derived MSCs (ASCs)) was affected by the printing process and if these stem cell grafts can be differentiated within the printed pattern.

MSCs can be found in many adult tissues and represent an attractive cell source due to their high proliferation capacity, self-renewing ability, and their mesodermal differentiation potential. MSCs are expected to regenerate many tissues, like bone and cartilage. Therefore, these cells are very attractive for tissue engineering applications.

For printing, the MSCs are embedded in a natural sol of autologous origin consisting of alginate and ethylenediaminetetraacetic (EDTA) blood plasma. Each printed layer was cross-linked with calcium chloride, to form a hydrogel as extracellular matrix for the grafts. This material is compatible with the cells and enables the exchange of nutrients and soluble factors. Thereby, material elasticity and forces have to be considered, since these parameters are known to influence stem cell differentiation (Hellström et al. 1999). Additionally, the differentiation of stem cells is dependent on cell density; in particular, chondrogenesis requires a high cell density. Therefore, for generating stem cell grafts, printing with defined, variable, and high cell density is required (Hui et al. 2008; Takagi et al. 2007).

Stem cells may undergo forces during the printing procedure that would not affect their proliferation ability but might induce uncontrolled differentiation (Clause et al. 2010). To screen out such negative effects of LaBP on stem cell behavior, several quantitative and qualitative investigations were carried out, showing that the differentiation potential of MSCs into osteogenic, adipogenic, and chondrogenic lineages is not affected by the printing procedure, and the printed MSC grafts can be differentiated toward bone, cartilage, and adipose tissue (Fig. 5). Accumulation of calcium phosphate shows osteogenic differentiation, lipid vacuoles indicate adipogenic differentiation, and collagen type II is specific to chondrogenesis.

Additionally, LaBP enables printing of cell densities high enough for the promotion of chondrogenesis. 3D scaffold-free autologous tissue grafts can be fabricated with LaBP, keeping their predefined shape even after several weeks in culture and also after removal of the alginate matrix material after 2 weeks in culture (Gruene et al. 2011b, c).

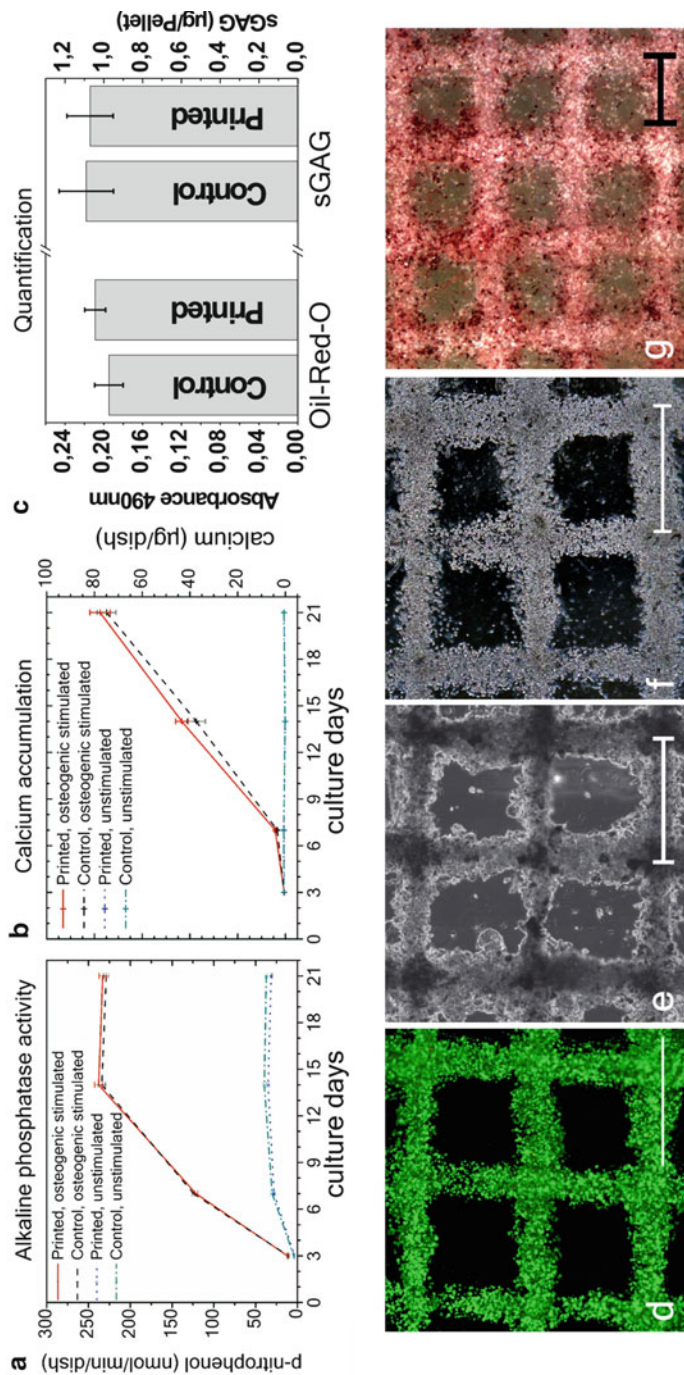


Fig. 5 Osteogenic, adipogenic, and chondrogenic differentiation potential of printed and nonprinted (control) mesenchymal stem cells (MSCs): (a, b) Quantitative assessments of (a) alkaline phosphatase activity and (b) calcium accumulation over a period of 21 days from printed and nonprinted control MSCs under osteogenic differentiation conditions in contrast to unstimulated stem cells (MSCs). Values are given as mean \pm SEM (n = 8). (c) *Left*: The quantity of the lipid accumulation from printed and nonprinted control cells after 21 days under adipogenic culture conditions was determined by Oil Red O staining and radiation absorbance at 490 nm wavelength. *Right*: Quantitative indication of sulfated glycosaminoglycans (sGAG) for chondrogenesis, by the 1,9-dimethyl-methylene dye-binding assay after 21 days under chondrogenic culture conditions. Values are given as mean \pm SEM (n = 5). (d-g) Printed 3D grid

5.2 Printed Multicellular Arrays for Cell–Cell Interaction Studies

Cellular microarrays have been developed for investigating cell responses in multiple parallel experiments (Fernandes et al. 2009) and to enable reproducible studies of the effects of proteins, growth factors, biomaterials, and drugs as well as the presence of other cells. Several studies indicate that cell behavior and tissue functionality are influenced or even controlled by local cell density, cellular spacing, cell–cell communication, and binding of cells to their 3D environment (Discher et al. 2009). The effect of the 3D environment on cellular behavior could be studied in printed 3D multicellular arrays. To prove the suitability of LaBP for generation of such arrays, Gruene et al. (2011d) printed arrays of droplets containing either human adipose-derived stem cells (ASCs) or endothelial colony-forming cells (ECFCs). These cells were chosen for investigation of vascular network formation, since recent studies indicate that these cell types represent suitable cell sources for therapeutic revascularization of ischemic tissues and can support the new vessel formation in engineered tissue constructs (Merfeld-Clauss et al. 2010; Wu et al. 2007; Gaebel et al. 2011). It was expected that the secretion of VEGF by the ASCs, which is well known for the promotion of endothelial cell proliferation, would lead to the outgrowth of ECFCs toward the ASCs along the VEGF gradient, as it was reported by other groups (Mirsky and Cohen 1995; Akeson et al. 2010). The cells were printed in 2D patterns of printed droplets on layers of fibrin hydrogel, each droplet containing one of both cell types, fibrinogen, and hyaluronic acid. Cultivated after printing in vascular endothelial growth factor-free (VEGF-free) medium for 10 days, cell–cell interactions were observed in arrays of separate droplets with ASCs and ECFCs as well as monoculture cell arrays containing only ASCs or only ECFCs as control. In each case, four independent cell arrays were printed.

As depicted in Fig. 6, the ASCs showed strong migration activity after 72 h, while the activity of ECFCs was very low. In the co-culture, the ASCs migrated toward the ECFC droplets, whereas the ECFCs showed negligible activity. After the ASCs got in direct contact with the ECFCs between days 3 and 5 (Gruene et al. 2011d), the activity of ECFCs strongly increased, and both cell types together began to form vascular-like networks with big branches. These networks were not observable either in the ASC or the ECFC controls. In all four independent co-culture cell arrays, these networks were formed and remained stable for 2 weeks under culture conditions. However, their formation did not occur at the same time.



Fig. 5 (continued) structure of MSCs: directly after printing (**d**), after 25 days under osteogenic (**e**), and after 21 days under chondrogenic (**f**), or adipogenic (**g**) culture conditions. Microscopic images with phase contrast (**e**, **f**), vitality staining (**d**, calcein AM), Oil Red O staining (**g**). Accumulation of calcium phosphate for osteogenic differentiation (**e**) and lipid vacuoles indicating adipogenic differentiation (**g**) can be seen (Reprinted from Gruene et al. (2011b) Copyright © 2011 Mary Ann Liebert, Inc. publishers and Gruene et al. (2011c) Copyright © 2010 IOP Publishing. Reproduced with permission. All rights reserved)

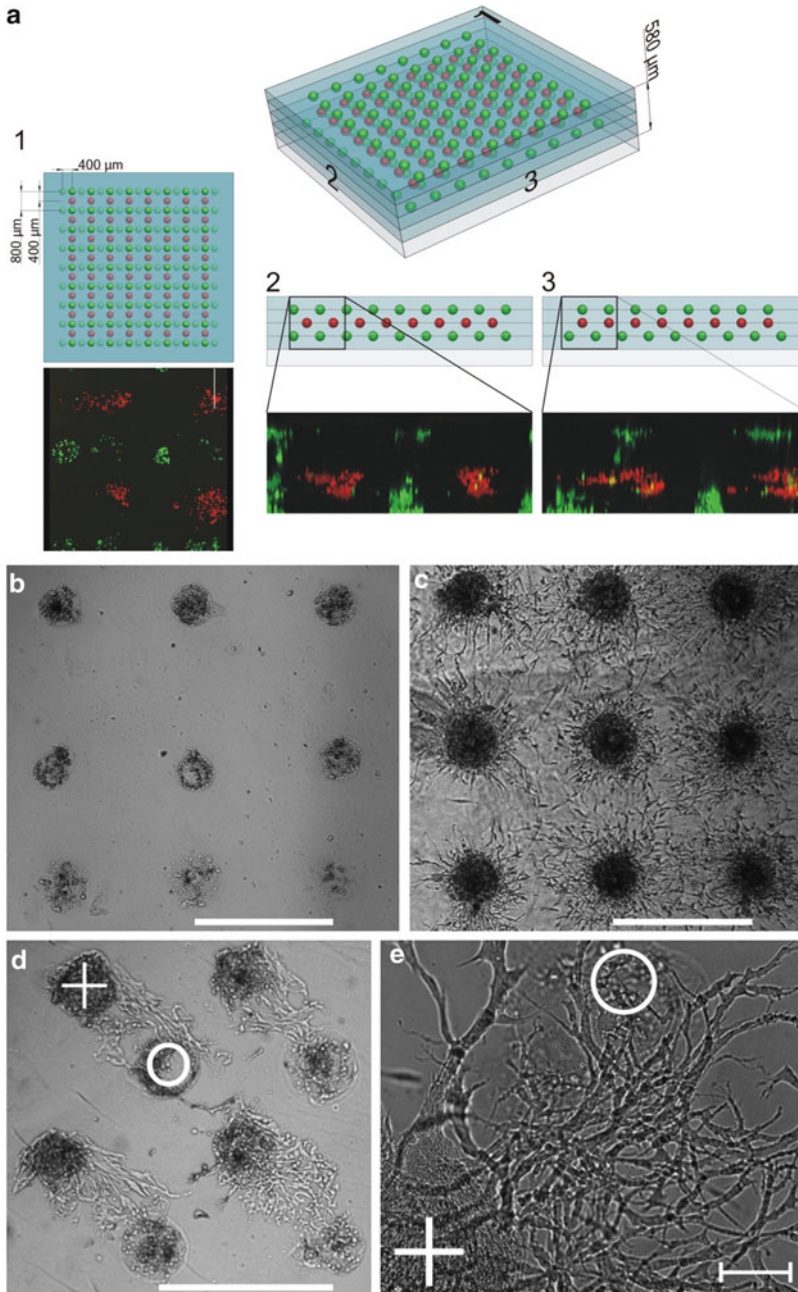


Fig. 6 (a) Three-dimensional reconstruction of the 3D cell array by means of confocal laser scanning microscopy and the corresponding CAD model. ECFCs were stained with calcein (green), and ASCs were stained with TAMRA-5 (red). (b–e) Visualization of cell–cell interactions by 3D cell arrays in mono- and co-cultures, cultivated for 5 days under VEGF-free conditions.

The migration of ASCs toward ECFCs may be due to a gradient of platelet-derived growth factor (PDGF). The subtype PDGF-BB is expressed in large amounts by ECFCs and is well known for the stimulation of ASC proliferation and migration (Hellström et al. 1999).

Gruene et al. (2011d) also printed 3D cell arrays with the same cell types as a multilayer pattern. A hydrogel consisting of a fibrin precursor (fibrinogen) and hyaluronic acid served as the bio-ink and extracellular matrix material. First, a layer of fibrin is produced on a glass slide by blade-coating a fibrinogen layer and subsequent cross-linking with thrombin; second, different cell types are printed on top of these fibrin layers in droplets with a predefined spot spacing by LaBP; and third, a second fibrin layer is deposited on top using the same procedure. Then, the second and third steps have been repeated several times to produce true 3D cell arrays.

By printing spots of ASCs and ECFCs, they demonstrated that (i) cell spots can be arranged layer by layer in a 3D array; (ii) any cell–cell ratio, cell quantity, cell-type combination, and spot spacing can be realized within this array; and (iii) the height of the 3D array is freely scalable. The fibrin-based environment could be replaced by any other hydrogel. Printed cell arrays are a suitable tool for investigating such complex interactions between different cell types like vascular network formation in engineered tissue constructs. In another study (Taidi et al. 2016), droplets of alginate containing yeast (*Saccharomyces cerevisiae* var. *bayanus*) or algae (*Chlorella vulgaris*) have been printed and co-cultured to study the interactions between oxygen-consuming yeast and oxygen-generating algae colonies. Thereby, successful printing of microorganisms has been demonstrated.

5.3 Stackable Biopapers with Printed Cells

For the generation of 3D cell constructs thicker than the diffusion limit of a few 100 μm , the application of so-called biopapers was proposed as an alternative to directly print cell-containing gels layer by layer. Biopapers are flat substrates, sometimes spongy or scaffold-like, that are also referred to as sheets. Onto each biopaper, cells are printed in a two-dimensional pattern, and later the biopapers are stacked to generate a 3D structure and 3D assembly of the cells.

This concept has been combined with LaBP by Pirlo et al. (2011) and Catros et al. (2012). As spongy substrates, they used 300 μm thick poly(lactic-co-glycolic acid) (PLGA) scaffolds coated with Matrigel™ (now Corning Inc., NY, USA) and 100 μm thick electrospun polycaprolactone (PCL) scaffolds, respectively. As 2D patterns, they printed human umbilical vein endothelial cells (HUVEC) onto the

Fig. 6 (continued) A circle indicates the printed ECFC spot and a cross the printed ASC spot. Interactions of ASCs and ECFCs (d, e) in comparison to separated arrays of ECFCs (b) and ASCs (c). A vascular-like network formation occurs after 5 days in the co-culture (e). Distance between spots with the same cell type is 800 μm . Scale bars are 250 μm (e) or 800 μm (b–d) (Reprinted from Gruene et al. (2011d), Copyright © 2011 Mary Ann Liebert, Inc. publishers)

Matrigel™-coated PLGA sheets and MG63 osteoblastic cells onto the PCL scaffolds, respectively. Later, they stacked these biopapers with printed cells to achieve 3D cell constructs. This technique enables cultivation of the 2D printed cells on the individual biopapers and cell formation with tissue-like intercellular junctions before stacking.

If generation of functional vascular networks on single biopapers is possible, this would be a very promising approach. The stacking of the biopapers could be carried out several days after printing, having enough time for vessel formation while the biopapers are in cell culture medium and the supply of cells with nutrients and oxygen is ensured. Stacking biopapers with functional vascular networks later would enable cell supply even in very thick 3D cell constructs. Additionally, requirements on the cell-embedding sol are reduced, since stiffness for three-dimensionality is not needed.

However, for generating predefined 3D patterns with high fidelity, precise stacking without any shift or rotation is essential. Furthermore, connections between cells and vascular networks of subsequent biopapers are required to achieve 3D tissue. Otherwise, cells would be involved in 2D cell patterns of single biopapers only, even if molecules like second messengers could diffuse through the biopapers. A further challenge would be to connect the vascular networks of several biopapers to some perfusion system. How far this method can be advanced remains to be seen.

5.4 Printed Skin Tissue

The major aim of cell printing is fabrication of functional tissues and organs with a wide area of application. Firstly, printed 3D patterns mimicking the placement of cells in specific tissues could improve our understanding of cell behavior, tissue functions, and regeneration. These complex interactions in 3D tissue and cell microenvironments *in vivo* cannot be simulated adequately with common *ex vivo* cell studies in two-dimensional cell cultures. Cell behavior differs radically in 3D.

Secondly, reproducibly printed 3D human tissue models can serve as test systems for studying effects and tolerability of chemical agents, cosmetics, or pharmaceuticals on tissues and organs. They could be integrated in so-called body-on-a-chip systems, more complex systems consisting of different tissue types combined in a micro-fluidic system. By using human cells, testing with such printed tissue models could even be more relevant than animal testing due to differences in the metabolism between animals and humans.

Of course, the ultimate goal of cell printing would be printing of complete human tissues and organs with full functionality as replacement organs for implantation to overcome the lack of donor organs. Organs, printed from autologous cells, someday may even outclass donor organs, since no rejection reaction is expected to occur and no lifelong intake of immunosuppressant is needed.

Currently, research is far away from printing fully functional organs. For such organs an integrated perfusable vascular network would be necessary to supply the printed cells with oxygen and nutrients, if the tissue size is above a few hundred microns. The vascular networks of natural tissue consist of vessels with diameters

between 10 μm and a few millimeters. Such perfusable networks have not been printed so far.

However, basic tissue has already been printed. Koch et al. (2012) printed simple skin tissue consisting of two cell types, murine fibroblast (NIH3T3) and human keratinocyte (HaCaT from adult human skin) cell lines. This combination of well-established cell lines can be found in other studies (Bigelow et al. 2005), too. 3T3 fibroblast cells are widely used in the cultivation of keratinocytes, because they are secreting growth factors favorable for keratinocytes (Linge 2004).

Koch et al. (2012) printed these cells from 20 layers of fibroblasts and 20 layers of keratinocytes, both embedded in collagen type I, to mimic the layered structure of natural skin with dermis and epidermis (Fig. 7). Collagen was used as bio-ink in order to approximate native skin as good as possible, since it is the main component of the extracellular matrix in the skin. A collagen–elastin matrix (Matriderm, Dr. Suwelack Skin & Health Care, Billerbeck, Germany) was used as the basic substrate to print onto.

The main goal of this study was investigating tissue formation by cells after laser printing. Therefore, the existence of intercellular junctions, adherens junctions (Niessen 2007), and gap junctions (Mese et al. 2007) was observed. Such junctions can be found as cell–cell and cell–matrix connections in all kinds of tissue, abundantly in epithelium like the epidermis. Adherens junctions are fundamental for tissue morphogenesis and cohesion; they consist mainly of cadherins (calcium-dependent adherent proteins). Gap junctions are cell–cell channels that allow intercellular communication by passing chemical signals; they consist of connexins (Richard 2000) and are known to have a fundamental role in differentiation, cell cycle progression, and cell survival (Schlie et al. 2010).

In the printed skin tissue, the extensive formation of intercellular adherens junctions between printed keratinocytes and a minor formation between fibroblasts could be observed after 10 days. This is expected, since there is typically (Niessen 2007) a higher level of junctions in the dermal epithelium (epidermis), formed by keratinocytes.

The formation of gap junctions has also been observed in the cell membranes between all adjacent cells 10 days after printing. The functionality of cell–cell communication via gap junction coupling has been verified in vital 3D cell constructs with a dye-transfer method. Thereby, it has been demonstrated with respect to adherens and gap junctions that tissue-specific functions are developed by printed skin cells in collagen.

Furthermore, the formation of a basement membrane between keratinocytes and fibroblasts has been observed (Fig. 7), as it exists between epidermis and dermis in natural skin.

The same skin constructs have also been implanted into full-thickness skin wounds in nude mice, applying a dorsal skinfold chamber (Michael et al. 2013). They were fully connected to the surrounding tissue after 11 days. A multilayered epidermis has been formed by the printed keratinocytes with beginning differentiation and stratum corneum. Blood vessels have been detected to grow from the wound bed and the wound edges into the printed cells.

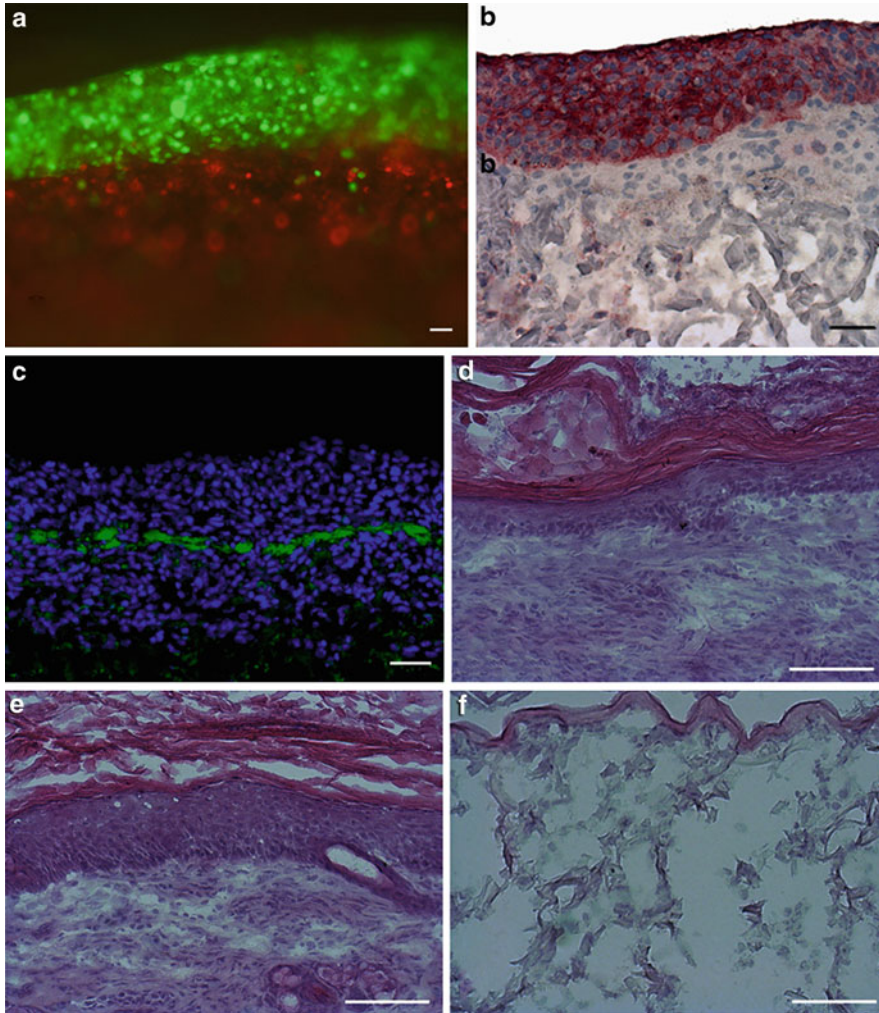


Fig. 7 Laser-printed skin tissue mimicking its bilayered structure: Embedded in collagen type I, 20 layers of murine fibroblasts and 20 layers of human keratinocytes were printed subsequently on a collagen–elastin substrate. **(a)** Section through the laser-printed construct with transduced fibroblasts (*red*) and keratinocytes (*green*), prepared directly after printing. **(b, c)** Cryostat sections, prepared 10 days after printing. Immunoperoxidase staining of cytokeratin 14 (**b**) depicts keratinocytes in *reddish brown* in the bilayered structure while all cell nuclei (fibroblasts and keratinocytes) are stained with hematoxylin in *light blue*. Image **(c)** shows an anti-laminin staining in *green* and all cell nuclei in *blue* (Hoechst 33342). Laminin is a major constituent of the basement membrane in the skin. **(d–f)** Hematoxylin–eosin staining of paraffin sections, prepared after implantation for 10 days in dorsal skin of nude mice. Printed skin cells **(d)**, on a collagen–elastin matrix; native dorsal mouse skin **(e)**; the collagen–elastin matrix **(f)**, implanted without cells, as a control. Scale bars are 50 μm (**a–c**) or 100 μm (**d–f**) (Partially reprinted from Koch et al. (2012), Copyright © 2012 Wiley Periodicals, Inc.)

However, natural mouse skin (Fig. 7e) is much more complex than the printed one (Fig. 7d). Figure 7f depicts Matriderm without printed cells after implantation for 11 days.

Actually no skin equivalent exists, which satisfactorily mimics native skins' functions (or appearance), like, e.g., the capability to control the body temperature with sweat glands, sensory skills, immunocompetence, or hair follicles. In future, LaBP might enable skin generation with all necessary cells in their specific micro-environment and the corresponding functions.

5.5 In Situ Printing

An alternative to implanting printed 3D cell constructs or tissue is printing cells directly into wounds or tissue defects. This has been demonstrated by Keriquel et al. (2010) by printing nano-hydroxyapatite (n-HA) slurry in mouse calvaria defect models *in vivo*. Hydroxyapatite is the major nonorganic component of bone and has been used in many studies on bone tissue engineering.

Two 4 mm diameter defects were generated with a trephine in the mouse skull. Into one defect the slurry has been printed, while the other one served as control. Thirty layers of the slurry containing n-HA and glycerol, with a thickness of about 20 μm each and 3 mm in diameter, have been printed layer by layer into one defect. Both defects were re-covered with soft tissue after printing.

After 3 months, in many defects with printed n-HA mature bone tissue has been observed, while bone repair has been incomplete in many mice's control defect (Fig. 8). However, from one mouse (sample) to another, bone regeneration was very inhomogeneous, and no statistical significance has been observed in bone repair enhancement by n-HA printing.

Besides the printing experiments, it has been investigated if tissue irradiated by infrared laser (1064 nm wavelength) during the printing might be harmed. Magnetic resonance imaging of directly irradiated dura mater, the outermost membrane enveloping the brain that is closest to the skull, displayed edema on the irradiated side after 1 week that has regressed after 2 weeks and has disappeared after 3 weeks. Therefore, it has been concluded that no deleterious effects are induced by the applied infrared laser on the brain tissue.

Although the experimental results have been heterogeneous and no cells have been printed, *in vivo* bioprinting has been successfully demonstrated. *In vivo* cell printing should be possible exactly the same way.

6 Discussion

Laser-assisted bioprinting (LaBP) has been applied for more than a decade for printing vital cells and different biomaterials in predefined two- and three-dimensional patterns.

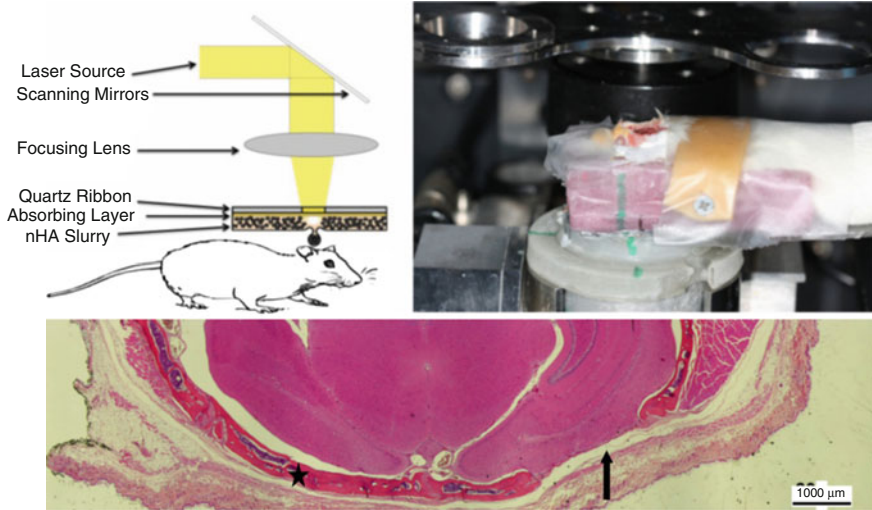


Fig. 8 In situ bioprinting in mouse model: *Top*: (a) Schematic setup for in vivo laser printing; (b) specific holder for in vivo printing in mouse calvaria defects. *Bottom*: Complete bone repair on the test side was observed in one sample after 3 months (*star*). The bone defect control site is not reconstructed in this picture (*arrow*) (Reprint from Keriquel et al. (2010), Copyright © 2010 IOP Publishing. Reproduced with permission. All rights reserved)

Various cell types (cell lines, primary cells, stem cells) have been printed, and different studies have consistently demonstrated that this technique does not harm the printed cells or influence the differentiation potential of stem cells.

LaBP allows printing of (i) cell amounts ranging from single to hundreds of cells per droplet, (ii) sols (hydrogel precursors) with a wide range of rheological properties, and (iii) cells with micrometer resolution in a high-throughput manner. Besides cells, also microorganisms like yeast or algae, DNA, growth factors, or biological agents can be printed.

Different lasers with wavelength from ultraviolet 193 nm to infrared 1064 nm and pulse durations from 500 fs to 30 ns have been used, demonstrating that no specific laser parameters are generally preferable. There is also a broad range of materials that have been applied as laser absorption layers; however, some materials require a specific laser wavelength range, like ultraviolet radiation for some polymers.

The optimal absorption layer material has not been found so far. The requirements are (i) easy to be disposed on a laser transparent substrate, (ii) to offer surface characteristics that allow to blade-coat very homogeneous sol layers on it, (iii) no side effects on cells, and (iv) no debris generation by laser vaporization.

Additionally, many different bio-inks have been applied with a wide range of rheological parameters. Typically, this is a sol mixture that is cross-linked after printing, but also printing with cell media has been demonstrated. The bio-ink always needs to be chosen with respect to the cell type and desired tissue to be printed. Some cells are affected in their behavior by specific sols or hydrogels, and so

far there is not one bio-ink that fits for all applications. However, the choice of bio-ink has also an effect on achievable printing resolution.

Besides the development of the laser-assisted bioprinting technique itself and testing of materials for laser absorption and as bio-inks, a wide range of applications have been demonstrated.

Printing of stem cells for fabrication of 3D scaffold-free autologous grafts was shown. Mesenchymal stem cells have been printed in 3D patterns and differentiated toward different lineages (osteogenic, chondrogenic, and adipogenic) within their predefined structure. Especially, human adipose-derived stem cells offer large clinical potential for autologous tissue reconstruction therapies due to the ease of their withdrawal from adipose tissue and their ability to differentiate down the mesenchymal and non-mesenchymal pathway (Schaeffler and Buechler 2007).

For cell–cell and cell–environment interaction studies, LaBP was used to precisely arrange different cells in 3D spot arrays. As a proof of concept, interactions between endothelial cells and stem cells toward generating new blood vessels were investigated.

For proving the formation of tissue by printed cells, skin cells have been laser-printed in 3D multicellular constructs analogous to native skin archetype. The involvement of intercellular adhesion and communication via adherens and gap junctions could be observed, which proves the tissue formation.

Reproducibly fabricated tissue equivalents could serve as 3D environments for studying cell behavior. By integrating further cell types, like endothelial cells for vascularization or dendritic cells in printed skin tissue for immune reactions, tissue equivalents may be developed further to their natural archetype. They could be used for testing cosmetics, pharmaceutical, or chemical agents reducing animal testing. Compared to animal testing, reproducibility of the printed skin tissue could become a significant advantage.

The tissue that has been printed with LaBP so far is relatively thin, which allows to supply cells with nutrients and oxygen by diffusion. For printing thicker tissue, a perfusable vascular network is required. This is the key challenge researchers are dealing with today in the tissue engineering field. Such a vascular network could be generated by printing blood vessel cells in a pattern integrated in the 3D printed structure. However, this network needs to be connected to an external pump and to be functional after a relatively short time period to supply the printed cells with nutrition.

For some tissue types, printing alone is not sufficient. If, for example, heart muscle tissue printing is intended, stimulation of the printed cell structure by mechanical forces is required, to induce a parallel orientation of the cells. A fabrication technique of very small cardiac tissue pieces already has been developed; for the fabrication of bigger tissue, it needs to be modified including the integration of a vascular network.

Additionally, for some organs even not all cell types are available, yet. Isolated from tissue and brought to conventional cell culture, cells may change their phenotype and lose their functionality. Some cell types still can't be cultivated outside their 3D microenvironment.

An alternative to scaffold-free printing of 3D cell constructs and tissue could be 3D stacking of biopapers, each with a printed 2D pattern on the biopaper surface. If a precise stacking is provided, this technique can enable the generation of well-defined 3D patterns within a 3D scaffold structure. Apart from some special scaffold geometries, this is not possible with conventional scaffolds, seeded with cells after fabrication. However, establishing vascular networks on 2D surfaces and integrating these 2D networks into a perfusable 3D vascular network will be very challenging.

Furthermore, direct printing into wounds of test animals was successfully tested. In the future, such an in situ printing might be applied in surgery for tissue repair, e. g., for cartilage or bone.

7 Conclusions

For generating replacement tissue and organs as well as cell-based therapies, an extensive understanding of interactions between different cells and their environment is essential. However, conventional cell studies *ex vivo* on two-dimensional cell culture plastic surfaces are limited significantly and are not appropriate to simulate complex interactions in cell microenvironments *in vivo* and in 3D tissue; cell behavior differs dramatically in 3D.

Thus, printed 3D cell models could enable better understanding of tissue-specific cell behavior and tissue regeneration. Really complex tissue, especially with an integrated vascular network, has not been printed so far. Nevertheless, first steps in this direction have already been taken. For future progress in tissue engineering, the development of reproducible well-defined 3D cell models is a key challenge. Since the structural dimensions in natural tissue are significantly lower than 100 μm , the ability to precisely position different cells in complex 3D patterns is essential.

There are other printing techniques under investigation, like techniques based on ink-jet printing, acoustic droplet ejection, or extrusion systems, which are described in other chapters of this book. Compared with them, laser-assisted bioprinting enables to print droplets of biomaterials (with or without cells) combining very low volumes with high viscosities (much higher than it can be done with the ink-jet printer or acoustic droplet ejection) and high cell densities. However, each technique has its advantages and disadvantages, and it is not clear yet if one technique will prevail in the future. Probably, there will be applications for all these techniques.

The ability of LaBP to precisely position various sols with a broad range of viscosities and high embedded cell densities in very small droplets is an important feature for future progress in printing complex tissue and organs.

Acknowledgments The authors acknowledge the financial support from Deutsche Forschungsgemeinschaft (DFG), the Cluster of Excellence *REBIRTH*, and project *Biofabrication for NIFE*, funded by State of Lower Saxony and Volkswagenstiftung.

References

- Akeson A, Herman A, Wiginton D, Greenberg J (2010) Endothelial cell activation in a VEGF-a gradient: relevance to cell fate decisions. *Microvasc Res* 80:65
- Barron JA, Ringeisen BR, Kim H, Spargo BJ, Chrisey DB (2004) Application of laser printing to mammalian cells. *Thin Solid Films* 453–454:383–387
- Barron JA, Young HD, Dlott DD, Darfler MM, Krizman DB, Ringeisen BR (2005a) Printing of protein microarrays via a capillary-free fluid jetting mechanism. *Proteomics* 5(16):4138–4144
- Barron JA, Krizman DB, Ringeisen BR (2005b) Laser printing of single cells: statistical analysis, cell viability, and stress. *Ann Biomed Eng* 33(2):121–130
- Baum M, Kim H, Alexeev I, Piqué A, Schmidt M (2013) Generation of transparent conductive electrodes by laser consolidation of LIFT printed ITO nanoparticle layers. *Appl Phys A* 111 (3):799–805. <https://doi.org/10.1007/s00339-013-7646-y>
- Bigelow RLH, Jen EY, Delehedde M, Chari NS, McDonnell TJ (2005) Sonic hedgehog induces epidermal growth factor dependent matrix infiltration in HaCaT keratinocytes. *J Invest Dermatol* 124:457
- Brown MS, Kattamis NT, Arnold CB (2010) Time-resolved study of polyimide absorption layers for blister-actuated laser-induced forward transfer. *J Appl Phys* 107:083103
- Brown MS, Brasz CF, Ventikos Y, Arnold CB (2012) Impulsively actuated jets from thin liquid films for high resolution printing applications. *J Fluid Mech* 709:341–370. <https://doi.org/10.1017/jfm.2012.337>
- Catros S, Guillemot F, Nandakumar A, Ziane S, Moroni L, Habibovic P, van Blitterswijk C, Rousseau B, Chassande O, Amédée J, Fricain J-C (2012) Layer-by-layer tissue microfabrication supports cell proliferation in vitro and in vivo. *Tissue Eng Part C Methods* 18(1):62–70
- Clause KC, Liu LJ, Tobita K (2010) Directed stem cell differentiation: the role of physical forces. *Cell Commun Adhes* 17(2):48–54
- Dinca V, Ranella A, Popescu A, Dinescu M, Farsari M, Fotakis C (2007) Parameters optimization for biological molecules patterning using 248-nm ultrafast lasers. *Appl Surf Sci* 254:1164–1168
- Dinca V, Farsari M, Kafetzopoulos D, Popescu A, Dinescu M, Fotakis C (2008) Patterning parameters for biomolecules microarrays constructed with nanosecond and femtosecond UV lasers. *Thin Solid Films* 516:6504–6511
- Discher DE, Mooney DJ, Zandstra PW (2009) Growth factors, matrices, and forces combine and control stem cells. *Science* 324:1673
- Duocastella M, Fernández-Pradas JM, Morenza JL, Serra P (2010a) Sessile droplet formation in the laser-induced forward transfer of liquids: a time-resolved imaging study. *Thin Solid Films* 518:5321–5325
- Duocastella M, Patrascioiu A, Fernández-Pradas JM, Morenza JL, Serra P (2010b) Film-free laser forward printing of transparent and weakly absorbing liquids. *Opt Express* 18(21):21815–21825
- Fernandes TG, Diogo MM, Clark DS, Dordick JS, Cabral JMS (2009) High-throughput cellular microarray platforms: applications in drug discovery, toxicology and stem cell research. *Trends Biotechnol* 27(6):342
- Gaebel R, Ma N, Liu J, Guan J, Koch L, Klopsch C, Gruene M, Toelk A, Wang W, Mark P, Wang F, Chichkov B, Li W, Steinhoff G (2011) Patterning human stem cells and endothelial cells with laser printing for cardiac regeneration. *Biomaterials* 32:9218–9230
- Gruene M, Unger C, Koch L, Deiwick A, Chichkov B (2011a) Dispensing picolitre of a natural hydrogel by laser-assisted bioprinting. *Biomed Eng Online* 10:19
- Gruene M, Deiwick A, Koch L, Schlie S, Unger C, Hofmann N, Bernemann I, Glasmacher B, Chichkov B (2011b) Laser printing of stem cells for biofabrication of scaffold-free autologous grafts. *Tissue Eng Part C Methods* 17:79–87
- Gruene M, Pflaum M, Deiwick A, Koch L, Schlie S, Unger C, Wilhelmi M, Haverich A, Chichkov B (2011c) Adipogenic differentiation of laser-printed 3D tissue grafts consisting of human adipose-derived stem cells. *Biofabrication* 3:015005

- Gruene M, Pflaum M, Hess C, Diamantouros S, Schlie S, Deiwick A, Koch L, Wilhelmi M, Jockenhoewel S, Haverich A, Chichkov B (2011d) Laser printing of three-dimensional multicellular arrays for studies of cell-cell and cell-environment interactions. *Tissue Eng Part C Methods* 17(10):973–982
- Hellström M, Kalén M, Lindahl P, Abramsson A, Betsholtz C (1999) Role of PDGF-B and PDGFR-beta in recruitment of vascular smooth muscle cells and pericytes during embryonic blood vessel formation in the mouse. *Development* 126:3047
- Hon KKB, Li L, Hutchings IM (2008) Direct writing technology—advances and developments. *CIRP Ann* 57:601–620
- Hopp B, Smausz T, Kresz N, Barna N, Bor Z, Kolozsvári L, Chrisey DB, Szabo A, Nogradi A (2005) Survival and proliferative ability of various living cell types after laser-induced forward transfer. *Tissue Eng* 11(11-12):1817–1823
- Hui TY, Cheung KMC, Cheung WL, Chan D, Chan BP (2008) In Vitro chondrogenic differentiation of human mesenchymal stem cells in collagen microspheres: influence of cell seeding density and collagen concentration. *Biomaterials* 29:3201
- Keriquel V, Guillemot F, Arnault I, Guillotin B, Miraux S, Amédée J, Fricain J-C, Catros S (2010) In vivo bioprinting for computer- and robotic-assisted medical intervention: preliminary study in mice. *Biofabrication* 2:014101
- Klopsch C, Gäbel R, Kaminski A, Mark P, Wang W, Toelk A, Delyagina E, Kleiner G, Koch L, Chichkov B, Mela P, Jockenhoewel S, Ma N, Steinhoff G (2012) Spray- and laser-assisted biomaterial processing for fast and efficient autologous cell-plus-matrix tissue engineering. *J Tissue Eng Regen Med* 9(12):E177–E190. <https://doi.org/10.1002/term.1657> Epub 2012 Dec 4 (2015)
- Koch L, Kuhn S, Sorg H, Gruene M, Schlie S, Gaebel R, Polchow B, Reimers K, Stoelting S, Ma N, Vogt PM, Steinhoff G, Chichkov B (2010) Laser printing of skin cells and human stem cells. *Tissue Eng Part C Methods* 16:847–854
- Koch L, Deiwick A, Schlie S, Michael S, Gruene M, Coger V, Zychlinski D, Schambach A, Reimers K, Vogt PM, Chichkov B (2012) Skin tissue generation by laser cell printing. *Biotechnol Bioeng* 109:1855–1863
- Lin Y, Huang Y, Chrisey DB (2009) Droplet formation in matrix-assisted pulsed-laser evaporation direct writing of glycerol-water solution. *J Appl Phys* 105(9):093111
- Lin Y, Huang Y, Chrisey DB (2011) Metallic foil-assisted laser cell printing. *J Biomech Eng* 133:025001
- Linge C (2004) Establishment and maintenance of normal human keratinocyte cultures. In: Picot J (ed) *Methods in molecular medicine*, vol 107, Human cell culture protocols. Humana Press, Totowa, p 1
- Merfeld-Clauss S, Gollahalli N, March KL, Traktuev DO (2010) Adipose tissue progenitor cells directly interact with endothelial cells to induce vascular network formation. *Tissue Eng Part A* 16(9):2953
- Mese G, Richard G, White TW (2007) Gap junctions: basic structure and function. *J Invest Dermatol* 127:2516–2524
- Michael S, Sorg H, Peck C-T, Koch L, Deiwick A, Chichkov B, Vogt PM, Reimers K (2013) Tissue engineered skin substitutes created by laser-assisted bioprinting form skin-like structures in the dorsal skin fold chamber in mice. *PLoS One* 8(3):e57741
- Mirsky N, Cohen Y (1995) VEGF and ECGF induce directed migration of endothelial cells: qualitative and quantitative assay. *Endothelium* 255:5444
- Niessen CM (2007) Tight junctions/adherens junctions: basic structure and function. *J Invest Dermatol* 127:2525–2532
- Odde DJ, Renn MJ (1999) Laser-guided direct writing for applications in biotechnology. *Trends Biotechnol* 17:385–389
- Othon CM, Wu X, Anders JJ, Ringeisen BR (2008) Single-cell printing to form three-dimensional lines of olfactory ensheathing cells. *Biomed Mater* 3:034101. <https://doi.org/10.1088/1748-6041/3/3/034101>

- Ovsianikov A, Gruene M, Pflaum M, Koch L, Maiorana F, Wilhelmi M, Haverich A, Chichkov B (2010) Laser printing of cells into 3D scaffolds. *Biofabrication* 2:014104
- Palla-Papavlu A, Paraico I, Shaw-Stewart J, Dinca V, Savopol T, Kovacs E, Lippert T, Wokaun A, Dinescu M (2011) Liposome micropatterning based on laser-induced forward transfer. *Appl Phys A* 102(3):651–659
- Pirlo RK, Wu P, Liu J, Ringeisen B (2011) PLGA/hydrogel biopapers as a stackable substrate for printing HUVEC networks via BioLPTM. *Biotechnol Bioeng* 109(1):262–273
- Richard G (2000) Connexins: a connection with the skin. *Exp Dermatol* 9:77
- Ringeisen BR, Kim H, Barron JA, Krizman DB, Chrisey DB, Jackman S, Auyeung RYC, Spargo BJ (2004) Laser printing of pluripotent embryonal carcinoma cells. *Tissue Eng* 10(3-4):483–491
- Ringeisen BR, Othon CM, Barron JA, Young D, Spargo BJ (2006) Jet-based methods to print living cells. *Biotechnol J* 1:930–948
- Schaeffler A, Buechler C (2007) Concise review: adipose tissue-derived stromal cells – basic and clinical implications for novel cell-based therapies. *Stem Cells* 25:818–827
- Schiele NR, Chrisey DB, Corr DT (2011) Gelatin-based laser direct-write technique for the precise spatial patterning of cells. *Tissue Eng Part C* 17(3):289–298
- Schlie S, Mazur K, Bintig W, Ngezahayo A (2010) Cell cycle dependent regulation of gap junction coupling and apoptosis in GFSHR-17 granulosa cells. *J Biomed Sci Eng* 3:884–891
- Taidi B, Leberne G, Koch L et al (2016) Colony development of laser printed eukaryotic (yeast and microalga) micro-organisms in co-culture. *Int J Bioprint* 2(2):146–152. <https://doi.org/10.18063/IJB.2016.02.001>
- Takagi M, Umetsu Y, Fujiwara M, Wakitani S (2007) High inoculation cell density could accelerate the differentiation of human bone marrow mesenchymal stem cells to chondrocyte cells. *J Biosci Bioeng* 103:98
- Unger C, Gruene M, Koch L, Koch J, Chichkov B (2011) Time-resolved imaging of hydrogel printing via laser-induced forward transfer. *Appl Phys A* 103:271–277
- Vogel A, Lorenz K, Horneffer V, Hüttmann G, von Smolinski D, Gebert A (2007) Mechanisms of laser-induced dissection and transport of histologic specimens. *Biophys J* 93:4481–4500
- Wu Y, Chen L, Scott PG, Tredget EE (2007) Mesenchymal stem cells enhance wound healing through differentiation and angiogenesis. *Stem Cells* 25(10):2648
- Yan J, Huang Y, Chrisey DB (2013) Laser-assisted printing of alginate long tubes and annular constructs. *Biofabrication* 5:015002



Development of Nanocellulose-Based Bioinks for 3D Bioprinting of Soft Tissue

Paul Gatenholm, Hector Martinez, Erdem Karabulut, Matteo Amoroso, Lars Kölby, Kajsa Markstedt, Erik Gatenholm, and Ida Henriksson

Contents

1	Introduction	332
1.1	Surgical Needs for Soft Tissue	332
1.2	Review of Bioinks for Soft Tissue	336
1.3	Evaluation of Bioinks	338
2	Commercialization of Novel Bioink for Soft Tissue Applications	346
3	Conclusions	348
	References	349

Abstract

3D bioprinting technology is expected to revolutionize the field of medicine and health care particularly within soft tissue repair and reconstruction. Surgical needs for soft tissue repair include nose, ear, meniscus, and cartilage in joints, as well as repair of damaged nerve tissue, and repair or replacement of damaged skin. 3D bioprinting technology includes a 3D bioprinter, cells, and bioink. Novel bioinks

P. Gatenholm (✉) · E. Karabulut · K. Markstedt · I. Henriksson
Chalmers University of Technology, 3D Bioprinting center Väst (BBV), Göteborg, Sweden
e-mail: paul.gatenholm@chalmers.se; erdemk@chalmers.se; kajsam@chalmers.se;
idahen@chalmers.se

H. Martinez
Chalmers University of Technology, 3D Bioprinting center Väst (BBV), Göteborg, Sweden
CELLINK AB, Göteborg, Sweden
e-mail: hm@cellink.com

M. Amoroso · L. Kölby
Sahlgrenska University Hospital, Plastic Surgery, Göteborg, Sweden
e-mail: matteo.amoroso@vgregion.se; lars.kolby@surgery.gu.se

E. Gatenholm
CELLINK AB, Göteborg, Sweden
e-mail: eg@cellink.com

which will be suitable for soft tissue repair need to be developed before 3D bioprinting technology can get into the clinic. Hydrogels and cell-laden hydrogels are very attractive for soft tissue application because of the similarity of mechanical properties and cell environment. The process of design and development of novel bioinks is described in detail in this chapter which includes rheology, printability, cross-linking, long-term stability in medium, cell viability, and stimulation of cells during tissue growth. The commercialization process of bioinks is also described.

1 Introduction

1.1 Surgical Needs for Soft Tissue

3D bioprinting technology has emerged as a new technology to create biologically active 3D constructs. The 3D bioprinting technology enables placement of multiple cell types, biomaterials, and biomolecules in a layer-by-layer fashion to generate predefined, biologically active 3D structures (Groll et al. 2016). This chapter addresses the potentials and limitations of bioprinting for soft tissue regeneration in three distinct areas: cartilage, nerve tissue, and the skin.

1.1.1 Bioprinted Cartilage Tissue

Cartilage is an avascular tissue that once degenerated or wounded has limited ability to heal. The demand for cartilage tissue restoration is therefore high. Current treatments for cartilage repair (Lindahl 2015) or replacement (Firmin and Marchac 2011) are often challenging. Auricular reconstructive surgery would, for example, greatly benefit from innovations brought by 3D bioprinting. The ear is a convoluted structure that is difficult to reproduce surgically because of its own complex architecture consisting of a delicate elastic cartilage core surrounded by a fine skin envelope.

The fundamental principle of current auricular reconstruction dates back to 1959 when Tanzer (Tanzer 1959) described the use of autologous costal cartilage to create a 3D auricular framework. Technical refinements have been applied during the years, and a two-stage auricular reconstruction using autologous costal cartilage framework is the current gold standard treatment (Luquetti et al. 2011). The rib cartilage is harvested from the patient's own ribs and 3D auricle framework is implanted subcutaneously (see Fig. 1). A second operation is required to obtain adequate projection. The limitations of this method are the multi-step and time-consuming nature of the procedure. Relatively inconsistent aesthetic results occur, due to contraction of the fibrous tissue surrounding the cartilage framework. Moreover, donor site morbidity can cause rib cage deformities in young patients. Serious problems are represented by pneumothorax, infections of the cartilage framework, or necrosis of the overlying skin flap leading to extrusion of the implant.

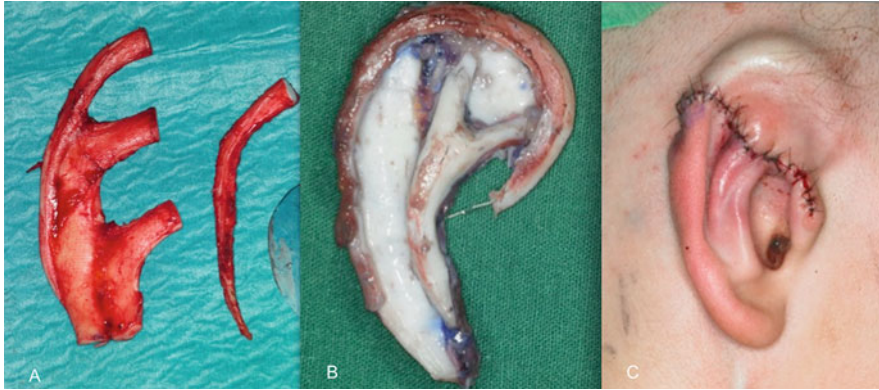


Fig. 1 Ear reconstruction with autologous rib cartilage graft. Harvesting of rib cartilage (a). Creation of an ear framework body (b). Insertion of the ear framework into a subcutaneous pocket (c) (By courtesy of Giovanni Maltese M.D., PhD, Craniofacial Surgery Unit, Sahlgrenska University Hospital, Göteborg, Sweden)

3D bioprinting is an emerging technology which has the potential to restore missing or destroyed cartilage tissue, such as the auricle, because of its ability to mimic the native biological and functional properties of the tissue and thus overcoming the current treatment limitations. The lack of structural organization and the inferior mechanical properties of the 3D bioprinted structure, compared to native cartilage, represent the main challenges and limitation of this technology. Key elements for the success and future clinical application of this regenerative technology are represented by the biological properties, mechanical characteristics, architectural structure, and shape stability of the 3D printed construct.

It has been widely demonstrated that the bioprinting process using extrusion, inkjet, or laser-based printing technologies does not hamper the viability or long-term performance of the deposited cells (Visser et al. 2013). In order to successfully generate 3D bioprinted cartilage constructs, the bioink has to meet specific prerequisites. Shape stability, mechanical strength, and biological properties are required properties of the bioink to enhance cell proliferation and extracellular matrix deposition and provide structural stability to the final construct. Moreover an additional requirement for an ideal bioink for in vivo use is long-term structural integrity. Hydrogels represent the most common materials used as bioink (Guillotin and Guillemot 2011). Although substantial progress has been made, the lack of mechanical and structural integrity of the 3D constructs still represent the major difficulties. In order to compensate the mechanical limitations, the hydrogel can be combined with supporting polymer (Markstedt et al. 2015) or with other materials such as gelatin (Schuurman et al. 2013).

Multiple cell types have been explored to generate a biologically active cartilage construct. The use of autologous chondrocytes has been investigated. Chondrocytes can be harvested from the patient's cartilage defect (Bekkers et al. 2013; Poole et al. 1988),

expanded in culture, and transplanted back to the patient. However, cell numbers are limited and the expansion in monolayer culture causes a fibroblastic dedifferentiation of the chondrocytes (Ma et al. 2013). The use of mesenchymal stem cells (MSCs) for cell-based cartilage repair has also been investigated. Their role is currently debated (Farrell et al. 2014) since the cartilage tissue formed is unstable and predisposed to mineralization and ossification in vivo (Scotti et al. 2013). More recent studies have evaluated the feasibility of co-culturing MSCs and chondrocytes (Hendriks et al. 2007). Cartilage matrix deposition was improved in co-cultures of MSCs and chondrocytes compared with the cultures of pure chondrocytes or MSCs (Gruber et al. 2010; Tsuchiya et al. 2005). The cellular mechanism responsible for the enhanced cartilage production in co-cultures has been debated. It was first suggested that increased cartilage formation in co-cultures was due to chondrogenic differentiation of MSCs stimulated by factors secreted by the chondrocytes. Recent studies have showed that the increased cartilage matrix formation is instead a result of trophic role of the MSCs in stimulating chondrocyte proliferation and matrix deposition (Wu et al. 2011).

The research on cartilage bioprinting is growing exponentially and the findings are very promising, but still no studies have yet demonstrated the superiority of this technology to the currently used clinical application. The clinical application of 3D bioprinted structures comparable to native human cartilage is still far. One way to increase clinical applicability would be to improve the bioprinting process itself. The poor structural organization of the engineered tissue and the poor mechanical properties compared to native cartilage are major challenges that must be overcome.

1.1.2 Bioprinted Nerve Tissue

The goal of nerve repair surgery is to minimize lost function due to nerve injury. The damage is best repaired by suturing the two ends of the injured nerve together without tension (Siemionow and Brzezicki 2009). However, if this is not possible, a nerve guide can be used as a bridge between the two ends of the injured nerve in order to support the axonal regeneration across the nerve gap and help the return of motor and sensory function. Currently, the gold standard for nerve repair requiring a conduit is an autograft, a nerve segment harvested from another site of the patient and transplanted to the damaged site. This type of repair, however, implies morbidity to the donor site, the risk of multiple surgeries (Siemionow and Brzezicki 2009), and problems matching nerve type (sensory vs. motor) and diameter (Wolford and Stevao 2003). Thus, efforts have focused on developing a conduit that mimics the biological properties of nerve tissue (Schmidt and Leach 2003).

Non-neuronal autologous tissues have been used to fill the gap. Autologous vein grafts resulted in good axonal regeneration and functional repair to an extent similar to autologous nerve grafts in 1 cm nerve gaps in rat models and in clinical application for gaps smaller than 3 cm (Chiu et al. 1988). Repair of larger gaps was unsuccessful since the vein graft collapsed due to contraction by surrounding scar tissue leaving some patients with lifelong disability and/or debilitating neuropathic pain (Tang et al. 1993). A potential solution would be filling the vein with graft of fresh muscle in order to favor the axonal growth (Meek et al. 2004).

More sophisticated methods are tubular constructs used as nerve guidance tubes. These tubular constructs are made from natural or synthetic polymers intended to mimic the ECM. The conduits are approved for clinical use by the FDA and are fabricated from biodegradable polymers such as polyglycolic acid or from the biological material collagen (Hadlock et al. 2001; Meek and Coert 2008). To create a permissive environment for cell growth, the guidance tubes can be filled with hydrogels (e.g., agarose, collagen, chitosan, hyaluronic acid, keratin) in association with ECM components (e.g., laminin, fibronectin, proteoglycans), neurotrophic factors (e.g., nerve growth factor, fibroblast growth factor) (Steed et al. 2011), and supporting cells such as Schwann cells (SC). Studies have been conducted on the effectiveness of seeding different cell types in the graft (Adams et al. 2012; Grimoldi et al. 2015; Hoffman 2006; Radtke et al. 2009). Neural stem cells and mesenchymal stem cells (MSCs) showed optimal properties as they can differentiate into any neural cell type. In particular, MSCs have the capacity to differentiate into neural and glial cells or glial-like cells that promote neurite extension *in vitro* (Brohlin et al. 2009; Ladak et al. 2011). An alternative approach would be to use a scaffold-free method, utilizing the self-organizing and self-assembly properties of cells and tissues to develop their own ECM. The use of fibroblast sheets, co-cultured with embryonic derived neural cells, resulting in a bi-layered sheet has been described. The sheet is pinned at two points and detached so that it rolls into a cylindrical conduit. The tube thus created represents a fully biological graft with cell neurotrophic factors (Baltich et al. 2010). These conduits have been tested *in vivo* and shown to restore normal conduction velocity after 28 days, suggesting a viable strategy for nerve repair (Adams et al. 2012).

Bioprinted nerve grafts have been functionally tested in a rat model (Marga et al. 2012). Biofabrication of nerve graft by bioprinting would represent a distinctive alternative; however obstacles toward this goal are still numerous.

1.1.3 Bioprinted Skin Tissue

The skin is the largest organ of the human body and it protects the body from external insults while maintaining homeostasis (Zulkifli et al. 2014). In humans, skin consists of different layers of cells. Keratinocytes and fibroblasts are the predominant cells of the epidermis and dermis, respectively, and collagen represent the dermal matrix of the skin. Current treatment methods for skin repair and replacement, including split-thickness grafts, xenografts, and acellular dermal substitutes, have all been developed with the intent to stabilize and heal a wound. Autologous donor skin sources are often scarce, and skin grafts can fall short in providing stable coverage and restoring the structure and function of the skin (Zulkifli et al. 2014). So far, there are no established models of artificial skin constructs that entirely replicate normal skin (Michael et al. 2013). To efficiently deposit the skin cells uniformly onto the wound, bioprinting technology has been proposed as a delivery method. Because this tissue consists of multiple cell types and layers, controlled placement of cells and biomaterials is required for 3D reconstruction of the multiple skin layers. Lee et al. (2009–2014) fabricated a biomimetic multilayered skin consisting of human skin fibroblasts and keratinocytes using the jetting-based bioprinting system and a collagen hydrogel (Lee et al. 2009; Lee et al. 2014). The printed 3D skin constructs were

cultured *in vitro*, and results showed the formation of distinctive dual-layered tissue resembling human skin. Koch et al. (Koch et al. 2012) bioprinted keratinocytes and fibroblasts in predefined patterns (Koch et al. 2012). Cells were embedded in collagen hydrogel to fabricate skin constructs with a layered configuration. Histological and immunohistochemical staining showed that cells developed intercellular adhesion indicating tissue formation.

Laser surface scanners have been proposed as an innovative technique for the creation and *in vivo* formation of a 3D tissue-like skin using cells and biomaterials deposited on the defected skin tissue for initial repair (Michael et al. 2013). A recent study used skin cells and amniotic fluid-derived stem cells and printed directly onto wounds in a rat model (Skardal et al. 2012). The results showed rapid re-epithelialization and accelerated wound healing of the printed wound. *In situ* bioprinting represents an alternative future trend, in which cells and materials are directly printed in or on the human body. With the increasing speed and resolution of 3D bioprinters, this approach may become viable for the *in vivo* regeneration of tissues. An alternative technique that is worth noting is the “spray skin” (Hu et al. 2015; Gilleard et al. 2013). With this technique, an autologous, heterogeneous skin cell suspension of keratinocytes, fibroblasts, and melanocytes is extracted from the dermal basal layer of the patient. The suspension is then applied onto the wounds before the application of a split-thickness autologous skin graft. The first clinical trial has shown promising results in terms of wound closure, healing rate, complications, and aesthetic outcome (Hu et al. 2015). The potential applications of skin bioprinting are exciting. Further studies are although needed to develop realistic printing treatment.

1.1.4 Advantages of 3D Bioprinting

The examples of soft tissue prepared by 3D bioprinting were recently presented in reviews (Murphy and Atala 2014; Kang et al. 2016). Hydrogels are preferred as biomaterial for 3D bioprinting of soft tissue because they resemble properties of extracellular matrix (Malda et al. 2013; Billiet et al. 2012). Soft tissue is composed of extracellular matrix such as collagen, elastin, and proteoglycans together with cells. The 3D bioprinting platform enables to spatially distribute different cell types and supporting biomaterial (bioink). The information about the cell type, cell density, and bioink needs to be provided to the 3D bioprinter through the CAD file. The CAD file can be prepared based on data from imaging of native and patient-specific tissue. With the CAD file, the 3D bioprinter can, in a reproducible and automated way, fabricate layer by layer the replica of the patient-specific tissue. In the near future, we will see 3D bioprinters which will be approved for use in the operation room and 3D bioprinting of patient-specific soft tissue will enter the clinic.

1.2 Review of Bioinks for Soft Tissue

1.2.1 Cell-Laden Hydrogels

The soft tissues in regenerative medicine are required to be designed as resembling the original tissue for ideal cell transplantation. The main function of a scaffold in

tissue engineering and regenerative medicine is to provide a structure for the proliferation of cells in a 3D network. The cells are arranged into 3D structures and surrounded by extracellular matrix (ECM) proteins such as fibrillary, collagen, elastin, glycosaminoglycans, and proteoglycans. Apart from being an adhesive substrate, the ECM regulates cell-to-cell communication and differentiation. The use of gels/hydrogels with appropriate properties (e.g., shear thinning, thickening, yield stress) in the 3D printers has been shown to be ideal to build up hierarchical scaffolds. Both natural and synthetic polymers have been used in various 3D printing applications. Although some of the synthetic polymers are useful in terms of printability (e.g., easy gelation after printing, less degradation, and operation advantage under various conditions), the natural biopolymers have been used to mimic the ECM conditions more suitably. A hydrogel can be formed by cross-linking of the polymer chains. The cross-linking occurs by either chemical or physical interaction. The chemical cross-linking is irreversible where the polymer chains are locked covalently. The physical interactions can be controlled as a function of pH, ionic strength and temperature, etc. In this chapter, the general properties of bioinks used in 3D bioprinting are discussed.

1.2.2 Bioink Properties for Bioprinting

An appropriate design of a bioink to be used in 3D bioprinting is crucial in terms of printability, cell viability, and support of forming tissue. A bioink must show an ideal viscoelasticity which allows printing of the target structure. The hydrogels are very attractive as bioinks because they provide a good combination of printability with optimal environment for the cells. When using hydrogels, mixing with cells to prepare cell-laden constructs is the most effective technology. The structure of a cell-laden bioink must be designed in such a way that the nutrients and oxygen are transferred within the hydrogel effectively. One of the most common structures is the 3D printed grid in which one or a few layers of lines are printed layer by layer. Several hydrogel materials have been evaluated as bioinks for cartilage and skin tissue, such as hyaluronic acid (Pescosolido et al. 2011), gelatin (Schiele et al. 2011), alginate (Khalil and Sun 2009), MatriDerm[®] (Michael et al. 2013), fibrinogen (Skardal et al. 2012), agarose (Campos et al. 2013), and polyethylene glycol (Gao et al. 2015a). Depending on the choice of material, different printing systems and cross-linking mechanisms are applicable. The printed scaffold has to be cross-linked in a facile way to keep its integrity and to demonstrate mechanical stiffness. Bioinks with low viscosity such as alginate need either a fast gelation process or be printed with a supporting material to obtain 3D constructs. Alternatively a double network can be printed where a second material provides the mechanical strength (Pescosolido et al. 2011; Shin et al. 2012) or a coaxial needle can print a core-shell structure (Colosi et al. 2016; Gao et al. 2015b).

1.2.3 Viscosity and Rheological Properties of Bioinks

In terms of printability, an ideal bioink should demonstrate a shear thinning behavior which allows a continuous flow and printability under high shear rate. When the shear force is increased, the viscosity of a hydrogel decreases due to the

rearrangement of the polymer chains into aligned form. When the shear force is withdrawn, the viscosity increases again resulting in a more solid-like gel. This is a typical property of a hydrogel that allows for printing under shear force, which is a pressure in many cases, and shape retaining after printing. The shear thinning behavior of silk fibroin gels as a function of applied shear rate has been demonstrated previously (Ghosh et al. 2008). Although the gels with relatively high viscosity improve the printability, longer printing times and the risk of cell death require novel bioinks with low viscosity. Colosi et al. used a low-viscosity bioink composed of a blend of alginate and gelatin methacrylate (GelMA) (Colosi et al. 2016). GelMA was used for cell encapsulation due to its ability to form a chemically stable hydrogel when exposed to light compared to ionically cross-linked alginate. One of the most important properties of a hydrogel used as bioink is to support cell viability by surrounding the soft cell aggregates. The viscosity of the hydrogel plays a significant role for the cell viability. The low viscosity bioinks are more suitable for high cell viability; however their printability and cross-linking capacity are low in most cases. Catros et al. have studied the influence of bioink viscosity on the viability of endothelial cells. The results have showed that increasing bioink viscosity of alginate improves cell viability after laser-assisted bioprinting (Catros et al. 2011).

1.3 Evaluation of Bioinks

1.3.1 Rheological Properties

Rheology describes the deformation behavior of a material when exposed to a force. Deformation is expressed differently depending on the matter; solids typically deform when a force is applied, while liquids and gases flow. Knowledge of the rheological properties is therefore necessary when studying the processability.

A shear viscosity curve describes the change in viscosity upon increasing shear stress and is thereby used to illustrate the flow behavior when dispensing the material through a printer head. A typical printable material for bioprinting has a pseudo-plastic flow behavior; the material is shear thinning, i.e., the viscosity decreases with increasing shear rate (Markstedt et al. 2015). Post printing, the shear forces are released whereby the viscosity increases and the printed construct does not flow. Common shear thinning materials are polymer melts, yoghurt, and ketchup.

Bioinks Based on Nanocellulose

Cellulose is a polysaccharide consisting of chains of 1,4-linked glucose monomers and is the most abundant polymer in nature. Although it is generally considered a plant material, some bacteria also produce cellulose. The cellulose polymers have the role of giving the plant strength and stiffness, where 40–50% of the cell wall consists of cellulose. Cellulose is insoluble in water and other common organic solvents, due to strong hydrogen bonds in the cellulose structure. Cellulose nanofibrils with widths in the nanosize range are very similar to collagen fibrils in regards to their morphology.

Bacterial Nanocellulose as a Biomaterial

In nature, cellulose-producing bacteria are found in rotten fruits and vegetables. Bacterial nanocellulose (BNC) is the extracellular product of *Gluconacetobacter xylinus*. These gram-negative aerobic bacteria produce pure nanocellulose fibrils in the presence of sugar and oxygen, where the production of cellulose occurs mainly at the air-liquid interface (Catros et al. 2011; Deinema and Zevenhuizen 1971).

BNC holds interesting properties for tissue engineering applications, as it is a biomaterial with excellent biocompatibility and remarkable tissue integration capability (Brown et al. 1976; Mello et al. 1997; Helenius et al. 2006; Andrade et al. 2013; Pertile et al. 2011). BNC has been evaluated for several TE strategies and has shown to support adhesion, proliferation, and differentiation of different cell types (Deinema and Zevenhuizen 1971; Brown et al. 1976; Mello et al. 1997; Helenius et al. 2006; Andrade et al. 2013; Pertile et al. 2011; Martínez Ávila et al. 2014). The past decade has seen a tremendous interest of scientists evaluating BNC for several tissue engineering applications with positive outcomes reported (Brown et al. 1976; Andrade et al. 2013; Pertile et al. 2011; Martínez Ávila et al. 2014; Svensson et al. 2005; Ahrem et al. 2014). The material-cell interaction and subsequent positive effects on cell fate processes could be attributed to the highly hydrated nanocellulose fibrils and their morphological similarity with extracellular matrix components such as collagen (Martínez Ávila et al. 2014). Several in vitro studies of BNC scaffolds seeded with bovine articular chondrocytes and human articular, auricular, and nasoseptal chondrocytes have also exhibited good cell adhesion and proliferation and, most importantly, have demonstrated the maintenance of chondrogenic phenotype—as confirmed by the synthesis of cartilage-specific ECM (Andrade et al. 2013; Pertile et al. 2011; Ahrem et al. 2014; Martinez et al. 2012).

Biomedical Applications of Bacterial Nanocellulose

BNC products, such as temporary skin, have been introduced into the wound care market. BNC films have found an application in the health care sector because of their unique absorption properties. Cellulose has been most commonly used in applications such as blood purification, anticoagulant, and plasma expander in aqueous systems. More recently, medical devices made from BNC are used in the clinic as wound and burn dressings (e.g., Dermafill[®], Bioprocess[®], XCell[®], and Biofill[®]), surgical meshes (e.g., Xylos[®], Macro-Porous Surgical Mesh, and Securian[®]), and dura mater substitutes (SyntheCel[®] Dura Repair), which have been used successfully to repair dural defects in 62 patients (Rosen et al. 2011).

Nanocellulose-Alginate Composite Biomaterial for Auricular Cartilage Tissue Engineering

Recently we evaluated the in vitro and in vivo performance of a novel composite scaffold made from nanocellulose and alginate for auricular cartilage TE (Martínez Ávila et al. 2015). Most studies that have used biodegradable materials to engineer auricular cartilage have resulted in poor structural integrity of the scaffold after implantation due to the short-lived chemical stability of the scaffold material. This

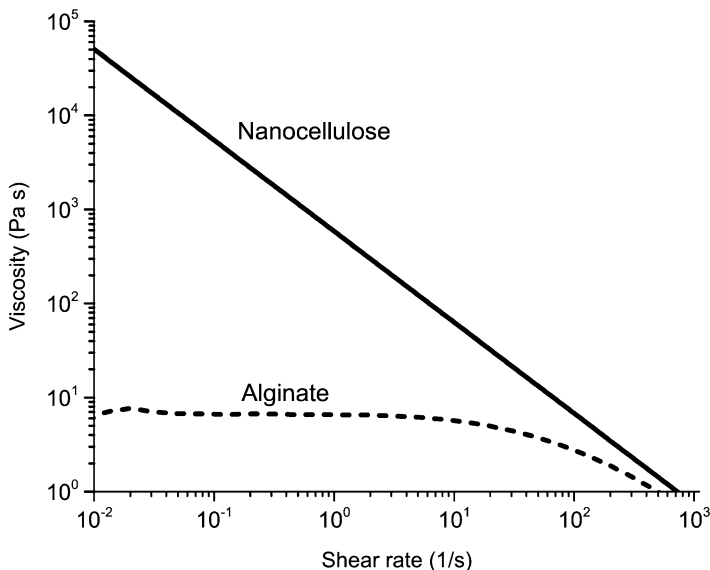


Fig. 2 Schematic of shear viscosity curves describing the general rheological behavior of a 3% nanocellulose dispersion and 3% alginate solution

nanocellulose-alginate composite scaffold was designed to be mechanically stable and maintain a long-term structural integrity while providing a porous architecture that supports cell ingrowth and neocartilage formation. Such composite scaffold provided a suitable environment for culture-expanded human nasoseptal chondrocytes (hNC) as well as freshly isolated hNCs combined with freshly isolated human mononuclear cells to form neocartilage *in vitro* and *in vivo*, as demonstrated by immunohistochemical, biochemical, and biomechanical analyses.

Dispersions of nanocellulose, with a dry content of 2–3%, are shear thinning (Paakko et al. 2007) and are therefore a suitable component in bioinks. Other hydrogels such as alginate are also shear thinning at high shear forces, but lack a high viscosity at zero shear rate, as seen in Fig. 2. The low viscosity makes it difficult to print 3D constructs unless the construct is solidified or gelled layer by layer while printing. Figure 3 demonstrates this where 3D bioprinted nanocellulose results in a higher resolution compared to Alginate.

To conclude, shear thinning properties and a sufficient viscosity at zero shear are essential for the printability of a material. However, after printing the material needs a certain mechanical strength to enable handling of the printed construct and to be further used for its aimed application in tissue engineering. Therefore, in nanocellulose-based bioinks, a cross-linking material is added which can hold together the printed construct even when mechanical force is applied. For this purpose, alginate is suitable due to its ability to cross-link by divalent ions.

The cross-linking time of the bioink can be defined by using a rheometer. Knowledge of the cross-linking time is especially important when printing a material

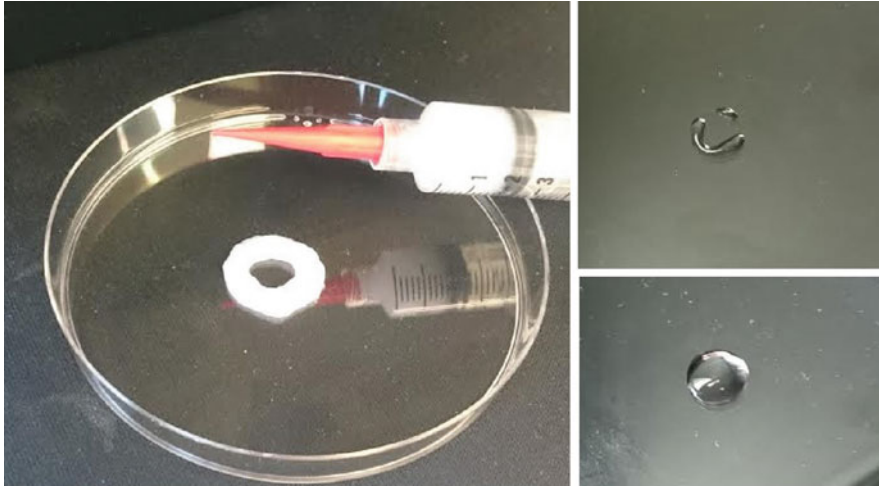


Fig. 3 Comparing printing fidelity by printing a circle: (a) nanocellulose and (b) alginate.

with cells since the cells may not survive at too long exposure times to the cross-linking agent. By performing an oscillation measurement, where stress is measured at a given strain and frequency (within the linear viscoelastic region), the storage and loss moduli can be followed over time as cross-linking agent is added. For a liquid, the loss modulus will be higher than the storage modulus, while for a viscoelastic solid, the storage modulus will dominate. The gelation point will be the time at which the storage modulus crosses the loss modulus (Weng et al. 2007). For very viscous bioinks, such as those based on nanocellulose, it is difficult to identify the cross-linking time since they respond as a gel in the oscillation measurement even before addition of cross-linking agent. However, the cross-linking can still be noticed by an increase of the storage modulus, as seen in Fig. 4 where the arrow indicates the time point when the cross-linking agent is added.

1.3.2 Bioink Printability

S-Test

The printability of the different biomaterials is evaluated by two methods. The first method compares the printability of different materials by varying the printer settings, for example, printing at different pressures as in Fig. 5. This method is called an S-test and identifies the printing fidelity of the material at a specific pressure, speed of printing, or needle size. The printer settings essentially control the flow, and by weighing the printed S, the weight and thus the flow of different biomaterials can be compared. A too high flow gives a high weight, and a too low flow gives a low weight. The weight of each print also depends on the material density, which is why a specific weight for the perfect printed S is difficult to define.

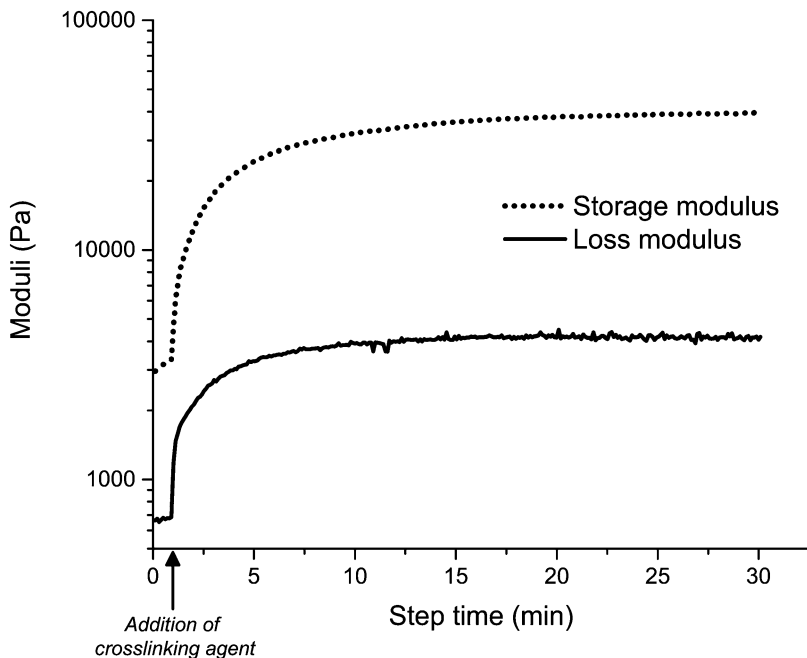


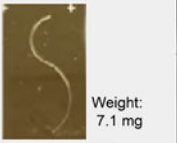



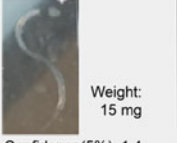
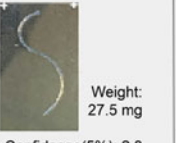
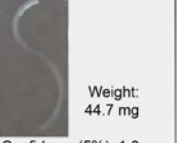

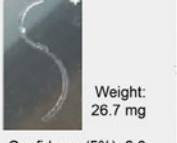
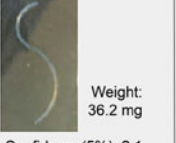
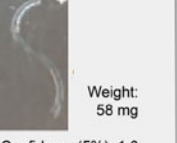
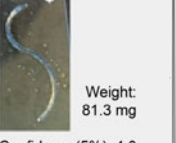
Fig. 4 Storage and loss modulus measured during cross-linking. The increase of the storage modulus indicates that the bioink is cross-linked. The arrow indicates the time point when the cross-linking agent is added

Printing Complex Construct

This test also defines the printability, but here a more complex construct is printed, which gives more information about the printing fidelity. The perfect settings are found in the S test, for example, used to 3D bioprint a tube which is 1 cm high with 5 mm in diameter. Depending on the final application, different constructs should be chosen to be printed in this test. In Fig. 6 an ear was 3D bioprinted and resulted in a high printing fidelity.

1.3.3 Bioink Cross-Linking Stability in Medium

The cell viability in the constructs are highly dependent on the encapsulation of the cells inside the bioink. Different cross-linking methods, for example, UV cross-linking, or ionic cross-linking, can be used to encapsulate the cells. The stability of the crosslinked constructs is therefore important to be tested. Typically, grids are printed, crosslinked, and put in medium in incubator at 37 °C. The stability of the constructs are controlled visually each week for at least 2 weeks (Fig. 7). If the encapsulation fails, the cells will leave the 3D scaffold and proliferate on the well plate, and the cells will not be 3D cultured.

	15% alg.	20% alg.	25% alg.	30% alg.
Pressure				
40 kPa	 Weight: 7.1 mg Confidence(5%): 1	 Weight: 12.6 mg Confidence(5%): 1.6	 Weight: 27.5 mg Confidence(5%): 2.7	 Weight: 47.5 mg Confidence(5%): 2.5
50 kPa	 Weight: 15 mg Confidence(5%): 1.4	 Weight: 27.5 mg Confidence(5%): 2.8	 Weight: 44.7 mg Confidence(5%): 1.8	 Weight: 71.1 mg Confidence(5%): 2.5
60 kPa	 Weight: 26.7 mg Confidence(5%): 2.0	 Weight: 36.2 mg Confidence(5%): 2.1	 Weight: 58 mg Confidence(5%): 1.6	 Weight: 81.3 mg Confidence(5%): 4.0

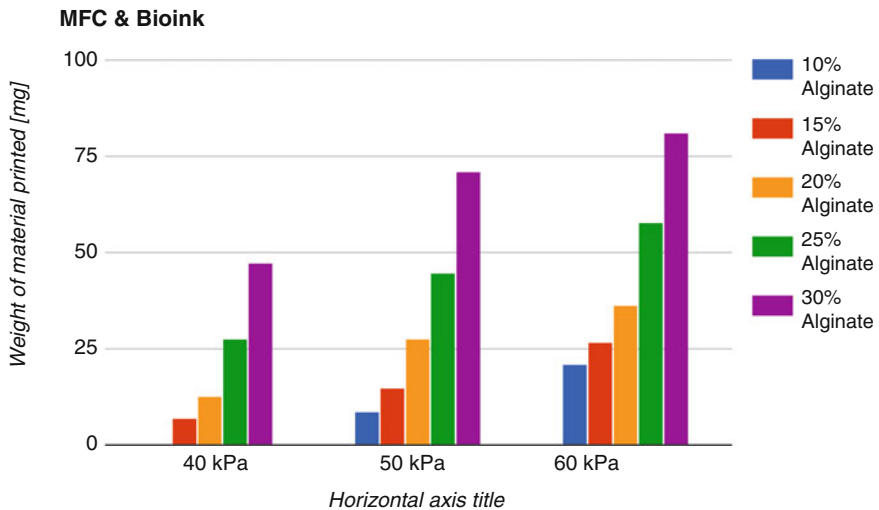


Fig. 5 To the *left*, a table of the S printed at different pressures for different bioink compositions. To the *right*, the weight of the printed material plotted against the pressure for each bioink

1.3.4 Mechanical Properties

Structural integrity of cell-laden constructs is of utmost importance since the constructs are incubated for long time, and in many cases the tissue development requires use of bioreactors. The cell-laden constructs can also be implanted in animal

Fig. 6 3D bioprinting of a complex construct. In this case an ear

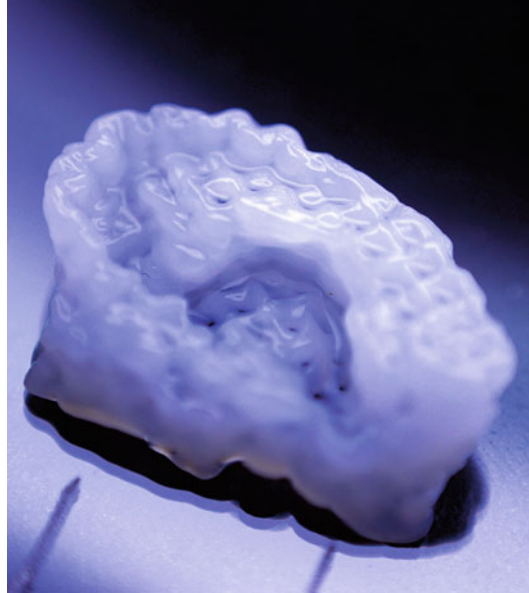
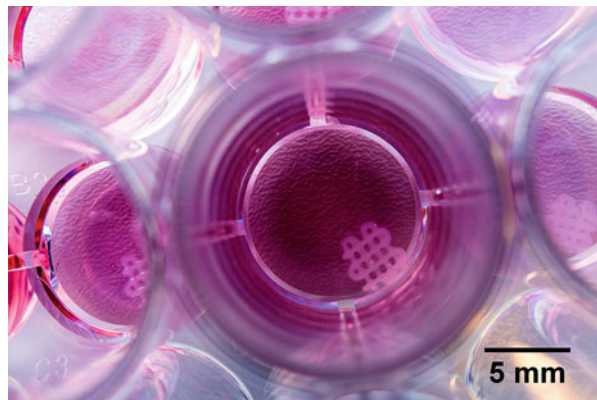


Fig. 7 Grids printed with nanocellulose mixed with alginate and cross-linked with 100 mM CaCl_2 are put in medium for stability test



for testing cell differentiation and tissue development and are aimed in the future to be implanted in humans. There are therefore requirements for good mechanical properties to provide structural integrity. This becomes critical when the architecture of the printed constructs has to satisfy oxygen and nutrient transport into the cells in the construct. The mechanical properties of the bioink which will be cross-linked during or after printing have to be selected, so good matching for the tissue which needs to be developed is achieved. Very stiff scaffolds might, for example, induce differentiation of cells toward bone. Determination and control of the mechanical properties is very important during development of novel bioinks. The available methods for mechanical testing are uniaxial tensile testing, compression testing,

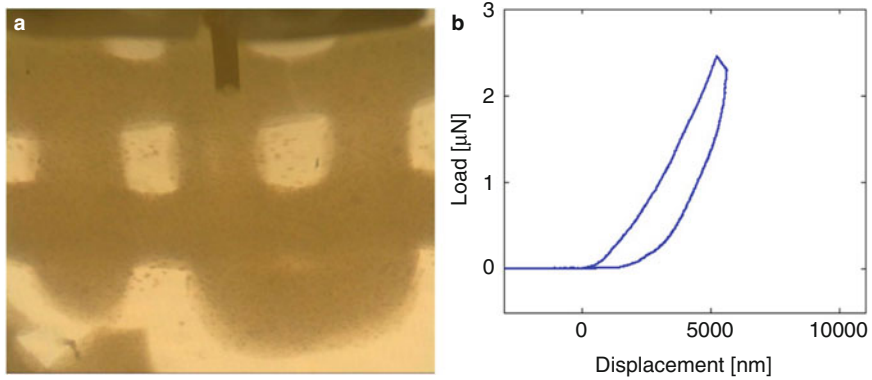


Fig. 8 Nanoindentation testing of printed grids. (a) The structure and (b) the results from nanoindentation testing

indentation, and dynamic mechanical testing. Tensile testing is not very applicable for hydrogels and cell-laden constructs. Compression testing is relatively simple to perform on uniform disks but is not very useful for characterization of samples with complex architecture particularly for macroporous structures such as grids. Nanoindentation is very attractive method, particularly with use of smaller size of indenter because the grids can be scanned in different directions (Fig. 8a) and also the effect of the development of the extracellular matrix can be analyze. Figure 8b shows results from nanoindentation testing of nanocellulose-alginate grids.

1.3.5 Bacterial Endotoxin and In Vitro Cytotoxicity Testing of Bioinks

The potential use of biocompatible bioinks as scaffold materials for cartilage regeneration requires, first and foremost, the depyrogenation of the biomaterial. That is, the removal of endotoxins, since these molecules are considered to be the most potent microbial pyrogens responsible for triggering the immune system (Williams 2007). High levels of endotoxins in the bloodstream trigger the production of excessive amounts of cytokines (IL-1 β , IL-1 α , IL-6, IL-8, and TNF), causing severe infection and inflammation that can lead to fatal septic shock (Heine et al. 2001; Hold and Bryant 2011). Due to the high risks associated with endotoxin contamination in medical devices, the United States Food and Drug Administration (FDA) has set guidelines for endotoxin limits in medical devices, which are no more than 0.5 endotoxin units (EU)/ml or 20 EU/device (Administration, U.S.F.a.D. 2012). Thus, it is of utmost importance to comply with these guidelines to guarantee the non-pyrogenicity of biomaterials. Our research group has developed and validated a depyrogenation process for large nanocellulose structures, where endotoxins are removed by rinsing the hydrogel material in sterile and non-pyrogenic conditions using endotoxin-free water with an endotoxin specification of <0.005 EU/ml (Martínez Ávila et al. 2014). An endotoxin-mediated pyrogen test is performed on extracts of the biomaterial to evaluate its potential to induce a pyrogenic response. This test can be performed

in vitro using the bacterial endotoxin test or in vivo using a rabbit model. Endotoxin extraction from the biomaterial in question should be performed in accordance to the international standard ISO 10993–12:2009. In brief, hydrogel samples can be incubated in endotoxin-free water, using the extraction ratio of 0.1 g of sample/ml of extraction medium, for 72 ± 2 h at 37 ± 1 °C under orbital motion. Endotoxicity of the extracted samples can then be determined using the PyroGene™ recombinant Factor C assay, where this assay has a minimum detection limit of 0.005 EU/ml.

In addition to evaluating the endotoxicity, the biomaterial should also be tested for cytotoxicity in order to determine the biological response of mammalian cells in vitro. The international standard ISO 10993–5:2009 (Biological evaluation of medical devices–Part 5: Tests for in vitro cytotoxicity) offers a valuable guidance when performing such test. This test is a common cytotoxicity test designed to assess the toxicity to cells of leachable components of the hydrogel. In brief, the biomaterial is incubated in cell culture media and then the extracts are placed in contact with a monolayer of L929 mouse fibroblast cells. Cells are incubated in standard culture conditions for an additional period of time, after which they are examined for indications of cytotoxicity. CellTiter 96® aqueous one solution cell proliferation assay (Promega, WI, USA) is widely used to determine the number of viable cells. The cytotoxic potential of the tested hydrogel is then identified based on the percentage of cell viability; classified as toxic when cell viability is below 50%, slightly cytotoxic when it is between 51 and 70%, and non-cytotoxic when cell viability is above 71%.

2 Commercialization of Novel Bioink for Soft Tissue Applications

Nanocellulose-alginate bioinks with remarkable printability have been recently developed and evaluated by our research group at Chalmers (Markstedt et al. 2015) and commercialized as CELLINK®. Such bioinks are composed of highly hydrated cellulose nanofibrils similar in size to extracellular matrix components. Thus, providing a biologically relevant 3D environment for cells. In Fig. 9 a summarized work flow during development of a bioink is illustrated including requirements of rheological properties, printability, cross-linkability, and bioink sterility. Another prerequisite for bioprinting is to be able to operate in an aqueous environment, which restricts the choice of materials (Malda et al. 2013; Pati et al. 2014). Porous, chondrocyte-laden constructs with high shape fidelity were successfully bioprinted due to the highly viscous, shear-thinning bioink composed of nanocellulose (CNF) and alginate (Markstedt et al. 2015). It is well known that CNF exhibits a high zero shear viscosity and shear-thinning behavior, even at low solid content. Moreover, the high viscosity is established instantaneously after shearing has stopped (Paakko et al. 2007; Bhattacharya et al. 2012). All these important rheological properties, combined with the rapid cross-linking property of alginate, are required for bioprinting the cell-laden hydrogel at a low pressure (e.g., <20 kPa), maintaining a high shape fidelity while and after bioprinting, and keeping the cells in a 3D environment after cross-linking the cell-laden constructs. Until now, hydrogels based on natural polymers have been regarded as having a suboptimal printability compared to synthetic hydrogels such as Pluronic (Fedorovich et al. 2009). However,

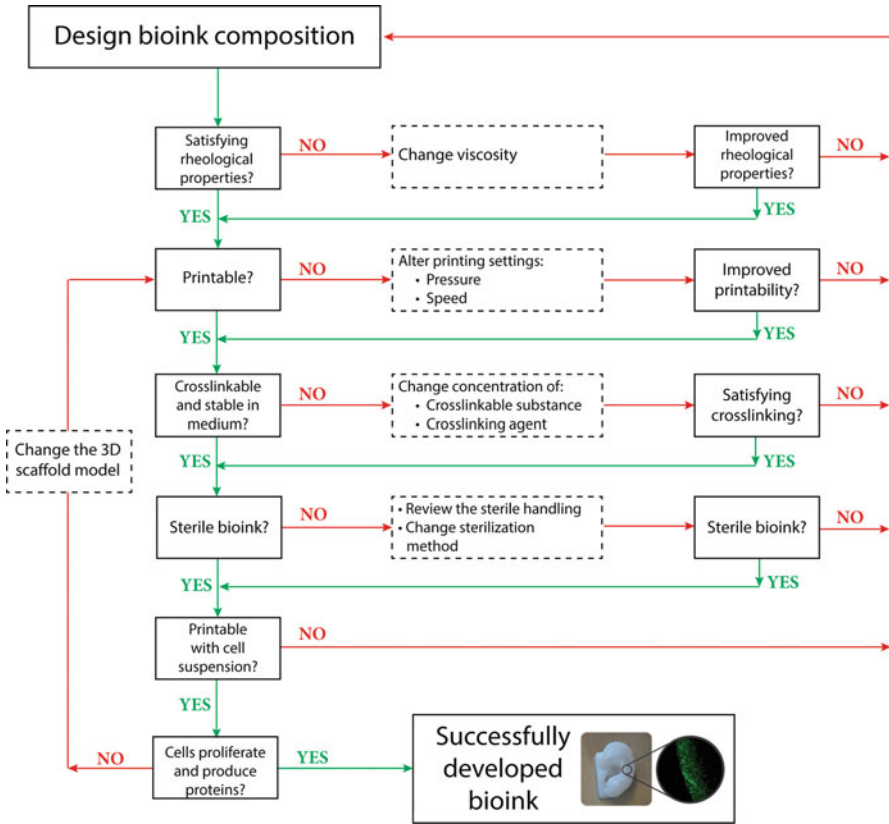


Fig. 9 Work flow chart of the development of bioink

this is not the case for nanocellulose-based bioinks. Furthermore, the mixing of the bioink with the cells is preferably done with the mixing unit CELLMIXER™, which provides a homogenous distribution of the cells in the bioink (see Fig. 10). A mixing unit consisting of a screw extrusion system is connected to two syringes. One syringe is filled with bioink and the other with cell suspension. The other end of the mixing unit is connected to the cartridge that is filled with the mixture of cells and bioink. The system keeps the bioink and cell mixture sterile during the mixing process.

The high zero shear viscosity of the nanocellulose-alginate bioink, coupled with its fast response to reestablish the high viscosity after extrusion, helps to improve the spatial resolution of the printed objects and maintain a high shape fidelity during the bioprinting process. These important rheological properties are illustrated by the end result of the complex, 3D anatomically shaped constructs, such as a human auricle and meniscus, bioprinted without the need of co-printing with sacrificial materials (see Fig. 6) (Markstedt et al. 2015). Furthermore, we have found that human nasal chondrocytes, hNCs bioprinted in nanocellulose-alginate bioink, show good viability after 7 days of 3D culture (85.7 ± 1.9%).

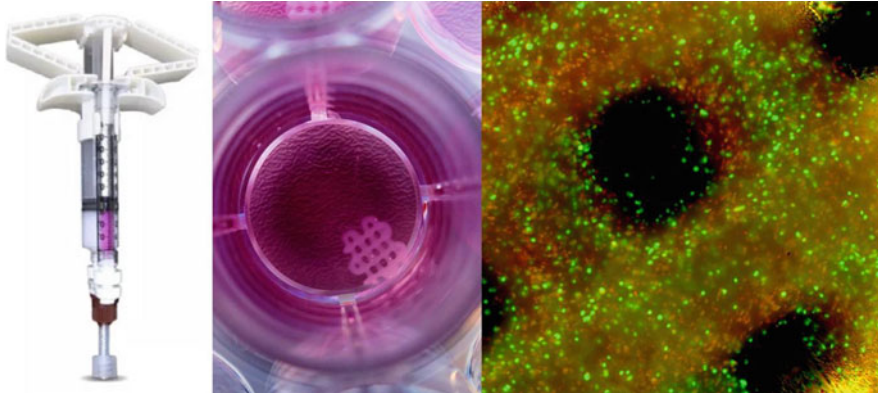


Fig. 10 CELLMIXER™ developed for getting an accurate mixture of bioink and cells. To the right, a confocal microscope picture of the fluorescent cells (green and red spots) in the 3D bioprinted constructs showing the homogenous distribution of cells

Our research group has also evaluated the biological functionality of CELLINK® in long-term 3D culture with culture-expanded hNCs and assessed their redifferentiation capacity (Martínez et al. 2016). In regard to stability, the cell-laden patient-specific auricular constructs showed an excellent shape and size stability after 28 days of culture. Furthermore, the biologically relevant 3D environment of CELLINK® provides the hNCs with a milieu that resembles their natural matrix. The hNCs proliferated and underwent chondrogenesis, which resulted in neo-synthesis and accumulation of cartilage-specific extracellular matrix around the cells, as demonstrated by gene expression and immunohistochemical and biochemical analyses. In conclusion, the nanocellulose-alginate bioink provides a biologically relevant environment that supports redifferentiation of human chondrocytes, reestablishing and maintaining their chondrogenic phenotype. This bioactive property, combined with excellent printability, make CELLINK® a promising bioink for cartilage TE applications.

The commercialization process included development of standard operating procedures (SOP) for aseptic production, sterilization, and packaging. The work is focused on reviewing all the process steps and defining the weak parts of the chain and improving them. This includes a lot of quality testing of each batch made. The documentation of each batch includes materials safety data sheet (MSDS), certificate of analysis, and production protocols.

3 Conclusions

3D bioprinting technology particularly cell-laden hydrogels has great potential to become surgical tool for repair and regeneration of soft tissue which includes the skin, cartilage, adipose tissue, and neural tissue. Novel bioinks have to be, however, developed and introduced to the market to facilitate this process. This chapter

describes the specifications for bioinks suitable for soft tissue engineering and the bioink development process. Rheological properties of bioinks are crucial since they determine the final printing fidelity which is critical for cell survival and tissue development. Cross-linking is an important part of the preparation of cell-laden hydrogel since it is contributing to the mechanical properties of the construct. Good mechanical properties are required to be able to handle the construct for culturing and/or implantation. The bioinks have to be endotoxin free and not cytotoxic. We described in this chapter how a novel bioink based on cellulose nanofibrils and alginate has been developed and introduced to the market as the first universal bioink under name CELLINK[®]. This bioink has unique printability at very low solid content due to shear-thinning properties and high zero shear viscosity of nanocellulose fibrils. Addition of alginate facilitates cross-linking which gives construct with double network architecture. This bioink has been evaluated in vitro and in vivo with human chondrocytes, human dermal fibroblasts and keratinocytes, neural cells, mesenchymal stem cells derived from bone marrow, and adipose tissue and iPSC cells derived from chondrocytes. All studies showed excellent cell viability and development of tissue in vitro and in vivo. The work is ongoing to bring next generation of biofunctional inks which will control cell adhesion and cell fate processes. The market introduction was successful because of scaling up of production process, development of protocols for sterilization, development of packaging system, and studies of shelf stability.

References

- Adams AM, Arruda EM, Larkin LM (2012) Use of adipose-derived stem cells to fabricate scaffoldless tissue-engineered neural conduits in vitro. *Neuroscience* 201:349–356
- Administration, U.S.F.a.D. (2012) Guidance for Industry – Pyrogen and Endotoxins Testing: Questions and Answers. U.S.D.o.H.H. Services, Editor. U.S. Food and Drug Administration, Silver Spring, p. 8
- Ahrem H et al (2014) Laser-structured bacterial nanocellulose hydrogels support ingrowth and differentiation of chondrocytes and show potential as cartilage implants. *Acta Biomater* 10(3): 1341–1353
- Andrade FK et al (2013) Studies on the biocompatibility of bacterial cellulose. *J Bioact Compat Polym* 28(1):97–112
- Baltich J et al (2010) Development of a scaffoldless three-dimensional engineered nerve using a nerve-fibroblast co-culture. *In Vitro Cell Dev Biol Anim* 46(5):438–444
- Bekkers JE et al (2013) Single-stage cell-based cartilage regeneration using a combination of chondrons and mesenchymal stromal cells: comparison with microfracture. *Am J Sports Med* 41(9):2158–2166
- Bhattacharya M et al (2012) Nanofibrillar cellulose hydrogel promotes three-dimensional liver cell culture. *J Control Release* 164(3):291–298
- Billiet T et al (2012) A review of trends and limitations in hydrogel-rapid prototyping for tissue engineering. *Biomaterials* 33(26):6020–6041
- Brohlin M et al (2009) Characterisation of human mesenchymal stem cells following differentiation into Schwann cell-like cells. *Neurosci Res* 64(1):41–49
- Brown RM Jr, Willison JH, Richardson CL (1976) Cellulose biosynthesis in *Acetobacter xylinum*: visualization of the site of synthesis and direct measurement of the in vivo process. *Proc Natl Acad Sci U S A* 73(12):4565–4569

- Campos DFD et al (2013) Three-dimensional printing of stem cell-laden hydrogels submerged in a hydrophobic high-density fluid. *Biofabrication* 5(1):015003
- Catros S et al (2011) Effect of laser energy, substrate film thickness and bioink viscosity on viability of endothelial cells printed by Laser-Assisted Bioprinting. *Appl Surf Sci* 257(12):5142–5147
- Chiu DT et al (1988) Comparative electrophysiologic evaluation of nerve grafts and autogenous vein grafts as nerve conduits: an experimental study. *J Reconstr Microsurg* 4(4):303–309 311–2
- Colosi C et al (2016) Microfluidic Bioprinting of Heterogeneous 3D Tissue Constructs Using Low-Viscosity Bioink. *Adv Mater* 28(4):677–684
- Deinema M, Zevenhuizen LPTM (1971) Formation of cellulose fibrils by gram-negative bacteria and their role in bacterial flocculation. *Arch Mikrobiol* 78(1):42–57
- Farrell MJ et al (2014) Functional properties of bone marrow-derived MSC-based engineered cartilage are unstable with very long-term in vitro culture. *J Biomech* 47(9):2173–2182
- Fedorovich NE et al (2009) Evaluation of photocrosslinked Lutrol hydrogel for tissue printing applications. *Biomacromolecules* 10(7):1689–1696
- Firmin F, Marchac A (2011) A novel algorithm for autologous ear reconstruction. *Semin Plast Surg* 25(4):257–264
- Gao G et al (2015a) Inkjet-bioprinted acrylated peptides and PEG hydrogel with human mesenchymal stem cells promote robust bone and cartilage formation with minimal printhead clogging. *Biotechnol J* 10(10):1568–1577
- Gao Q et al (2015b) Coaxial nozzle-assisted 3D bioprinting with built-in microchannels for nutrients delivery. *Biomaterials* 61:203–215
- Ghosh S et al (2008) Direct-write assembly of microperiodic silk fibroin scaffolds for tissue engineering applications. *Adv Funct Mater* 18:1883–1889
- Gilleard O, Segaren N, Healy C (2013) Experience of ReCell in skin cancer reconstruction. *Arch Plast Surg* 40(5):627–629
- Grimoldi N et al (2015) Stem cell salvage of injured peripheral nerve. *Cell Transplant* 24(2):213–222
- Groll J et al (2016) Biofabrication: reappraising the definition of an evolving field. *Biofabrication* 8(1):013001
- Gruber HE et al (2010) Human adipose-derived mesenchymal stem cells: direction to a phenotype sharing similarities with the disc, gene expression profiling, and coculture with human annulus cells. *Tissue Eng Part A* 16(9):2843–2860
- Guillotin B, Guillemot F (2011) Cell patterning technologies for organotypic tissue fabrication. *Trends Biotechnol* 29(4):183–190
- Hadlock TA et al (2001) A new artificial nerve graft containing rolled Schwann cell monolayers. *Microsurgery* 21(3):96–101
- Heine H, Rietschel ET, Ulmer AJ (2001) The biology of endotoxin. *Mol Biotechnol* 19(3):279–296
- Helenius G et al (2006) In vivo biocompatibility of bacterial cellulose. *J Biomed Mater Res A* 76(2):431–438
- Hendriks J, Riesle J, van Blitterswijk CA (2007) Co-culture in cartilage tissue engineering. *J Tissue Eng Regen Med* 1(3):170–178
- Hoffman RM (2006) The pluripotency of hair follicle stem cells. *Cell Cycle* 5(3):232–233
- Hold GL, Bryant CE (2011) The molecular basis of lipid a toll-like receptor 4 interactions. In: *Bacterial lipopolysaccharides*. Springer, Vienna, pp 371–387
- Hu ZC et al (2015) Randomized clinical trial of autologous skin cell suspension combined with skin grafting for chronic wounds. *Br J Surg* 102(2):e117–e123
- Kang HW et al (2016) A 3D bioprinting system to produce human-scale tissue constructs with structural integrity. *Nat Biotechnol* 34(3):312–319
- Khalil S, Sun W (2009) Bioprinting Endothelial Cells With Alginate for 3D Tissue Constructs. *J Biomech Eng* 131(11):111002–111002
- Koch L et al (2012) Skin tissue generation by laser cell printing. *Biotechnol Bioeng* 109(7):1855–1863
- Ladak A et al (2011) Differentiation of mesenchymal stem cells to support peripheral nerve regeneration in a rat model. *Exp Neurol* 228(2):242–252

- Lee W et al (2009) Multi-layered culture of human skin fibroblasts and keratinocytes through three-dimensional freeform fabrication. *Biomaterials* 30(8):1587–1595
- Lee DH et al (2014) Recombinant growth factor mixtures induce cell cycle progression and the upregulation of type I collagen in human skin fibroblasts, resulting in the acceleration of wound healing processes. *Int J Mol Med* 33(5):1147–1152
- Lee V et al (2014) Design and fabrication of human skin by three-dimensional bioprinting. *Tissue Eng Part C Methods* 20(6):473–484
- Lindahl A (2015) From gristle to chondrocyte transplantation: treatment of cartilage injuries. *Philos Trans R Soc Lond B Biol Sci* 370(1680):20140369
- Luquetti DV, Leoncini E, Mastroiacovo P (2011) Microtia-anotia: a global review of prevalence rates. *Birth Defects Res A Clin Mol Teratol* 91(9):813–822
- Ma B et al (2013) Gene expression profiling of dedifferentiated human articular chondrocytes in monolayer culture. *Osteoarthritis Cartilage* 21(4):599–603
- Malda J et al (2013) 25th anniversary article: Engineering hydrogels for biofabrication. *Adv Mater* 25(36):5011–5028
- Markstedt K et al (2015) 3D bioprinting human chondrocytes with nanocellulose–alginate bioink for cartilage tissue engineering applications. *Biomacromolecules* 16(5):1489–1496
- Marga F et al (2012) Toward engineering functional organ modules by additive manufacturing. *Biofabrication* 4(2):022001
- Martínez Ávila H et al (2014) Biocompatibility evaluation of densified bacterial nanocellulose hydrogel as an implant material for auricular cartilage regeneration. *Appl Microbiol Biotechnol* 98(17):7423–7435
- Martínez Ávila H et al (2015) Novel bilayer bacterial nanocellulose scaffold supports neocartilage formation in vitro and in vivo. *Biomaterials* 44(0):122–133
- Martínez H et al (2012) Mechanical stimulation of fibroblasts in micro-channeled bacterial cellulose scaffolds enhances production of oriented collagen fibers. *J Biomed Mater Res A* 100(4):948–957
- Martínez Ávila H, Schwarz S, Rotter N, Gatenholm P (2016) 3D bioprinting of human chondrocyte-laden nanocellulose hydrogel for patient-specific auricular cartilage regeneration. *Bioprinting*
- Meek MF, Coert JH (2008) US Food and Drug Administration /Conformit Europe- approved absorbable nerve conduits for clinical repair of peripheral and cranial nerves. *Ann Plast Surg* 60(4):466–472
- Meek MF, Varejao AS, Geuna S (2004) Use of skeletal muscle tissue in peripheral nerve repair: review of the literature. *Tissue Eng* 10(7–8):1027–1036
- Mello LR et al (1997) Duraplasty with biosynthetic cellulose: an experimental study. *J Neurosurg* 86(1):143–150
- Michael S et al (2013) Tissue engineered skin substitutes created by laser-assisted bioprinting form skin-like structures in the dorsal skin fold chamber in mice. *PLoS One* 8(3):e57741
- Murphy SV, Atala A (2014) 3D bioprinting of tissues and organs. *Nat Biotechnol* 32(8):773–785
- Paakko M et al (2007) Enzymatic hydrolysis combined with mechanical shearing and high-pressure homogenization for nanoscale cellulose fibrils and strong gels. *Biomacromolecules* 8(6):1934–1941
- Pati F et al (2014) Printing three-dimensional tissue analogues with decellularized extracellular matrix bioink. *Nat Commun* 5:3935
- Pertile RA et al (2011) Bacterial cellulose: long-term biocompatibility studies. *J Biomater Sci Polym Ed* 23(10):1339–1354
- Pescosolido L et al (2011) Hyaluronic acid and dextran-based semi-IPN hydrogels as biomaterials for bioprinting. *Biomacromolecules* 12(5):1831–1838
- Poole CA, Ayad S, Schofield JR (1988) Chondrons from articular cartilage: I. Immunolocalization of type VI collagen in the pericellular capsule of isolated canine tibial chondrons. *J Cell Sci* 90(Pt 4):635–643

- Rosen CL, Steinberg GK, DeMonte F, Delashaw JB, Lewis SB, Shaffrey ME et al (2011) Results of the prospective, randomized, multicenter clinical trial evaluating a biosynthesized cellulose graft for repair of dural defects. *Neurosurgery* 69:1093–1103
- Radtke C et al (2009) Transplantation of olfactory ensheathing cells enhances peripheral nerve regeneration after microsurgical nerve repair. *Brain Res* 1254:10–17
- Schiele NR, Chrisey DB, Corr DT (2011) Gelatin-based laser direct-write technique for the precise spatial patterning of cells. *Tissue Eng Part C Methods* 17(3):289–298
- Schmidt CE, Leach JB (2003) Neural tissue engineering: strategies for repair and regeneration. *Annu Rev Biomed Eng* 5:293–347
- Schuurman W et al (2013) Gelatin-methacrylamide hydrogels as potential biomaterials for fabrication of tissue-engineered cartilage constructs. *Macromol Biosci* 13(5):551–561
- Scotti C et al (2013) Engineering of a functional bone organ through endochondral ossification. *Proc Natl Acad Sci U S A* 110(10):3997–4002
- Shin H, Olsen BD, Khademhosseini A (2012) The mechanical properties and cytotoxicity of cell-laden double-network hydrogels based on photocrosslinkable gelatin and gellan gum biomacromolecules. *Biomaterials* 33(11):3143–3152
- Siemionow M, Brzezicki G (2009) Chapter 8: current techniques and concepts in peripheral nerve repair. *Int Rev Neurobiol* 87:141–172
- Skardal A et al (2012) Bioprinted amniotic fluid-derived stem cells accelerate healing of large skin wounds. *Stem Cells Transl Med* 1(11):792–802
- Steed M et al (2011) Advances in bioengineered conduits for peripheral nerve regeneration. *Atlas Oral Maxillofac Surg Clin North Am* 19(1):119–130
- Svensson A et al (2005) Bacterial cellulose as a potential scaffold for tissue engineering of cartilage. *Biomaterials* 26(4):419–431
- Tang JB, Gu YQ, Song YS (1993) Repair of digital nerve defect with autogenous vein graft during flexor tendon surgery in zone 2. *J Hand Surg Br* 18(4):449–453
- Tanzer RC (1959) Total reconstruction of the external ear. *Plast Reconstr Surg Transplant Bull* 23(1):1–15
- Tsuchiya T et al (2005) Characterization of microglia induced from mouse embryonic stem cells and their migration into the brain parenchyma. *J Neuroimmunol* 160(1–2):210–218
- Visser J et al (2013) Biofabrication of multi-material anatomically shaped tissue constructs. *Biofabrication* 5(3):035007
- Weng L, Chen X, Chen W (2007) Rheological Characterization of in Situ Crosslinkable Hydrogels Formulated from Oxidized Dextran and N-Carboxyethyl Chitosan. *Biomacromolecules* 8(4):1109–1115
- Williams, KL (2007) Fever and the host response. In: Williams KL, (ed) *Endotoxins*. CRC Press, Florida, USA. p. 47–66
- Wolford LM, Stevao EL (2003) Considerations in nerve repair. *Proc (Bayl Univ Med Cent)* 16(2):152–156
- Wu L et al (2011) Trophic effects of mesenchymal stem cells increase chondrocyte proliferation and matrix formation. *Tissue Eng Part A* 17(9–10):1425–1436
- Zulkifli FH et al (2014) Nanostructured materials from hydroxyethyl cellulose for skin tissue engineering. *Carbohydr Polym* 114:238–245



Photopolymerizable Materials for Cell Encapsulation

L. Tytgat, Stefan Baudis, H. Ottevaere, R. Liska, H. Thienpont, P. Dubruel, and S. Van Vlierberghe

Contents

1	Introduction	354
2	Overview of Commonly Applied Photoinitiators for Cell Encapsulation Purposes	356
2.1	Type I One-Photon-Initiators	357
2.2	Type II One-Photon-Initiators	358
2.3	Two-Photon-Initiators	360
3	Overview of Relevant Photopolymerizable Materials for Cell Encapsulation	363
3.1	Overview of Natural Materials	364
3.2	Overview of Synthetic Materials	378
4	Conclusions and Future Perspectives	387
	References	388

L. Tytgat · H. Thienpont · S. Van Vlierberghe (✉)

Polymer Chemistry and Biomaterials Group, Ghent University, Ghent, Belgium

Brussels Photonics (B-PHOT), Department of Applied Physics and Photonics, Vrije Universiteit Brussel, Brussels, Belgium

e-mail: Liesbeth.Tytgat@UGent.be; hthienpo@vub.ac.be; sandra.vanvlierberghe@ugent.be; svvlierb@b-phot.org

S. Baudis · R. Liska

Institute of Applied Synthetic Chemistry, Technische Universität Wien (TU Wien), Vienna, Austria

e-mail: stefan.baudis@tuwien.ac.at; robert.liska@tuwien.ac.at

H. Ottevaere

Brussels Photonics (B-PHOT), Department of Applied Physics and Photonics, Vrije Universiteit Brussel, Brussels, Belgium

e-mail: hottevae@b-phot.org

P. Dubruel

Polymer Chemistry and Biomaterials Group, Ghent University, Ghent, Belgium

e-mail: peter.dubruel@ugent.be

Abstract

Photopolymerization of hydrogels in the presence of cells is a frequently applied technique to realize tissue engineering and regeneration due to the fact that the reaction can take place under cell-friendly physiological conditions. Photopolymerization can be subdivided into three modes, including radical, cationic, and anionic photopolymerization, according to the reactive species which are formed during initiation and propagation. However, radical photoinitiators are the only species suitable for hydrogel formation since ionic photopolymerization inevitably leads to termination of the reactive species as a result of the presence of water. Hydrogels are promising materials due to their capability to absorb large amounts of water and biological fluids without dissolving, their ability to become photopolymerized in the presence of cells, and their close resemblance to the extracellular matrix of native tissue. The present chapter aims to provide an overview of commonly applied photoinitiators as well as photopolymerizable natural and synthetic polymers which are frequently used for cell encapsulation purposes.

1 Introduction

Hydrogels are promising materials for tissue engineering applications due to their similarities to the native extracellular matrix (ECM) and their ability to become photopolymerized in the presence of cells (Vlierberghe et al. 2011b; Anseth 2015). Hydrogels are natural or synthetic crosslinked networks that are capable of absorbing large amounts of water or biological fluids without dissolving (Peppas et al. 2000; Vlierberghe et al. 2011). Crosslinking can occur either physically or chemically (Drury and Mooney 2003). Physically crosslinked networks are reversible due to the occurrence of high molecular chain entanglements, ionic interactions, hydrogen bonds, and/or hydrophobic interactions, while on the other hand chemically crosslinked hydrogels are irreversible as a result of the introduced covalent bonds (Vlierberghe et al. 2011; Malda et al. 2013; Ullah et al. 2015). The latter can be formed by several methods including Michael-type addition reactions (Fu and Kao 2011), enzyme-mediated reactions (Moreira Teixeira et al. 2012), click chemistry (Sivashanmugam et al. 2015), and photopolymerization reactions (Ovsianikov et al. 2011a).

A photopolymerization reaction is driven by a light-sensitive compound also referred to as photoinitiator (Sect. 2), which results in the formation of radicals upon light exposure of a specific wavelength (Williams et al. 2005). Next, the radicals initiate the polymerization of a crosslinkable material resulting in a crosslinked hydrogel network (Nguyen and West 2002; Fouassier et al. 2003). Most photopolymerization reactions are triggered by the absorption of UV or visible light, but recently researchers also developed systems which are suitable to become activated

by near-infrared light (Fouassier et al. 2003). Photopolymerization holds several advantages over the alternative conventional polymerization techniques. It provides (i) spatiotemporal control over the hydrogel formation, (ii) the curing rates are fast (cfr. generally seconds up to minutes), (iii) the reaction can be performed at room or physiological temperature, and (iv) only a minimal amount of heat is released (Nguyen and West 2002; Anseth 2015). The main advantage associated with this technique is that crosslinked hydrogels can be produced under physiological conditions implying that hydrogel formation can occur in the presence of cells (Anseth 2015).

Highly water-swollen hydrogels provide an excellent platform to encapsulate cells as they closely resemble the ECM of living tissue (Peppas et al. 2000; Vlierberghe et al. 2011). The ECM is a dynamic and complex environment which ensures structural support for the embedded cells and stimulates cellular functions including cell adhesion, migration, proliferation, and differentiation (Torgersen et al. 2013). Hydrogels are soft and rubbery materials and have a high water content which contributes to their excellent biocompatibility (Vlierberghe et al. 2011). In addition, hydrogels are porous networks rendering them permeable for oxygen and nutrient transport (Nguyen and West 2002). Generally, synthetic hydrogels do not exert cell-interactive properties. Therefore, natural polymers such as collagen, gelatin, glycosaminoglycans, and/or peptide sequences (Sect. 3.1) containing arginine-glycine-aspartic acid (RGD) are often incorporated in those material types to introduce cell adhesion (Hern and Hubbell 1998).

A drawback of the photopolymerization process is that the generated radicals in the hydrogel can be harmful for the encapsulated cells. The cells can be directly damaged by the radicals through the oxidation of their lipid bilayer or indirectly through the generated oxidative stress to their DNA which results in instability of their genome (Burhans and Weinberger 2007; Lin et al. 2011). The produced radicals can also react with reactive oxygen species (ROS). These ROS including superoxide anions (SO_x), nitric oxide (NO_x), superoxide radicals (O_2), hydroxyl radicals (OH), singlet oxygen ($^1\text{O}_2$), and ozone (O_3) can also react with the lipid bilayer of the cells resulting in the peroxidation of the lipid (Mihaila et al. 2013; Lim et al. 2015). It is known from literature that lipid peroxidation causes disruption of the cell membrane resulting eventually in damaged DNA, upregulation of the enzymes responsible for tissue degradation, as well as the formation of toxic products (Halliwell and Chirico 1993; Greenberg et al. 2008).

Recently, there has been an increasing interest in hydrogels based on natural (e.g., collagen, gelatin, hyaluronic acid, etc.) (Sect. 3.1) and/or synthetic polymers (e.g., poly(ethylene glycol) (PEG) (meth)acrylate derivatives, poly(vinyl alcohol) (PVA) derivatives, etc.) (Sect. 3.2) for cell encapsulation targeting tissue engineering and regeneration (Hoffman 2001; Nguyen and West 2002). The current book chapter provides an overview of commonly applied photoinitiators as well as photopolymerizable materials which are frequently used to enable photopolymerization reactions in the presence of cells.

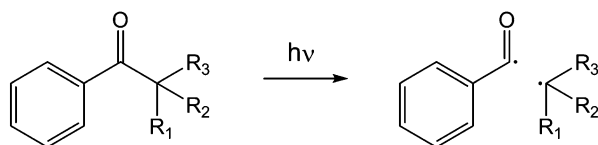
2 Overview of Commonly Applied Photoinitiators for Cell Encapsulation Purposes

Photopolymerization is a versatile technology tool. It enables spatiotemporal control over phase transitions. In most of the applications, a liquid formulation is transferred into a solid material by the formation of an insoluble network within seconds upon irradiation with light of a suitable wavelength (Fouassier 1995). Generally, photopolymerization can be subdivided into three modes, determined by the reactive species generated during the initiation and propagation of the polymerization reaction. However, the two ionic modes – cationic and anionic photopolymerization – are not suitable for the application in hydrogel formation as water inevitably leads to termination of the polymerization. Hence, only the remaining mode – the radical photopolymerization – is of relevance for the encapsulation of cells. The key substance of hydrogel precursor formulations is the radical photoinitiator (PI). The PI transfers the electromagnetic energy of light into chemical energy by the generation of radical species, which initiate the polymerization. Radical PIs can be classified in one-photon-initiators (1PIs) (Dietliker 2002; Green 2010) and multi-photon-initiators (MPIs) (Selimis et al. 2015), whereas to date, two-photon-initiators (2PIs) have the highest relevance in the group of MPIs. The group of 1PIs is subdivided into Type I (Sect. 2.1) and Type II (Sect. 2.2) (Fouassier 1995). Type I 1PIs are excited by light to triplet state and subsequently undergo a cleavage process to form two radicals. Typical structure elements of Type I 1PIs are aryl ketones, which photocleave in α -position to form highly reactive benzoyl radicals (Fig. 1).

Type II 1PIs, however, do not undergo cleavage reactions after being excited to the triplet state. Instead, the energy is transferred from the photosensitizer to a co-initiator and radicals are generated either by direct hydrogen abstraction or by electron transfer followed by proton transfer from the co-initiator to the Type II 1PIs (Fig. 2).

Radicals formed by the co-initiator initiate the polymerization while radicals formed by the photosensitizer couple with radicals from growing chains. Owing to the bimolecular mechanism, Type II 1PIs are generally less efficient compared to Type I 1PIs. In contrast to 1PIs, 2PIs (Sect. 2.3) are photoactive molecules that absorb two photons with half of the energy (i.e., twice of the wavelength) simultaneously by a nonlinear excitation mechanism (two-photon-absorption, 2PA) proposed by Maria Göppert-Mayer (1931). This implies two important things. First, due to the doubling of the excitation wavelength, near-infrared light (NIR) is used for the activation of the 2PI. Generally, natural materials (i.e., cells and tissues) are transparent to NIR. Consequently, irradiation through cells and tissues is enabled. Secondly, owing to the nonlinear nature of 2PA, 2PI activation is only attained at very high photon densities within the focal point of femtosecond pulsed lasers. Thus,

Fig. 1 α -Photocleavage of Type I one-photon-initiators



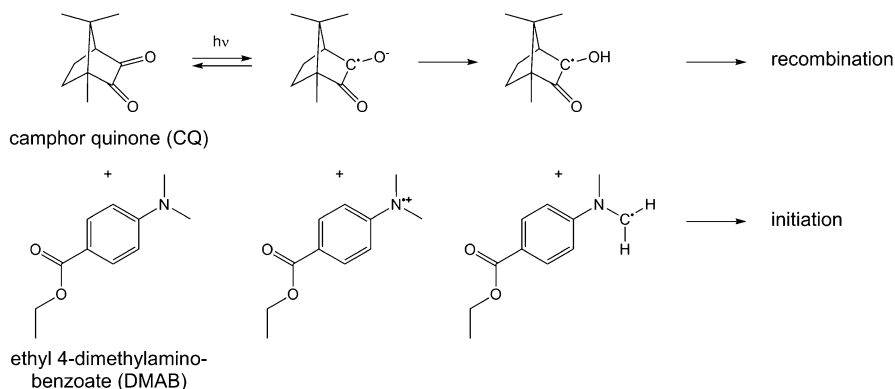


Fig. 2 Generation of radicals in Type II photoinitiator systems

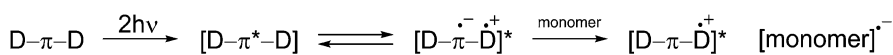


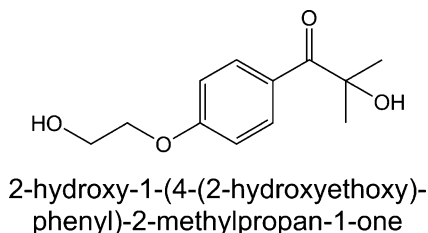
Fig. 3 Two-photon-absorption induced radical generation on the example of a donor- π -donor (D- π -D) type 2PI (Lu et al. 2004)

two-photon-polymerization (2PP) only takes place in the focus of the laser, enabling real 3D writing (Cumpston et al. 1999). Although the exact mechanism of 2PA induced radical generation is not yet fully understood, a very similar mechanism compared to Type II 1PIs is proposed (Lu et al. 2004). 2PIs have highly conjugated π -systems, a good coplanarity and strong donor/acceptor groups (Rumi et al. 2000; Lee et al. 2008; He et al. 2011). The excited triplet state of the 2PI (2PI*) leads to intra- and intermolecular charge transfer interactions between 2PI* and monomer, and radicals are formed by electron transfer to initiate the polymerization (Fig. 3).

2.1 Type I One-Photon-Initiators

Most of the commercially available 1PIs are not or hardly soluble in water, thereby prohibiting their application in hydrogel precursor formulations (Dietliker 2002; Green 2010). This is essentially due to their main application field in the coatings industry. In order to increase water solubility and to enable cell encapsulation, hydrophilic moieties are often attached to the molecular structure of the 1PIs (Liska 2002; Ullrich et al. 2005). However, suitable spacers like alkyl-chains are usually required to avoid shifting of the electronic structure, which would otherwise lead to a significant change in photoactivity. Important solubilizing groups are hydroxyl groups as found in 2-hydroxy-1-(4-(2-hydroxyethoxy)phenyl)-2-methylpropan-1-one (Irgacure 2959, Fig. 4), currently almost exclusively used when water solubility is desired (Bryant et al. 2000; Cheng et al. 2014; Liu et al. 2014; Lobry et al. 2014).

Fig. 4 Commercial water-soluble Type I one-photon-initiator Irgacure 2959



However, the water solubility of Irgacure 2959 is still very limited (<0.5 wt%). Taken together with the relatively poor photoreactivity of this 1PI (compared to organo-soluble 1PIs (Schuster et al. 2007)) and the considerable cytotoxicity at even lower concentrations (Williams et al. 2005; Mironi-Harpaz et al. 2012; Dua and Ramaswamy 2013), this is a very severe restriction for crosslink efficacy of hydrogels. Moreover, the activation wavelength of Irgacure 2959 is below 360 nm (UV-A radiation). In this region, substantial cell damage is caused by the radiation. Additionally, this region is not covered by common LED lamps, used for instance in digital light processing stereolithography (DLP-SLA) for 3D printing applications, of which emission maxima lie between 400 and 500 nm. For these reasons the demand arose for alternative 1PIs with increased water solubility, bathochromic shift of activation wavelength, and enhanced photoreactivity. The common design approach for such alternative 1PIs is to use efficient organo-soluble 1PIs, like monoacylphosphineoxide (MAPO) and bisacylphosphineoxide (BAPO) as a template and transfer them into lithium or sodium salts, respectively (Fig. 5; Majima et al. 1991; Fairbanks et al. 2009a; Lin et al. 2013; Benedikt et al. 2015; Mueller et al. 2015).

Besides the superior water solubility of the salt based 1PIs (an order of magnitude higher than Irgacure 2959) and cytocompatibility (Benedikt et al. 2015), the absorbance above 400 nm enables efficient visible light polymerization, ideal for cell encapsulation (Fairbanks et al. 2009a). Another approach in the field of Type I 1PIs is to use azo compounds known as thermal initiators, which readily cleave at wavelengths lower than 390 nm. However, besides the issue with harsh UV radiation, the generation of nitrogen bubbles might be an unwanted effect during hydrogel crosslinking. A very common azo-based 1PI used for cell encapsulation experiments is 2,2'-azobis[2-methyl-*N*-(2-hydroxyethyl)propionamide] (VA-086, Fig. 6) (Occhetta et al. 2015).

2.2 Type II One-Photon-Initiators

Introduction of solubilizing moieties like salts or hydroxyl groups also leads to water-soluble Type II 1PIs. Here, benzophenone (Allen et al. 1990) and thioxanthone derivatives (Corrales et al. 2006) are of highest relevance. 3-(4-Benzoylphenoxy)-2-hydroxy-*N,N,N*-trimethyl-1-propanaminium-chloride (Quantacure BPQ) (Liska 2002) and 2-hydroxy-*N,N,N*-trimethyl-3-((9-oxo-9H-thioxanthen-3-yl)oxy)propan-1-aminium chloride (Lougnot and Fouassier 1988; Lougnot et al. 1989) are important examples for these types of water-soluble Type II 1PI (Fig. 7).

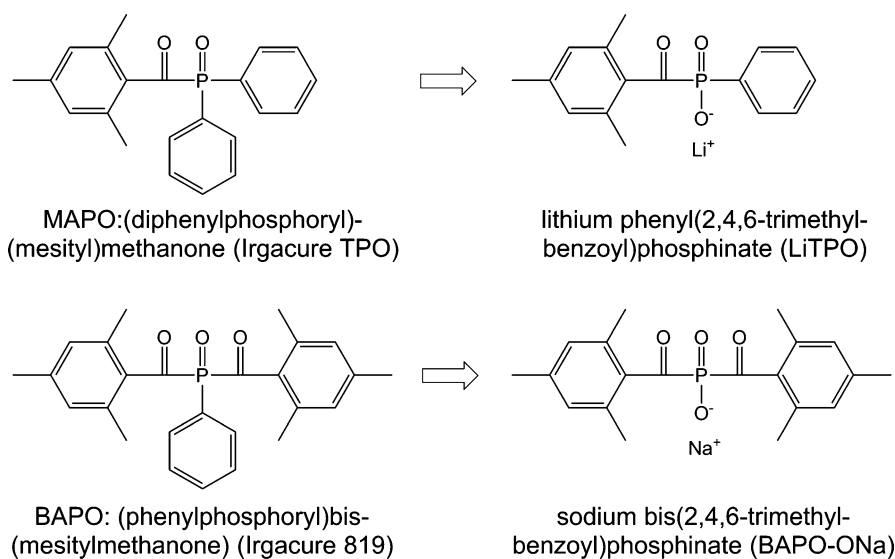
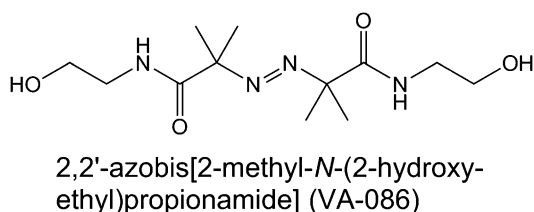


Fig. 5 Monoacylphosphineoxide (*MAPO*) and bisacylphosphineoxide (*BAPO*) photoinitiators and the derived water soluble salts

Fig. 6 Azo-based one-photon-initiator



These photoinitiators show good water solubility. However, their biocompatibility is rather poor, especially for the tertiary ammonium salts as these infiltrate and impair the function of cell membranes. Additionally, they suffer from lower reactivity owing to the bimolecular Type II photoinitiation mechanism and the solvent cage effect (Ullrich et al. 2005). Among the group of salt-based water soluble photosensitizers, eosin Y is a potent visible light Type II 1PI. An optimized three-component system composed of eosin Y, triethanolamine, and *N*-vinyl-2-pyrrolidone (Fig. 8) was found to support viability during cell encapsulation (Bahney et al. 2011).

Another possibility to enhance water solubility is the complexation of the photosensitizing component of Type II 1PIs. Naphthalimid derivative 5-amino-2-benzyl-1H-benzo[de]isoquinoline-1,3(2H)-dione was complexed with 2,6-di-*O*-methyl- β -cyclodextrin and combined with *N*-methyldiethanolamine (MDEA) to a Type II 1PI system for the polymerization of a 2-hydroxyethyl acrylate hydrogel with a very high efficiency (Fig. 9; Zhang et al. 2015).

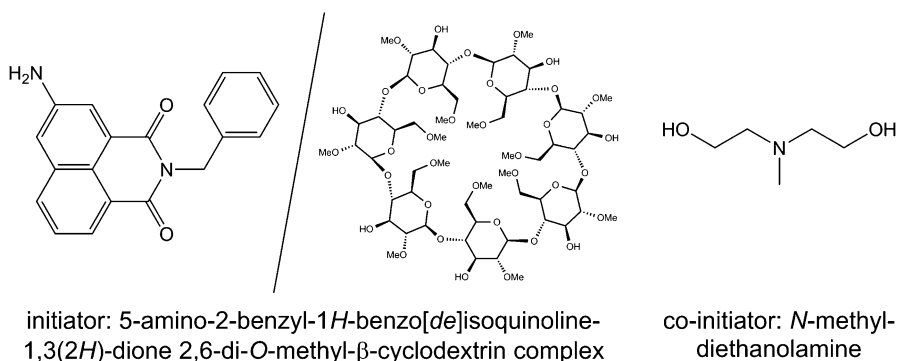


Fig. 9 Naphthalimid-based cyclodextrin complexed Type II IPI with water-soluble co-initiator *N*-methyl-diethanolamine

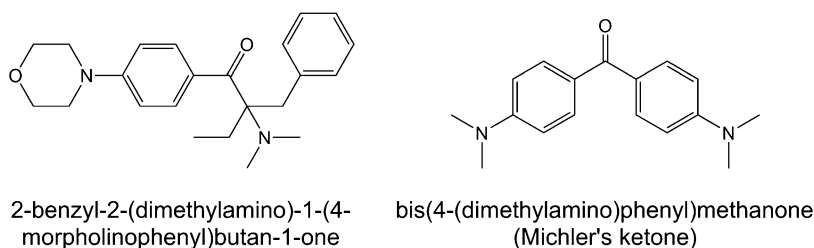


Fig. 10 One-photon-initiator Irgacure 369 (*left*) and Michler's ketone (*right*) used as two-photon-initiator

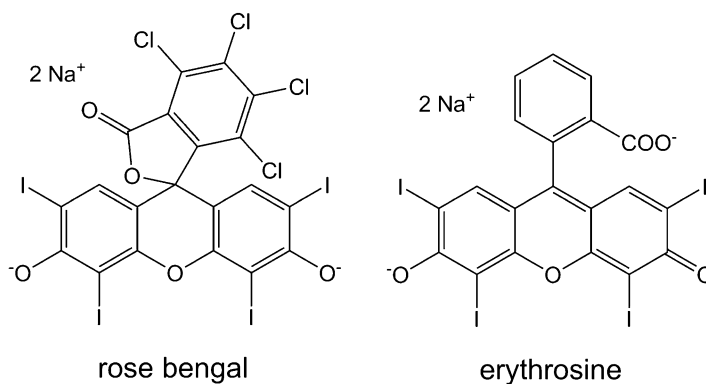


Fig. 11 Hydrophilic dyes as two-photon-initiators (in combination with amines)

wavelength above 400 nm were favorable as this corresponds to a 2PA absorption wavelength of 800 nm at which biological material is transparent. Combinations of commercially available hydrophilic dyes, like eosin Y (Fig. 8; Farsari et al. 2006), rose bengal, and erythrosine (Fig. 11; Campagnola et al. 2000), with amines as

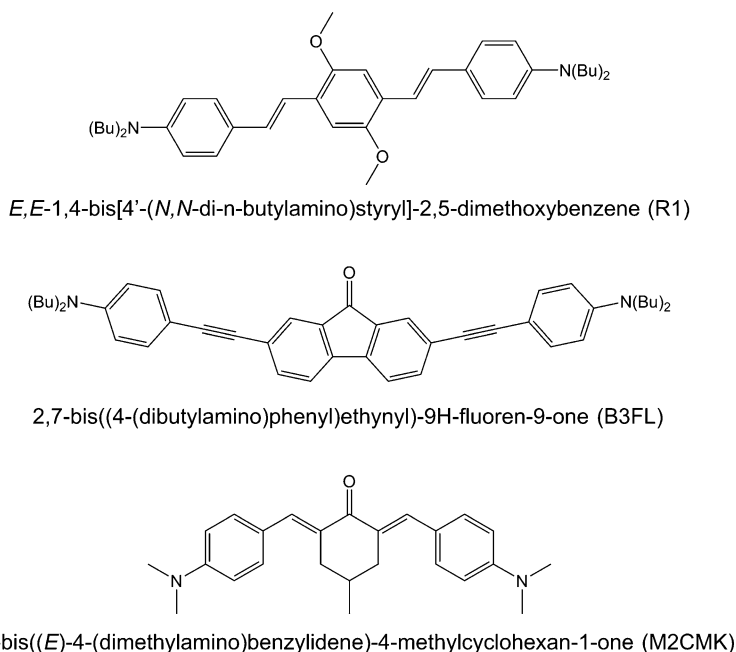


Fig. 12 Highly efficient two-photon-initiators

co-initiator enabled the 2PP fabrication of hydrogels. Nevertheless, very high laser intensities and low writing speeds are required in order to compensate for the small 2PA cross-sections of the dyes.

In order to increase the 2PA cross-section of 2PIs for an efficient hydrogel crosslinking at moderate laser powers and fast writing speeds, a fundamental understanding of structure-properties relationships is required. However, it is mandatory to avoid high quantum yields for fluorescence as found for 2PA active hydrophilic dyes for bioimaging applications (Hayek et al. 2006; Liu et al. 2012) since this energy is lost for polymerization initiation leading to a low crosslink efficacy despite large 2PA cross-sections. By combination of different structure elements to enhance the intramolecular charge transfer, which is assumed to be the key element for a good 2PI (Nguyen et al. 2006; Ramakrishna and Goodson 2007), new and highly efficient 2PIs (R1, B3FL, and M2CMK, Fig. 12) have been identified with wide structuring processing windows (He et al. 2011; Li et al. 2011, 2013a).

However, these effective 2PIs have a very poor water solubility. Along the common concept, water solubility was enhanced by the introduction of salt moieties. Quaternary ammonium cations were installed on the distyrylbenzene chromophore of R1 in order to obtain the water-soluble highly efficient 2PI WSPI (Woo et al. 2005; Fig. 13), which enables the fabrication of a 3D hydrogel construct in the presence of living organisms (Torgersen et al. 2012). By the incorporation of hydrophilic carboxylate groups onto efficient 2PI chromophores, other water-soluble 2PIs have been obtained and described in literature BSEA (Wan et al. 2009) including P2CK and

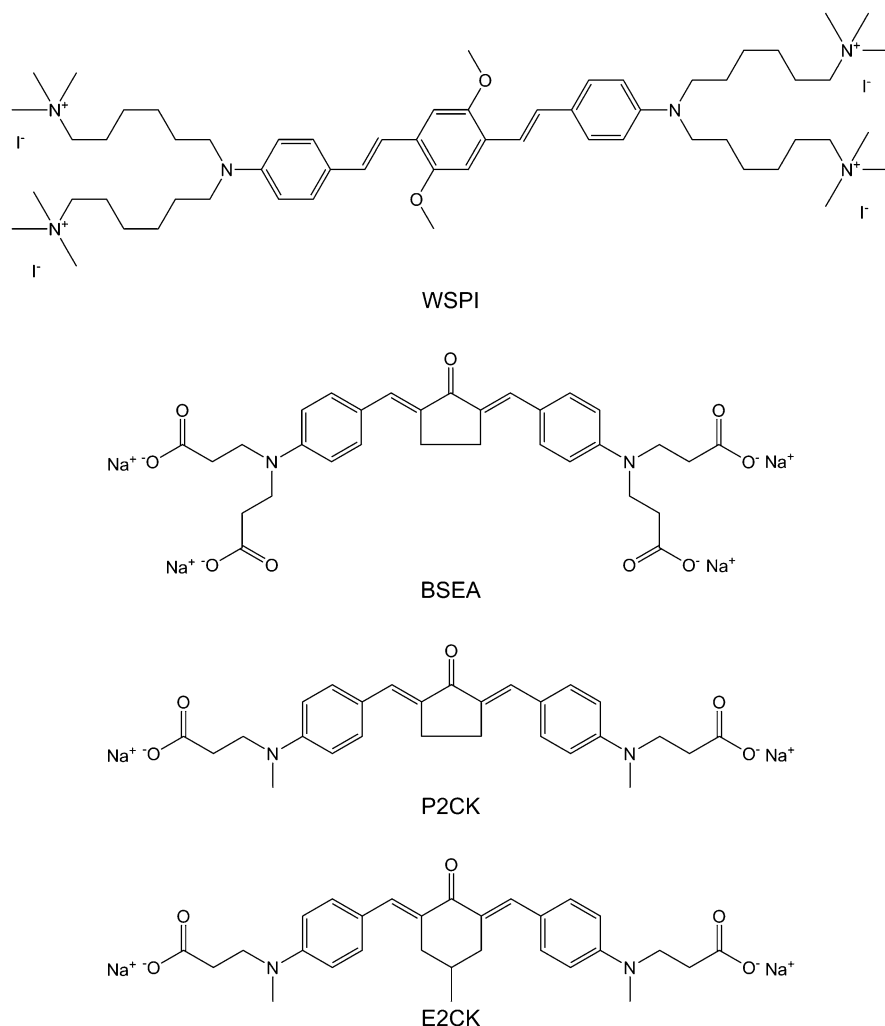


Fig. 13 Water-soluble, cytocompatible two-photon-initiators

E2CK (Li et al. 2013b; Fig. 13). It was demonstrated that the cytocompatibility of these 2PIs (tested with MG63) is comparable with the established Irgacure 2959.

3 Overview of Relevant Photopolymerizable Materials for Cell Encapsulation

Photopolymerizable hydrogels for cell encapsulation purposes are generally composed of macromolecular hydrogel building blocks since most of the monomers which are photopolymerizable are cytotoxic toward the encapsulated cells (Nguyen and West 2002). Ideally, the precursors should be water-soluble, biocompatible, and

biodegradable in order to create an excellent mimic of the ECM. Generally, the polymers are functionalized to introduce suitable moieties which can be photopolymerized in the presence of cells.

To date, various photopolymerizable materials have already been developed to be used as hydrogel scaffolds for cell encapsulation applications. These compounds can be subdivided into two groups: the natural polymers including proteins and polysaccharides (Sect. 3.1) versus the synthetic materials such as PEG and PVA (Sect. 3.2) derivatives (Xu et al. 2012; Fu et al. 2015; Sivashanmugam et al. 2015). Synthetic hydrogels applied for these purposes are non-toxic and exhibit minimal batch-to-batch variations (Xu et al. 2012). Furthermore, these materials are characterized by tuneable mechanical and degradation properties (Xu et al. 2012). However, the main disadvantage associated with synthetic polymers is their lack of natural biofunctionality which stimulates cell adhesion, migration, proliferation, and/or differentiation (Fu et al. 2015). Therefore, conjugation chemistry is often applied to introduce cell-interactive properties (Xu et al. 2012). Conversely, the processing of natural materials into their final design tend to be difficult due to the fact that they are generally mechanically less robust (Fu et al. 2015; Sivashanmugam et al. 2015). Another challenge includes the maintenance of compositional consistency due to the heterogeneity often associated with natural materials (Fu et al. 2015). A hybrid hydrogel based on natural and synthetic polymers is often a promising approach toward regenerative medicine, because it combines the bioactive properties of natural compounds with the tuneable mechanical characteristics of synthetic polymers (Xu et al. 2012; Fu et al. 2015; Sivashanmugam et al. 2015). In what follows, an overview of the most frequently applied photocrosslinkable materials in regenerative medicine is given together with a nonexhaustive overview of the different cells used to date for cell encapsulation (Table 1).

3.1 Overview of Natural Materials

3.1.1 Description of Proteins

Collagen which is the main component of the ECM and gelatin which is obtained by the basic or acidic hydrolytic degradation of collagen are the most frequently used proteins for biomedical applications (Gomez-Guillen et al. 2011; Vlierberghe et al. 2011). The interest in collagen has decreased over the years because there is one major drawback associated with the use of collagen-based hydrogels (Xu et al. 2012). Collagen exhibits extensive contraction upon encapsulating cells (Lewus and Nauman 2005). Contraction of collagen hydrogels is caused by the collagen concentration, cell density, and the amount of serum in the medium (Feng et al. 2003; Gentleman et al. 2004). This process generally results in a decreased hydrogel size which makes it difficult to produce patient-specific scaffolds (Gentleman et al. 2004). Furthermore, hydrogel contraction decreases the permeability of the constructs resulting in limited diffusion of oxygen and nutrients and slow proliferation, and induces apoptosis of the embedded cells (Gentleman et al. 2004).

Table 1 Overview of photopolymerizable hydrogel materials together with the type of cells encapsulated

Hydrogel starting material	Hydrogel composition	Encapsulated cell type	Ref.
Proteins	Gelatin methacrylamide	Hepatocarcinoma cells Human osteosarcoma cells	(Billiet et al. 2014) (Ovsianikov et al. 2014)
	Gelatin methacrylamide/gellan gum methacrylate	NIH-3T3 fibroblasts	(Shin et al. 2012)
	Gelatin norbornene	Human mesenchymal stem cells	(Munoz et al. 2014)
Polysaccharides	Gelatin styrene Gelatin methacrylated ethanalamide/ hyaluronic acid methacrylate	Chondrocytes Hepatocarcinoma cells Human intestinal epithelial cells Murine fibroblasts	(Hoshikawa et al. 2006) (Skardal et al. 2010) (Skardal et al. 2010) (Skardal et al. 2010)
	Alginate methacrylate	Nucleous pulposus cells	(Chou and Nicoll 2009)
	Carboxymethylcellulose methacrylate	Nucleous pulposus cells	(Reza and Nicoll 2010)
	Carrageenan methacrylate	NIH-3T3 fibroblasts MC3T3 E1-4 preosteoblasts Human mesenchymal stem cells	(Mihaila et al. 2013) (Mihaila et al. 2013) (Mihaila et al. 2013)
PEG	Dextran methacrylate + lysine/gelatin methacrylamine	Human umbilical artery smooth muscle cells	(Liu and Chan-Park 2010)
	Hyaluronic acid methacrylate	Cardiac valvular interstitial cells	(Masters et al. 2005)
	Thiolated heparin/PEG diacrylate	3T3 fibroblasts	(Fu et al. 2015)
	Chondroitin sulfate methacrylate	Chondrocytes	(Li et al. 2004)
	PEG diacrylate/RGD	Chondrocytes	(Bryant et al. 2008)
	PEG acrylate/ dexamethasone	Human mesenchymal stem cells	(Nuttelman et al. 2006)
PEG	PEG dimethacrylate	Chondrocytes	(Cui et al. 2012)
	PEG dimethacrylate/ RGD/MMP	Human mesenchymal stem cells	(Gao et al. 2015)
	PEG diacrylate/thiolated gelatin	Neonatal human dermal fibroblasts	(Xu et al. 2012)
	PEG diacrylate/ fibrinogen	Human pluripotent stem cells	(Kerscher et al. 2015)
	PEG tetranorbornene/ chymotrypsin-degradable peptide	Human mesenchymal stem cells	(Fairbanks et al. 2009b)

(continued)

Table 1 (continued)

Hydrogel starting material	Hydrogel composition	Encapsulated cell type	Ref.
PVA	PVA methacrylate/ chondroitin sulfate methacrylate	Chondrocytes	(Bryant et al. 2004)
	PVA methacrylate/ heparin methacrylate	L929 murine fibroblasts	(Young et al. 2013)
	PVA tyraminated/ gelatin/sericin	L929 murine fibroblasts	(Lim et al. 2015)
Poloxamer	F127 diacrylate	NIH-3T3 fibroblasts	(Lee and Tae 2007)
	F127 diacrylate/ fibrinogen	Human dermal fibroblasts	(Shachaf et al. 2010)

Nowadays, gelatin is a widely used biomaterial due to its unique properties (Vlierberghe et al. 2011; Van Hoorick et al. 2015; Yue et al. 2015). Gelatin exhibits cell-interactive properties as a result of the presence of tripeptide sequences of arginine (Arg), glycine (Gly), and aspartic acid (Asp) (RGD) present in the protein backbone (Chang et al. 2013; Van Hoorick et al. 2015). Furthermore, gelatin forms a transparent physical hydrogel below its sol-gel transition temperature (around 30 °C depending on the gelatin concentration, cfr. upper critical solution temperature (UCST) behavior) (Van Den Bulcke et al. 2000). Consequently, gelatin has to be chemically crosslinked to avoid dissolution at body temperature. The different amino acids constituting gelatin provide this protein with a large variety of functionalities, which can be modified with a plethora of photocrosslinkable moieties (Van Den Bulcke et al. 2000; Vlierberghe et al. 2011; Lin et al. 2015; Van Hoorick et al. 2015).

To date, one of the most frequently studied gelatin derivatives is the one of which the primary amine groups are modified with methacrylamide (MA) moieties (Gel-MOD) (Ovsianikov et al. 2011a, 2014; Billiet et al. 2014; Graulus et al. 2015; Van Hoorick et al. 2015). These MA groups are introduced by the reaction of the amine groups of gelatin with methacrylic anhydride. This reaction is generally performed at 40 °C in a phosphate buffer at pH 7.8 (Fig. 14; Van Den Bulcke et al. 2000; Yue et al. 2015). Gel-MOD forms a hydrogel when the MA functionalities are exposed to light irradiation in the presence of a suitable photoinitiator (Sect. 2) (Van Den Bulcke et al. 2000). The mechanical properties of the hydrogel can be tuned by varying the degree of methacrylation. Gel-MOD is a suitable hydrogel to encapsulate cells since, despite the incorporated MA groups, Gel-MOD remains an excellent mimic of the ECM due to the presence of the cell-interactive RGD sequences (Yue et al. 2015). In summary, Gel-MOD combines the biomimetic characteristics of gelatin with the tuneable mechanical properties of synthetic polymers.

Billiet et al. studied the effect of 3D printed Gel-MOD-based scaffolds on embedded hepatocarcinoma cells (HepG2) (Billiet et al. 2014). The authors used the additive manufacturing (RP) Bioplotter technique for the 3D printing of cell-laden Gel-MOD hydrogels. This three-axis dispensing machine deposits hydrogel precursors combined with the cells in the presence of a photoinitiator pneumatically

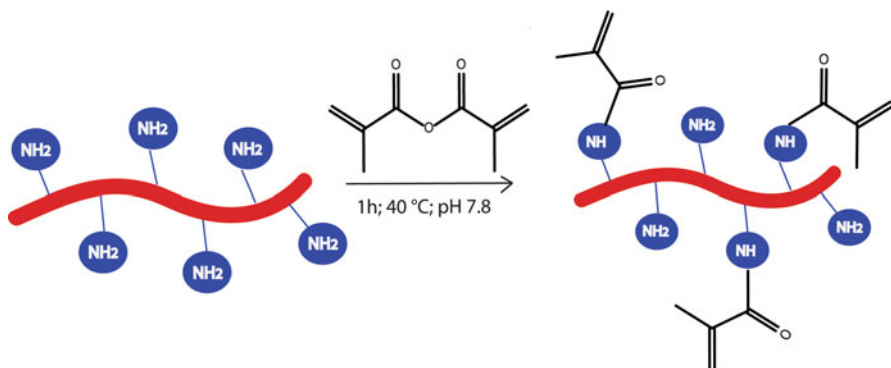


Fig. 14 Modification of gelatin with methacrylic anhydride to introduce crosslinkable methacrylamide moieties

onto a stationary platform. The inlet pressure, the curing irradiation dose, as well as the applied photoinitiator (Irgacure 2959 or VA-086) have an influence on the cell viability of the HepG2 cells (Billiet et al. 2014). The highest cell viability (i.e., >97%) was obtained by using low dispensing pressure (≤ 1 bar) (Billiet et al. 2014). Long-term (14 days) stable cell-laden constructs were produced using UV-A irradiation (1800 mJ/cm^2) (Billiet et al. 2014). The usage of the VA-086 photoinitiator resulted in a higher cell survival (>97%) compared to the Irgacure 2959 photoinitiator (83%) due to the lower cytotoxicity of the generated VA-086 radicals (Billiet et al. 2014). The study showed that the cells maintained their potential to express liver-specific functions including the production of albumin and the storage of glycogen. The latter implies that the produced hydrogels can result into promising scaffolds for liver tissue engineering.

Ovsianikov et al. also investigated the usage of cell-laden Gel-MOD-based hydrogels (Ovsianikov et al. 2014). Two-photon polymerization (2PP) was employed to produce these hydrogel-based scaffolds. With 2PP, localized crosslinking of the photopolymer is induced in the focal point of a femtosecond pulsed laser by the simultaneous absorption of two photons by a two-photon active photoinitiator (Ciuciu and Cywiński 2014). 2PP employs a near-IR laser with a wavelength of around 800 nm which has the capability of penetrating into the cell-containing material without damaging the embedded cells. The latter is a result of the transparency properties of tissues and cells at this wavelength (Ovsianikov et al. 2014). A critical factor for 2PP is the biocompatibility and the water-solubility of the photoinitiator (Ciuciu and Cywiński 2014). The authors selected the benzylidene cycloketone-based two-photon photoinitiator P2CK, which was in-house synthesized, to fabricate Gel-MOD-based “Yin Yang” structures in the presence of human osteosarcoma cells (MG63) (Ovsianikov et al. 2014). Their results demonstrated that only the MG63 cells located in the immediate vicinity of the exposure region survived the photopolymerization process and while the cells that came in close contact with the laser beam did not (Fig. 15; Ovsianikov et al. 2014).

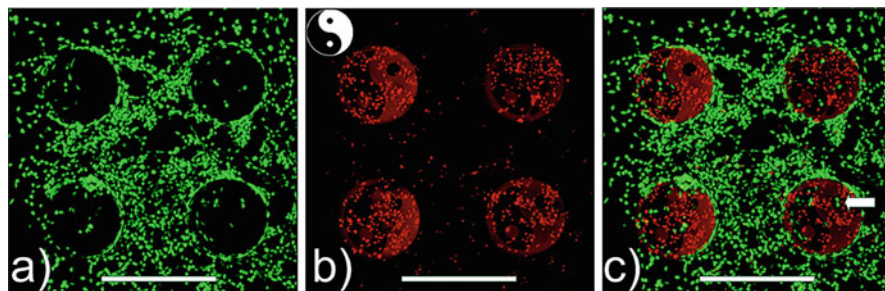


Fig. 15 Viability of cells encapsulated in a gelatin-based hydrogel structures produced by two-photon polymerization (2PP): (a) *green*-stained live cells; (b) *red*-stained dead cells; (c) overlay, with an *arrow* indicating two live cells trapped with a cylindrical void. Scale bar represents 500 μm (Ovsianikov et al. 2014) (<http://pubs.acs.org/doi/full/10.1021/la402346z>)

Ovsianikov et al. observed that it was not the laser itself that damaged the cells, but rather the reactive oxygen species produced during the 2PP process (Ovsianikov et al. 2014). Furthermore, the cell-laden Gel-MOD scaffolds were stable in cell culture for at least 3 weeks and the cells were able to proliferate resulting in the occupation of the available spaces within the 3D hydrogel constructs (Ovsianikov et al. 2014). These scaffolds have the potential to become used for bone tissue engineering applications.

The mechanical strength of Gel-MOD-based hydrogels is often too weak to be suitable for extensive load-bearing tissue engineering applications. Therefore, an increasing interest has emerged for double-network (DN) hydrogels which exhibit high fracture toughness and stress (Shin et al. 2012). DN hydrogels are interpenetrating networks (IPNs), which are composed of two independently crosslinked networks with opposing mechanical properties (Na et al. 2004). One network is stiff and brittle while on the other hand the second one is soft and ductile (Na et al. 2004; Shin et al. 2012). To prevent crack development in the hydrogel, the rigid network will sustain the stress throughout the material while the loosely crosslinked second network dissipates the fracture energy by effective relaxation of the stress (Na et al. 2004; Shin et al. 2012). To date, a wide range of DN hydrogels have already been reported. However, these materials are not suitable for in situ cell encapsulation, because the crosslinking mechanisms often require the usage of toxic crosslinkers (Gong et al. 2003; Nakayama et al. 2004; Weng et al. 2008; Zhu and Marchant 2011). Nevertheless, Shin et al. modified two natural biopolymers including gelatin and gellan gum, via a two-step photopolymerization to develop DN hydrogels with high mechanical strength while preserving the ability to encapsulate cells (Shin et al. 2012). Gellan gum is a polysaccharide produced by the Gram-negative bacteria *Sphingomonas elodea* (Shin et al. 2012; Moxon and Smith 2016). It is composed of repeating tetrasaccharide units consisting of L-rhamnose, D-glucuronic acid, and two residues of D-glucose (Moxon and Smith 2016). Gellan gum forms strong hydrogels due to the interaction of divalent cations with the negative charges of the carboxylic acids

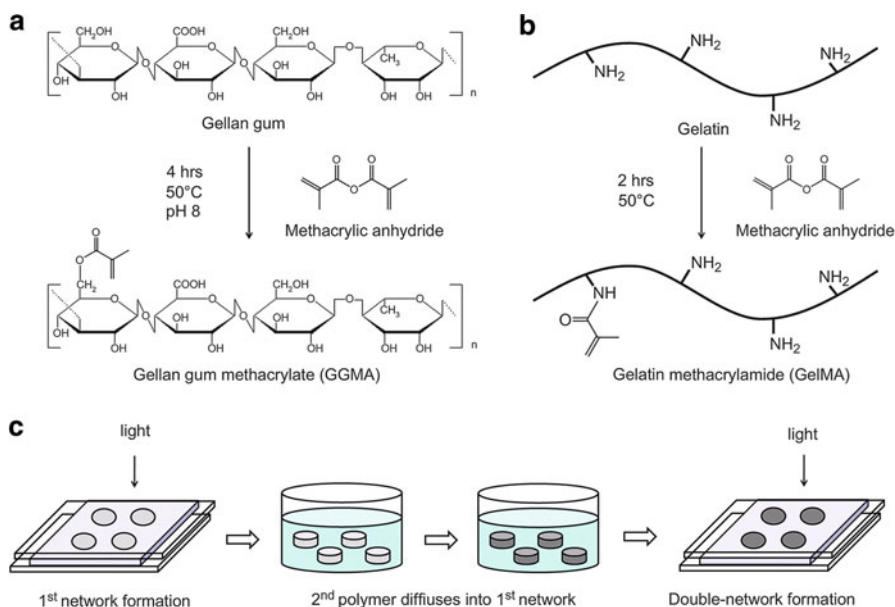


Fig. 16 The modification of (a) gellan gum methacrylate (GG-MOD) and (b) methacrylamide-modified gelatin (Gel-MOD). (c) An overview of the fabrication of DN hydrogels through two-step photocrosslinking (Shin et al. 2012)

of the glucuronic acid units and upon cooling below the sol-gel temperature (UCST behavior) (Moxon and Smith 2016). Gellan gum is a Food and Drug Administration (FDA)-approved food additive and has recently gained a lot of interest for tissue engineering purposes (Shin et al. 2012). Both gellan gum and gelatin were modified with photocrosslinkable methacrylate (GG-MOD) and methacrylamide groups (Gel-MOD), respectively. The DN hydrogels were formed by exposing first a mixture of GG-MOD, cells, and Irgacure 2959 to light (300–500 nm, ~ 7 mW/cm²) for 120s (Fig. 16; Shin et al. 2012). Then, the GG-MOD gels were immersed in Gel-MOD solutions containing the photoinitiator to allow the Gel-MOD to diffuse into the GG-MOD (Shin et al. 2012). Finally, the system was again exposed to light to produce the DN hydrogels (Shin et al. 2012). GG-MOD results in stiff hydrogels, while Gel-MOD hydrogels provide soft and ductile networks (Shin et al. 2012). The authors developed DN hydrogels with high mechanical strength (~ 7 MPa) suitable for the encapsulation of NIH-3T3 fibroblasts (Shin et al. 2012). Their results showed that the hydrogels were cytocompatible resulting in a cell viability of 71% after 3 days (Shin et al. 2012). The DN hydrogels are thus excellent scaffolds for hard tissue engineering applications such as cartilage engineering.

Recent studies, which have already been mentioned in earlier sections, have shown that photopolymerized Gel-MOD hydrogels are excellent scaffolds for regenerative medicine applications (Billiet et al. 2014; Ovsianikov et al. 2014). However, a major disadvantage associated with these hydrogels is that its crosslinking

mechanism is based on radical-mediated chain-growth photopolymerization which yields a high initial radical concentration (Lin et al. 2011; McCall and Anseth 2012). The latter is not ideal for cell types that are susceptible to radical-mediated damage (Lin et al. 2008; McCall and Anseth 2012). This problem could potentially be solved by using “click chemistry” (Lin et al. 2015).

Munoz et al. developed norbornene-functionalized gelatine (Gel-NB) by reacting gelatin with carbic anhydride in aqueous buffered solution (Munoz et al. 2014). Gel-NB can be orthogonally crosslinked via step-growth thiol-ene photo-click chemistry using multifunctional thiols as crosslinkers (dithiothreitol (DTT) or tetra-thiolated PEG (PEG4SH)) (Munoz et al. 2014). The photoinitiator lithium arylphosphinate (1 mM) was used to initiate hydrogel formation (365 nm, 10 mW/cm², 5 min). From literature, it is known that, unlike chain-growth photopolymerization, thiol-ene photo-click reactions are not inhibited by oxygen. Furthermore, thiol-ene photo-click chemistry requires only small amounts of radicals for initiation which results in extremely fast crosslinking (cfr. a few seconds) (Lin et al. 2011, 2015; McCall and Anseth 2012). The results showed that step-growth Gel-NB hydrogels were cytocompatible for in situ cell encapsulation of human mesenchymal stem cells (Munoz et al. 2014). Furthermore, the viability of the stem cells encapsulated in the Gel-NB hydrogels (~91% in 4 wt% Gel-NB) was higher compared to that of the cells encapsulated in the Gel-MOD hydrogels (~85% in 4 wt% Gel-MOD) (Munoz et al. 2014). In addition, the degree of cell spreading was more pronounced in Gel-NB hydrogels compared to Gel-MOD hydrogels (Munoz et al. 2014).

Another gelatin derivative that can be used for the encapsulation of cells is styrenated gelatin. Hoshikawa et al. modified gelatin with photocrosslinkable styrene moieties which can be employed as carrier for chondrocyte transplantation (Hoshikawa et al. 2006). Styrenated gelatin was synthesized by the condensation reaction between the amine groups of the amino acid lysine and the carboxylic acid groups of 4-vinylbenzoic acid (Hannoyer et al. 1999; Hoshikawa et al. 2006). Cell-laden gelatin constructs were made by the irradiation of a mixture of gelatin, chondrocytes, and the photoinitiator camphorquinone, which is a dental photoinitiator, with visible light (400–520 nm) for 2 min (Hoshikawa et al. 2006). The results showed that an average of 26% of the encapsulated chondrocytes survived the irradiation process (Hoshikawa et al. 2006). Furthermore, most of these cells were still viable after 21 days of culture. The viable chondrocytes maintained their phenotype and kept on producing the cartilaginous matrix (Hoshikawa et al. 2006). Therefore, the study indicated the feasibility of using the styrenated gelatin hydrogels as cell carriers for cartilage engineering purposes.

Not only the amine groups of gelatin can be methacrylated but also the carboxylic acid moieties are excellent functionalities for modification. Skardal et al. developed a two-step bioprinting method based on extrusion bioprinting and photopolymerization to fabricate scaffolds for tissue engineering applications (Skardal et al. 2010). The hydrogel was based on a methacrylated ethanolamide derivative of gelatin (Gel-AEMA) and methacrylated hyaluronic acid (Skardal et al. 2010). Gel-AEMA was developed by modifying the carboxylic acid groups of aspartic acid and glutamic acid with ethanolamine. Next, the hydroxyl groups have been

methacrylated to introduce photocrosslinkable moieties. Methacrylated hyaluronic acid (HA-MOD) also contains photopolymerizable functional groups. Therefore, the two materials could be first partially photopolymerized (365 nm, 180 mW/cm², 2,2-dimethoxy-2-phenyl-acetophenone in *N*-vinylpyrrolidone as photoinitiator stock solution (300 mg/mL)) to obtain a printable, extrudable gel-like bioink which was a combination of the hydrogel material and the embedded cells (Skardal et al. 2010). Afterwards, the scaffolds could be produced with extrusion-based bioprinting. The results indicated that the cell-laden constructs were biocompatible, promoting cell attachment and proliferation of encapsulated HepG2, human intestinal epithelial cells (Int-407), and murine fibroblasts (NIH 3T3) (Skardal et al. 2010). In addition, no inflammatory response was observed when the hydrogels were subcutaneously injected into nude mice (Skardal et al. 2010).

3.1.2 Description of Polysaccharides

Alginates are interesting biopolymers for biomedical applications due to their straightforward fabrication, biocompatibility, biodegradability, and non-immunogenic properties (Yang et al. 2011; Jaikumar et al. 2015). Alginate is an anionic polysaccharide derived from brown seaweed (Hunt and Grover 2010; Graulus et al. 2015). It is composed of D-mannuronic acid (M block) and L-guluronic acid (G block) units which are organized into an irregular, block-wise pattern of varying proportions of GG, MG, and MM blocks linked by 1,4-glycosidic bonds (Yang et al. 2011; Graulus et al. 2015). The G block forms β -(1,4) linkages resulting in a linear and flexible conformation, while the M block gives rise to α -(1,4) linkages thereby introducing steric hindrance around the carboxylic acid groups (Yang et al. 2011; Graulus et al. 2015). As a result, the M block domains are associated with the rigid and stiff molecular chains (Yang et al. 2011). Alginate rapidly forms physical hydrogels upon addition of multivalent cations (Yang et al. 2011; Jaikumar et al. 2015). The G block has more affinity to become crosslinked with divalent cations including Ca²⁺, Ba²⁺, etc., compared to the M block (Yang et al. 2011; Graulus et al. 2015; Jaikumar et al. 2015). However, the gelation mechanism of alginate is not easy to control and often results in a nonuniform structure (Graulus et al. 2015).

Traditionally, calcium-crosslinked alginate hydrogels are a frequently used biomaterial for nucleus pulposus tissue engineering (cfr. as a treatment for intervertebral disc (IVD) degeneration) (Chou and Nicoll 2009; Reza and Nicoll 2010). IVD is a fibro-cartilaginous tissue composed of two interdependent tissues (Rannou et al. 2004). A gelatinous, semi-fluid nucleus pulposus (NP) center is surrounded by a coaxial, lamellar annulus fibrosus (AF) (Rannou et al. 2004). This unique feature allows the IVD to support and distribute loads and permits motion of the spine (Rannou et al. 2004). The degeneration of the IVD plays an important role in the manifestation of lower back pain (Rannou et al. 2004). However, studies have already shown that reversible, ionically crosslinked hydrogels lose their structural integrity over time (Chou and Nicoll 2009; Reza and Nicoll 2010). Therefore, researchers started with the investigation of photopolymerization methods for the production of covalently crosslinked hydrogels that maintain the structural and mechanical integrity of the 3D constructs (Chou and Nicoll 2009; Reza and Nicoll 2010).

Chou et al. already developed photocrosslinkable alginate hydrogels by the introduction of photopolymerizable methacrylate moieties (Chou and Nicoll 2009). Methacrylated alginate (Alg-MOD) was synthesized through esterification of the hydroxyl groups (Smeds and Grinstaff 2001; Chou and Nicoll 2009). A 20-fold excess of methacrylic anhydride was added dropwise to the reaction mixture (Smeds and Grinstaff 2001). The reaction (~24 h) was performed in deionized water at 48 °C and adjusted to pH 8 using 5N NaOH (Smeds and Grinstaff 2001). Hydrogel formation was achieved by UV photopolymerization (368 nm, 1.2 W) of a mixture of Alg-MOD, NP cells, and Irgacure 2959. Both the material properties of the photocrosslinked alginate hydrogels, including equilibrium swelling ratios and Young's moduli, as well as the viability of the encapsulated NP cells were evaluated. The alginate hydrogels, exhibiting different substitution degrees (i.e., 3.1, 4.6, and 6.9%) and starting from different polymer concentrations (2 and 3 w/v%) displayed equilibrium swellings ratios and Young's moduli of 30.52 ± 1.782 kPa up to 43.50 ± 1.345 kPa and 0.5850 ± 1.701 kPa up to 8.824 ± 0.6014 kPa, respectively (Chou and Nicoll 2009). The cell viability was the highest in the hydrogels with the lowest degree of methacrylation. The results indicated that an increased methacrylation degree and polymer concentration resulted in a decrease of the swelling ratio, an increase in the Young's modulus, and in a decrease of the viability of the cells (Chou and Nicoll 2009). The study showed that photocrosslinkable alginate hydrogels with tuneable material properties depending on the envisaged application can be employed for cell encapsulation purposes (Chou and Nicoll 2009).

Another photocrosslinkable material investigated for its potential use in nucleus pulposus tissue engineering is methacrylated carboxymethylcellulose (CMC) (Reza and Nicoll 2010). CMC is one of the most important derivatives of *cellulose*, a linear polysaccharide, which is a very important structural component of the primary cell wall of plants (Reza and Nicoll 2010; Su et al. 2010). CMC is a low-cost alternative for other natural polysaccharides which is commercially available (Reza and Nicoll 2010). Due to its biocompatibility, biodegradability, and hydrophilicity properties, CMC hydrogels are suitable for tissue engineering purposes (Reza and Nicoll 2010). Furthermore, CMC is an FDA-approved material that is composed of linear $\beta(1,4)$ -linked glucopyranose residues (Reza and Nicoll 2010; Su et al. 2010). The hydrophobic polysaccharide backbone of CMC contains many hydrophilic carboxylic acid and hydroxyl moieties that can be modified with photopolymerizable groups (Reza and Nicoll 2010; Su et al. 2010).

Reza et al. have investigated the potential of novel photocrosslinked CMC hydrogels for the encapsulation of NP cells (Reza and Nicoll 2010). Two different molecular weight CMC polymers (90 and 250 kDa) were modified with methacrylate moieties. Afterwards, the polysaccharides were photocrosslinked in the presence of cells to produce hydrogels. The results showed that the encapsulated NP cells were still viable after 7 days (Reza and Nicoll 2010). The swelling ratio and the Young's modulus were determined by analyzing cell-laden and cell-free CMC hydrogels (4 w/v% and molecular weight (MW) 90 kDa versus 2 w/v% and MW 250 kDa) (Reza and Nicoll 2010). The authors observed that there was no significant difference in swelling between the two hydrogel types for either molecular weight

(i.e., $46.45 \pm 3.15\%$ and $48.55 \pm 2.91\%$ for MWs of 90 kDa and 250 kDa, respectively) (Reza and Nicoll 2010). A decreased Young's modulus for all cell-laden and the cell-free hydrogels was observed which indicates an interplay between limited hydrolysis of inter-chain crosslinks as well as the development of a functional matrix (Reza and Nicoll 2010). Histological analyses performed on CMC constructs with a DS of 3 w/v% and a MW of 250 kDa resulted in the presence of rounded cells in lacunae and the pericellular deposition of chondroitin sulfate proteoglycan which is a phenotypic NP marker (Reza and Nicoll 2010). The study supported the use of photocrosslinked CMC hydrogels as tuneable biomaterials for NP cell encapsulation (Reza and Nicoll 2010).

Another interesting polysaccharide which has more scarcely been reported on is *carrageenan*, which is a generic name for the family of linear sulfated polysaccharides which are extracted from red seaweed of the Rhodophyceae class (Campo et al. 2009; Prajapati et al. 2014). It is widely used in the pharmaceutical and food industry as gelling, thickening, emulsifying, or stabilizing agent (Campo et al. 2009). The different carrageenan structures are classified according to the location and the number of sulfated groups on the repetitive disaccharide units. K-carrageenan (κ -CAR), which is composed of alternating 3,6-anhydro-D-galactose and β -D-galactose-4-sulfate units, is a suitable candidate for tissue engineering applications because of its gelation properties and its mechanical strength while it closely resembles glycosaminoglycans (GAGs) which also play an important role in the ECM (Campo et al. 2009; Mihaila et al. 2013; Prajapati et al. 2014). The gelation of κ -CAR is based on cooling (UCST behavior) and the presence of mainly potassium ions (Rocha et al. 2011). The formed hydrogels are firm but brittle, which dissolve when heated. To prevent the dissolution of the hydrogels at physiological conditions, κ -CAR can be modified with (photo-)crosslinkable functionalities followed by polymerization (Mihaila et al. 2013).

Mihaila et al. have synthesized methacrylated κ -CAR (CAR-MOD) through reacting κ -CAR with methacrylic anhydride in water at 50 °C and with pH 8 (Mihaila et al. 2013). CAR-MOD is able to form hydrogels through ionic interactions with potassium ions as well as through chemical crosslinking induced by UV-irradiation in the presence of a suitable photo-initiator. The authors created a dual-crosslinkable hydrogel platform for cell encapsulation applications (Mihaila et al. 2013). The cell viability of encapsulated NIH-3T3 fibroblast cells, MC3T3 E1-4 pre-osteoblast cells, and human mesenchymal stem cells was evaluated within the dually crosslinked CAR-MOD hydrogels (Mihaila et al. 2013). The results showed that the UV exposure time, the photoinitiator concentration, and the degree of methacrylation had no significant effect on the viability of the encapsulated cells (~75%) (Mihaila et al. 2013). The latter indicated that CAR-MOD hydrogels are suitable scaffolds for a wide range of tissue engineering applications.

Dextran is a natural, highly hydrophilic, and high molecular weight polysaccharide consisting of α -1,6 linked D-glucopyranose residues (Liu and Chan-Park 2009; Hennink and van Nostrum 2012). It is often applied for tissue engineering applications, because the polysaccharide is similar to glycosaminoglycans which are important constituents of the ECM (Liu and Chan-Park 2010). Dextran is frequently used as

an alternative for PEG hydrogels (Liu and Chan-Park 2009, 2010). PEG is a synthetic, nonbiodegradable polymer with only terminal functionalizable groups, while dextran is a biodegradable biopolymer with abundant pendant hydroxyl groups amenable to chemical modification (Liu and Chan-Park 2009, 2010). The only disadvantage associated with the usage of dextran is its lack of bioactive sites (Liu and Chan-Park 2009). Therefore, dextran is often functionalized with RGD peptide sequences or a hybrid hydrogel system is developed to enhance the cell-interactive properties of the polysaccharide (Ferreira et al. 2007; Liu and Chan-Park 2010).

Liu et al. investigated a combination of a polysaccharide and a protein in a hybrid hydrogel system to closely mimic the natural composition and function of the ECM (Liu and Chan-Park 2010). The polysaccharide dextran was functionalized with methacrylate and lysine moieties and methacrylamide-modified gelatin (Gel-MOD) was selected as protein (Liu and Chan-Park 2010). First, dextran was modified with methacrylate and aldehyde groups (Dex-MA-AD). The reaction was performed in anhydrous DMSO under nitrogen atmosphere, followed by the addition of the catalyst 4-dimethylaminopyridine (DMAP) (Liu and Chan-Park 2009, 2010). Then, glycidyl methacrylate (GMA) was added to the solution to produce methacrylated dextran (Dex-MA) (Liu and Chan-Park 2009, 2010). The degree of substitution could be adapted by varying the amount of GMA as well as the reaction time. By oxidizing Dex-MA with sodium periodate at room temperature in the absence of light, aldehyde groups were introduced (Dex-MA-AD) (Liu and Chan-Park 2009, 2010). Finally, the Dex-MA-AD solutions were added dropwise to L-lysine solution (twofold molar excess with respect to the aldehyde functionalities) (Liu and Chan-Park 2010). The modification of gelatin with methacrylamide groups has already been described above (Sect. 3.1.1). The hydrogel blends encapsulating human umbilical artery smooth muscle cells (SMCs) were crosslinked by exposure of the precursor solutions to UV light ($\lambda = 365 \text{ nm}$, 20 mW/cm^2 , Irgacure 2959) for 5 min under argon atmosphere (Liu and Chan-Park 2010). The results showed that the degree of crosslinking of dextran and gelatin as well the concentration/composition of the precursor solution have an influence on the mechanical stiffness and the degree of swelling of the hydrogels (Liu and Chan-Park 2010). The results showed that SMCs spreading and proliferation is sensitive to the hydrogel mechanics (Liu and Chan-Park 2010). Soft hydrogels with shear storage moduli ranging from 898 Pa to 3124 Pa promote fast cell spreading, proliferation, and extensive 3D cellular network formation, while the cell viability of stiffer hydrogels with shear storage moduli ranging from 4026 Pa to 6075 Pa declined by 50% over 2 weeks of culture time (Liu and Chan-Park 2010). Stiffer hydrogels form denser networks that are more obstructive toward cell spreading and proliferation (Liu and Chan-Park 2010). This indicated that the hydrogel blends based on dextran and gelatin are excellent candidates for further development as biomimetic scaffolds for usage in vascular tissue engineering and regeneration (Liu and Chan-Park 2010).

Glycosaminoglycans

Hyaluronic acid is a biocompatible, biodegradable, and nonimmunogenic glycosaminoglycan found in the ECM of many tissue types (Oudshoorn et al. 2007; Collins

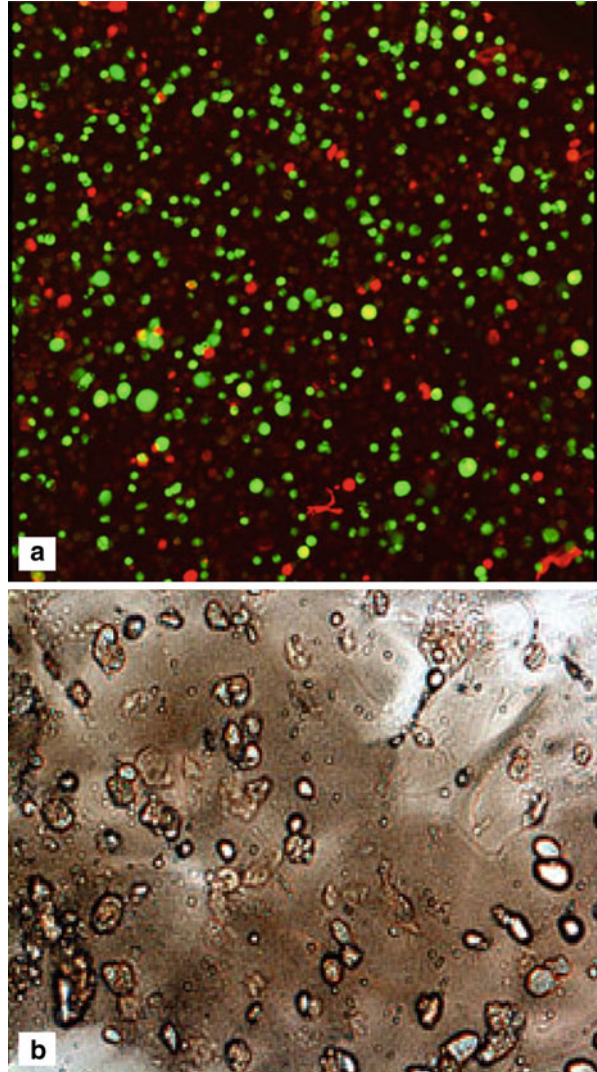
and Birkinshaw 2013). All these properties render hyaluronic acid an attractive candidate for various biomedical applications (Masters et al. 2005). Hyaluronic acid consists of repeating disaccharide units which are composed of $\beta(1,4)$ -linked *N*-acetyl-D-glucosamine and $\beta(1,3)$ -linked D-glucuronic acid (Oudshoorn et al. 2007). Modification of the hydroxyl and carboxylic acid moieties can result in the incorporation of photocrosslinkable groups which can be photopolymerized in the presence of cells (Oudshoorn et al. 2007; Collins and Birkinshaw 2013).

One modification strategy was elaborated by Masters et al. to develop photocrosslinkable, methacrylated hyaluronic acid (HyA-MA) hydrogels suitable for the encapsulation of cardiac valvular interstitial cells (VICs) (Masters et al. 2005). VICs are a good mimic of myofibroblasts which are present in many tissues in the body and contribute to tissue remodeling (Masters et al. 2005). The methacrylation of HyA-MA is similar to that of CAR-MOD (Masters et al. 2005; Mihaila et al. 2013). The reaction is performed in an aqueous environment at pH 8 and an excess of methacrylic anhydride is added with respect to the hydroxyl functionalities of hyaluronic acid (Oudshoorn et al. 2007). The HyA-MA gels were formed by exposing the polymer precursor solution together with the embedded cells to UV light at an intensity of 5 mW/cm^2 for 3 min (Masters et al. 2005). The reaction was carried out in the presence of Irgacure 2959 (Masters et al. 2005). The authors observed that the degradation products of HyA-MA hydrogels significantly increased the proliferation of the embedded VICs (Masters et al. 2005). Their study also showed that after 6 weeks, the encapsulated VICs were still viable and that there was a significant production of elastin which is an elastic protein present in the ECM (Fig. 17; Masters et al. 2005). The results indicated that HyA-MA hydrogels are promising scaffolds for heart valve tissue engineering applications (Masters et al. 2005).

Heparin is a highly sulfated, anionic polysaccharide that is found in the human body (Guimond et al. 2006; Tae et al. 2007). It is composed of repeating disaccharide units consisting of (1,4)-linked glucosamine and uronic acid (Tae et al. 2007). Heparin exhibits anticoagulant properties which are mediated through a pentasaccharide sequence that binds antithrombin III (Tae et al. 2007). The polysaccharide is capable of interacting with a variety of proteins including many growth factors, through the specific heparin-binding domains present on the proteins (Tae et al. 2007; Fu et al. 2015). Therefore, incorporating heparin into hydrogels provides an efficient way to introduce growth factors in its structure without an associated loss of activity (Fu et al. 2015).

Fu et al. investigated the potential of a heparin-based hydrogel which can be cured using visible light (Fig. 18; Fu et al. 2015), as it was shown earlier that many cell types including osteoblasts and corneal epithelial cells are very sensitive to UV-irradiation. UV-light can compromise the cytocompatibility of a system due to the production of cytotoxic free radicals (Cerutti 1985). These radicals can damage cellular proteins and DNA (Cerutti 1985). The authors developed thiol-functionalized heparin (Hep-SH) that can react with PEG-diacrylate (PEG-DA) when green light (525 nm) is applied to excite the photoinitiator eosin Y (EY) in the presence of the electron-donor triethanolamine (TEOA) (Fig. 18; Fu et al. 2015). Hep-SH was synthesized by modifying 40% of the carboxylic acid groups of

Fig. 17 Live/dead staining images of VICs encapsulated in HyA-MA hydrogels indicated that the cells (a) remained viable after 1 week of culture and (b) produced significant amounts of elastin after 6 weeks in culture (displayed by reddish-brown staining throughout hydrogel sections (Masters et al. 2005)



heparin. First, 1-ethyl-3-[3-dimethylamino]propyl]carbodiimide (EDC) and 1-hydroxy-benzotriazole hydrate (HOBt) were added to activate the carboxylic acid moieties (Tae et al. 2007). Then, cysteamine was used to introduce thiol groups and dithiothreitol was added to reduce the oxidized disulfide groups to free thiol groups (Tae et al. 2007). The hydrogels were formed by photopolymerization of the precursor solution containing 3T3 fibroblast cells upon exposure to green LED light (525 nm, 5–100 mW/cm²) (Fu et al. 2015). The gelation was achieved via Michael-type addition between the thiol groups of Hep-SH and the acrylate moieties of PEG-DA. The mechanical properties, the gelation kinetics, and the swelling ratios

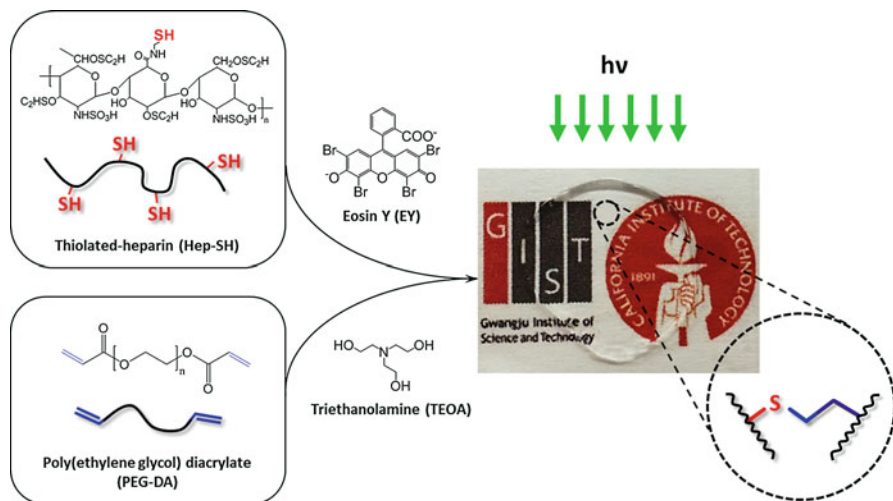


Fig. 18 Schematic overview of visible-light-activated heparin-based hydrogel formation. Green light was used to excite the photoinitiator EY in the presence of the electron-donor TEOA, which induces the reaction of Hep-SH with PEG-DA. The GIST and Caltech logos have been used with permission from the Gwangju Institute of Science and Technology and the California Institute of Technology, respectively (Fu et al. 2015) (Reprinted with permission from Fu et al. Copyright 2016 American Chemical Society)

of the hydrogel system could be adapted by modulating the precursor concentration and the degree of substitution (Fu et al. 2015). The results indicated that 96% of the encapsulated 3T3 fibroblasts were viable (Fu et al. 2015). Furthermore, proliferation of the embedded cells was also observed in the constructs. It seemed that the addition of fibrinogen, a glycoprotein, enhanced the proliferation of the cells more than five times (Fu et al. 2015). In vitro analysis of the epidermal growth factor released from the hydrogel confirmed that the growth factor remained bioactive (Fu et al. 2015). Thus, the developed system with the ability to deliver growth factors and exhibiting fast gelation kinetics upon exposure to green visible light rendered the hydrogels promising candidates to be applied for regenerative medicine purposes.

Chondroitin sulfate (CS) is a natural glycosaminoglycan which is present in the ECM of cartilage tissue (Lee et al. 2005). It is composed of the alternating disaccharide units D-glucuronic acid and N-acetyl-D-galactosamine (Jerosch 2011). When CS binds with core proteins, it can produce either the highly absorbing aggrecan, which is a major component inside cartilage and acts as a shock absorber, or it can produce syndecan which is a cell receptor that can interact with adhesion proteins, cells, and ECM (Lee et al. 2005). It is the negative charge of CS which is responsible for the water retention in cartilage tissue rendering it more resistant toward pressure (Jerosch 2011). The hydroxyl groups of CS can be modified with photocrosslinkable functionalities to fabricate chemically crosslinked hydrogels suitable for cell encapsulation purposes (Van Vlierbergh et al. 2011).

Li et al. have developed methacrylated chondroitin sulfate hydrogels (CS-MA) by the reaction of CS with glycidyl methacrylate (Li et al. 2004). The reaction was performed in a phosphate-buffered saline (PBS, pH 7.4). The hydrogels were prepared by the photopolymerization ($\lambda = 365 \text{ nm}$, $\sim 10 \text{ mW/cm}^2$) of the CS-MA-based solution containing chondrocytes using Irgacure 2959 as photoinitiator (Li et al. 2004). The results indicated that the gels exhibited viscoelastic behavior typical for hydrogels. Furthermore, the CS hydrogels remained degradable in the presence of the enzyme chondroitinase (Li et al. 2004). The live/dead staining and the 3-(4,5-dimethylthiazol-2-yl)-2,5-diphenyltetrazolium bromide (MTT) assay showed that the chondrocytes remained viable after photoencapsulation and incubation in the CS hydrogels (Li et al. 2004). This indicated the potential of CS hydrogels as scaffolds for cartilage tissue engineering.

3.2 Overview of Synthetic Materials

Throughout the years, the potential of various synthetic hydrogels for tissue engineering applications has been evaluated (Alexandridis and Alan Hatton 1995; Bryant et al. 2004; Nuttelman et al. 2006). Not all synthetic materials are suitable candidates for these purposes, because several requirements have to be fulfilled including water-solubility, biodegradability, and biocompatibility of the hydrogels as well as their degradation products (Zustiak and Leach 2011). The well-known copolymer of lactic and glycolic acid (PLGA) is, for example, not an appropriate scaffold material to mimic the natural ECM due to its hydrophobicity, which often results in protein denaturation and/or adsorption as well as potential inflammation as a result of the acidic degradation products (Jiang et al. 2002; Pai et al. 2009; Anderson and Shive 2012). Synthetic hydrogel materials including PEG- and PVA-based materials do exhibit, often after modification, the required characteristics for tissue engineering (Young et al. 2013; Kerscher et al. 2015).

3.2.1 PEG Derivatives

An attractive feature of synthetic hydrogels is their ability to control the macroscopic characteristics including design, swelling properties, compressive modulus, and diffusion-related parameters by varying the crosslinking degree (Bryant et al. 2008). Bryant et al. developed PEG-based hydrogels with different crosslinking densities to regulate biomedical cues and tissue growth for cartilage tissue engineering (Bryant et al. 2008). PEG diacrylate (PEG-DA) was synthesized via the reaction of PEG with acryloyl chloride in the presence of trimethylamine. To enhance the cell-interactive properties of the hydrogels, RGD sequences were incorporated in the hydrogel structure. Hydrogel formation was induced by photopolymerization (365 nm, 6 mW/cm², 10 min) of the macromer solution combined with Irgacure 2959 encapsulating chondrocyte cells (Bryant et al. 2008). The results showed that cell deformation was depending on the crosslink density. It seems that a high crosslinking degree results in the highest cell deformation (Bryant et al. 2008). During cartilage homeostasis, chondrocytes are responsible for the turnover of

new matrix meaning that there is a balance between anabolic and catabolic activities. Different loading regimes were studied to evaluate the chondrocyte activity. It seemed that in the absence of a loading regime, anabolic activity was moderately upregulated while catabolic activity was significantly inhibited. Continuous loading inhibited catabolic activity while intermittent loading stimulated catabolic activity and dynamic loading enhanced anabolic activity (Bryant et al. 2008). The incorporation of RGD introduced cell-matrix interactions but did not affect the mechanical properties nor the water content of the hydrogel (Bryant et al. 2008). The authors demonstrated that by varying the crosslink densities, the biomedical cues for cartilage tissue engineering could be regulated.

PEG-based hydrogels can also be applied to develop a dexamethasone-releasing scaffold for osteogenic differentiation of encapsulated human mesenchymal stem cells (hMSCs) (Nuttelman et al. 2006). Dexamethasone is a synthetic corticosteroid that stimulates osteogenic differentiation by binding to specific regulatory proteins within the cell and activation transcription of osteoblast-specific genes (Atmani et al. 2002; Liu et al. 2002). Nuttelman et al. covalently linked dexamethasone to a photoreactive mono-acrylated PEG via a degradable lactide linkage (Nuttelman et al. 2006). Next, this molecule was incorporated in the PEG hydrogel structure during photopolymerization (upon UV (365 nm) exposure in the presence of Irgacure 2959) (Nuttelman et al. 2006). Over time, dexamethasone was released from the hydrogels due to the hydrolysis of the ester bonds. The rate at which dexamethasone was released could be controlled by altering the length of the lactide spacer (Nuttelman et al. 2006). The results showed that a sustained release of dexamethasone occurred over a month (Nuttelman et al. 2006). Live/dead staining tests indicated that hMSCs were viable up to at least 1 week in vitro after photo-encapsulation. More specifically, the results showed that after 1 week, more than 97% of the encapsulated hMSCs were still viable (Nuttelman et al. 2006), implying that the hydrogel environment was suitable for the delivery of hMSCs. Also osteogenic differentiation was observed in the dexamethasone-modified PEG hydrogels, as indicated by the 2.3-fold elevation in core binding factor alpha 1, which is a common marker for osteogenic differentiation (Nuttelman et al. 2006). The authors thus developed a cytocompatible hydrogel system for the sustained and localized release of dexamethasone to hMSCs embedded in PEG-based hydrogels.

3D inkjet bioprinting combined with simultaneous photopolymerization is one of the most promising additive manufacturing techniques for tissue engineering due to its high speed, high resolution, and low cost (Cui et al. 2012; Gao et al. 2015). An inkjet bioprinter delivers small droplets of bioink (1–100 picoliters; 10–50 μm diameter), which is a mixture of biomaterials and cells, on predefined locations of a substrate (Pereira and Bártolo 2015). To form the ink droplets, the bioink is heated for less than 2 μs which results in a temperature increase of 4–10 $^{\circ}\text{C}$ giving rise to a biocompatible printing process associated with an average cell viability exceeding 90% (Gao et al. 2015). Cui et al. developed this novel bioprinting platform with simultaneous photopolymerization for the fabrication of 3D scaffolds starting from PEG methacrylate (PEG-MA) (Cui et al. 2012). The compressive modulus of the photocrosslinked hydrogels encapsulating chondrocytes was 395.73 ± 80.40 kPa

(Cui et al. 2012). This value is close to the mechanical characteristics of native human articular cartilage (Cui et al. 2012). Furthermore, the embedded chondrocytes showed excellent tissue formation (Gao et al. 2015). However, the usage of autologous differentiated cells is associated with a major drawback. Only a limited number of cells can be harvested during a biopsy. Therefore, bone marrow or adipose tissue-derived human mesenchymal stem cells gained increasing interest, because they are relatively abundant and are able to differentiate into adipose, chondrogenic, osteogenic, myogenic, and other mesenchymal pathways upon implementing appropriate induction (Mackay et al. 1998). However, bioprinted hMSCs-PEG-based constructs lack the potential to produce the full cartilage matrix (Gao et al. 2015). These scaffolds require additional cellular or matrix signals for optimal hMSCs differentiation (Salinas and Anseth 2009). A combination of natural hydrogels with PEG could enhance the cell response of the constructs, but these mixtures have not always been suitable for inkjet bioprinting due to the dramatically increased viscosity of the bioink which can easily clog the printing head of the bioprinter (Van Den Bulcke et al. 2000; Galis and Khatri 2002). Therefore, Gao et al. conjugated biomimetic peptides onto a PEG hydrogel to enhance the biocompatibility and biodegradability of the constructs while maintaining an easy-printable bioink (Gao et al. 2015). By using the inkjet bioprinting technique combined with simultaneous UV photopolymerization, the crosslinking of the PEG backbone could be performed together with the covalent incorporation of acrylated RGD and acrylated matrix metalloproteinase (MMP)-sensitive peptides as well as the encapsulation of hMSCs, while fabricating a layer-by-layer construct. The produced peptide-conjugated PEG scaffolds demonstrated excellent biocompatibility and cell viability (i.e., $87.9 \pm 5.3\%$) (Gao et al. 2015). Clogging of the printing head was minimized due to the low viscosity of the PEG-based bioink (Gao et al. 2015). Furthermore, the results showed osteogenic and chondrogenic differentiation of the embedded stem cells as well as significantly increased mechanical properties (Gao et al. 2015). The bioprinted scaffolds also dramatically inhibited hMSC hypertrophy during chondrogenic differentiation (Gao et al. 2015). In summary, the bioprinted PEG-peptide scaffolds and hMSCs significantly enhanced osteogenic and chondrogenic differentiation toward bone and cartilage formation and was associated with minimal nozzle clogging.

Xu et al. developed a thiol-ene based hybrid biomatrix combining mechanically robust synthetic materials with cell-interactive biopolymers for 3D cell culture (Xu et al. 2012). Gelatin was modified with L-cysteine which is an amino acid that is absent in the primary structure of gelatin, via a homobifunctional PEG-bis-NHS linker (Gel-PEG-Cys) (Fig. 19). This thiolated gelatin material can be covalently linked with PEG-DA via thiol-ene photopolymerization (Irgacure 2959, 365 nm, 10 mW/cm², 90s) to avoid dissolution of gelatin at body temperature (Fig. 19; Xu et al. 2012). The reaction can be performed in the presence of neonatal human dermal fibroblasts to achieve cell encapsulation.

The relative ratio of PEG-DA and Gel-PEG-Cys in the hydrogel starting formulation influenced the bulk and local environment of the scaffold (Xu et al. 2012). It seemed that the bulk viscoelastic characteristics were affected by the PEG-DA

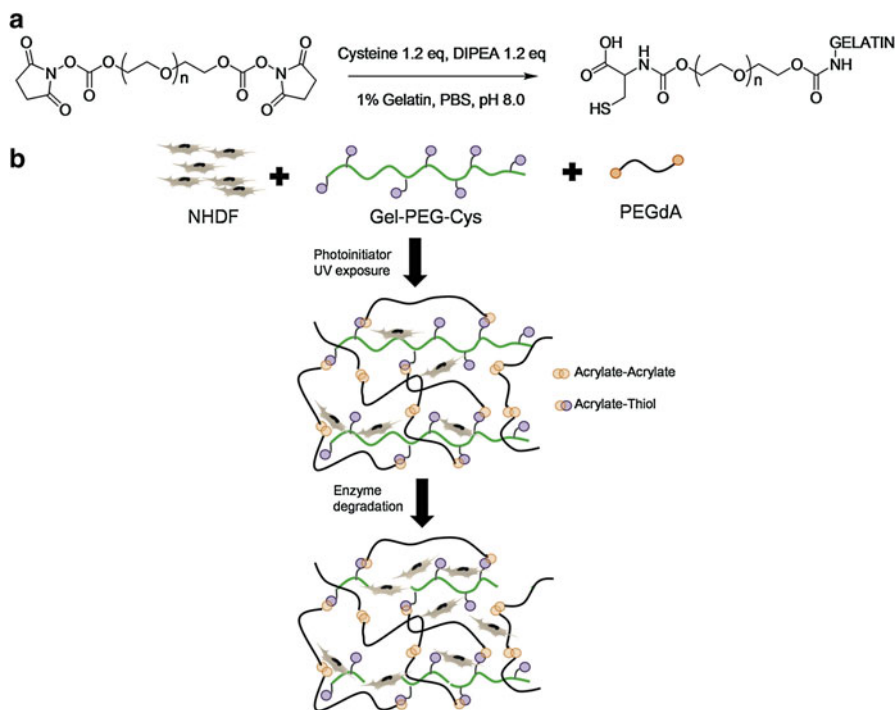


Fig. 19 (a) Schematic representation of the synthesis of PEG/cysteine-modified gelatin (Gel-PEG-Cys). (b) Overview of the scaffold structure of gelatin-PEG matrix for living cell encapsulation. Two possible crosslinks, acrylate–acrylate and acrylate–thiol, can occur simultaneously (Xu et al. 2012)

concentration and the total water content, while the swelling properties were depending on the Gel-PEG-Cys concentration (Xu et al. 2012). The polymer concentration was responsible for the micro-viscoelastic properties of the hydrogel (Xu et al. 2012). The embedded fibroblasts were spread and formed extensions after 2 weeks cell culture into a soft hydrogel. In stiffer hydrogels, no cell spreading was observed (Xu et al. 2012). Furthermore, a higher gelatin concentration provided more binding sites for the cells thereby stimulating cell spreading and proliferation (Xu et al. 2012). The authors developed a hybrid hydrogel for cell and drug delivery applications.

Hydrogels based on PEG can also be combined with fibrinogen to produce a biomatrix for tissue engineering applications. Kresher et al. encapsulated directly human pluripotent stem cells (hPSCs) in a hydrogel to stimulate ontogeny-mimicking (i.e., ontomimetic) differentiation and growth of engineered human heart tissue (Kerscher et al. 2015). hPSCs were able to differentiate into large amounts of physiologically relevant, species-specific, and even patient-specific cardiomyocytes (CMs) (Kerscher et al. 2015). PEG-fibrinogen hydrogels were synthesized by the reaction of PEG-DA with fibrinogen which was modified with phosphine hydrochloride in a urea solution. Hydrogel formation was achieved by the

visible light photopolymerization of the PEG-fibrinogen precursor solution combined with hPSCs and eosin Y photoinitiator (Kerscher et al. 2015). The results showed that the encapsulated hPSCs were able to grow and differentiate into cardiac tissue in the 3D microenvironment of the PEG-fibrinogen hydrogels (Kerscher et al. 2015). This method was extensible to a variety of tissue sizes and designs thereby resulting in a substantial and straightforward improvement of cardiac tissue formation (Kerscher et al. 2015). In addition, this approach even showed potential to fabricate human heart tissue in the long term.

PEG hydrogels for cell-based photoencapsulation purposes are commonly produced by the photopolymerization of linear PEG chains modified on either end with acrylate or methacrylate functional groups. However, thiol-norbornene step-growth polymerization can also be applied for the development of PEG-based hydrogels for tissue engineering applications (Fairbanks et al. 2009b). This type of polymerization results in homogeneous networks that exhibit superior strength and strain tolerance compared to the heterogeneous networks formed by conventional radical-chain-growth polymerization (Malkoch et al. 2006). Fairbanks et al. developed a hydrogel based on PEG-tetranorbornene and the chymotrypsin-degradable peptide to fabricate a versatile synthetic mimic of the ECM (Fairbanks et al. 2009b). The norbornene-derivative of PEG was synthesized by the addition of norbornene acid combined with *N,N'*-dicyclohexylcarbodiimide (DCC). The thiol-ene hydrogels were formed by photocrosslinking the precursor solution containing the PEG derivative in the presence of Irgacure 2959 and hMSCs (352 nm, 7–10 mw/cm²). The mechanical properties of the swollen hydrogels were related to the monomer concentration. The shear elastic moduli of the scaffolds were in the range of 300 ± 20 Pa up to 1700 ± 360 Pa for 3–10 wt% polymer concentrations, which corresponds to the values for physiologically relevant tissues (Discher et al. 2005). The PEG-based hydrogels could be enzymatically degraded by chymotrypsin due to the presence of the chymotrypsin-sensitive peptide crosslinkers (Fairbanks et al. 2009b). Cleavage of the crosslinks decreased the elastic shear moduli over time (Fairbanks et al. 2009b). Live/dead staining results indicated that the thiol-ene hydrogels were cytocompatible, because the cell viability of the encapsulated hMSCs exceeded 95% after 24 h (Fairbanks et al. 2009b). By using thiol-ene photocrosslinkable chemistry, versatile, tailorable, and bioresponsive hydrogels could be fabricated to be applied for cell biology, drug delivery, and regenerative medicine applications.

3.2.2 PVA Derivatives

Poly(vinyl alcohol) (PVA) is a synthetic polymer which is also often used as a hydrogel for biomedical applications because it is water-soluble and biocompatible (Bryant et al. 2004; Young et al. 2013; Lim et al. 2015). PVA has several modifiable hydroxyl groups making this polymer suitable for photopolymerization purposes (Bryant et al. 2004). Bryant et al. modified the hydroxyl moieties of PVA with methacrylates via the reaction with 2-isocyanatoethyl methacrylate in dimethyl sulfoxide (DMSO) (Bryant et al. 2004). To enhance the bioactive properties of the PVA derivative, the authors incorporated methacrylate-modified chondroitin sulfate (ChSA) in the hydrogel structure (Bryant et al. 2004). ChSA was selected to mimic

the native biochemical environment of cartilage and to introduce charges into the network (Bryant et al. 2004). The latter results in an increased water content and stiffness of the hydrogel. In addition, the presence of ChSA can also help to promote cartilage tissue formation through increased cell proliferation and stimulated proteoglycan secretion (Bryant et al. 2004). The cell-hydrogel constructs were fabricated by UV-induced photopolymerization (365 nm, 10 mW/cm²) of the precursor solution containing the methacrylated PVA and ChSA macromers as well as the chondrocytes and the photo-initiator Irgacure 2959 (Bryant et al. 2004). Because the low crosslinking density of the produced hydrogels resulted in highly swollen gels, an adhesive RGD peptide sequence was incorporated in the hydrogel structure to stimulate retention of the encapsulated chondrocytes (Bryant et al. 2004). The RGD sequence was conjugated to a monoacrylated PEG chain (MW 3400) and mixed with the precursor solution prior to photopolymerization. Although no quantitative results could be obtained with respect to the ECM production (Bryant et al. 2004), the embedded chondrocytes appeared to be healthy and rounded and produced their characteristic lacunae (Bryant et al. 2004). Furthermore, the copolymerization of PVA and ChSA produced hydrogels which were degradable in the presence of chondroitinase ABC (Bryant et al. 2004). The study of hydrogel scaffolds, constituting a synthetic PVA component, native glycosaminoglycan found in cartilage tissue, and a cell-interactive RGD peptide sequence, showed that the constructs could be employed for the photoencapsulation of chondrocytes (Bryant et al. 2004). The hydrogels stimulated the natural cell function as observed morphologically (Bryant et al. 2004).

Young et al. investigated the potential of PVA hydrogel microspheres combined with another glycosaminoglycan, heparin, for cell-based photoencapsulation applications (Young et al. 2013). These hydrogel microspheres link the favorable and tuneable mechanical properties of the synthetic polymer PVA with the cell-interactive characteristics of heparin. PVA was modified with methacrylate groups according to the protocol of Bryant et al. (2004). Heparin was also modified with methacrylate moieties by adding glycidyl methacrylate to a heparin solution under vigorous stirring. The reaction was left to react, protected from light at room temperature for 14 days. A capillary-based microfluidic droplet generation device combined with a photopolymerization method was employed to produce the hydrogels (Young et al. 2013). The cell-laden hydrogel microspheres were fabricated by UV-induced photopolymerization (300–500 nm, 30 mW/cm²) of the precursor solution containing methacrylated PVA and heparin, L929 murine fibroblast cells, and the photoinitiator Irgacure 2959 (Young et al. 2013). The modulus of the produced microspheres was 335 kPa for the PVA/heparin. The incorporated heparin did not affect the size and the morphology of the microspheres (Young et al. 2013). The viability of the encapsulated mammalian cells was also evaluated. After 24 h, 90% of the cells remained viable and even after 28 days, over 90% of the cells were still alive (Young et al. 2013). The results showed that the use of a biosynthetic hydrogel offers an improved approach for long-term cell encapsulation purposes (Young et al. 2013).

Covalent incorporation of proteins in the hydrogel structure is a frequently used approach to obtain a biosynthetic hydrogel, because the physical blending of proteins, such as collagen and laminin, with synthetic hydrogels results in rapid leaching

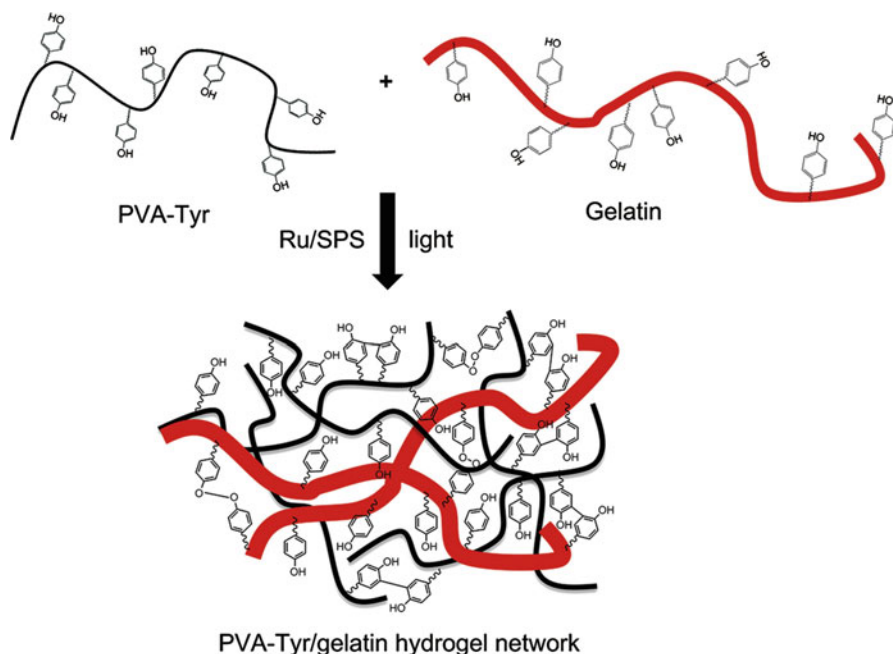


Fig. 20 Schematic representation of the copolymerization of PVA-Tyr and gelatin using Ru/SPS and visible light (Lim et al. 2013)

of proteins from the hydrogel (Zustiak and Leach 2011). However, the covalent incorporation of proteins is also associated with disadvantages. The grafting of functional moieties, such as acrylates and methacrylates, onto proteins to covalently link natural and synthetic polymers causes often disruption of the protein side chains required for the bioactivity properties of the hydrogel (Nilasaroya et al. 2012). Therefore, Lim et al. searched for new approaches eliminating the use of harsh chemicals which did not require prior modification of the protein backbone (Lim et al. 2015). The study proposed a new method to obtain a biosynthetic hydrogel by introducing tyrosine-like moieties such as tyramine onto PVA and crosslinking them with the tyrosine residues of proteins (Fig. 20; Lim et al. 2015). Tyraminated-PVA (PVA-Tyr) was synthesized via a two-step reaction. First, PVA was functionalized with carboxylic acid groups by using succinic anhydride and triethylamine. In a second step, the tyramine groups were coupled to the carboxylic acids of PVA via conventional carbodiimide coupling reaction in the presence of 1,3-dicyclohexylcarbodiimide (DCC) and *N*-hydroxysuccinimide (NHS).

For the visible light photopolymerization of the PVA-Tyr hydrogels, a two-component initiator system consisting of a ruthenium (Ru) and sodium persulfate (SPS) was used (Lim et al. 2015). First, Ru^{2+} is oxidized to Ru^{3+} by donating an electron to SPS (Elvin et al. 2010). Then, Ru^{3+} reacts with the tyramine groups on PVA thereby generating tyrosyl radicals which create crosslinks with the nearby tyramine groups of PVA-Tyr (Elvin et al. 2010; Lim et al. 2015). At the same time,

the parallel dissociation of SPS into sulfate anions and sulfate radicals occurs after accepting electrons from Ru^{2+} (Elvin et al. 2010). The authors also hypothesized that the radicals generated during photoencapsulation might induce oxidative stress to the cells (Lim et al. 2015). Therefore, two antioxidative proteins, gelatin and sericin, were incorporated in the PVA-Tyr structure to scavenge the radicals and ROS potentially formed during the process. By incorporating gelatin at low concentrations in the PVA-Tyr, no significant improvement of the viability of the encapsulated murine dermal fibroblast (L929) cells was observed (Lim et al. 2015). However, it seemed that the embedded cells were able to survive the photopolymerization process when higher concentrations of gelatin (5 w/v%, sample name “5G”) were used (Lim et al. 2015). For sericin, the fibroblast cells were only viable upon applying 1 w/v% (1S) and 5 w/v% sericin concentrations (5S). Combining 1 w/v% gelatin with 1 w/v% sericin (1G/1S) resulted in a high cell viability (>80%) of the embedded fibroblasts (Lim et al. 2015). However, there was a difference observed between 1S and 1G/1S hydrogels with respect to cell proliferation. It seemed that 1S did not stimulate cell aggregation formation compared to 1G/1S, because the encapsulated cells in 1G/1S hydrogels formed clusters associated with the deposition of laminin and collagen after 21 days but these aggregates were not observed in 1G hydrogels (Lim et al. 2015). This result suggested that only gelatin promoted cell proliferation and aggregation as the hydrogel degraded. A possible reason for this phenomenon was that the protein sericin does not contain RGD structures in its protein backbone (Lim et al. 2015). The study showed that the PVA-Tyr hydrogels combined with gelatin and sericin are promising candidates for long-term tissue engineering applications.

3.2.3 Poloxamer

Reversible thermo-responsive polymers such as Poloxamers are also promising candidates for tissue engineering applications (Shachaf et al. 2010). Poloxamers or Pluronics are nonionic copolymers consisting of poly(ethylene oxide)-poly(propylene oxide)-poly(ethylene oxide) (PEO-PPO-PEO) triblocks (Bohorquez et al. 1999; Shachaf et al. 2010). One of the most widely used Poloxamer is Pluronic F127 (F127), which has a nominal molecular weight of 12,500 Da and a PEO/PPO ratio of 2:1 by weight (Bohorquez et al. 1999). An important characteristic of Poloxamer and in particular F127 is its thermoreversible gelation behavior at concentrations exceeding 20% (Bohorquez et al. 1999; Cohn et al. 2005). At ambient temperature, a low viscosity aqueous solution is formed, while a hydrogel is produced by increasing the temperature (cfr. low critical solution temperature (LCST) behavior) (Cohn et al. 2005). The endothermal sol-gel transition is the result of an increase in entropy caused by the release of water molecules bound to the PPO segments as the temperature increases (Alexandridis and Alan Hatton 1995). However, the application potential of Poloxamer has been limited due to its fast dissolution after physical gelation. Therefore, a photopolymerizable Poloxamer system has already been developed to overcome this drawback (Lee and Tae 2007).

Lee et al. modified F127 with diacrylate groups (DA-F127) to produce hydrogels that can be made without the need for UV light to induce photopolymerization after injection (Lee and Tae 2007). First, DA-F127 was photopolymerized at molecular level by UV

light (Lee and Tae 2007). Next, the solution was injected into the target site by macroscopic gelation before it showed significant increase in viscosity (Lee and Tae 2007). This new injection method eliminated the commonly observed problems including damage to normal cells and tissues around the injected polymer due to direct UV exposure during photocrosslinking (Lee et al. 2004). DA-F127 was synthesized by acrylating the hydroxyl groups of F127 by reaction with a tenfold molar excess of both acryloyl chloride and trimethylamine in dichloromethane (Lee and Tae 2007). The reaction was allowed to stir overnight under argon (Lee and Tae 2007). The degree of acylation determined by $^1\text{H-NMR}$ spectroscopy was 98%. DA-F127 was photopolymerized using UV light (1.3 mW/cm^2) in the presence of NIH 3T3 fibroblasts (Lee and Tae 2007). The results showed that the usage of the photoinitiator Irgacure 2959 did not affect the proliferation of the cells whatsoever (Lee and Tae 2007). Furthermore, the majority of the encapsulated cells remained viable after the photopolymerization process (Lee and Tae 2007). A cell viability exceeding 95% was observed (Lee and Tae 2007). Therefore, the study suggested that this injection method can be applicable for in vivo biomedical purposes without major issues (Lee and Tae 2007).

Poloxamer-based hydrogels are synthetic polymers without bioactive properties. Therefore, Shachaf et al. developed a temperature-responsive biomaterial with enhanced cell-interactive characteristics by combining the protein fibrinogen with F127 (Shachaf et al. 2010). F127 was end-functionalized with acrylate groups by reaction with acryloyl chloride. Next, denatured fibrinogen reacted via a Michael-type addition reaction to form a biosynthetic copolymer (FF127). The hydrogel constructs were made by photocrosslinking the precursor solution in the presence of human dermal fibroblasts upon UV-exposure (365 nm, $4\text{--}5 \text{ mW/cm}^2$) (Shachaf et al. 2010). The FF127 displayed a reversible temperature-induced physical sol-gel transition and irreversible chemical photocrosslinking characteristics (Fig. 21; Shachaf et al. 2010). The results of the cell viability test showed that at day 0, 88% of the embedded cells were viable and that at day 3 more than 85% of the cells were still alive (Shachaf et al. 2010). Furthermore, it seemed that the protease degradation and consequent cell-mediated remodeling could be controlled by the F127 constituent, because F127 elicits less steric interactions that could shield the protein backbone from proteolysis (Shachaf et al. 2010). The hydrogels exhibited also biomimetic properties, because the bioactive sites on the fibrinogen backbone

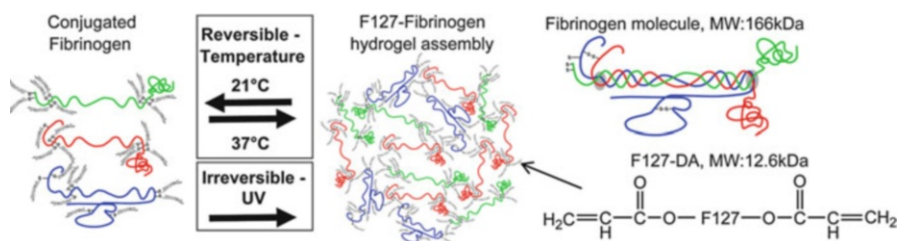


Fig. 21 Schematic representation of the reversible physical and irreversible chemical crosslinking of FF127 (Shachaf et al. 2010)

were able to send inductive signals to the cells (Shachaf et al. 2010). The results of the study suggested that the hydrogel constructs are suitable to be used for tissue engineering applications.

4 Conclusions and Future Perspectives

The current chapter clearly shows that a variety of photopolymerizable hydrogels including natural and synthetic polymers are promising candidates for cell encapsulation targeting tissue engineering and regeneration applications. Photopolymerization holds several advantages over alternative conventional crosslinking methods since a liquid formulation can be crosslinked in situ into an insoluble hydrogel network under cell-friendly, physiological conditions. Furthermore, the process provides spatiotemporal control over the phase transitions implying that complex shapes can be produced. Only radically induced photopolymerization using 1PIs and 2PIs is suitable for photocrosslinking of hydrogels, since the reactive species of ionic photoinitiators will be immediately terminated in the presence of water. The two main advantages of 2PIs compared to 1PIs include that near-infrared light, for which cells and tissue are transparent, can be used for their activation and that 2PP only takes place in the focus of the laser, enabling real 3D writing. Both natural and synthetic materials are employed for cell encapsulation. The most commonly applied natural polymers are proteins and polysaccharides as these are the main constituents of the ECM of native tissue. Synthetic hydrogels, on the other hand, generally exhibit superior and tuneable mechanical properties, but lack cell-interactive properties and are therefore often functionalized with bioactive moieties including natural polymers and RGD peptide sequences to stimulate cell adhesion and to tune their response and organ-specific tissue formation. Therefore, a hybrid hydrogel based on natural and synthetic polymers is a promising approach toward regenerative medicine, since it combines the bioactive properties of natural materials with the tuneable mechanical properties of synthetic polymers.

To date, the photoinitiator Irgacure 2959 has already been frequently used for cell encapsulation purposes due to its relatively low cytotoxicity. However, since the activation wavelength of this 1PI is below 360 nm, substantial cell damage is generally caused.

In order to further reduce PI toxicity, scarce attempts have also been reported on the development of macromolecular PIs. It can be anticipated that the latter pathway will also be further pursued in future work. Ideally, photopolymerizable materials could be developed which can be polymerized in the absence of a photoinitiator which is likely to result in a more biocompatible approach toward cell encapsulation.

Acknowledgments This work was supported in part by FWO (G008413N, G044516N, G005616N, G0F0516N, FWOKN273), BELSPO IAP Photonics@be, the Methusalem and Hercules foundations, Flanders Make, the OZR of the Vrije Universiteit Brussel (VUB), and Ghent University (UGent). The work of L.Tytgat was supported by the Research Foundation Flanders (FWO) through a PhD grant. The work of S.Baudis was supported by the Austrian Research Promotion Agency (FFG, Project Number 849787).

References

- Alexandridis P, Alan Hatton T (1995) Poly(ethylene oxide)poly(propylene oxide)poly(ethylene oxide) block copolymer surfactants in aqueous solutions and at interfaces: thermodynamics, structure, dynamics, and modeling. *Colloids Surf A Physicochem Eng Asp* 96:1–46. [https://doi.org/10.1016/0927-7757\(94\)03028-X](https://doi.org/10.1016/0927-7757(94)03028-X)
- Allen NS, Catalina F, Mateo JL et al (1990) Photochemistry and photopolymerization activity of water-soluble benzophenone initiators. In: *Radiation curing of polymeric materials*. ACS symposium series 417:72–81. <https://doi.org/10.1021/bk-1990-0417.ch006>
- Anderson JM, Shive MS (2012) Biodegradation and biocompatibility of PLA and PLGA microspheres. *Adv Drug Deliv Rev* 64:72–82. <https://doi.org/10.1016/j.addr.2012.09.004>
- Anseth K (2015) Photoencapsulation of chondrocytes in poly (ether oxide) -based semi-interpenetrating networks photoencapsulation of chondrocytes in poly (ethylene oxide) -based semi-interpenetrating networks. *J Biomed Mater Res*. [https://doi.org/10.1002/\(SICI\)1097-4636\(200008\)51](https://doi.org/10.1002/(SICI)1097-4636(200008)51)
- Atmani H, Audrain C, Mercier L et al (2002) Phenotypic effects of continuous or discontinuous treatment with dexamethasone and/or calcitriol on osteoblasts differentiated from rat bone marrow stromal cells. *J Cell Biochem* 85:640–650. <https://doi.org/10.1002/jcb.10165>
- Bahney CS, Lujan TJ, Hsu CW et al (2011) Visible light photoinitiation of mesenchymal stem cell-laden bioresponsive hydrogels. *Eur Cell Mater* 22:43–55
- Benedikt S, Wang J, Markovic M et al (2015) Highly efficient water-soluble visible light photoinitiators. *J Polym Sci A Polym Chem* 54:473–479. <https://doi.org/10.1002/pola.27903>
- Billiet T, Gevaert E, De Schryver T et al (2014) The 3D printing of gelatin methacrylamide cell-laden tissue-engineered constructs with high cell viability. *Biomaterials* 35:49–62. <https://doi.org/10.1016/j.biomaterials.2013.09.078>
- Bohorquez M, Koch C, Trygstad T, Pandit N (1999) A study of the temperature-dependent micellization of Pluronic F127. *J Colloid Interface Sci* 216:34–40. <https://doi.org/10.1006/jcis.1999.6273>
- Bryant SJ, Nuttelman CR, Anseth KS (2000) Cytocompatibility of UV and visible light photoinitiating systems on cultured NIH/3T3 fibroblasts in vitro. *J Biomater Sci Polym Ed* 11:439–457. <https://doi.org/10.1163/156856200743805>
- Bryant SJ, Davis-Arehart KA, Luo N et al (2004) Synthesis and characterization of photopolymerized multifunctional hydrogels: water-soluble poly(vinyl alcohol) and chondroitin sulfate macromers for chondrocyte encapsulation. *Macromolecules* 37:6726–6733. <https://doi.org/10.1021/ma0499324>
- Bryant SJ, Nicodemus GD, Villanueva I (2008) Designing 3D photopolymer hydrogels to regulate biomechanical cues and tissue growth for cartilage tissue engineering. *Pharm Res* 25:2379–2386
- Burhans WC, Weinberger M (2007) DNA replication stress, genome instability and aging. *Nucleic Acids Res* 35:7545–7556. <https://doi.org/10.1093/nar/gkm1059>
- Campagnola PJ, Delguidice DM, Epling GA et al (2000) 3-dimensional submicron polymerization of acrylamide by multiphoton excitation of xanthene dyes. *Macromolecules* 33:1511–1513. <https://doi.org/10.1021/ma991042e>
- Campo VL, Kawano DF, da Silva DB, Carvalho I (2009) Carrageenans: biological properties, chemical modifications and structural analysis – a review. *Carbohydr Polym* 77:167–180. <https://doi.org/10.1016/j.carbpol.2009.01.020>
- Cerutti PA (1985) Prooxidant states and tumor promotion. *Science* 227:375–381. <https://doi.org/10.1126/science.2981433>
- Chang K-H, Liao H-T, Chen J-P (2013) Preparation and characterization of gelatin/hyaluronic acid cryogels for adipose tissue engineering: in vitro and in vivo studies. *Acta Biomater* 9:9012–9026. <https://doi.org/10.1016/j.actbio.2013.06.046>
- Cheng J, Jiang S, Gao Y et al (2014) Tuning gradient property and initiating gradient photopolymerization of acrylamide aqueous solution of a hydrosoluble photocleavage polysiloxane-based photoinitiator. *Polym Adv Technol* 25:1412–1418. <https://doi.org/10.1002/pat.3378>

- Chou AI, Nicoll SB (2009) Characterization of photocrosslinked alginate hydrogels for nucleus pulposus cell encapsulation. *J Biomed Mater Res A* 91:187–194. <https://doi.org/10.1002/jbm.a.32191>
- Ciuciu AI, Cywiński PJ (2014) Two-photon polymerization of hydrogels – versatile solutions to fabricate well-defined 3D structures. *RSC Adv* 4:45504–45516. <https://doi.org/10.1039/C4RA06892K>
- Claeysens F, Hasan EA, Gaidukeviciute A et al (2009) Three-dimensional biodegradable structures fabricated by two-photon polymerization. *Langmuir* 25:3219–3223. <https://doi.org/10.1021/la803803m>
- Cohn D, Sosnik A, Garty S (2005) Smart hydrogels for in situ generated implants. *Biomacromolecules* 6:1168–1175. <https://doi.org/10.1021/bm0495250>
- Collins MN, Birkinshaw C (2013) Hyaluronic acid based scaffolds for tissue engineering – a review. *Carbohydr Polym* 92:1262–1279. <https://doi.org/10.1016/j.carbpol.2012.10.028>
- Corrales T, Catalina F, Allen NS, Peinado C (2006) Photochemistry and photoinduced polymerisation activity of thioxanthone initiators: an overview of recent advances. *Photochem UV Curing New Trends* 1:31–44
- Cui X, Breitenkamp K, Finn MG et al (2012) Direct human cartilage repair using 3D bioprinting technology. *Tissue Eng* 18:1304–1312. <https://doi.org/10.1089/ten.tea.2011.0543>
- Cumpston BH, Ananthavel SP, Barlow S et al (1999) Two-photon polymerization initiators for three-dimensional optical data storage and microfabrication. *Nature* 398:51–54
- Dietliker K (2002) A compilation of Photoinitiators commercially available for UV today. SITA Technology Limited, Edinburgh
- Discher DE, Janmey P, Wang Y-L (2005) Tissue cells feel and respond to the stiffness of their substrate. *Science* 310:1139–1143. <https://doi.org/10.1126/science.1116995>
- Doraiswamy A, Jin C, Narayan RJ et al (2006) Two photon induced polymerization of organic–inorganic hybrid biomaterials for microstructured medical devices. *Acta Biomater* 2:267–275. <https://doi.org/10.1016/j.actbio.2006.01.004>
- Drury JL, Mooney DJ (2003) Hydrogels for tissue engineering: scaffold design variables and applications. *Biomaterials* 24:4337–4351. [https://doi.org/10.1016/S0142-9612\(03\)00340-5](https://doi.org/10.1016/S0142-9612(03)00340-5)
- Dua R, Ramaswamy S (2013) Relative survivability of human osteoblasts is enhanced by 39 °C and ascorbic acid after exposure to photopolymerization ingredients. *Cytotechnology* 65:587–596. <https://doi.org/10.1007/s10616-012-9512-8>
- Elvin CM, Vuocolo T, Brownlee AG et al (2010) A highly elastic tissue sealant based on photopolymerised gelatin. *Biomaterials* 31:8323–8331. <https://doi.org/10.1016/j.biomaterials.2010.07.032>
- Fairbanks BD, Schwartz MP, Bowman CN, Anseth KS (2009a) Photoinitiated polymerization of PEG-diacrylate with lithium phenyl-2,4,6-trimethylbenzoylphosphine: polymerization rate and cytocompatibility. *Biomaterials* 30:6702–6707. <https://doi.org/10.1016/j.biomaterials.2009.08.055>
- Fairbanks BD, Schwartz MP, Halevi AE et al (2009b) A versatile synthetic extracellular matrix mimic via thiol-norbornene photopolymerization. *Adv Mater* 21:5005–5010. <https://doi.org/10.1002/adma.200901808>
- Farsari M, Filippidis G, Sambani K et al (2006) Two-photon polymerization of an Eosin Y-sensitized acrylate composite. *J Photochem Photobiol A Chem* 181:132–135. <https://doi.org/10.1016/j.jphotochem.2005.11.025>
- Feng Z, Yamato M, Akutsu T et al (2003) Investigation on the mechanical properties of contracted collagen gels as a scaffold for tissue engineering. *Artif Organs* 27:84–91. <https://doi.org/10.1046/j.1525-1594.2003.07187.x>
- Ferreira LS, Gerecht S, Fuller J et al (2007) Bioactive hydrogel scaffolds for controllable vascular differentiation of human embryonic stem cells. *Biomaterials* 28:2706–2717. <https://doi.org/10.1016/j.biomaterials.2007.01.021>
- Fouassier J-P (1995) Photoinitiation, photopolymerization, and photocuring: fundamentals and applications. Hanser, Munich

- Fouassier JP, Allonas X, Burget D (2003) Photopolymerization reactions under visible lights: principle, mechanisms and examples of applications. *Prog Org Coat* 47:16–36. [https://doi.org/10.1016/S0300-9440\(03\)00011-0](https://doi.org/10.1016/S0300-9440(03)00011-0)
- Fu Y, Kao WJ (2011) In situ forming poly(ethylene glycol)-based hydrogels via thiol-maleimide Michael-type addition. *J Biomed Mater Res A* 98(A):201–211. <https://doi.org/10.1002/jbm.a.33106>
- Fu A, Gwon K, Kim M et al (2015) Visible-light-initiated thiol-acrylate photopolymerization of heparin-based hydrogels. *Biomacromolecules* 16:497–506. <https://doi.org/10.1021/bm501543a>
- Galis ZS, Khatri JJ (2002) Matrix metalloproteinases in vascular remodeling and atherogenesis: the good, the bad, and the ugly. *Circ Res* 90:251–262. <https://doi.org/10.1161/hh0302.105345>
- Gao G, Yonezawa T, Hubbell K et al (2015) Inkjet-bioprinted acrylated peptides and PEG hydrogel with human mesenchymal stem cells promote robust bone and cartilage formation with minimal printhead clogging. *Biotechnol J* 10:1568–1577. <https://doi.org/10.1002/biot.201400635>
- Gentleman E, Nauman EA, Dee KC, Livesay GA (2004) Short collagen fibers provide control of contraction and permeability in fibroblast-seeded collagen gels. *Tissue Eng* 10:421–427. <https://doi.org/10.1089/107632704323061780>
- Gomez-Guillen MC, Gimenez B, Lopez-Caballero ME, Montero MP (2011) Functional and bioactive properties of collagen and gelatin from alternative sources: a review. *Food Hydrocoll* 25:1813–1827. <https://doi.org/10.1016/j.foodhyd.2011.02.007>
- Gong JP, Katsuyama Y, Kurokawa T, Osada Y (2003) Double-network hydrogels with extremely high mechanical strength. *Adv Mater* 15:1155–1158. <https://doi.org/10.1002/adma.200304907>
- Göppert-Mayer M (1931) Über Elementarakte mit zwei Quantensprüngen. *Ann Phys* 401:273–295
- Graulus G-J, Mignon A, Van Vlierberghe S et al (2015) Cross-linkable alginate-graft-gelatin copolymers for tissue engineering applications. *Eur Polym J* 72:494–506. <https://doi.org/10.1016/j.eurpolymj.2015.06.033>
- Green WA (2010) Industrial photoinitiators: a technical guide. CRC Press, Boca Raton
- Greenberg ME, Li XM, Gugiu BG et al (2008) The lipid whisker model of the structure of oxidized cell membranes. *J Biol Chem* 283:2385–2396. <https://doi.org/10.1074/jbc.M707348200>
- Guimond SE, Turnbull JE, Yates EA (2006) Engineered bio-active polysaccharides from heparin. *Macromol Biosci* 6:681–686. <https://doi.org/10.1002/mabi.200600042>
- Halliwell B, Chirico S (1993) Lipid peroxidation: its mechanism, measurement and significance. *Am J Clin Nutr* 57:715S–725S
- Hannoyer B, Balmain J, Hannoyer B, Lopez E (1999) Photocurable surgical tissue adhesive glues composed of photoreactive gelatin and poly(ethylene glycol) diacrylate. *J Biomed Mater Res* 4636:10421698. [https://doi.org/10.1002/\(SICI\)1097-4636\(1999\)48](https://doi.org/10.1002/(SICI)1097-4636(1999)48)
- Hayek A, Bolze F, Nicoud J-F et al (2006) Synthesis and characterization of water-soluble two-photon excited blue fluorescent chromophores for bioimaging. *Photochem Photobiol Sci* 5:102–106. <https://doi.org/10.1039/B509843B>
- He GS, Zhu J, Baev A et al (2011) Twisted π -system chromophores for all-optical switching. *J Am Chem Soc* 133:6675–6680. <https://doi.org/10.1021/ja1113112>
- Hennink WE, van Nostrum CF (2012) Novel crosslinking methods to design hydrogels. *Adv Drug Deliv Rev* 64:223–236. <https://doi.org/10.1016/j.addr.2012.09.009>
- Hern DL, Hubbell JA (1998) Incorporation of adhesion peptides into nonadhesive hydrogels useful for tissue resurfacing. *J Biomed Mater Res* 39:266–276. [https://doi.org/10.1002/\(SICI\)1097-4636\(199802\)39:2<266::AID-JBM14>3.0.CO;2-B](https://doi.org/10.1002/(SICI)1097-4636(199802)39:2<266::AID-JBM14>3.0.CO;2-B)
- Hoffman AS (2001) Hydrogels for biomedical applications. *Ann N Y Acad Sci* 944:62–73. <https://doi.org/10.1016/j.addr.2012.09.010>
- Hoshikawa A, Nakayama Y, Matsuda T et al (2006) Encapsulation of chondrocytes in photopolymerizable styrenated gelatin for cartilage tissue engineering. *Tissue Eng* 12:2333–2341. <https://doi.org/10.1089/ten.2006.12.2333>

- Hunt NC, Grover LM (2010) Cell encapsulation using biopolymer gels for regenerative medicine. *Biotechnol Lett* 32:733–742. <https://doi.org/10.1007/s10529-010-0221-0>
- Jaikumar D, Sajesh KM, Soumya S et al (2015) Injectable alginate-*O*-carboxymethyl chitosan/nano fibrin composite hydrogels for adipose tissue engineering. *Int J Biol Macromol* 74:318–326. <https://doi.org/10.1016/j.ijbiomac.2014.12.037>
- Jerosch J (2011) Effects of glucosamine and chondroitin sulfate on cartilage metabolism in OA: outlook on other nutrient partners especially omega-3 fatty acids. *Int J Rheumatol*. <https://doi.org/10.1155/2011/969012>
- Jiang G, Woo BH, Kang F et al (2002) Assessment of protein release kinetics, stability and protein polymer interaction of lysozyme encapsulated poly(D,L-lactide-co-glycolide) microspheres. *J Control Release* 79:137–145. [https://doi.org/10.1016/S0168-3659\(01\)00533-8](https://doi.org/10.1016/S0168-3659(01)00533-8)
- Kerscher P, Turnbull IC, Hodge AJ et al (2015) Direct hydrogel encapsulation of pluripotent stem cells enables ontomimetic differentiation and growth of engineered human heart tissues. *Biomaterials* 83:383–395. <https://doi.org/10.1016/j.biomaterials.2015.12.011>
- Klein F, Striebel T, Fischer J et al (2010) Elastic fully three-dimensional microstructure scaffolds for cell force measurements. *Adv Mater* 22:868–871. <https://doi.org/10.1002/adma.200902515>
- Lee SY, Tae G (2007) Formulation and in vitro characterization of an in situ gelable, photopolymerizable Pluronic hydrogel suitable for injection. *J Control Release* 119:313–319. <https://doi.org/10.1016/j.jconrel.2007.03.007>
- Lee JB, Yoon JJ, Lee DS, Park TG (2004) Photo-crosslinkable, thermo-sensitive and biodegradable Pluronic hydrogels for sustained release of protein. *J Biomater Sci Polym Ed* 15:1571–1583
- Lee CT, Kung PH, Der Lee Y (2005) Preparation of poly(vinyl alcohol)-chondroitin sulfate hydrogel as matrices in tissue engineering. *Carbohydr Polym* 61:348–354. <https://doi.org/10.1016/j.carbpol.2005.06.018>
- Lee K-S, Kim RH, Yang D-Y, Park SH (2008) Advances in 3D nano/microfabrication using two-photon initiated polymerization. *Prog Polym Sci* 33:631–681. <https://doi.org/10.1016/j.progpolymsci.2008.01.001>
- Leitz G, Fällman E, Tuck S, Axner O (2002) Stress response in *Caenorhabditis elegans* caused by optical tweezers: wavelength, power, and time dependence. *Biophys J* 82:2224–2231. [https://doi.org/10.1016/S0006-3495\(02\)75568-9](https://doi.org/10.1016/S0006-3495(02)75568-9)
- Lewus KE, Nauman EA (2005) In vitro characterization of a bone marrow stem cell-seeded collagen gel composite for soft tissue grafts: effects of fiber number and serum concentration. *Tissue Eng* 11:1015–1022. <https://doi.org/10.1089/ten.2005.11.1015>
- Li Q, Williams CG, Sun DDN et al (2004) Photocrosslinkable polysaccharides based on chondroitin sulfate. *J Biomed Mater Res A* 68:28–33. <https://doi.org/10.1002/jbm.a.20007>
- Li Z, Siklos M, Pucher N et al (2011) Synthesis and structure-activity relationship of several aromatic ketone-based two-photon initiators. *J Polym Sci A Polym Chem* 49:3688–3699. <https://doi.org/10.1002/pola.24806>
- Li Z, Pucher N, Cicha K et al (2013a) A straightforward synthesis and structure–activity relationship of highly efficient initiators for two-photon polymerization. *Macromolecules* 46:352–361. <https://doi.org/10.1021/ma301770a>
- Li Z, Torgersen J, Ajami A et al (2013b) Initiation efficiency and cytotoxicity of novel water-soluble two-photon photoinitiators for direct 3D microfabrication of hydrogels. *RSC Adv* 3:15939–15946. <https://doi.org/10.1039/C3RA42918K>
- Lim KS, Alves MH, Poole-Warren LA, Martens PJ (2013) Covalent incorporation of non-chemically modified gelatin into degradable PVA-tyramine hydrogels. *Biomaterials* 34:7097–7105. <https://doi.org/10.1016/j.biomaterials.2013.06.005>
- Lim KS, Ramaswamy Y, Roberts JJ et al (2015) Promoting cell survival and proliferation in degradable poly(vinyl alcohol)-tyramine hydrogels. *Macromol Biosci* 15:1423–1432. <https://doi.org/10.1002/mabi.201500121>

- Lin CC, Sawicki SM, Metters AT (2008) Free-radical-mediated protein inactivation and recovery during protein photoencapsulation. *Biomacromolecules* 9:75–83. <https://doi.org/10.1021/bm700782c>
- Lin CC, Raza A, Shih H (2011) PEG hydrogels formed by thiol-ene photo-click chemistry and their effect on the formation and recovery of insulin-secreting cell spheroids. *Biomaterials* 32:9685–9695. <https://doi.org/10.1016/j.biomaterials.2011.08.083>
- Lin H, Zhang D, Alexander PG et al (2013) Application of visible light-based projection stereo-lithography for live cell-scaffold fabrication with designed architecture. *Biomaterials* 34:331–339. <https://doi.org/10.1016/j.biomaterials.2012.09.048>
- Lin CC, Ki CS, Shih H (2015) Thiol-norbornene photoclick hydrogels for tissue engineering applications. *J Appl Polym Sci* 132:1–11. <https://doi.org/10.1002/app.41563>
- Liska R (2002) Photoinitiators with functional groups. V. New water-soluble photoinitiators containing carbohydrate residues and copolymerizable derivatives thereof. *J Polym Sci A Polym Chem* 40:1504–1518. <https://doi.org/10.1002/pola.10232>
- Liu Y, Chan-Park MB (2009) Hydrogel based on interpenetrating polymer networks of dextran and gelatin for vascular tissue engineering. *Biomaterials* 30:196–207. <https://doi.org/10.1016/j.biomaterials.2008.09.041>
- Liu Y, Chan-Park MB (2010) A biomimetic hydrogel based on methacrylated dextran-graft-lysine and gelatin for 3D smooth muscle cell culture. *Biomaterials* 31:1158–1170. <https://doi.org/10.1016/j.biomaterials.2009.10.040>
- Liu F, Aubin JE, Malaval L (2002) Expression of leukemia inhibitory factor (LIF)/interleukin-6 family cytokines and receptors during in vitro osteogenesis: differential regulation by dexamethasone and LIF. *Bone* 31:212–219. [https://doi.org/10.1016/S8756-3282\(02\)00806-2](https://doi.org/10.1016/S8756-3282(02)00806-2)
- Liu Y, Dong X, Sun J et al (2012) Two-photon fluorescent probe for cadmium imaging in cells. *Analyst* 137:1837–1845. <https://doi.org/10.1039/C2AN16254G>
- Liu M, Li M-D, Xue J, Phillips DL (2014) Time-resolved spectroscopic and density functional theory study of the photochemistry of irgacure-2959 in an aqueous solution. *J Phys Chem A* 118:8701–8707. <https://doi.org/10.1021/jp506099n>
- Lobry E, Jasinski F, Penconi M et al (2014) Continuous-flow synthesis of polymer nanoparticles in a microreactor via miniemulsion photopolymerization. *RSC Adv* 4:43756–43759. <https://doi.org/10.1039/C4RA06814A>
- Loungnot DJ, Fouassier JP (1988) Comparative reactivity of water soluble photoinitiators as viewed in terms of excited states processes. *J Polym Sci A Polym Chem* 26:1021–1033. <https://doi.org/10.1002/pola.1988.080260407>
- Loungnot DJ, Turck C, Fouassier JP (1989) Water-soluble polymerization initiators based on the thioxanthone structure: a spectroscopic and laser photolysis study. *Macromolecules* 22:108–116. <https://doi.org/10.1021/ma00191a022>
- Lu Y, Hasegawa F, Goto T et al (2004) Highly sensitive measurement in two-photon absorption cross section and investigation of the mechanism of two-photon-induced polymerization. *JOL* 110:1–10. <https://doi.org/10.1016/j.jlumin.2004.02.012>
- Mackay A, Beck S, Murphy J et al (1998) Chondrogenic differentiation of cultured human mesenchymal stem cells from marrow. *Tissue Eng* 4:415–428. <https://doi.org/10.1089/ten.1998.4.415>
- Majima T, Schnabel W, Weber W (1991) Phenyl-2,4,6-trimethylbenzoylphosphinates as water-soluble photoinitiators. Generation and reactivity of $O=\dot{P}(C_6H_5)(O^-)$ radical anions. *Die Makromol Chemie* 192:2307–2315. <https://doi.org/10.1002/macp.1991.021921010>
- Malda J, Visser J, Melchels FP et al (2013) 25th anniversary article: engineering hydrogels for biofabrication. *Adv Mater* 25:5011–5028. <https://doi.org/10.1002/adma.201302042>
- Malkoch M, Vestberg R, Gupta N et al (2006) Synthesis of well-defined hydrogel networks using click chemistry. *Chem Commun* 2006:2774–2776. <https://doi.org/10.1039/b603438a>
- Masters KS, Shah DN, Leinwand LA, Anseth KS (2005) Crosslinked hyaluronan scaffolds as a biologically active carrier for valvular interstitial cells. *Biomaterials* 26:2517–2525. <https://doi.org/10.1016/j.biomaterials.2004.07.018>

- McCall JD, Anseth KS (2012) Thiol-ene photopolymerizations provide a facile method to encapsulate proteins and maintain their bioactivity. *Biomacromolecules* 13:2410–2417. <https://doi.org/10.1021/bm300671s>
- Mihaila SM, Gaharwar AK, Reis RL et al (2013) Photocrosslinkable *Kappa*-carrageenan hydrogels for tissue engineering applications. *Adv Healthc Mater* 2:895–907. <https://doi.org/10.1002/adhm.201200317>
- Mironi-Harpaz I, Wang DY, Venkatraman S, Seliktar D (2012) Photopolymerization of cell-encapsulating hydrogels: crosslinking efficiency versus cytotoxicity. *Acta Biomater* 8:1838–1848. <https://doi.org/10.1016/j.actbio.2011.12.034>
- Moreira Teixeira LS, Feijen J, van Blitterswijk CA et al (2012) Enzyme-catalyzed crosslinkable hydrogels: emerging strategies for tissue engineering. *Biomaterials* 33:1281–1290. <https://doi.org/10.1016/j.biomaterials.2011.10.067>
- Moxon SR, Smith AM (2016) Controlling the rheology of gellan gum hydrogels in cell culture conditions. *Int J Biol Macromol* 84:79–86. <https://doi.org/10.1016/j.ijbiomac.2015.12.007>
- Mueller G, Zalibera M, Gescheidt G et al (2015) Simple one-pot syntheses of water-soluble bis (acyl)phosphane oxide photoinitiators and their application in surfactant-free emulsion polymerization. *Macromol Rapid Commun*. <https://doi.org/10.1002/marc.201400743>
- Munoz Z, Shih H, Lin C-C (2014) Gelatin hydrogels formed by orthogonal thiol-norbornene photochemistry for cell encapsulation. *Biomater Sci* 2:1063–1072. <https://doi.org/10.1039/c4bm00070f>
- Na YH, Kurokawa T, Katsuyama Y et al (2004) Structural characteristics of double network gels with extremely high mechanical strength. *Macromolecules* 37:5370–5374. <https://doi.org/10.1021/ma049506i>
- Nakayama A, Kakugo A, Gong JP et al (2004) High mechanical strength double-network hydrogel with bacterial cellulose. *Adv Funct Mater* 14:1124–1128. <https://doi.org/10.1002/adfm.200305197>
- Nguyen KT, West JL (2002) Photopolymerizable hydrogels for tissue engineering applications. *Biomaterials* 23:4307–4314. [https://doi.org/10.1016/S0142-9612\(02\)00175-8](https://doi.org/10.1016/S0142-9612(02)00175-8)
- Nguyen KA, Rogers JE, Slagle JE et al (2006) Effects of conjugation in length and dimension on spectroscopic properties of fluorene-based chromophores from experiment and theory. *J Phys Chem A* 110:13172–13182. <https://doi.org/10.1021/jp0642645>
- Nilasaroya A, Martens PJ, Whitelock JM (2012) Enzymatic degradation of heparin-modified hydrogels and its effect on bioactivity. *Biomaterials* 33:5534–5540. <https://doi.org/10.1016/j.biomaterials.2012.04.022>
- Nuttelman CR, Tripodi MC, Anseth KS (2006) Dexamethasone-functionalized gels induce osteogenic differentiation of encapsulated hMSCs. *J Biomed Mater Res A* 76:183–195. <https://doi.org/10.1002/jbm.a.30537>
- Occhetta P, Visone R, Russo L et al (2015) VA-086 methacrylate gelatine photopolymerizable hydrogels: a parametric study for highly biocompatible 3D cell embedding. *J Biomed Mater Res A* 103:2109–2117. <https://doi.org/10.1002/jbm.a.35346>
- Oudshoorn MHM, Rissmann R, Bouwstra JA, Hennink WE (2007) Synthesis of methacrylated hyaluronic acid with tailored degree of substitution. *Polymer (Guildf)* 48:1915–1920. <https://doi.org/10.1016/j.polymer.2007.01.068>
- Ovsianikov A, Schlie S, Ngezahayo A et al (2007) Two-photon polymerization technique for microfabrication of CAD-designed 3D scaffolds from commercially available photosensitive materials. *J Tissue Eng Regen Med* 1:443–449. <https://doi.org/10.1002/term.57>
- Ovsianikov A, Deiwick A, Van Vlierberghe S et al (2011a) Laser fabrication of 3D gelatin scaffolds for the generation of bioartificial tissues. *Materials (Basel)* 4:288–299. <https://doi.org/10.3390/ma4010288>
- Ovsianikov A, Deiwick A, Van Vlierberghe S et al (2011b) Laser fabrication of three-dimensional CAD scaffolds from photosensitive gelatin for applications in tissue engineering. *Biomacromolecules* 12:851–858. <https://doi.org/10.1021/bm1015305>

- Ovsianikov A, Malinauskas M, Schlie S et al (2011c) Three-dimensional laser micro- and nano-structuring of acrylated poly(ethylene glycol) materials and evaluation of their cytotoxicity for tissue engineering applications. *Acta Biomater* 7:967–974. <https://doi.org/10.1016/j.actbio.2010.10.023>
- Ovsianikov A, Mühleder S, Torgersen J et al (2014) Laser photofabrication of cell-containing hydrogel constructs. *Langmuir* 30:3787–3794. <https://doi.org/10.1021/la402346z>
- Pai SS, Tilton RD, Przybycien TM (2009) Poly(ethylene glycol)-modified proteins: implications for poly(lactide-co-glycolide)-based microsphere delivery. *AAPS J* 11:88–98. <https://doi.org/10.1208/s12248-009-9081-8>
- Peppas NA, Bures P, Leobandung W, Ichikawa H (2000) Hydrogels in pharmaceutical formulations. *Eur J Pharm Biopharm* 50:27–46. [https://doi.org/10.1016/S0939-6411\(00\)00090-4](https://doi.org/10.1016/S0939-6411(00)00090-4)
- Pereira RF, Bártolo PJ (2015) 3D bioprinting of photocrosslinkable hydrogel constructs. *J Appl Polym Sci*. <https://doi.org/10.1002/app.42458>
- Prajapati VD, Maheriya PM, Jani GK, Solanki HK (2014) Carrageenan: a natural seaweed polysaccharide and its applications. *Carbohydr Polym* 105:97–112. <https://doi.org/10.1016/j.carbpol.2014.01.067>
- Ramakrishna G, Goodson T (2007) Excited-state deactivation of branched two-photon absorbing chromophores: a femtosecond transient absorption investigation. *J Phys Chem A* 111:993–1000. <https://doi.org/10.1021/jp064004n>
- Rannou F, Lee T-S, Zhou R-H et al (2004) Intervertebral disc degeneration: the role of the mitochondrial pathway in annulus fibrosus cell apoptosis induced by overload. *Am J Pathol* 164:915–924. [https://doi.org/10.1016/S0002-9440\(10\)63179-3](https://doi.org/10.1016/S0002-9440(10)63179-3)
- Reza AT, Nicoll SB (2010) Characterization of novel photocrosslinked carboxymethylcellulose hydrogels for encapsulation of nucleus pulposus cells. *Acta Biomater* 6:179–186. <https://doi.org/10.1016/j.actbio.2009.06.004>
- Rocha PM, Santo VE, Gomes ME et al (2011) Encapsulation of adipose-derived stem cells and transforming growth factor-1 in carrageenan-based hydrogels for cartilage tissue engineering. *J Bioact Compat Polym* 26:493–507. <https://doi.org/10.1177/0883911511420700>
- Rumi M, Ehrlich JE, Heikal AA et al (2000) Structure–property relationships for two-photon absorbing chromophores: bis-donor diphenylpolyene and bis(styryl)benzene derivatives. *J Am Chem Soc* 122:9500–9510. <https://doi.org/10.1021/ja994497s>
- Salinas CN, Anseth KS (2009) Decorin moieties tethered into PEG networks induce chondrogenesis of human mesenchymal stem cells. *J Biomed Mater Res A* 90:456–464. <https://doi.org/10.1002/jbm.a.32112>
- Schafer KJ, Hales JM, Balu M et al (2004) Two-photon absorption cross-sections of common photoinitiators. *J Photochem Photobiol A Chem* 162:497–502. [https://doi.org/10.1016/S1010-6030\(03\)00394-0](https://doi.org/10.1016/S1010-6030(03)00394-0)
- Schuster M, Turecek C, Kaiser B et al (2007) Evaluation of biocompatible photopolymers I: photoreactivity and mechanical properties of reactive diluents. *J Macromol Sci Part A* 44:547–557. <https://doi.org/10.1080/10601320701235958>
- Selimis A, Mironov V, Farsari M (2015) Direct laser writing: principles and materials for scaffold 3D printing. *Microelectron Eng* 132:83–89. <https://doi.org/10.1016/j.mee.2014.10.001>
- Shachaf Y, Gonen-Wadmany M, Seliktar D (2010) The biocompatibility of Pluronic F127 fibrinogen-based hydrogels. *Biomaterials* 31:2836–2847. <https://doi.org/10.1016/j.biomaterials.2009.12.050>
- Shin H, Olsen BD, Khademhosseini A (2012) The mechanical properties and cytotoxicity of cell-laden double-network hydrogels based on photocrosslinkable gelatin and gellan gum biomacromolecules. *Biomaterials* 33:3143–3152. <https://doi.org/10.1016/j.biomaterials.2011.12.050>
- Sivashanmugam A, Arun Kumar R, Vishnu Priya M et al (2015) An overview of injectable polymeric hydrogels for tissue engineering. *Eur Polym J* 72:543–565. <https://doi.org/10.1016/j.eurpolymj.2015.05.014>
- Skardal A, Zhang J, McCoard L et al (2010) Photocrosslinkable hyaluronan-gelatin hydrogels for two-step bioprinting. *Tissue Eng Part A* 16:2675–2685. <https://doi.org/10.1089/ten.tea.2009.0798>

- Smeds KA, Grinstaff MW (2001) Photocrosslinkable polysaccharides for in situ hydrogel formation. *J BioMed Mater Res* 54(1):155–121. [https://doi.org/10.1002/1097-4636\(200101\)54:1<115::AID-JBM14>3.0.CO;2-Q](https://doi.org/10.1002/1097-4636(200101)54:1<115::AID-JBM14>3.0.CO;2-Q)
- Su JF, Huang Z, Yuan XY et al (2010) Structure and properties of carboxymethyl cellulose/soy protein isolate blend edible films crosslinked by Maillard reactions. *Carbohydr Polym* 79:145–153. <https://doi.org/10.1016/j.carbpol.2009.07.035>
- Tae G, Kim YJ, Choi WI et al (2007) Formation of a novel heparin-based hydrogel in the presence of heparin-binding biomolecules. *Biomacromolecules* 8:1979–1986. <https://doi.org/10.1021/bm0701189>
- Torgersen J, Ovsianikov A, Mironov V et al (2012) Photo-sensitive hydrogels for three-dimensional laser microfabrication in the presence of whole organisms. *J Biomed Opt* 17:105008. <https://doi.org/10.1117/1.JBO.17.10.105008>
- Torgersen J, Qin XH, Li Z et al (2013) Hydrogels for two-photon polymerization: a toolbox for mimicking the extracellular matrix. *Adv Funct Mater* 23:4542–4554. <https://doi.org/10.1002/adfm.201203880>
- Ullah F, Bisyrul M, Javed F, Akil H (2015) Classification, processing and application of hydrogels: a review. *Mater Sci Eng A* 57:414–433. <https://doi.org/10.1016/j.msec.2015.07.053>
- Ullrich G, Burtcher P, Salz U et al (2005) Phenylglycine derivatives as coinitiators for the radical photopolymerization of acidic aqueous formulations. *J Polym Sci A Polym Chem* 44:115–125. <https://doi.org/10.1002/pola.21139>
- Van Den Bulcke AI, Bogdanov B, De Rooze N et al (2000) Structural and rheological properties of methacrylamide modified gelatin hydrogels. *Biomacromolecules* 1:31–38. <https://doi.org/10.1021/bm990017d>
- Van Hoorick J, Declercq H, De Muynck A et al (2015) Indirect additive manufacturing as an elegant tool for the production of self-supporting low density gelatin scaffolds. *J Mater Sci Mater Med* 26:247. <https://doi.org/10.1007/s10856-015-5566-4>
- Van Vlierberghe S, Samal SK, Dubruel P (2011a) Development of mechanically tailored gelatin-chondroitin sulphate hydrogel films. *Macromol Symp* 309–310:173–181. <https://doi.org/10.1002/masy.201100030>
- Van Vlierberghe S, Dubruel P, Schacht E (2011b) Biopolymer-based hydrogels as scaffolds for tissue engineering applications: a review. *Biomacromolecules* 12:1387–1408
- Vogel A, Venugopalan V (2003) Mechanisms of pulsed laser ablation of biological tissues. *Chem Rev* 103:577–644. <https://doi.org/10.1021/cr010379n>
- Wan X, Zhao Y, Xue J et al (2009) Water-soluble benzylidene cyclopentanone dye for two-photon photopolymerization. *J Photochem Photobiol A Chem* 202:74–79. <https://doi.org/10.1016/j.jphotochem.2008.10.029>
- Weng L, Gouldstone A, Wu Y, Chen W (2008) Mechanically strong double network photo-crosslinked hydrogels from *N,N*-dimethylacrylamide and glycidyl methacrylated hyaluronan. *Biomaterials* 29:2153–2163. <https://doi.org/10.1016/j.biomaterials.2008.01.012>
- Williams CG, Malik AN, Kim TK et al (2005) Variable cytocompatibility of six cell lines with photoinitiators used for polymerizing hydrogels and cell encapsulation. *Biomaterials* 26:1211–1218. <https://doi.org/10.1016/j.biomaterials.2004.04.024>
- Woo HY, Liu B, Kohler B et al (2005) Solvent effects on the two-photon absorption of distyrylbenzene chromophores. *J Am Chem Soc* 127:14721–14729. <https://doi.org/10.1021/ja052906g>
- Xu K, Fu Y, Chung W et al (2012) Thiol-ene-based biological/synthetic hybrid biomatrix for 3-D living cell culture. *Acta Biomater* 8:2504–2516. <https://doi.org/10.1016/j.actbio.2012.03.049>
- Yang JS, Xie YJ, He W (2011) Research progress on chemical modification of alginate: a review. *Carbohydr Polym* 84:33–39. <https://doi.org/10.1016/j.carbpol.2010.11.048>
- Young C, Rozario K, Serra C et al (2013) Poly(vinyl alcohol)-heparin biosynthetic microspheres produced by microfluidics and ultraviolet photopolymerisation. *Biomicrofluidics* 7:1–13. <https://doi.org/10.1063/1.4816714>

- Yue K, Trujillo-De Santiago G, Mois Es Alvarez M et al (2015) Synthesis, properties, and biomedical applications of gelatin methacryloyl (GelMA) hydrogels. *Biomaterials* 73:254–271. <https://doi.org/10.1016/j.biomaterials.2015.08.045>
- Zhang J, Dumur F, Xiao P et al (2015) Structure design of naphthalimide derivatives: toward versatile photoinitiators for near-UV/visible LEDs, 3D printing, and water-soluble photoinitiating systems. *Macromol (Washington, DC, US)* 48:2054–2063. <https://doi.org/10.1021/acs.macromol.5b00201>
- Zhu J, Marchant RE (2011) Design properties of hydrogel tissue-engineering scaffolds. *Expert Rev Med Devices* 8:607–626. <https://doi.org/10.1586/erd.11.27>
- Zustiak SP, Leach JB (2011) Characterization of protein release from hydrolytically degradable poly(ethylene glycol) hydrogels. *Biotechnol Bioeng* 108:197–206. <https://doi.org/10.1002/bit.22911>



Fabrication and Printing of Multi-material Hydrogels

Navein Arumugasaamy, Hannah B. Baker, David S. Kaplan,
Peter C. W. Kim, and John P. Fisher

Contents

1	Introduction	398
2	Challenges Associated with Hydrogel Bioprinting	399
2.1	Choice of Bioprinter	400
2.2	Mechanical Support and Printability	402
2.3	Stress in Cell-Laden Hydrogels	404
3	Methods for Polymer Crosslinking	405
3.1	Photo-crosslinking	405

N. Arumugasaamy · J. P. Fisher (✉)

Fischell Department of Bioengineering, University of Maryland, College Park, MD, USA

Sheikh Zayed Institute for Pediatric Surgical Innovation, Children’s National Health System,
Washington, DC, USA

e-mail: navein@umd.edu; jpfisher@umd.edu

H. B. Baker

Fischell Department of Bioengineering, University of Maryland, College Park, MD, USA

Center for Devices and Radiological Health, U.S. Food and Drug Administration, Silver Spring,
MD, USA

e-mail: hbaker1@umd.edu

D. S. Kaplan

Center for Devices and Radiological Health, U.S. Food and Drug Administration, Silver Spring,
MD, USA

e-mail: David.Kaplan@fda.hhs.gov

P. C. W. Kim

Sheikh Zayed Institute for Pediatric Surgical Innovation, Children’s National Health System,
Washington, DC, USA

School of Medicine and Health Sciences, The George Washington University, Washington, DC,
USA

e-mail: PKim@childrensnational.org

© This is a U.S. Government work and not under copyright protection in the US;
foreign copyright protection may apply 2018

397

A. Ovsianikov et al. (eds.), *3D Printing and Biofabrication*, Reference Series in
Biomedical Engineering, https://doi.org/10.1007/978-3-319-45444-3_13

3.2	Thermal Crosslinking	408
3.3	Ionic Crosslinking	408
4	Multi-material Hydrogel Printing	409
4.1	Material Selection	409
4.2	Common Materials in Hydrogel Bioprinting	411
4.3	Single Bioink Bioprinting	414
4.4	Multiple Bioink Bioprinting	420
5	Summary and Future Directions	422
	References	423

Abstract

Bioprinting has emerged over the past decade as a prominent technology in the field of tissue engineering. This enables fabrication of cell-laden hydrogels with precise control over the architecture of the scaffold and the location of cells, growth factors, and other biological cues of interest. We first discuss the challenges that exist in terms of choosing a bioprinter, ensuring mechanical support and printability of a material, and minimizing cellular stress for cell-laden prints. We then explain the different crosslinking methods commonly used in hydrogel printing and approaches to alter bioink crosslinking mechanisms. We discuss material selection for bioprinting with elaboration on common materials that have been used and a review of multi-material prints involving hydrogels. We also explore the use of a single, mixed bioink to fabricate complex but homogeneous constructs and multiple, independent bioinks to fabricate complex heterogeneous tissue constructs within the multi-material review. We conclude with a summary of the current state of the field and an outlook on future research.

1 Introduction

Hydrogels are networks of crosslinked, hydrophilic polymers capable of absorbing water and swelling in size. They have long been used in a variety of applications, such as for drug delivery, where their ability to swell and degrade can be utilized to deliver molecules of various sizes and chemical structure, and in tissue engineering, where hydrogels provide a support environment for encapsulating and growing cells in a 3D biomimetic environment (Qiu and Park 2001; Hoare and Kohane 2008; Burdick and Prestwich 2011; Murphy and Atala 2014; Pereira and Bártolo 2015). In particular, hydrogels have become prominent in applications involving cells, due to the capacity to mimic the native *in vivo* cellular environment. For this reason, hydrogels have become common as an alternative to traditional solid material scaffolds for cell growth and assays in a 3D environment. In applications using solid scaffolds, cells are grown on the surface of the material wherein the bulk material properties, such as porosity and pore size, influence cell growth and behavior. With hydrogels, cells can be fully encapsulated in the material, providing cells with a means to directly interact with their scaffold in three dimensions. This differs from traditional scaffolds, in which cells interact with the scaffold via cell-scaffold

adhesion points on the surface. Further, it is worth noting that many groups have investigated the use of cell suspensions alone as bioinks to generate patterns and to spatially arrange multiple cell types on one substrate (Roth et al. 2004; Nakamura et al. 2005; Xu et al. 2013b, 2005, 2006; Carolina 2012; Ferris et al. 2013a, b; Skardal and Atala 2015). However, these approaches when used without a supporting matrix are better suited for sheet-like applications, such as drug delivery, and cannot offer the same therapeutic capacity enabled by support materials (Chan et al. 2010; Cha et al. 2014; Akkineni et al. 2015; Elomaa et al. 2015; Park et al. 2015; Gao et al. 2015b; Tabriz et al. 2015; Ferlin et al. 2016). Thus, it becomes clear that hydrogels may provide an enhanced biomimetic microenvironment through improved cell-scaffold interfaces.

Fabricating hydrogels has commonly been done through the use of molds and casting, but the emergence of 3D printing (3DP) technology has allowed for significantly more spatial control of the architecture and design of the hydrogel network. Fabricating hydrogels in a mold involves filling a predefined bulk architecture with the material being used to synthesize the hydrogel, followed by crosslinking of the hydrogel within the mold such that the material transitions from liquid to solid and maintains that bulk geometry. 3DP overcomes this key limitation by depositing and crosslinking material, layer by layer, in order to control both the micro- and macro-architecture of the gel. This allows for precision, defined by the resolution of the individual bioprinter, which can go down to the microscale. Furthermore, bioprinting incorporates cells and other biological components in order to create a system for studying biological phenomena or for tissue regeneration. As a result, bioprinting enables precise control over where cells or other factors are located within the gel, as well as allowing for the use of multiple, distinct bioinks composed of unique materials or cells.

With that in mind, this chapter seeks to provide an overview of cell-laden printing of hydrogels. In particular, we discuss the current challenges in hydrogel printing and the key aspects of cell bioprinting. We provide an overview of materials commonly used, show examples of what has been done using multiple materials with different 3DP systems, and finish with commentary about what is in store for the future of hydrogel bioprinting.

2 Challenges Associated with Hydrogel Bioprinting

Although hydrogels provide a biomimetic environment for cells similar to that found *in vivo*, challenges remain in printing hydrogels with highly controlled architecture, maintaining mechanical support, crosslinking the polymer network while maintaining cell viability, and minimizing cellular exposure to stress. While 3DP provides precise and accurate control over the architecture, the level of precision and accuracy are largely determined by the printer used. Further, to maintain the desired level of precision and accuracy, structural support is necessary throughout the duration of the printing process. This mechanical support comes from the viscosity of the gelatinous material in the cartridge during the printing process and through the use of crosslinking,

either layer by layer or on the bulk geometry, during the printing process. Finally, the mechanism of crosslinking and the imparted shear stress need to be considered when printing cells in order to reduce cytotoxicity and mechanical damage to the cells.

2.1 Choice of Bioprinter

Currently, there are four common types of bioprinters used for 3DP hydrogels. These are inkjet bioprinters, laser-assisted bioprinters, extrusion (or micro-extrusion) bioprinters, and stereolithography (SLA) printers. Each type has been thoroughly described in recent reviews (Murphy and Atala 2014; Pereira and Bártolo 2015); thus, our emphasis here is the advantages and disadvantages of each type in printing cell-laden hydrogels. The four printing methods are depicted in Fig. 1.

Inkjet bioprinters function by dispensing small droplets of bioink onto a platform. Early inkjet printers were commercially available printers, such as Hewlett-Packard printers, modified in order to control the z-axis (Xu et al. 2005). Ink cartridges are replaced with bioink, and all parts of the printer are sterilized prior to printing (Xu et al. 2013b). As with traditional inkjet printing, small volumes (picoliters) of liquid are dispensed onto a substrate. In addition, cell viability has been shown to generally be high (>90%) (Xu et al. 2013b, 2005). Thus, this platform is benefitted by a low capital cost, comparatively fast printing speed, ease of modification for printing biological components, and demonstrated high cell viability. However, droplets are forced out using high temperatures or an applied voltage, which may lead to stresses up to 20 kPa being induced on the cells (He et al. 2014). Cells may be capable of surviving stress up to 2 MPa, but the mechanical deformation resulting from stresses this high decreases cell viability significantly (down to less than 5%), indicating care should be taken to avoid mechanical damage to cells during the printing process (Ringeisen et al. 2004; Wang et al. 2008). In addition, due to the size of the droplets and the force needed to allow for printing to occur, both cell density (on the order of 1,000,000 cells/mL) and viscosity of bioink is limited (Xu et al. 2005).

Laser-assisted bioprinters operate based upon laser-induced forward transfer (Koch et al. 2012). In essence, a laser is used to propel material from a donor substrate onto a receiving platform (Barron et al. 2004; Ovsianikov et al. 2010). Similar to inkjet printing, small droplets of bioink (down to femtoliters) are transferred from donor to receiver (Koch et al. 2012). However, in comparison to inkjet printers, laser-assisted bioprinters are capable of much higher cell densities (on the order of 100,000,000 cells/mL) as well as a wide range of viscosities (Koch et al. 2012). In contrast, these types of printers are significantly more expensive (Murphy and Atala 2014).

Extrusion (or micro-extrusion) bioprinters use pressure to extrude continuous strands of bioink onto a platform. Like inkjet printing, it has become common for many groups to build their own bioprinters, indicating the ease of using this type of printer. One trait of extrusion bioprinters is that they shear the material during the printing process as the material is forced through a needle. As a result, care must be taken to ensure cells remain viable, as numerous factors, including pressure, needle size, and rheological properties of the material, can lead to low cell viabilities (<50%)

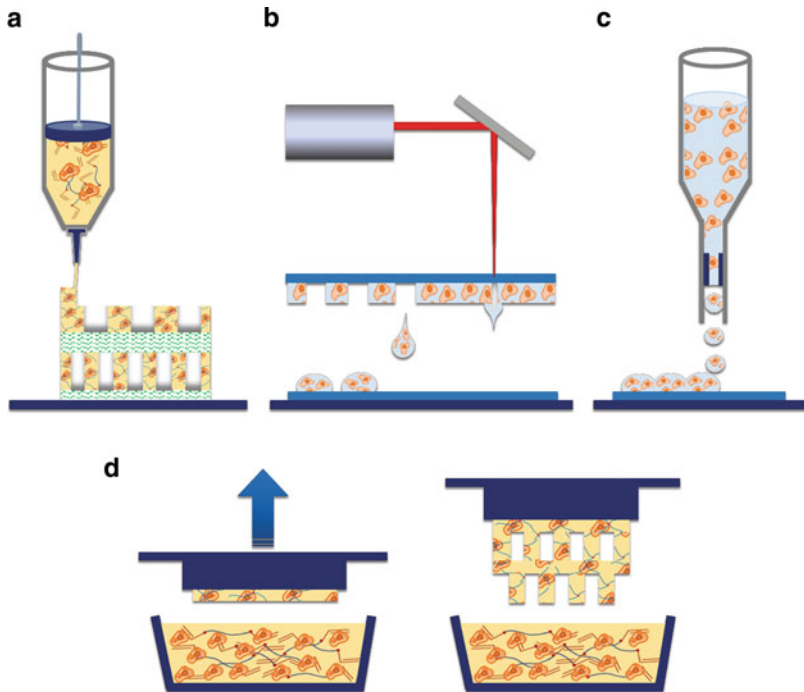


Fig. 1 Schematic of 3D printing methods for cell-laden hydrogels. There are several available 3D printing methods which can be used for cell-laden hydrogels. **(a)** Extrusion printing. Extrusion 3DP entails the use of pressure to extrude continuous strands of bioink onto a platform. Shown here, a piston applies force to cell-laden material which is extruded onto a platform. Multiple bioink cartridges may be used as shown here where the cell-laden material is *yellow* and a second material is shown in *green* and *white*. **(b)** Laser-assisted bioprinting (LAB). LAB uses laser diode and a mirror to direct the laser onto specific points of a platform. The laser contacts a laser-sensitive material which results in the release of the cell-laden material onto a collection platform. **(c)** Inkjet Printing. Inkjet bioprinters function using thermal or piezoelectric forces (*dark blue plates* within the nozzle) to dispense droplets of bioink onto a platform. **(d)** Stereolithography (SLA). SLA printing entails projection of a light source through a specially designed mask to crosslink material one layer at a time. In the setup depicted here, the platform moves upward as each layer is crosslinked and added onto the structure

(Yu et al. 2013). In addition, they are comparatively slow and tend to have lower resolution than inkjet or laser-assisted bioprinters since continuous strands, not droplets, are being deposited (Murphy and Atala 2014).

Stereolithography (SLA) is a less frequently used approach for 3DP of cell-laden hydrogels (Melchels et al. 2010). In this method of 3DP, cell-laden gel solutions are selectively crosslinked according to an image mask or by scanning laser beam layer by layer with ultraviolet (UV) light, or visible light using a projector and digital light processors (DLP) (Melchels et al. 2010). The use of SLA for printing hydrogels implies the need for photo-crosslinkable polymers and as such limits the materials which may be used in this application (Melchels et al. 2010). Moreover,

photo-crosslinkable polymers can entail exposure of cells to potentially harmful UV radiation, and careful selection of photoinitiators is necessary to minimize harm to cells (Bryant et al. 2000; Melchels et al. 2010). Finally, SLA approaches to encapsulate cells require the use of a high volume of cell-laden working solution, which is both expensive and time consuming (Melchels et al. 2010; Lin et al. 2013). Nonetheless, several groups have demonstrated the ability to generate cell-laden, layered constructs with complex geometries and viable cell populations (Dhariwala et al. 2004; Mapili et al. 2005; Arcaute et al. 2006; Chan et al. 2010; Lin et al. 2013).

In comparing the four types of printers, and the body of current literature, it is clear that inkjet and extrusion bioprinters are dominant for hydrogel bioprinting. Both are capable of reaching high cell viability with cell densities comparable to that of traditional hydrogel fabrication methods, both can be used with a wide variety of materials, and, importantly, both are inexpensive and relatively easy to build using off-the-shelf parts. In fact, numerous groups have built their own inkjet or extrusion bioprinters (Yan et al. 2005; Lee et al. 2009, 2014; Cui et al. 2012; Xu et al. 2013a; Melchels et al. 2014; Xu and Wang 2015). Thus, both provide options for beginning to bioprint hydrogels and can be made more complex later on to increase the complexity of printed constructs. While LAB and SLA offer some advantages over inkjet and extrusion printers, such as handling higher viscosity materials and generally having higher cell viability, these have yet to be used to fullest capability. For example, LAB may be used in printing complex tissues, such as the placenta, bone tissue, or lymph nodes, with high cell densities to make improved *in vitro* models for understanding cell-cell interactions and bulk properties of the tissue. Figure 2 provides a flow chart to aid in choosing the right type of bioprinter.

Resolution of a printed gel often is dependent upon the printer, which could impact the choice of bioprinter needed. Both inkjet printers and laser-assisted bioprinters are limited by the size of the droplet being transferred while extrusion printers are limited by the needle size. These are technological limitations. However, resolution is also dictated by material used. Highly viscous materials, for example, may not be capable of being transferred or extruded using the smallest size droplet or needle. Cells within the bioink may also limit resolution. For example, inkjet printing small droplets at a high cell density may result in cells being sheared, and possibly dying, as they fall onto the platform surface, as may be a similar case for trying to extrude large cells through a small needle in an extrusion bioprinter. Further, resolution is important to consider in the context of the desired end goal. For example, the resolution desired in printing biologically active molecules may be different than the resolution needed to print the scaffold without biological additives. Thus, both bioink composition and printer resolution should be considered when considering the resolution of bioprinters.

2.2 Mechanical Support and Printability

The key aspect of 3DP is the ability to control the overall structure and micro-architecture of the final, printed product. Here, we will refer to that control as “printability.” If a material or design is printable, then the accuracy of fabricated

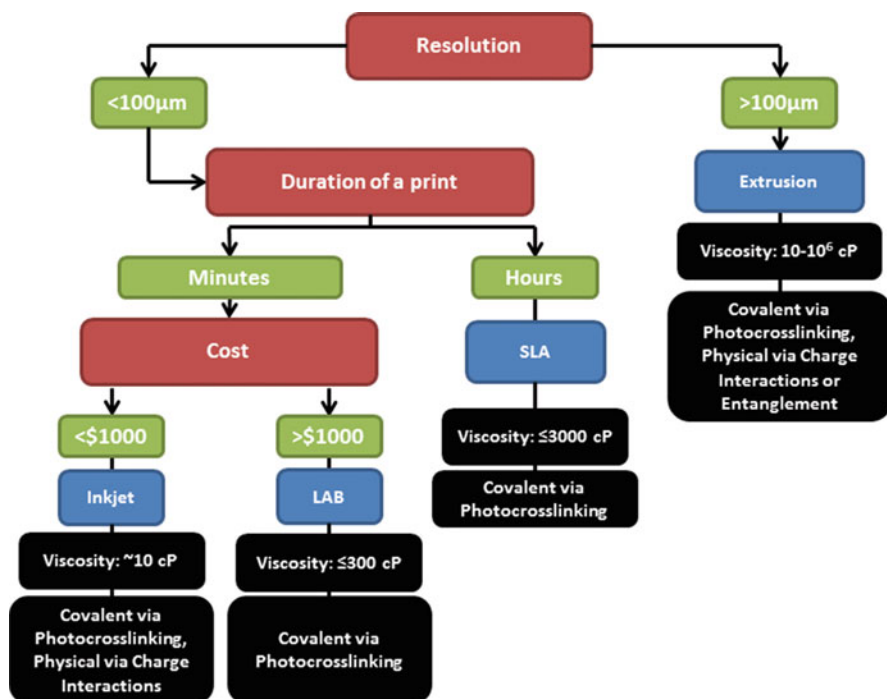


Fig. 2 Flow chart for choosing a bioprinter. The four primary types of bioprinters vary in achievable resolution, duration of a print (the time from start to finish), cost, capable viscosities, and methods of crosslinking polymers that can be used with the 3DP. To aid in choosing a printer, these key factors are broken down. *Red boxes* indicate a decision that must be made, *green boxes* indicate options for that decision, *blue boxes* indicate printer choices, and *black boxes* indicate details related to the printer choice. For example, extrusion printers offer the lowest resolution but can print the highest viscosity bioinks and offer the widest range of polymer crosslinking methods. Inkjet, laser-assisted bioprinters, and stereolithography (SLA) all offer better resolution and can be further chosen based upon duration of a print and cost

product with regard to theoretical and intended design will be high. While printability is often considered largely driven by design, it is also driven by the bioink and material being used. In some cases, it is necessary to use a support material that can later be sacrificed in order to get the final, desired structure (Kolesky et al. 2014; Hinton et al. 2015). These sacrificial materials help support architectural features within the design that are intended to be surrounded by open space. This is a common approach in trying to create vascularized tissue constructs, where sacrificial materials are used during the printing process, evacuated post-printing to create channels, and those channels later seeded with endothelial cells (Kolesky et al. 2014; Bertassoni et al. 2014b). In addition to support materials, printability is also determined by the viscosity of the bioink itself.

Natural polymers, meaning polymers (or their products) commonly derived from an organism, tend to be widely used in bioprinting. However, sometimes their

viscosity presents an issue in the printing process (Shim et al. 2012; Kolesky et al. 2014). This is particularly true for hydrogels, since gelation is based upon the viscosity of the material. A sharp increase in viscosity generally indicates that gelation has occurred. Two materials commonly used in bioprinting that exhibit different viscosities depending on exogenous variables are gelatin and alginate. Gelatin is similar to its precursor, collagen, in that both exhibit temperature-dependent rheological properties (Pietrucha 2005; Florián-Algarín et al. 2008). Thus, bioink formulations that use gelatin as the polymer may need to be printed at a temperature that allows the ink to be viscous enough to print and not spill as a liquid, yet not so viscous as to prevent the material from being printed (Kolesky et al. 2014). Alginate is another natural polymer; however, it exhibits shear-dependent rheological behavior (Rezende et al. 2009). As a result, printing alginate may require some optimization in order to get an appropriate fluid viscosity, with or without a support structure, such that the bioink becomes printable (Shim et al. 2012). Thus, in hydrogel printing, it is important to consider the viscosity of the bioink to ensure that it will be printable, as well as taking into account any support structure that will be needed to achieve an intended design.

2.3 Stress in Cell-Laden Hydrogels

As alluded to previously, bioprinting of cell-laden hydrogel bioinks exposes cells to stress atypical of traditional methods of fabricating hydrogels. In LAB and inkjet printing, cells are exposed to shear stress as strands are extruded out of the needle. Finally, while stereolithography overcomes the limitation of shear stress introduction, cells undergo other stresses as a result of this fabrication method. Potentially harmful stresses associated with can include exposure to UV and photoinitiator chemicals associated with crosslinking the hydrogels and discussed in depth in the next section. Recently, a few studies have looked at how printing impacts cell viability.

A study by Xu et al. was among the first to show inkjet printing is capable of keeping mammalian cells alive (Xu et al. 2005). In this study, Chinese hamster ovary (CHO) cells were suspended in $3 \times$ Dulbecco's PBS at a concentration of 5,000,000 cells/mL and printed onto soy agar or collagen. They modified a Hewlett-Packard desktop printer (HP 550C) and HP ink cartridge (51626a) to print their cell suspensions. They compared cell death as a function of bioink formulation and printing processing. They found that, on average, $3.3 \pm 3.7\%$ of the cells lysed as a result of the printing process compared to the $18.6 \pm 3.7\%$ cells lysing due to bioink formulation. This indicated that the vast majority of the cells were able to live, regardless of the potential damage done by the inkjet printing process. Others have evaluated similar parameters for extrusion-based bioprinters (Nair et al. 2009; Yu et al. 2013; Blaeser et al. 2016).

In a study done by Blaeser et al., cells were exposed to varying levels of shear stress, which was then correlated with the cell viability (Blaeser et al. 2016). Using L929 mouse fibroblast cells encapsulated in alginate, prints were conducted in three

experimental groups, based upon shear stress: lower than 5 kPa, between 5 and 10 kPa, and greater than 10 kPa. The lowest shear stress group (<5 kPa) resulted in 96% cell viability, indicating minimal impact on the overall cell population. However, viability decreased to 91% for the middle group (shear stress between 5 and 10 kPa) and 76% for the higher group (shear stress >10 kPa), indicating an inverse correlation between shear stress and cell viability. A similar correlation was obtained with human mesenchymal stem cells (hMSCs), where cells were 94% viable for a shear stress of 4 kPa, 92% for 9 kPa, and 86% for 18 kPa. This group further investigated the impact of shear stress on cells by evaluating cell function after exposure to printing-associated shear stress. Again, using hMSCs and low (<5 kPa), medium (5–10 kPa), and high (>10 kPa) shear stress experimental groups, cell-laden hydrogels were stained for vimentin, an intermediate filament mesenchymal marker, and CD34, an endothelial marker, and showed no change in phenotype over the course of 7 days. Other groups have looked at cell viability as a function of printing parameters, such as nozzle size, and found that parameters that would increase shear stress, such as small needles or higher printing pressures, resulted in more cell injury or cell death (Nair et al. 2009; Yu et al. 2013). One study done by Zhao et al. looked at the impact of holding time, meaning how long a bioink was held at set conditions prior to printing, and temperature on cell viability (Zhao et al. 2015). In this study, longer holding times and lower temperatures resulted in significantly lower cell viability (in some cases down to 72%), indicating that some printing parameters are significantly more important than others when considering the impact on cell viability and functionality post-printing.

3 Methods for Polymer Crosslinking

In bioprinting hydrogels, one aspect that is fundamental to the printability of a bioink is the method for crosslinking the polymer. There are a few common methods for crosslinking a polymer, but not all of them may be amenable to bioprinting. The simplest method, in terms of printing, is photo-crosslinking initiated by ultraviolet (UV) or visible light, whereby polymer chains are covalently bonded together. Temperature-induced gelation of hydrogels can also be utilized as a method for solidifying materials. Lastly, hydrogels may also be ionically crosslinked, whereby molecular interactions maintain structural integrity. Here we will consider how each method affects the bioprinting of cells with a summary of the mechanisms depicted in Fig. 3.

3.1 Photo-crosslinking

Photo-crosslinking is commonly used because it can rapidly crosslink a large hydrogel. Briefly, photo-crosslinking uses a photoinitiator to create a free radical within the polymer network. This radical rapidly penetrates throughout the network, causing chemical bonds to form between neighboring polymer chains until

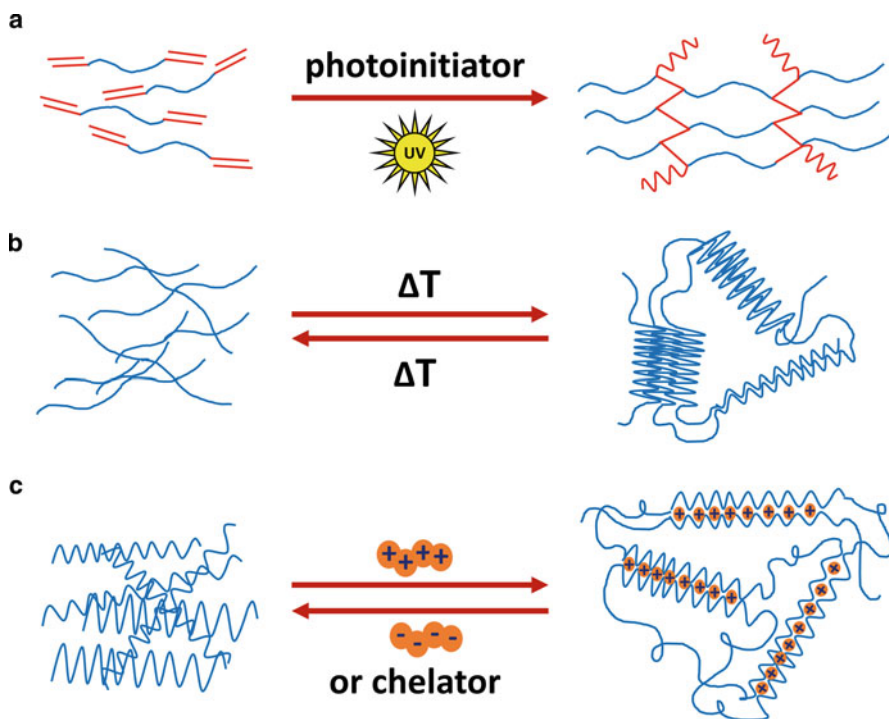


Fig. 3 Methods for generating hydrogel networks. Hydrogels may form networks through both physical and chemical interactions which can be reversible or permanent. (a) Photo-crosslinking uses a photoinitiator coupled with a light source (such as UV shown here) to generate free radicals. The free radicals rapidly propagate throughout the network, causing chemical bonds to form between the susceptible moieties of neighboring polymer chains (depicted in red). (b) Temperature-dependent physical entanglement occurs when materials exhibit thermoreversible gelation, with the bulk material solidifying at low temperatures and liquefying at higher temperatures. (c) Ionic crosslinking entails the use of charged compounds (depicted in orange) as crosslinkers to create ionic interactions between sites exhibiting the opposite net charge of the crosslinkers. These interactions may be reversed with oppositely charged particles or chelators

the free radicals can no longer propagate. While this method can successfully maintain the structure of the printed gel, it can lead to problems in terms of cell viability. Radical initiators, extended exposure to UV light, and the power of UV irradiation may lead to a decrease in cell viability (Rouillard et al. 2011; Mironi-Harpaz et al. 2012; Billiet et al. 2014). In spite of these concerns, photo-crosslinking is still rapid and can yield cell viabilities that are sufficient for many applications (Rouillard et al. 2011; Billiet et al. 2014). Further, photo-crosslinking allows for control over the rate and degree of crosslinking, allowing for more controlled design of the hydrogel (Skardal et al. 2010).

In some cases, materials are functionalized in order to add groups that can undergo a radical reaction to enable photo-crosslinking of the hydrogel network.

One common example of this is the addition of acrylate or methacrylate groups to the polymer backbone. This has utilized with gelatin (Skardal et al. 2010; Schuurman et al. 2013; Bertassoni et al. 2014a; Billiet et al. 2014; Gao et al. 2015a), hyaluronic acid (Skardal et al. 2010; Duan et al. 2014), poly(ethylene glycol) (Ovsianikov et al. 2010; Cui et al. 2012; Hockaday et al. 2012; Hong et al. 2015; Gao et al. 2015b), and polyvinyl alcohol (PVA) (Schmedlen et al. 2002). These materials are biocompatible and support cell growth and proliferation on their own. Thus, functionalization provides the advantages of their inherent properties with the added benefit of having significantly better control over crosslinking.

Free radical-mediated photo-crosslinking or photopolymerization of a given material requires the presence of a photo-crosslinkable functional group and a photoinitiator (Andrzejewska 2001; Ifkovits and Burdick 2007). The selection of initiators must be carefully considered when bioprinting hydrogels in order to optimize cell viability and printed construct mechanical and physical properties (Bryant et al. 2000; Williams et al. 2005; Pereira and Bártolo 2015). In particular, light radiation and the presence of free radicals and unreacted double bonds can be detrimental to cell viability (Bryant et al. 2000; Williams et al. 2005; Wallace et al. 2014). To reduce damage from such factors, it is important to choose an efficient and minimally cytotoxic photoinitiator wherein light intensity and exposure time can be minimized (Pereira and Bártolo 2015). This can be achieved by closely matching the photoinitiator absorption spectra to the emitting light source wavelength and further by selecting a photoinitiator with cytocompatibility throughout the reaction process (Bryant et al. 2000; Andrzejewska 2001). A handful of commercially available photoinitiators have been found to be cytocompatible for use with a variety of cell types including 2-hydroxy-1-[4-(hydroxyethoxy)phenyl]-2-methyl-1-propanone (Irgacure 2959), lithium phenyl-2,4,6-trimethylbenzoylphosphinate (LAP), and riboflavin (Bryant et al. 2000; Williams et al. 2005; Hu et al. 2012; Chen et al. 2012; Li et al. 2015; Davey et al. 2015; Ahearne and Coyle 2016). In stereolithography applications, undesirable free radical propagation can extend beyond the illuminated area intended to be crosslinked, negatively impacting feature resolution, crosslinking density, and subsequently impacting mechanical properties (Elomaa et al. 2011; Wallace et al. 2014; Wang et al. 2015b). The addition of photoinhibitors and absorbing dyes has been shown to mitigate these concerns in cell-free photo-crosslinking applications (Melchels et al. 2009; Elomaa et al. 2011; Wallace et al. 2014). Photoinhibitors such as vitamin E and hydroquinone prevent premature crosslinking by quenching free radicals (Melchels et al. 2009; Elomaa et al. 2011; Wang et al. 2015a). The addition of dyes or pigments such as Orasol Orange G, 2-hydroxy-4-butanoic acid (HMB), and titanium dioxide blocks penetration of radiation to prevent undesired radical generation and crosslinking (Elomaa et al. 2011; Wang et al. 2015b). Unfortunately, while several photoinitiators have been shown to be cytocompatible, to the best of the authors' knowledge, the use of inhibitors and dyes in cell-laden bioprinting has not been investigated, indicating the need for further work in this area (Wallace et al. 2014).

3.2 Thermal Crosslinking

Temperature-induced gelation is another method for crosslinking materials, though it is limited by the material and the printer. In terms of materials, gelatin is a commonly used material that exhibits thermoreversible gelation, with the bulk material solidifying at low temperatures and liquefying at higher temperatures (Hinton et al. 2015). In terms of printers, extrusion-based printers are generally the only type capable of printing a material that can later be crosslinked by temperature (Smith et al. 2007; Khalil and Sun 2007).

In addition, there is a limitation in terms of gelation kinetics. As previously discussed, printing hydrogel materials requires that the bioink be sufficiently viscous to maintain its structure as printing occurs. After completion of the printing process, a structure is generally allowed to fully undergo crosslinking – here that means that the structure would be placed at an appropriate temperature to allow a complete transition to the solid state. However, thermal gelation often occurs at a rate that is too low in order to both maintain an appropriate viscosity for printing and be viscous enough to maintain its structure during the printing process (Moraes et al. 2013; Tsai et al. 2015; Lee et al. 2016). In addition, allowing gelation to occur within the syringe for too long may clog the printer tip due to the increased viscosity of the bioink and the lower temperature of the printer tip, compared to the syringe (Hinton et al. 2015). A recent study found it took 170 s in order to fully gel a novel, thermo-responsive polyurethane, which may still be too long, leading to difficulty in the printing process (Tsai et al. 2015). However, this is still notable as being relatively quick compared to other polymers. Collagen, for example, generally takes 30 min at 37 °C to fully gel (Moraes et al. 2013; Lee et al. 2016). As a result, those who have printed collagen have needed a framework in order to maintain the structure of the collagen (Lee et al. 2016). In general, thermo-responsive polymers have been difficult to print due to the slow gelation kinetics. Thus, this is an area in need of novel approaches, such as synthesizing new polymers with improved gelation kinetics (Tsai et al. 2015).

3.3 Ionic Crosslinking

Ionic crosslinking uses charged compounds to create crosslinks within a polymer network. The most common example of this is alginate, wherein calcium chloride is commonly used as the crosslinker (Song et al. 2011; Shim et al. 2012; Yu et al. 2013; Hong et al. 2015). In this system, alginate chains interact with calcium ions to form a polymer network. In bioprinting, different methods have been used when crosslinking alginate. Shim et al. used an extrusion system to create a support structure, deposit alginate, and later crosslink the alginate using calcium chloride, in the presence of sodium chloride, for 10 min (Shim et al. 2012). In contrast, Yu et al. used a coaxial nozzle system in an extrusion printer (Yu et al. 2013). In this system, the biomaterial and the crosslinker solution were kept at different flow rates, but began to mix at the tip of the needle or the interface where the needle meets the

printing platform. This “double-barrel” style of syringe allowed for controlled printing without the need for later crosslinking via solution. Alginate has also been used in an inkjet-style printer. Faulkner-Jones et al. created a system that dispensed nanoliters of printing solution onto a platform (Faulkner-Jones et al. 2015). Here, an alginate solution and calcium solution were printed next to each other, with crosslinking occurring at the interface of the two solutions. This indicates feasibility of using this crosslinking method in multiple types of bioprinters. Further, while this mechanism has primarily been used for alginate, chitosan is another polymer that has been extensively used and can ionically crosslink, indicating potential for chitosan to become useful as a bioprintable material in future applications (Berger et al. 2004).

4 Multi-material Hydrogel Printing

By this point, it should be clear what the major challenges are in bioprinting cell-laden hydrogels, common methods for addressing some of these challenges, and limitations that stem from the fundamental biology and chemistry of the intended system. Here, we explore selection of an appropriate material, discuss some commonly used materials, and showcase examples of how these materials interact in multi-material printing of hydrogels.

4.1 Material Selection

A key aspect of hydrogel bioprinting is determining which material will be used for printing. Up to this point, we have mainly discussed applications using gelatin, hyaluronic acid, PEG, and alginate (Skardal et al. 2010; Hockaday et al. 2012; Duan et al. 2013; Hinton et al. 2015; Hong et al. 2015; Gaetani et al. 2015; Zhao et al. 2015). The benefits of these materials include, but are not limited to, biocompatibility, functionalization capacity, and ease of crosslinking into a gel. However, there are other materials which have been shown to successfully generate cell-laden hydrogel scaffolds. Examples of commonly used materials will be discussed in detail later, but some other less commonly used include fibrin or fibrinogen (Lee et al. 2010; Xu et al. 2013a; Xu and Wang 2015), gellan gum (GG) (Melchels et al. 2014; Levato et al. 2014), Pluronic F127 (Smith et al. 2004; Kolesky et al. 2014; Müller et al. 2015), polyurethanes (Hsieh et al. 2015), PVA (Schmedlen et al. 2002), and decellularized tissue (Pati et al. 2014, 2015). Each of these materials has unique benefits, which ultimately dictates why they may be chosen over other materials for a given application. For example, fibrin is the polymerized form of the protein fibrinogen that is a part of the blood coagulation cascade and thus can be a good environment for endothelial cells to spread and proliferate. Another example is the use of GG, which has been shown to increase the viscosity of the bioink to help improve its printability (Melchels et al. 2014). Ultimately, in each investigation described herein, materials were chosen with a particular end goal in mind. The question thus becomes: What should be considered when choosing a material?

As in choosing a bioprinter, each material has its advantages and disadvantages. The first question is whether to use a natural polymer or a synthetic polymer. Natural polymers are advantageous due to their biocompatibility, yet often have the drawback of weak mechanical properties (Gao et al. 2015a; Kundu et al. 2015). In addition, the intrinsic crosslinking method of a natural polymer may cause printing to be difficult. In contrast, synthetic polymers are easy to process and/or modify, yet may be cytotoxic to cells (Murphy and Atala 2014). While the vast majority of hydrogels used in bioprinting applications are composed of natural polymers (Fedorovich et al. 2008; Rutz et al. 2015; Ouyang et al. 2015a; Tabriz et al. 2015; Pereira and Bártolo 2015), there have been examples where synthetic polymers were used (Visser et al. 2013; Zhang et al. 2015). Beyond just the broad material classification, further rationale is needed for selection of a material. This includes consideration of a material's mechanical properties and how that may affect the cells embedded, the presence of binding sites, and the ability of cells to spread and adhere to the material, as well as the printability of the material. Fibronectin, for example, is commonly employed to enhance cell adhesion, yet has not been widely used as the primary material for bioprinting (Fedorovich et al. 2011). Poly(2-hydroxyethyl methacrylate), or pHEMA for short, has been commonly used in various applications, such as for soft contact lenses (Galante et al. 2015; García-Millán et al. 2015), but is less commonly used in 3DP applications (Hanson Shepherd et al. 2011; Mohanty et al. 2016). The sparse use of materials such as fibronectin and pHEMA is in contrast with the numerous alginate applications, including both extrusion and inkjet bioprinting (Song et al. 2011; Shim et al. 2012; Pataky et al. 2012; Yu et al. 2013; Faulkner-Jones et al. 2015; Markstedt et al. 2015). Thus, the extent of existing literature and expertise with a material should inform the material selection in bioprinting cell-laden hydrogels. Materials and some of their properties are outlined in Fig. 4 to aid in material selection.

One interesting avenue that is emerging both in the broader context of tissue engineering and more specifically within hydrogel bioprinting is the use of decellularized tissue (Pati et al. 2014, 2015). In essence, the bioink is formed from whole tissue that has, as the name implies, the cells removed, leaving only the extracellular matrix (ECM). The ECM is then solubilized to form a viscous solution for the bioink. Fundamentally, using decellularized tissue ECM as the material for printing provides a significantly enhanced biomimetic environment for encapsulated cells, in terms of material composition. Specifically, ECM proteins are rich in cell adhesion moieties such as GFOGER and RGD peptide sequences found in triple helical collagen and fibronectin, respectively (Petit and Thiery 2000; Hynes 2002; Takada et al. 2007). Studies have also shown enhanced tissue-specific cell differentiation through the use of ECM derived from the tissue of interest (Pati et al. 2014). In these studies, the primary bioink materials investigated were decellularized adipose, cartilage, and heart tissues. As a supportive material, to help with maintaining the structural integrity of the printed hydrogel, polycaprolactone (PCL) was used as a framework. The investigators first looked at differentiating human adipose-derived stem cells (hASCs) and human inferior turbinate tissue-derived mesenchymal stromal cells (hTMSCs) toward chondrogenic (cartilage)

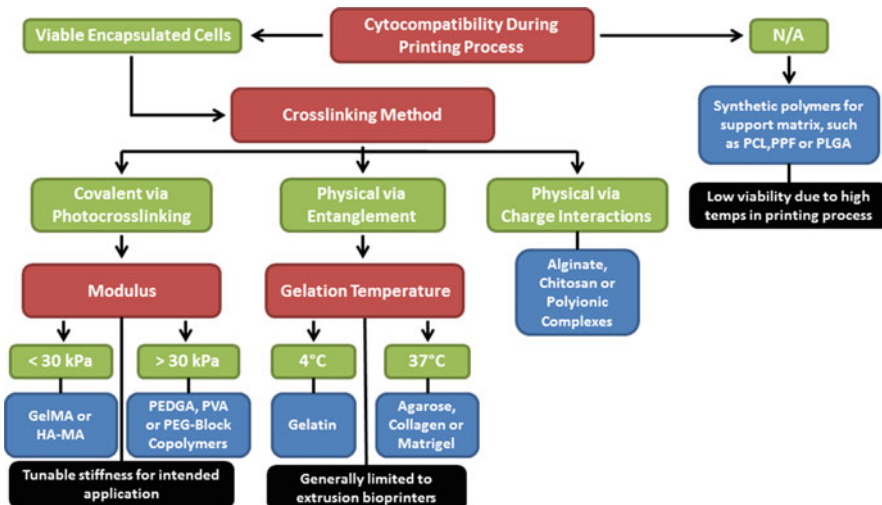


Fig. 4 Flow chart for choosing a material. Material selection can be informed by cytocompatibility during the printing process, method of crosslinking the polymer, mechanical properties, and, in the case of entangled polymers, gelation temperature. *Red boxes* indicate a decision that must be made, *green boxes* indicate options for each decision, *blue boxes* indicate the resulting materials, and *black boxes* indicate comments related to a decision or material. For example, wanting a highly cytocompatible material that can be thermally crosslinked at 37 °C indicates that agarose, collagen, or Matrigel should be used. In addition, the use of thermally crosslinked polymers is generally limited to extrusion-based bioprinters, thus limiting the choice of 3DP

and adipogenic (fat) lineages (Pati et al. 2014). Interestingly, they found that the decellularized tissue associated with each of those lineages enhanced the cellular differentiation, indicating the benefit of using tissue-specific ECM. In a later study, the group sought to see if printed constructs using adipose tissue ECM supported fat tissue growth (Pati et al. 2015). They decellularized adipose tissue, printed dome-shaped constructs using the material, and ultimately implanted the constructs into mice. The group found that the constructs did not cause inflammation and supported formation and constructive remodeling of the tissue. This recent work indicates the potential for using decellularized tissue as the primary material in bioink formulations for bioprinting hydrogels that can advance the field of tissue engineering and regenerative medicine.

4.2 Common Materials in Hydrogel Bioprinting

Hydrogel bioprinting has been investigated for over a decade (Barron et al. 2004; Xu et al. 2005). This longevity might imply the field has advanced to using a vast selection of materials, yet literature shows only a handful are regularly used. As previously mentioned, four of the most commonly used materials are (1) alginate (Cohen et al. 2010; Song et al. 2011; Shim et al. 2012; Fedorovich et al. 2012; Pataky

Table 1 Common materials used in hydrogel bioprinting. Alginate, GelMA, HA-MA, and PEGDA are among the most commonly used materials in bioprinting hydrogels. Key characteristics of these materials include their mechanical properties, cell compatibility, mechanisms for crosslinking, printers that have been used with each material, and their associated resolution

Material	Mechanical properties	Cell compatibility	Crosslinking methods	Printers	Resolution
Alginate	Elastic modulus: 5–30 kPa	75–96% viability	Ionic	Inkjet, extrusion, laser	10–100 μm (inkjet), 320–640 μm (extrusion), 500 μm (laser)
Gelatin methacrylate (GelMA)	Modulus: 3–60 kPa	60–90% viability	Photo-initiated, thermal	Inkjet, extrusion	150–200 μm
Hyaluronic acid methacrylate (HA-MA)	Modulus: 4–12 kPa	>90% viability	Photo-initiated	Extrusion	<1 mm
Poly (ethylene glycol)-diacrylate (PEGDA)	Compressive modulus: 30–395 kPa	90% viability	Photo-initiated	Inkjet, extrusion	20–85 μm (inkjet), 500 μm (extrusion)

et al. 2012; Yu et al. 2013; Zhang et al. 2013; Faulkner-Jones et al. 2015; Tabriz et al. 2015; Blaeser et al. 2016), (2) gelatin (Schuurman et al. 2013; Bertassoni et al. 2014a; Billiet et al. 2014; Melchels et al. 2014; Ma et al. 2015), (3) hyaluronic acid (Skardal et al. 2010; Duan et al. 2014; Highley et al. 2015; Kesti et al. 2015), and (4) poly(ethylene glycol) (PEG) (Cui et al. 2012; Hockaday et al. 2012; Hong et al. 2015; Ma et al. 2015; Gao et al. 2015a). Some characteristics of these materials are outlined in Table 1. Here, we will elaborate on studies involving each of these materials more in depth.

Alginate is perhaps the most common material used in hydrogel printing and has been shown to work using both inkjet printers and extrusion-based printers (Pataky et al. 2012; Faulkner-Jones et al. 2015; Sher et al. 2015; Tabriz et al. 2015). Alginate is biocompatible, is non-immunogenic, can be crosslinked in a reversible and controlled manner, and can form highly porous structures that support cells (Faulkner-Jones et al. 2015; Tabriz et al. 2015). As previously discussed, alginate crosslinks through the use of calcium ions that cause chains of alginate to interact, with strong enough interactions to result in the formation of a hydrogel network (Yu et al. 2013; Hong et al. 2015). In printing alginate, multiple approaches have been taken. In one method, an inkjet-style printer was used to print an alginate solution followed by a calcium solution, thus allowing for crosslinking to occur at the interface (Faulkner-Jones et al. 2015). Another approach using an inkjet printer was to embed calcium ions into a gelatin-based gel substrate and allow for the

diffusion of calcium ions from the substrate to crosslink the alginate as it is being deposited on top (Pataky et al. 2012). An interesting approach taken by Tabriz et al. used a modified Fab@Home extrusion printer to print cell-laden alginate onto a substrate that was on a z-axis controlled platform (Tabriz et al. 2015). As the printing continued, the platform would move downward into a solution of calcium chloride-enriched culture media. Interestingly, this method would allow for continuous crosslinking of the bottom portion of the structure, perhaps leading to a mechanically enhanced structure, assuming alginate chains are still available for crosslinking. Other groups have also printed alginate solutions into a calcium solution in order to crosslink their hydrogels (Blaeser et al. 2016). In addition to variability in crosslinking approaches used, the concentration of alginate has varied in applications from 0.5 to 6% w/v (Zhang et al. 2013; Blaeser et al. 2016). These differences have been shown to impact cell viability and solution viscosity (Yu et al. 2013; Blaeser et al. 2016), indicating a need to optimize the composition of the alginate bioink for its intended application.

Gelatin is another commonly used material that is biocompatible, is biodegradable, and exhibits thermoreversible gelation (Schuurman et al. 2013). Gelatin naturally gels at low temperature and liquefies at high temperature. Some groups have used unmodified gelatin (Ouyang et al. 2015b; Zhao et al. 2015), while others have functionalized gelatin, most commonly by adding methacrylate groups (Schuurman et al. 2013; Bertassoni et al. 2014a). When using unmodified gelatin, efforts were made to ensure printing occurred within the temperature range for gelation to occur (Ouyang et al. 2015b; Zhao et al. 2015). While this approach ensures integrity of the bioink and the printed structure throughout the printing process, using unmodified gelatin may lead to degradation of the hydrogel during the growth and culture of cells at 37 °C. Interestingly, one study using a gelatin-alginate hydrogel found that cell growth continued in patterns mimicking the initial printed structure, showing it may be possible to maintain a printed design when combining gelatin with another material (Ouyang et al. 2015b). In contrast, functionalized gelatin, specifically methacrylated gelatin (GelMA), can form a hydrogel network through photocrosslinking. GelMA provides the benefits of gelatin along with the capacity for rapid and controlled polymerization. Bioinks using gelatin or GelMA have typically used 5–20% w/v within the final bioink formulation (Schuurman et al. 2013; Bertassoni et al. 2014a; Zhao et al. 2015). One study showed that the compressive modulus of GelMA hydrogels varied depending on gelatin concentration and gelation temperature. Their work illustrated that 10% w/v and 20% w/v GelMA had a modulus of 30–50 kPa and 200–300 kPa, respectively, when crosslinked at 37 °C or room temperature (Schuurman et al. 2013). These examples serve to showcase the wide range of material properties which can be achieved with gelatin-based bioinks which have resulted in the wide use of these materials in hydrogel bioprinting applications.

Hyaluronic acid (HA), or hyaluronan, is a natural, linear, anionic glycosaminoglycan that is capable of forming a hydrogel network (Pietrucha 2005; Burdick and Prestwich 2011). However, it is less commonly used in bioprinting than either alginate or gelatin, perhaps due to the fact that it is inherently difficult to print

(Burdick and Prestwich 2011). Printing of HA necessitates the use of soluble additives such as dextran to tune the viscosity and functionalization with moieties and proteins to enable crosslinking and enhance cell adhesion (Skardal et al. 2010; Duan et al. 2014). HA network formation is dependent upon functionalization and established mechanisms for functionalizing and crosslinking HA have been thoroughly reviewed (Burdick and Prestwich 2011). A recent investigation by Duan et al. added a methacrylate group to HA, thus making hyaluronic acid methacrylate (HA-MA) (Duan et al. 2014). In this study, the group combined HA-MA with GelMA and found that increasing the HA-MA content from 2% to 6% increased the stiffness of the hydrogel when using 6% GelMA. However, these differences were not apparent using higher amounts of GelMA (10% and 12%). This indicates that HA may be useful as an additive in hydrogels, but may not be the most suitable primary material. This finding was further supported by a group that used HA-MA as a barrier for cell migration, wherein their results indicated that HA-MA did not enable cell adhesion to the matrix without another material present (Skardal et al. 2010). Regardless, HA is a prominent molecule within cartilage tissue and thus may be advantageous for cartilage-focused tissue constructs (Kesti et al. 2015).

Poly(ethylene glycol) (PEG) is a synthetic polymer that has been used in a variety of therapeutic applications approved by the US Food and Drug Administration (FDA) and as such has become increasingly prevalent in translational tissue engineering investigations. Further, PEG is biocompatible and can be easily modified for specific applications (Hockaday et al. 2012). In bioprinting, acrylate-modified PEG, poly(ethylene glycol)-diacrylate (PEGDA), is commonly used to enable photo-crosslinking of the polymer (Cui et al. 2012; Gao et al. 2015a). Furthermore, the mechanical properties of PEGDA are tunable for use in a wide variety of applications (Cui et al. 2012; Hockaday et al. 2012). In using synthetic polymers, such as PEG, not only is polymer concentration important but also the molecular weight (MW) of polymer used. In particular, when using cell-laden hydrogels, the MW of PEGDA can impact cell viability. Specifically, one group showed that MW < 3 kDa resulted in decreased viability of encapsulated cells compared with higher MW PEGDA hydrogels (Chan et al. 2010). Using the same polymer with different MW can also yield different bulk material properties. One example of this is that the MW of PEG tends to correlate with the stiffness of the gel, meaning lower MW polymers lead to softer gels (Hockaday et al. 2012). Groups have used PEGDA that ranged from 0.7 to 20 kDa and from 10% to 20% w/v polymer in bioink solution (Cui et al. 2012; Hockaday et al. 2012; Hong et al. 2015; Gao et al. 2015a). In addition, PEG is one of the only materials used in all four major types of bioprinters, truly indicating its versatility (Ovsianikov et al. 2010; Cui et al. 2012; Hockaday et al. 2012; Hong et al. 2015; Gao et al. 2015a).

4.3 Single Bioink Bioprinting

In printing multi-material hydrogels, the use of a single bioink has distinct advantages and disadvantages over the use of multiple, separate bioinks. A depiction of the differences between single and multi-bioinks of homogenous and heterogeneous resins

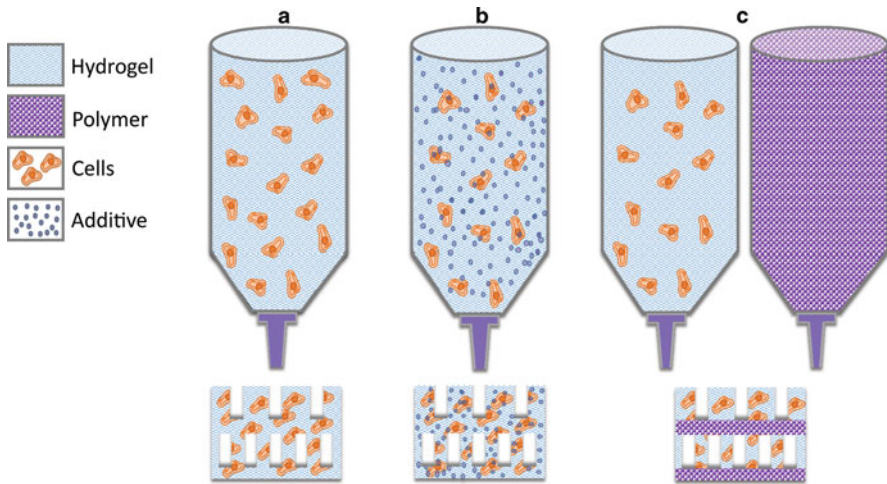


Fig. 5 Single and multi-bioink resins. Multi-material single bioinks benefit cell-laden hydrogel 3D printing by including additives to enhance material viscosity for printing or which can be beneficial to cell viability and target behavior. Cell-laden hydrogels have been printed in a variety of single material hydrogel bioink resins (a) and single resins made of multiple materials (b). The use of multiple, separated bioinks can benefit 3DP of hydrogels by enhancing the mechanical integrity of printed structures by including stiffer materials such as printable polymers (c)

can be seen in Fig. 5. A single bioink will be homogeneous and require only one cartridge. In addition, “hard-to-print” materials can be incorporated into “easy-to-print” materials. For example, hyaluronic acid can be incorporated into a gelatin methacrylate bioink (Skardal et al. 2010). However, using a single bioink prevents the construct from being heterogeneous. This does not prevent investigators from fabricating single bioink constructs for various applications though, as outlined in Table 2.

One set of single bioink examples comes from incorporating GG into a GelMA hydrogel (Melchels et al. 2014; Levato et al. 2014). In two studies, GG was included at a low concentration (0.75–1% w/v) to improve the printing of GelMA. In the study by Melchels et al., they compared the viscosity of four bioinks: (1) 0.75% GG, (2) 10% GelMA, (3) 10% GelMA + 0.75% GG, and (4) 10% GelMA + 0.75% GG + 24 mM cations (Melchels et al. 2014). (To clarify, the 24 mM cations are of any valence and promote the formation of a more brittle GG gel.) Over the range of shear rates tested to investigate the viscosity (0.01–1,000 s^{-1}), they found the GelMA alone and GG alone to be similar, while the combination of both together was generally an order of magnitude higher than either alone. This difference in viscosity was spread even further when including cations, which resulted in nearly an order of magnitude higher viscosity than the combined material and thus two orders of magnitude higher than either material alone (Melchels et al. 2014). In a study done by Levato et al., microcarriers were used in a 10% GelMA/1% GG system to enhance the GelMA matrix that was being printed. Briefly, poly(lactic acid) (PLA) microparticles were coated with collagen and had cells seeded onto them prior to

Table 2 Multi-material hydrogels using a single, homogeneous bioink. Examples of multi-component bioinks are listed here, including the materials used in the bioink; the printer used; the intended application for each material; results of interest, including mechanical properties, and results related to 3DP of the bioink; and the reference information for each study

Materials	Printer	Application	Results of interest	Reference
Agar/acrylamide/alginate	Extrusion	Tough hydrogel	Modulus: 70–870 kPa Strength: 402–1,096 kPa	Wei et al. (2015)
Acrylamide/alginate	Extrusion	Tough hydrogel	Young's modulus: 90–170 kPa Failure strain: 90–300%	Bakarich et al. (2013)
Alginate/collagen	Inkjet	Vascularized bone	Compressive modulus increases to over 2 MPa after 18 weeks implantation, one of the first prints using multiple cell types in a single construct	Xu et al. (2013b)
Alginate/gelatin	Extrusion	Embryoid bodies	>90% cell viability with retention of pluripotent stem cell markers after printing	Ouyang et al. (2015b)
Alginate/gelatin	Extrusion		Storage modulus: 1–100 Pa Loss modulus: 0.1–10 kPa Increased holding time; storage modulus decreased cell viability but increased printability	Zhao et al. (2015)
Alginate/gelatin	Extrusion	Aortic valve	Modulus remains between 0.9 and 1.1 MPa over 7 days of incubation, cell-laden gels have lower moduli than cell-free gels, hydrogel's tensile strength and modulus decrease over time in culture	Duan et al. (2013)

(continued)

Table 2 (continued)

Materials	Printer	Application	Results of interest	Reference
Alginate/gelatin/fibrin	Extrusion	Embryonic tissues	Cells maintained function and proliferated within the architecture of the printed	Ouyang et al. (2015a)
Alginate/gelatin/fibrin	Extrusion	Model of energy metabolic system	Cells printed in 3D constructs had higher levels of metabolic activity than those in 2D	Xu et al. (2010)
Alginate/gelatin/fibrin	Extrusion	Cervical tumor model	Observed chemoresistance in 3D printed gels, but not in 2D culture studies	Zhao et al. (2014)
Collagen/fibrin	Inkjet	Cartilage	Young's modulus: 0.77 MPa Combined with electrospun PCL to make a strong scaffold	Xu et al. (2013a)
Gelatin/chitosan	Extrusion	Liver tissue	Showed liver cells maintain some functionality after being printed in a matrix	Yan et al. (2005)
GelMA/GG	Extrusion		Compressive modulus: 15–60 kPa (dose dependent on GG concentration)	Melchels et al. (2014)
GelMA/GG/PLA microcarriers (MCs)	Extrusion	Articular cartilage	Compressive modulus: 27–50 kPa (dose dependent on MC concentration) Cells remained on the surface and did not penetrate into MCs	Levato et al. (2014)
GelMA/HA	Extrusion	Cardiovascular patch	Patches help improve cardiac remodeling after 1 month in vivo	Gaetani et al. (2015)
HA-MA/adamantane/ β -cyclodextrin	Extrusion	Self-healing hydrogels	Printed structures with hollow geometries are self-supporting	Highley et al. (2015)

(continued)

Table 2 (continued)

Materials	Printer	Application	Results of interest	Reference
			after removal of support matrix	
HA-MA/gelatin ethanolamide methacrylate	Extrusion	Organ printing	Storage modulus: 10–90 Pa (dependent on crosslinking time)	Skardal et al. (2010)
HA-MA/GelMA	Extrusion	Heart valve	Modulus: 4–12 kPa Increasing GelMA concentration decreased modulus (contrary to most studies)	Duan et al. (2014)
PEGDA/acrylated peptides	Inkjet	Bone and cartilage	Initial compressive modulus: 35 kPa (increased to 50–70 kPa after osteo- or chondrogenesis for 21 days), decreased hMSC hypertrophy in chondrogenic differentiation on scaffolds	Gao et al. (2015b)
PEGDA/alginate	Extrusion	Aortic valves	Modulus: 10–75 kPa (dependent on ratio of MW 700 to MW 800 PEGDA) Printed constructs 1 cm in size with high cell viability	Hockaday et al. (2012)
PEGDA/alginate/nanoclay	Extrusion	Tough, complex hydrogels	Material returns to nominal shape after relaxation of uniaxial stretching 3× its size or 95% compressive strain	Hong et al. (2015)
PEGDA/GelMA	Inkjet	Bone and cartilage	Initial compressive modulus: 30–40 kPa (increased to 50–70 kPa after osteo- or chondrogenesis for 21 days)	Gao et al. (2015a)

(continued)

Table 2 (continued)

Materials	Printer	Application	Results of interest	Reference
PEGDA/GelMA	Inkjet	Periodontal ligament	Saw positive correlation between cell viability and GelMA to PEGDA ratio	Ma et al. (2015)
Silk fibroin/gelatin	Extrusion	Stem cell-laden tissue constructs	Storage modulus: 166–221 kPa (at 37 °C) and 530–751 kPa (at 18 °C) Tyrosinase crosslinked gels had higher moduli and were more stable long term than sonication crosslinked gels	Das et al. (2015)

being mixed in with the GelMA/GG bioink. This provided a dose-dependent mechanical enhancement of the matrix. The compressive modulus for the matrix was 27–28 kPa without microparticles, but increased to over 50 kPa with the addition of microparticles at a dose of 50 mg/mL (Levato et al. 2014). Thus, this system provided a homogeneous bioink that could enhance the mechanical properties of the printed material by using microcarriers, which in itself has potential applications in numerous areas for both growing cells and delivering growth factors. Both studies illustrated the utility of GelMA–GG bioinks in 3DP.

Another system used in several studies is alginate-gelatin combination bioinks (Chung et al. 2013; Duan et al. 2013; Ouyang et al. 2015b; Zhao et al. 2015). This combination is benefitted by the biocompatibility of both materials, the straightforward crosslinking capacity offered by alginate, and the thermo-controllable properties and cell adhesion provided by the gelatin in one system. One study by Zhao et al. sought to characterize the gelation ability of these types of bioinks and the rheological properties at a temperature of 20 °C (Zhao et al. 2015). They found that with minimal changes in alginate concentration (from 0% to 2%), the gelation temperature only minimally changed (from 21 to 22.5 °C). They also found that cell viability was dependent upon the holding temperature, i.e., the temperature at which the bioink was held prior to printing, as well as how long it was held at that temperature. Viability increased with increasing temperatures (from 10 to 20 °C), but decreased with longer holding times (from 5 to 30 min) (Zhao et al. 2015). A similar correlation was found in a study done by Ouyang et al. (2015b). In this investigation, the results showed that cell distribution was well maintained within the printed structure, even though the water-soluble gelatin was not modified to be crosslinkable (Ouyang et al. 2015b). Other studies have also looked at gelatin-alginate hybrids with the addition

of fibrinogen (Zhao et al. 2014; Ouyang et al. 2015a). A system of alginate-gelatin-fibrinogen provides the same benefits as an alginate-gelatin system, but the addition of fibrinogen further helps to stabilize the bioink and may offer an enhanced biomimetic environment through the formation of fibrin from the added fibrinogen (Zhao et al. 2014; Ouyang et al. 2015a). In another study by Ouyang et al., gelatin-alginate and a gelatin-alginate-fibrinogen scaffolds were compared, revealing minor differences in pore size (i.e., the distance between printed strands), thread diameter (i.e., the thickness of a printed strand), and distance between pores (Ouyang et al. 2015a). Hybrid single bioinks, such as the gelatin-alginate and gelatin-alginate-fibrinogen systems described here, have allowed investigators to capitalize on the synergy of material properties, showing potential in a wide range of applications.

4.4 Multiple Bioink Bioprinting

In contrast to a single bioink with multiple materials, multiple bioinks provide more room for complexity in design. Different regions within a single printed construct can be made from a unique bioink, without or without cells, to create localized environments (i.e., a heterogeneous tissue constructs). This provides advantages in engineering complex tissue structures such as interface tissues, wherein multiple microenvironments exist within a single tissue (Fedorovich et al. 2012). In addition, beyond simply printing soft hydrogels, further support materials and structures can be included in order to fabricate constructs with varied mechanical properties, which is advantageous in regenerative medicine applications for hard tissues. Here, we discuss examples of heterogeneous tissue applications, some of which are shown in Table 3.

An example of a multi-material and multi-bioink system is the printing of alginate with PCL (Schuurman et al. 2011; Lee et al. 2013; Kundu et al. 2015; Jung et al. 2016). In these examples, PCL was printed first as a hard material to support the structure of the alginate over the time course of the study (Schuurman et al. 2011; Lee et al. 2013; Kundu et al. 2015; Jung et al. 2016). Initial viability studies of the cells (C20A4, a chondrocyte cell line, and MC3T3-E1, preosteoblast cells) encapsulated in the alginate indicated that approximately 80% of the cells were alive (Schuurman et al. 2011; Lee et al. 2013). Interestingly, this viability decreased over a few days, toward 60%, which the authors hypothesized to be a result of heat shock from the printed PCL cooling (Schuurman et al. 2011). However, the PCL did result in improved mechanical properties of the larger construct. Printing PCL alongside alginate resulted in a higher Young's modulus for the construct (Schuurman et al. 2011; Lee et al. 2013). This method for enhancing mechanical properties of a construct, by providing a hard support structure, enables the printing of difficult to print hydrogel materials. This concept was also demonstrated in a study by Visser et al. in which thermoplastic materials were printed with hydrogels to form mechanically improved structures that better mimicked the anatomically important features of vascular trees and the right ear (Visser et al. 2013). In contrast, there are a handful of studies that have looked at using two different hydrogel materials to fabricate complex 3DP constructs.

Table 3 Multi-material hydrogels using multiple bioinks. Examples of studies that have used multiple bioinks for a single construct are listed here. This includes the materials used, the interactions of the materials, the printer used, the intended application, and results of interest, including mechanical properties, and results related to the use of multiple bioinks, as well as reference information

Materials	Material interactions	Printer	Application	Results of interest	Reference
Alginate/ alginate +biphasic calcium phosphate particles	Two distinct matrices side by side, interfacing on one side	Extrusion	Osteochondral grafts	Modulus: 4.5–15 kPa Saw heterogeneous tissue formation after implanting in vivo in nude mice	Fedorovich et al. (2012)
Gelatin/ ECM mix (collagen type 1/Matrigel/ fibrinogen/ HA)	ECM mix printed into gelatin slurry	Extrusion	Complex biological structures	Printed structures were similar to design parameters, such as the angle between arterial tree branches	Hinton et al. (2015)
GelMA/ Pluronic F127	Sacrificial networks (Pluronic F127) were surrounded by GelMA	Extrusion	Vascularized tissue	Cells in different bioinks only interacted with other cells/ materials at the interface of printed structures	Kolesky et al. (2014)
GelMA/ gellan/ PCL or alginate	PCL or alginate served as a sacrificial matrix for final hydrogel	Extrusion	Model of a distal femur (PCL) of box with tubes (alginate)	Hydrogel constructs were 1–4 cm in length/ width, indicating large constructs could be fabricated	Visser et al. (2013)
Matrigel/ alginate/ biphasic calcium particles	Two distinct matrices side by side, interfacing on one side	Extrusion	Vascularized bone	Saw distinct tissue formation in each matrix after 2 and 6 weeks implantation in vivo	Fedorovich et al. (2011)

One example using multiple hydrogel bioinks comes from a study by Kolesky et al. where the goal was to print a multi-material and multicellular tissue construct with pre-vasculature structures (Kolesky et al. 2014). GelMA (15% w/v) was used as the bulk material, while Pluronic F127 (40% w/v) was printed to later be sacrificed, in order to allow for channels that could later be lined with endothelial cells. Irgacure 2529 was used as a photoinitiator for UV crosslinking of the GelMA at 0.3% w/w in

the bioink. GelMA without cells was used to print the portions of the design that were not meant to contain cells. Cells used in the printing process included C3H/10T1/2 Clone 8 (10T1/2) cells, a fibroblast cell population, from ATCC, and human neonatal dermal fibroblasts (HDNFs) at densities of 2×10^6 cells/mL. Once the Pluronic F127 was sacrificed, human umbilical vein endothelial cells (HUVECs) were injected into the space at a density of 1×10^7 cells/mL. This innovative research illustrated the ability of cells to maintain and localize within a printed structure. In addition, printed gels showed a viability of 60–70% within a day after printing, which continued to increase to approximately 80% by 7 days after printing (Kolesky et al. 2014). This promising and innovative effort further highlighted 3DP technologies as a means for generating complex and multifaceted constructs consisting of multiple materials and cell types. As such, this investigation provides impetus for further investigation of multi-material and multicell hydrogel bioprinting.

One last example is from a study by Fedorovich et al. that aimed to create a heterogeneous scaffold to see if this heterogeneity is maintained after implantation in vivo (Fedorovich et al. 2011). To do this, two cell populations were used – goat endothelial progenitor cells (EPCs) and goat mesenchymal stem cells (MSCs). For materials, BD Matrigel was used to encapsulate EPCs at a density of 5×10^6 cells/mL gel, while MSCs were encapsulated in either alginate or growth factor-depleted Matrigel at a density of 5×10^6 cells/mL gel. The MSC-laden gel also included osteoinductive biphasic calcium phosphate (BCP) microparticles (106–212 μm in size) at 10% w/v to encourage formation of bone tissue. Calcium chloride solution (102 mM) was used to crosslink the alginate, while Matrigel formed a gel at room temperature. As with the vascularized tissue study, this group was able to show that each cell population stayed within the bounds of the printed area of its own bioink, with little to no interactions between the two cell types/materials. For the in vivo portion of the study, the group explanted the scaffolds at 2 and 6 weeks after implantation in subcutaneous dorsal pockets of nude mice and found that the construct maintained its heterogeneity. Blood vessels began to form after 2 weeks within the EPC-laden part of the construct, while bone and cartilage tissue formation were identified in the MSC-laden part of the construct. This study further indicates the promise of heterogeneous 3DP scaffolds by showing the ability of such constructs to be implanted in vivo while maintaining the heterogeneity of the construct.

5 Summary and Future Directions

Bioprinting of hydrogels has made great strides in the last decade. Four major bioprinting modalities have emerged in inkjet bioprinting, extrusion bioprinting, LAB, and SLA. While the former two have become extensively used by various labs with plenty of examples of custom-built bioprinters, the latter two are still in the growth stages and have yet to be fully exploited in their capabilities. Studies have been done to characterize the parameters associated with hydrogel bioprinting, but

more work can be done to further characterize and expand upon these studies for different materials and different cell populations. In addition, research is currently being carried out to better control the crosslinking of various biomaterials by trying new crosslinking methods, as well as attempting to enhance the precise control over thermal and ionically crosslinked polymers (Zhang et al. 2013; Bertassoni et al. 2014a; Highley et al. 2015; Hinton et al. 2015; Zhao et al. 2015). Future work is necessary to investigate modifications to materials which have the potential to provide a useful biomimetic environment, but are presently difficult to print, in order to fully utilize these materials as 3DP bioinks.

For multi-material hydrogels, work has been done evaluating both single, multi-component bioinks and multiple bioinks for generating complex heterogeneous constructs. While much of this work has been done using alginate, gelatin, HA, and/or PEG as the primary polymer, there remain other choices which could enhance the characteristics of the printed constructs. Using other natural polymers, such as collagen, Matrigel, fibrin, or ECM, in combination with synthetic polymers, such as polyurethanes or PEG copolymers, may result in improved printability and, ultimately, regenerative capacity of printed constructs (Fedorovich et al. 2008; Schuurman et al. 2011; Pati et al. 2014, 2015; Rutz et al. 2015; Tsai et al. 2015; Zhang et al. 2015; Hsieh et al. 2015; Lee et al. 2016).

Functionally, little of this work has been translated into the clinic. To date, a therapeutic device consisting of a bioprinted hydrogel construct containing cells, with or without the addition of other growth factors or signals, has yet to be approved by the FDA for clinical application. However, many groups have investigated printed constructs in animal models, indicating the significant progress made toward the goal of clinical translation (Fedorovich et al. 2011, 2012; Xu et al. 2013b; Pati et al. 2015). To this end, it is probable that future work will continue to focus on improved bioprinted tissue functionality with a greater extent of complex approaches being employed such as multicellular heterogeneous tissue constructs and 4D printing.

As it stands, hydrogel bioprinting has become established and continues to move forward, with many groups seeking to expand the limits of current bioprinting capabilities. With continued research in this area, we may find better solutions to existing problems and improve the outlook of the field of 3DP and tissue engineering as a whole.

Acknowledgments This work was supported by a seed grant from the Sheikh Zayed Institute for Pediatric Surgical Innovation at Children's National Medical Center and the A. James Clark School of Engineering at the University of Maryland. Additional funding was provided by the National Science Foundation/US Food and Drug Administration Scholar in Residence Program (CBET1445700). The content is solely the responsibility of the authors and does not necessarily represent the official views of these funding sources.

References

- Ahearne M, Coyle A (2016) Application of UVA-riboflavin crosslinking to enhance the mechanical properties of extracellular matrix derived hydrogels. *J Mech Behav Biomed Mater* 54:259–267. <https://doi.org/10.1016/j.jmbbm.2015.09.035>

- Akkineni AR, Luo Y, Schumacher M, Nies B, Lode A, Gelinsky M (2015) 3D plotting of growth factor loaded calcium phosphate cement scaffolds. *Acta Biomater* 27:264–274. <https://doi.org/10.1016/j.actbio.2015.08.036>
- Andrzejewska E (2001) Photopolymerization kinetics of multifunctional monomers. *Prog Polym Sci* 26:605–665. [https://doi.org/10.1016/S0079-6700\(01\)00004-1](https://doi.org/10.1016/S0079-6700(01)00004-1)
- Arcaute K, Mann BK, Wicker RB (2006) Stereolithography of three-dimensional bioactive poly (ethylene glycol) constructs with encapsulated cells. *Ann Biomed Eng* 34:1429–1441. <https://doi.org/10.1007/s10439-006-9156-y>
- Bakarich SE, in het Panhuis M, Beirne S, Wallace GG, Spinks GM (2013) Extrusion printing of ionic-covalent entanglement hydrogels with high toughness. *J Mater Chem B* 1:4939. <https://doi.org/10.1039/c3tb21159b>
- Barron JA, Ringeisen BR, Kim H, Spargo BJ, Chrisey DB (2004) Application of laser printing to mammalian cells. *Thin Solid Films* 453–454:383–387. <https://doi.org/10.1016/j.tsf.2003.11.161>
- Berger J, Reist M, Mayer JM, Felt O, Peppas NA, Gurny R (2004) Structure and interactions in covalently and ionically crosslinked chitosan hydrogels for biomedical applications. *Eur J Pharm Biopharm* 57:19–34. [https://doi.org/10.1016/S0939-6411\(03\)00161-9](https://doi.org/10.1016/S0939-6411(03)00161-9)
- Bertassoni LE, Cardoso JC, Manoharan V, Cristino AL, Bhise NS, Araujo WA, Zorlutuna P, Vrana NE, Ghaemmaghami AM, Dokmeci MR, Khademhosseini A (2014a) Direct-write bioprinting of cell-laden methacrylated gelatin hydrogels. *Biofabrication* 6:024105. <https://doi.org/10.1088/1758-5082/6/2/024105>
- Bertassoni LE, Cecconi M, Manoharan V, Nikkhah M, Hjortnaes J, Cristino AL, Barabaschi G, Demarchi D, Dokmeci MR, Yang Y, Khademhosseini A (2014b) Hydrogel bioprinted micro-channel networks for vascularization of tissue engineering constructs. *Lab Chip* 14:2202–2211. <https://doi.org/10.1039/c4lc00030g>
- Billiet T, Gevaert E, De Schryver T, Cornelissen M, Dubruel P (2014) The 3D printing of gelatin methacrylamide cell-laden tissue-engineered constructs with high cell viability. *Biomaterials* 35:49–62. <https://doi.org/10.1016/j.biomaterials.2013.09.078>
- Blaeser A, Duarte Campos DF, Puster U, Richtering W, Stevens MM, Fischer H (2016) Controlling shear stress in 3D bioprinting is a key factor to balance printing resolution and stem cell integrity. *Adv Healthc Mater* 3:326–333
- Bryant SJ, Nuttelman CR, Anseth KS (2000) Cytocompatibility of UV and visible light photo-initiating systems on cultured NIH/3T3 fibroblasts in vitro. *J Biomater Sci Polym Ed* 11:439–457. <https://doi.org/10.1163/156856200743805>
- Burdick JA, Prestwich GD (2011) Hyaluronic acid hydrogels for biomedical applications. *Adv Mater* 23:41–56. <https://doi.org/10.1002/adma.201003963>
- Carolina N (2012) Bioprinted amniotic fluid-derived stem cells accelerate healing of large skin wounds. *Stem Cells Transl Med* 1:792–802. <https://doi.org/10.5966/sctm.2012-0088>
- Cha C, Soman P, Zhu W, Nikkhah M, Camci-Unal G, Chen S, Khademhosseini A (2014) Structural reinforcement of cell-laden hydrogels with microfabricated three dimensional scaffolds. *Biomater Sci* 2:703–709. <https://doi.org/10.1039/C3BM60210A>
- Chan V, Zorlutuna P, Jeong JH, Kong H, Bashir R (2010) Three-dimensional photopatterning of hydrogels using stereolithography for long-term cell encapsulation. *Lab Chip* 10:2062–2070. <https://doi.org/10.1039/c004285d>
- Chen Y-C, Lin R-Z, Qi H, Yang Y, Bae H, Melero-Martin JM, Khademhosseini A (2012) Functional human vascular network generated in photocrosslinkable gelatin methacrylate hydrogels. *Adv Funct Mater* 22:2027–2039. <https://doi.org/10.1002/adfm.201101662>
- Chung JHY, Naficy S, Yue Z, Kapsa R, Quigley A, Moulton SE, Wallace GG (2013) Bio-ink properties and printability for extrusion printing living cells. *Biomater Sci* 1:763. <https://doi.org/10.1039/c3bm00012e>
- Cohen DL, Lipton JI, Bonassar LJ, Lipson H (2010) Additive manufacturing for in situ repair of osteochondral defects. *Biofabrication* 2:035004. <https://doi.org/10.1088/1758-5082/2/3/035004>
- Cui X, Breitenkamp K, Finn MG, Lotz M, D’Lima DD (2012) Direct human cartilage repair using three-dimensional bioprinting technology. *Tissue Eng Part A* 18:1304–1312. <https://doi.org/10.1089/ten.TEA.2011.0543>

- Das S, Pati F, Choi YJ, Rijal G, Shim JH, Kim SW, Ray AR, Cho DW, Ghosh S (2015) Bioprintable, cell-laden silk fibroin-gelatin hydrogel supporting multilineage differentiation of stem cells for fabrication of three-dimensional tissue constructs. *Acta Biomater* 11:233–246. <https://doi.org/10.1016/j.actbio.2014.09.023>
- Davey SK, Aung A, Agrawal G, Lim HL, Kar M, Varghese S (2015) Embedded 3D photopatterning of hydrogels with diverse and complex architectures for tissue engineering and disease models. *Tissue Eng Part C Methods* 21:1188–1196. <https://doi.org/10.1089/ten.TEC.2015.0179>
- Dhariwala B, Hunt E, Boland T (2004) Rapid prototyping of tissue-engineering constructs, using photopolymerizable hydrogels and stereolithography. *Tissue Eng* 10:1316–1322. <https://doi.org/10.1089/ten.2004.10.1316>
- Duan B, Hockaday LA, Kang KH, Butcher JT (2013) 3D Bioprinting of heterogeneous aortic valve conduits with alginate/gelatin hydrogels. *J Biomed Mater Res A* 101 A:1255–1264. <https://doi.org/10.1002/jbm.a.34420>
- Duan B, Kapetanovic E, Hockaday LA, Butcher JT (2014) Three-dimensional printed trileaflet valve conduits using biological hydrogels and human valve interstitial cells. *Acta Biomater* 10:1836–1846. <https://doi.org/10.1016/j.actbio.2013.12.005>
- Elomaa L, Teixeira S, Hakala R, Korhonen H, Grijpma DW, Seppälä JV (2011) Preparation of poly(ϵ -caprolactone)-based tissue engineering scaffolds by stereolithography. *Acta Biomater* 7:3850–3856. <https://doi.org/10.1016/j.actbio.2011.06.039>
- Elomaa L, Pan C-C, Shanjani Y, Malkovskiy A, Seppälä JV, Yang Y (2015) Three-dimensional fabrication of cell-laden biodegradable poly(ethylene glycol-co-depsipeptide) hydrogels by visible light stereolithography. *J Mater Chem B* 3:8348–8358. <https://doi.org/10.1039/C5TB01468A>
- Faulkner-Jones A, Fyfe C, Cornelissen D-J, Gardner J, King J, Courtney A, Shu W (2015) Bioprinting of human pluripotent stem cells and their directed differentiation into hepatocyte-like cells for the generation of mini-livers in 3D. *Biofabrication* 7:044102. <https://doi.org/10.1088/1758-5090/7/4/044102>
- Fedorovich NE, De Wijn JR, Verbout AJ, Alblas J, Dhert WJA (2008) Three-dimensional fiber deposition of cell-laden, viable, patterned constructs for bone tissue printing. *Tissue Eng Part A* 14:127–133. <https://doi.org/10.1089/ten.a.2007.0158>
- Fedorovich NE, Wijnberg HM, Dhert WJ, Alblas J (2011) Distinct tissue formation by heterogeneous printing of osteo – and endothelial progenitor cells. *Tissue Eng Part A* 17:2113–2121. <https://doi.org/10.1089/ten.tea.2011.0019>
- Fedorovich NE, Schuurman W, Wijnberg HM, Prins H-J, van Weeren PR, Malda J, Alblas J, Dhert WJA (2012) Biofabrication of osteochondral tissue equivalents by printing topologically defined, cell-laden hydrogel scaffolds. *Tissue Eng Part C Methods* 18:33–44. <https://doi.org/10.1089/ten.TEC.2011.0060>
- Ferlin KM, Prendergast ME, Miller ML, Kaplan DS, Fisher JP (2016) Influence of 3D printed porous architecture on mesenchymal stem cell enrichment and differentiation. *Acta Biomater* 32:161–169. <https://doi.org/10.1016/j.actbio.2016.01.007>
- Ferris CJ, Gilmore KG, Wallace GG, In Het Panhuis M (2013a) Biofabrication: an overview of the approaches used for printing of living cells. *Appl Microbiol Biotechnol* 97:4243–4258
- Ferris CJ, Gilmore KJ, Beirne S, McCallum D, Wallace GG, in het Panhuis M (2013b) Bio-ink for on-demand printing of living cells. *Biomater Sci* 1:224. <https://doi.org/10.1039/c2bm00114d>
- Florián-Algarín V, Acevedo-Rullán A, Co A, Leal GL, Colby RH, Giacomini AJ (2008) Rheology and gelation temperature of aqueous gelatin and sodium alginate solutions. In: *AIP Conference Proceedings*. AIP, pp 618–620
- Gaetani R, Feyen DAM, Verhage V, Slaats R, Messina E, Christman KL, Giacomello A, Doevendans PAFM, Sluijter JPG (2015) Epicardial application of cardiac progenitor cells in a 3D-printed gelatin/hyaluronic acid patch preserves cardiac function after myocardial infarction. *Biomaterials* 61:339–348. <https://doi.org/10.1016/j.biomaterials.2015.05.005>
- Galante R, Paradiso P, Moutinho MG, Fernandes AI, Mata JLG, Matos APA, Colaço R, Saramago B, Serro AP (2015) About the effect of eye blinking on drug release from pHEMA-based hydrogels: an in vitro study. *J Biomater Sci Polym Ed* 26:235–251. <https://doi.org/10.1080/09205063.2014.994948>

- Gao G, Schilling AF, Hubbell K, Yonezawa T, Truong D, Hong Y, Dai G, Cui X (2015a) Improved properties of bone and cartilage tissue from 3D inkjet-bioprinted human mesenchymal stem cells by simultaneous deposition and photocrosslinking in PEG-GelMA. *Biotechnol Lett* 37:2349–2355. <https://doi.org/10.1007/s10529-015-1921-2>
- Gao G, Yonezawa T, Hubbell K, Dai G, Cui X (2015b) Inkjet-bioprinted acrylated peptides and PEG hydrogel with human mesenchymal stem cells promote robust bone and cartilage formation with minimal printhead clogging. *Biotechnol J* 10:1568–1577. <https://doi.org/10.1002/biot.201400635>
- García-Millán E, Koprivnik S, Otero-Espinar FJ (2015) Drug loading optimization and extended drug delivery of corticoids from pHEMA based soft contact lenses hydrogels via chemical and microstructural modifications. *Int J Pharm* 487:260–269. <https://doi.org/10.1016/j.ijpharm.2015.04.037>
- Hanson Shepherd JN, Parker ST, Shepherd RF, Gillette MU, Lewis JA, Nuzzo RG (2011) 3D microperiodic hydrogel scaffolds for robust neuronal cultures. *Adv Funct Mater* 21:47–54. <https://doi.org/10.1002/adfm.201001746>
- He P, Liu Y, Qiao R (2014) Fluid dynamics of the droplet impact processes in cell printing. *Microfluid Nanofluidics* 18:569–585. <https://doi.org/10.1007/s10404-014-1470-3>
- Highley CB, Rodell CB, Burdick JA (2015) Direct 3D printing of shear-thinning hydrogels into self-healing hydrogels. *Adv Mater* 27:5075–5079. <https://doi.org/10.1002/adma.201501234>
- Hinton TJ, Jallerat Q, Palchesko RN, Park JH, Grodzicki MS, Shue H-J, Ramadan MH, Hudson AR, Feinberg AW (2015) Three-dimensional printing of complex biological structures by freeform reversible embedding of suspended hydrogels. *Sci Adv* 1:1–10. <https://doi.org/10.1126/sciadv.1500758>
- Hoare TR, Kohane DS (2008) Hydrogels in drug delivery: progress and challenges. *Polymer (Guildf)* 49:1993–2007. <https://doi.org/10.1016/j.polymer.2008.01.027>
- Hockaday LA, Kang KH, Colangelo NW, Cheung PYC, Duan B, Malone E, Wu J, Girardi LN, Bonassar LJ, Lipson H, Chu CC, Butcher JT (2012) Rapid 3D printing of anatomically accurate and mechanically heterogeneous aortic valve hydrogel scaffolds. *Biofabrication* 4:035005. <https://doi.org/10.1088/1758-5082/4/3/035005>
- Hong S, Sycks D, Chan HF, Lin S, Lopez GP, Guilak F, Leong KW, Zhao X (2015) 3D printing of highly stretchable and tough hydrogels into complex, cellularized structures. *Adv Mater* 27:4035–4040. <https://doi.org/10.1002/adma.201501099>
- Hsieh F-Y, Lin H-H, Hsu S-H (2015) 3D bioprinting of neural stem cell-laden thermoresponsive biodegradable polyurethane hydrogel and potential in central nervous system repair. *Biomaterials* 71:48–57. <https://doi.org/10.1016/j.biomaterials.2015.08.028>
- Hu J, Hou Y, Park H, Choi B, Hou S, Chung A, Lee M (2012) Visible light crosslinkable chitosan hydrogels for tissue engineering. *Acta Biomater* 8:1730–1738. <https://doi.org/10.1016/j.actbio.2012.01.029>
- Hynes RO (2002) Integrins: bidirectional, allosteric signaling machines. *Cell* 110:673–687. [https://doi.org/10.1016/S0092-8674\(02\)00971-6](https://doi.org/10.1016/S0092-8674(02)00971-6)
- Ifkovits JL, Burdick JA (2007) Review: photopolymerizable and degradable biomaterials for tissue engineering applications. *Tissue Eng* 13:2369–2385. <https://doi.org/10.1089/ten.2007.0093>
- Jung JW, Lee J-S, Cho D-W (2016) Computer-aided multiple-head 3D printing system for printing of heterogeneous organ/tissue constructs. *Sci Rep* 6:21685. <https://doi.org/10.1038/srep21685>
- Kesti M, Müller M, Becher J, Schnabelrauch M, D'Este M, Eglin D, Zenobi-Wong M (2015) A versatile bioink for three-dimensional printing of cellular scaffolds based on thermally and photo-triggered tandem gelation. *Acta Biomater* 11:162–172. <https://doi.org/10.1016/j.actbio.2014.09.033>
- Khalil S, Sun W (2007) Biopolymer deposition for freeform fabrication of hydrogel tissue constructs. *Mater Sci Eng C* 27:469–478. <https://doi.org/10.1016/j.msec.2006.05.023>
- Koch L, Deiwick A, Schlie S, Michael S, Gruene M, Coger V, Zychlinski D, Schambach A, Reimers K, Vogt PM, Chichkov B (2012) Skin tissue generation by laser cell printing. *Biotechnol Bioeng* 109:1855–1863. <https://doi.org/10.1002/bit.24455>

- Kolesky DB, Truby RL, Gladman AS, Busbee TA, Homan KA, Lewis JA (2014) 3D bioprinting of vascularized, heterogeneous cell-laden tissue constructs. *Adv Mater* 26:3124–3130. <https://doi.org/10.1002/adma.201305506>
- Kundu J, Shim J-H, Jang J, Kim S-W, Cho D-W (2015) An additive manufacturing-based PCL-alginate-chondrocyte bioprinted scaffold for cartilage tissue engineering. *J Tissue Eng Regen Med* 9:1286–1297. <https://doi.org/10.1002/term.1682>
- Lee W, Debasitis JC, Lee VK, Lee J-H, Fischer K, Edminster K, Park J-K, Yoo S-S (2009) Multi-layered culture of human skin fibroblasts and keratinocytes through three-dimensional freeform fabrication. *Biomaterials* 30:1587–1595. <https://doi.org/10.1016/j.biomaterials.2008.12.009>
- Lee Y-B, Polio S, Lee W, Dai G, Menon L, Carroll RS, Yoo S-S (2010) Bio-printing of collagen and VEGF-releasing fibrin gel scaffolds for neural stem cell culture. *Exp Neurol* 223:645–652. <https://doi.org/10.1016/j.expneurol.2010.02.014>
- Lee H, Ahn S, Bonassar LJ, Kim G (2013) Cell(MC3T3-E1)-printed poly(ϵ -caprolactone)/alginate hybrid scaffolds for tissue regeneration. *Macromol Rapid Commun* 34:142–149. <https://doi.org/10.1002/marc.201200524>
- Lee VK, Lanzi AM, Ngo H, Yoo SS, Vincent PA, Dai G (2014) Generation of multi-scale vascular network system within 3D hydrogel using 3D bio-printing technology. *Cell Mol Bioeng* 7:460–472. <https://doi.org/10.1007/s12195-014-0340-0>
- Lee JW, Choi YJ, Yong WJ, Pati F, Shim JH, Kang KS, Kang IH, Park J, Cho DW (2016) Development of a 3D cell printed construct considering angiogenesis for liver tissue engineering. *Biofabrication* 8:15007. <https://doi.org/10.1088/1758-5090/8/1/015007>
- Levato R, Visser J, Planell JA, Engel E, Malda J, Mateos-Timoneda MA (2014) Biofabrication of tissue constructs by 3D bioprinting of cell-laden microcarriers. *Biofabrication* 6:035020. <https://doi.org/10.1088/1758-5082/6/3/035020>
- Li B, Wang L, Xu F, Gang X, Demirci U, Wei D, Li Y, Feng Y, Jia D, Zhou Y (2015) Hydrosoluble, UV-crosslinkable and injectable chitosan for patterned cell-laden microgel and rapid transdermal curing hydrogel in vivo. *Acta Biomater* 22:59–69. <https://doi.org/10.1016/j.actbio.2015.04.026>
- Lin H, Zhang D, Alexander PG, Yang G, Tan J, Cheng AW-M, Tuan RS (2013) Application of visible light-based projection stereolithography for live cell-scaffold fabrication with designed architecture. *Biomaterials* 34:331–339. <https://doi.org/10.1016/j.biomaterials.2012.09.048>
- Ma Y, Ji Y, Huang G, Ling K, Zhang X, Xu F (2015) Bioprinting 3D cell-laden hydrogel microarray for screening human periodontal ligament stem cell response to extracellular matrix. *Biofabrication* 7:044105. <https://doi.org/10.1088/1758-5090/7/4/044105>
- Mapili G, Lu Y, Chen S, Roy K (2005) Laser-layered microfabrication of spatially patterned functionalized tissue-engineering scaffolds. *J Biomed Mater Res B Appl Biomater* 75:414–424. <https://doi.org/10.1002/jbm.b.30325>
- Markstedt K, Mantas A, Tournier I, Martínez Ávila H, Hägg D, Gatenholm P (2015) 3D bioprinting human chondrocytes with nanocellulose-alginate bioink for cartilage tissue engineering applications. *Biomacromolecules* 16:1489–1496. <https://doi.org/10.1021/acs.biomac.5b00188>
- Melchels FPW, Feijen J, Grijpma DW (2009) A poly(D,L-lactide) resin for the preparation of tissue engineering scaffolds by stereolithography. *Biomaterials* 30:3801–3809. <https://doi.org/10.1016/j.biomaterials.2009.03.055>
- Melchels FPW, Feijen J, Grijpma DW (2010) A review on stereolithography and its applications in biomedical engineering. *Biomaterials* 31:6121–6130. <https://doi.org/10.1016/j.biomaterials.2010.04.050>
- Melchels FPW, Dhert WJA, Huttmacher DW, Malda J (2014) Development and characterisation of a new bioink for additive tissue manufacturing. *J Mater Chem B* 2:2282. <https://doi.org/10.1039/c3tb21280g>
- Mironi-Harpaz I, Wang DY, Venkatraman S, Seliktar D (2012) Photopolymerization of cell-encapsulating hydrogels: crosslinking efficiency versus cytotoxicity. *Acta Biomater* 8:1838–1848. <https://doi.org/10.1016/j.actbio.2011.12.034>

- Mohanty S, Alm M, Hemmingsen M, Dolatshahi-Pirouz A, Trifol J, Thomsen P, Dufva M, Wolff A, Emnéus J (2016) 3D printed silicone-hydrogel scaffold with enhanced physicochemical properties. *Biomacromolecules* 17:1321. <https://doi.org/10.1021/acs.biomac.5b01722>
- Moraes C, Simon AB, Putnam AJ, Takayama S (2013) Aqueous two-phase printing of cell-containing contractile collagen microgels. *Biomaterials* 34:9623–9631. <https://doi.org/10.1016/j.biomaterials.2013.08.046>
- Müller M, Becher J, Schnabelrauch M, Zenobi-Wong M (2015) Nanostructured pluronic hydrogels as bioinks for 3D bioprinting. *Biofabrication* 7:035006. <https://doi.org/10.1088/1758-5090/7/3/035006>
- Murphy SV, Atala A (2014) 3D bioprinting of tissues and organs. *Nat Biotechnol* 32:773–785. <https://doi.org/10.1038/nbt.2958>
- Nair K, Gandhi M, Khalil S, Yan KC, Marcolongo M, Barbee K, Sun W (2009) Characterization of cell viability during bioprinting processes. *Biotechnol J* 4:1168–1177. <https://doi.org/10.1002/biot.200900004>
- Nakamura M, Kobayashi A, Takagi F, Watanabe A, Hiruma Y, Ohuchi K, Iwasaki Y, Horie M, Morita I, Takatani S (2005) Biocompatible inkjet printing technique for designed seeding of individual living cells. *Tissue Eng* 11:1658–1666. <https://doi.org/10.1089/ten.2005.11.1658>
- Ouyang L, Yao R, Chen X, Na J, Sun W (2015a) 3D printing of HEK 293FT cell-laden hydrogel into macroporous constructs with high cell viability and normal biological functions. *Biofabrication* 7:015010. <https://doi.org/10.1088/1758-5090/7/1/015010>
- Ouyang L, Yao R, Mao S, Chen X, Na J, Sun W (2015b) Three-dimensional bioprinting of embryonic stem cells directs highly uniform embryoid body formation. *Biofabrication* 7:044101. <https://doi.org/10.1088/1758-5090/7/4/044101>
- Ovsianikov A, Gruene M, Pflaum M, Koch L, Maiorana F, Wilhelmi M, Haverich A, Chichkov B (2010) Laser printing of cells into 3D scaffolds. *Biofabrication* 2:014104. <https://doi.org/10.1088/1758-5082/2/1/014104>
- Park JY, Shim J-H, Choi S-A, Jang J, Kim M, Lee SH, Cho D-W (2015) 3D printing technology to control BMP-2 and VEGF delivery spatially and temporally to promote large-volume bone regeneration. *J Mater Chem B* 3:5415–5425. <https://doi.org/10.1039/C5TB00637F>
- Pataky K, Braschler T, Negro A, Renaud P, Lutolf MP, Brugger J (2012) Microdrop printing of hydrogel bioinks into 3D tissue-like geometries. *Adv Mater* 24:391–396. <https://doi.org/10.1002/adma.201102800>
- Pati F, Jang J, Ha D-H, Won Kim S, Rhie J-W, Shim J-H, Kim D-H, Cho D-W (2014) Printing three-dimensional tissue analogues with decellularized extracellular matrix bioink. *Nat Commun* 5:3935. <https://doi.org/10.1038/ncomms4935>
- Pati F, Ha D-H, Jang J, Han HH, Rhie JW, Cho DW (2015) Biomimetic 3D tissue printing for soft tissue regeneration. *Biomaterials* 62:164–175. <https://doi.org/10.1016/j.biomaterials.2015.05.043>
- Pereira RF, Bártolo PJ (2015) 3D bioprinting of photocrosslinkable hydrogel constructs. *J Appl Polym Sci* 132. <https://doi.org/10.1002/app.42458>
- Petit V, Thiery J-P (2000) Focal adhesions: structure and dynamics. *Biol Cell* 92:477–494. [https://doi.org/10.1016/S0248-4900\(00\)01101-1](https://doi.org/10.1016/S0248-4900(00)01101-1)
- Pietrucha K (2005) Changes in denaturation and rheological properties of collagen-hyaluronic acid scaffolds as a result of temperature dependencies. *Int J Biol Macromol* 36:299–304. <https://doi.org/10.1016/j.ijbiomac.2005.07.004>
- Qiu Y, Park K (2001) Environment-sensitive hydrogels for drug delivery. *Adv Drug Deliv Rev* 53:321–339. [https://doi.org/10.1016/S0169-409X\(01\)00203-4](https://doi.org/10.1016/S0169-409X(01)00203-4)
- Rezende RA, Bártolo PJ, Mendes A, Filho RM (2009) Rheological behavior of alginate solutions for biomanufacturing. *J Appl Polym Sci* 113:3866–3871. <https://doi.org/10.1002/app.30170>
- Ringeisen BR, Kim H, Barron JA, Krizman DB, Chrisey DB, Jackman S, Auyeung RYC, Spargo BJ (2004) Laser printing of pluripotent embryonal carcinoma cells. *Tissue Eng* 10:483–491. <https://doi.org/10.1089/107632704323061843>

- Roth EA, Xu T, Das M, Gregory C, Hickman JJ, Boland T (2004) Inkjet printing for high-throughput cell patterning. *Biomaterials* 25:3707–3715. <https://doi.org/10.1016/j.biomaterials.2003.10.052>
- Rouillard AD, Berglund CM, Lee JY, Polacheck WJ, Tsui Y, Bonassar LJ, Kirby BJ (2011) Methods for photocrosslinking alginate hydrogel scaffolds with high cell viability. *Tissue Eng Part C Methods* 17:173–179. <https://doi.org/10.1089/ten.TEC.2009.0582>
- Rutz AL, Hyland KE, Jakus AE, Burghardt WR, Shah RN (2015) A multimaterial bioink method for 3D printing tunable, cell-compatible hydrogels. *Adv Mater* 27:1607–1614. <https://doi.org/10.1002/adma.201405076>
- Schmedlen RH, Masters KS, West JL (2002) Photocrosslinkable polyvinyl alcohol hydrogels that can be modified with cell adhesion peptides for use in tissue engineering. *Biomaterials* 23:4325–4332. [https://doi.org/10.1016/S0142-9612\(02\)00177-1](https://doi.org/10.1016/S0142-9612(02)00177-1)
- Schuurman W, Khristov V, Pot MW, van Weeren PR, Dhert WJA, Malda J (2011) Bioprinting of hybrid tissue constructs with tailorable mechanical properties. *Biofabrication* 3:021001. <https://doi.org/10.1088/1758-5082/3/2/021001>
- Schuurman W, Levett PA, Pot MW, van Weeren PR, Dhert WJA, Huttmacher DW, Melchels FPW, Klein TJ, Malda J (2013) Gelatin-methacrylamide hydrogels as potential biomaterials for fabrication of tissue-engineered cartilage constructs. *Macromol Biosci* 13:551–561. <https://doi.org/10.1002/mabi.201200471>
- Sher P, Oliveira SM, Borges J, Mano JF (2015) Assembly of cell-laden hydrogel fiber into non-liquefied and liquefied 3D spiral constructs by perfusion-based layer-by-layer technique. *Biofabrication* 7:011001. <https://doi.org/10.1088/1758-5090/7/1/011001>
- Shim J-H, Lee J-S, Kim JY, Cho D-W (2012) Bioprinting of a mechanically enhanced three-dimensional dual cell-laden construct for osteochondral tissue engineering using a multi-head tissue/organ building system. *J Micromech Microeng* 22:085014. <https://doi.org/10.1088/0960-1317/22/8/085014>
- Skardal A, Atala A (2015) Biomaterials for integration with 3-D bioprinting. *Ann Biomed Eng* 43:730–746. <https://doi.org/10.1007/s10439-014-1207-1>
- Skardal A, Zhang J, McCoard L, Xu X, Oottamasathien S, Prestwich GD (2010) Photocrosslinkable hyaluronan-gelatin hydrogels for two-step bioprinting. *Tissue Eng Part A* 16:2675–2685. <https://doi.org/10.1089/ten.TEA.2009.0798>
- Smith CM, Stone AL, Parkhill RL, Stewart RL, Simpkins MW, Kachurin AM, Warren WL, Williams SK (2004) Three-dimensional bioassembly tool for generating viable tissue-engineered constructs. *Tissue Eng* 10:1566–1576. <https://doi.org/10.1089/ten.2004.10.1566>
- Smith CM, Christian JJ, Warren WL, Williams SK (2007) Characterizing environmental factors that impact the viability of tissue-engineered constructs fabricated by a direct-write bioassembly tool. *Tissue Eng* 13:373–383. <https://doi.org/10.1089/ten.2006.0101>
- Song SJ, Choi J, Park YD, Hong S, Lee JJ, Ahn CB, Choi H, Sun K (2011) Sodium alginate hydrogel-based bioprinting using a novel multinozzle bioprinting system. *Artif Organs* 35:1132–1136. <https://doi.org/10.1111/j.1525-1594.2011.01377.x>
- Tabriz AG, Hermida MA, Leslie NR, Shu W (2015) Three-dimensional bioprinting of complex cell laden alginate hydrogel structures. *Biofabrication* 7:045012. <https://doi.org/10.1088/1758-5090/7/4/045012>
- Takada Y, Ye X, Simon S (2007) The integrins. *Genome Biol* 8(215). <https://doi.org/10.1186/gb-2007-8-5-215>
- Tsai YC, Li S, SG H, Chang WC, Jeng US, Hsu SH (2015) Synthesis of thermoresponsive amphiphilic polyurethane gel as a new cell printing material near body temperature. *ACS Appl Mater Interfaces* 7:27613–27623. <https://doi.org/10.1021/acsami.5b10697>
- Visser J, Peters B, Burger TJ, Boomstra J, Dhert WJA, Melchels FPW, Malda J (2013) Biofabrication of multi-material anatomically shaped tissue constructs. *Biofabrication* 5:035007. <https://doi.org/10.1088/1758-5082/5/3/035007>
- Wallace J, Wang MO, Thompson P, Busso M, Belle V, Mammoser N, Kim K, Fisher JP, Siblani A, Xu Y, Welter JF, Lennon DP, Sun J, Caplan AI, Dean D (2014) Validating continuous digital

- light processing (cDLP) additive manufacturing accuracy and tissue engineering utility of a dye-initiator package. *Biofabrication* 6:015003. <https://doi.org/10.1088/1758-5082/6/1/015003>
- Wang W, Huang Y, Grujicic M, Chrisey DB (2008) Study of impact-induced mechanical effects in cell direct writing using smooth particle hydrodynamic method. *J Manuf Sci Eng* 130:021012. <https://doi.org/10.1115/1.2896118>
- Wang MO, Piard CM, Melchiorri A, Dreher ML, Fisher JP (2015a) Evaluating changes in structure and cytotoxicity during in vitro degradation of three-dimensional printed scaffolds. *Tissue Eng Part A* 21:1642–1653. <https://doi.org/10.1089/ten.TEA.2014.0495>
- Wang Z, Zhang Y, Zhu J, Dong S, Jiang T, Zhou Y, Zhang X (2015b) In vitro investigation of a tissue-engineered cell-tendon complex mimicking the transitional architecture at the ligament-bone interface. *J Biomater Appl* 29:1180–1192. <https://doi.org/10.1177/0885328214555168>
- Wei J, Wang J, Su S, Wang S, Qiu J, Zhang Z, Christopher G, Ning F, Cong W (2015) 3D printing of an extremely tough hydrogel. *RSC Adv* 5:81324–81329. <https://doi.org/10.1039/C5RA16362E>
- Williams CG, Malik AN, Kim TK, Manson PN, Elisseff JH (2005) Variable cytocompatibility of six cell lines with photoinitiators used for polymerizing hydrogels and cell encapsulation. *Biomaterials* 26:1211–1218. <https://doi.org/10.1016/j.biomaterials.2004.04.024>
- Xu Y, Wang X (2015) Fluid and cell behaviors along a 3D printed alginate/gelatin/fibrin channel. *Biotechnol Bioeng* 112:1683–1695. <https://doi.org/10.1002/bit.25579>
- Xu T, Jin J, Gregory C, Hickman JJJ, Boland T (2005) Inkjet printing of viable mammalian cells. *Biomaterials* 26:93–99. <https://doi.org/10.1016/j.biomaterials.2004.04.011>
- Xu T, Zhao W, Atala A, Yoo JJ, Forest W, Salem W (2006) Bio-printing of living organized tissues using an inkjet technology. *FASEB J* 21:131–134
- Xu M, Wang X, Yan Y, Yao R, Ge Y (2010) An cell-assembly derived physiological 3D model of the metabolic syndrome, based on adipose-derived stromal cells and a gelatin/alginate/fibrinogen matrix. *Biomaterials* 31:3868–3877. <https://doi.org/10.1016/j.biomaterials.2010.01.111>
- Xu T, Zhao W, Zhu JM, Albanna MZ, Yoo JJ, Atala A (2013a) Complex heterogeneous tissue constructs containing multiple cell types prepared by inkjet printing technology. *Biomaterials* 34:130–139. <https://doi.org/10.1016/j.biomaterials.2012.09.035>
- Xu T, Binder KW, Albanna MZ, Dice D, Zhao W, Yoo JJ, Atala A (2013b) Hybrid printing of mechanically and biologically improved constructs for cartilage tissue engineering applications. *Biofabrication* 5:015001. <https://doi.org/10.1088/1758-5082/5/1/015001>
- Yan Y, Wang X, Pan Y, Liu H, Cheng J, Xiong Z, Lin F, Wu R, Zhang R, Lu Q (2005) Fabrication of viable tissue-engineered constructs with 3D cell-assembly technique. *Biomaterials* 26:5864–5871. <https://doi.org/10.1016/j.biomaterials.2005.02.027>
- Yu Y, Zhang Y, Martin JA, Ozbolat IT (2013) Evaluation of cell viability and functionality in vessel-like bioprintable cell-laden tubular channels. *J Biomech Eng* 135:91011. <https://doi.org/10.1115/1.4024575>
- Zhang Y, Yu Y, Chen H, Ozbolat IT (2013) Characterization of printable cellular micro-fluidic channels for tissue engineering. *Biofabrication* 5:025004. <https://doi.org/10.1088/1758-5082/5/2/025004>
- Zhang M, Vora A, Han W, Wojtecki RJ, Maune H, Le ABA, Thompson LE, McClelland GM, Ribet F, Engler AC, Nelson A (2015) Dual-responsive hydrogels for direct-write 3D printing. *Macromolecules* 48:6482–6488. <https://doi.org/10.1021/acs.macromol.5b01550>
- Zhao Y, Yao R, Ouyang L, Ding H, Zhang T, Zhang K, Cheng S, Sun W (2014) Three-dimensional printing of Hela cells for cervical tumor model in vitro. *Biofabrication* 6:035001. <https://doi.org/10.1088/1758-5082/6/3/035001>
- Zhao Y, Li Y, Mao S, Sun W, Yao R (2015) The influence of printing parameters on cell survival rate and printability in microextrusion-based 3D cell printing technology. *Biofabrication* 7:045002. <https://doi.org/10.1088/1758-5090/7/4/045002>



Scaffold-Free Biofabrication

Ana Raquel Verissimo and Koichi Nakayama

Contents

1	Introduction	432
2	Scaffold-Free Tissue Engineering	432
3	Classification of Existing Scaffold-Free Systems	434
4	Aggregation/Spheroid-Based Approaches	435
5	Preparation of Multicellular Spheroids and Construct Design	437
6	Bioprinting Methods and Equipment	439
7	Applications	440
7.1	Blood Vessels	440
7.2	Kidney	441
7.3	Liver Regeneration	442
7.4	Periodontal Regeneration	442
7.5	Cartilage	443
8	Advantages and Challenges	443
9	Conclusions	445
	References	446

Electronic supplementary material: The online version of this chapter (https://doi.org/10.1007/978-3-319-45444-3_16) contains supplementary material, which is available to authorized users.

A. R. Verissimo (✉)

Department of Regenerative Medicine and Biomedical Engineering, Faculty of Medicine, Saga University, Saga, Japan

Vascular Surgery Group, Department of Cardiovascular Sciences, University of Leicester, Leicester, UK

e-mail: ana.verissimo@nakayama-labs.com; av127@le.ac.uk

K. Nakayama

Department of Regenerative Medicine and Biomedical Engineering, Faculty of Medicine, Saga University, Saga, Japan

e-mail: ko.nakayama@gmail.com

Abstract

Tissue engineering and regenerative medicine have met great scientific, medical, and technological advances in the past decade. Most methods combine scaffolds, such as polymers, and living cells to make implantable structures that will integrate and heal the host's tissues. More recently, alternative scaffold-free approaches have started to emerge. This chapter provides an overview of the current scaffold-free systems, advantages, challenges, methods, and applications. Scaffold-free tissue artificially produced in the lab using patients' own cells has already been successfully used in heart and blood vessel regeneration at a small scale. New techniques and approaches are being developed, not only in terms of assembling cells and structures but also in terms of new equipment, namely for 3D bioprinting. Both primary and stem or iPSC-derived cells are used to assemble artificial tissues that are currently being tested *in vivo* and *in vitro*. These engineered constructs have numerous applications, such as regenerative medicine, disease models, and drug testing.

1 Introduction

Until recently, most studies on tissue function, whether normal or in pathological conditions, were performed using either *in vivo* models that do not always behave in the same way as the human body does and can at times raise ethical issues (Festing and Wilkinson 2007; Mak et al. 2014; Denayer et al. 2014) or 2D *in vitro* models, which fail to provide the adequate environment for cells to maintain their normal features and behavior. A step forward was taken when 3D cultures were developed where cells are cultured with or without exogenous extracellular matrix, in a much more *in vivo*-like environment (Edmondson et al. 2014).

In recent years, the fields of tissue engineering and tissue regeneration have undergone rapid growth and evolution to overcome these difficulties and create more realistic models and solutions. Many materials have been developed as scaffolds, which provide a template, with predefined geometry, where cells can attach, expand, and even differentiate (O'Brien 2011). Alternative approaches, termed scaffold-free, are also employed in regenerative medicine and tissue engineering.

2 Scaffold-Free Tissue Engineering

Scaffold-free methods had their infancy in the early 1990s (Yamada et al. 1990) but have somewhat developed slower than those using scaffolds, mainly due to the structural challenges of building complex geometries and relatively big structures without rigid support (Czajka et al. 2014). The advent of new technologies and better understanding of developmental processes and cell manipulation have led to advances and expansion of these methodologies.

The definition of scaffold-free tissue engineering still remains unclear and controversial, loosely meaning the production of living tissue using cells only and relying on them to produce their own matrix and architecture. Athanasiou et al. (2013) have stated that “scaffoldless tissue engineering refers to any platform that does not require cell seeding or adherence within an exogenous, three-dimensional material.”

In a review concerning current scaffold-based and scaffold-free bioprinting methods, decellularized matrix components, as well as hydrogels and microcarriers, were classed as scaffold-based bioprinting. As for the scaffoldless counterpart, it was pointed out that the absence of hydrogels and higher cell density, more similar to naturally occurring tissues, affords quicker fusion and maturation (Ozbolat 2015). Elsewhere, it is stated that the current two methods for making scaffold-free tissue engineered vascular grafts are sheet seeding and decellularizing/recellularizing (Lee et al. 2016). The latter was considered scaffold-free, as the scaffold used to create the vessel was highly degradable, leaving behind a robust tissue that could be decellularized and applied *in vivo*, with or without recellularization. Complete organ decellularization has also been achieved for kidney, liver, lung, and heart (Orlando et al. 2013; Gilpin et al. 2014; Guyette et al. 2014; Mazza et al. 2015). If the first example, after decellularization, is considered a scaffold-free approach, by comparison, so should the latter ones. However, using a scaffold, even if of natural origin, to produce a scaffold-free structure seems rather contradictory. Additionally, hepatocyte spheroids aggregated without the addition of exogenous scaffolds and then encapsulated in hydrogels for further assemblage and implantation (without a bioprinting step) were also classed as scaffold-free. The distinction used in this chapter, whether referring to the initial process of cell aggregation or subsequent steps, such as bioprinting, accepts that the final tissue should remain scaffold-free at the time of implantation or testing. Temporary scaffold or hydrogel materials may be used, so long as they do not form part of the final tissue. They only lend structural support to keep the structure together until the cells or spheroids start to grow and fuse. Ideally, these substances should remain in the living structures for as little as possible and be easily removable by either physical peel or chemical or thermal processes.

Another concept, or area of research, that relates to tissue engineering and regenerative medicine is biofabrication. With the recent explosion in the development and availability of 3D bioprinters and associated methods, materials, equipment, and accessories, “biofabrication” has expanded accordingly. Presently, and in this context, biofabrication has been widely used as synonymous of 3D bioprinting and terminology is somewhat confusing. However, the concept is not new and represents different processes and materials in different disciplines. A definition harmonizing bioprinting and bioassembly for tissue engineering and regenerative medicine has been recently proposed as “the automated generation of biologically functional products with structural organization from living cells, bioactive molecules, biomaterials, cell aggregates such as micro-tissues, or hybrid cell-material constructs, through Bioprinting or Bioassembly and subsequent tissue maturation processes” (Groll et al. 2016). Thus, the two concepts are complementary.

In the same way, more traditional definitions of tissue engineering, such as “understanding the principles of tissue growth, and applying this to produce functional replacement tissue for clinical use” (MacArthur and Oreffo 2005), are now being expanded to other applications, such as *in vitro* models for disease or drug screening (Vunjak et al. 2014). As the tissues made for clinical uses are becoming more realistic, it makes sense that they can also be used as *in vitro* models. Therefore, in a wider interpretation of these notions, scaffold-free stand-alone functional models, such as organoids, that do not necessarily constitute the building blocks for bigger structures or are produced by automated methods will also be discussed in this chapter.

3 Classification of Existing Scaffold-Free Systems

Existing scaffold-free systems can be classified according to the type of building blocks used (cell sheets, isolated single cells or spheroid cell aggregates) or the processes involved in the formation of the artificial tissues or building blocks.

Self-organization is achieved by using external forces (for example, bioprinting and cell sheets), and self-assembly relies on spontaneous events without any external forces (nonadherent substrates are used so that the cells can carry out all the events with minimal intervention, such as spheroid formation). Both processes of self-organization and self-assembly produce highly biomimetic tissues that are capable of looking and behaving in a similar fashion to the native tissues they recreate, thus holding potential for clinical applications (Athanasidou et al. 2013).

The very first cell sheets for clinical application were developed by Rheinwald and Green in 1975. They used keratinocytes to produce sheets that were applied onto sites of severe burns. Over the years, these grafts have been refined and are now in clinical use, approved by the FDA (Phillips 1998).

Fifteen years later, an enzyme-free method for cell sheet detachment was developed, using poly(*N*-isopropylacrylamide), which is temperature-responsive (Fig. 1a). Below 32 °C the material becomes hydrophilic, which results in cell detachment (Yamada et al. 1990; Okano et al. 1993). The method can be used for more fragile sheets and does not require feeder cells. This has successfully been used to produce implantable engineered tissues for clinical repair, such as skin (O'Connor et al. 1981), cornea (Nishida et al. 2004), esophagus (Ohki et al. 2009), and heart muscle (Sawa et al. 2012). Recently, the same group has developed an automated cell culture system and fabricated corneal epithelial cell sheets were successfully implanted into rabbits, allowing regeneration on a limbal epithelial stem cell deficiency model (Kobayashi et al. 2013).

Cell sheets can be produced individually and then rolled on top of each other (Fig. 1b). Initial studies have shown that it was possible to build blood vessel-like structures without the use of scaffolds. Overlaying a sheet of fibroblasts over a sheet of smooth muscle cells and then seeding endothelial cells on the lumen produced a three-layered structure, able of synthesizing extracellular matrix proteins usually found in blood vessels, such as elastin and collagen. Furthermore, the cells expressed the correct cell differentiation markers and were able to perform functions such as platelet adhesion inhibition (L'Heureux et al. 1998). The most notable advancement

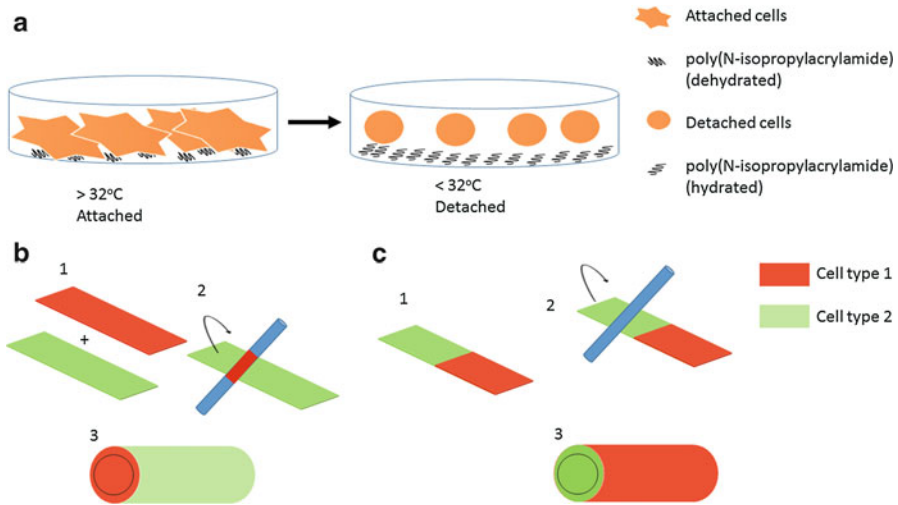


Fig. 1 Scaffold-free systems: cell sheets. (a) Poly(*N*-isopropylacrylamide) is a temperature-responsive polymer that is used to coat cell culture dishes. In aqueous solutions, above 32 °C, the molecule is dehydrated, which allows cell attachment. Below that lower critical solution temperature, the molecule will be hydrated and swollen, which results in cell detachment. (b) Cell sheets of the same or different cell types can be detached from the culture vessel and rolled on top of each other to form multilayered tissues. (c) Alternatively, two or more cell types can be grown in different areas of the same sheet, and then rolled onto each other in a single-step procedure

was the strength of the construct, which could cope with physiological pressure and allowed in vivo grafting. This was where promising earlier attempts had failed (Weinberg and Bell 1986; L’Heureux et al. 1993; Hirai and Matsuda 1996). When this approach was first developed, it would take around 5 months to obtain the final product. This technique is still widely used and has been refined along the years.

An alternative single-step method has also been developed, where two cell types, vascular smooth muscle cells and fibroblasts in this case, were separately seeded on each half of a gelatin-coated plate, divided by a spacer, which was removed 24 h later. The cells were allowed to grow and migrate towards each other, to form a continuous monolayer with two distinct halves. When ready, the sheet was rolled onto a tubular support, allowing the fibroblasts to be placed on top of the smooth muscle cells, without the need for extra steps (Fig. 1c). Compared to the traditional two-step method, apart from saving time, these constructs showed improved mechanical properties, such as strength and viscoelastic behavior (Gauvin et al. 2010).

4 Aggregation/Spheroid-Based Approaches

Self-assembly approaches such as spheroid formation can use one (homocellular) or multiple (heterocellular) cell types to produce spheroids of controllable size and shape. The aggregates can form by a variety of methods, such as the rotating wall

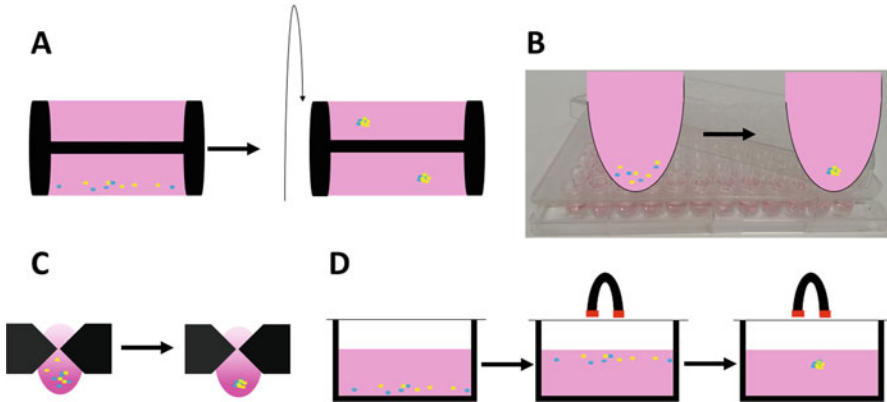


Fig. 2 Scaffold-free systems: spheroids. Homo- or heterocellular spheroids can be obtained by a variety of methods. **(a)** The rotating wall vessel consists of a cylinder containing culture medium and cells, with a gas-permeable membrane at the center and revolves around a horizontal axis. This allows the cells to experience a free-fall environment and form aggregates, with or without microcarriers. **(b)** Ultralow attachment wells are coated with hydrophilic molecules that do not allow cell attachment to the bottom or the walls. Due to this inability and gravity, seeded individual cells will converge at the bottom and form spheroids. **(c)** The hanging drop method consists of placing drops of cell suspension at the bottom of a tissue culture dish lid or a specialized multiwell plate so that they are suspended. Then, the individual cells will cluster to form aggregates. **(d)** Cells can also be preincubated with magnetic particles and levitate in the presence of a magnet. They will subsequently spontaneously aggregate and form spheroids

vessel, micromolding, ultralow attachment plates, pellet, hanging drop, and magnetic levitation.

The rotating wall vessel bioreactor was devised by NASA to produce cartilage in a microgravity environment, which is simulated by the rotation of a circular vessel around a horizontal axis (Freed et al. 1997). Isolated individual cells added to the system, mixed with porous beads or without beads, have access to fluid shear, oxygen and nutrients and slowly start to form 3D structures. These have been made for a selection of tissues and used for a wide variety of studies, such as small intestine, bladder, lung, and liver (Barrila et al. 2010) (Fig. 2a).

Some cells, when confluent, have the capacity to produce high amounts of extracellular matrix. This property has been explored to create scaffold-free, matrix self-producing 3D structures made up from chondrocytes, treated with transforming growth factor-beta and other growth factors and matured into shape in molds. Proteoglycan and collagen were identified and the overall strength allowed implantation into a pig articular cartilage defect model, which was well integrated (Miyazaki et al. 2010).

Cells seeded onto U-shaped polystyrene plates, which do not allow cell attachment, will deposit onto the bottom and form spheroids (Kelm et al. 2010) (Fig. 2b). Depending on the combination of cell types, the resulting architectures may be more or less organized (Mironov et al. 2009). A variation of this method includes spinning the cells down, forcing them to form spheroids (Baraniak and McDevitt 2012).

Another way of obtaining spheroids consists of adding PBS to a petri dish, to generate a wet chamber and pipetting drops of cell suspension onto the inside of the lid, hanging upside down. Due to the effect of gravity, the cells will spontaneously aggregate (Foty 2011; Jorgensen et al. 2014). An automated version of this method, using a 384-well plate with upper and lower reservoirs for PBS and the hanging drops, has been developed (Tung et al. 2011) (Fig. 2c).

Super paramagnetic iron oxide nanoparticles can be incubated with cells so that they get internalized. After that, the cells are harvested and transferred into ultralow attachment plates. Then, aggregates can immediately start forming by holding a magnet either on top or under the plates for a few hours (Tseng et al. 2015; Leonard and Godin 2016) (Fig. 2d).

Complex scaffoldless structures may in some cases be more challenging to achieve than if scaffolding materials were to be used to provide support and shape. Therefore, the latter rely on the cells' ability to build their own 3D network. The final structure can be achieved by either placing the cells in molds until they aggregate and form a structure that will hold on its own, or small aggregates can be combined by bioprinting.

Spheroids obtained by any of the methods described above are suitable for subsequent bioprinting, into bigger and more complex structures. Depending on the method/equipment used, they need to be within a strict amplitude of values for size and shape, compatible with the software and nozzle. If they are to be printed, aggregates must be only a few days old, otherwise they will lose the ability to fuse. Bioprinting of scaffold-free cell materials can be expensive and time-consuming when making the spheroids, as a very high number of cells are required. However, these support faster and better tissue growth.

Spheroids themselves can also be used as models for tumors or even simplified organs or functional units of organs. Cells in 3D cultures exhibit higher expression of adhesion molecules (among others) and the native tumor microenvironment and matrix, as well as cell interactions, are more closely recreated than in their 2D counterparts. Spheroid tumor models are currently done with or without scaffolds. These spheroids can acquire very different shapes, varying from round to stellate and depend on the cell type/state used and culture conditions. Structurally, spheroids can resemble a tumor, with hypoxia, necrosis, and metabolite accumulation at the core region, a middle layer of quiescent cells, and an outer proliferating rim (Nath and Devi 2016).

5 Preparation of Multicellular Spheroids and Construct Design

Scaffold-free approaches largely rely on the cells' intrinsic ability to spontaneously remodel and differentiate into naturally occurring systems, as happens during embryonic development. The preparation of spheroids can be done by several methods, but they all rely on the fact that dissociated cells can regroup to form aggregates. This is a survival mechanism that prevents anoikis (apoptosis due to the lack of correct cell/matrix attachment). Depending on the cell type, culture

conditions and method chosen, aggregation normally takes between 24 and 72 h. The formation of a spheroid in an ultralow attachment well can be visualized on Video 1.

3D bioprinting has made depositing cells or cell aggregates easier, faster, more accurate, and reproducible than by hand. With the aid of software, users can design the structures they want to obtain and the equipment will then deposit the various materials at very precise positions. There are three main stages to consider when designing and fabricating 3D bioprinted tissue: preprocessing (digital design of the final construct), processing (the actual printing step), and postprocessing (maturation stage) (Mironov et al. 2003). Computer-aided design software can be used to freehand design simple structures, such as a tube composed of 20 rows of 32 spheroids each, or more complex designs based on 3D images acquired from patients, for example, CT scan, MRI, angiography, and echography (Sun and Lal 2002; Murphy and Atala 2014).

Printing can be achieved by using cells only or cells combined with a material that will confer initial structure but that can be quickly removed (thermo-reversible, dissolved chemically or physically pulled away). Flat tissues are easier to print than tubular or more intricate shapes. Vascularization, especially an internal network of microcapillaries required to keep the tissue alive and healthy, is still a challenge. Also, during this step, it is important to choose methods/equipment and materials that ensure cell viability. The design will have to take all these factors into account.

When printing scaffoldless structures, spheroid fusion, cell migration, and remodeling, as well as deposition of extracellular matrix and eventually cell differentiation, are expected to occur spontaneously. A vast body of literature currently describes how these processes occur during development and tissue engineering is now even considered a branch of applied developmental biology (Ingber et al. 2006). Embryonic tissue (or spheroids for bioprinting), composed of different cell types, can be compared to a viscoelastic fluid. When two immiscible liquids are mixed together, they will sort themselves apart. In the same way, different cell types mixed together in a spheroid will migrate until one surrounds the other, a process driven by surface tension and adhesive interactions (Beysens et al. 2000). When designing the final construct, building blocks can be made all the same or with different cell compositions, and deposited at distinct locations, which accelerates the sorting process. Depending on the printing equipment, spheroids may be picked up individually (Itoh et al. 2015), combined with agarose rods (Norotte et al. 2009), or mixed with a hydrogel.

Additionally, before printing, it is important to prepare the building blocks in advance (cells or spheroids) and any additional materials required. Depending on the resources available, construct size and intended application, different cell types and sources can be used (for example, iPSC, primary cells, cell lines, or adult stem cells).

Construct design will depend on the software available, printer resolution, type and size of printing material, application, cell origin and differentiation status, type of printer, bioink, building blocks, and assembly method. In vitro models, at least for some structures, will need finer detail than structures printed for transplantation, where the host can provide the right environment and colonizing cells (Itoh et al. 2015).

6 Bioprinting Methods and Equipment

Since the first mention of using a computer-assisted inkjet printer to deposit cells and proteins at precise positions (Klebe 1988), technology has flourished and recent years have seen an enormous progress in 3D bioprinting methods and equipment, both scaffold-based and scaffold-free. Printing living, viable cells, however, is more complex than printing nonliving materials, such as plastic or metal.

Bioprinters can be classified according to their use of laser, into laser-assisted or laser-free (inkjet, microextrusion). Variations of the latter are used for scaffold-free 3D bioprinting, most commonly mechanical microextrusion (Murphy and Atala 2014). Ideally, in scaffold-free printing methods, living cells are deposited directly onto a substrate, without the addition of other materials. Then, expansion, fusion, and migration processes occur to produce the final structure. In this case, the “bioinks” would be cell pellets, tissue spheroids, or tissue strands. Methods using these starting materials print high cell densities, which means cell fusion and remodeling, as well as extracellular matrix production, can start right after printing (Achilli et al. 2012).

A wider nozzle than those of inkjet printers allows for a larger number of cells to be printed at one time. With the addition of extra nozzles, different materials can be printed usually sequentially or in alternation. Cells or spheroids can be printed between layers of hydrogel, which confer structure and will then be removed after maturation, rendering the constructs scaffold-free. In other cases, cells can be printed together with hydrogels or oils.

The most widely used printers use extrusion, where cell spheroids are first loaded into a tubular reservoir/dispenser, ready for printing. With this method, variable amounts of oils or a hydrogel that does not allow cell adhesion usually need to be added. This is because cell culture medium would be too liquid to both deposit the cell materials in accurate positions or to keep them homogeneously distributed while on the cartridge. On the other hand, this technology is not compatible with printing cell masses on their own. The cell material to other materials ratio is still much higher than in bioprinting methods that are classed as scaffold-based. Another difference is that in scaffold-based printing the scaffold is there to be part of the structure and keep the cells in place. On the other hand, carrier liquids used in scaffold-free bioprinting are used to keep the building blocks from fusing prematurely, as well as an extrusion medium. They are not intended to be part of the final product (Marga et al. 2011).

After loading, cells and carrier are extruded by means of mechanical pressure. As they make their way out of the pipette, they are deposited onto a mold (which will not be part of the final construct), so that they can fuse, mature, and acquire a predetermined architecture. This information will have been previously inserted into the program (usually CAD-based), so that the printer can deposit the cells at the correct locations. The same approach can be used to print less mature aggregates of cells and even cell strands (Ozolat 2015).

Apart from the need of a carrier medium where the cells are delivered, loading the dispensers can be challenging. When loading all the spheroids into the pipette/

cartridge at once, time is of essence, as they may start to fuse while inside the dispenser, despite the low adhesion medium. Conversely, after printing, they need to be close enough to fuse to each other, or else gaps will be left.

Microcarriers will have degradation issues similar to those of hydrogels. Additionally, they need to be adhesive enough for fusion after printing and not too adhesive as not to block the nozzle.

A newer method, called the Kenzan method, does not rely on scaffolds, molds, or even carrier liquids to ensure correct spheroid positioning. Needle arrays (Kenzan) with different sizes and arrangements are placed in PBS and a nozzle will aspirate each spheroid individually and place it in the correct xyz coordinates, as determined by the design program. The stainless steel needles have a diameter of 100–200 μm and a pitch of 300–400 μm . Before and during printing, the bioprinter (Regenova) is able to check the spheroids for several parameters, such as size (diameter) and smoothness (roundness). This allows the machine to decide which spheroids are suitable for aspiration and which ones are not. Depending on the spheroid size, weight, and robustness, aspiration parameters may also be adjusted. The collected spheroids are skewered through the needles and when the process is completed the needle array is transferred into culture medium and incubated for initial maturation, after which the needles are removed. Therefore, this printing method does not use any chemicals that make up bioinks, nor does it put the cells through great temperature changes, which increase cell viability. Another advantage is that the spheroids are produced and printed individually, so they will not start fusing while being manipulated and loaded for printing.

7 Applications

Scaffold-free approaches are now being employed to generate artificial tissue representative of many different organs, resorting to a variety of techniques. Below are a few examples of scaffoldless tissues that have been developed and are currently being used for both research and clinical applications.

7.1 Blood Vessels

Engineered blood vessels can be used as vascular grafts, models for disease and drug discovery or as part of vascularized structures for research or therapy.

Mesenchymal stem cells are an attractive source of material because they can differentiate into several cell types, such as endothelial cells, smooth muscle cells (Silva et al. 2005), osteocytes, and chondrocytes (Pittenger et al. 1999), among others. In 2012, tissue-engineered vascular grafts made from rabbit mesenchymal cell sheets were autologously implanted into the common carotid artery. After 4 weeks, the graft showed good patency and had successfully integrated the native vessel. Endothelialization was confirmed and the overall structure was similar to that of a real artery (Zhao et al. 2012). Since this discovery, many others have used these

cells. Jung et al. (2015), for example, have produced 1 mm inner diameter tubular structures using human mesenchymal cell sheets cultured on a rotating wall bioreactor. They later added human endothelial progenitor cells to form an endothelium, and further cultured them in a perfusion system. The constructs showed vasoconstriction and vasodilation, as well as nitric oxide release and adhesion of HL-60 to the lumen, a promyelocytic leukemia cell line.

A different strategy consisted of using spheroids made from primary human umbilical vein endothelial cells (40%), human aortic smooth muscle cells (10%), and normal human dermal fibroblasts (50%) to bioprint tubular tissues using the Kenzan method. These were matured in a perfusion system and implanted into the abdominal aortae of nude rats. After histological analyses, it was confirmed that both remodeling and lumen endothelialization had occurred (Itoh et al. 2015).

Human vascular grafts produced by the cell sheet method have been used in clinical trials as access for hemodialysis (McAllister et al. 2009). After a 6 month follow-up of the first 10 patients, patency remained 60% after initial 78% at 1 month postoperation. These results are encouraging; however, faster and cheaper methods need to be developed, as it took 6–9 months to produce these grafts.

7.2 Kidney

Kidneys are complex organs, composed of approximately 30 different cell types, required to create diverse structures, in order to perform functions such as pH regulation, electrolyte and fluid balance, hormone production, mineral absorption, filtering, and waste excretion (Guimaraes-Souza et al. 2009).

So far, kidney regeneration strategies have relied on the use of scaffolds to make grafts, especially those obtained from decellularized kidneys deemed not suitable for transplant (Orlando et al. 2013; Karczewski and Malkiewicz 2015; Moon et al. 2016). Injection of adipocyte derived stem cells, which are a source of mesenchymal stem cells, has shown some promise, as it resulted in reduced renal dysfunction and increased tubular regeneration after injury on a unilateral severe ischemia mouse model (Almeida et al. 2013). Other cell sources, such as primary kidney cells (Guimaraes-Souza et al. 2012), induced pluripotent stem cells, adult bone marrow, embryonic and placental stem cells, have also shown to be suitable to produce or differentiate into kidney structures, either by environment manipulation or seeding on scaffolds (Little 2006; Karczewski and Malkiewicz 2015).

Due to its structural complexity, scaffold-free approaches have not yet produced suitable *in vitro* models or kidney grafts adequate for tissue regeneration. However, a recent study has taken us one step closer to producing functional organoids. The authors have shown that it is possible to direct human embryonic stem cells or human induced pluripotent stem cells to differentiate into different renal structures *in vitro*, depending on the timing and duration of exposure to small molecules which modified the initial Wnt signal (GSK-3 inhibitor) or promoted the growth of specific cells (FGF-9) (Takasato et al. 2015). The concept itself is not new (Mae et al. 2013), but these organoids resemble human embryonic kidneys and are comprised of four

compartments, showing evidence of functional maturation: the collecting duct (GATA3⁺, ECAD⁺), distal tubule (GATA3⁻, ECAD⁺, LTL⁻), proximal tubule (ECAD⁻, LTL⁺), and the glomerulus (WT1⁺). This has allowed not only the production of a more realistic model but also helped to elucidate these events during embryogenesis (Takasato et al. 2015).

7.3 Liver Regeneration

Similarly to kidney, extracellular matrix scaffolding provided by decellularization is now also possible for liver. The material is amenable to repopulation by hepatic cells and is not rejected when implanted into mice (Mazza et al. 2015). Although promising, these strategies rely on the availability of actual livers and potential problems such as accidental disease transmission may arise. Manipulation of the extracellular matrix during the decellularization process may also cause alterations that result in mis-repopulation or mis-differentiation once implanted in vivo or when used for in vitro studies.

Scaffold-free approaches have also been developed. Primary hepatocytes were cultured on temperature-responsive poly(*N*-isopropylacrylamide)-coated plates and used to produce cell sheets. These were treated with basic fibroblast growth factor (to stimulate neovascularization) and transplanted into the subcutaneous space of mice, where they remained well integrated for over 200 days. Furthermore, the tissue showed hepatic functionality and histological analysis of the 3D organization of sheets revealed liver-like appearance (Ohashi et al. 2007).

A different methodology consists of transplanting hepatocytes encapsulated in hydrogels into rodent models of acute liver failure. Human hepatocyte beads surrounded by alginate were well tolerated, showed absence of immune cells on their surface, and contained viable and functional liver cells, while improving liver damage (Jitraruch et al. 2014). Microliver tissue encapsulated in collagen-alginate was implanted in 90% partial hepatectomized mice and promoted regeneration of the caudate lobe, as well as improved survival (80%, compared to 10% observed in the controls) (No da et al. 2014).

7.4 Periodontal Regeneration

Human periodontal ligament cells harvested from extracted teeth were used to prepare sheets that were transplanted onto a mesial dehiscence rat model. Tissue regeneration has occurred and fibrils as well as an acellular cementum-like layer were present (Huang and Zhang 2011). The same type of cell sheets had previously been applied to dogs with surgically created dehiscence defects, where bone formation, periodontal ligament, and cementum were observed (Akizuki et al. 2005).

Regarding clinical trials using scaffold-free materials, there is one on www.clinicaltrials.gov (study ID NCT01814436) that is currently recruiting. Scaffold-free pellets of stem cells from human exfoliated deciduous teeth will be used to

assess safety and regenerative efficacy in patients with avulsed immature permanent teeth and pulp necrosis.

The same group of researchers has recently demonstrated that scaffold-free stem cell sheet-derived pellets from dental root apical papilla can form a vascularized pulp/dentine complex in empty root canals. The pellets contained extracellular matrix and exhibited higher expression of both bone and dentine sialoprotein, alkaline phosphatase, and runt-related gene 2 compared to traditional cell sheets, showing higher osteogenic potential (Na et al. 2016).

7.5 Cartilage

Cartilage regeneration still poses a challenge for both surgeons and researchers. Strategies to develop suitable solutions have spanned from cell-free approaches (Gille et al. 2010), to a mixture of cells and scaffolds to, more recently, scaffold-free methods.

Laryngotracheal reconstruction was attempted by using cartilage sheets made from autologous rabbit chondrocytes isolated from auricular cartilage. Although some signs of mechanical failure were observed, the structures were well integrated, did not elicit inflammatory reaction, and were covered in mucosal epithelium. This suggests that stronger constructs may be suitable for grafting (Gilpin et al. 2010).

A clinical trial, in Japan (study ID UMIN000017944), is also recruiting volunteers to evaluate the safety and osteochondral regeneration using implanted high-density mesenchymal scaffold-free stem cell autologous constructs derived from adipose tissue for donor site of mosaic plasty plugs. This follows on from encouraging preclinical studies where cartilage and subchondral bone regeneration were achieved in rabbits knees (Ishihara et al. 2014).

Most of the clinical trials currently underway using tissue engineering rely on the use of directly injected or applied stem cells or structures containing cells and scaffolds, with various degrees of predicted or demonstrated reabsorption. Search for the term “scaffold-free” has only retrieved one study, the abovementioned trial using pellets of stem cells from human exfoliated deciduous teeth. Cell sheets are being used in clinical trials for phase I, phase II, and phase III studies for a wide range of applications, such as healing of esophagus mucosal defects after endoscopic resection (NCT02455648), heart failure (for example, NCT02672163), articular cartilage defects (for example, NCT01694823), and ocular surface disease (NCT01123044).

8 Advantages and Challenges

In a similar fashion to their counterparts that use scaffolds, scaffold-free structures allow cell differentiation, cell-cell and cell-matrix interactions, remodeling, and assembly. It may be argued that, in fact, some of these processes can occur faster in scaffold-free structures, as there is no physical barrier to cell-cell communication,

cell and small molecules migration/diffusion and fusion. When a scaffold is present, time may be required for it to degrade, so that cells can move or make connections. These may be with host tissue in the course of integration or with each other during the maturation phase.

An exception to this may be the regeneration of periodontal tooth supporting structures that require selective wound healing and membranes are used to protect them from blood clots and connective tissue, which would interfere with the process (El Haddad et al. 2014).

Complex architectures and bigger structures may be more technically challenging to put together, in the absence of rigid templates with defined shapes. Tissue deformation, partly caused by tension on the actin cytoskeleton, can be reduced by the addition of Y-27632, a selective inhibitor of ROCK phosphorylation (Czajka et al. 2014). Although still a challenge, studies that specifically look at this problem and how to increase intrinsic resistance, as well as the development of creative solutions where a scaffold or a mold can provide support but does not become an integral part of the structure, may push the capabilities of scaffold-free tissue engineering further.

In some cases, scaffolds are able to encourage or direct differentiation and homing of different cells to distinct areas. Self-assembled structures must produce their own extracellular matrix and chemical cues in order to obtain the correct degree of cell differentiation and structural organization. Scaffold-free assemblage seems to rely on processes similar to those naturally occurring during development. The resulting microenvironment, without exogenous structures and barriers to cell-cell/cell-matrix interactions and migration brings the process closer to physiological conditions. Also, the degradation of scaffolds may hinder remodeling and integration, not only in terms of time but also in terms of release of undesirable compounds. Thus, scaffold-free structures have the potential to make the process faster and safer/more reliable. For example, the addition of enzymes or other molecules seems to contribute to the formation of new tissue (Responde et al. 2012). One drawback is the possible lack of knowledge of all the factors involved, but in recent years there has been an increasing body of new literature on developmental processes and cell (re) programming.

The absence of a physical barrier may also influence mechanotransduction, as it can begin immediately after assembly or transplantation. The presence of structures, however temporary they may be, with a stiffness different to what cells might encounter in an *in vivo* situation may have an influence on cell morphology and behavior beyond the life span of the scaffold. Studies have shown that cells grown on a certain surface, harvested and then seeded on a different surface are able to retain a memory of the previous conditions, affecting their future behavior.

The fact that scaffold-free structures are able to begin fusion and remodeling more promptly, as well as are more permeable to small signaling molecules than those containing scaffolds, may confer them an advantage in terms of graft survival *in vivo*, which is crucial for the success of surgical implantation. However, everything comes at a cost. Scaffold-based structures use less cells, so the process is slower, as they need to expand. Starting with high cell numbers is beneficial to

achieve conditions similar to those in nature, but cells are usually expensive both to buy and maintain.

An important aspect to consider when using scaffolds is the unknown effects of the scaffolding materials or their interactions with living cells. These can be chemical, thus altering normal signaling and cell behavior, as well as physical, as mentioned above. For pharmaceutical studies, unknown chemical interactions between the drugs and scaffold materials may occur that can result in incorrect data. The material itself may be toxic to the cells or its physical presence may interfere with cell migration or access to shear stress. From the point of view of transplantation of artificial engineered tissue into patients, scaffold-free structures may offer advantages in terms of not eliciting an inflammatory reaction, which causes graft death and rejection.

Structures that are made from cells only and their products, such as extracellular matrix, are cultured in aseptic conditions with no addition of exogenous materials, except for sterile media and supplements. This affords less risk of infection by microorganisms that may lead to septicemia.

The process of obtaining constructs itself is less punishing on the cells as they do not need to be exposed to so many steps, chemicals, compression, temperature, and manipulation. This results in higher cell viability and less overall disturbance in terms of signaling and behavior.

Cell sheets collected from thermoresponsive substrates do not require the use of enzymes for detachment, which may have negative effects on them. They will adhere to host tissue, eliminating the need for suturing or glue (Huang and Zhang 2011).

Both technologies have advantages and disadvantages, which may render them more or less appropriate, depending on the application. The increasing understanding of cellular and molecular processes, as well as developments in materials (both biological and nonbiological) and equipment, is shaping the way tissue engineering is done and progress will continue towards more realistic and effective therapies, as well as *in vitro* models.

9 Conclusions

Recent advances in the manufacturing industry, scaffold materials, and biodegradable hydrogels, as well as the understanding of developmental and cell biology, have led to the current rapid growth of 3D bioprinting and its applications. Two main approaches have emerged: those using scaffolds and scaffold-free processes. The definition of “scaffold-free” can be confusing at times, as temporary scaffolding may be used, but the final biological product should be scaffoldless at the time of implantation or testing.

Various scaffold-free systems have been developed, such as cell sheets (and variations), those using single cells as building blocks or spheroid aggregates. There is a selection of methods that can be employed to obtain spheroids but, after the cells aggregate, remodeling and extracellular matrix deposition will occur by self-assembly. This is similar to the natural processes occurring during development.

Seminal studies in this field, as well as more recent literature, have provided valuable insights into how cells are regulated by their microenvironment, namely which factors contribute to cell differentiation, migration, adhesion, coalescence, and interactions with other cells, molecules, and matrix.

Printing living cells to form tissue is more complex than printing plastic or metal objects. However, new biocompatible materials and bioprinting techniques are being developed, including those able to produce scaffold-free structures. These require a higher number of cells and are more difficult to obtain due to the lack of structural stiffness but have several advantages over their counterparts containing scaffolds. These include faster remodeling, extracellular matrix deposition and integration with host tissue if implanted, absence of potentially hazardous chemicals, as well as a physical barrier within the tissue.

Although complex structure, especially that of solid organs that comprise many different cell types and an intricate microvascular network is still a challenge, the multidisciplinary nature of the field allows for the development of innovative solutions that would take longer to achieve from a single point of view. Currently, there are several scaffold-free 3D bioprinted structures that are already being used for research and clinical applications throughout a variety of specialties, from the cardiovascular system to dentistry. Also, the number of ongoing and recruiting clinical trials using tissue created with this technology has been increasing in the past few years. Therefore, it is reasonable to expect this upwards trend to continue in the future, with more tissue-based therapies and *in vitro* tools being trialed and put into practical use.

References

- Achilli T-M, Meyer J, Morgan JR (2012) Advances in the formation use and understanding of multi-cellular spheroids. *Exp Opin Biol Ther* 12(10):1347–1360
- Akizuki T, Oda S, Komaki M, Tsuchioka H, Kawakatsu N, Kikuhi A, Yamato M, Okano T, Ishikawa I (2005) Application of periodontal ligament cell sheet for periodontal regeneration: a pilot study in beagle dogs. *J Periodontal Res* 40(3):245–251
- Almeida DC, Donizetti-Oliveira C, Barbossa-Costa P, Origassa CS, Camara NO (2013) In search of mechanisms associated with mesenchymal stem cell-based therapies for acute kidney injury. *Clin Biochem Rev* 34:131–144
- Athanasiou KA, Eswaramoorthy R, Hadidi P, Hu JC (2013) Self-organization and the self-assembling process in tissue engineering. *Annu Rev Biomed Eng* 15:115–136
- Baraniak PR, McDevitt TC (2012) Scaffold-free culture of mesenchymal stem cell spheroids in suspension preserves multilineage potential. *Cell Tissue Res* 347:701–711
- Barrila J, Radtke AL, Crabbe A, Sarker SF, Herbst-Kralovetz MM, Ott CM, Nickerson CA (2010) Organotypic 3D cell culture models: using the rotating wall vessel to study host–pathogen interactions. *Nat Rev Microbiol* 8(11):791–801
- Beysens DA, Forgacs G, Glazier JA (2000) Cell sorting is analogous to phase separation in fluids. *Proc Natl Acad Sci U S A* 97:9467–9471
- Czajka CA, Mehesz AN, Trusk TC, Yost MJ, Drake CJ (2014) Scaffold-free tissue engineering: organization of the tissue cytoskeleton and its effects on tissue shape. *Ann Biomed Eng* 42(5):1049–1061

- Denayer T, Stöhr T, Van Roy M (2014) Animal models in translational medicine: validation and prediction. *New Horiz Transl Med* 2(1):5–11
- Edmondson R, Broglie JJ, Adcock AF, Yang L (2014) Three-dimensional cell culture systems and their applications in drug discovery and cell-based biosensors. *Assay Drug Dev Technol* 12(4):207–218
- El Haddad E, Lauritano D, Candotto V, Carinci F (2014) Guided bone regeneration is a reliable technique in implant dentistry: an overview and a case report. *OA Dentist* 2(1):5–8
- Festing S, Wilkinson R (2007) The ethics of animal research. Talking point on the use of animals in scientific research. *EMBO Rep* 8(6):526–530
- Foty R (2011) A simple hanging drop cell culture protocol for generation of 3D spheroids. *J Vis Exp* 51:2720
- Freed LE, Langer R, Martin I, Pellis NR, Vunjak-Novakovic G (1997) Tissue engineering of cartilage in space. *Proc Natl Acad Sci U S A* 94(25):13885–13890
- Gauvin R, Ahsan T, Larouche D, Lévesque P, Dubé J, Auger FA, Nerem RM, Germain L (2010) A novel single-step self-assembly approach for the fabrication of tissue-engineered vascular constructs. *Tissue Eng Part A* 16(5):1737–1747
- Gille J, Schuseil E, Wimmer J, Gellissen J, Schulz AP, Behrens P (2010) Mid-term results of autologous matrix-induced chondrogenesis for treatment of focal cartilage defects in the knee. *Knee Surg Sports Traumatol Arthrosc* 18(11):1456–1464
- Gilpin DA, Weidenbecher MS, Dennis JE (2010) Scaffold-free tissue-engineered cartilage implants for laryngotracheal reconstruction. *Laryngoscope* 120(3):612–617
- Gilpin SE, Guyette JP, Gonzalez G, Ren X, Asara JM, Mathisen DJ, Vacanti JP, Ott HC (2014) Perfusion decellularization of human and porcine lungs: bringing the matrix to clinical scale. *J Heart Lung Transplant* 33(3):298–308
- Groll J, Boland T, Blunk T, Burdick JA, Cho D-W, Dalton PD, Derby B, Forgacs G, Li Q, Mironov VA, Moroni L, Nakamura M, Shu W, Takeuchi S, Vozzi G, Woodfield TBF, Xu T, Yoo JJ, Malda J (2016) Biofabrication: reappraising the definition of an evolving field. *Biofabrication* 8:013001
- Guimaraes-Souza N, Soler R, Yoo JJ (2009) Regenerative medicine of the kidney. In: Denstedt J, Atala A (eds) *Biomaterials and tissue engineering in urology*, 1st edn. CRC Press LLC, Boca Raton, pp 502–517
- Guimaraes-Souza NK, Yamaleyeva LM, AbouShwareb T, Atala A, Yoo JJ (2012) In vitro reconstitution of human kidney structures for renal cell therapy. *Nephrol Dial Transplant* 27(8):3082–3090
- Guyette JP, Gilpin SE, Charest JM, Tapias LF, Ren X, Ott HC (2014) Perfusion decellularization of whole organs. *Nat Protocols* 9:1451–1468
- Hirai J, Matsuda T (1996) Venous reconstruction using hybrid vascular tissue composed of vascular cells and collagen tissue regeneration process. *Cell Transplant* 5:93–105
- Huang SY, Zhang DS (2011) Periodontal ligament cell sheet engineering: a new possible strategy to promote periodontal regeneration of dental implants. *Dent Hypothesis* 2(1):23–30
- Ingber DE, Mow VC, Butler D, Niklason L, Huard J, Mao J, Yannas I, Kaplan D, Vunjak-Novakovic G (2006) Tissue engineering and developmental biology: going biomimetic. *Tissue Eng* 12:3265–3283
- Ishihara K, Nakayama K, Akieda S, Matsuda S, Iwamoto Y (2014) Simultaneous regeneration of full-thickness cartilage and subchondral bone defects in vivo using a three-dimensional scaffold-free autologous construct derived from high-density bone marrow-derived mesenchymal stem cells. *J Orthop Surg Res* 9:98
- Itoh M, Nakayama K, Noguchi R, Kamohara K, Furukawa K, Uchihashi K, Toda S, Oyama J, Node K, Morita S (2015) Scaffold-free tubular tissues created by a bio-3D printer undergo remodeling and endothelialization when implanted in rat aortae. *PLoS One* 10(12):e0145971
- Jitraruch S, Dhawan A, Hughes RD, Filippi C, Soong D, Philippees C, Lehec SC, Heaton ND, Longhi MS, Mitry RR (2014) Alginate microencapsulated hepatocytes optimised for transplantation in acute liver failure. *PLoS One* 10(3):e0119226

- Jorgensen A, Young J, Nielsen JE, Joensen UN, Toft BG, Rajpert-De Meyts E, Loveland KL (2014) Hanging drop cultures of human testis and testis cancersamples: a model used to investigate activin treatment effects in a preserved niche. *Br J Cancer* 110:2604–2614
- Jung Y, Ji HY, Chen Z, Chan HF, Atchison L, Klitzman B, Truskey G, Leong KW (2015) Scaffold-free, human mesenchymal stem cell-based tissue engineered blood vessels. *Nat Sci Rep* 5:15116
- Karczewski M, Malkiewicz T (2015) Scaffolds from surgically removed kidneys as a potential source of organ transplantation. *Biomed Res Int* 2015:1–8. Article ID 325029
- Kelm JM, Lorber V, Snedeker JG, Schmidt D, Broggini-Tenzer A, Weisstanner M, Odermatt B, Mol A, Zünd G, Hoerstrup SP (2010) A novel concept for scaffold-free vessel tissue engineering: self-assembly of microtissue building blocks. *J Biotechnol* 148(1):46–55
- Klebe RJ (1988) Cytoscribing: a method for micropositioning cells and the construction of two- and three-dimensional synthetic tissues. *Exp Cell Res* 179:362–373
- Kobayashi T, Kana K, Nishida K, Yamato M, Okano T (2013) Corneal regeneration by transplantation of corneal epithelial cell sheets fabricated with automated cell culture system in rabbit model. *Biomaterials* 34(36):9010–9017
- L'Heureux N, Germain L, Labbe R, Auger FA (1993) In vitro construction of a human blood vessel from cultured vascular cells: a morphologic study. *J Vasc Surg* 17:499–509
- L'Heureux NPS, Labbé R, Germain L, Auger FA (1998) A completely biological tissue-engineered human blood vessel. *FASEB J* 12:47–56
- Lee AY, Lee Y-U, Mahler N, Best C, Tara S, Breuer CK (2016) Regenerative implants for cardiovascular tissue engineering. In: Laurence J (ed) *Translating regenerative medicine to the clinic*, 1st edn. Academic, London, pp 52–57
- Leonard F, Godin B (2016) 3D in vitro model for breast cancer research using magnetic levitation and bioprinting method. *Methods Mol Biol* 1406:239–251
- Little MH (2006) Regrow or repair: potential regenerative therapies for the kidney. *J Am Soc Nephrol* 17:2390–2401
- MacArthur BD, Oreffo ROC (2005) Bridging the gap. *Nature* 433(7021):19
- Mae S, Shono A, Shiota F, Yasuno T, Kajiwara M, Gotoda-Nishimura N, Arai S, Sato-Otubo A, Toyoda T, Takahashi K, Nakayama N, Cowan CA, Aoi T, Ogawa S, McMahon AP, Yamanaka S, Osafune K (2013) Monitoring and robust induction of nephrogenic intermediate mesoderm from human pluripotent stem cells. *Nat Commun* 4:1367
- Mak IWY, Evaniew N, Ghert M (2014) Lost in translation: animal models and clinical trials in cancer treatment. *Am J Transl Res* 6(2):114–118
- Marga F, Jakab K, Khatiwala C, Shephard B, Dorfman S, Forgacs G (2011) Organ printing: a novel tissue engineering paradigm. *5th Eur Conf IFMBE Proc* 37:27–30
- Mazza G, Rombouts K, Hall AR, Urbani L, Vinh Luong T, Al-Akkad W, Longato L, Brown D, Magsoudlou P, Dhillon AP, Fuller B, Davidson B, Moore K, Dhar D, De Coppi P, Malago M, Porginzani M (2015) Decellularized human liver as a natural 3D-scaffold for liver bioengineering and transplantation. *Sci Rep* 5:13079
- McAllister TN, Maruszewski M, Garrido SA, Wystrychowski W, Dusserre N, Marini A, Zagalski K, Fiorillo A, Avila H, Manglano X, Antonelli J, Kocher A, Zembala M, Cierpka L, de la Fuente LM, L'heureux N (2009) Effectiveness of haemodialysis access with an autologous tissue-engineered vascular graft: a multicentre cohort study. *Lancet* 373:1440–1446
- Mironov V, Boland T, Trusk T, Forgacs G, Markwald RR (2003) Organ printing: computer-aided jet-based 3D tissue engineering. *Trends Biotechnol* 21(4):157–161
- Mironov V, Visconti RP, Kasyanov V, Forgacs G, Drake CJ, Markwald RR (2009) Organ printing: tissue spheroids as building blocks. *Biomaterials* 30:164–2174
- Miyazaki T, Miyauchi S, Matsuzaka S (2010) Formation of proteoglycan and collagen-rich scaffold-free stiff cartilaginous tissue using two-step culture methods with combinations of growth factors. *Tissue* 16(5):1575–1584
- Moon KH, Ko IK, Yoo JJ, Atala A (2016) Kidney diseases and tissue engineering. *Methods* 99:112–119
- Murphy SV, Atala A (2014) 3D bioprinting of tissues and organs. *Nat Biotechnol* 32(8):773–785

- Na S, Zhang H, Huang F, Wang W, Ding Y, Li D, Jin Y (2016) Regeneration of dental pulp/dentine complex with a three-dimensional and scaffold-free stem-cell sheet-derived pellet. *J Tissue Eng Regen Med* 10(3):261–270
- Nath S, Devi GR (2016) Three-dimensional culture systems in cancer research: focus on tumor spheroid model. *Pharmacol Ther* 163:94–108
- Nishida K, Yamato M, Hayashida Y, Watanabe K, Yamamoto K, Adachi E, Nagai S, Kikuchi A, Maeda N, Watanabe H, Okano T, Tano Y (2004) Corneal reconstruction with tissue-engineered cell sheets composed of autologous oral mucosal epithelium. *N Engl J Med* 351(12):1187–1196
- No da Y, Jeong GS, Lee SH (2014) Immune-protected xenogeneic bioartificial livers with liver-specific microarchitecture and hydrogel-encapsulated cells. *Biomaterials* 35(32):8983–8991
- Norotte C, Marga F, Niklason L, Forgacs G (2009) Scaffold-free vascular tissue engineering using bioprinting. *Biomaterials* 30(30):5910–5917
- O'Brien FJ (2011) Biomaterials and scaffolds for tissue engineering. *Mater Today* 14(3):88–95
- O'Connor N, Mulliken J, Banks-Schlegel S, Kehinde O, Green H (1981) Grafting of burns with cultured epithelium prepared from autologous epidermal cells. *Lancet* 317(8211):75–78
- Ohashi K, Yokoyama T, Yamato M, Kuge H, Kanehiro H, Tsutsumi M, Amanuma T, Iwata H, Yang J, Okano T, Nakajima Y (2007) Engineering functional two- and three-dimensional liver systems in vivo using hepatic tissue sheets. *Nat Med* 13(7):880–885
- Ohki T, Yamato M, Ota M, Murakami D, Takagi R, Kondo M, Nakamura T, Okano T, Yamamoto M (2009) Endoscopic transplantation of human oral mucosal epithelial cell sheets—world's first case of regenerative medicine applied to endoscopic treatment. *Gastrointest Endosc* 69(5):AB253–AB254
- Okano T, Yamada N, Sakai H, Sakurai Y (1993) A novel recovery system for cultured cells using plasma-treated polystyrene dishes grafted with poly(*N*-isopropylacrylamide). *J Biomed Mater Res* 27(10):1243–1251
- Orlando G, Booth C, Wang Z, Totonelli G, Ross CL, Moran E, Salvatori M, Maghsoudlou P, Turmaine M, Delario G, Al-Shraideh Y, Farooq U, Farney AC, Rogers J, Iskandar SS, Burns A, Marini FC, De Coppi P, Stratta RJ, Soker S (2013) Discarded human kidneys as a source of ECM scaffold for kidney regeneration technologies. *Biomaterials* 34:5915–5925
- Ozbolat IT (2015) Scaffold-based or scaffold-free bioprinting: competing or complementing approaches? *J Nanotechnol Eng Med* 6(2):024701
- Phillips TJ (1998) New skin for old: developments in biological skin substitutes. *Arch Dermatol* 134(3):344–349
- Pittenger MF, Mackay AM, Beck SC, Jaiswal RK, Douglas R, Mosca JD, Moorman MA, Simonetti DW, Craig S, Marshak DR (1999) Multilineage potential of adult human mesenchymal stem cells. *Science* 284(5411):143–147
- Responde DJ, Arzi B, Natoli RM, Hu JC, Athanasiou KA (2012) Mechanisms underlying the synergistic enhancement of self-assembled neocartilage treated with chondroitinase-ABC and TGF- β 1. *Biomaterials* 33(11):3187–3194
- Rheinwald JG, Green H (1975) Serial cultivation of strains of human epidermal keratinocytes: the formation of keratinizing colonies from single cells. *Cell* 6(3):331–343
- Sawa Y, Miyagawa S, Sakaguchi T, Fujita T, Matsuyama A, Saito A, Shimizu T, Okano T (2012) Tissue engineered myoblast sheets improved cardiac function sufficiently to discontinue LVAS in a patient with DCM: report of a case. *Surg Today* 42(2):181–184
- Silva GV, Litovsky S, Assad JA, Sousa AL, Martin BJ, Vela D, Coulter SC, Lin J, Ober J, Vaughn WK, Branco RV, Oliveira EM, He R, Geng YJ, Willerson JT, Perin EC (2005) Mesenchymal stem cells differentiate into an endothelial phenotype, enhance vascular density, and improve heart function in a canine chronic ischemia model. *Circulation* 111:150–156
- Sun W, Lal P (2002) Recent development on computer aided tissue engineering – a review. *Comput Methods Prog Biomed* 67:85–103
- Takasato M, Er PX, Chiu HS, Maier B, Baillie GJ, Ferguson C, Parton RG, Wolvetang EJ, Roost MS, Lopes SMCS, Little MH (2015) Kidney organoids from human iPS cells contain multiple lineages and model human nephrogenesis. *Nature* 526(7574):564–568

- Tseng H, Gage JA, Shen T, Haisler WL, Neeley SK, Shiao S, Chen J, Desai PK, Liao A, Hebel C, Raphael RM, Becker JL, Souza GR (2015) A spheroid toxicity assay using magnetic 3D bioprinting and real-time mobile device-based imaging. *Sci Rep* 5:13987
- Tung Y-C, Hsiao AY, Allen SG, Torisawa Y-S, Ho M, Takayama S (2011) High-throughput 3D spheroid culture and drug testing using a 384 hanging drop array. *Analyst* 136(3):473–478
- Vunjak NG, Eschenhagen T, Mummery C (2014) Myocardial tissue engineering: in vitro models. *Cold Spring Harb Perspect Med* 4(3):pii: a014076
- Weinberg CB, Bell E (1986) A blood vessel model constructed from collagen and cultured vascular cells. *Science* 231:397–400
- Yamada N, Okano T, Sakai H, Karikusa F, Sawasaki Y, Sakurai Y (1990) Thermo-responsive polymeric surfaces; control of attachment and detachment of cultured cells. *Makromol Chem Rapid Commun* 11(11):571–576
- Zhao J, Liu L, Wei J, Ma D, Geng W, Yan X, Zhu J, Du H, Liu Y, Li L, Chen F (2012) A novel strategy to engineer small-diameter vascular grafts from marrow-derived mesenchymal stem cells. *Artif Organs* 36(1):93–101



Translation and Applications of Biofabrication

Ji Hyun Kim, Anthony Atala, and James Yoo

Contents

1	Introduction	452
2	Bioprinting of Tissues and Organs for Implantation In Vivo	454
2.1	Bone	459
2.2	Cartilage	461
2.3	Skin	464
2.4	Nerve	466
2.5	Blood Vessels and Vascular Networks	468
2.6	Cardiac Tissue and Heart Valve	470
3	Biofabrication of In Vitro Tissue/Organ Models	471
3.1	Drug Discovery and Toxicity Testing	472
3.2	Cancer Research	476
4	Current Challenges and Future Perspectives	477
5	Conclusions	479
	References	480

Abstract

Three-dimensional (3D) bioprinting is an emerging field that holds promise for creating functional living tissues and organs. Bioprinting enables to fabricate structurally complex 3D tissue constructs by precise positioning and spatially separated patterns of multiple types of cells, biomaterials, and bioactive molecules within a single construct. With recent advances in bioprinting strategies, 3D bioprinting has been applied in various research areas, including tissue engineering and regenerative medicine, biology, physiology, drug discovery, and cancer/stem cell research. In tissue engineering and regenerative medicine, many types

J. H. Kim · A. Atala · J. Yoo (✉)

Wake Forest Institute for Regenerative Medicine, Wake Forest School of Medicine, Winston-Salem, NC, USA

e-mail: jihkim@wakehealth.edu; aatala@wakehealth.edu;
jyoo@wakehealth.edu

of 3D tissue constructs have been bioprinted to generate functional tissues for implantation, with the ultimate goal of clinical use. In addition, 3D bioprinting has been used as a tool to create *in vitro* tissue/organ models for drug discovery and cancer research, enabling deeper understanding of physiological phenomena of specific tissues/organs and more accurate prediction of drug or toxicity responses. In this chapter, we discuss recent applications of 3D bioprinting; first to create tissues and organs for the purposes of tissue engineering and regenerative medicine and then as platforms for *in vitro* tissue/organ models in drug discovery/toxicity testing and cancer research. We also discuss current challenges and future perspectives for practical applications of 3D bioprinting.

1 Introduction

Bioprinting technology enables the creation of three-dimensional (3D) living tissue and organ constructs with potential use in a variety of applications. Bioprinting allows for precise positioning of different tissue elements, such as living cells, biomaterials, and bioactive molecules, in a spatially organized pattern within a single structure through computer-aided design and manufacturing (CAD/CAM) (Arslan-Yildiz et al. 2016; Mandrycky et al. 2015; Ozbolat 2015). 3D living tissue constructs are fabricated during the printing process by direct patterning and stacking of cell-laden bioinks, one layer at a time (Murphy and Atala 2014). Because of its detailed nature, 3D bioprinted structures have the potential to accurately mimic the complex structure and function of native tissues, as compared to traditional fabrication methods of 3D scaffolds (Arslan-Yildiz et al. 2016).

To create 3D living tissue constructs with the desired structural and functional mimicry of target tissues, many factors need to be considered, including the type of bioprinter, cells, and bioinks. Commonly used bioprinting methods are inkjet-, extrusion-, and laser-based bioprinting. The features, advantages, and drawbacks of each printing modality are summarized in Table 1 (Arslan-Yildiz et al. 2016; Mandrycky et al. 2015; Murphy and Atala 2014; Sears et al. 2016). Recently, bioprinting systems have been combined with other fabrication technologies to enhance outcomes (Chang et al. 2010; Kolesky et al. 2016). To achieve the biological functions of target tissues, selection of cells is critical. A variety of primary/immortalized cells and progenitor/stem cells have been used for bioprinting (Murphy and Atala 2014). Heterogeneous tissue constructs with spatially organized patterns of multiple cell types have been created to engineer more complex and functional tissue constructs (Duan et al. 2013; Fedorovich et al. 2011; Kolesky et al. 2014; Xu et al. 2013b). Bioinks also have been refined in recent years. Naturally derived hydrogels, such as fibrinogen, collagen, hyaluronic acid (HA), and gelatin, are mainly used because they can provide superior cell survival and proliferation (Stanton et al. 2015). In addition, synthetic polymers such as polyethylene glycol (PEG), polycaprolactone (PCL), and polyurethane (PU) have been used as bioinks (Cui et al. 2012), or have been patterned as a supporting architecture within the tissue

Table 1 Comparison of bioprinting technologies

	Inkjet	Extrusion	Laser	References
Resolution	50–300 μm	200 μm	>20 μm	(Arslan-Yildiz et al. 2016; Ozbolat and Yu 2013; Sears et al. 2016)
Fabrication speed	Fast (1–10000 droplet/s)	Slow-medium (10–50 $\mu\text{m/s}$)	Medium-fast (200–1600 mm/s)	(Demirci and Montesano 2007; Guillotin et al. 2010; Nair et al. 2009; Smith et al. 2004)
Scalability	Medium	High	Low	(Mandrycky et al. 2015; Wang et al. 2015)
Material viscosity	3.5–12 mPa/s	30–6 $\times 10^7$ mPa/s	1–300 mPa/s	(Chang et al. 2011; Guillemot et al. 2010; Guillotin and Guillemot 2011; Kim et al. 2010)
Gelation methods	Chemical, photo-cross-linking, temperature	Chemical, photo-cross-linking, shear thinning, temperature	Chemical, photo-cross-linking	(Koch et al. 2010; Michael et al. 2013; Murphy et al. 2013; Smith et al. 2007)
Cell viability	>85%	>40–95%	>95%	(Campbell et al. 2005; Guillotin et al. 2010; Kang et al. 2016; Phillippi et al. 2008; Smith et al. 2004)
Cell density	Low, 10^6 – 10^7 cells/ml	High, cell spheroids	Medium-high, 10^6 – 10^8 cells/ml	(Arslan-Yildiz et al. 2016; Guillotin et al. 2010; Marga et al. 2012; Mironov et al. 2011; Xu et al. 2005)
Cost	Low	Medium	High	(Jones 2012; Mandrycky et al. 2015)
Advantages	Relatively low cost High printing speed High cell viability	Multiple cells/ material delivery High cell densities with an acceptable cell viability Possibility of tissue fabrication large enough for clinical use	High resolution High cell densities High printing speed	(Bajaj et al. 2014; Jiao et al. 2014; Lu et al. 2013; Mandrycky et al. 2015; Murphy and Atala 2014)

(continued)

Table 1 (continued)

	Inkjet	Extrusion	Laser	References
Disadvantages	Limited material selectivity (low viscosity) Clogging of the printer ejector Low mechanical properties of printed structures	Relatively low fabrication resolution Shear stress-induced cell damage	High cost Difficulty in scale-up	(Ballyns et al. 2008; Jiao et al. 2014; Lu et al. 2013; Mandrycky et al. 2015; Zheng et al. 2012)

constructs to enhance their mechanical properties (Kang et al. 2016; Merceron et al. 2015).

3D bioprinting technology has been used in various fields, including tissue engineering and regenerative medicine, pharmaceutical, drug discovery, cancer, and personalized medicine research (Arslan-Yildiz et al. 2016; Knowlton et al. 2015; Ozbolat et al. 2016). Several types of tissue constructs have been bioprinted with tissue-specific cells or stem cells and successfully implanted *in vivo*. In addition, 3D bioprinted *in vitro* tissue/organ models offer new opportunities for drug discovery and toxicity testing, as well as for cancer research (Pati et al. 2016). As such, 3D bioprinting technology presents with an enormous potential to change the way science and medicine is practiced.

In this chapter, the current development efforts and utility of 3D bioprinting technology will be discussed. These include bioprinting of tissue and organ constructs for reconstruction and development of *in vitro* tissue and organ models for drug discovery and screening. Furthermore, we discuss current challenges and future perspectives in advancing 3D bioprinting technology for translational applications.

2 Bioprinting of Tissues and Organs for Implantation *In Vivo*

The ability of 3D bioprinting to create living tissues and organs with complex geometry and function has led to translational applications in tissue engineering and regenerative medicine. With 3D bioprinting technology, investigators have created tissue constructs such as the bone (Tang et al. 2016), cartilage (Kang et al. 2016), skin (Skardal et al. 2012), nerve tissue (Owens et al. 2013), cardiac tissue (Duan 2016) and heart valve (Jana and Lerman 2015), and blood vessels (Hoch et al. 2014) for structural and functional repair of damaged tissues (Table 2). Currently, 3D bioprinted tissue constructs have been applied to various animal models, which show potential for functional tissue regeneration (Box 1) (Arslan-Yildiz et al. 2016; Ozbolat et al. 2016; Seol et al. 2014). By combining medical imaging and

Table 2 Bioprinting strategies to produce tissues and organs for transplantation

Tissue/organ type	Application model	Bioprinting technology	Cell type	Bioink	Size	Outcome	References
Bone	Calvarial bone defect model in rats	Extrusion	hAFSCs	Fibrinogen, gelatin, HA, glycerol	8 mm diameter × 1.2 mm thickness	Matured and vascularized bone tissue formation in vivo	(Kang et al. 2016)
	–	Extrusion	hAFSCs	Fibrinogen, gelatin, HA, glycerol	3.6 × 3.0 × 1.6 cm ³	Human mandible defect-shaped bone constructs Calcium deposition in vitro	(Kang et al. 2016)
Cartilage	Subcutaneous implantation in mice	Bioscaffolder (extrusion)	Goat MSCs, goat EPCs	Matrigel Alginate	10 × 10 mm ²	Vascularized bone tissue formation in vivo	(Fedorovich et al. 2011)
	Subcutaneous implantation in mice	Extrusion	Rabbit ear chondrocytes	Fibrinogen, gelatin, HA, glycerol	3.2 × 1.6 × 0.9 cm ³	Human ear-shaped cartilage tissue reconstruction	(Kang et al. 2016)
	Subcutaneous implantation in mice	Hybrid inkjet	Rabbit elastic chondrocytes	Fibrin/ collagen	1 mm thickness (five layers)	Cartilage-like tissues formation	(Xu et al. 2013a)
Osteochondral composite	Subcutaneous implantation in mice	Bioscaffolder (extrusion)	Human chondrocytes, osteogenic progenitors	Alginate	1 × 2 cm ²	Spatially organized heterogeneous tissue formation	(Fedorovich et al. 2012)

(continued)

Table 2 (continued)

Tissue/organ type	Application model	Bioprinting technology	Cell type	Bioink	Size	Outcome	References
Skin	Full-thickness excision in mice ($1 \times 1 \text{ cm}^2$)	Extrusion	Epidermal keratinocytes, hDFBs	Collagen	$5 \times 5 \text{ mm}^2 \times 4 \text{ layers}$	Multilayered skin constructs Effective proliferation and migration of keratinocytes and fibroblasts	(Yoon et al. 2016)
	Full thickness wound model in mice ($2 \times 2 \text{ cm}^2$)	Extrusion	AFSCs	Fibrin/collagen	In situ skin printing	In situ skin printing Full-thickness wound closure Neovascularization	(Skardal et al. 2012)
	Full-thickness wound model in mice	Laser-assisted bioprinting (Laser)	Human keratinocyte, fibroblasts	Collagen	$2.3 \times 2.3 \text{ cm}^2$	Multilayered epidermis tissue construction	(Koch et al. 2012; Michael et al. 2013)
	Full-thickness skin wound model in mice	Inkjet	Human microvascular ECs, hNDFs, epidermal keratinocytes	Collagen	$1.7 \times 1.7 \text{ cm}^2$	Microvasculature in a bi-layer skin graft Improved wound contraction	(Yanez et al. 2015)

Nerve graft	Rat sciatic nerve injury model	Extrusion	Schwamm cells, BMSCs	–	2 mm in diameter × 1 cm long	Three-channel nerve graft construct	(Marga et al. 2012; Owens et al. 2013)
Vessel	–	Extrusion	hASMCs, hAECs, hDFBs	–	–	Perfused and matured vascular grafts	(Marga et al. 2012; Norotte et al. 2009; Owens et al. 2013)
	Abdominal aortas in rats	Bio-3D printer	HUVEC, hASMCs, hDFBs,	–	Inner diameter of 1.5 mm	Scaffold-free tubular tissue Remodeling and endothelialization after implantation	(Itoh et al. 2015)
	–	Inkjet	HUVECs	Gelatin	0.7–1.5 mm × 0.5–1.2 mm in height	Perfused functional vascular channels	(Lee et al. 2014)
	–	Extrusion	Fibroblasts, HUVECs, hNDFs	Fugitive Pluronic F127, GelMA	–	Vascularized heterogeneous tissue constructs	(Kolesky et al. 2014)
	–	Extrusion	hMSCs, hNDFs, HUVECs	Gelatin, Fibrinogen	<1 cm	Thick vascularized tissue on a perfusion chip	(Kolesky et al. 2016)

(continued)

Table 2 (continued)

Tissue/organ type	Application model	Bioprinting technology	Cell type	Bioink	Size	Outcome	References
Cardiac tissue	Myocardial infarction in rats	Laser	hMSCs, HUVECs	PEUU	$26 \times 26 \times 1 \text{ mm}^3$	Enhanced blood vessels formation Preservation of cardiac function	(Gaebel et al. 2011)
	—	Bioscaffold (extrusion)	hCMPCs	Alginate	—	Homogenous distribution of cells Expression of early cardiac transcription factors	(Gaetani et al. 2012)
Heart valve	—	Extrusion	Aortic root sinus SMCs, Aortic VICs	Alginate/Gelatin	—	Anatomically complex aortic valve conduits	(Duan et al. 2013)
	—	Extrusion	Human aortic VICs	Me-HA/Me-Gel hybrid hydrogels	$5 \times 5 \times 1.5 \text{ mm}^3$	Bioprinted trileaflet valve conduits	(Duan et al. 2014)

AFSCs amniotic fluid stem cells, BMSCs bone marrow stem cells, ECs endothelial cells, EPCs endothelial progenitor cells, Gel/MA gelatin methacrylate, HA hyaluronic acid, hAECs human aortic endothelial cells, hASMCs human aortic smooth muscle cells, hCMPCs human cardiac-derived cardiomyocyte progenitor cells, hDFBs human dermal fibroblasts, hNDFs human neonatal dermal fibroblasts, HUVECs human umbilical vein endothelial cells, Me-Gel methacrylated gelatin, Me-HA methacrylated hyaluronic acid, MSCs mesenchymal stem cells, PEUU poly(ethylene urethane urea), SMCs smooth muscle cells, VICs valve leaflet interstitial cells

CAD/CAM technology, investigators are able to engineer anatomically accurate, patient-specific tissue constructs for reconstructive procedures (Kang et al. 2016; Murphy and Atala 2014).

Despite great progress, current applications of 3D bioprinted tissues are mainly limited to implantation in small animals (Ozbolat et al. 2016). To build clinically relevant sized tissue constructs for application, many challenges have to be addressed (see Sect. 4). In this section, we review recent applications of 3D bioprinting in tissue engineering and regenerative medicine and discuss 3D bioprinting strategies for mimicking tissue-specific properties of structure and function and their biological outcomes.

Box 1

Advantages of 3D bioprinting for transplantation:

- Engineers 3D living tissue/organ constructs that mimic natural structure and function
- Forms complex tissues by direct patterning and precise placement of living cells on specific locations
- Creates anatomically shaped, patient-specific tissue constructs by combining medical imaging and CAD/CAM technologies
- Rapidly produces tissues and organs compared with traditional tissue engineering scaffold fabrication methods

2.1 Bone

The bone supports the body structure, controls movement, and protects other organs (Cohen 2006). The bone is known to possess relatively good regenerative and self-repair capacity when defects are small. However, when bone is subjected to injury from trauma, cancer, pathological fractures, infection, or arthritis and other rheumatic diseases, its ability to fully regenerate is impaired and can lead to loss of function. Current surgical treatment options for bony defects include autograft, allograft, or prosthetic procedures. Autografts are considered as the best option for treating extensive bone defects, but it is expected that approximately 60% of them will fail within 10 years (Cancedda et al. 2007). As an alternative, engineered bone scaffolds have been actively explored in the tissue engineering and regenerative medicine areas. Most of these scaffold are composed of homogeneous mixtures of biomaterials, bioactive molecules (e.g., osteogenic factors), and cells. Cell-free scaffolds have been translated into the clinic, but are limited by inadequate integration into native bone and bone tissue formation (Gibbs et al. 2014). Recently, cell-based bone tissue constructs have been engineered, but it remains difficult to create clinically relevant tissue constructs, in terms of shape and size with conventional fabrication techniques (Amini et al. 2012).

Bioprinting technology has become an emerging method for bone graft generation. Grafts created via 3D bioprinting contain cellular and noncellular components in a single construct, thereby mimicking the complex structure and functionality of native bone tissue. Bioprinted bone constructs with cell-laden biomaterials have been successfully implanted into animal models of bony defects (Tang et al. 2016). In a recent report, bone tissue constructs were fabricated using an integrated tissue-organ printer (ITOP) system consisting of multi-dispensing modules; bone tissue formation was successful in their animal model (Kang et al. 2016). Calvarial bone constructs (8 mm diameter \times 1.2 mm thickness) were fabricated with PCL/tricalcium phosphate (TCP) mixture and human amniotic fluid-derived stem cells (hAFSCs) (Fig. 1a–b). In this study, composite hydrogels consisting of fibrinogen, gelatin, HA, and glycerol were used to deliver hAFSCs. To mimic the mechanical properties and structural stability of 3D bone constructs, multiple layers of PCL/TCP patterns were placed in between hAFSC patterns. By patterning Pluronic F-127 in outer layers of the constructs as a sacrificial material, the complex 3D structure was maintained during the entire printing process. The Pluronic F-127 was then dissolved out after cross-linking of fibrinogen with thrombin. Micro-channels ($500 \times 300 \mu\text{m}^2$) created within the construct were essential to maintain viability of cells by supplying adequate oxygen and nutrients supplement to the volumetric construct through diffusion. The printed bone constructs were then

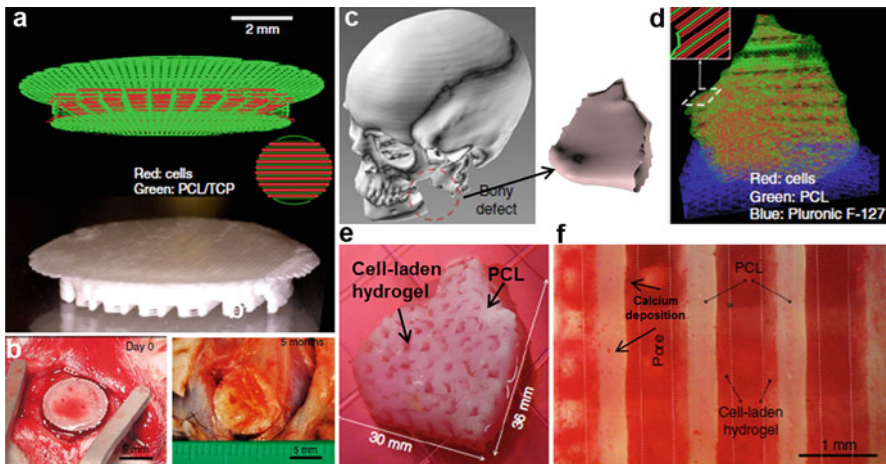


Fig. 1 Bioprinting of the bone. (a–b) Calvarial bone reconstruction (Kang et al. 2016). (a) Visualized motion program for bioprinting calvarial bone construct (top) and 3D bioprinted calvarial bone construct (bottom). (b) Photographs of implanted calvarial bone constructs in calvarial bone defect model in rats at day 0 and month 5. (c–f) Mandible bone reconstruction (Kang et al. 2016). (e) 3D bioprinted mandible bone construct after 28 days of in vitro culture. (f) Osteogenic differentiation of hAFSCs in the mandible bone constructs as evidenced by calcium deposition with Alizarin Red S staining (red color) (Figures reprinted with permission from Kang et al. (2016))

implanted to a calvarial bone defect region in Sprague Dawley rats. Five months later, new bone formation was observed in the implanted constructs with adequate vascular integration, demonstrating the feasibility of using 3D bioprinted bone constructs for calvarial bone tissue reconstruction.

For bone tissue reconstruction and regeneration, customized and personalized tissue constructions to fit patient-specific defects in size and shape would be desirable. Unlike other tissues, the bone is relatively hard, so a mismatch in shape and size between defects and implants may lead to failure of implantation or unfavorable outcomes (Shafiee and Atala 2016). 3D bioprinting enables to fabricate anatomically accurate patient-specific tissue constructs. Kang et al. fabricated a customized mandible bone construct based on a CT scan of a human mandible defect for mandible bone reconstruction (Fig. 1c–f) (Kang et al. 2016). The mandible bone construct was fabricated using hAFSC-laden composite hydrogels (final dimensions 3.6 cm × 3.0 cm × 1.6 cm), and osteogenic differentiation of hAFSCs was observed *in vitro*.

Small bone constructs containing cells (mm scale) have been fabricated via 3D bioprinting technologies and successfully implanted in animal models. However, larger-scale bone constructs for translational applications in large animal models and eventual clinical translation are still challenged by poor cell survival due to limited vascularization. To prevent cell death and achieve successful bone formation of 3D bioprinted bone constructs, adequate supply of oxygen and nutrients is necessary; thus, one approach is to fabricate pre-vascularized bone constructs (Liu et al. 2013). Fedorovich et al. printed heterogeneous constructs containing two different cell types with a BioScaffolder™ pneumatic dispensing system (Fedorovich et al. 2011). Porous constructs containing spatially organized mesenchymal stem cells (MSCs) and endothelial progenitor cells (EPCs) were printed. The constructs were implanted subcutaneously, and tissue formation by each type of cell was evaluated. In their study, the printed constructs maintained cellular heterogeneity after implantation; bone formation and mature blood vessel formation were observed in constructs containing MSCs and EPCs at 6 weeks post-implantation. This study illustrates that functional vascularized bone grafts can be created by bioprinting, which may eventually be used for treating larger bone defects in patients.

2.2 Cartilage

With the increasing numbers of aging people in our population, and the greater numbers of obese individuals, more people have cartilage damage and osteoarthritis than ever before (Li et al. 2013). Current treatments for articular cartilage repair include mosaicplasty, microfracture, autologous chondrocyte transplantation, and osteochondral allograft transplantation. Unfortunately, these treatments often result in structural and mechanical mismatches between regenerated tissues and surrounding native cartilage (Jeong and Atala 2015; Schuurman et al. 2015).

Articular cartilage is heterogeneous and composed of zonally differentiated cells and extracellular matrix (ECM); each zone has different biological and mechanical

properties. Tissue engineering approaches aim to mimic the zonal structure and function of the articular cartilage to recapitulate normal cartilage; however, recreating zonally stratified articular cartilage tissue remains a challenge. To this end, 3D bioprinting technology has been utilized to engineer articular cartilage constructs with zonally different cells and ECMs composition. Schuurman et al. designed a 3D zonal architecture of cartilage tissues composed of different cells contained in hydrogel and thermoplastic fibers in patterns with different mechanical stiffnesses, with the goal of improving clinical outcomes following implantation (Schuurman et al. 2011, 2015).

Current tissue engineering approaches for osteochondral implants to regenerate cartilage and subchondral bone are limited by insufficient tissue formation and poor integration between layers of cartilage and bone. In conventional strategies for engineering osteochondral composite tissues, two different types of scaffolds, one for cartilage and the other for bone, were created and then combined physically or chemically (Noeaid et al. 2012). However, the two scaffolds were easily separated following implantation, leading to insufficient osteochondral tissue formation (Schaefer et al. 2000).

Bioprinting technology is expected to address these issues because it allows for controlled spatial organization of multiple cell types and biomaterials in a single contiguous construct. Fedorovich et al. fabricated a cell-laden, heterogeneous osteochondral graft by introducing a 3D fiber deposition technique (Fedorovich et al. 2012). Alginate bioinks combined with chondrocytes and osteogenic progenitor cells were deposited directly adjacent to each other, with dimensions of 1 cm × 2 cm. The spatially organized cells remained in the initially printed region during *in vitro* culture. Six weeks after subcutaneous implantation in mice, heterogeneous tissue formation with a specific organization and matrix composition was observed, as evidenced by osteocalcin and collagen production. This study demonstrates the feasibility of engineering centimeter-scaled, porous, heterogeneous constructs using 3D fiber deposition technology to regenerate osteochondral defects.

Naturally derived biomaterials are widely used as cell-carrier materials in bioprinting due to their structural and biological resemblance to native tissues. However, these biomaterials have low to moderate mechanical properties that limit their utility in bioprinting of load-bearing tissues such as the bone and cartilage (Schuurman et al. 2011). Therefore, Xu et al. introduced a hybrid inkjet/electrospinning system to generate durable tissue constructs (Fig. 2a) (Xu et al. 2013a). They constructed electrospun PCL fibers and printed rabbit elastic chondrocytes in fibrin-collagen hydrogels deposited in alternating layers of 1 mm thickness. The hybrid constructs demonstrated enhanced mechanical properties compared to the constructs fabricated using inkjet printing alone, and the constructs formed cartilage-like tissue after subcutaneous implantation in mice.

3D printing also has been used to fabricate human auricular prostheses, and clinical applications for patients have been reported (Watson and Hatamleh 2014). However, 3D bioprinting of cell-laden ear structures remains challenging because it is difficult to print mechanically stable, human-scale tissue constructs with 3D complex architecture by using cell-laden hydrogel platforms. Very recently, Kang

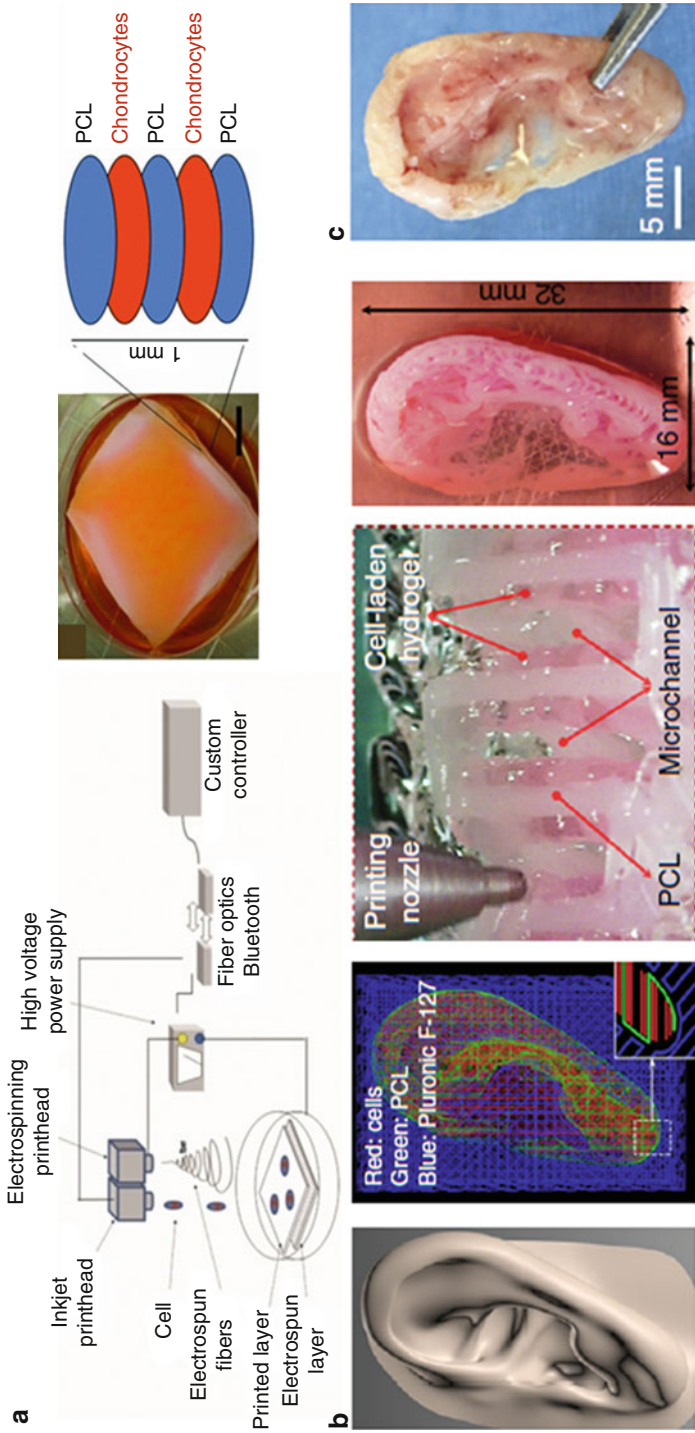


Fig. 2 Bioprinting of the cartilage. **(a)** Bioprinting of hybrid cartilage tissue construct by combining inkjet printing and electrospinning technologies (Xu et al. 2013a). **(b-c)** Human ear-shaped cartilage reconstruction (Kang et al. 2016). **(b)** 3D bioprinting of human ear by using the ITOP system and **(c)** cartilage formation in vivo (Figures reprinted with permission from Xu et al. (2013a) and Kang et al. (2016))

et al. successfully fabricated a human-sized external ear construct by using the ITOP system guided by CT images of the human ear (Fig. 2b) (Kang et al. 2016). The system contains multi-dispensing modules that can print chondrocyte-laden composite hydrogel and PCL layers in a single construct. The multiple PCL patterns prevented the collapse of cell-laden hydrogel patterns, resulting in construction of a structurally stable human ear (3.2 cm × 1.6 cm × 0.9 cm) with cartilaginous matrix formation *in vitro*. The anatomically shaped human ear was implanted in dorsal subcutaneous tissues in mice for 2 months; cartilage formation in the implants and structural maintenance were observed (Fig. 2c). This work brings the creation of 3D bioprinted biological ear cartilage constructs closer to human applications.

2.3 Skin

The skin is the largest organ in the body and plays an important role in the protection from the external environment and maintaining homeostasis (Bouwstra et al. 2003). Current treatment methods for skin injuries mainly caused by extensive burn injuries and full-thickness skin wounds include autologous split-thickness skin grafts, allografts, and xenografts. Despite some successful results in clinical applications, these treatments are still limited by the size of donor sites, immune rejection, and poor cosmetic outcomes (Sheridan and Greenhalgh 2014; Skardal and Atala 2015). One alternative is the use of acellular dermal skin substitutes such as Integra[®] and MatriDerm[®]. Although these substitutes can overcome some limitations and achieve efficient re-epithelialization and revascularization of the damaged skin, regeneration of damaged skin is a lengthy process (Pereira et al. 2007; Pham et al. 2007). Thus, cell-based skin substitutes, such as Dermagraft[®], Apligraf[®], and TransCyte[™], have been used to accelerate wound repair of large skin defects. These products require several weeks to culture cells *in vitro* prior to clinical use (Pham et al. 2007; Skardal et al. 2012). An alternative strategy, cell spraying, delivers cells directly to the wound, which is effective for superficial and partial-thickness burns, but further advances are needed (Gerlach et al. 2011).

One of the promising methods for cell-based therapy of skin injuries is skin bioprinting. Skin bioprinting can mimic the proper anatomic configuration of skin, which composed of multiple layers containing different cell types. The skin is comprised of two layers of dermis and epidermis, of which the main cell type is fibroblasts and keratinocytes (Bouwstra et al. 2003). To mimic normal human skin, Yoon et al. developed 3D skin grafts by modifying rapid prototyping methods and cell printing techniques (Fig. 3a) (Yoon et al. 2016). The bioprinted skin graft was composed of four layers of cell-laden collagen hydrogels. The top layer was printed with keratinocytes as an epidermis, and the other three layers of the bottom were fabricated with fibroblasts as a dermis. The printed scaffolds with dimensions of 5 × 5 mm² were transplanted to the full-thickness excision model of mice and demonstrated human skin-like tissue reconstruction and effective proliferation and migration of keratinocytes and fibroblasts. Another study by Michael et al. created a multilayered, cellularized skin substrate via a laser-assisted bioprinting technique

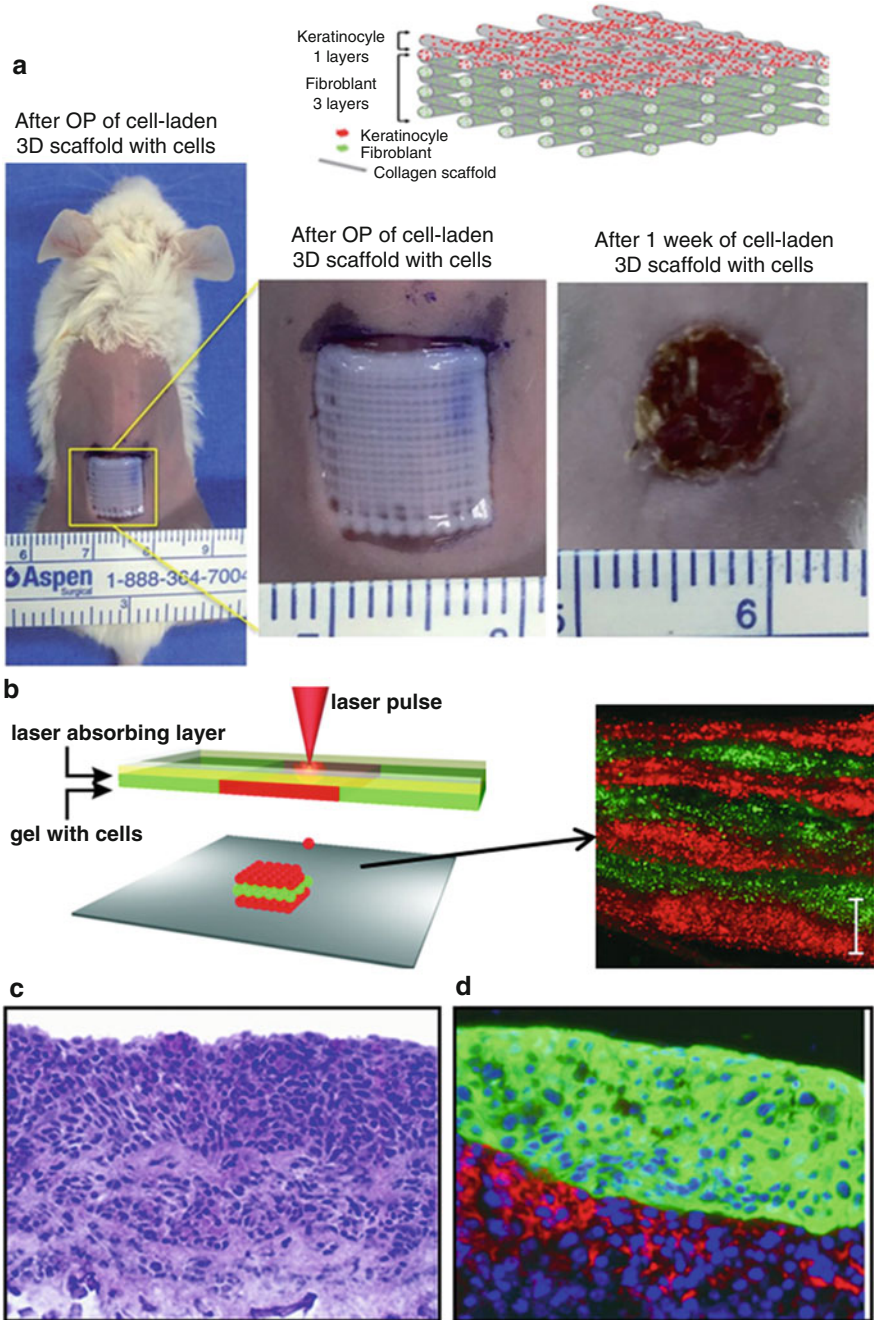


Fig. 3 Bioprinting of the skin. (a) Multilayered, cell-laden 3D skin scaffold composed of one layer of keratinocytes and three layers of fibroblasts (top) and transplantation of the bioprinted skin scaffold in full-thickness skin excision model in a mouse (bottom) (Yoon et al. 2016).

(Fig. 3b–d) (Koch et al. 2012). The skin substrates were fabricated by depositing 20 layers each of fibroblast- and keratinocyte-embedded collagen matrices onto a sheet of Matriderm[®] (2.3 cm × 2.3 cm), a commercialized acellular skin graft. The skin substitutes were fully connected to the host skin tissue and formed a stratified epidermis with differentiation and formation of the *stratum corneum* when they were transplanted to the full-thickness skin wounds on dorsa of mice (Michael et al. 2013).

Recently, in situ bioprinting of stratified skin substitutes has been proposed as a technique to apply skin cells directly onto the wound surface. In situ skin bioprinting technology can rapidly and uniformly cover wounds with different composition of cells and ECMs and geometry, depending on the wound sites. Skardal et al. used a skin bioprinter for in situ regeneration of large-scale wounds and burns (Skardal et al. 2012). Using in situ 3D bioprinting, skin substitutes composed of two layers of AFSCs-laden fibrin-collagen hydrogels were bioprinted directly onto full-thickness wounds in mice. Wound closure with re-epithelialization and microvascularization was achieved. For cross-linking, two layers of fibrin-collagen gel, used as a skin substitute, were printed by alternatively depositing thrombin and fibrinogen/collagen layers. AFSCs have a high proliferation rate, can differentiate to multiple lineages, and are nonimmunogenic.

A skin printer is currently being developed and optimized (Atala and Yoo 2015). The skin printer is built into a portable frame that is easily accessible for patients in the operating room. A scanning system is incorporated into the skin printer, scans the topography and dimensions of the wound, and guides the printer to deposit cells and extracellular matrix in layers to approximate the anatomic skin configuration. By introducing multiple-dispensing modules, skin substitutes composed of fibroblast- and keratinocyte-laden fibrin/collagen gel layers can be bioprinted in situ (Atala and Yoo 2015). Wound healing capacity of the in situ bioprinted skin substitutes is being investigated in full-thickness wound models in pigs before being tested in clinical applications.

2.4 Nerve

Clinically, the goal of surgery of damaged or severed nerve is to minimize loss of function by suturing the ends of the nerves. If this is not possible, a nerve guide is required to bridge the severed nerve ends to regrow axons and restore motor and sensory function. The gold standard for repair of nerve tissue is an autologous graft, but it is limited by donor site morbidity and mismatches between diameters and



Fig. 3 (continued) (b–d) Bi-layered skin tissue generated by laser cell printing (Koch et al. 2012). (b) Micropatterning capacity of the laser printing. (c) Hematoxylin and eosin stained images and (d) fluorescent images of skin mimicking a bi-layered construct composed of 20 layers of fibroblasts (red) and two layers of human keratinocytes (green) (Figures reprinted with permission from Yoon et al. (2016) and Koch et al. (2012))

mechanical properties of the nerve (Wolford and Stevao 2003). Autologous vein grafts, as a non-neural autologous tissue, have been used clinically and show axonal regeneration with functional repair, but these effects are not proven for gaps larger than 3 cm (Wolford and Stevao 2003). Most grafts currently in clinical use are noncellular grafts composed of synthetic polymers (e.g., PEG, PCL) or collagen (Gu et al. 2014). These materials allow control of graft size and address the shortage of the autologous grafts. However, noncellular grafts could not fully regenerate severed nerve tissues without cellular components. Thus, developing a cellular nerve graft is required for nerve repair, but it is still a challenge for tissue engineering and regenerative medicine.

Current neural tissue engineering has been focused on constructing straight tubular structures to guide nerve and cell growth. In particular, 3D bioprinting techniques enable control of the diameter and length of the nerve grafts as well as geometrical parameters. By applying 3D bioprinting techniques, Marga et al. developed a fully cellular bioprinted nerve graft for repair of peripheral nerve injury (Fig. 4) (Marga et al. 2012; Owens et al. 2013). They used a scaffold-free, self-assembly-based method to construct 3D nerve grafts, which had structures with multi-lumen channels. To create cellular cylinders, cellular spheroids (~500 μm) composed of Schwann cells and bone marrow stem cells (BMSCs) were printed, together with agarose support rods, by an extrusion-based bioprinting system (Fig. 4a–b). The printed cellular spheroids fused over time, resulting in formation of continuous tubes. After maturation for 7 days, the supporting agarose rods were

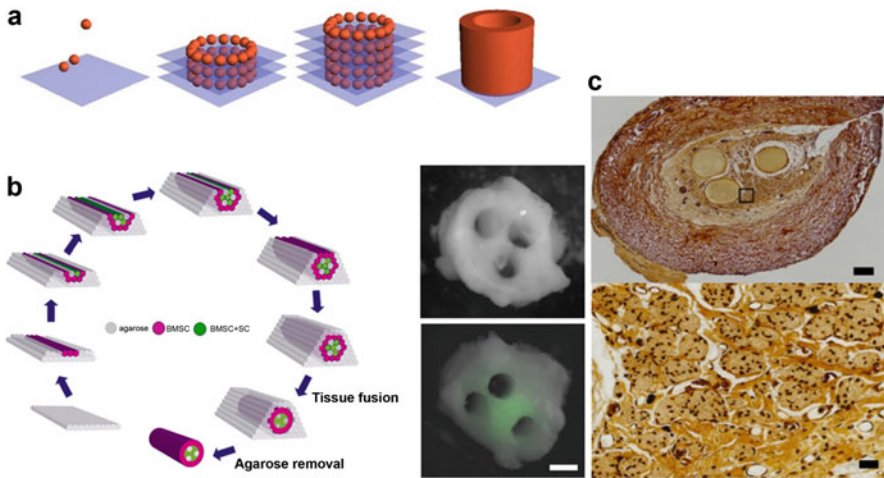


Fig. 4 Bioprinting of fully cellular nerve grafts (Marga et al. 2012; Owens et al. 2013). (a) Schematic diagram to create tubular structures with cellular spheroids and arrangement. (b) Schematics of bioprinting strategy for multicellular, cylinder-shaped nerve grafts (*left*) and photographs of bioprinted nerve grafts (*right*). (c) Bielschowsky's staining of histological sections of a bioprinted nerve graft, which was transplanted in the sciatic nerve damage model in a rat, showing axonal regeneration in the graft at week 40 (Figures reprinted with permission from Marga et al. (2012) and Owens et al. (2013))

removed for implantation (Fig. 4c). Histologic and functional repair of the fully biological nerve grafts was evaluated in a rat model of sciatic nerve injury model. The injury model was created by excision of 1 cm of sciatic nerve and then bridging the resulting gap with the bioprinted nerve graft. After 3 weeks of follow-up, about 40% of axons crossed the implanted nerve graft (Marga et al. 2012). This model showed functional repair of motor and sensory neurons at 40 weeks post-implantation, demonstrating the potential of a fully cellular bioprinted nerve graft for regenerating damaged or severed nerves (Owens et al. 2013).

2.5 Blood Vessels and Vascular Networks

Blood vessels and microvascular networks are essential to transfer oxygen and nutrients and remove metabolic wastes in the body (Novosel et al. 2011). In the field of tissue engineering and regenerative medicine, the ability to engineer functional blood vessels and vascular networks is required for viable tissues (Novosel et al. 2011). Any types of cell cannot survive in large volumetric tissue constructs for a long time without vascular networks, since the maximum diffusion distance of oxygen and nutrients is only about 200 μm (Novosel et al. 2011). Success in transplantation of bioprinted scale-up tissues and organs also may depend on vascularization which provides oxygen and nutrient supply to the cells for their survival and thereby exerting normal function. However, engineering of the vascular structure within 3D constructs remains a significant challenge in 3D tissues and organs. Several methods have been developed for fabricating vascular and microvascular structures by using 3D bioprinting technology (Hoch et al. 2014). Even though only a few have been tested in vivo, several approaches have potential use for in vivo applications on their own, or for creating vascularized complex tissue constructs.

A scaffold-free, self-assembly-based bioprinting approach similar to that used for nerves (mentioned in the previous section) was also used to engineer vascular grafts (Fig. 5a, b) (Marga et al. 2012; Norotte et al. 2009). To fabricate a cylindrical vascular graft, cell spheroids including human aortic smooth muscle cells, human aortic endothelial cells, and human dermal fibroblasts were printed in the agarose templates (Fig. 5a). The printed multicellular cell spheroids were fused and self-assembled into tubular structures at the post-printing stages (Fig. 5b, c), and the vascular graft was perfused in the bioreactor for vessel conditioning and maturation up to 3 weeks. This study yielded fully functional perfused and clinically relevant vascular grafts, which are applicable in vivo (Fig. 5d). A scaffold-free vascular tissue was generated by combining needle-assay technology and 3D bioprinting by Itoh et al. (Itoh et al. 2015). The 3D bioprinter placed multicellular spheroids in the needle-array system to have a 3D tube-shaped structure, and then it was matured in a perfusion system. The 3D printed vascular tissues of 1.5 mm in diameter and 7 mm in length were implanted into abdominal aortas of rats showing remodeling and endothelialization. In another study by Lee et al., a functional vascular channel with a perfused open lumen was created by combining 3D bioprinting with a flow chamber perfusion system (Lee et al. 2014). To fabricate the vascular channel, a

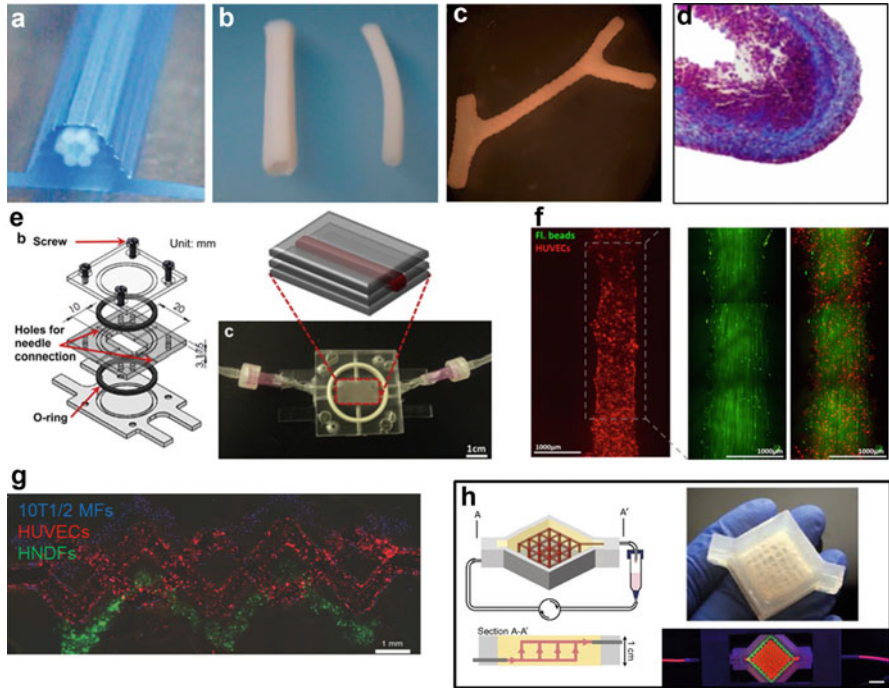


Fig. 5 Bioprinting of blood vessels and microvascular networks. (a–d) Bioprinting scaffold-free tubular structures for engineering blood vessels (Marga et al. 2012; Norotte et al. 2009). (a) The printed construct by layer-by-layer deposition of agarose rods and cells spheroids. (b) Photographs of bioprinted blood vessels resulted after 3 days of post-printed fusion. (c) The branched tubular construct after 6 days of post-printed fusion. (d) Masson’s trichrome staining of bioprinted blood vessels at day 21 of in vitro culture. (e–f) Perfused functional vascular channels (Lee et al. 2014). (e) Schematics of the bioprinted vascular channel construction connected to a custom-designed flow chamber. (f) Fluorescent images of vascular channel system on in vitro dynamic flow culture indicating the creation of perfused open lumen. (g) 3D printed vascularized, heterogeneous cell-laden tissue constructs (Kolesky et al. 2014). (h) 3D vascularized thick tissue housed within a perfusion chamber (Kolesky et al. 2016) (Figures reprinted with permission from Marga et al. (2012), Norotte et al. (2009), Lee et al. (2014), and Kolesky et al.(2016))

mixture of gelatin and human umbilical vein endothelial cells (HUVECs) was printed within a thick collagen matrix, and the printed constructs were then transferred to a custom-designed flow chamber. The resulting vascular grafts had a lumen structure covered with viable, aligned endothelial lining. The structure was maintained for up to 2 weeks under dynamic flow conditions (Fig. 5e, f).

Very recently, Kolesky et al. bioprinted a 3D cell-laden, vascularized thick tissue (>1 cm) that could be perfused for over 6 weeks (Kolesky et al. 2016). They also demonstrated the ability to create 3D bioprinted microvascular networks by using extrusion printing (Fig. 5g) (Kolesky et al. 2014). In that study, they integrated parenchyma, stroma, and endothelium into a single engineered 3D tissue model by co-printing multiple bioinks composed of human MSCs (hMSCs) and human

neonatal dermal fibroblasts in which vasculature was embedded (Fig. 5h). To create vascular networks within the customized and multicellular perfusion chip, acellular Pluronic F127 was used as a fugitive ink. After washing out the ink using cold cell media, HUVECs were injected to fill the vascular network. This 3D microvasculature perfused growth factors, which promoted differentiation of hMSCs toward an osteogenic lineage in situ. This study proposed a strategy to fabricate a physiologically relevant 3D vascularized thick tissue model using biofabrication technology with potential use for in vivo applications.

2.6 Cardiac Tissue and Heart Valve

Engineered cardiac tissue constructs for damaged cardiac muscles have been developed in tissue engineering and regenerative medicine, but very little success has been achieved in clinical trials due to significant biologic and physiologic challenges (Buikema et al. 2013; Jawad et al. 2008). In addition, traditional fabrication methods are inadequate to create cardiac constructs that mimic the complex anatomy of myocardial organization and beating property. Therefore, 3D bioprinting of cardiac tissue is promising in cardiac tissue reconstruction and repair (Duan 2016). For instance, Gaebel et al. fabricated a geometrically patterned cardiac patch by using a laser-based printer for treatment of myocardial infarction (Gaebel et al. 2011). The cardiac patch was patterned with hMSCs and HUVECs on polyester urethane urea (PEUU) and transplanted to the infarcted area in a rat after ligation of left anterior descending coronary artery (Fig. 6a). This bioprinted cardiac patch enhanced vessel

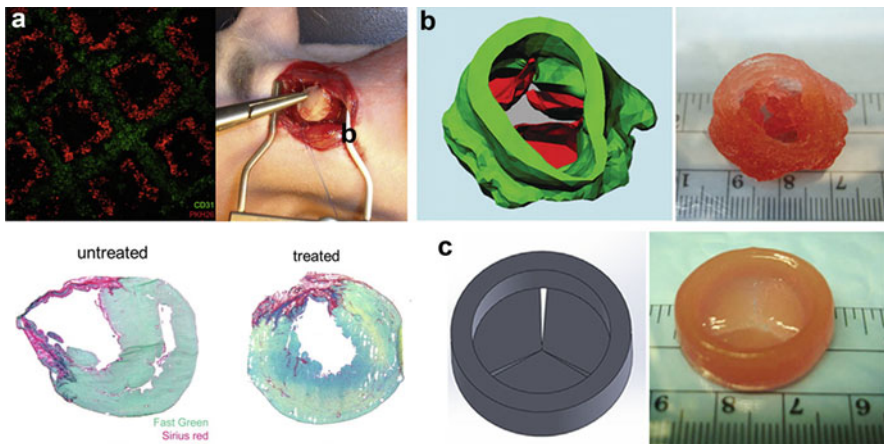


Fig. 6 Bioprinting of the cardiac tissue and heart valve. (a) Bioprinted cardiac patch with HUVECs and hMSCs in a defined pattern and cardiac repair evidenced by increased infarct wall thickness (Fast Green FCF/Sirius Red staining images) (Gaebel et al. 2011). (b) 3D bioprinted heterogeneous aortic valve conduit (Duan et al. 2013). (c) 3D bioprinted trileaflet valve conduit (Duan et al. 2014) (Figures reprinted with permission from Gaebel et al. (2011) and Duan et al. (2013))

formation and preservation of cardiac function. This group also showed the printability of human cardiac-derived cardiomyocyte progenitor cells (hCMPCs) by using a BioScaffolder (Gaetani et al. 2012). Printed hCMPCs were highly viable after at least 7 days *in vitro* culture and showed cardiac lineage phenotypes, as evidenced by gene expression of early cardiac transcription factors.

Heart valves are complex, with very limited regeneration capacity. Mechanical or biological prostheses have been used to replace damaged heart valves, but have been plagued by thrombogenicity and calcification (Jana and Lerman 2015). By contrast, 3D bioprinting technology can fabricate functional and cellular heart valves that mimic the native anatomic complexity. Duan et al. printed anatomically complex, heterogeneous aortic valve conduits using extrusion-based, dual-nozzle bioprinters (Duan et al. 2013). The valve root and leaflet were patterned with aortic root sinus smooth muscle cells and aortic valve leaflet interstitial cells, encapsulated on alginate/gelatin composite hydrogels, respectively (Fig. 6b). Printed cells were over 80% viable at 7 days *in vitro* culture within the 3D structure, with phenotypic retention. This group later fabricated a trileaflet valve conduit using human aortic valvular interstitial cells and encapsulated hybrid hydrogels (Fig. 6c) (Duan et al. 2014). By controlling the concentration and ratio of methacrylated hyaluronic acid and methacrylated gelatin in the hybrid hydrogel, they could fabricate anatomically accurate trileaflet valves that were highly viable and had remodeling potential.

3 Biofabrication of In Vitro Tissue/Organ Models

In vitro tissue/organ models can provide platforms for development of drugs and specific therapeutics and for understanding biological phenomena. Current 2D culture models cannot provide the tissue-specific, physiologically relevant functions of 3D models due to lack of cell-cell and cell-microenvironment interactions (Griffith and Swartz 2006). With the marked advances in 3D tissue fabrication/culture methods within the last decade, 3D *in vitro* tissue/organ models can now provide more realistic environments that mimic spatial and chemical complexity of living tissues and tissue-specific functions (Pampaloni et al. 2007). Various types of 3D tissue/organ models have been developed, such as randomly distributed or spatially separated cell-encapsulated hydrogel constructs, cellular spheroids, and mini-organs or organoids (tissue-like masses mimicking parts of an organ's functions). In addition, microfluidic organs on chips have been developed by combining 3D culture techniques with microfluidic systems (Bhatia and Ingber 2014). However, most *in vitro* 3D tissue/organ models are still unable to create highly controllable, multicellular, spatially and functionally complex microscale architecture (Pati et al. 2016). Therefore, 3D bioprinting techniques have been introduced to develop 3D *in vitro* tissue/organ models (Arslan-Yildiz et al. 2016; Cancedda et al. 2007; Pati et al. 2016). Although 3D bioprinted *in vitro* tissue/organ models are relatively new, they offer platforms for deeper understanding of physiological phenomena of tissues/organs and more accurate prediction of therapeutic/toxic responses. Advantages

of 3D bioprinted in vitro tissue/organ models are described in Box 2 (Arslan-Yildiz et al. 2016; Mandrycky et al. 2015; Ozbolat et al. 2016; Pati et al. 2016). In the next section, we introduce and discuss 3D bioprinted tissue/organ models for drug discovery and toxicity testing and cancer research (Table 3).

Box 2

Advantages of 3D bioprinted in vitro tissue/organ models:

- Realistic 3D mimicry of complex morphological, pathological, and physiological structure and functions of living tissue in vitro
- Multiple cell types and biomaterials at targeted locations with high precision
- Creates cell-cell interactions, cell-extracellular matrix environments, and tissue-tissue interfaces
- Rapid production and high-throughput screening
- Accurately predictable and cost-effective preclinical drug discovery/screening tools
- Elucidates basic mechanisms of tissue/organ physiology, pathophysiology, and tumorigenesis, reducing need for animal studies and facilitating translation of drugs into clinics
- Possible customization and personalization of specific tissue models for drug discovery and therapeutics

3.1 Drug Discovery and Toxicity Testing

The use of 3D bioprinted in vitro tissue/organ models is promising in drug discovery and toxicity test studies with various advantages. These models can be more realistic than traditional 2D culture and 3D tissue models. 3D bioprinting can fabricate complex tissues/organs, either normal or diseased, by controlling specific locations of several cell types and materials, which could improve accuracy of drug response. The development of in vitro human tissue/organ models with high precision can reduce the numbers of preclinical animal studies needed for drug testing, thereby reducing time and costs and accelerating translation of drugs to clinical applications (Pati et al. 2016). Therefore, 3D bioprinted in vitro tissue/organ models can offer an accurate, reproducible, highly controllable, and cost-effective tool for drug discovery.

Liver tissue/organ models are increasingly of interest in drug testing and high-throughput screening because the liver plays a primary role in drug metabolism in the body (Bernal and Wendon 2013). For instance, Chang et al. developed a 3D liver micro-organ device as an in vitro model for drug discovery and metabolism test (Chang et al. 2008). They combined 3D bioprinting with microfluidics to apply continued perfusion flow to the bioprinted liver micro-organ. For creating a liver micro-organ chamber, hepatocyte-laden alginate hydrogels were directly bioprinted

Table 3 3D bioprinting of in vitro tissue/organ models for drug screening/toxicity tests and cancer research

Application model	Biofabrication technology	Cell type	Bioink	Outcome	References
3D liver micro-organ	Extrusion	Hepatocytes	Alginate	3D liver micro-organ model combined with microfluidics Continuous perfusion drug flow	(Chang et al. 2008, 2010)
exVive3D™	NovoGen MIMX Bioprinter™ (Extrusion)	Human hepatocytes, Hepatic stellate, ECs	–	Albumin secretion Clinical trial for drug toxicity testing	(Vaidya 2015)
Mini-liver	Inkjet	hiPSCs	Alginate	Animal-free drug discovery and personalized medicine Hepatocyte-like cells differentiation Albumin secretion	(Faulkner-Jones et al. 2015)
Skin model	Extrusion	Human skin fibroblasts and keratinocytes	Collagen	Dermal/epidermal-like distinctive layers	(Lee et al. 2009)
Human air-blood tissue barrier model	Inkjet	Alveolar epithelial cells, ECs,	Matrigel	Realistic 3D in vitro alveolar model	(Horvath et al. 2015)
3D cell assays	Laser	hASCs, ECFCs	Fibrin precursors, HA	Mimicry of 3D cell-microenvironments	(Grune et al. 2011)
Cervical tumor model	Extrusion	HeLa cells	Gelatin/alginate/fibrin	Cellular spheroid formation Chemoresistance in 3D model	(Zhao et al. 2014)
Ovarian cancer co-culture model	Inkjet	Human ovarian cancer cells, Normal fibroblasts	–	Spontaneous multicellular actini formation High-throughput screening	(Xu et al. 2011)
Human breast cancer model	NovoGen Bioprinting™ (Extrusion)	Breast cancer cell, Mammary fibroblasts, ECs, Adipocytes	–	Viable breast neo-tissue Chemotherapeutic drug response	(King et al. 2014)

ECs endothelial cells, ECFCs endothelial colony-forming cells, HA hyaluronic acid, hASCs human adipose-derived stem cells, hiPSCs human-induced pluripotent stem cell

within the microfluidic chamber of the polydimethylsiloxane substrate. The 3D bioprinted liver micro-organ device showed predictable cell viability and proliferation outcomes and enhanced liver cell-specific function, such as urea synthesis, compared to traditional 2D culture method. In addition, they showed effective drug metabolic function compared to the static culture condition. These results demonstrated feasibility of the 3D bioprinted liver micro-organ device for a drug-testing platform.

A single-tissue model sometimes yields false-positive or false-negative results for drug tests, because some drugs are metabolized and converted to the active or inactive forms before reaching the target tissues. Therefore, to facilitate cell-cell interaction and more closely mimic downstream effects of metabolism on the target liver tissue, a multiple-tissue model has been used. Amifostine, for example, is an anti-radiation drug which is converted to an active form by epithelial cells. To model pathogenesis *in vivo*, Snyder et al. (Snyder et al. 2011) created a dual-tissue microfluidic chip (Fig. 7a) to test the conversion and radioprotective effects of amifostine on the target liver tissue. The dual-tissue microfluidic chip was created

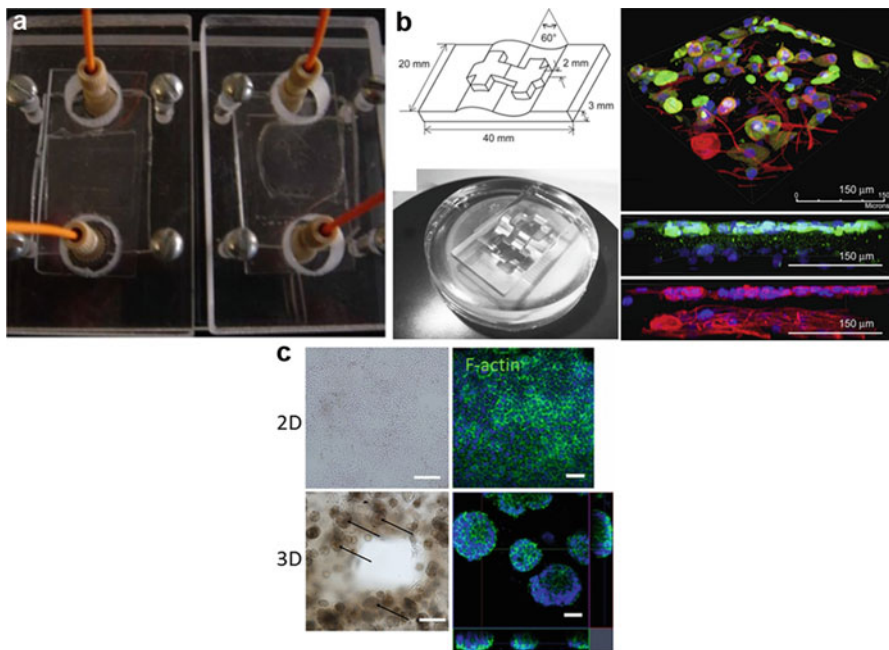


Fig. 7 Bioprinting of 3D *in vitro* tissue/organ model. (a) Dual-tissue microfluidic chip (Snyder et al. 2011). (b) Fabrication of 3D skin wound model (Lee et al. 2009). 3D PDMS mold having non-planar surface for printing multiple layers of skin cells (left). Immunofluorescent images of multilayered printing of keratinocytes and fibroblasts (Keratin: green, β -tubulin: red). (c) Bioprinted cervical cancer model. Cell spheroids formation in 3D constructs at day 8 (Zhao et al. 2014) (Figures reprinted with permission from Snyder et al. (2011), Lee et al. (2009), and Zhao et al. (2014))

by direct printing of epithelial cell- and hepatocyte-encapsulated Matrigel within each microfluidic chamber. After radiation exposure, the injected drug passed the epithelial cell-laden chamber before reaching the hepatocyte-laden chamber in this chip, as the drug would pass endothelial cells from the blood stream to the target tissue *in vivo*. Enhanced radioprotective effects of the testing drug were reported compared to the single-tissue system.

Recently, the 3D printed exVive3D™ platform was tested for use in drug toxicity tests for liver tissue (Vaidya 2015). A scaffold-free liver tissue model consisting of pellets of human hepatocytes, hepatic stellate and endothelial cells was printed using a NovoGen MMX Bioprinter™. It had a liver-like structure and long-term function, as shown by secretion of liver-specific albumin protein up to 42 days. This model has now been used in clinical trials for drug toxicity testing, making a breakthrough toward commercialization of a 3D bioprinted model of liver.

Faulkner-Jones et al. bioprinted 3D mini-livers for the first time by using human-induced pluripotent stem cells (hiPSCs) (Faulkner-Jones et al. 2015). By using alginate hydrogel as a cell-encapsulating material and a dual-head valve-based inkjet printer, the hiPSCs can be bioprinted, maintaining cell viability and pluripotency. In this study, post-printing differentiation of printed hiPSCs into hepatocyte-like cells was reported, as shown by expression of hepatocyte markers, including hepatocyte nuclear factor 4 alpha (HNF4 α) and albumin secretion. Their work showed the potential to bioprint tissues or organs containing patient-specific cells for animal-free drug discovery and eventually for personalized medicine.

Bioprinting of lung tissue is relatively new, and a realistic 3D *in vitro* alveolar model is not yet available. An advanced 3D lung model was created using BioFactory® (regenHU) for drug testing (Horvath et al. 2015). To mimic the microenvironment of the native tissue, an *in vitro* human air-blood barrier architecture was fabricated composed of zonally stratified endothelial cells, basement membrane, and epithelial cell layers. By using 3D bioprinting, very thin layers of Matrigel were used as a basement membrane and uniform cell layers were generated compared to the conventional manual seeding method. This bioprinted 3D lung tissue model is expected to provide an excellent tool for high-throughput screening for drug screening and toxicity tests.

In the pharmaceutical and cosmetics industries, 3D bioprinting technology has been applied to engineer human skin tissue substitutes for testing specific drugs or products. For instance, to create a more realistic 3D skin wound model, Lee et al. printed multilayered skin tissues on the PDMS mold having non-planar surface (Fig. 7b) (Lee et al. 2009). The 3D bioprinted skin tissue model had dermal/epidermal-like distinctive layers consisting of human skin fibroblasts and keratinocytes, showing that biologically comparable skin tissue printing is possible. This study showed the potential to create a tailored skin tissue model in wound shape for disease models and drug tests. Recently, cosmetic companies began to introduce 3D bioprinted skin tissue models to test cosmetics. L’Oreal USA announced a partnership with Organovo to develop 3D bioprinted skin tissue (Markin 2016).

Their collaboration is expected to provide more advanced skin tissue models for prescription drug and toxicity tests.

3.2 Cancer Research

2D models have been used for cancer research *in vitro*, but they provide very limited information due to lack of biomimicry of natural tumor environments. Therefore, a 3D tissue model that can mimic/represent complex tumor environments of cell-cell and cell-matrix interactions *in vivo* is needed for better understanding of cancer biology before effective treatments can be developed (Kim 2005; Padron et al. 2000). Bioprinting holds promise to fabricate 3D *in vitro* cancer tissue models that more closely imitate the complex and physiological environments of tumors. 3D bioprinting to create cancer tissue models *in vitro* is an emerging field, and only a few studies have been reported so far.

In one example, a 3D cervical tumor model was recently created by 3D bioprinting (Zhao et al. 2014). The *in vitro* cervical tumor model (dimensions of $10 \times 10 \times 2 \text{ mm}^3$) was extrusion printed by patterning HeLa cells derived from cervical cancer tissues. To mimic the extracellular matrix of cervical cancer tissue, a composite hydrogel composed of gelatin, alginate, and fibrinogen was used as a bioink. The printed HeLa cells showed viability of over 90% and formed spheroids in the 3D environment (Fig. 7c). This is promising because 3D cellular spheroids are commonly used *in vitro* as 3D tumor models for antitumor therapy (Friedrich et al. 2007). The possibility of 3D bioprinting of *in vitro* cancer model was further demonstrated by increased cell proliferation, indicating factors of tumor metastasis and chemoresistance compared to a 2D culture model.

Physiologically relevant 3D co-culture models of fibroblasts and ovarian cancer cells are needed because fibroblasts are closely related to the growth and progression of ovarian cancer (Kenny et al. 2007). However, precise control and patterning of each cell type are difficult in conventional 3D tissue models. Therefore, an *in vitro* 3D ovarian cancer co-culture model was developed with a bioprinting system (Xu et al. 2011). This group printed human ovarian cancer cells and normal fibroblasts on Matrigel platforms. Cell density per droplet, droplet size, and spatial distance between droplets of each cell types were controlled. Spontaneous multicellular acini formations of printed cells were observed; these proliferated within the 3D patterned co-culture model. This study demonstrated the ability to create an *in vitro* ovarian cancer co-culture model via bioprinting technology for future cancer research and high-throughput screening.

A scaffold-free human breast cancer model (the NovoGen Bioprinting™ Platform) was created for therapeutic drug screening (King et al. 2014). To mimic the tumor microenvironment, the models were composed of breast cancer cells in the core as well as breast stromal cells such as mammary fibroblasts, endothelial cells and adipose cells. The 3D breast neo-tissue was then directly printed into multi-well

plates for high-throughput screening of chemotherapeutic drugs. The bioprinted breast cancer neo-tissue was viable for 2 weeks and less susceptible to chemotherapeutic agents than breast cancer cells in 2D culture. The therapeutic effect of anticancer drugs is frequently overestimated in the 2D cancer tissue models because cells in 2D react quickly and are more sensitive than cells in the complex 3D microenvironments. Therefore, the results demonstrated that this 3D bioprinted breast cancer model could be an effective tool for development of anticancer therapeutics and drug screening.

4 Current Challenges and Future Perspectives

3D bioprinting has shown great progress and promise for creating 3D living tissues and organs. Several types of 3D bioprinted tissues and organs that mimic structural and functional characteristics of natural tissues and organs have been created by spatial patterning of cell-laden bioinks with inkjet-, extrusion-, or laser-based bioprinters. In tissue engineering and regenerative medicine, 3D bioprinted living tissues (including bone, cartilage, skin, nerve, and cardiac tissue, heart valve, blood vessel and microvascular networks) have been constructed. Some of them have successfully been transplanted to animals. Furthermore, 3D bioprinting has been widely applied in areas such as physiology, oncology, and pathology and in the cosmetics and pharmaceutical industries. The 3D bioprinted *in vitro* tissues/organ models offer a drug discovery and screening platform, enabling an accurate prediction of preclinical effects of drugs and a tool for understanding basic mechanisms of tissue/organ physiology and tumorigenesis. However, despite the great progress and broad applications of 3D bioprinting, there remain many challenges to be addressed for further applications and eventual translation to clinical use (Box 3).

Current applications for implantation of 3D bioprinted tissues in tissue engineering and regenerative medicine are mainly limited to small animals, and none of the bioprinted tissues has been used clinically. The ability to scale up tissues and organs via bioprinting techniques is needed for rapid clinical transplantation. To do so, issues related to cell viability and long-term structural stability should be addressed. In large-sized tissues, supplying oxygen and nutrient supplies to the cells are difficult. To overcome this limitation, vascularization of bioprinted tissues is a possible strategy. Incorporation of vascular patterns such as bioprinted blood vessels or microvascular networks into bioprinted tissue constructs can be a potential solution for maintaining cell survival. Incorporation of biological factors for promoting angiogenesis within the bioprinted tissues can be an alternative approach. In addition, porosity and pore size of scaffolds could be redesigned to provide sufficient space for formation of vascular networks and accelerate angiogenesis.

To fabricate tissues large enough for clinical use, biologically functional and mechanically robust bioinks are needed. Current printable bioinks are mainly natural

hydrogel-based biomaterials and their composites. The hydrogel-based bioinks provide 3D microenvironments for the cells to survive and proliferate long-term within the bioprinted tissue constructs. However, they have weak mechanical properties after cross-linking (Stanton et al. 2015). Synthetic biomaterials used as bioinks are mechanically stable and easily controllable compared to the natural-derived hydrogels, but they have relatively long degradation times and low cytocompatibility that results in delayed tissue formation *in vitro* and *in vivo* (Skardal and Atala 2015). Therefore, optimizing bioinks that can support cell functions and mechanical properties may be a key factor for advancement in 3D bioprinting technologies.

Cell source and quality also need to be addressed for translation of 3D bioprinted tissues and organs into clinical uses and pharmaceutical applications. In the tissue engineering and regenerative medicine fields, the usage of patient-specific primary cells isolated has been recommended for implantation to reduce immunogenic risks. *In vitro* 3D tissue/organ models using patient-specific cells would enable diagnostics and development of patient-specific drugs/therapies in personalized medicine. For further application of 3D bioprinted tissues and organs, clinically relevant and reproducible cell sources are needed that can be expanded in large quantities and are well characterized. Although stem cells such as hAFSCs and hiPSCs have currently been used as patient-specific cell sources (Skardal et al. 2012; Yoshida and Yamanaka 2010), more refinements are needed to better control differentiation of stem cells with specific lineages or functions within the 3D bioprinted tissues and organs. In addition, multiple cell types are needed to more closely mimic the highly complex anatomy and function of native tissues.

Although the 3D bioprinters such as extrusion-, inkjet-, and laser-based bioprinters have seen significant improvements for fabricating 3D living tissues and organs, several issues remain to be addressed. To fabricate more complex tissue constructs, high-resolution bioprinters ($<10\ \mu\text{m}$) is needed. In addition, integration of multi-dispensing systems into the bioprinter facilitates a simultaneous bioprinting of multiple cell types and biomaterials to fabricate complex tissues with desired function (Kang et al. 2016). For fabricating tissues large enough for clinical use, high-resolution bioprinters are required to increase the speed of the printing process. Since cells are exposed to stressful conditions (e.g., limited oxygen and nutrient supply) in the cartilage, and high pressure and shear stress during the printing process, a longer printing time leads to more cell death. In addition, mechanical properties of bioinks, especially hydrogels, can change during long printing process, impairing printing resolution. Therefore, a real-time monitoring/controlling system of the printing environment is needed in future 3D bioprinting technologies. New types of bioprinters in which several types of bioprinting modalities are integrated or other biofabrication technologies are combined (i.e., microfluidics, electrospinning, microfabrication) are among the potential solutions to overcome current technical limitations of 3D bioprinting (Kolesky et al. 2016; Snyder et al. 2011; Visser et al. 2015; Xu et al. 2013a).

Challenges facing the 3D bioprinting technologies related to technical, mechanical, biological, and biomaterial issues can be addressed through close collaborations

among engineers, scientists, and clinicians. This multidisciplinary approach can offer solutions for advancements in 3D bioprinting and accelerate translation and applications.

Box 3

Future perspectives of 3D bioprinting tissues and organs:

- Bioprinting of vascular networks for scaling up 3D tissues or organs for clinical translation
- Development of biologically functional and mechanically robust bioinks for use in bioprinting
- Clinically relevant, well-characterized, reproducible cell sources
- Bioprinting of 3D tissues and organs with multiple cell types to mimic highly complex anatomy and function of native tissues
- Advanced bioprinting technologies with increased resolution and speed and automatic monitoring/controlling system
- Combinations with other biofabrication technologies to overcome current technical challenges
- Standardization and optimization of bioprinting processes to enable manufacturing and commercialization
- Collaboration with engineers, basic scientists, clinicians, and manufacturers

5 Conclusions

3D bioprinting is an advanced technology for fabricating 3D living tissues and organs with great potential in a variety of applications. This technique can fabricate several types of complex and functional tissue and organ constructs and has shown great regenerative capacity in animal transplantation. It also provides a tool for drug discovery, toxicity tests, and cancer research. The 3D bioprinted in vitro tissue/organ models can facilitate future investigations of physiological phenomena of normal/diseased/tumorigenic tissues and enables accurate prediction and fast screening of drugs/therapies. Even though 3D bioprinting technology is still in its infancy and faces many challenges to be addressed for clinical translation, multidisciplinary research and close collaboration between engineer, scientists, and clinicians will be able to overcome the challenges and realize the potential of 3D printing in translation and applications to a variety of areas.

Acknowledgments This research was supported, in part, by the Basic Science Research Program through the Research Foundation of Korea (NRF), funded by the Ministry of Education, Science and Technology (NRF-2012R1A6A3A03040684). The authors thank Karen Klein, MA, at the Wake Forest Clinical and Translational Science Institute (UL1 TR001420; PI: Li) for editorial assistance.

References

- Amini AR, Laurencin CT, Nukavarapu SP (2012) Bone tissue engineering: recent advances and challenges. *Crit Rev Biomed Eng* 40:363–408
- Arslan-Yildiz A, Assal RE, Chen P, Guven S, Inci F, Demirci U (2016) Towards artificial tissue models: past, present, and future of 3D bioprinting. *Biofabrication* 8:014103
- Atala A, Yoo J (2015) *Essentials of 3D biofabrication and translation*. Elsevier, London
- Bajaj P, Schweller RM, Khademhosseini A, West JL, Bashir R (2014) 3D biofabrication strategies for tissue engineering and regenerative medicine. *Annu Rev Biomed Eng* 16:247–276
- Ballyns JJ, Gleghorn JP, Niebrzydowski V, Rawlinson JJ, Potter HG, Maher SA, Wright TM, Bonassar LJ (2008) Image-guided tissue engineering of anatomically shaped implants via MRI and micro-CT using injection molding. *Tissue Eng Part A* 14:1195–1202
- Bernal W, Wendon J (2013) Acute liver failure. *N Engl J Med* 369:2525–2534
- Bhatia SN, Ingber DE (2014) Microfluidic organs-on-chips. *Nat Biotechnol* 32:760–772
- Bouwstra JA, Honeywell-Nguyen PL, Gooris GS, Ponc M (2003) Structure of the skin barrier and its modulation by vesicular formulations. *Prog Lipid Res* 42:1–36
- Buikema JW, Van Der Meer P, Sluijter JP, Domian IJ (2013) Concise review: engineering myocardial tissue: the convergence of stem cells biology and tissue engineering technology. *Stem Cells* 31:2587–2598
- Campbell PG, Miller ED, Fisher GW, Walker LM, Weiss LE (2005) Engineered spatial patterns of FGF-2 immobilized on fibrin direct cell organization. *Biomaterials* 26:6762–6770
- Cancedda R, Giannoni P, Mastrogiacomo M (2007) A tissue engineering approach to bone repair in large animal models and in clinical practice. *Biomaterials* 28:4240–4250
- Chang R, Nam J, Sun W (2008) Direct cell writing of 3D microorgan for in vitro pharmacokinetic model. *Tissue Eng Part C Methods* 14:157–166
- Chang R, Emami K, Wu H, Sun W (2010) Biofabrication of a three-dimensional liver micro-organ as an in vitro drug metabolism model. *Biofabrication* 2:045004
- Chang CC, Boland ED, Williams SK, Hoying JB (2011) Direct-write bioprinting three-dimensional biohybrid systems for future regenerative therapies. *J Biomed Mater Res B Appl Biomater* 98:160–170
- Cohen MM Jr (2006) The new bone biology: pathologic, molecular, and clinical correlates. *Am J Med Genet A* 140:2646–2706
- Cui XF, Breitenkamp K, Finn MG, Lotz M, D’Lima DD (2012) Direct human cartilage repair using three-dimensional bioprinting technology. *Tissue Eng Part A* 18:1304–1312
- Demirci U, Montesano G (2007) Single cell epitaxy by acoustic picolitre droplets. *Lab Chip* 7:1139–1145
- Duan B (2016) State-of-the-art review of 3D bioprinting for cardiovascular tissue engineering. *Ann Biomed Eng*. <https://doi.org/10.1007/s10439-016-1607-5>
- Duan B, Hockaday LA, Kang KH, Butcher JT (2013) 3D bioprinting of heterogeneous aortic valve conduits with alginate/gelatin hydrogels. *J Biomed Mater Res A* 101:1255–1264
- Duan B, Kapetanovic E, Hockaday LA, Butcher JT (2014) Three-dimensional printed trileaflet valve conduits using biological hydrogels and human valve interstitial cells. *Acta Biomater* 10:1836–1846
- Faulkner-Jones A, Fyfe C, Cornelissen DJ, Gardner J, King J, Courtney A, Shu W (2015) Bioprinting of human pluripotent stem cells and their directed differentiation into hepatocyte-like cells for the generation of mini-livers in 3D. *Biofabrication* 7:044102
- Fedorovich NE, Wijnberg HM, Dhert WJ, Alblas J (2011) Distinct tissue formation by heterogeneous printing of osteo- and endothelial progenitor cells. *Tissue Eng Part A* 17:2113–2121
- Fedorovich NE, Schuurman W, Wijnberg HM, Prins HJ, van Weeren PR, Malda J, Alblas J, Dhert WJ (2012) Biofabrication of osteochondral tissue equivalents by printing topologically defined, cell-laden hydrogel scaffolds. *Tissue Eng Part C Methods* 18:33–44
- Friedrich J, Ebner R, Kunz-Schughart LA (2007) Experimental anti-tumor therapy in 3-D: spheroids – old hat or new challenge? *Int J Radiat Biol* 83:849–871

- Gaebel R, Ma N, Liu J, Guan J, Koch L, Klopsch C, Gruene M, Toelk A, Wang W, Mark P et al (2011) Patterning human stem cells and endothelial cells with laser printing for cardiac regeneration. *Biomaterials* 32:9218–9230
- Gaetani R, Doevendans PA, Metz CH, Alblas J, Messina E, Giacomello A, Sluijter JP (2012) Cardiac tissue engineering using tissue printing technology and human cardiac progenitor cells. *Biomaterials* 33:1782–1790
- Gerlach JC, Johnen C, McCoy E, Brautigam K, Plettig J, Corcos A (2011) Autologous skin cell spray-transplantation for a deep dermal burn patient in an ambulatory treatment room setting. *Burns* 37:e19–e23
- Gibbs DM, Vaezi M, Yang S, Oreffo RO (2014) Hope versus hype: what can additive manufacturing realistically offer trauma and orthopedic surgery? *Regen Med* 9:535–549
- Griffith LG, Swartz MA (2006) Capturing complex 3D tissue physiology in vitro. *Nat Rev Mol Cell Biol* 7:211–224
- Gruene M, Pflaum M, Hess C, Diamantouros S, Schlie S, Deiwick A, Koch L, Wilhelmi M, Jockenhoevel S, Haverich A et al (2011) Laser printing of three-dimensional multicellular arrays for studies of cell-cell and cell-environment interactions. *Tissue Eng Part C Methods* 17:973–982
- Gu X, Ding F, Williams DF (2014) Neural tissue engineering options for peripheral nerve regeneration. *Biomaterials* 35:6143–6156
- Guillemot F, Souquet A, Catros S, Guillotin B, Lopez J, Faucon M, Pippenger B, Bareille R, Remy M, Bellance S et al (2010) High-throughput laser printing of cells and biomaterials for tissue engineering. *Acta Biomater* 6:2494–2500
- Guillotin B, Guillemot F (2011) Cell patterning technologies for organotypic tissue fabrication. *Trends Biotechnol* 29:183–190
- Guillotin B, Souquet A, Catros S, Duocastella M, Pippenger B, Bellance S, Bareille R, Remy M, Bordenave L, Amedee J et al (2010) Laser assisted bioprinting of engineered tissue with high cell density and microscale organization. *Biomaterials* 31:7250–7256
- Hoch E, Tovar GE, Borchers K (2014) Bioprinting of artificial blood vessels: current approaches towards a demanding goal. *Eur J Cardiothorac Surg* 46:767–778
- Horvath L, Umehara Y, Jud C, Blank F, Petri-Fink A, Rothen-Rutishauser B (2015) Engineering an in vitro air-blood barrier by 3D bioprinting. *Sci Rep* 5:7974
- Itoh M, Nakayama K, Noguchi R, Kamohara K, Furukawa K, Uchihashi K, Toda S, Oyama J, Node K, Morita S (2015) Correction: scaffold-free tubular tissues created by a bio-3D printer undergo remodeling and endothelialization when implanted in rat aortae. *PLoS One* 10:e0145971
- Jana S, Lerman A (2015) Bioprinting a cardiac valve. *Biotechnol Adv* 33:1503–1521
- Jawad H, Lyon AR, Harding SE, Ali NN, Boccaccini AR (2008) Myocardial tissue engineering. *Br Med Bull* 87:31–47
- Jeong CG, Atala A (2015) 3D printing and biofabrication for load bearing tissue engineering. *Adv Exp Med Biol* 881:3–14
- Jiao A, Trosper NE, Yang HS, Kim J, Tsui JH, Frankel SD, Murry CE, Kim DH (2014) Thermo-responsive nanofabricated substratum for the engineering of three-dimensional tissues with layer-by-layer architectural control. *ACS Nano* 8:4430–4439
- Jones N (2012) Science in three dimensions: the print revolution. *Nature* 487:22–23
- Kang HW, Lee SJ, Ko IK, Kengla C, Yoo JJ, Atala A (2016) A 3D bioprinting system to produce human-scale tissue constructs with structural integrity. *Nat Biotechnol* 34:312–319
- Kenny HA, Krausz T, Yamada SD, Lengyel E (2007) Use of a novel 3D culture model to elucidate the role of mesothelial cells, fibroblasts and extra-cellular matrices on adhesion and invasion of ovarian cancer cells to the omentum. *Int J Cancer* 121:1463–1472
- Kim JB (2005) Three-dimensional tissue culture models in cancer biology. *Semin Cancer Biol* 15:365–377
- Kim JD, Choi JS, Kim BS, Choi YC, Cho YW (2010) Piezoelectric inkjet printing of polymers: stem cell patterning on polymer substrates. *Polymer* 51:2147–2154

- King SM, Presnell SC, Nguyen DG (2014) Development of 3D bioprinted human breast cancer for in vitro drug screening. *Cancer Res* 74:2034
- Knowlton S, Onal S, Yu CH, Zhao JJ, Tasoglu S (2015) Bioprinting for cancer research. *Trends Biotechnol* 33:504–513
- Koch L, Kuhn S, Sorg H, Gruene M, Schlie S, Gaebel R, Polchow B, Reimers K, Stoelting S, Ma N et al (2010) Laser printing of skin cells and human stem cells. *Tissue Eng Part C Methods* 16:847–854
- Koch L, Deiwick A, Schlie S, Michael S, Gruene M, Coger V, Zychlinski D, Schambach A, Reimers K, Vogt PM (2012) Skin tissue generation by laser cell printing. *Biotechnol Bioeng* 109:1855–1863
- Kolesky DB, Truby RL, Gladman AS, Busbee TA, Homan KA, Lewis JA (2014) 3D bioprinting of vascularized, heterogeneous cell-laden tissue constructs. *Adv Mater* 26:3124–3130
- Kolesky DB, Homan KA, Skylar-Scott MA, Lewis JA (2016) Three-dimensional bioprinting of thick vascularized tissues. *Proc Natl Acad Sci U S A* 113:3179–3184
- Lee W, Debasitis JC, Lee VK, Lee JH, Fischer K, Edminster K, Park JK, Yoo SS (2009) Multi-layered culture of human skin fibroblasts and keratinocytes through three-dimensional freeform fabrication. *Biomaterials* 30:1587–1595
- Lee VK, Kim DY, Ngo H, Lee Y, Seo L, Yoo SS, Vincent PA, Dai G (2014) Creating perfused functional vascular channels using 3D bio-printing technology. *Biomaterials* 35:8092–8102
- Li Y, Wei X, Zhou J, Wei L (2013) The age-related changes in cartilage and osteoarthritis. *Biomed Res Int* 2013:916530
- Liu Y, Lim J, Teoh SH (2013) Review: development of clinically relevant scaffolds for vascularised bone tissue engineering. *Biotechnol Adv* 31:688–705
- Lu T, Li Y, Chen T (2013) Techniques for fabrication and construction of three-dimensional scaffolds for tissue engineering. *Int J Nanomedicine* 8:337–350
- Mandrycky C, Wang Z, Kim K, Kim DH (2015) 3D bioprinting for engineering complex tissues. *Biotechnol Adv* 34:422
- Marga F, Jakab K, Khatiwala C, Shepherd B, Dorfman S, Hubbard B, Colbert S, Gabor F (2012) Toward engineering functional organ modules by additive manufacturing. *Biofabrication* 4:022001
- Markin CA (2016) News: recognitions, societies, and academia. *Regen Eng Transl Med* 2:51–52
- Merceron TK, Burt M, Seol YJ, Kang HW, Lee SJ, Yoo JJ, Atala A (2015) A 3D bioprinted complex structure for engineering the muscle-tendon unit. *Biofabrication* 7:035003
- Michael S, Sorg H, Peck CT, Koch L, Deiwick A, Chichkov B, Vogt PM, Reimers K (2013) Tissue engineered skin substitutes created by laser-assisted bioprinting form skin-like structures in the dorsal skin fold chamber in mice. *PLoS One* 8:e57741
- Mironov V, Kasyanov V, Markwald RR (2011) Organ printing: from bioprinter to organ biofabrication line. *Curr Opin Biotechnol* 22:667–673
- Murphy SV, Atala A (2014) 3D bioprinting of tissues and organs. *Nat Biotechnol* 32:773–785
- Murphy SV, Skardal A, Atala A (2013) Evaluation of hydrogels for bio-printing applications. *J Biomed Mater Res A* 101:272–284
- Nair K, Gandhi M, Khalil S, Yan KC, Marcolongo M, Barbee K, Sun W (2009) Characterization of cell viability during bioprinting processes. *Biotechnol J* 4:1168–1177
- Noeaid P, Salih V, Beier JP, Boccaccini AR (2012) Osteochondral tissue engineering: scaffolds, stem cells and applications. *J Cell Mol Med* 16:2247–2270
- Norotte C, Marga FS, Niklason LE, Forgacs G (2009) Scaffold-free vascular tissue engineering using bioprinting. *Biomaterials* 30:5910–5917
- Novosel EC, Kleinhans C, Kluger PJ (2011) Vascularization is the key challenge in tissue engineering. *Adv Drug Deliv Rev* 63:300–311
- Owens CM, Marga F, Forgacs G, Heesch CM (2013) Biofabrication and testing of a fully cellular nerve graft. *Biofabrication* 5:045007
- Ozbolat IT (2015) Bioprinting scale-up tissue and organ constructs for transplantation. *Trends Biotechnol* 33:395–400

- Ozbolat IT, Yu Y (2013) Bioprinting toward organ fabrication: challenges and future trends. *IEEE Trans Biomed Eng* 60:691–699
- Ozbolat IT, Peng W, Ozbolat V (2016) Application areas of 3D bioprinting. *Drug Discov Today* 21:1257
- Padron JM, van der Wilt CL, Smid K, Smitskamp-Wilms E, Backus HH, Pizao PE, Giaccone G, Peters GJ (2000) The multilayered postconfluent cell culture as a model for drug screening. *Crit Rev Oncol Hematol* 36:141–157
- Pampaloni F, Reynaud EG, Stelzer EH (2007) The third dimension bridges the gap between cell culture and live tissue. *Nat Rev Mol Cell Biol* 8:839–845
- Pati F, Gantelius J, Svahn HA (2016) 3D bioprinting of tissue/organ models. *Angew Chem Int Ed Engl* 55:4650–4665
- Pereira C, Gold W, Herndon D (2007) Review paper: burn coverage technologies: current concepts and future directions. *J Biomater Appl* 22:101–121
- Pham C, Greenwood J, Cleland H, Woodruff P, Maddern G (2007) Bioengineered skin substitutes for the management of burns: a systematic review. *Burns* 33:946–957
- Phillippi JA, Miller E, Weiss L, Huard J, Waggoner A, Campbell P (2008) Microenvironments engineered by inkjet bioprinting spatially direct adult stem cells toward muscle- and bone-like subpopulations. *Stem Cells* 26:127–134
- Schaefer D, Martin I, Shastri P, Padera RF, Langer R, Freed LE, Vunjak-Novakovic G (2000) In vitro generation of osteochondral composites. *Biomaterials* 21:2599–2606
- Schuurman W, Khristov V, Pot MW, van Weeren PR, Dhert WJ, Malda J (2011) Bioprinting of hybrid tissue constructs with tailorable mechanical properties. *Biofabrication* 3:021001
- Schuurman W, Klein TJ, Dhert WJ, van Weeren PR, Huttmacher DW, Malda J (2015) Cartilage regeneration using zonal chondrocyte subpopulations: a promising approach or an over-complicated strategy? *J Tissue Eng Regen Med* 9:669–678
- Sears NA, Seshadri DR, Dhavalikar PS, Cosgriff-Hernandez E (2016) A review of three-dimensional printing in tissue engineering. *Tissue Eng Part B Rev* 22:298
- Seol YJ, Kang HW, Lee SJ, Atala A, Yoo JJ (2014) Bioprinting technology and its applications. *Eur J Cardiothorac Surg* 46:342–348
- Shafiee A, Atala A (2016) Printing technologies for medical applications. *Trends Mol Med* 22:254–265
- Sheridan RL, Greenhalgh D (2014) Special problems in burns. *Surg Clin North Am* 94:781–791
- Skardal A, Atala A (2015) Biomaterials for integration with 3-D bioprinting. *Ann Biomed Eng* 43:730–746
- Skardal A, Mack D, Kapetanovic E, Atala A, Jackson JD, Yoo J, Soker S (2012) Bioprinted amniotic fluid-derived stem cells accelerate healing of large skin wounds. *Stem Cells Transl Med* 1:792–802
- Smith CM, Stone AL, Parkhill RL, Stewart RL, Simpkins MW, Kachurin AM, Warren WL, Williams SK (2004) Three-dimensional bioassembly tool for generating viable tissue-engineered constructs. *Tissue Eng* 10:1566–1576
- Smith CM, Christian JJ, Warren WL, Williams SK (2007) Characterizing environmental factors that impact the viability of tissue-engineered constructs fabricated by a direct-write bioassembly tool. *Tissue Eng* 13:373–383
- Snyder JE, Hamid Q, Wang C, Chang R, Emami K, Wu H, Sun W (2011) Bioprinting cell-laden matrigel for radioprotection study of liver by pro-drug conversion in a dual-tissue microfluidic chip. *Biofabrication* 3:034112
- Stanton MM, Samitier J, Sanchez S (2015) Bioprinting of 3D hydrogels. *Lab Chip* 15:3111–3115
- Tang D, Tare RS, Yang LY, Williams DF, Ou KL, Oreffo RO (2016) Biofabrication of bone tissue: approaches, challenges and translation for bone regeneration. *Biomaterials* 83:363–382
- Vaidya M (2015) Startups tout commercially 3D-printed tissue for drug screening. *Nat Med* 21:2
- Visser J, Melchels FP, Jeon JE, van Bussel EM, Kimpton LS, Byrne HM, Dhert WJ, Dalton PD, Huttmacher DW, Malda J (2015) Reinforcement of hydrogels using three-dimensionally printed microfibres. *Nat Commun* 6:6933

- Wang Z, Abdulla R, Parker B, Samanipour R, Ghosh S, Kim K (2015) A simple and high-resolution stereolithography-based 3D bioprinting system using visible light crosslinkable bioinks. *Biofabrication* 7:045009
- Watson J, Hatamleh MM (2014) Complete integration of technology for improved reproduction of auricular prostheses. *J Prosthet Dent* 111:430–436
- Wolford LM, Stevao EL (2003) Considerations in nerve repair. *Proc (Bayl Univ Med Cent)* 16:152–156
- Xu T, Jin J, Gregory C, Hickman JJ, Boland T (2005) Inkjet printing of viable mammalian cells. *Biomaterials* 26:93–99
- Xu F, Celli J, Rizvi I, Moon S, Hasan T, Demirci U (2011) A three-dimensional in vitro ovarian cancer coculture model using a high-throughput cell patterning platform. *Biotechnol J* 6:204–212
- Xu T, Binder KW, Albanna MZ, Dice D, Zhao W, Yoo JJ, Atala A (2013a) Hybrid printing of mechanically and biologically improved constructs for cartilage tissue engineering applications. *Biofabrication* 5:015001
- Xu T, Zhao W, Zhu JM, Albanna MZ, Yoo JJ, Atala A (2013b) Complex heterogeneous tissue constructs containing multiple cell types prepared by inkjet printing technology. *Biomaterials* 34:130–139
- Yanez M, Rincon J, Dones A, De Maria C, Gonzales R, Boland T (2015) In vivo assessment of printed microvasculature in a bilayer skin graft to treat full-thickness wounds. *Tissue Eng Part A* 21:224–233
- Yoon H, Lee JS, Yim H, Kim G, Chun W (2016) Development of cell-laden 3D scaffolds for efficient engineered skin substitutes by collagen gelation. *Rsc Adv* 6:21439–21447
- Yoshida Y, Yamanaka S (2010) Recent stem cell advances: induced pluripotent stem cells for disease modeling and stem cell-based regeneration. *Circulation* 122:80–87
- Zhao Y, Yao R, Ouyang L, Ding H, Zhang T, Zhang K, Cheng S, Sun W (2014) Three-dimensional printing of HeLa cells for cervical tumor model in vitro. *Biofabrication* 6:035001
- Zheng Y, Chen J, Craven M, Choi NW, Totorica S, Diaz-Santana A, Kermani P, Hempstead B, Fischbach-Teschl C, Lopez JA et al (2012) In vitro microvessels for the study of angiogenesis and thrombosis. *Proc Natl Acad Sci U S A* 109:9342–9347



Bioprinting: The Intellectual Property Landscape

Robert W. Esmond and Deborah Sterling

Contents

1	Introduction	486
2	Bioprinting	486
3	Intellectual Property (IP) Protection	487
4	3D Bioprinting Patent Landscape	493
4.1	Bioimaging ± CAD ± Blueprint Patents	496
4.2	Bio-ink ± Bio-paper ± Bioprinter Patents	499
4.3	Maturongens ± Biomonitoring ± Bioreactor	509
5	There Is Room for Additional Patentable Innovations	510
6	Existing Patent Filings May Not Impede Commercialization of Bioprinted Organs: Exceptions to Patent Infringement	510
7	Conclusion	511
	References	511

Abstract

The patenting of bioprinting techniques to make tissues and organs has quietly been going on for more than a decade. Anyone seeking to develop a product or service based upon bioprinting must be concerned about the patent landscape. This chapter will first discuss the various options available to protect the different aspects of bioprinting. Then, it will provide a summary of the landscape of utility patents that protect innovation in each of the three stages of bioprinting: (i) bioimaging + CAD + blueprint, (ii) bi-oink + bio-paper + bioprinter, and (iii) maturogens + biomonitoring + bioreactor. Lastly, the chapter will discuss certain exceptions to patent infringement for the development of bioprinted tissues and organs.

R. W. Esmond (✉) · D. Sterling

Biotechnology/Chemical Group, Sterne, Kessler, Goldstein & Fox P.L.L.C., Washington, DC, USA
e-mail: resmond@skgf.com; dsterlin@skgf.com

1 Introduction

Bioprinting of tissues and organs has been big news recently. However, the patenting of bioprinting techniques to make organs and tissues has quietly been going on for years. Anyone seeking to develop a product or service based upon bioprinting must be concerned about the patent landscape. This chapter will focus on the ways bioprinting innovations have been protected, patent and trademark filings on bioprinting innovations and the opportunities for further patenting, and certain exceptions to patent infringement for the development of bioprinted tissues and organs.

2 Bioprinting

Additive manufacturing (or 3D printing, as is known more widely) is driving major innovations in many areas, such as engineering, manufacturing, art, education, and medicine. Recent advances have enabled 3D printing of biocompatible materials, cells, and supporting components into complex 3D functional living tissues. Indeed, several uses of 3D bioprinting are already generating revenue as viable businesses, such as research tools, drug screening, dental applications, prosthetics, and hearing devices.

Bioprinting technology, in general, involves depositing consecutive layers of cells as “bio-ink” in a desired pattern and controlling cell aggregations, fusions, and differentiations until a living three-dimensional structure with specialized compartments (such as cavities and vasculature) or specialized cell types (such as smooth muscle cells, endothelial cells, connective tissue cells, lung cells, or liver cells) is produced.

Organs-on-a-chip recapitulates the multicellular architectures, tissue-tissue interfaces, physicochemical microenvironments, and vascular perfusion of the body to produce levels of tissue and organ functionality not possible with conventional 2D or 3D culture systems. The simplest organs-on-a-chip are microfluidic devices that contain a single, perfused microfluidic chamber containing a single type of cultured cell that exhibits the functions of a single tissue type. More complex devices contain two or more channels or chambers that are connected by porous membranes which are lined on opposite sides by different types of cells in an attempt to mimic interfaces between different tissue types. These devices can incorporate physical forces such as cellular interactions, liquid flow, and liquid residence parameters, allowing analysis of organ-specific responses. They also enable high-resolution, real-time imaging, and *in vitro* analysis of biochemical, genetic, and metabolic activities of living cells in a functional tissue and organ context. This technology has great potential to advance the study of tissue development, organ physiology, and disease etiology. In the context of drug discovery and development, it should be especially valuable for the study of molecular mechanisms of action, prioritization of lead candidates, toxicity testing, and biomarker identification. Bioprinting is one method that can be used to make organs-on-a-chip.

3D bioprinting is also being applied to regenerative medicine to address the need for tissues and organs suitable for transplantation. Growing tissues and organs on demand, using stem cells and iPS cells derived from patients themselves, could

eliminate the lengthy wait that people in need of a transplant are often forced to endure before one becomes available. It could also reduce the risk of a patient's immune system rejecting the transplant, since the tissue could be grown from the patient's own cells.

Compared with nonbiological printing, 3D bioprinting involves additional complexities, such as the choice of materials, cell types, growth and differentiation factors, and technical challenges related to the sensitivities of living cells and the construction of tissues. Addressing these complexities requires the integration of technologies from the fields of engineering, biomaterials science, cell biology, physics, and medicine.

3 Intellectual Property (IP) Protection

IP law fosters advancements in science by providing mechanisms to protect research and innovation from copycats, even accidental copycats. Such protections incentivize innovators and investors to spend the time and money needed to develop innovations and improvements that benefit society. Patent protection in particular provides inventors and investors with the capability to capitalize on investment in research and development by deterring, or at least slowing down, competitors.

Protecting IP is particularly important in the medical industry. This is because anything that is to be used on or in a human body is subject to rigorous testing to ensure biocompatibility and to evaluate and minimize side effects. This testing substantially increases the costs of new drugs or implants. Consequently, innovators experimenting with new materials bear the burden of significant research costs. Innovators hope that a successful product will be approved, go on sale, and generate enough revenue to recoup the research and development costs incurred – and preferably to also make a profit. Patent protection makes this possible.

Typical intellectual property rights are listed in the table below.

IP right	Nature of right	Limitations
Copyright	Protects means of expression of an idea. Useful to protect software, code, CAD drawings, sculptures, and 3D models. Easy and cost-effective to obtain. Statutory damages are available in many countries	Protection does not extend to the utilitarian features of a product. Difficult and expensive to enforce in court
Design patent	Protects novel ornamental features of a product, i.e., the way an article “looks.” Easy and inexpensive to obtain	Protection does not extend to the utilitarian features of a product. Difficult and expensive to enforce in court
Trade dress	Protects the visual appearance of a product that indicates the source of origin. No filings required	Protection does not extend to the utilitarian features of a product. Difficult and expensive to enforce in court
Trademark	Protects indication of source of origin and protects consumers from being	Protection is limited to the mark and does not extend to the utilitarian

(continued)

IP right	Nature of right	Limitations
	confused by the origins of a product. Easy and inexpensive to obtain	features of the product. Difficult and expensive to enforce in court
Trade secret	Protects against misappropriation of secret information about a product maintained as a secret. Such information may include design plans, software, and code used to make the product. No filings required but steps must be taken to ensure secrecy of the information	Competitors can reverse engineer the product and method of manufacture. Unless trade secret misappropriated, there is no protection once the information is no longer “secret.” Difficult and expensive to enforce in court
Utility patent	Grants limited right (generally 20 years) to exclude others from making, using, and selling claimed a product or process	Expensive and time-consuming to obtain. Difficult and expensive to enforce

Generally, products of commerce may be protected by any one of these IP rights, each of which is briefly addressed next.

Copyright: Copyright law protects the esthetic and decorative aspects of printed objects such as original print and patterns, unique color arrangements, and novel combinations of elements (protectable or non-protectable) but, in most cases, not the utilitarian aspects of such objects. In other words, the software and code used to manufacture a bioprinted tissue or organ may be protected by copyright. But given that the tissues and organs themselves are utilitarian, the bioprinted tissue itself typically would not be eligible for copyright protection.

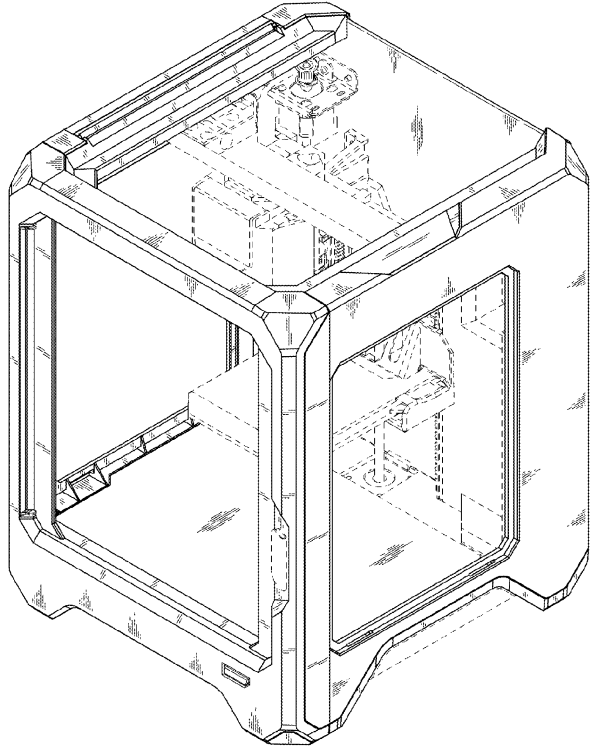
Design patent: Design patent term varies around the world. A US design patent, for example, provides 14 or 15 years – depending on when it was filed¹ – of exclusive industrial design rights for new and nonobvious ornamental designs of articles of manufacture. In Europe and Hong Kong, a registered design lasts 5 years from the date of filing and can be renewed at 5-year intervals for a total term of up to 25 years from filing. An industrial design patent in Japan or South Korea provides 20 years of protection, while Australia, Canada, and China provide at most 10 years.

In every jurisdiction, a design consists of the visual ornamental characteristics embodied in, or applied to, an article of manufacture. Since a design is manifested in appearance, the subject matter of a design patent application may relate to the configuration or shape of an article, to the surface ornamentation applied to an article, or to the combination of configuration and surface ornamentation. But, just like with copyrights, design patents cannot protect utilitarian aspects of an article. In other words, if the unique or distinctive shape or appearance of the article is dictated by the function that it performs, then it will not be eligible for design patent protection.

While a bioprinted tissue is distinctly utilitarian in nature, that does not mean that a 3D manufacturer cannot avail itself of design protection. Any unique configuration

¹“Patents issued from design applications filed on or after May 13, 2015 shall be granted for the term of 15 years from the date of grant. Patents issued from design applications filed before May 13, 2015 shall be granted for the term of 14 years from the date of grant.” 35 USC § 173.

Fig. 1 Figure 1 from D752,661 S



or shape of a bioprinter or of an organ microchip may be eligible for design patent protection as long as it is not tied to the utility of the printer or microchip. Such unique designs can go a long way to creating market brand protection and loyalty, which can long outlast the life of a utility patent. Indeed, some additive manufacturers have already taken advantage of design patents to protect the appearance of their 3D printers. Here are a few examples of US design patents:

US Design Patent No. D752,661 S: “Three-Dimensional Printer Frame” (Exp. Date: March 29, 2030)

Exemplary Fig. 1:

US Design Patent No. D739,885 S: “3D Printer” (Exp. Date: September 29, 2029).

Exemplary Fig. 2:

Trademark: Trademarks or brands are a shorthand way of communicating everything that is great about a company or a product. Market analysts often estimate that the consumer goodwill associated with brand identities account for an average of one-third of shareholder value. Unlike patents, trademarks can remain in force for as long as they are in use and can differentiate a product from a competitor for the life of the product.

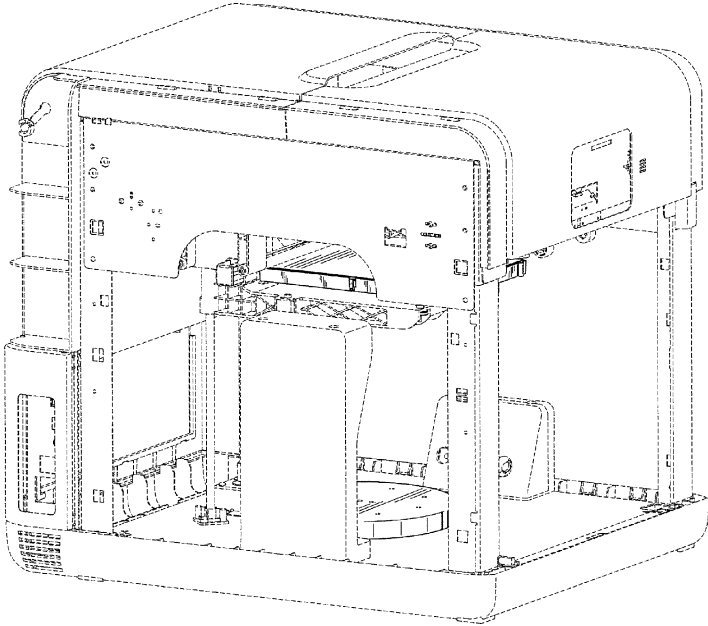


Fig. 2 Figure 2 from D739,885 S

For originators, a strong brand can serve as an effective market buffer between the first approved product and a later-coming generic. For follow-on products, it can serve as an efficient way to communicate why a particular follow-on is superior to the originator or to competing follow-ons. For any company, strong and enforceable trademarks are the most effective tool for staving off challenges from infringers and counterfeiters. Strong brand identity is also critical for capturing modern market-places – such as online platforms.

The US Trademark Act does not provide protection for three-dimensional designs or objects per se. Instead, trademark law protects brand names, logos, symbols, designs, and other elements of such items. For example, the brand name on a 3D object could be registered as a protectable trademark in the USA. The USA is in the minority though as many other countries, such as Australia, Japan, China, Colombia, Mexico, Peru, Venezuela, and the European Union, accept the registration of three-dimensional trademarks, i.e., trademarks consisting of the shape of products or their packaging.

While implanted devices may have some kind of brand marking, printed tissues or organs likely will not carry logos or branding (although one can never underestimate the advances of science). At this time, trademarks are most applicable to branding hardware and software used in 3D bioprinting as well as microchips.

Example trademarks in the 3D bioprinting market include

Company	Trademark	Example “goods and services” description
Organovo, Inc.	NOVOGEN BIOPRINTER	Laboratory apparatus for fabrication of three-dimensional tissues and organs
Organovo, Inc.	NOVOTISSUES	Engineered biological tissues and tissue arrays, namely, human and animal organ, connective, epithelial, muscular, and nervous tissues, and tissue arrays, for use in scientific and medical research
Organovo, Inc.	NOVOGEL	Non-pharmaceutical inert gel for use with three-dimensional bioprinting and other three-dimensional fabrication systems used by bioengineers and tissue engineers for the creation of biological tissues for surgical implantation, transplantation, or extracorporeal use for therapeutic purposes
Organovo, Inc.	3D QUALIFIED	Providing evaluation in the nature of determining the suitability by testing and analysis of nonbiologic reagents, biologic materials, scientific apparatuses, tissues, and scientific and medical research services of others for use in three-dimensional biology applications for the purpose of certification
Tengion, Inc.	TENGION	Bioengineered human and other mammalian tissues for subsequent implantation
Tengion, Inc.	NEO- ESOPHAGUS	Bioengineered human and other mammalian tissues and organs for medical research
Tengion, Inc.	NEO- BLADDER	Bioengineered human and other mammalian tissues and organs for medical research
Fluicell AB	FLUICELL	Apparatus and instruments for use in 3D bioprinting, namely, 3D printers
Fluicell AB	LAB-ON-A-TIP	Apparatus and instruments for use in 3D bioprinting, namely, 3D printers
Fluicell AB	SYNCHRO	Apparatus and instruments for use in 3D bioprinting, namely, 3D printers
Fluicell AB	BIOPEN	Apparatus and instruments for use in 3D bioprinting, namely, 3D printers
Advanced Polymer Technology AB Corporation	CELLINK	Cellulose nanofibril-based preparations for use in 3D bioprinting of tissues and organs

Trade dress: Trade dress law protects the overall commercial image of a product or service and can consist of nonfunctional elements such as a product configuration or shape, inner and outer packaging (e.g., cartons, vials, etc.), labeling, color, and even texture. Trade dress protection is intended to protect consumers from packaging or appearance of products that are designed to imitate other products and to prevent a consumer from buying one product under the belief that it is another. To gain

registration in the Principal Register or common law protection under the US Lanham Act,² a trade dress must be “distinctive.” This means that consumers perceive a particular trade dress as identifying a source of a product. A classic example of trade dress is Pfizer’s registration of the blue color and diamond shape of its VIAGRA erectile dysfunction tablet. Another is the distinctive shape of a Coca-Cola bottle. Like trademarks, trade dress is currently most applicable to branding hardware and software used in 3D bioprinting, as well as microchips. But if one were to develop a particularly distinctive bioprinted tissue, trade dress protection should not be overlooked.

Trade secret: Broadly speaking, any confidential business information, which provides a company with a competitive edge, may be considered a trade secret. Trade secrets include manufacturing or industrial secrets and commercial secrets. The unauthorized use of that information by persons other than the holder is considered unfair practice and a violation of the trade secret. Depending on the legal system, trade secret protection forms part of the general concept of protection against unfair competition or is based on specific provisions or case law on the protection of confidential information.

In contrast to patents, copyrights and trademarks, trade secrets are protected without registration, that is, there are no procedural formalities needed to obtain trade secret protection. Consequently, a trade secret can be protected for an unlimited period of time. There are, however, some conditions for the information to be considered a trade secret:

- The information is generally not known to the public (i.e., it is not readily accessible to circles that normally deal with the kind of information in question).
- It must have been subject to reasonable efforts to keep the information secret (e.g., through confidentiality agreements).
- It must have commercial value because it is a secret.

Trade secrets are an invisible component of a company’s IP. Being invisible, their contribution to a company’s value is hard to measure. Coca-Cola once again provides a good example here; its recipe being a trade secret since it was first invented in 1886.

Because protection of trade secrets can, in principle, extend indefinitely, it therefore may provide an advantage over patent protection, which lasts only for a specific duration. The disadvantage, however, is that there is no protection once information protected as trade secret is uncovered by third parties, such as through reverse engineering. In addition, trade secret protection for a bioprinted tissue or organ will provide little protection in view of national regulations that require the disclosure of the methods of making approved biologics and medical devices.

²Trade dress registration and common law protection vary from country to country. A company seeking to rely upon trade dress protection should seek legal counsel in the countries in which it plans to market.

Utility patents: Utility patents are the most common type of patent application. Utility patents may protect the underlying specialized biomaterials used in bioprinting, methods of printing biological tissue, methods of manufacturing bioprinted materials/devices, and methods of engineering tissue or of forming arrays of viable cells, for example. Utility patents may also protect various aspects of the bioprinting hardware such as the bioprinter itself, or software³ for controlling the bioprinter.

Utility patents are issued for the invention of a new and useful process, machine, manufacture, or composition of matter, or a new and useful improvement of the same. Simply owning a patent does not give one the right to practice the invention that is claimed. Instead, a utility patent generally permits its owner to exclude others from making, using, or selling the claimed invention for a period of up to 20 years from the date of filing the patent application. To obtain patent protection, a company must submit a separate patent application for each country in which it wishes to protect its investment and invention. The time, money, and effort required to obtain national and international patents are important considerations because the process to obtain a patent requires a significant investment.

While patents are expensive and time-consuming to obtain and difficult to enforce, regulatory approval for a bioprinted tissue or organ is also very expensive and time-consuming. There is little incentive to invest in obtaining regulatory approval if the bioprinted tissue or organ can be knocked off once approved for marketing. Consequently, patents are critical. If the 3D bioprinting device or bioprinted product is patentable (and once it has been patented), the company will be able to (i) create legal barriers to entry for competing devices by preventing others from copying, selling, or manufacturing the product, (ii) license the claimed technology to generate revenue and (iii) enhance the value of the proprietary company by building equity in the company and creating assets that may attract other investments.

4 3D Bioprinting Patent Landscape

There are several aspects of 3D bioprinting that warrant utility patent protection:

Materials: The basic materials in bioprinting include the “bio-ink” made up of specialized cell types (such as smooth muscle cells, endothelial cells, connective tissue cells, lung cells, liver cells, and aggregates thereof). In addition to outputting cells and cell aggregates, most bioprinters also output a dissolvable gel to support

³The standard for patenting software varies around the world. Software is difficult to patent in the USA. And patenting software in China, Taiwan, Korea, and Japan, for example, is possible only when the claims recite the use of software working in concert with specific hardware, particularly when the invention resolves a technical problem and achieves a technical result.

and protect cells during printing, sometimes called a “bio-paper.” Once the relevant cells and cell aggregates are placed in roughly the right place, they appear to be capable of rearranging themselves and fuse together into a final living tissue. Other bio-papers include scaffold materials, biodegradable polymers, and ceramics that may be used to support and help form artificial organs or even substitute for bone. Because the bio-ink and bio-paper materials are consumed during the use of the printer, very much like the ink-jet cartridge marketplace, having a defensible IP position on these basic materials may be key to financial success in this marketplace.

Methods: Unlike most of the rest of the world, “laws of nature, physical phenomena, and abstract ideas” are not considered patent eligible in the USA under 35 USC §101. Bioprinting process claims and technologies typically pass the patent-eligible subject matter test of 35 USC §101, as they fall under “process, machine, manufacture, [or] composition of matter.” Patent practitioners drafting patent bioprinting claims should encompass various aspects of the bioprinting process and technology including the process of printing activity, methods of tissue engineering, methods of manufacturing bioprinted devices and implants, methods of engineering tissue, and methods of forming arrays of viable cells, among many others.

These types of bioprinting claims are patent eligible and, assuming they meet the other statutory requirements, may be patentable.

Hardware: The hardware is the printer and its components. A 3D printer has some similarities to and some differences from a standard, 2D ink-jet printer. Similar to a 2D ink-jet printer, a bioprinter has a print head, which may function to spray droplets or extrude bio-ink. But unlike a 2D ink-jet printer, the bioprinted article is built up layer by layer, in three dimensions on a 3D printer. The printer structure must accommodate an X, Y, and Z axes. Because printers are typically structural in nature, the main issue faced in pursuing utility patent protection is whether the components are in a configuration that is novel and not obvious over prior art 3D printers. If the printer has a specific configuration or shape, surface ornamentation, or a combination of configuration and surface ornamentation, then design patent protection would be another option. Some examples are discussed above.

Software: The process of printing and processing living tissue is complex and involves many factors that must be tightly controlled. Typically, the complex, repetitive steps implemented by bioprinting are performed automatically by the programmed 3D printer and controlled by software. As discussed above, copyright protection prevents someone from copying source code from the author’s program and pasting it into a different program without the author’s consent. Patent protection offers broader coverage because it allows the innovator to prevent others from copying source code and “tweaking” it to avoid copyright protection, or from developing equivalent software using different code.

Protecting software requires special attention as patent protection for software has been challenged in the USA. The question that US courts have struggled with is

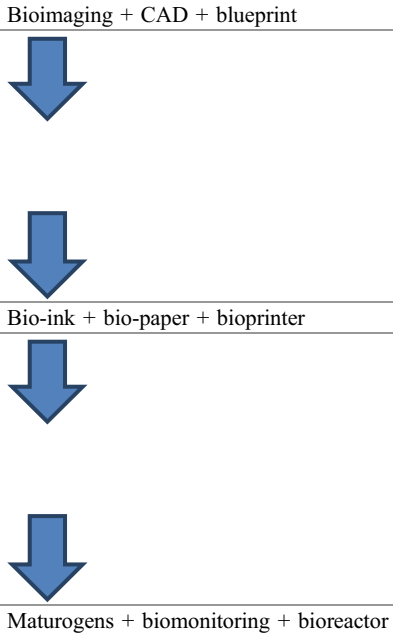
whether a computer software program should be considered like a mathematical formula and therefore unpatentable subject matter, or more like a modification to an electrical device and therefore eligible for patent protection. In other words, if software merely implements an abstract idea, then a claim to that software will likely be considered invalid because it is directed to an unpatentable abstract idea. In contrast, if the software is designed to improve the functioning of a computer or some other type of technology, then that software should be considered patent eligible. In many cases, unfortunately, an invention falls in between these two ends of the spectrum, making patent protection uncertain.

Product: While bioprinting process claims for engineering bioprinted materials/devices such as the human skin, organs, or 3D-printed body parts may be patentable, the same is not always true for bioprinting product claims. In the USA, the question key to patentability is whether the bioprinted product claim passes the patent-eligible subject matter test of 35 USC §101, i.e., whether the bioprinted product is a “process, machine, manufacture, [or] composition of matter” and not “laws of nature, physical phenomena, and abstract ideas,” and whether it passes the “product of nature” test. To pass the “product of nature” test, a claimed bioprinted product must be (1) a product of human ingenuity and (2) nonnaturally occurring. While, technically, all bioprinting technologies and resulting bioprinted constructs are manmade, the difficulty arises in situations wherein the bioprinted medical device or organ/organism is essentially an identical copy of the naturally occurring organ/tissue.

In addition, the Leahy-Smith America Invents Act (AIA), signed into US law in September 2011, clearly states that “no patent may issue on a claim directed to or encompassing a human organism.” The AIA did not specifically define the term “human organism.” Consequently, and until US courts decide what “human organism” means, patent examiners could reject any bioprinting claim “directed to” or “encompassing” something “human” under the broadest reasonable interpretation. With the lack of clarity of the AIA regarding “human organism” and following the guidelines of the two-prong test discussed above, patent practitioners should draft bioprinting product claims carefully, to ensure that the claimed product is more clearly a redesign of another naturally occurring organism (and distinguishable in some ways) and not an exact copy.

In order to determine what patents might dominate the making, using, and selling of bioprinted tissues and organs, we carried out a patent landscape search. The landscape search did not attempt to cover all patents filed on additive manufacturing techniques, of which there are thousands. Instead, the search was limited to issued US patents (the claims in published patent applications not being a clear predictor of what the US Patent and Trademark Office deems patentable) in the field of 3D bioprinting. Even then, this is a representative listing of patents in the field and is not exhaustive.

The search results were categorized into a preprocessing or design phase, production phase, and postproduction maturation phase (Mironov et al. 2008).



Several important issued patents in each category are discussed below.

4.1 Bioimaging ± CAD ± Blueprint Patents

US 8,579,620: “Single-action three-dimensional model printing methods” (Exp. Date: May 30, 2031).

Exemplary Claim:

1. A system for printing a 3D physical model from an image data set, comprising: a display component for displaying one or more printing templates; and a single-action data processing component that, in response to a printing template selected by a single action by a user, executes the selected printing template to take the image data set as input and generates a geometric representation for use as input to a 3D printer; wherein the selected printing template comprises predefined instructions for processing the image data set.

The owner of this patent is not known. It was filed only in the USA. This patent appears to cover a system for 3D printing any product from an image data set in response to a printing template selected by a single action by a user. The patent specification makes clear that bioprinted organs are contemplated: “Fig. 14 illustrates an example of printing a physical model of selected organs. . .”

US 8,639,484: “Method and Apparatus for Computer-Aided Tissue Engineering . . .” (Exp. Date: November 17, 2024).

Exemplary Claim:

1. A process for multi-nozzle biopolymer deposition of heterogeneous materials . . . having at least one biomimetic and at least one non-biomimetic feature comprising importing data from MRI, CT or other patient specific data into a CAD environment; utilizing the CAD environment [and] using at least of Boolean, scaling, smoothing, and mirroring CAD operations; converting the CAD design into a . . . format suitable for three-dimensional, multi-nozzle printing. . . ; printing the composite assembly . . . herein the simultaneous depositing includes direct deposition of cells.

This patent is assigned to Drexel University. Equivalent patents were filed in Canada and the European Patent Office. This patent appears to cover a method for 3D printing a composite biopolymer by importing patient-specific data from an MRI or CT scan, for example, into the CAD environment and converting the CAD design into a 3D model suitable for printing.

US 7,174,282: “Design methodology for tissue engineering scaffolds and biomaterial implants” (Exp. Date: September 27, 2024).

Exemplary Claim:

21. A method of designing a tissue scaffold for replacing native tissue in a patient comprising: determining a native tissue effective stiffness; determining a native tissue regeneration requirement; creating a first set of databases representing a plurality of microstructure designs for said scaffold in image based format; for each of the plurality of microstructure designs, calculating a scaffold effective stiffness of a resultant scaffold incorporating the microstructure design and a regenerate tissue effective stiffness of regenerate tissue that will grow into the scaffold incorporating the microstructure design; selecting a desired microstructure design for the scaffold, said selecting step including: selecting the microstructure design which yields the resultant scaffold most closely matching scaffold effective stiffness and regenerate tissue effective stiffness with native tissue effective stiffness while satisfying the native tissue regeneration requirement; creating a second database representing a scaffold exterior geometry desired to replace the native tissue in the patient in image based format; and merging the databases representing the desired microstructure design with the second database into an image-based design of the scaffold.

The owner of this patent is unknown. An equivalent patent was filed in Australia. This patent appears to cover a method of designing a tissue scaffold for replacing native tissue in a patient. The method creates all designs using voxel-based design techniques. The voxel-based design techniques allow combination of any scaffold or implant microstructure database with any complex 3D anatomic shape created by CT or MRI scanners. These designs can be readily converted to formats for layered manufacturing or casting.

US 7,509,183: “Integrated global layout and local microstructure topology optimization approach for spinal cage design and fabrication” (Exp. Date: April 22, 2024).

Exemplary Claim:

1. A method of designing an interbody fusion cage comprising: defining operational parameters for the cage; defining a macroscopic structural layout for the cage satisfying the operational parameters; dividing the macroscopic structural layout of the cage into a plurality of discreet sub-segments; defining a density distribution of the macroscopic structural layout by determining a density level for each sub-segment; defining a microscopic structural layout for the cage by assigning pre-selected microstructures to the sub-segments in accordance with the density level of each sub-segment; and outputting an integrated design topology solution for fabrication of the interbody fusion case in response to the macroscopic structural layout and the microscopic structural layout.

This patent is assigned to the Regents of the University of Michigan and was filed only in the USA. The claimed method uses topology optimization algorithms to define the structural layout and the inner microstructures of the cage. After the structural layout is defined, a density distribution process is performed. Based on the density distribution, the inner microstructures of the cage are defined.

US 7,445,441: “Three-dimensional printing apparatus and methods of manufacture including sterilization or disinfection, for example, using ultraviolet light” (Exp. Date: January 21, 2026).

Exemplary Claim:

1. A three-dimensional printing machine comprising at least one ultraviolet light source suitable to kill or damage microorganisms, wherein at least one ultraviolet source is substantially stationary.

This patent is owned by Therics, LLC. It was filed only in the US. According to the patent specification, the invention includes a 3D printing machine that has at least one ultraviolet (UV) light source directed at powder or slurry being processed by the 3D printing machine or directed at any of various surfaces or machine components, in a manner suitable to kill or damage microorganisms. The UV light can also provide sources for a combination of polymerization/cross-linking in addition to sterilization/disinfection.

US 6,993,406: “Method for making a bio-compatible scaffold” (Exp. Date: April 23, 2024).

Exemplary Claim:

1. A method for making a three-dimensional, bio-compatible scaffold structure, comprising: designing a three-dimensional geometry of a scaffolding structure utilizing software implemented by a computer; said software selected from the group consisting of mass transport software and solid mechanics software to match a pre-selected property, said property selected from the group consisting of compressive modulus, compressive strength, porosity of the porous structure, tortuosity of the porous structure, and mass transport characteristics of the porous structure; and depositing a bio-compatible slurry as discrete elements in said three-dimensional geometry using a robocasting rapid-prototyping method to construct a three-dimensional, porous structure, said three-dimensional porous structure comprising macroporosity between approximately 0 and 80%, microporosity of said discrete elements between 0 and 70% and nanoporosity of said discrete elements between approximately 0 and 60%.

This patent is assigned to Sandia Corporation and was filed only in the USA. The patent appears to cover a method for forming a three-dimensional, biocompatible, porous scaffold structure using a solid freeform fabrication technique, which the patent calls “robocasting,” that is driven by particular software. According to the patent, the scaffold structure can be used as a medical implant, such as a bone implant or graft.

4.2 Bio-ink ± Bio-paper ± Bioprinter Patents

US 8,241,905: “Self-assembling cell aggregates and methods of making engineered tissue using the same” (Exp. Date: March 11, 2028).

Exemplary Claim:

1. A three-dimensional layered structure comprising: at least one layer of a matrix; and a plurality of cell aggregates, each cell aggregate comprising a plurality of living cells; wherein the cell aggregates are embedded in the at least one layer of matrix in a non-random predetermined pattern, the cell aggregates having predetermined positions in the pattern.

This patent is assigned to the Curators of the University of Missouri. This patent is reportedly licensed to Organovo, Inc. (Organovo 2012). It was filed only in the USA. This patent appears to cover a tissue or organ containing layers of matrix and a plurality of living cell aggregates embedded in the layers of the matrix in predetermined positions in a pattern.

US 8,143,055: “Self-assembling multicellular bodies and methods of producing a three-dimensional biological structure using the same” (Exp. Date: June 24, 2029).

Exemplary Claim:

1. A three-dimensional structure comprising: a plurality of multicellular bodies, each multicellular body comprising a plurality of living cells cohered to one another; and a plurality of discrete filler bodies, each filler body comprising a biocompatible material that resists migration and ingrowth of cells from the multicellular bodies into the filler bodies and resists adherence of cells in the multicellular bodies to the filler bodies, wherein the multicellular bodies and filler bodies are arranged in a pattern in which each multicellular body contacts at least one other multicellular body or at least one filler body.

This patent is assigned to the Curators of the University of Missouri (this patent may also be licensed to Organovo, Inc.). Equivalent patents were also filed in Australia, Canada, China, the European Patent Office, Japan, and South Korea. This patent appears to cover bioprinted tissues and organs containing patterned discrete filler bodies that resist migration and ingrowth of patterned multicellular bodies containing living cells. Such filler bodies may include sacrificial hydrogels that form tubular engineered blood vessels inside tissues and organs.

US 8,852,932: “Self-Assembling Cell Aggregates and Methods of Making Engineered Tissue Using the Same” (Exp. Date: June 24, 2029).

Exemplary Claim:

1. A method of producing a three-dimensional engineered biological tissue, the method comprising: arranging a plurality of cell aggregates according to a pattern such that each of the cell aggregates contacts at least one other cell aggregate, wherein each cell aggregate comprises a plurality of living cells, and allowing at least one of the cell aggregates to fuse with at least one other cell aggregate to produce a three-dimensional engineered biological tissue.

This patent is assigned to the Curators of the University of Missouri (this patent may also be licensed to Organovo, Inc.). Equivalent patents were also filed in Australia, Canada, China, the European Patent Office, Japan, and South Korea. This patent is related to US 8,143,055, discussed above. This patent appears to cover methods of making bioprinted tissues and organs by arranging cell aggregates in such a way that allows the aggregates to fuse to produce a tissue.

US 8,747,880: “Engineered Biological Nerve Graft, Fabrication and Application Thereof” (Expiration date May 28, 2031).

What is claimed is:

1. A multicellular construct consisting essentially of: a multicellular region comprising: a plurality of living cells cohered to one another to form an elongate graft for restoring neural connection between the ends of a severed nerve; a plurality of acellular channels extending axially through the multicellular region; and wherein the multicellular construct does not comprise any scaffold material at the time of implantation into a living organism having a nervous system.

This patent is assigned to the Curators of the University of Missouri (this patent may also be licensed to Organovo, Inc.). Equivalent patents were also filed in Australia, Canada, China, the European Patent Office, Israel, Japan, and Russia. This patent covers a nerve graft that may be made using bioprinting techniques.

US 7,051,654 “Ink-Jet Printing Of Viable Cells” (Exp. Date: May 22, 2024).

Exemplary Claim:

36. A method for forming an array of viable cells, said method comprising:
 - supplying a cellular composition containing cells to at least one printer head of an ink-jet printer, said printer head defining an orifice through which said cellular composition is capable of flowing;
 - forming one or more droplets from said cellular composition;
 - flowing the droplets through said orifice so that said cells are printed onto a substrate;
 - and depositing a support compound onto said substrate for supporting said cells, said support compound forming a gel after being deposited onto said substrate.

This patent is assigned to Clemson University and was filed only in the USA. This patent appears to cover a method of preparing a bioprinted tissue or organ by ink-jet printing a cellular composition containing cells and forming a gel after deposition.

US 7,625,198: “Modular Fabrication Systems and Methods” (Exp. Date: Aug. 10, 2025).

Exemplary Claim:

1. An article fabrication system comprising: a plurality of material deposition tools containing one or more materials useful in fabricating the article; a material deposition device having a tool interface for receiving said material deposition tools, the tool interface of said material deposition device being movable in various paths . . . relative to a substrate to dispense material . . . a system controller operably connected to said material deposition device . . . and a tool rack comprising tool mounts. . .

This patent is assigned to Cornell University. This patent was filed only in the USA. This patent appears to cover an ink-jet printer that may be used for bioprinting. The specification makes clear that it may be configured for deposition of a hydrogel with seeded cells and that a “further aspect of the present invention relates to a method of fabricating a living three-dimensional structure.”

US 9,242,031: “Modular Fabrication Systems and Methods” (Exp. Date: Aug. 10, 2025).

Exemplary Claim:

1. A method of fabricating a living three-dimensional structure, said method comprising: providing a data set representing a living three-dimensional structure to be fabricated; providing a printable composition comprising a hydrogel seeded with cells, wherein the hydrogel comprises collagen; and printing the printable composition onto a substrate in layers in a pattern in accordance with the data set suitable to fabricate the living three-dimensional structure without the need to provide a negative template; wherein the printable composition is capable of bonding between printed layers; and wherein $94 \pm 5\%$ of the cells in the fabricated living three-dimensional structure are viable.

This patent is in the same family as US 7,625,198. It appears to claim a method of fabricating a tissue or organ by bioprinting a hydrogel containing cells and collagen, wherein $94 \pm 5\%$ of the cells remain viable.

US 8,728,807: “Self-Assembling Multicellular Bodies and Methods of Producing a Three-Dimensional Biological Structure Using the Same” (Exp. Date: June 24, 2029).

Exemplary Claim:

1. A method of producing a three-dimensional biological engineered tissue, the method comprising: arranging a plurality of multicellular bodies on a substrate according to a pattern such that each of the multicellular bodies contacts at least one other multicellular body, wherein each multicellular body comprises a plurality of living cells, arranging one or more filler bodies in the pattern with the multicellular bodies so that each filler body contacts at least one multicellular body or another filler body, each filler body comprising a biocompatible material that resists migration and ingrown of cells from the multicellular bodies into the filler bodies and resists adherence of cells in the multicellular bodies to the filler bodies, and allowing at least one of the multicellular bodies to fuse with at least one other multicellular body to produce a three-dimensional biological engineered tissue.

This patent is assigned to the Curators of the University of Missouri (this patent may also be licensed to Organovo, Inc.). Equivalent patents were also filed in Australia, Canada, China, the European Patent Office, Hong Kong, Israel, Japan, and South Korea. This patent appears to cover methods of making bioprinted tissues

by arranging a pattern of multicellular bodies and filler bodies that resist migration and ingrowth of the multicellular bodies containing living cells in a way that allows the multicellular bodies to fuse forming a three-dimensional tissue.

US 8,198,086: “Method for production of three-dimensional structure of cells” (Exp. Date: December 13, 2028).

Exemplary Claim:

1. A method for the production of a structure made of cells, comprising: a) forming a plurality of cell clusters; b) arranging the cell clusters on a support comprising a substrate and a plurality of puncturing structures suitable for puncturing cell clusters selected from thread-shaped and needle-shaped materials, wherein the cell clusters are arranged on the support by penetrating individual cell clusters with a puncturing structure of the support; c) causing each penetrated cell cluster to contact at least one other cell cluster, wherein the contact between any two cell clusters occurs either between cell clusters on the same puncturing structure, or between cell clusters on adjacent puncturing structures; d) allowing the contacted cell clusters to adhere to each other to form a structure made of cells; and e) removing the structure made of cells from the support.

This patent is assigned to Kyushu University and National University Corporation. Equivalent patents were filed in China, the European Patent Office, Japan, and Korea. It appears to cover a method for making a structure of cells by using certain needlelike arrangements onto which cell clusters are speared. The way the needle structures are arranged determines how the cells adhere to form certain structures. Figures 3 and 4 below show exemplary figures from the patent that show how the cell clusters are arranged:

US 6,767,928: “Mineralization and biological modification of biomaterial surfaces” (Exp. Date: March 17, 2020).

Exemplary Claim:

1. A method for generating an extended, osteoconductive mineral coating on a surface of a biomaterial, comprising functionalizing at least a first surface of a biomaterial to create a plurality of polar oxygen groups on the biomaterial surface and contacting the functionalized biomaterial surface with an amount of a mineral-containing solution effective to form a mineralized biomaterial that comprises an extended, osteoconductive mineral coating at the functionalized biomaterial surface; wherein said biomaterial comprises at least a first porous, biodegradable polymer portion that has an interconnected pore structure and that is degradable over a controllable time scale and wherein said biomaterial comprises at least a first portion that is prepared by a process comprising gas foaming and particulate leaching.

This patent is assigned to the Regents of the University of Michigan. An equivalent patent was filed in Australia, Canada, and the European Patent Office. In Europe, a patent has granted in Austria, Germany, Denmark, and Spain. This patent appears to cover methods for patterning or mineralizing biomaterial surfaces. According to the patent, the claimed methods are useful for generating three-dimensional or contoured bioimplant materials with modified surface features

Fig. 3 Figure 2A from US 8,198,086

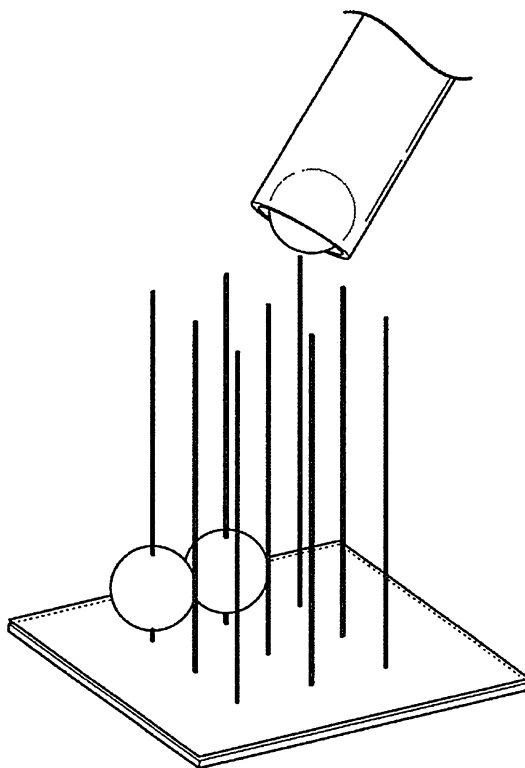
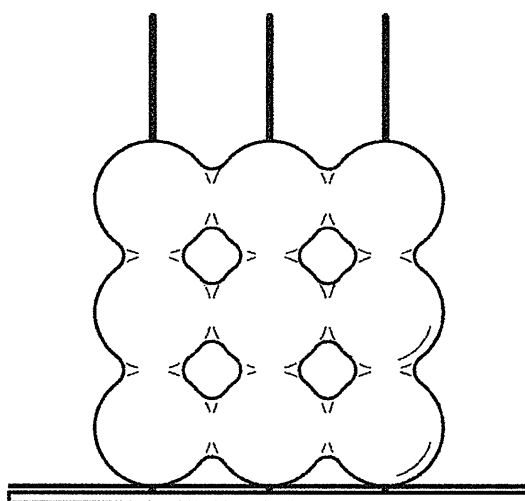


Fig. 4 Figure 3B from US 8,198,086



including surfaces incorporating bioactive factors and/or cells. The methods are particularly useful for bone tissue engineering and vascularization.

US 8,691,974: “Three-dimensional bioprinting of biosynthetic cellulose (BC) implants and scaffolds for tissue engineering” (Exp. Date: October 6, 2030).

Exemplary Claim:

1. A method of producing 3-D nano-cellulose based structures comprising: providing bacteria capable of producing nano-cellulose; providing media capable of sustaining the bacteria for the production of nano-cellulose; controlling microbial production rate by administering media with a microfluidic device, for a sufficient amount of time, and under conditions sufficient for the bacteria to produce nano-cellulose at a desired rate; continuing the administering of the media until a target three-dimensional structure with a target thickness and target strength is formed which has a morphology defined by a network of multiple layers of interconnected biosynthetic cellulose.

The patent is assigned to Virginia Tech Intellectual Properties, Inc. and was filed only in the USA. It appears to cover a method to grow biosynthetic cellulose, which can be used to make implants and scaffolds for tissue engineering. According to the patent, the method uses a 3D bioprinting process to make an alginate structure. The structure is placed into a media in which biosynthetic cellulose-producing bacteria are grown. The bacteria grow up along the printed alginate structure producing an entangled cellulose nanofibril network in the same shape as the alginate structure, which can be removed once the culturing is complete.

US 7,615,373: “Electroprocessed collagen and tissue engineering” (Exp. Date: August 31, 2019).

Exemplary Claim:

1. Synthetic electrospun collagen fibers electrospun from a solvent comprising a halogenated alcohol comprising a repeated longitudinal banding pattern, wherein the repeated banding pattern occurs at a spacing of about 65 nm to about 67 nm; wherein the synthetic electrospun collagen fibers comprise a matrix and the matrix has an elastic modulus between about 0.5 and about 10 MPa when hydrated.

This patent is assigned to Organogenesis, Inc. and Virginia Commonwealth University Intellectual Property Foundation. Equivalent patents were filed in Austria, Australia, Brazil, Canada, Germany, the European Patent Office, Spain, Japan, Mexico, Poland, and Singapore. This patent appears to cover synthetic electrospun collagen fibers. The patent specification makes clear that bioprinted organs are contemplated: “The invention is directed to formation and use of electroprocessed collagen, including use as an extracellular matrix and, together with cells, its use in forming engineered tissue. The engineered tissue can include the synthetic manufacture of specific organs or tissues which may be implanted into a recipient.”

US 7,780,897: “Hydrogel constructs using stereolithography” (Exp. Date: January 5, 2029).

Exemplary Claim:

1. A method of fabricating a hydrogel construct comprising: solidifying a first solution into a first hydrogel construct layer with a first energy dosage using stereolithography, the first solution comprising: a first hydrogel polymer having a first polymer concentration; and a first photoinitiator having a first photoinitiator concentration; where the first polymer concentration, first photoinitiator concentration, and first energy dosage are configured such that the cure depth of the first solution is less than or equal to two millimeters; and forming a second hydrogel construct layer using stereolithography.

This patent is assigned to Keck Graduate Institute and the Board of Regents of the University of Texas Systems. An equivalent patent was filed in Japan and the European Patent Office. The patent appears to cover a method of fabricating a hydrogel using stereolithography.

US 9,242,031: “Modular Fabrication Systems and Methods” (Exp. Date: August 10, 2025).

Exemplary Claim:

1. A method of fabricating a living three-dimensional structure, said method comprising: providing a data set representing a living three-dimensional structure to be fabricated; providing a printable composition comprising a hydrogel seeded with cells, wherein the hydrogel comprises collagen; and printing the printable composition onto a substrate in layers in a pattern in accordance with the data set suitable to fabricate the living three-dimensional structure without the need to provide a negative template; wherein the printable composition is capable of bonding between printed layers; and wherein $94 \pm 5\%$ of the cells in the fabricated living three-dimensional structure are viable.

This patent is assigned to Cornell Research Foundation Inc. and was filed only in the USA. It appears to cover a method of making a 3D bioprinted structure using a bio-ink seeded with cells that makes a structure in which a high cell content remains viable.

US 6,942,830: “Device and method for the production of three-dimensional objects” (Exp. Date: Nov 1, 2021).

Exemplary Claim:

1. A process for producing a three-dimensional object, the process comprising: . . . providing a three-dimensionally movable dispenser having an outlet opening to dispense a material comprising one or more components; positioning the outlet opening of the three-dimensionally movable dispenser in the medium; discharging of the material through the outlet of the dispenser into the medium; allowing the material to form a solid structure; and moving the dispenser to the points within the medium which correspond to a structure of a three-dimensional object and repeating the steps of discharging the material and allowing the material form a solid structure at each point, thereby forming a solid three-dimensional structure; wherein the material, after being discharged into the medium, forms a solid structure due to the contact with the medium without irradiation.

This patent is assigned to Envisiontec GmbH. Equivalent patents were filed in Australia, China, the European Patent Office, Israel, and Japan. European patents have granted in Austria, Germany, Denmark, Spain, and Portugal. The patent

appears to cover printing a 3D object by depositing an “ink” into a medium wherein a solid structure is formed by contacting the “ink” to the medium as opposed to using irradiation. The patent specification shows that the inventors contemplate that the method can be used in bioprinting: “The process of the invention does not require thermal or chemical after-treatment of the three-dimensional object formed. . . . This facilitates the use of temperature-sensitive, biologically or pharmaceutically active materials . . . such as for example proteins, growth factors and living cells, Hence, for the first time biocompatible and biodegradable excipients, which have a defined, freely selectable form and contain thermally and toxicologically highly sensitive materials or structures, may be produced in one step. Excipients of this type have considerable importance for the field of tissue engineering.”

US 9,005,972: “Inkjet printing of tissues and cells” (Exp. Date: February 13, 2029).

Exemplary Claim:

1. A method of making a biodegradable scaffold having cells seeded therein, comprising:
 - (a) forming a biodegradable substrate by electrospinning; and then
 - (b) printing viable cells on said substrate with an inkjet printing device, to make said biodegradable scaffold,wherein said method is carried out by an apparatus for printing cells comprising:
 - (i) an electrospinning device, said electrospinning device comprising a high voltage power supply;
 - (ii) an inkjet printing device operatively associated with said electrospinning device;
 - (iii) a controller operatively connected with said inkjet printing device; and
 - (iv) a three-dimensional plotter operatively connected with an inkjet head of said inkjet printing device and an electrospinning head of said electrospinning device,wherein said high voltage power supply is conductively isolated from said controller, and wherein said electrospinning head and said inkjet head are both simultaneously mounted over said plotter.

This patent is assigned to Wake Forest University Health Sciences and was filed only in the USA. The claim is self-explanatory and appears to cover a method of making a biodegradable scaffold that has cells seeded in it. The cells include cartilage cells, bone cells, muscle cells, and skin cells.

US 9,149,952: “Devices, systems and methods for the fabrication of tissue” (Exp. Date: September 27, 2031).

Exemplary Claim:

1. A bioprinter comprising:
 - a) one or more printer heads, wherein each printer head comprises a means for receiving and holding at least one cartridge, and wherein each cartridge comprises a deposition orifice and a bio-ink, the bio-ink comprising a solid or semi-solid composition comprising living cells;
 - b) a means for dispensing the bio-ink of a selected cartridge by application of pressure to extrude the bio-ink of the selected cartridge through the deposition orifice;
 - c) a means for determining a position of the selected cartridge in space; and
 - d) a programmable computer processor for regulating the dispensing of the bio-ink communicatively coupled to the means for determining a position of the selected cartridge and the means for dispensing the bio-ink.

This patent is assigned to Organovo, Inc. Equivalent patents were filed in Australia, Brazil, Canada, China, the European Patent Office, India, Japan, and Korea. The claims appear to cover a 3D bioprinter, which has cartridges comprising a deposition orifice and a bio-ink and is connected to a programmable computer.

US 8,931,880: “Devices, systems and methods for the fabrication of tissue” (Exp. Date: September 27, 2031).

Exemplary Claim:

1. A three-dimensional bioprinter comprising:
 - a. one or more printer heads, wherein a printer head comprises a means for receiving and holding at least one cartridge, wherein a cartridge comprises at least one deposition orifice and contents comprising a bio-ink, wherein the bio-ink comprises solid or semi-solid aggregates of living cells;
 - b. a means for calibrating a position in space of the at least one cartridge or the at least one deposition orifice utilizing a laser and a laser detector;
 - c. a means for extruding the contents of the at least one cartridge by application of pressure, utilizing a piston;
 - d. a receiving surface for receiving the extruded contents of the at least one cartridge; and
 - e. a programmable computer processor communicatively connected to the means for calibrating and the means for extruding, the programmable computer processor for positioning the one or more printer heads in three dimensions and regulating the extrusion of the contents of the at least one cartridge.

This patent is assigned to Organovo, Inc. and is related to US 9,149,952 and US 9,227,339.

US 9,039,998: “Bioprinting Station, Assembly Comprising Such Bioprinting Station and Bioprinting Method” (Exp. Date: March 4, 2031)

Exemplary Claim:

1. Bioprinting station comprising:
 - i) a bioprinting device adapted to deposit a pattern of biological material onto an area of interest of a substrate, . . . said bioprinting device comprising: at least one biological material dispenser . . . and a positioning system adapted to . . . position the area of interest with respect to the dispenser, wherein the dispenser comprises:
 - a) a holding device for holding at least one ribbon containing the biological material, . . .and b) a laser system arranged for emitting a laser beam adapted to transfer the biological material from the ribbon to the substrate, . . .
 - ii) an imaging system configured to acquire an image of the substrate . . . and
 - iii) an electronic control unit configured to: first, drive the imaging system according to an optical pathway to acquire an image of the substrate, . . . second, process the acquired image of the substrate so as to detect the revealed area of interest on the acquired image, third, determine the pattern corresponding to the area of interest detected on the acquired image, fourth, drive the holding device and the positioning system relative to one another so that the opened working space faces the area of interest, fifth, deposit the biological material according to the pattern within the opened working space by driving the laser system and the positioning system relative to one another.

This patent is assigned to Institut National de la Sante et de la Recherche Medical (INSERM). Equivalent patents were filed in Japan and the European Patent Office. The claims appear to cover a bioprinting device coupled to an imaging system that assists in depositing the biological material in a desired pattern.

US 8,691,274: “Inkjet printing of tissues and cells” (Exp. Date: July 9, 2030).

Exemplary Claim:

1. An apparatus for printing cells comprising:
 - (a) an electrospinning device, said electrospinning device comprising a high voltage power supply;
 - (b) an inkjet printing device operatively associated with said electrospinning device;
 - (c) a controller operatively connected with said inkjet printing device; and
 - (d) a three-dimensional plotter operatively connected with an inkjet head of said inkjet printing device and an electrospinning head of said electrospinning device. . .

This patent is assigned to Wake Forest University Health Sciences and was filed only in the USA. Additional claims specify that “device further comprises a composition to be printed in said printer cartridge, said composition comprising cells” (claim 6); “wherein said cells are stem cells” (claim 22); “progenitor cells” (claim 23); “cartilage cells, bone cells, muscle cells, skin cells, pancreatic cells, kidney cells, nerve cells or liver cells” (claim 24); and “chondrocytes” (claim 25).

US 7,857,756: “Architecture tools and methods of use” (Exp. Date: August 23, 2032).

Exemplary Claim:

1. A tool for performing biological, tissue engineering and/or medical procedures involving at least the placement of at least one constituent material at a target area within a body from a supply of the constituent material, comprising:
 - a. at least one material dispenser, which dispenses constituent materials forming biocompatible scaffold material, said material dispenser being configured to include an opening, and being controlled by a computer-controlled location control device, such that said constituent material is deposited in a three-dimensional pattern or shape which three-dimensional pattern or shape defines a cell growth template within said body, and
 - b. at least one imaging device, wherein the tool is sized and shaped to at least partially enter the body through an opening therein. . .

This patent is assigned to nscript, Inc. and an equivalent was filed in Australia. The claims appear to cover 3D bioprinting directly into a body.

US 6,986,739: “Architecture tools and methods of use” (Exp. Date: October 9, 2022).

Exemplary Claim:

1. An apparatus for depositing a material on a substrate, comprising:
 - a) at least one material dispenser, comprising:
 - i) a tip orifice defining an opening through which the material exits the dispenser,
 - ii) at least one elongate feed channel having an inlet and a spaced outlet adjacent the tip orifice, . . .
 - iii) a valve for controlling the flow of material through the outlet of the at least one feed channel, . . .
 - iv) an actuator operatively coupled to the valve for selectively moving the valve between the open position and the closed position,
 - v) wherein the material is displaced forward as the valve moves to the open position and the material is sucked back as the valve is moved to the closed position.

The patent is assigned to Sciperio, Inc. An equivalent patent was also filed in Australia. The patent appears to cover a printing apparatus. The patent specification indicates that the inventors contemplated the apparatus useful in bioprinting: “The direct-write technologies [DWDT] may be used to construct purely inorganic materials, purely organic materials, biological materials and/or any combination thereof . . . he DWDT may be used to perform biological, medical, bioengineering, bioelectronic, and tissue-engineering procedures . . .”

4.3 Maturongens ± Biomonitoring ± Bioreactor

The utility patent landscape is developing in the post processing steps of bioprinting; our search found mostly pending applications. But we also identified one relevant patent.

US 8,507,263: “Rotating Bioreactor” (Exp. Date: March 4, 2030).

Exemplary Claim:

1. A bioreactor, comprising:
 - a vessel;
 - a cylindrical scaffold defining an outer wall of an inner chamber and an inner wall of an outer chamber, wherein the scaffold is removably positioned within the vessel and configured to rotate relative to the vessel about a central axis extending through the inner chamber;
 - a shaft positioned within the inner chamber, the shaft comprising an opening defining a first inlet for introducing a liquid into the inner chamber;
 - a removable flange which is operatively connected to the shaft, wherein the scaffold is attached to the flange, and wherein the flange is configured to rotate with the scaffold about the central axis;
 - one or more mixing elements that are connected to the flange such that they are positioned within the outer chamber and co-rotate with the scaffold to enhance fluid motion and mixing in the outer chamber;
 - a first outlet in fluid communication with the inner chamber; and
 - an opening in fluid communication with the outer chamber for introducing and/or removing a liquid from the outer chamber.

This patent is assigned to Harvard Bioscience, Inc. An equivalent patent was filed in Germany and the European Patent Office. The patent specification indicates that the claimed bioreactor is useful for forming and growing tissues and organs: “Articles and methods for growing tissues and organs using bioreactors, including rotating bioreactors, are provided. In some embodiments, a . . . wall of the bioreactor defining the two chambers may be formed at least in part from a scaffold derived from a length of a hollow or tubular tissue or organ. Such a bioreactor can be used to form biocompatible structures for tissue engineering and organ replacement, such as cellular tissues, organ-like structures, and/or complete organs, within the bioreactor.”

5 There Is Room for Additional Patentable Innovations

While it may seem that it is too late to start filing patent applications on bioprinting innovations, there remains room for further patentable improvements. A number of researchers have questioned whether it will be possible to create a functioning bioprinted organ. For example, Dr. Darryl D’Lima, a researcher at the University of Manchester in Britain, has been quoted as saying that “Nobody who has any credibility claims they can print organs, or believes in their heart of hearts that that will happen in the next 20 years,” (Fountain 2013). In view of this skepticism, if one discovers a method of bioprinting a functional organ, the patenting of such a method should be a patentable innovation, assuming one can craft claims that distinguish the printed organ from a natural organ.

6 Existing Patent Filings May Not Impede Commercialization of Bioprinted Organs: Exceptions to Patent Infringement

It will be many years before a functioning bioprinted organ is made and approved by regulatory authorities. In the meantime, the basic patents may expire. Even if not expired, many countries have an exception to patent infringement under what is called the experimental use exception.

One who uses a patented invention without authorization from the patent holder is liable for patent infringement. However, an accused infringer can escape a finding of infringement by invoking the common-law experimental use exception, which permits a de minimis use of a patented invention where the use was motivated by an experimental purpose. In the USA, the exception is narrow and unavailable in most practical circumstances.

In *Embrex v. Service Engineering Corp.*, 216 F.3d 1343 (Fed. Cir. 2000) the US Court of Appeals for the Federal Circuit narrowly construed the experimental use exception. While recognizing that early precedent carved out a narrow defense “for amusement, to satisfy idle curiosity, or for strictly philosophical inquiry,” the court held that tests conducted in furtherance of a business venture were not protected by the experimental use exception. In other words, the experimental use exception is only available to noncommercial uses of a patented invention. Similar to *Embrex*, *Madey v. Duke University*, 307 F.3d 1351 (Fed. Cir. 2002), asked the question of whether the accused use is “in furtherance of the alleged infringer’s legitimate business.” If it is, it cannot qualify as experimental use for purposes of the exception. Because the patented invention was being used for educational purposes in *Madey*, it was considered, at least in part, in furtherance of a legitimate business purpose and ineligible for an exception to infringement. These cases show how narrow the experimental use exception truly is. And it is not something that a business should consider relying upon.

In the pharmaceutical industry, however, an additional exception to infringement exists. For this exemption, despite the patent rights, performing research and tests for preparing regulatory approval, for instance, by the Food and Drug Administration (“FDA”) in the USA, does not constitute infringement for a limited term before the

end of patent term. This exemption allows generic manufacturers to prepare generic drugs in advance of the patent expiration.

In the USA, this exemption is called § 271(e)(1) exemption or Hatch-Waxman exemption. In the European Union, equivalent exemptions are allowed under the terms of EC Directives 2001/82/EC (as amended by Directive 2004/28/EC) and 2001/83/EC (as amended by Directives 2002/98/EC, 2003/63/EC, 2004/24/EC, and 2004/27/EC). In Canada, this exemption is known as the Bolar provision or Roche-Bolar provision, named after the case *Roche Products v. Bolar Pharmaceutical Co., Inc.*, 733 F.2d 858 (Fed. Cir. 1984), which held that the use of a patented invention to collect information for compliance with FDA approval process for generic drugs was not covered by the experimental exception to infringement. In reaction to the *Roche* decision, Congress passed an amendment to the patent statute exempting certain uses, including performing research and tests for preparing regulatory approval, from infringement.

Thus, in many countries, one can carry out clinical testing of a patented bioprinted organ or tissue without fear of patent infringement, as long as the clinical testing is to collect information for compliance with government approval.

However, if a bioprinted tissue is used as a research tool, e.g., to screen drugs, there will be no exception to patent infringement. And the use of a patented bioprinter to make a bioprinted organ or tissue will not be exempt from infringement. Any company or institution contemplating use of a bioprinted tissue as a research tool must consider the patent landscape and seek licenses where available.

7 Conclusion

There have been many patent applications filed and patents issued that cover various aspects of bioprinting. Most of the patent applications were filed first in the USA by US companies and institutions, and some were then filed in foreign countries. These patents and ordered injunction will prohibit the commercialization of the product or service. Applications, their expiration dates, considered prior to undertaking and the countries in which they have been filed must be the development of a product or service based upon bioprinting. Failure to do so may lead to liability for patent infringement, costly damage awards to the patent owners, and possible court-ordered injunction that would prohibit the commercialization of the product on service.

References

- Fountain H. At the printer, living tissue, N.Y. Times, 18 Aug 2013. http://www.nytimes.com/2013/08/20/science/next-out-of-the-printer-living-tissue.html?pagewanted=all&_r=1&
- Mironov V et al (2008) Organ printing: promises and challenges. *Regen Med* 3:93–103
- Press Release, Organovo Holdings, Inc., Organovo announces two issued patents, First Company Patent and Key Founder Patent (9 July 2012) (on file with author). <http://ir.organovo.com/news/press-releases/press-releases-details/2012/Organovo-Announces-Two-Issued-Patents-First-Company-Patent-and-Key-Founder-Patent1130104/>



Emerging Business Models Toward Commercialization of Bioprinting Technology

Yakov M. Balakhovsky, Alexander Yu. Ostrovskiy, and Yusef D. Khesuani

Contents

1	Introduction	514
2	Bioprinting Industry and Market Development	515
3	3D Bioprinting Market Segments and Business Models	518
4	Legal Issues of 3D Bioprinting	525
5	Opportunities for Raising Financing	527
6	Porter's Analysis of 3D Bioprinting Industry Development	528
7	Conclusion	531
	References	533

Abstract

After breaking out from the confines of purely academic research, 3D bioprinting technology is quickly developing as a commercial industry and exhibiting the qualities of a mature market with immense potential. We are currently witnessing not only growth in the number of companies and their geographical reach, but also the market's segmentation. The main models of 3D bioprinting technology commercialization seem to be selling bioprinters and bioinks, services of bioprinting 3D functional tissue constructs – including for drug discovery and disease modeling – selling software, and technological consulting. As the

Y. M. Balakhovsky (✉)
Vivax Bio, LLC, New York, NY, USA
e-mail: yb@vivaxbio.com

A. Y. Ostrovskiy
Independent Laboratory INVITRO, Moscow, Russian Federation
e-mail: aos@invitro.ru

Y. D. Khesuani
Vivax Bio, LLC, New York, NY, USA

The Laboratory of Biotechnical Research 3D Bioprinting Solutions, Moscow, Russian Federation
e-mail: usefhesuani@yandex.ru

industry advances, so does the legal regulation of the relevant issues. A number of companies are already successfully monetizing the technology and are able to raise financing through various paths. In the near future, we should expect the start of industry consolidation. At this stage of the technology development, rivalries within the industry do not represent a significant threat. The industry is currently characterized by stakeholders joining efforts in order to expedite its advancement and reach the commercial application stage. To accomplish this, the industry must overcome a number of significant hurdles, including achieving the standardization of bioprinting methods, software, and materials.

1 Introduction

3D bioprinting, an additive robotic biofabrication of functional tissue and organ constructs on the basis of digital models and using live cells as a printing material, is a very young, yet rapidly advancing technology that holds the promise of addressing some of the most pressing needs in life science (Mironov et al. 2003).

Aging, cancer, cardiovascular diseases, and high injury rate are the main causes of acute or gradually developing structural and functional atrophy of critical organs and tissues. In the US and Europe alone, more than 100 million people currently suffer from chronic kidney insufficiency (American Kidney Fund 2015) (European Renal Association – European Dialysis and Transplant Association 2016) and more than 60 million people have kidney problems (European Renal Care Providers Association 2015). As things stand today, it does not appear possible to achieve complete structural and functional restoration of human organs. The progress of regenerative medicine and tissue engineering has led to the development of approaches to transplantation of 3D microtissues, which, according to many studies, has a number of significant advantages compared to transplantation of cell suspension (Huang et al. 2013; Manabu Itoh et al. 2015; Delphine Antoni et al. 2015).

The demand for organ transplantation is extremely high and so is the market for human organs. There are more than 120,000 people on the organ transplant waiting list in the United States, and 20 people die every day while waiting for a donor (National Kidney Foundation 2016). In China, there are 1,500,000 people on the waiting list and less than 1% of patients needing organ transplants were treated (Jiayang Fan 2014). The situation is somewhat better in certain European countries. In Italy and France, for example, the cadaveric donation rate is 25–27 per 1 million of population per year. In Spain and Croatia, the rate is more than 40 (Spanish Ministry of Health 2016). This is not an indication of “artificial” donor creation (the so-called “black market transplantology”), but a rational approach to the problem.

Nevertheless, the gap between the demand for organ transplants and supply is growing, and, therefore, a “black market” for human organs and the so-called “transplantation tourism,” when patients needing organ transplantation travel to some developing countries which do not observe international conventions on organ transplantation, are present-day realities. There is hope that bioprinting will

help resolve this problem, as well as the associated unethical situation where millions of people worldwide are waiting for the death of others.

Another problem where bioprinting may help is the obvious imperfection of 2D models and animal tests currently used in preclinical drug testing. The pharmaceutical industry could strongly benefit from having the means of early detection for negative side effects of potential drugs. With such means at hand, pharmacologists could discard blind-alley formulations before too much time and money have been spent (not to mention the possibility of avoiding or drastically decreasing the chances of a drug, having passed all tests and received all permits, being recalled because of a dangerous side effect, which was revealed only after the drugs had been released to the market). Tests on 3D tissue and organ constructs could become and, are already becoming a good alternative to conventional preclinical drug discovery methods and methods of disease modeling. A separate field of application is cosmetic formulations testing, where the goal is complete exclusion of animal tests. Incidentally, such tests are forbidden in the EU since 2013 (European Commission 2013).

2 Bioprinting Industry and Market Development

Although 3D printing technology has been known since the 1980s, it was only in the early 2000s when additive technologies involving the use of live material were first applied in tissue engineering. The latter technologies quickly made their way from research labs to commercial companies.

Currently, the main components of bioprinting technology include the bioprinter, an automatic device capable of printing 3D objects, scaffold, or substrate for cell material, and cell material itself (Murphy and Atala 2014). Each of these components may be of interest from the commercial viewpoint and may be a separate line of business for a company. Since bioprinting is a relatively young technology, it appears advisable to track its birth and evolution in Gartner's Hype Cycle annual reports.

Gartner is a research and consulting company specializing in information technologies. In 1995, Gartner introduced the term "*Hype Cycle*," which is widely used by market analysts for explaining or forecasting various trends related to the appearance of a new technology. In a nutshell, the term is used for illustrating that in its development to maturity, each technology passes through several phases. During these phases, the interest in the technology from specialists and the broader public is different:

- Technology trigger – the appearance of an innovation, first publications about a new technology
- Peak of inflated expectations – the time when a new technology becomes popular, widely discussed by the public, and expected to lead to revolutionary developments
- Trough of disillusionment – the time when a technology ceases to be new, its drawbacks are revealed, and the public demonstrates disappointment
- Slope of enlightenment – main drawbacks are rectified, interest slowly returns, commercial use of the technology begins

- Plateau of productivity – the technology reaches maturity and is adopted by the mainstream with full awareness of its advantages and limitations

It is stressed that not all technologies are destined to reach *peak of inflated expectations* or *slope of enlightenment*, because their cycle can finish earlier without any prospects for productive use. On Hype Cycle graphs plotted for certain dates and certain market segments, Gartner analysts ascribe a point to each new technology which corresponds to its phase of development. With the help of special symbols, this illustrates the prognosis for technologies to reach maturity and mainstream acceptance.

The first appearance of 3D bioprinting in Gartner reports dates back to 2011, when the technology appeared under the name “3D bioprinting” and was attributed to the “technology trigger” phase (Fig. 1).

In Gartner’s report for 2014, the technology appeared under the name “3D bioprinting systems,” and moved a bit further along the curve, but still remained within the “technology trigger” phase (Fig. 2).

In 2015, the technology was once again renamed and appeared as “3D bioprinting systems for organ transplant” (Fig. 3).

In the same year, Gartner published a special report highlighting 3D printing, and for the first time two directions for the technology’s development were specified on the Hype Cycle graph: “3D bioprinting systems for organ transplant” and “3D bioprinting for life science R&D.” The second direction appeared at the intersection of the “technology trigger” and “peak of inflated expectations” phases (Fig. 4).

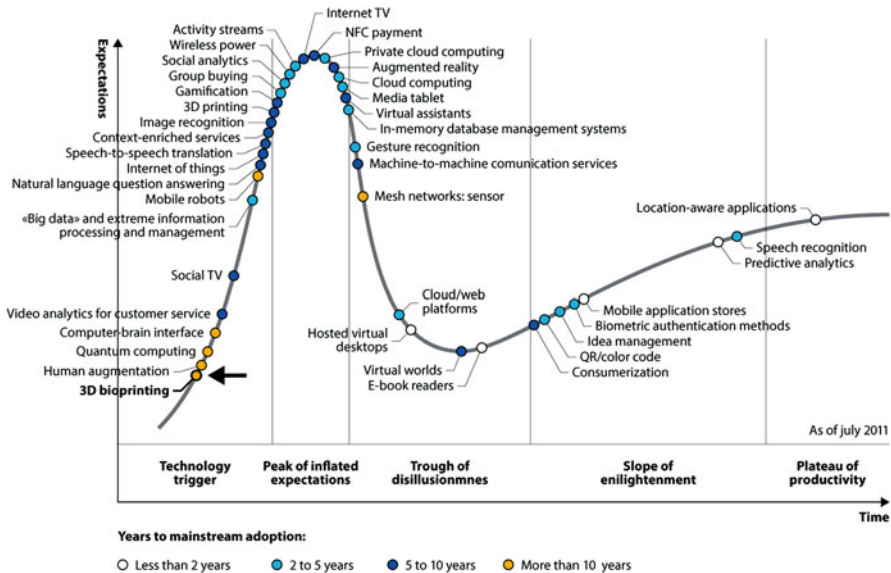


Fig. 1 Gartner’s Hype Cycle for the technology, 2011

Judging by Gartner’s publications, 3D bioprinting technology is developing quite rapidly and acquiring the traits of maturity.

Also indirectly pointing to the technology’s maturity are numerous market reviews, which have begun to appear very frequently recently. They have different forecasting horizons, and feature, among other topics, the appearance of new bioprinting methods,

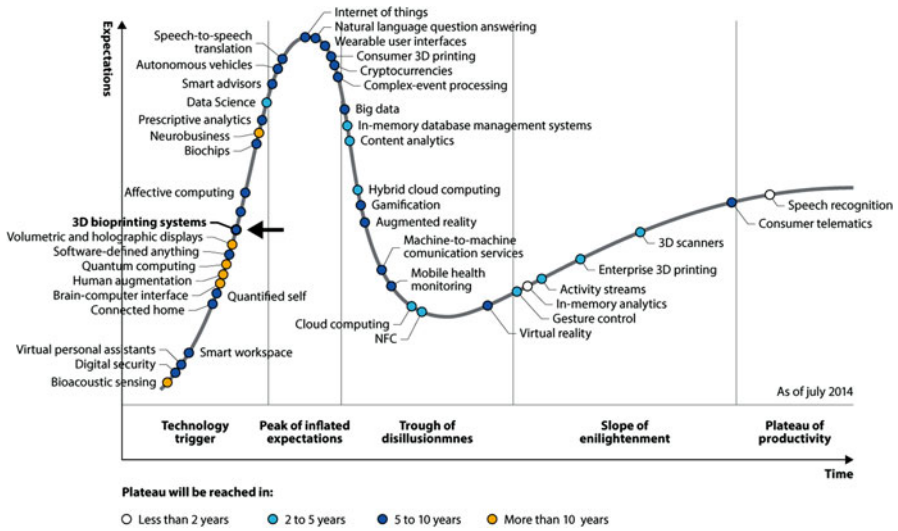


Fig. 2 Gartner’s Hype Cycle for the technology, 2014

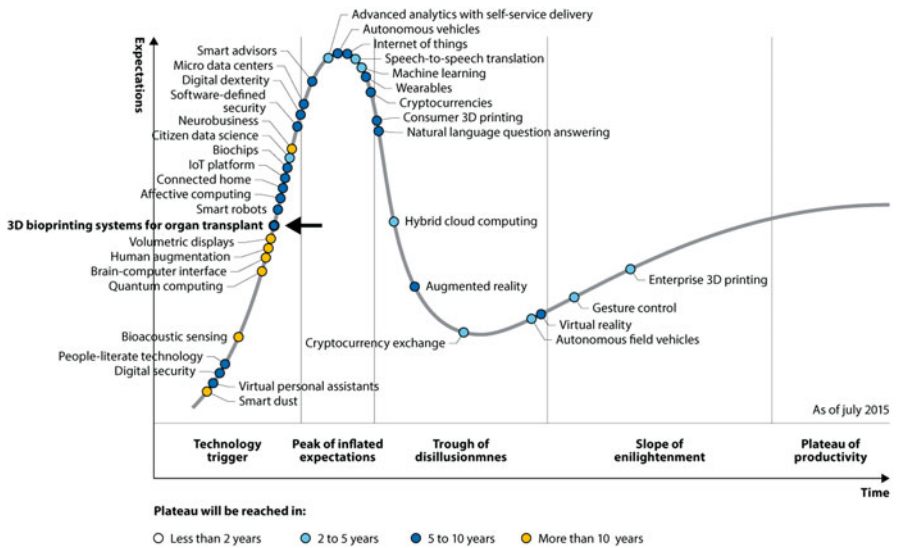


Fig. 3 Gartner’s Hype Cycle for the technology, 2015

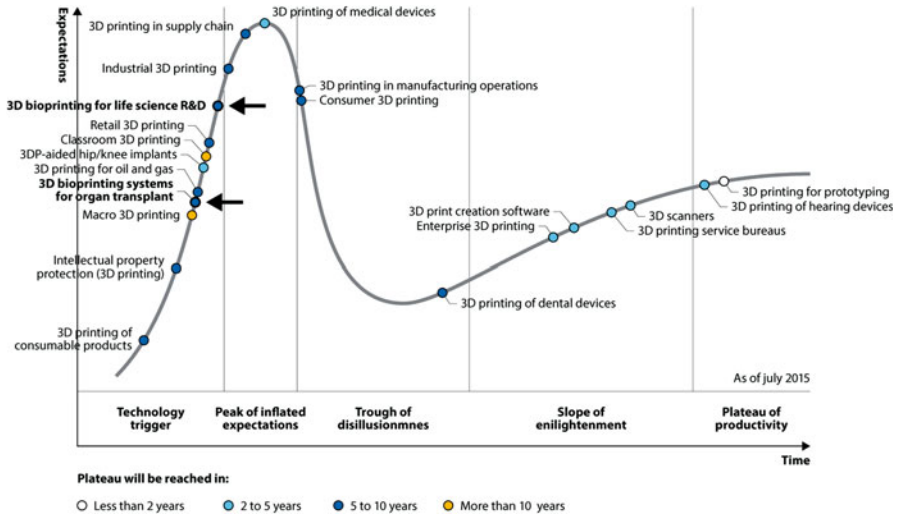


Fig. 4 Gartner’s Hype Cycle for the 3D printing technology, 2015

such as acoustic and magnetic bioprinting. They also tend to become more segmented, for example, highlighting the market of equipment for bioprinting.

While forecasts of 3D bioprinting market growth (including all its segments) vary widely, most reports seem to indicate that it will reach \$1–1.8 billion within the next 5 years and up to \$10–12 billion (\$12 billion being an optimistic scenario) by 2030. Different reports contain a wide range for the applied market compound annual growth rate (CAGR) – anywhere from 18% to 36%. This is not surprising, because the reports disagree not only on the magnitude of the market growth but also on the starting market volume numbers.

3 3D Bioprinting Market Segments and Business Models

It is, therefore, obvious that 3D bioprinting technology is becoming the basis for the creation of new markets. One new market is bioprinters – automated devices for printing 3D live constructs (Table 1).

As things stand today, more than 30 commercial companies are involved in the business of bioprinter manufacturing. They represent different countries and continents, and what is most interesting is different bioprinting methods. Most commercially available bioprinters employ the extrusion bioprinting method. At the same time, some companies are developing laser bioprinters (Poietis, France) and inkjet bioprinters (Nano Dimension, Israel). Bioprinters manufactured by Cyfuse Biomedical (Japan) and 3D Bioprinting Solutions (Russia) allow printing with tissue spheroids, which has a number of obvious advantages. They include higher printing speed, and the possibility of making 3D constructs with high cell densities and

Table 1 Main bioprinter manufacturers

Company	Country	Name of product
RegenHu	Switzerland	3D Biofactory
EnvisionTec	USA	Bioplotter
Neatco	Canada	Laboratory Bioprinter
Regenovo	China	Regenovo Bioprinter
Bio3D Technologies	Singapore	Explorer
GeSim	Germany	Bioscaffolder
The Technology Partnership	United Kingdom	Vista 3D
Cyfuse Biomedical	Japan	Regenovo Bioprinter
Advanced Solution Life Sciences	USA	BioassemblyBot
Poietis	France	Laser-assisted bioprinter
Ourobotics	Ireland	Revolution 3D Bioprinter
Cellink	Sweden	Inkredible
BioBots	USA	BioBot bioprinter
3D Bioprinting Solutions/Vivax Bio	Russia/USA	FABION

correct tissue architecture, higher stress resistance of cells, etc. (Mironov et al. 2009; Moldovan et al. 2017).

Bioprinter prices vary widely depending on their functionality and complexity: From \$10,000 to over \$200,000. According to public sources, prices of bioprinters manufactured by 3Dynamic Systems, CELLINK, and BioBots are in the range of \$10,000–\$23,000 USD; bioprinters from 3D Bioprinting Solutions and Advanced Solutions are \$100,000–160,000; and bioprinters from RegenHu, EnvisionTEC, and Cyfuse Biomedical cost more than \$200,000 (Davide Sher 2015).

Of course, bioprinters need special software to create models of the constructs being printed and to control the printing process. Most of the currently available bioprinters are based on extrusion technology. All materials used in bioprinting are readily available, but each bioprinter uses its own software. This means there is no such thing as a standard file format for bioprinting, and, therefore, results obtained in one laboratory cannot be reproduced in others (or, at least, such reproduction is extremely difficult). This problem is holding back the development of bioprinting as an industrial sector. It should be noted that other innovative areas such as robotics and artificial intelligence research confront the same problem with a lack of information exchange standards.

Necessary conditions for 3D bioprinting to become widespread include a radical simplification of the entire process and achieving a flawlessly smooth materialization of 3D computer designs. 3D printing successfully achieves this goal thanks to its ability to slice and connect 2D layers. However, using a digital control system for layer slicing is a more complicated technology, and not all users are familiar with it at the moment. Each step requires a special approach and creative selection of a special set of tools by the operator. The actual complexity of the problems being tackled lies somewhere between the digital control system planning and additive 3D bioprinting scheme. Bioprinting software should account for the diversity of technical approaches and characteristics of the materials used. For example, if a bioprinter

performs extrusion printing (analogous printing) with additive allocation of tissue spheroids and simultaneously employs UV polymerization, its software must be adequately flexible and modular to support these tasks. At the same time, software must be compatible with the bioprinter's kinematic design and be easily adaptable to its changes. The option of creating and storing test reports in the same computer program would be an additional convenience for users.

Therefore, the main engineering challenges can be summarized as follows:

- Lack of a standard bioprinting file format – not STL or AFM 3D files, but a format compatible with any bioprinter model
- Lack of bioprinting planning software powerful enough to ensure a complete and simultaneously intuitive control of the printer's operation
- Lack of standardized bioprinting software and process

Another market associated with bioprinting is bioink. For the purposes of this discussion, we are narrowing our focus on bioink as temporary scaffolds for cell material, thus leaving out the integral component of bioink – the cell material itself, which is extensively discussed in various other chapters of the book. Most often, bioink (as defined above) is produced on the basis of biological or synthetic hydrogels, or their combinations (Skardal and Atala 2015) (Table 2).

As a rule, bioinks are manufactured by bioprinter makers, but recently companies specializing exclusively in bioink manufacturing have begun to appear, which means a deviation from the vertical integration in favor of “niche” products (Table 3).

Another widespread business model in the field of bioprinting is selling the services of testing various pharmaceutical preparations using 3D structures. Bioprinting allows automated manufacturing of standardized and, therefore, reproducible structures with preset properties (Tables 4 and 5).

It is known that cells of the same type may demonstrate very different properties, even at different gene expression levels, in 3D structures compared to monolayers. It has been demonstrated that a more complex and natural organization of the extracellular matrix in 3D structures leads to radically different cell responses to external influences *in vitro*. The high density of cells, extracellular matrix synthesis, and tissue architectonics formation are factors that make this direction of work

Table 2 Primary types of bioink

Synthetic	Natural
Polyethyleneglycol (PEG) - PEG-diacrylate (PEGDA) - PEG-dimethacrylate (PEGDMA)	Agarose
Multiaim PEG (maPEG): PEG peptide, maPEG acrylate, maPEG azide, maPEG thiol	Alginate
Polyacrylamide (PAm)	Collagen
Poly (N-isopropylacrylamide) (PNIPAAm)	Fibrin
Poly (2-hydroxyethyl methacrylate) (PHEMA)	Gelatin
Poly methyl methacrylate	Hyaluronic acid

Table 3 Primary manufacturers of bioink

Company	Country	Product	Base material
Bioink Solutions	South Korea	Gel4Cell Gel4Cell-BMP Gel4Cell-VEGF Gel4Cell-TGF	Gelatin
Cellink	Sweden	CELLINK	Cellulose-alginate mixture
RegenHU	Switzerland	BioInk	No data
		Osteoink	Calcium phosphate paste
Biobot	USA	Bio127	Pluronic F-127
		BioGel	Gelatin methacrylate
Collplant	Israel	rhCollagen	Recombinant collagen
Advanced Biomatrix	USA	LifeInk 100	Methacrylated Type I Collagen
		LifeInk 200	Type I Collagen

Table 4 Advantages of using 3D structures for testing pharmacological preparations

	Cells on scaffolds	Spheroids	Bioprinted constructs
High cell density	–	+	+
3 Dimensional Space without any exogenous materials	–	+	+
Multiple cell types	+	+	+
Tissue-like architectonics	–	±	+
High repeatability, automated process	–	–	+

particularly promising. Apart from testing pharmacological properties of drug candidates, such as predictive toxicology, ADME, and efficiency, 3D constructs are increasingly used for disease modeling like inflammation, tumor development, fibrosis, genetic disorders, etc. (Knowlton et al. 2015; Nguyen et al. 2016). Work has also been reported on placenta bioprinting for studying the permeability of drugs through placental barrier (Che-Ying Kuo et al. 2016).

Therefore, the main models of 3D bioprinting commercialization seem to be:

1. Sale of bioprinters and their components and/or licensing their manufacturing
2. Sale of hydrogel- and cell-based bioinks
3. Sale of the services of bioprinting 3D functional tissue constructs, including for drug discovery and disease modeling
4. Sale of bioprinting software
5. Technological consulting, setting up turn-key bioprinting labs, lab infrastructure maintenance

Primary customers for these services today are academia, research institutions and laboratories, pharmaceutical and chemical companies, and the military.

Table 5 Comparison of cell properties in 2D and 3D structure

	Cells in 2D (monolayer)	Cells in 3D
Cell Shape	Spread and stretched	Polarized, ellipsoid
Contact region of cell surface	50% with liquid phase (culture media), 50% with plastic	80% cell-cell interaction or cell-matrix interaction, 20% interaction with liquid phase (culture media)
Types of cell contacts	Integrins – extracellular matrix	All the variety of adhesive contacts: - Desmosomes - Gap junctions - Tight junctions - Integrins – extracellular matrix

Bioprinters also appear in hospitals. For example, a bioprinting center has opened in Brisbane, Australia (Institute of Health and Biomedical Innovation 2017). These developments have led to a business model where constructs are printed not in special labs, but in situ, directly at the patient's hospital bed. Such technical solutions have already been implemented and demonstrated for skin defects treatment at the Wake Forest Institute for Regenerative Medicine (Wake Forest Institute for Regenerative Medicine 2016). Without a doubt, the full-fledged use of bioprinted products and services at hospitals can be expected only at a later phase, when reliable mass printing of fully functional human organs, or at least constructs to “patch” affected organs, is mastered. One possible commercialization option is a bioprinter company that does not merely sell its products, but offers a service agreement to set up a “turn-key” biofabrication line in a hospital and provide consulting services for a set amount of time after the line's commissioning.

Obviously, 3D bioprinted fully functional organ constructs for transplantology would have the biggest commercial potential. However, we believe in the short- to intermediate-term perspective; the market segmentation will look as follows (Fig. 5).

There are already some well-known examples of successful technology commercialization (Table 6).

These services are in high demand from pharmacological companies due to the possibility of using human cells in 3D structures, pathology modeling, and a standardization of approaches (Ozbolat et al. 2016). 3D bioprinting technology is a part of regenerative medicine. It can be described as an automated process that precisely places cells and tissue spheroids onto scaffolds to form 3D constructs. Laboratories working in the field must have access to cell material and be competent working with live objects.

One of the factors holding back the development of regenerative medicine is often the lack of quality, safe cell material. It is not surprising that an increasing number of bioprinter developers tend to cooperate with cell and cell line producers. The best-known examples of such cooperation are Nano Dimension with Accelta and Cyfuse Biomedical with Cell Applications. Interestingly, some companies offer “ready-to-print” kits, which, in addition to hydrogels, include a certain type of cells. One

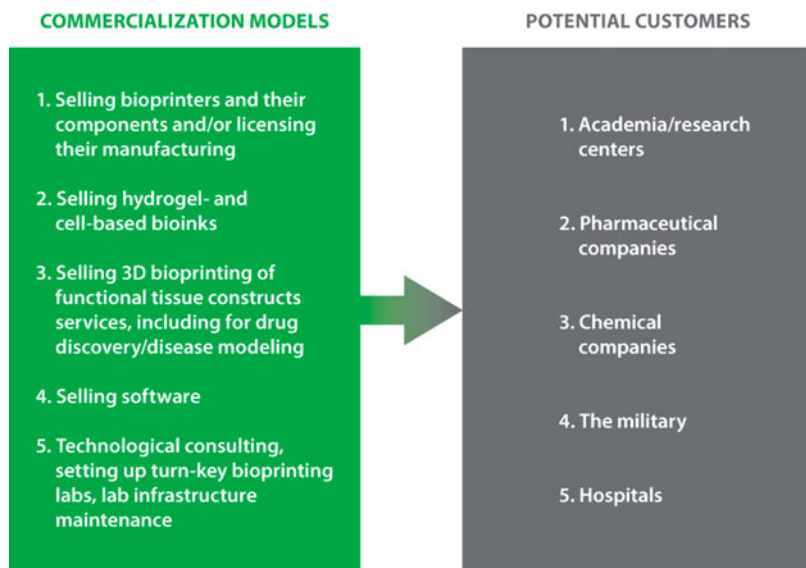


Fig. 5 Market segmentation

Table 6 Examples of service commercialization options

Seller Company	Buyer Company	Product/Service
Organovo	Merck	Liver Construct
Organovo	Janssen Research and Development	Liver Construct
Organovo	Bristol-Myers Squibb Co	Liver Construct
Organovo	Astellas Pharma	Liver Construct
Organovo	Ardea Biosciences (subsidiary of Astra Zeneca)	Kidney construct
Organovo	La Jolla Pharmaceutical	Kidney construct
Organovo	L'Oreal	Bioprinted skin
Poietis	L'Oreal	Bioprinting of hair
Poietis	BASF	Bioprinted skin
Aspect Biosystems	Johnson & Johnson	Bioprinting of cartilage

example is the product made by RoosterBio, which is based on stem cells in combination with Cellink's hydrogels.

The tendency for cooperation between bioprinter developers and cell and cell line producers will grow further, along with traditional strategic cooperation between commercial companies and research institutions. Already, we have witnessed examples of international integration, such as the merger of an American company, Vivax Bio, with a Russian company, 3D Bioprinting Solutions. These mergers aim to achieve the most efficient allocation of qualified and economically effective human resources, engineering, and production bases (the above-mentioned merger

of Vivax Bio and 3D Bioprinting Solutions also involved the use of Austrian and German engineering resources), potential client bases, and capital markets. It seems possible in the future we will witness the emergence of new multinational chains of companies – biofabrication technology integrators.

Another notable trend is the change of business models. For example, shifting from selling bioprinters to providing services (Organovo). Clearly, selling bioprinters involves a maintenance agreement, which requires having a significant number of engineers to ensure an adequate customer support. The service provision model requires rigid standardization of procedures and precise compliance with the customer's conditions.

As we noted above, technologies are usually born in research laboratories and make their way to commercial organizations. However, a reverse direction of cooperation is also possible. For example, a number of commercial companies (3D Bioprinting Solutions, nScript in cooperation with Bioficial Organs, and Nano3D Biosciences Innovate in cooperation with Greiner Bio-One North America) are preparing to conduct several experiments on the International Space Station (ISS). This will require manufacturing new specialized equipment, developing means of biological material delivery, preparation of specialized documentation, and obtaining relevant permits. Obviously, these experiments will also require employing several systems and installations from the ISS standard set of equipment used for biological experiments at the station, establishing an online monitoring and control system, and, in certain cases, training the personnel for performing this work in space. Therefore, cooperation with such companies as Roscosmos, NASA, Techshot, and several others to put the necessary infrastructure in place is critically important. Following the acquisition of relevant experience, commercial companies will be able to provide “turn-key” B2S (business-to-science) services for conducting such experiments at research institutions.

In addition to the medical services market, bioprinting may be used in the food industry and even in the fashion industry. Today, there are billions of cattle and poultry in the world to satisfy our needs for meat, dairy products, eggs, and hides (Thornton 2010). Farm livestock is currently the major consumer of land and fresh water resources, and one of the main sources of greenhouse gases. Furthermore, a considerable part of the world population (vegetarians) refuses to eat such products for ethical or other reasons. There are a number of companies around the world involved in the business of developing the production of artificial animal products. They include Memphis Meats (plans to launch commercial production and sale of artificial croquettes, chicken breasts, and steaks in the next 2–5 years), SuperMeat (an Israeli company specializing in the production of kosher chicken liver), Clara Foods (egg whites synthesis), and more. Only a few of them, such as Mosa Meats and Modern Meadow, plan to use 3D bioprinting technology for meat production (Modern Meadow's primary objective is biofabrication of leather for manufacturing clothes). Without a doubt, organoleptic characteristics, such as taste, odor, texture, color, appearance, are important in the business of artificial food production (using bioprinting or other biofabrication technologies). So too are production costs. It is too early to talk about that economy at this point. The cost of bioprinted products is

currently too high for commercial use, but will decrease with time and is expected to reach an acceptable level. One conclusion can definitely be made: The industry of biofabrication has colossal potential. The capacity of the world meat market is hundreds of billions of dollars.

In addition to the manufacturing of leather with preset characteristics (thickness, rigidity, stretching, etc.), the approach proposed by MIT Media Lab researchers for the fashion industry appears interesting. MIT researchers have discovered that ancient bacteria from Japanese fermented soybeans are capable of dilatation and contraction in response to changes of ambient temperature and humidity. The project, which was launched in cooperation with fashion designers from the Royal College of Arts and sports brand New Balance, sets the goal of creating a biohybrid material, named “bioLogic,” to be used as bioink for 3D bioprinting technology. The plan is to use the material for both traditional clothes and sportswear.

The technology is based on applying cells derived from *Bacillus subtilis* natto bacteria onto synthetic material (spandex) using a bioprinter. Natto bacteria, which live on dry rice stems, are very susceptible to humidity and heat. They change their size and form in response to changes in ambient conditions. Natto bacteria’s ability to expand and contract in response to humidity changes suggests they can be used as “ventilation holes,” which can close or open in response to human body conditions. As humidity increases, each natto cell can quickly expand, adding up to 50% of its original size. The bioLogic team developed its own high-resolution bioprinter capable of printing natto cells directly into spandex textiles.

Such biohybrid material may have other potential applications. For example, a teabag tag with bioprinted natto cells can serve as a readiness indicator; similarly treated flowers will close or open their petals or even change color under the influence of sunlight; and a lampshade with natto cells planted on its surface will change its form under the influence of heat irradiated by the light bulb.

At the 2016 Summer Olympics in Rio de Janeiro, Brazil, athletes wore sports shoes made by using a 3D printer (Hall 2016). In the future, we could see athletes dressed in sportswear made of biohybrid materials produced with the help of bioprinters.

4 Legal Issues of 3D Bioprinting

Naturally, having invested enormous creative energy, human and financial resources in the research and development of their products, devices, methods, manufacturing processes, and designs, the inventors are trying to protect their intellectual property rights by filing patent applications both nationally and internationally. As reported last year, an updated patent search on 3D bioprinting showed a 36% increase of 3D bioprinting patents in 2016 (950), compared to a similar search conducted in 2015. The companies that owned the most patents included Organovo, Koninklijke Philips, HP, Medprin Regenerative Medical Technologies, and Corning. Alternatively, these same companies are active buyers of licenses from other patent holders (Hornick and Rajan 2016).

The issue of what exactly can be protected by patents as it applies to the industry is rather complicated, the pertinent law is still evolving, and the matter is largely beyond the scope of this writing. Having said that, let us note the basic legal principle, at least in the United States, is a “human organism” or any “naturally occurring” object, i.e., a product of nature, is not patent eligible. In other words, the closer a printed organ or a tissue mimics the real human organ, the lower its chances to be patentable. Inevitably, as the 3D bioprinting technology advances, and the problem becomes more pressing, the courts (or Congress) will have to clarify the law in this regard. Obviously, industry-related products such as hardware, processes or methods, chemical materials/compounds, software, designs, and trademarks do enjoy respective IP protection. In fact, the sale of patents and licenses has been an important way for academia and commercial companies to monetize the results of their R&D. In other words, protecting an IP serves the dual purpose of barring IP infringement and benefitting financially from its licensing to interested third parties.

Aside from purely protecting the IP rights of inventors, an impressive IP portfolio adds certain prestige to the company’s image and seems to be required by venture capitalists considering an investment. Because of these factors, we should expect to see an ever-growing number of patent filings in 3D bioprinting in the foreseeable future.

A number of issues have arisen in connection with the existing IP protection situation in 3D bioprinting, even if we leave aside a broad discussion of the value of IP protection versus, as its critics would argue, its stifling effect on innovation and technological progress, which has created an anti-IP protection backlash in favor of open source development. Any patent application filed in the United States is usually not published for the next 18 months. Accordingly, during this 18-month period, everybody working on related products is operating in the dark. In a young, rapidly developing industry, 18 months represents a significant amount of time to work on a product which ultimately may infringe on a competitor’s IP rights.

On the other hand, despite the fact that some early industry players have filed a number of broad, basic patents, ostensibly precluding anybody else from independently developing many (if not most) 3D bioprinting products, we do not currently observe any significant patent litigation in the industry. This may be explained by a number of factors: (1) the industry as a whole is very young, and even the more established companies do not yet represent a “deep pocket” target for any litigation; (2) some patent holders realize their patents are overly broad and do not want to risk having a court cancel them in response to an infringement lawsuit; (3) at this point in the nascent industry’s development, its participants realize that cooperation, not litigation, represents a more productive path going forward. This includes potential industry consolidation (and thus, IP portfolios consolidation) where companies will be merging both vertically and horizontally.

At this point, the bulk of the industry products and services remain beyond the realm of the FDA in the United States or similar regulatory bodies in other countries. For instance, in drug discovery using 3D assays, the onus is rather on the side of industry clients presenting their final product for FDA approval. However, as the industry reaches the stage of developing fully functional human organs for transplantation, or at least, in the interim, some organ “patches” as a transplantation stopgap solution, these new industry products will inevitably become the subject of FDA scrutiny.

The creation of 3D constructs (for drug testing or for disease modeling) and the use of 3D bioprinting technology has created a number of ethical and legal issues. 3D organ and tissue constructs are fabricated using cells taken from people, who possess certain legal rights. Therefore, the performance of such studies in any country should be regulated by unified legal procedures adopted for handling biological material taken from patients. Relevant consent should be obtained from patients before using their cells for research purposes. The same rules should apply to 3D tissue and organ constructs.

5 Opportunities for Raising Financing

While the 3D bioprinting industry's big payday is still at least 15–20 years away, when fully functioning printed human organs will reach the market for transplantation, a few companies are already successfully monetizing the technology and are able to raise financing through various paths. (In this section, we are leaving out any forms of financing from government, quasigovernment, and nonprofit sources (such as grants, etc.), which is clearly a well-established way of financing for academia and the industry alike.)

Until recently, Organovo – the pioneer in industrial-scale drug testing using its 3D printed organ constructs – was the only publicly traded 3D bioprinting company (it still remains the only American public company in the industry). Organovo went public in February 2012 through a reverse IPO (reverse merger). It subsequently raised about \$128 million through a few rounds of offerings in the following years. This represents an important breakthrough, not only for the company itself but for the industry as a whole. The company's market capitalization fluctuated significantly during the last 5 years from around \$230 million to just under \$1 billion.¹ Organovo shares are quite volatile (volatility is a statistical financial measure of the dispersion

¹For a regular IPO, (initial public offering, the offering of a company's shares to the public for the first time to raise capital) the financial advisers/investment banking firms hired by the company guide it through the process, assist in determining the offering price, the type and the amount of securities to be issued, the proper timing of the IPO, and help draw the markets' interest to the offering. Despite all of the obvious benefits, the process is lengthy, complex, and quite costly. Meanwhile, a reverse IPO, a.k.a. reverse merger or reverse takeover, is a much simpler, speedier, and less expensive way for a private company to go public through buying a majority of the shares of a publicly traded shell company (normally, this shell company is in bad financial shape, dormant or fully defunct, while still maintaining its listing on a stock exchange) and merging it with their private company. The combined company keeps the public status (listing on a stock exchange) of the original shell company, while its business and assets are essentially those of the former private company. Obviously, unlike the case of a conventional IPO, the company using a reverse IPO does not immediately raise capital through this process, but rather changes its status to become public, thus allowing it the access to public capital markets through subsequent offerings, providing liquidity, etc. Some critics argue, however, that a reverse IPO has an important downside and should be considered a somewhat inferior alternative to a regular IPO – it misses substantial strategic guidance from experienced financial advisers and lacks a certain “stamp of approval” from the investment community. This may lead to the company's shares not being properly valued, add downward pressure on the valuation, and add to the stock's volatility.

of prices for a stock). We believe that, among other things, this is due to the lack of any adequate comparables on the market, i.e., any other similar public companies from the same industry. Accordingly, to a certain extent, the stock fluctuates both with other biotech companies' stock and with those of 3D printing companies (such as 3D Systems and Stratasys).

On November 3, 2016, Cellink AB, a Swedish-American bioink company founded in January of the same year, began trading on Nasdaq First North in Stockholm. Its IPO raised SEK 23 million (approximately \$2.5 million as of the date of the offering), valuing the company at SEK 152 million (approx. \$16.8 million) (Vilhelm Carlström 2016). Despite the limited size of the offering and its trading on an exchange which is not considered one of the main global markets, this, again, is a significant milestone for the company and the industry.

In February of 2015, Cyfuse Biomedical K.K., the Japanese manufacturer of Regenova 3D bioprinters, closed its Series B private placement funding raising 1.4 billion yen (approx. \$12.5 million). That brought the total amount of capital invested in the company to 1.98 billion yen (approx. \$17.8 million).

The limited number of initial public offerings of 3D bioprinting companies' stock to date, in our view, is attributable to the industry not yet reaching the necessary maturity, and the technology not reaching a broad market adoption. It probably also reflects the generally observed recent trend of "the dearth of initial public offerings" in favor of other paths to raise capital (Steven Davidoff Solomon 2017). In the near future, we could expect the start of industry consolidation through mergers and acquisitions of smaller start-ups by strategic buyers, as industry insiders are able to better appreciate potential business and technology synergies as well as the value of target companies than the broader capital markets. This would also reflect a general trend, especially in the biotech industry, of a visible increase in M&A activity.

6 Porter's Analysis of 3D Bioprinting Industry Development

It appears useful from a methodological viewpoint to apply Porter's Five Forces Model to the bioprinting industry. Porter's Five Forces Model is a method used for analyzing industry sectors and formulating business strategies. The method was developed by Michael Porter at the Harvard Business School in 1979 (Porter 1979).

Porter's Five Forces include:

- Threat of substitutes
- Threat of new entrants
- Bargaining power of suppliers
- Bargaining power of buyers
- Industry rivalry

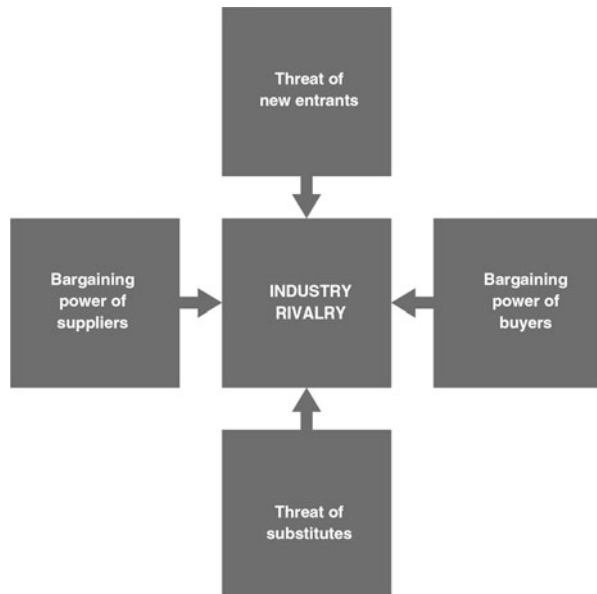
According to Porter, in order to determine a company's place in its industrial sector, the Five Forces Analysis should be performed on a microeconomic level. The

method is not designed to be applied to several industrial sectors at a time, or to any part of one industrial sector. A monoline company should perform at least one Porter's Five Forces Analysis for its line of business. For diversified companies, the fundamental point of corporate strategy is the choice of business lines in which the company will compete, according to Porter. A separate, industry-specific Five Forces Analysis should be performed for each business direction. A change in any of the five forces usually means the company should reconsider its place in the sector and the market. A sufficiently attractive sector does not mean all companies belonging to it will make equal profit. Companies should seek to use their key strengths, business models, or sale networks in a way that makes their profits higher than the industrial average. A good example is air passenger transportation. Though the business is characterized by a rather low profit margin, some companies manage to harvest higher profits thanks to unique business models (Fig. 6).

If we apply Porter's model to 3D bioprinting technology, it will look as follows (Fig. 7):

1. Threat of substitutes comes, in our opinion, from the appearance of techniques to "repair" organs or tissues using gene-editing methods, such as CRISPR/Cas9, without the need to grow organ or tissue constructs. Recovery is achieved through organism stimulation.
2. Threat of new entrants is most likely the threat of large companies specializing in 3D printer manufacturing, such as 3D Systems, Stratasys, or Hewlett-Packard, or major software developers like Autodesk or Microsoft taking up the business of biofabrication. Given their mighty R&D centers and abilities with additive technologies, these companies may combine bioprinter fabrication with

Fig. 6 Porter's Five Forces Model



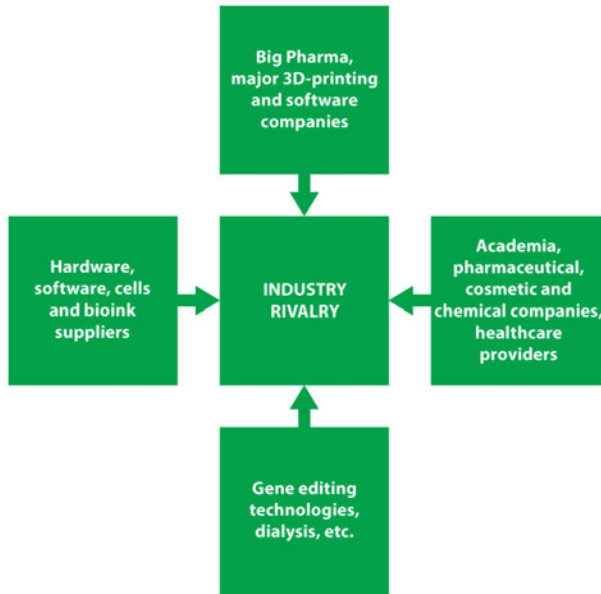


Fig. 7 Porter's Five Forces Model as it applies to the bioprinting industry

providing bioprinting services. Another potential threat is the possibility of pharmaceutical companies deciding to perform drug tests in house without inviting third party contractors.

3. Bargaining power of suppliers of hardware, software, and scaffold materials is, in our opinion, not very strong. The same cannot be said about suppliers of cell material. Therefore, a likely trend is the further strengthening of cooperation ties between such companies as Nano Dimension and Accelta, or Cyfuse Biomedical and Cell Applications (as noted above). Organovo has demonstrated an alternative approach. It receives cell material from its subsidiary, Samsara, i.e., the problem is resolved in house by setting up specialized business units. An example of cooperation in the field of hardware and software is Zhuhai CTC Electronic Co., Ltd. (CTC), a Chinese manufacturer of 3D printers, and South Korean company, ROKIT, in a project of joint development of a new generation bioprinter based on laser stereolithography (SLA) technology, which will use CTC Electronic's RiverOS.
4. Bargaining power of customers appears to be fairly strong today. As noted above, the main customers of 3D bioprinting technology are research institutions, pharmacological and chemical companies, military departments and, in the long run, hospitals. As things stand, customers demand customized approaches to bioprinter development, fabrication of materials, and performance of tests, depending on their specific interests. In other words, products and services have to be strongly client-specific, which is inconvenient for manufacturers as it

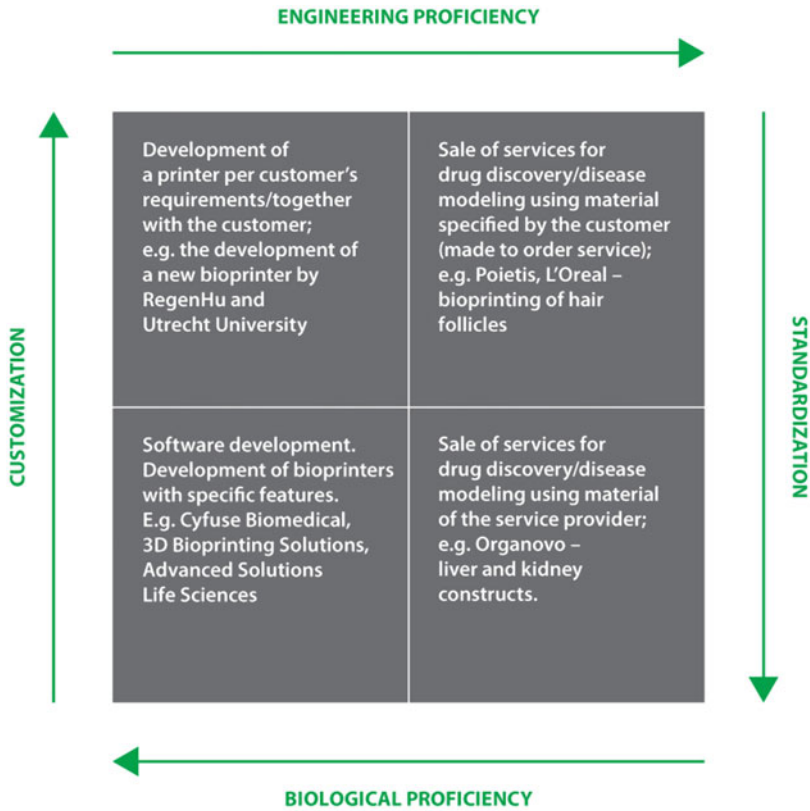


Fig. 8 The interplay of products/services and required proficiencies

obstructs standardization and the economy of scale, making it impossible to achieve any drastic reductions in production costs.

5. Industry rivalry. At this stage of technology development, industry rivalry is not a problem. Moreover, industry participants (commercial companies and research institutions) prefer joining efforts to competition in order to expedite the achievement of sufficient maturity for commercial application (Fig. 8).

7 Conclusion

First research reports on 3D bioprinting technology appeared in the early 2000s. Experiments were performed on bioprinters assembled at laboratories. During the several years that followed, bioprinters, as well as services based on 3D bioprinting technology, became commercially available.

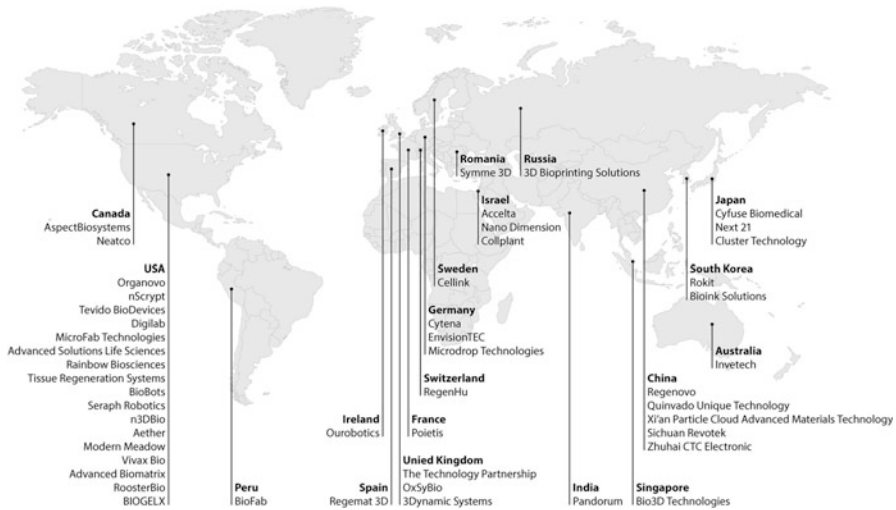


Fig. 9 The geography of 3D bioprinting industry

As things stand today, biofabrication is a rapidly developing industry with fantastic potential, and it has already entered the commercial application phase. In addition to the growing number of companies entering the industry and the number of countries they represent, we are witnessing the process of segmentation, i.e., the appearance of companies specializing in specific kinds of products or services, which is also indicative of the industry's overall progress (Fig. 9).

Of course, 3D bioprinting industry still has a way to go to reach the plateau of productivity, i.e., become mature enough to be perceived by the public with full awareness of its advantages and limitations. Naturally, the most important challenges the industry is facing lie in the realm of the scientific progress: Advances in vascularization and nerve regeneration are two examples. However, these problems are beyond the scope of this chapter, where we focus on the industrial and commercial side of 3D bioprinting. As we see it, 3D bioprinting technology needs standardization for bioprinting methods, software, and materials. Lack of standardization is a natural development problem. Eventually, the best competitive approaches (in terms of both technology and economy) will become industry standards. The main condition for 3D bioprinting companies to become profitable is the market's adoption of the technology (products and services) as the solution for its needs (for example, testing pharmaceutical characteristics of drugs being developed).

Consolidation (mergers and partnering relations between market participants) and establishment of legal regulation are definitely positive and beneficial developments for the industry. The examples of successful capital attraction point to the existence of investor interest in the technology. However, real financial success for 3D bioprinting will come when 3D organ constructs enter clinical use, i.e., when the technology starts helping millions of people suffering from organ dysfunction. Our common objective is to make this time arrive sooner.

References

- American Kidney Fund (2015) <http://www.kidneyfund.org/assets/pdf/kidney-disease-statistics.pdf>
- Antoni D, Burckel H, Josset E, Noel G (2015) Three-dimensional cell culture: a breakthrough in vivo. *Int. J. Mol. Sci.* 16(3):5517–5527
- Carlström V (2016). <http://nordic.businessinsider.com/from-idea-to-nasdaq-in-less-than-a-year—cellink-is-swedens-newest-international-success-2016-11/>
- European Commission (2013) https://ec.europa.eu/growth/sectors/cosmetics/animal-testing_en
- European Renal Association – European Dialysis and Transplant Association (2016) http://eraedta.org/press/160104_CKD_Prevalance_Press.pdf
- European Renal Care Providers Association (2015) <http://ercpa.eu/wp-content/uploads/2015/09/Infograph-final-version-updated.pdf>
- Fan J (2014) <http://www.newyorker.com/news/news-desk/can-china-stop-organ-trafficking>
- Hall N (2016) <http://3dprintingindustry.com/news/nike-powers-olympic-champion-3d-printing-91474/>
- Hornick JF, Rajan K (2016) <https://3dprintingindustry.com/news/3d-bioprinting-patent-landscape-takes-shape-ip-leaders-emerge-84541/>
- Huang G-S, Tseng C-S, Linju YB, Dai L-G, Hsu S-H (2013) Solid freeform-fabricated scaffolds designed to carry multicellular mesenchymal stem cell spheroids. *European cells and materials* 26:179–194
- Institute of Health and Biomedical Innovation (2017). <https://www.qut.edu.au/institute-of-health-and-biomedical-innovation/facilities/herston-biofabrication-institute>
- Itoh M, Nakayama K, Morita S (2015) Bio-3D printer undergo Remodeling and endothelialization when implanted in rat aortae. *PLoS One* 10:1–15
- Knowlton S, Onal S, Yu CH, Zhao JJ, Tasoglu S (2015) Bioprinting for cancer research. *Trends Biotechnol* 33(9):504–513
- Kuo C-Y, Eranki A, Placone JK, Rhodes KR, Aranda-Espinoza H, Fernandes R, Fisher JP, Kim PCW (2016) Development of a 3D printed, bioengineered placenta model to evaluate the role of trophoblast migration in preeclampsia. *ACS Biomater Sci Eng* 2(10):1817–1826
- Mironov V, Boland T, Trusk T, Forgacs G, Markwald RR (2003) Organ printing: computer-aided jet-based 3D tissue engineering. *Trends Biotechnol* 21(4):57–61
- Mironov V, Visconti RP, Kasyanov V, Forgacs G, Drake CJ, Markwald RR (2009) Organ printing: tissue spheroids as building blocks. *Biomaterials* 30(12):2164–2174
- Moldovan NI, Hibino N, Nakayama K (2017) Principles of the Kenzan method for robotic cell spheroid-based three-dimensional bioprinting. *Tissue Eng Part B Rev* 23:237–244
- Murphy SV, Atala A (2014) 3D bioprinting of tissues and organs. *Nat Biotechnol* 32(8):773–785
- National Kidney Foundation (2016) <https://www.kidney.org/news/newsroom/factsheets/Organ-Donation-and-Transplantation-Stats>
- Nguyen DG, Funk J, Robbins JB, Crogan-Grundy C, Presnell SC, Singer T, Roth AB (2016) Bioprinted 3D primary liver tissues allow assessment of organ-level response to clinical drug induced toxicity in vitro. *PLoS One* 11(7):e0158674
- Ozbolat IT, Peng W, Ozbolat V (2016) Application areas of 3D bioprinting. *Drug Discov Today* 21(8):1257–1271
- Porter ME (1979) How Competitive Forces Shape Strategy. *Harvard Business Review*. <https://hbr.org/1979/03/how-competitive-forces-shape-strategy>
- Sher D (2015). The Top 15 Bioprinters. <https://3dprintingindustry.com/news/top-10-bioprinters-55699/>
- Skardal A, Atala A (2015) Biomaterials for integration with 3-D bioprinting. *Ann Biomed Eng* 43(3):730–746
- Solomon SD (2017) <https://www.nytimes.com/2017/03/28/business/dealbook/fewer-ipos-regulation-stock-market.html>
- Spanish Ministry of Health (2016) <http://www.ont.es/Documents/PresentaciónDatos2016-17.pdf>
- Thornton PK (2010) Livestock production: recent trends, future prospects. *Philos Trans R Soc Lond Ser B Biol Sci* 365(1554):2853–2867
- Wake Forest Institute for Regenerative Medicine (2016) <http://www.wakehealth.edu/Research/WFIRM/Research/Military-Applications/Printing-Skin-Cells-On-Burn-Wounds.htm>



Commercial 3D Bioprinters

Frederico David A. S. Pereira, Vladislav Parfenov, Yusef D. Khesuani, Aleksandr Ovsianikov, and Vladimir Mironov

Contents

1	Introduction	536
2	Definition of 3D Bioprinters	536
3	Anatomy of 3D Bioprinters	538
4	Classification of 3D Bioprinters	539
5	Ink-Jet 3D Bioprinters	540
6	Extrusion-Based 3D Bioprinters	540
7	Laser-Based Bioprinters	542
8	Organ Biofabrication Line	543
9	In Situ Bioprinters and Biofabricators	545
10	Emerging Trends in the Design and Functionalities of Commercial 3D Bioprinters	545
11	Challenges and Future Perspectives	546
	References	547

F. D. A. S. Pereira · V. Parfenov
The Laboratory of Biotechnological Research, 3D Bioprinting Solutions, Moscow, Russia
e-mail: freddasp@gmail.com; vapar@mail.ru

Y. D. Khesuani
Vivax Bio, LLC, New York, NY, USA

The Laboratory of Biotechnological Research, 3D Bioprinting Solutions, Moscow, Russian Federation

A. Ovsianikov
Institute of Materials Science and Technology, Technische Universität Wien (TU Wien), Vienna, Austria
e-mail: Aleksandr.Ovsianikov@tuwien.ac.at

V. Mironov (✉)
3D Bioprinting Solutions (3D Bio), The Laboratory of Biotechnological Research, Moscow, Russia
Institute for Regenerative Medicine, Sechenov Medical University, Moscow, Russia
e-mail: vladimir.mironov54@gmail.com

Abstract

The bioprinters are robotic devices, which enable 3D bioprinting. In this chapter, we provide classification of already existing commercially available 3D bioprinters and outline basic principles of their construction and functionalities. The emerging trends in the design and development of 3D bioprinters, perspectives of creation of new types of commercial 3D bioprinters based on new physical principles, including in situ bioprinters, as well as completely integrated organ biofabrication lines or “human organ factories” will be also discussed.

1 Introduction

Bioprinting is a rapidly emerging and very promising biomedical field. Availability of commercial 3D bioprinters is one of the main enabling factors for rapidly spreading the principles of 3D bioprinting among industrial and academic R&D groups. According to our best knowledge, the first commercial 3D bioprinter has been developed in Germany with strong tradition in precision engineering and well-developed rapid prototyping/additive manufacturing industry at Freiburg University at Prof. Ralf Mulhaupt’s group, and it has been successfully commercialized later (<https://envisiontec.com>). The problem with first generation of commercial 3D bioprinters was that they were extremely expensive. Second generation of bioprinting companies identified the strong demand in the reasonably priced affordable 3D bioprinters and explored this market niche. The number of companies producing commercial 3D bioprinters continues to grow (Table 1). The right choice of commercial available 3D bioprinters requires certain systematization, which includes definition and classification of three bioprinters, description of principles of their work, and functionalities as well as understanding of emerging trends in their design and reminding limitations, challenges, and perspectives which we will address here.

2 Definition of 3D Bioprinters

One possible definition of a 3D bioprinter is an automated device for robotic additive biofabrication of 3D functional tissue and organs based on digital models. This definition implies following criteria for such devices. First, it must be automated and robotic device. In this context, manually controlled biomaterials, cells, or minitissues dispensing and/or cell spraying do not fit to definition. Second, it must be able to produce not just 2D cell patterning but rather 3D tissue and organ constructs. Third, it must enable bioprinting both biomaterials (printable bioinks) and living cells or minitissues. Thus, certain robotic devices, for example, 3D printer based on so-called fused deposition modeling or melt electrospinning,

Table 1 List of leading bioprinting companies producing commercial bioprinters (<https://3dprintingindustry.com/news/top-10-bioprinters-55699/>)

1.	EnvisionTech (Germany) https://envisiontec.com
2.	RegenHu (Switzerland) https://www.regenhu.com
3.	Poetis (France) http://poetis.com
4.	Organovo (USA) http://organovo.com
5.	Sciperio/nScript (USA) http://www.sciperio.com
6.	Cellink (Sweden/USA) https://cellink.com
7.	Allevi (formerly BioBots) (USA) https://biobots.io
8.	TeVido BioDevices (USA) http://tevidobiodevices.com
9.	3Dynamics systems (USA) http://www.bioprintingsystems.com
10.	Aspect BioSystems (Canada) https://www.aspectbiosystems.com
11.	Rokit (South Korea) http://en.3disonprinter.com
12.	3D Bioprinting solutions (Russia) http://www.bioprinting.ru
14.	Cyfuse Biomedics (Japan) https://www.cyfusebio.com/en/
15.	Rikoh (Japan) (https://www.rioh.com)
16.	Regenovo (China) http://regenovo.com/english/
17.	SunP biotech international (China/USA) http://sunpbiochem.com/about-us-2/

After discussion and consultations with several companies producing commercial bioprinters, we decided not to indicate prices of 3D bioprinters because they are subjects of changes based on market demand and constant 3D bioprinters upgrading. Thus, for updated bioprinters pricing information, we direct readers to correspondent companies' websites

which can print cell-free scaffolds and are not able to print or dispense living cells should not be considered as 3D bioprinters. Finally, bioprinting process is based on using digital models. Manually controlled dispensing, pipetting, or spraying even using hydrogel containing living cells without employment digital model (usually in STL file) does not exactly fit to our definition. Moreover, as it will be shown later, there are new 3D biofabrication methods based on using novel physical principles which do not fit to the above definition. It does not mean that these methods have disadvantages, but merely that the main focus of this chapter is on commercial 3D bioprinters as we have defined them. There are many different types of bioprinting devices, and popular hybridization of technological approaches constantly creates new types of devices, which could be eventually commercialized. For the sake of focus, we limit our scope only to consideration devices, which are already implemented and commercially available or at least under development. There are several textbooks on bioprinting (Lee et al. 2015; Ringeisen et al. 2010; Zhang et al. 2015; Atala and Yoo 2015; Chua and Yeong 2015; Ozbolat 2016) as well as excellent reviews (Mironov et al. 2009a; Derby 2012; Murphy and Atala 2014; Mandrycky et al. 2016; Mironov et al. 2008; Mironov et al. 2003; Mironov et al. 2009b; Melchels et al. 2012) where readers will be able to find all necessary information about the most recent developments in this sector. Finally, we also do not review in this chapter related patents which readers could find elsewhere.

3 Anatomy of 3D Bioprinters

Beside obvious diversity of commercially available 3D bioprinters, they also have certain commonly shared general characteristics. It is logical to describe these common characteristics before we will start to characterize specific types of commercial devices. In order to describe main components of typical or conventional 3D bioprinter, we will use anatomy-like approach (Fig. 1). The typical 3D bioprinter includes at least five main structural functional components: (i) X-Y-Z axis robotic positioning system or usually Cartesian-type robot although there are already devices with articulated type of robots; (ii) nozzle or dispenser or extrusion mechanism, usually automated syringes; (iii) operational or controlling device usually, including a PC with according operation software; (iv) collector for placing of bioprinted tissue and organ constructs (the simplest option is a standard Petri dish); and (v) finally, for sterility purposes bioprinting devices must either have their own sterile cabinet or at least be placed into sterile cell culture hood or laminar.

The sizes of bioprinting devices are different, but again the limiting factors are functional specifications related to desirable bioprinted tissue or organ construct size (Fig. 2). The shape and size of specific device is also a function of the selected form of robot. The number of nozzles is also dictated by functional specifications. Some commercial 3D bioprinters claim to have as many as 10 nozzles. Number of nozzles could be optimized by using pick and place mechanism or revolver-like mechanism. The evolving standard is a commercial 3D bioprinter with minimum two nozzles: one for printing solid scaffold using fused deposition modeling and another for bioprinting of hydrogel loaded with living cells. However, increasing the number of nozzles is a well-established trend. There are not yet standard software and control systems. Finally, there are no certified commercial bioprinting devices approved for clinical application yet. Moreover, correspondent FDA regulations are practically absent.

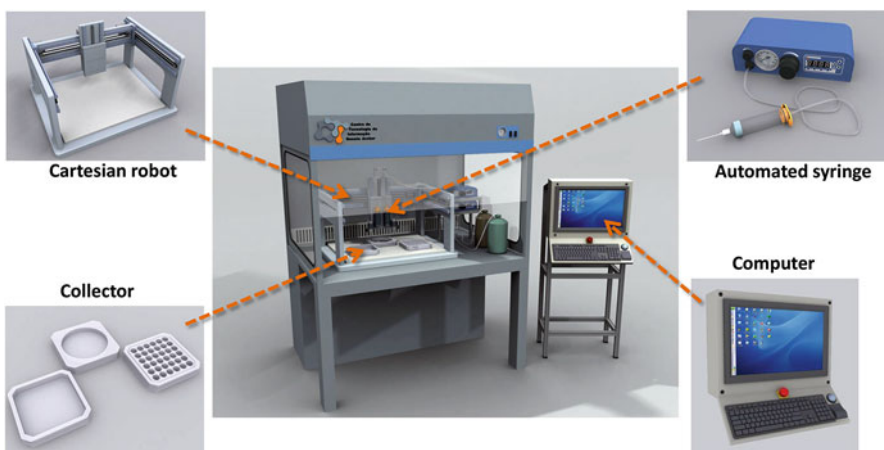


Fig. 1 Anatomy of 3D bioprinter (scheme)

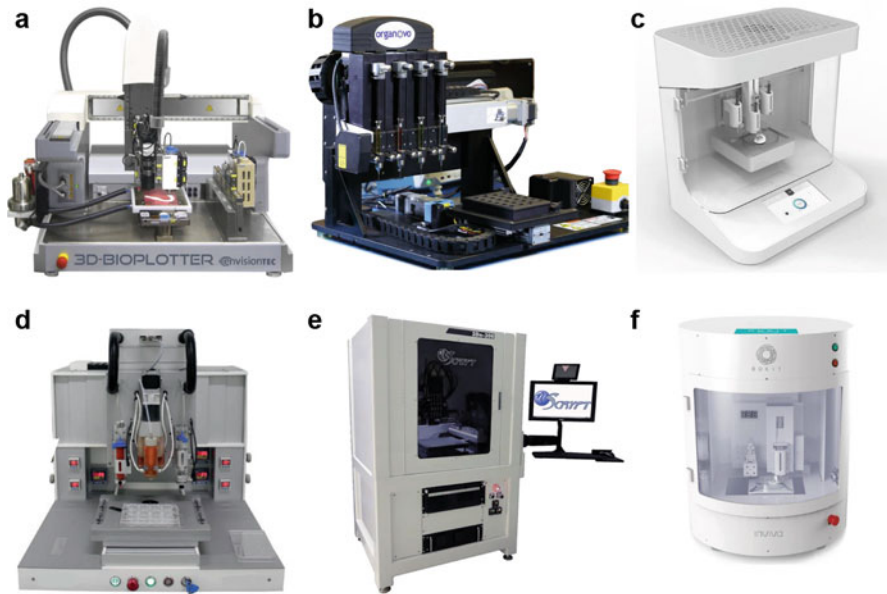


Fig. 2 Extrusion-based commercial 3D bioprinters (photo). (a) EnvisionteC (Germany). (b) Organovo (USA). (c) Cellink (Sweden/USA). (d) RegenHu (Switzerland). (e) Sciperio/nScript (USA). (f) RokiT (South Korea)

4 Classification of 3D Bioprinters

The classification is a logical part of systematization of any types of knowledge. It is already generally accepted classification of 3D bioprinters on three main groups: (i) ink-jet bioprinters, (ii) extrusion-based bioprinters, and (iii) laser-based bioprinters (Melchels et al. 2012). Some authors and especially industry reports often include an additional group of so-called magnetic bioprinting technology developed and commercialized by USA company **n3D Biosciences, USA** (<http://www.n3dbio.com/products/magnetic-levitation/>). However, devices which are working without digital model do not fit our definition of bioprinters.

Although magnetic (Durmus et al. 2015; Tasoglu et al. 2015; Tocchio et al. 2018) and acoustic levitations (Bouyer et al. 2016) as well as dielectrophoresis (Albrecht et al. 2004; Lin et al. 2006) and using electric field have enormous potential for development of new types of 3D bioprinters or more correctly say 3D biofabricators or 3D assemblers, according our best knowledge there is no published evidence for any attempts of commercialization of these very perspective biofabrication technologies yet. The potential advantage of these technologies is using magnetic, acoustic, and electric fields as some sort of temporal and removable support which we (using obvious analogy with scaffold which is usually defined as a temporal and removable or biodegradable support) suggest to call **scaffolds-based bioassembly**.

3D Bioprinting Solutions (Russia) is now developing a first commercial variant of magnetic and acoustic bioprinting devices based on the principles of diamagnetic and acoustic levitational bioassembly. However, for using nontoxic concentration of paramagnetic salts (such as gadolinium salts) which are enabling diamagnetic levitation, it is necessary either to use very expensive supermagnets (30 Tesla) on the Earth or to perform magnetic levitation in the condition of microgravity in Space at The International Space Station, which is also very expensive.

Although they often employ digital models, it would be more logical to call such new evolving types of devices **3D bioassemblers**.

5 Ink-Jet 3D Bioprinters

The first ink-jet bioprinter has been developed by Thomas Boland at **Clemson University** (USA) using modified standard **Hewlett-Packard** 2D ink-jet printer (Wilson Jr and Boland 2003) and related patent belongs to company **Organovo** (USA). However, according our best knowledge until now there were no indications of commercialization and developing production of ink-jet 3D bioprinters by this company. An early attempt to develop a multinozzle ink-jet cell printer has also been reported in California, USA, at the famous **Xerox Institute**, but again they chose not to commercialize technology due to the absence of obvious market at that time. Similarly, Japanese company **Canon** tried to develop an ink-jet bioprinters, but decided to focus their attention of using ink-jet technology for 2D protein and cell patterning. The main technological impediment for development of commercial ink-jet technology was transition from 2D to 3D printing. Although world leaders in the development of ink-jet bioprinting technology such as Thomas Boland (USA), Brain Derby (UK), and Makoto Nakamura (Japan) (Boland et al. 2006; Arai et al. 2011; Saunders et al. 2008) made great efforts in the advancing this technology, they were not able to move it to the market with commercial product. However, there are some good news. Thomas Boland recently co-founded a new startup 3D bioprinting company **TeVido Biodevices** (<http://tevidobiodevices.com>) in Texas (USA), and it is logical to expect the development of commercial ink-jet bioprinter by this company in the nearest future. Even more interesting and exciting developments are ongoing now in Japan. At recent biofabrication meeting in Austria, representative of printing company **Ricoh (Japan)** (<https://www.ricoh.com>) for first time reported publicly about the development of a new modified ink-jet 3D bioprinting technology and its potential commercialization. The great advantage of presented technology is that they elegantly solved the problem of transition from 2D to 3D ink-jet bioprinting using as printable biomaterials gelatin microbeads. Cheap commercially available ink-jet 3D bioprinters are highly desirable.

6 Extrusion-Based 3D Bioprinters

The extrusion-based bioprinters are most popular versions of 3D bioprinters. A publication by Robert Klebe from the University of Texas in San Antonio (Texas, USA) about so-called **cytoscribing** published in 1988 is often mistakenly considered

as a first pioneering publication about 3D bioprinting technology (Klebe 1988). Robert Klebe is also a holder of first patent about extrusion-type 3D bioprinter named **apparatus for the precise positioning of cells** (Klebe 1987). However, the careful reading of his publication indicates, beside the title of his paper, that he used printing of proteins for 2D cell patterning and never actually bioprint living cells or 3D tissues. Moreover, what is most important in the context of this chapter that his cytoscribing technology has never been commercialized.

The adaptation of fused deposition modeling for 3D printing of at first biodegradable tissue engineered scaffold and later hydrogel was the next important step and simultaneously developed by Dietmar Hutmacher's group in National University of Singapore (Singapore) (Zein et al. 2002), Anthony Mikos's group in Rice University in Texas (USA) (Cooke et al. 2003), and Ralf Mulhaupt's group in University of Freiburg (Germany) (Landers et al. 2002). However, only the German group was able to successfully commercialize their **bioplotter** technology through German company **Envisiontec** (<https://envisiontec.com>). Envisiontec 3D bioplotter became a first commercial 3D bioprinter. Modified fused deposition modeling technology for fabrication of solid biodegradable scaffold was not truly bioprinting technology because cell was seeded on printed scaffold later not by robotic bioprinter but simply manually. Hydrogel-based extrusion type bioprinter could not provide desirable initial high cell density, and material properties of construct were also inferior.

The next main advance developed initially by Jos Malda's group in Utrecht University (The Netherlands) (Schuurman et al. 2011) and later by Antony Atala's group in Wake Forest University in NC, USA (Kang et al. 2016), was based on using hybrid approach or combination of fused deposition modeling of solid biodegradable scaffold with simultaneous bioprinting of hydrogel loaded with living cells. This technology has been successfully commercialized and became a standard for the most advanced extrusion-type commercial 3D bioprinters.

The low initial cell density forced some researchers to think about possible alternatives to extrusion bioprinting based on using original concept of **organ printing** introduced by Vladimir Mironov et al. in 2003, using tissue spheroids as building blocks (Mironov et al. 2009c). According our best knowledge at least several groups and companies tried to develop bioprinting technology based on using tissue spheroid as building blocks. **Organovo** (USA) which holds the original patent on this technology developed jointly by Gabor Forgacs's group at University of Missouri (Columbia, USA) and Vladimir Mironov's group at The Medical University of South Carolina (Charleston, USA) failed to develop a reproducible tissue spheroid-based biotechnology because tissue spheroids usually fused before they have a chance to be dispensed. Thus, Gabor Forgacs's group and Organovo later switched to development of rod-like continuous dispensing (Owens et al. 2013).

The company **Cyfuse Biomedical** (Japan) (<https://www.cyfusebio.com/en/>) introduced and successfully commercialized a novel scaffold-free "**Kenzan**" platform technology based on an array of surgical needles for robotic assembly of tissue spheroids using robotic pick and place device according to predesigned digital model (Yanagi et al. 2017). Finally, at least three groups including Timothy Woodfield group at University of Otago (New Zealand) (Mekhileri et al. 2017),

Stefan Zimmermann and Peter Koltay group at University of Freiburg (Germany) (Gutzweiler et al. 2017), and Vladimir Mironov group in the company **3D bioprinting Solutions** (Russia) (Bulanova et al. 2017) tried to develop extrusion type 3D bioprinters capable to dispensing one spheroid a time using built-in microfluidic device (Fig. 3). Two latter groups are on their way to commercialization of this advanced type of extrusion 3D bioprinters which in combination with previously already achieved functionalities could become a *new industrial standard* with three different functionalities: 3D printing of solid biodegradable scaffold, 3D bioprinting of living cells loaded hydrogel, and 3D bioprinting of tissue spheroids.

7 Laser-Based Bioprinters

Among the most commercially ripe methods is laser-induced forward transfer (LIFT), also referred to as biological laser printing. We refer the readers to the chapter “Laser-Based Cell Printing” of this book for detailed introduction and overview of the current state of the art of this method. One of the main advantages of LIFT is its relatively high bioprinting resolution (down to several picoliters and one cell per drop) and the fact that it is a nozzle-free technology, avoiding shear-forces potentially damaging to cells. The printing resolution of LIFT depends on several factors, which include laser pulse energy, repetition rate, thickness of the bioprintable material layer and its viscosity, the distance between donor and collector substrates, and the substrate wettability. This technology was in fact successfully commercialized by a French company **Poetis** founded by Fabien Guillemot (<http://www.poetis.com>). However, **Poetis** decided do not sell their

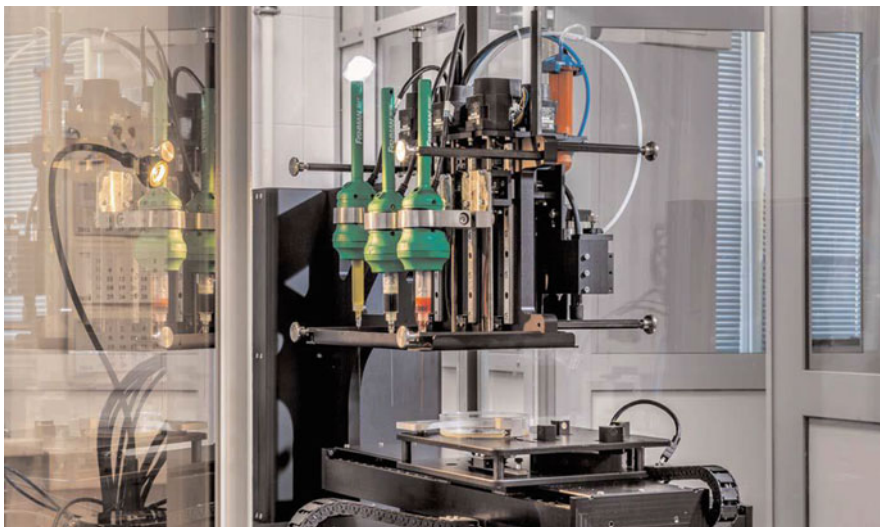


Fig. 3 Commercial 3D bioprinter Fabion (photo according to 3D Bioprinting Solutions)

bioprinters because their business model is based on providing bioprinting service such as bioprinting of human skin to the large cosmetic, chemical, and pharmacological companies (see Chapter “Emerging Business Models Toward Commercialization of Bioprinting Technology” of this book).

In 1999 David Odde from University of Minnesota (USA) introduced a laser-assisted bioprinting method using optical cell strapping (Odde and Renn 1999). This laser-guided direct writing approach was demonstrated to be capable of producing 2D cell patterns. However, the subsequent attempts to adapt it for 3D bioprinting practically failed, and to the best of our best knowledge this technology has been never commercialized.

Stereolithography (SLA) was also shown to produce complex 3D constructs from photopolymerizable materials containing living cells (Chan et al. 2010). This photopatterning technique can be adapted to process multiple material types and potentially offers spatial resolution superior to extrusion-based methods. Digital light processing (DLP) is another lithography-based technique, which can be conveniently adapted to live cell patterning (Ma et al. 2016). Despite the fact that SLA and DLP are among of the most advanced technologies very widespread throughout industrial 3D printing market, their use for 3D bioprinting has not been commercialized so far. A combination of optical trapping and stereolithography for cell patterning has also been reported in the literature (Linnenberger et al. 2013).

Multiphoton processing, often referred to as two-photon polymerization (2PP) or multiphoton-excited microfabrication, is a lithography-based technique providing even higher spatial resolution down to subcellular level (Ovsianikov et al. 2012). The group of Paul Campagnola demonstrated already in 2005 that this method can be used for cross-linking of cytoplasmic proteins in live cells (Basu et al. 2005). Interestingly, among the main bottlenecks for developing 2PP towards biofabrication is again its high spatial resolution, resulting in long processing times when it comes to the 3D constructs of tissue-relevant size. The need to substantially increase the throughput of this method for bioprinting necessitates the development of novel biomaterials and highly efficient photoinitiators (Qin et al. 2014). A recent report has demonstrated that macromolecular photoinitiators, designed to exhibit large two-photon absorption cross-sections, can be used for efficient 2PP in the presence of cells (Tromayer et al. 2017). Despite the fact that several companies sell 2PP-based devices, none of them is currently suitable for bioprinting.

8 Organ Biofabrication Line

Several years ago Mironov et al. published a short review (Mironov et al. 2011) arguing that the use of 3D bioprinters alone will not be enough for biofabrication of human organs. The proposed concept of so-called *organ biofabrication line* (or organ factory) implies that beside the obvious need of employment of 3D bioprinters in organ printing technology the whole organ biofabrication line must be developed, implemented, and commercialized. The ideal organ biofabrication line must be automated and robotized (Fig. 4). It must include devices for all steps of organ biofabrication including:



Fig. 4 Organ biofabrication line (scheme)

(i) preprocessing using clinical cell sorting, stem cells propagation in special bioreactor, and tissue spheroids biofabrication using robotic biofabricators; (ii) processing or actual printing using 3D bioprinters; and (iii) postprocessing using perfusion bioreactor with nondestructive and noninvasive biomonitoring.

In 2011 this concept indeed looked a little bit futuristic and even close to domain of science fiction rather than to profit-oriented pragmatic and realistic commercialization. Now it is possible to state that practically all components of this proposed integrated organ biofabrication line are commercially available. Moreover, according to **Rokit** (South Korea) a similar concept of integrated tissue and organ factory is currently under commercial development. It is safe to predict now that similar approach will be explored by other European and USA companies. It is interesting that in this context there is a room for potentially very interesting and potentially very profitable emerging business model when one intermediate service company will collect and integrate all necessary for 3D tissue and organ biofabrication devices developed by other companies into one integrated and automated organ biofabrication line and will sell it including necessary service as one package at a very good price to all hospitals and clinics interested in well-equipped intrahospital GMP facilities for regenerative medicine, biofabrication, and 3D bioprinting.

9 In Situ Bioprinters and Biofabricators

Surgery of twenty-first century ideally must be minimally invasive, cost-effective, and increasingly biology-based or, at least, biology-inspired. The stunning clinical and commercial success of robotic surgery with using a sophisticated semi-robotic device such as a legendary **Da Vinci Surgical Systems** (Intuitive Surgery, USA <https://www.intuitivesurgical.com>) strongly suggests the possibility of combining surgical robotics with 3D bioprinting technologies. There are already several commercial medical devices for in situ biofabrication using simultaneous cells and hydrogel spraying **Duplo-jet** (**Baxter**, Austria), **Vivostat** (**Vivostat**, Denmark), and **Skingun** (**Renovacare**, USA). Specialists from **Regenerative Medicine Institute** in Pittsburg (USA) have developed **CellGun**. Australian scientists and engineers are very close to starting commercialization of their device for extrusion hydrogel loaded with living cells so-called **BioPen** (O'Connell et al. 2016). **Duplojet** loaded with fibrin hydrogel containing living cells have been used for tissue engineering by German surgeons (Klopsch et al. 2015). However, all these devices even commercially available do not fit to definition of 3D bioprinting because they are basically manually controlled and do not use digital models. The concept of truly in situ 3D bioprinters has been explored initially by Antony Atala's group in USA (Tarassoli et al. 2017) and by Paulo Bartolo's group in UK (Pereira et al. 2013). According our best knowledge, these attempts do not yet lead to commercial development of 3D bioprinters. Brazilian scientists at **Renato Archer Center for information Technology** in Campinas, Brazil, together with first and last authors of this paper developed a conceptual mocked model of 3D bioprinter using Swiss articulated robot. Finally, Russian company **3D Bioprinting Solutions** (Moscow, Russia) together with Russian experts in robotics and computer science has developed working model of in situ 3D bioprinter using commercial articulated robots (**Kuka**, Germany and **Fanuc**, Japan), USA automated syringe (**Fishman**, USA), and Russian software and already successfully tested its functionality on phantom oral cavity (Fig. 5). Next logical step is a commercialization of in situ bioprinting technology.

10 Emerging Trends in the Design and Functionalities of Commercial 3D Bioprinters

The fact that there are already several dozens of 3D bioprinting companies around the world already producing commercially available 3D bioprinters is a direct manifestation and objective evidence that we are facing the emerging and rapid development of new very perspective bioengineering industry. Thus, all these conversations about bioprinting as some sort of *science fiction* and statement that bioprinting technology is still in infancy are in essence nothing more than a subjective opinion which is probably based either on insufficient knowledge or on limited access to objective information. We hope that this review provides at least some objective documented evidence against this still persisting view. Instead of dealing

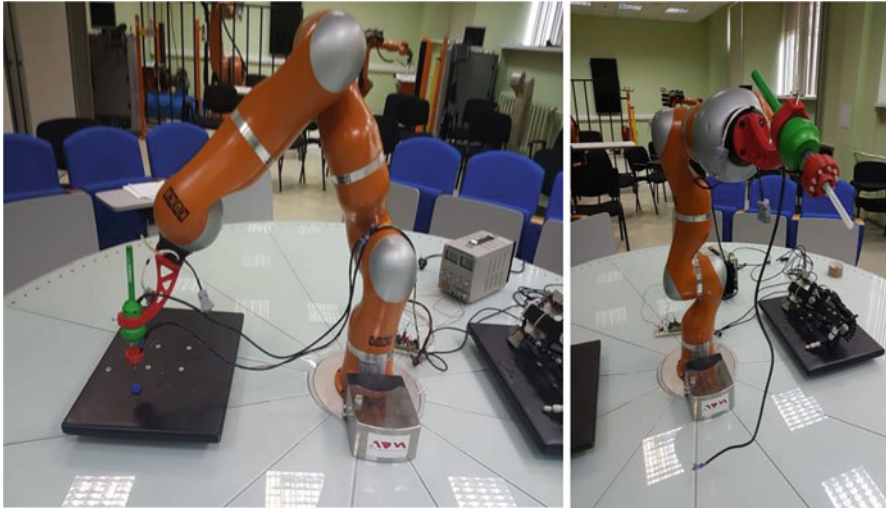


Fig. 5 In situ 3D bioprinter (according to 3D Bioprinting Solutions)

with such types of baseless and often unprofessional futuristic predictions and similar statements about enormous complexity of human tissues and organs is much more productive actually to work hard on the development of 3D bioprinting technology and, thus, advance this exciting and perspective field.

Moreover, the analysis of the development of commercial 3D bioprinters can also show some emerging important trends in the designing of commercial 3D bioprinters. The first trend strongly indicates on obvious fact that number of commercial 3D bioprinters as well as number companies and countries producing 3D bioprinters continue to grow and that 3D bioprinting technology is already in the process of global commercialization. Thus, we are observing the emergence of new bioprinting and biofabrication industry. The second trend clearly demonstrates that there are different types of 3D bioprinters based on different physical principles of their work. The third recent trend demonstrates that companies started to develop not only expensive but also affordable 3D bioprinters which will enable further spreading of this very popular technology in the academic circles. The hybridization of bioprinting technologies as well as increasing functionalities of commercially available 3D bioprinters are the next evolving trends.

11 Challenges and Future Perspectives

The started commercialization of 3D bioprinting technology does not automatically mean that there are no problems and challenges left. It just indicates that bioprinting technology is already mature enough to initiate potentially profitable commercialization. However, relatively young 3D bioprinting technology still has a lot of problems and limitations. First of all, there are no bioprinted human organs and

certified 3D bioprinters approved for clinical use. The bioprinting resolution and speed need further improvement. There are at least several basic questions related to commercial 3D bioprinters which we will face in nearest future.

First such question – Can we use one type of commercial bioprinter for bioprinting of any types of human tissue and organs? The answer is probably no. The second question – Is it enough just 3D bioprinter to print tissue and organ constructs? The answer is also probably no. As we argued in previous sections just development of only 3D bioprinters is not enough and we will need development of integrated ideally automated and robotic organ biofabrication line. The third question – Did we already discover and systematically explore all possible physical principles for 3D bioprinting and biofabrication of human tissue and organs? The answer is again no, at least not yet. Another interesting but still unanswered question – Do we need one bioprinter to print whole entire organ in one step or we need several distributed biofabricators, bioassemblers, and bioprinters which will print at first small living building blocks such a minitissues, tissue modules, organ lobules, and even lobes and then we will need to design some types of bioassemblers which will put these building blocks together? Final question – Do we need to create all human tissue and organs only *ex vivo* and only then transplant them into human body or we must try to print at least some of human tissue directly in vivo in operation room combining advanced surgical robotics with 3D bioprinting and 3D biofabrication? The answer is we must definitely try to develop in vivo bioprinting.

The sufficient and long term sustainable funding, properly orchestrated multidisciplinary efforts, creation of national centers of excellence in bioprinting and biofabrication as well as transnational and may be even global initiatives are essential for success. The well-funded multidisciplinary efforts as well as competition between emerging 3D bioprinting companies will guarantee that transplantation of bioprinted functional and vascularized 3D human tissues and organs will eventually become a highly desirable clinical reality and will ensure that commercialization of 3D bioprinting technology will be successful. It is safe to predict that second generation of commercial 3D bioprinters will be more advanced and sophisticated and we will face the emerging of profitable bioprinting industry.

References

- Albrecht DR, Sah RL, Bhatia SN (2004) Geometric and material determinants of patterning efficiency by dielectrophoresis. *Biophys J* 87(4):2131–2147
- Arai K, Iwanaga S, Toda H, Genci C, Nishiyama Y, Nakamura M (2011) Three-dimensional inkjet biofabrication based on designed images. *Biofabrication* 3(3):034113
- Atala A, Yoo JJ (eds) (2015) *Essentials of 3D Biofabrication and translation*. Academic Press, Boston. 440 pages
- Basu S, Rodionov V, Terasaki M, Campagnola PJ (2005) Multiphoton-excited microfabrication in live cells via rose Bengal cross-linking of cytoplasmic proteins. *Opt Lett* 30(2):159–161
- Boland T, Xu T, Damon B, Cui X (2006) Application of inkjet printing to tissue engineering. *Biotechnol J* 1(9):910–917
- Bouyer C, Chen P, Güven S, Demirtaş TT, Nieland TJ, Padilla F, Demirci U (2016) A bio-acoustic Levitational (BAL) assembly method for engineering of multilayered, 3D brain-like

- constructs, using human embryonic stem cell derived neuro-progenitors. *Adv Mater* 28(1): 161–167
- Bulanova EA, Koudan EV, Degosserie J, Heymans C, Pereira FD, Parfenov VA, Sun Y, Wang Q, Akhmedova SA, Sviridova IK, Sergeeva NS, Frank GA, Khesuani YD, Pierreux CE, Mironov VA (2017) Bioprinting of a functional vascularized mouse thyroid gland construct. *Biofabrication* 9(3):034105
- Chan V, Zorlutuna P, Jeong JH, Kong H, Bashir R (2010) Three-dimensional photopatterning of hydrogels using stereolithography for long-term cell encapsulation. *Lab Chip* 10(16):2062–2070
- Chua CK, Yeong WY (2015) *Bioprinting: principles and applications*. World Scientific Publishing, Singapore. 296 pages
- Cooke MN, Fisher JP, Dean D, Rinnac C, Mikos AG (2003) Use of stereolithography to manufacture critical-sized 3D biodegradable scaffolds for bone ingrowth. *J Biomed Mater Res B Appl Biomater* 64(2):65–69
- Derby B (2012) Printing and prototyping of tissues and scaffolds. *Science* 338(6109):921–926
- Durmus NG, Tekin HC, Guven S, Sridhar K, Arslan Yildiz A, Calibas G, Ghiran I, Davis RW, Steinmetz LM, Demirci U (2015) Magnetic levitation of single cells. *Proc Natl Acad Sci USA* 112(28):E3661–E3668
- Gutzweiler L, Kartmann S, Troendle K, Benning L, Finkenzeller G, Zengerle R, Koltay P, Stark GB, Zimmermann S (2017) Large scale production and controlled deposition of single HUVEC spheroids for bioprinting applications. *Biofabrication* 9(2):025027
- Kang HW, Lee SJ, Ko IK, Kengla C, Yoo JJ, Atala A (2016) A 3D bioprinting system to produce human-scale tissue constructs with structural integrity. *Nat Biotechnol* 34(3):312–319
- Klebe RJ (1987) Apparatus for the precise positioning of cells. US patent 5,108,926 A, 8 Sept 1987
- Klebe RJ (1988) Cytoscribing: a method for micropositioning cells and the construction of two- and three-dimensional synthetic tissues. *Exp Cell Res* 179(2):362–373
- Klopsch C, Gäbel R, Kaminski A, Mark P, Wang W, Toelk A, Delyagina E, Kleiner G, Koch L, Chichkov B, Mela P, Jockenhoevel S, Ma N, Steinhoff G (2015) Spray- and laser-assisted biomaterial processing for fast and efficient autologous cell-plus-matrix tissue engineering. *J Tissue Eng Regen Med* 9(12):E177–E190
- Landers R, Hübner U, Schmelzeisen R, Mülhaupt R (2002) Rapid prototyping of scaffolds derived from thermoreversible hydrogels and tailored for applications in tissue engineering. *Biomaterials* 23(23):4437–4447
- Lee J-S, Pati F, Jung JW (2015) *Organ printing*. Morgan & Claypool, San Rafael. 92 pages
- Lin RZ, Ho CT, Liu CH, Chang HY (2006) Dielectrophoresis based-cell patterning for tissue engineering. *Biotechnol J* 1(9):949–957
- Linnenberger A, Bodine MI, Fiedler C, Roberts JJ, Skaalure SC, Quinn JP, Bryant SJ, Cole M, McLeod RR (2013) Three dimensional live cell lithography. *Opt Express* 21(8):10269–10277
- Ma X, Qu X, Zhu W, Li YS, Yuan S, Zhang H, Liu J, Wang P, Lai CS, Zanella F, Feng GS, Sheikh F, Chien S, Chen S (2016) Deterministically patterned biomimetic human iPSC-derived hepatic model via rapid 3D bioprinting. *Proc Natl Acad Sci U S A* 113(8):2206–2211
- Mandrycky C, Wang Z, Kim K, Kim DH (2016) 3D bioprinting for engineering complex tissues. *Biotechnol Adv* 34(4):422–434
- Mekhileri NV, Lim K, Brown GCJ, Mutreja I, Schon BS, Hooper GJ, Woodfield TBF (2018) Automated 3D bioassembly of micro-tissues for biofabrication of hybrid tissue engineered constructs. *Biofabrication*. 10(2):024103. <https://doi.org/10.1088/1758-5090/aa9ef1>. PubMed PMID: 29199637
- Melchels FPW, Domingos MAN, Klein TJ, Malda J, Bartolo P, Huttmacher D (2012) Additive manufacturing of tissues and organs. *Prog Polym Sci* 37(31):1079–1104
- Mironov V, Boland T, Trusk T, Forgacs G, Markwald RR (2003) Organ printing: computer-aided jet-based 3D tissue engineering. *Trends Biotechnol* 21(4):157–161
- Mironov V, Kasyanov V, Drake C, Markwald RR (2008) Organ printing: promises and challenges. *Regen Med* 3(1):93–103

- Mironov V, Trusk T, Kasyanov V, Little S, Swaja R, Markwald R (2009a) Biofabrication: a 21st century manufacturing paradigm. *Biofabrication* 1(2):022001. <https://doi.org/10.1088/1758-5082/1/2/022001>
- Mironov V, Visconti RP, Kasyanov V, Forgacs G, Drake CJ, Markwald RR (2009b) Organ printing: tissue spheroids as building blocks. *Biomaterials* 30(12):2164–2174
- Mironov V, Kasyanov V, Markwald RR (2011) Organ printing: from bioprinter to organ bio-fabrication line. *Curr Opin Biotechnol* 22(5):667–673
- Murphy SV, Atala A (2014) 3D bioprinting of tissues and organs. *Nat Biotechnol* 32(8):773–785
- O'Connell CD, Di Bella C, Thompson F, Augustine C, Beirne S, Cornock R, Richards CJ, Chung J, Gambhir S, Yue Z, Bourke J, Zhang B, Taylor A, Quigley A, Kapsa R, Choong P, Wallace GG (2016) Development of the Biopen: a handheld device for surgical printing of adipose stem cells at a chondral wound site. *Biofabrication* 8(1):015019
- Odde DJ, Renn MJ (1999) Laser-guided direct writing for applications in biotechnology. *Trends Biotechnol* 17(10):385–389
- Ovsianikov A, Mironov V, Stampf J, Liska R (2012) Engineering 3D cell-culture matrices: multiphoton processing technologies for biological and tissue engineering applications. *Expert Rev Med Devices* 9(6):613–633
- Owens CM, Marga F, Forgacs G, Biofabrication HCM (2013) Testing of a fully cellular nerve graft. *Biofabrication* 5(4):045007
- Ozbolat IT (2016) 3D Bioprinting: fundamentals, principles and applications. Academic Press, Boston. 356 pages
- Pereira RF, Barrias CC, Granja PL, Bartolo PJ (2013) Advanced biofabrication strategies for skin regeneration and repair. *Nanomedicine (Lond)* 8(4):603–621
- Qin XH, Aleksandr Ovsianikov A, Stampf J, Liska R (2014) Additive manufacturing of photo-sensitive hydrogels for tissue engineering applications. *BioNanoMat* 15(3-4):49–70
- Ringeisen BR, Spargo BJ, Wu PK (eds) (2010) Cell and organ printing. Springer, Dordrecht. 260 pages
- Saunders RE, Gough JE, Derby B (2008) Delivery of human fibroblast cells by piezoelectric drop-on-demand inkjet printing. *Biomaterials* 29(2):193–203
- Schuurman W, Khristov V, Pot MW, van Weeren PR, Dhert WJ, Malda J (2011) Bioprinting of hybrid tissue constructs with tailorable mechanical properties. *Biofabrication* 3(2):021001
- Tarassoli SP, Jessop ZM, Al-Sabah A, Gao N, Whitaker S, Doak S, Whitaker IS (2017) Skin tissue engineering using 3D bioprinting: an evolving research field. *J Plast Reconstr Aesthet Surg*. pii: S1748-6815(17)30505-3. <https://doi.org/10.1016/j.bjps.2017.12.006>. [Epub ahead of print] Review. PubMed PMID: 29306639
- Tasoglu S, Yu CH, Liaudanskaya V, Guven S, Migliaresi C, Demirci U (2015) Magnetic Levitational assembly for living material fabrication. *Adv Healthc Mater* 4(10):1469–1476
- Tocchio A, Durmus NG, Sridhar K, Mani V, Coskun B, El Assal R, Demirci U (2018) Magnetically guided self-assembly and coding of 3D living architectures. *Adv Mater* 30(4):1705034
- Tromayer M, Gruber P, Markovic M, Rosspeintner A, Vauthey E, Redl H, Ovsianikov A, Liska RA (2017) Biocompatible macromolecular two-photon initiator based on hyaluronan. *Polym Chem* 8(2):451–460
- Wilson WC Jr, Boland T (2003) Cell and organ printing 1: protein and cell printers. *Anat Rec A Discov Mol Cell Evol Biol* 272(2):491–496
- Yanagi Y, Nakayama K, Taguchi T, Enosawa S, Tamura T, Yoshimaru K, Matsuura T, Hayashida M, Kohashi K, Oda Y, Yamaza T, Kobayashi E (2017) In vivo and ex vivo methods of growing a liver bud through tissue connection. *Sci Rep* 7(1):14085
- Zein I, Huttmacher DW, Tan KC, Teoh SH (2002) Fused deposition modeling of novel scaffold architectures for tissue engineering applications. *Biomaterials* 23(4):1169–1185
- Zhang LG, Fisher JP, Leong K (eds) (2015) 3D Bioprinting and nanotechnology in tissue engineering and regenerative medicine. Academic Press, Boston. 392 pages

Index

A

- Additive manufactured scaffolds
 - biological properties characterization, 72–74
 - electrical properties characterization, 72
 - geometry on degradation kinetics, 62
 - imaging-based characterization, 59–62
 - mechanical properties characterization, 62–65
 - permeability, 70–72
 - porosity and pore characterization, 58–59
 - surface properties characterization, 66–69
 - wettability, 69–70
- Additive manufacturing (AM) techniques, 5,
165, 174, 178, 184, 212
 - advantage, 7
 - biomaterials, 6
 - bone, 9–12
 - bottom-up approach, 5
 - cardiovascular system, 37
 - cartilage, 24
 - cartilage tissue, 8
 - cartilage tissue regeneration, 27
 - ligament and tendon scaffold synthesis, 36
 - muscle scaffold synthesis, 34
 - skeletal muscle regeneration, 26
 - tendon and ligament reconstruction, 31
- Additives, 402, 414, 415
- Agarose, 267
- Alginate, 261–264, 338, 371, 404, 408,
412–413, 416, 418–421, 423
- Alumina, 162, 163
- America Invents Act (AIA), 495
- Anastomosis, 97, 99
- Anatomic model, 228
- Angiogenesis, 98
- Antioxidative proteins, 385

- Apparent tissue surface tension
(ATST), 38
- Atomic-force microscopy (AFM) analysis, 67
- Auricular reconstructive surgery, 332–333
- Average Intensity Projection (AIP), 209

B

- Bacterial nanocellulose (BNC), 339
- Bathochromic shift, 358, 360
- Binder jetting, 22
- Bioactive glass, 163, 174, 175, 177
- Bioactive properties, 386
- Bioceramics
 - bioactive, 162, 163
 - bioresorbable, 162
 - clinical and economic relevance, 164
 - historic perspective, 163–164
 - load-bearing implants, 166–167
 - passive, 162, 166
 - synthetic bone grafts (*see* Synthetic bone grafts, bioceramics)
 - void filling, bone substitutes for, 167
- Bio-compatible scaffold, 498
- Biodegradation, 108
- Biofabrication, 196, 211, 214, 216, 470–472
 - nerve graft, 335
- Bioglass[®], 162, 163
- Bioimaging, 496–499
- Bioimplant materials, 504
- Bio inks, 261–270, 309–310, 399, 401–405,
408, 410, 413–422, 452, 477, 493,
499–502
 - bacterial endotoxin and in vitro cytotoxicity testing, 345–346
 - cell laden hydrogels, 336–338
 - commercialization, 346–348

- Bio inks (*cont.*)
- complex constructs, 342, 344
 - crosslinking, 342–344
 - crosslinking time, 340
 - development work flow chart, 347
 - growth factor, 419, 422, 423
 - heterogeneous, 414, 420, 423
 - mechanical properties, 343–345
 - primary manufacturers of, 521
 - printability, 341–344
 - properties, 337
 - rheological properties, 338–342
 - S-test, 341
 - viscosity and rheological properties, 337–338
- Biological heart valve prostheses, 40
- bioLogic team, 525
- Biomaterial implants, 497
- Biomimetic, 217
- Biomimicry, 217
- Biomodels, 212
- Biomonitoring, 509–510
- Biopaper(s), 319, 499–502
- Bioplotters, 18, 33, 261
- Bioprinter(s), 452, 507
- patents, 499–502
 - prices, 519
 - software, 519
- Bioprinting
- additional patentable innovation, 510
 - cartilage tissue, 332–334
 - 3D patent landscape, 5, 9, 37, 56, 87, 196, 214, 216, 304, 399, 452, 486–487, 493–495
 - nerve tissue, 334–335
 - industry and market development, 515–518
 - in-situ, 266, 273
 - skin tissue, 335–336
 - technology, 515–532
- Bioprinting Station, 507
- Bioreactor, 509–510
- Bioresorbable airway splint, 136
- Biphasic calcium phosphate (BCP), 168, 177
- Bisacrylphosphineoxide (BAPO), 358
- Bladder, 80
- Blood vessels, 440–441, 468–470
- Blueprint patents, 496–499
- Body-on-a-chip systems, 320
- Bone, 459–461
- bioceramics (*see* Synthetic bone grafts, bioceramics)
- Bone morphogenetic protein 2, 91
- Bone tissue engineering scaffolds
- multi-scale modeling, 112–121
 - numerical modeling approaches, 110–112
- C**
- Calcium phosphate, 163, 168, 177
- Calcium sulfate, 186
- Cancer research, 473, 476–477
- Cannulation, 100
- Capillaries, 84, 97, 98
- Carboxylic acid moieties, 370, 375, 376
- Cardiac tissue, 470–471
- Carrageenan, 373
- Cartilage, 80, 443, 461–464
- tissue engineering, 24
- Cell aggregates, 270
- scaffold-free, 271
- Cell-cell interaction studies, 317–319
- CELLINK, 348
- Cell laden hydrogels, 336–337, 401, 404
- Cell-laden scaffolds, 26
- CELLMIXER, 346–348
- Cell properties, in 2D and 3D structure, 522
- Cell sheets, 434, 435, 440, 442, 443, 445
- Cell sorting, 38
- Cell source, 478
- Cellulose, 338, 372
- Cell viability, 338, 346, 400, 402, 404–407, 413, 416, 419, 420
- Chain-growth photopolymerization, 370
- Chemotaxis, 98
- Chitosan, 266–267
- Chondrocytes, 383
- Chondroitin sulphate (CS), 377, 378
- Clinical design hypothesis (CDH), 135–137
- Clinical trials, 441, 443
- Coaxial extrusion, 87–89
- Collagen, 310, 364
- Collagen type I, 265
- crosslinking mechanism, 265
 - fabrication, 265
- Computer aided design (CAD), 496–499
- models, 247
- Computer-aided tissue engineering, 497
- Confocal laser scanning microscopy, 68
- Construct design, 437–438
- Continuous inkjet (CIJ) printers, 284
- Contrast enhancement, 200, 203, 204
- Copyright, 488
- Cornea, 80
- Covalent incorporation of proteins, 383
- Creep and stress relaxation tests, 65

Crosslink, 398–401, 405–410, 412, 414, 419, 422
 alginate, 412
 entangle, 406, 411
 ionic, 405, 406, 408–409, 412, 423
 thermal, 408, 411, 412, 423
 Customized porous scaffold, 10
 Cyborg organs, 274

D

Darcy equation, 110
 Decell, 409–411
 Decellularized extracellular matrix, 271
 Dental implant, 167
 Depyrogenation, 345
 Design control waterfall, 135
 Design model output (DMO), 148–149
 Design patent, 488–489
 Design verification, 134
 Dexamethasone, 379
 Dextran, 373
 Dicalcium silicate, 183
 DICOM format, 199, 200
 Digital image correlation (DIC), 64
 Digital light processing (DLP), 14, 178, 543
 Digital micromirror device (DMD), 93
 Digital volume correlation (DVC), 64
 3D inkjet bioprinting, 379
 Direct ink writing/robocasting (DIW), 175
 Direct metal laser sintering (DMLS), 22
 Direct micromirror device (DMD), 175, 178
 Direct volume rendering, 207–211
 Direct-write technologies [DWDT], 509
 Direct writing, 10
 Distinctive, 492
 Double-network (DN), 368, 369
 Droplet-based bioprinting, 273
 Droplet-based printing, 286
 Droplet volume control, 311–313
 Drug delivery, 398, 399
 Drug discovery, 472
 Drug formulation, 296
 Drug screening, 473
 Dynamic mechanical analysis, 65
 Dynamic release layer, 308–309

E

ECM, *see* Extracellular matrix (ECM)
 Edge detection, 200, 202
 Electron beam melting (EBM), 7, 18
 Electroprocessed collagen, 504, 505

Electrospinning (ELS), 81, 92, 175, 176, 508
 Electrostatic inkjet printing, 285, 286
 Encompassing, 495
 Endotoxin-mediated pyrogen test, 345
 Energy dispersive X-ray spectroscopy, 60
 Engineered biological nerve graft, 500
 Environmental scanning electron microscopy (ESEM), 60
 Envisiontec, 506
 Eosin Y, 359, 361, 375, 382
 Extracellular matrix (ECM), 354, 364, 366, 373, 375, 377, 378, 382, 383, 387
 Extrusion-based bioprinting, 540–542
 biomaterials, 257
 3D constructs, 260
 dispensing, 257
 3D scaffold, 256, 257–261
 gelation, 272
 printing stage, 261
 shear-thinning, 260
 tissue construct, 257
 Extrusion-based manufacturing, 30
 Extrusion bioprinters, 400, 402, 404, 408, 410, 412, 416, 421, 422
 Extrusion printing, 304

F

Failure mode effects analysis (FMEA), 143
 Fibrin, 265–266, 409, 423
 in-situ bioprinting, 266
 Fibrin gel, 310
 Fibrinogen, 381, 386, 409, 420, 421
 Finite element modelling, 66
 Fractal, 85
 Fused deposition modeling (FDM), 16, 25, 171, 175, 176, 536
 Fused filament fabrication (FFF) method, 11

G

Gartner's Hype Cycle, 515, 518
 Gas foaming, 81
 Gelatin, 264–265, 366, 399, 404, 407, 409, 412, 413, 415, 417, 419, 421, 423
 Gelatin methacrylamide Gel-MOD, 360, 366, 369, 374
 Gelatin methacrylate (GelMA), 338, 412, 414–419, 421
 Gelation, 272
 Gellan gum, 368
 Geometric transformations, 206

Granular, hydroxyapatite-based biomaterial,
114–121
Growing technique, 205

H

Hardware, 494
Heart valve, 470–471
Heparin, 375
Heterotypic interactions, 89
Hierarchical branching, 84, 89, 93, 95
High throughput screening and cancer research,
295
Hip, 163, 178
Homogenization
 of conglomerate stiffness, 117–119
 of granule stiffness, 117
 of hydroxyapatite matrix stiffness, 116–117
Humanitarian device exemption (HDE), 134,
137, 155
Human mesenchymal stem cells, 380
Human nasoseptal chondrocytes (hNC), 340
Human organism, 495
Hyaluronic acid (HA), 268–269, 374,
413–414, 423
Hyaluronic acid methacrylate (HA-MA), 414
Hybrid hydrogel, 374
Hydrogel(s), 333, 336, 354, 355, 357, 358, 360,
363, 366, 368, 375, 378, 380, 385,
399–405
 cell laden, 336, 346
 characteristics and limitations, 261
 constructs using stereolithography, 505
 degradation, 270
 multi-chamber single-nozzle unit, 269
 multi-material printing, 265
 synthetic, 269
Hydroxyapatite (HAP), 162, 163, 167, 169,
174, 176, 177
2-Hydroxyethyl acrylate, 359

I

Image preprocessing, 200
Image registration, 206
Image segmentation, 205
Imaging techniques, 196, 197
Inflammation, 101
Inkjet bioprinters, 400–402, 410, 412, 416, 418,
422, 540
Inkjet-mediated gene transfection (IMGT), 294
Inkjet printing (3DP), 174, 175, 304
 applications, 295

 characteristics, 287
 cytocompatibility of, 290
 and functional repair, 297
 planar cell patterns, 288
 print proteins, 292
 regenerative medicine in, 296
 and structural repair, 296
 technology, 24
 technology map, 284, 285
 of tissues and cells, 506, 508
 2D and 3D cell pattern fabrication, 86, 291
 of viable cells, 500
In situ biofabrication, 545
In-situ bioprinting, 266, 273, 545
In situ printing, 323
Integrated global layout, 498
Intellectual property (IP) protection, 487–493
 copyright, 488
 design patent, 488
 hardware, 494
 materials, 493
 methods, 494
 product, 495
 software, 494
 trade dress, 491
 trade mark, 489
 trade secret, 492
 utility patents, 493
InVesalius, 196
In vitro bioprinted muscle, 32
In vitro tissue/organ model, 471–473
Irgacure 2959, 357, 358, 360, 363, 367, 369,
372, 374, 375, 378, 380, 382, 383,
386, 387
Isosurface rendering, 207–208

J

Joint replacement (arthroplasty), 163, 178

K

Kenzan method, 440, 441
Kidneys, 441–442
Knee, 163, 178

L

Laser-assisted bioprinters (LABs), 323, 400,
402, 403, 412
Laser-based biofabrication, 256
Laser-based bioprinters, 542–543
Laser-based cell printing techniques

- applications, 314–323
 - laser-guided direct write, 305–306
 - laser-induced forward transfer, 306–308
- Laser Doppler, 99
- Laser-guided direct write (LGDW), 305–306
- Laser-induced forward transfer (LIFT), 306–308, 542
- Laser parameters, 310–311
- Laser printing, 12
- Laser surface scanners, 336
- Liquid-frozen deposition manufacturing (LFDM), 25, 26
- Liver, 442
- Local microstructure topology optimization, 498
- Low-temperature deposition manufacturing (LDM), 18
- Low-temperature deposition modeling (LDM), 175

M

- Macroporosity, 499
- Magnetic bioprinting technology, 539
- Magnetic resonance imaging (MRI), 257
- Manufacturing process compatibility and bioceramics, *see* Bioceramics
- Material extrusion
 - bioplotter and 3D plotter, 18
 - fused deposition modeling, 16
 - LDM, 18
 - precision extruding deposition, 17
 - robocasting, 16
- Matrigel, 267–268, 319, 411, 421–423
- Maturongens, 509–510
- Maximum intensity difference accumulation (MIDA), 209
- Maximum intensity projection (MIP), 209
- Mechanical micro-extrusion, 259
- Mechanotransduction, 98
- Medical imaging, modalities, 196
- Melt electrospinning (MES), 175, 176, 536
- Melt extrusion, 81, 92
- Mesenchymal stem cells (MSCs), 334, 335
- Methacrylate, 372
- Methylcellulose (MC), 269–270
- Michael-type addition, 354, 376, 386
- Microcarriers, 270
- Micro computed tomography, 61
- Microfluidic organs-on-a-chips, 471
- Microporosity, 499
- Microwave sintering, 11
- Minimum intensity projection (MinIP), 209

- Mini-organs, 471
- Modification of biomaterial surfaces, 502
- Modular fabrication systems and methods, 501, 505
- Modular implant manufacturing, 7
- Modular tissue engineering, 8
- Modulus, 412, 413, 416, 420, 421
- Mohr-Coulomb-type criteria, 113
- Monoacylphosphineoxide (MAPO), 358
- Multicellular aggregates, 86
- Multi-material hydrogels, 409–422
- Multi-photon polymerization, 95
- Multi-photon processing, 543
- Multi-scale modeling, bone tissue engineering
 - bone regeneration kinetics, 120
 - micromechanical model representation, 114–115
 - micromechanical stiffness estimation, 116–119
 - micromechanical strength estimation, 119
 - motivation, 112
 - numerical studies, 120–121, 123–125

N

- Nanocellulose, 338
 - alginate composite biomaterial, 339
 - biomedical application, bacterial, 339
 - viscosity curves, 340
- Nanocellulose-alginate bioinks, 346
- Nano-hydroxyapatite, 183, 188, 323
- Nanoindentation, 345
- Nanoporosity, 499
- Near-infrared light (NIR), 356
- Near-infrared (NIR) lasers, 311
- Needle arrays, 440
- Neovascularization, 3D printed and engineered tissues, 271
- Nerve, 466–468
- Noise filtering, 200, 202
- Non-adhesive scaffold surface, 67
- Non-neuronal autologous tissues, 334
- Nuclear magnetic resonance imaging, 61
- Nucleus pulposus tissue engineering, 371

O

- Octacalcium phosphate, 173
- One-photon-initiators (1PIs), 356, 357
- Organ biofabrication line, 217, 543–544
- Organ fabrication, 272
- Organ modules, 274
- Organoids, 471

- Organ-on-a-chip devices, 274
Organ printing, 215, 217
Organ transplants, demand for, 514
Osteogenic differentiation, 90, 91
- P**
- 2PA cross-section, 360, 362
Parenchyma, 38, 91, 469
P2CK, 362, 367
PEG diacrylate (PEG-DA), 375, 378, 380
Perfusion culture, 81, 82, 87, 91, 94
Periodontal regeneration, 442–443
Pharmaceuticals, 273
Photo-crosslinkable, 401, 407
Photoencapsulation, 382
Photoinitiators (PIs), 87, 354, 402, 404, 406, 407, 421
 two-photon-initiators, 360
 type I one-photon-initiators, 357
 type II one-photon-initiators, 358
Photolithography, 82, 84
Photonic explorers by biologically localized embedding (PEBBLEs), 68
Photopolymerizable materials, cell encapsulation
 PEG derivatives, 378
 and photoinitiators, 356
 poloxamer, 385
 polysaccharides, 371
 proteins, 364
 PVA derivatives, 382
Photopolymerization, 354, 355, 368, 370, 371, 376, 378, 380, 382, 384, 387
Piezoelectric inkjet printing method, 286
PIs, *see* Photoinitiators (PIs)
Pluronic F127, 409, 422
Pluronic[®] polymer, 90, 266
Pneumatic-based extrusion, 257
Poloxamer, 385
Polyamide, 183
Polycaprolactone, 183, 186, 188
Poly(ethylene glycol) (PEG), 268, 378, 409, 412, 414, 418, 419, 423
Polylactide acid, 186, 188
Poly(L-lactide-co-D,L-lactide), 186
Poly(propylene fumarate), 188
Polysaccharides, 371
Poly(vinyl alcohol) (PVA), 382
Porosity, 58
Porous PLA screw-like scaffold with hydroxyapatite coating, 35
Powder bed and inkjet, 3D printing (PBIH), 22
Powder bed fusion
 DMLS, 22
 electron beam melting, 18
 selective heat sintering, 21
 selective laser sintering, 19
Precision extruding deposition (PED), 17, 175
Pre-market approval (PMA) pathway, 134
Pressure assisted dispensing (PAD), 175
Pressure-assisted micro syringe (PAM) method, 11
Printed multicellular arrays, 317–319
Printed skin tissue, 320–323
Printed stem cell grafts, 315
Process impact, cells, 313–314
Production of three-dimensional structure of cells, 502
Product of nature, 495
Progenitor cells, 508
Proteins, 364
PVA-Tyr hydrogels, 384
- R**
- Radiometric transformations, 206
Rapid prototyping, 212
Reconstructive surgery, 167
Regeneration, 454
Regenerative medicine, 454
Regenova, 440
Replica molding, 83–85
Representative volume element (RVE), 112, 115, 118
Reverse transcription polymerase chain reaction (RT-PCR) analysis, 73
Rheology, 338
Robocasting, 16, 499
Rotating bioreactor, 509, 510
Runge-Kutta method, 110
- S**
- Sacrificial templating, 89–92
Scaffold(s), 214, 217, 360
Scaffold design, 247
 computer-aided porous, 227
 heterogeneous porous, 225, 228, 229
Scaffold fabrication, 30
Scaffold-free
 advantages and challenges, 443–445
 aggregation/spheroid-based approaches, 435–437
 bioprinting methods and equipment, 438–440

- blood vessels, 440
 - cartilage, 443
 - classification, 434–435
 - kidney, 441
 - liver regeneration, 442
 - multicellular spheroids and construct design, 437–438
 - periodontal regeneration, 442
 - tissue engineering, 432–434
 - Scaffold's tensile stress ratio, 238
 - Scanning electron microscopy, 60
 - Schoen surfaces, 235, 238, 242, 245, 246
 - Schwarz surfaces, 234, 238
 - Selective heat sintering (SHS), 21
 - Selective laser melting (SLM), 174, 175
 - scaffolds, 71
 - Selective laser sintering (SLS), 11, 19, 96, 175
 - Self-assembling cell aggregates, 499, 500
 - Self-assembling multicellular bodies, 499
 - Self-assembly, 434, 435, 445
 - Self-organization, 434
 - Sericin, 385
 - Shear stress, 272
 - Shear-thinning, 91, 260
 - Shear viscosity curve, 338
 - Single-action three-dimensional model printing methods, 496
 - Skeleton, 179
 - Skin, 80, 464–466
 - Slide, 173
 - Slurry, 95, 96
 - Soft lithography, 84, 85, 100
 - Software, 494–495
 - Solenoid micro-extrusion, 259
 - Solid-scaffold-free, 214
 - Sphere-shaped scaffold model, 232
 - Spherical cellular bioinks, 39
 - Spheroid, 435–438
 - Splint design model, 147
 - Spray skin, 336
 - Sr-hardystonite, 183
 - Stackable biopapers, printed cells, 319–320
 - Stereolithography (SLA), 13, 93, 94, 175, 400–404, 407, 543
 - Stress, 399, 400, 404–405
 - Stroma, 91
 - Styrenated gelatin, 370
 - Support, 95, 398, 399, 402–404, 407, 410, 411, 420
 - Suture strength, 92
 - Synthetic bone grafts, bioceramics, 167–170
 - additive manufacturing methods, 174–177
 - graded materials, 178–179
 - high resolution manufacturing processes and composites, 178
 - molds, bioceramic devices in, 173–174
 - morphology and mechanical properties of scaffolds, 170–172
 - standardized in vivo testing, 179
 - surface treatment methods, 177
 - Synthetic hydrogels, 269, 378
- T**
- Technology trigger phase, 516
 - Tensile/compressive testing, 63–65
 - Tetracalcium phosphate, 186
 - Thermal inkjet printer, 285, 286
 - Thiol-ene photopolymerization, 380
 - 3D bioprinters, 478, 536
 - components, 538
 - definition of, 536–537
 - design and functionality of, 545–546
 - extrusion-based bioprinters, 540–542
 - ink-jet technology, 540
 - in situ* biofabrication, 545
 - laser-based bioprinters, 542–543
 - organ biofabrication line, 543–544
 - shape and size of, 538
 - 3D bioprinting, 514
 - of biosynthetic cellulose (BC), 504
 - commercialization, 521
 - in Gartner reports, 516
 - legal issues of, 525–527
 - market segments and business models, 518–525
 - methods and equipment, 439
 - opportunities, 527–528
 - Porter's analysis, industry development, 528–531
 - technology, 332, 333, 336, 337, 344 (*see also* Bio inks)
 - 3D Bioprinting Patent Landscape, 493–495
 - Three-dimensional (3D) models, 196
 - Three-dimensional printing, 498
 - Three-dimensional visualization, 197
 - 3D Plotter, 18
 - 3D printed patient specific devices
 - clinical objectives and clinical design hypothesis, 135
 - design and manufacturing processes, 147–151
 - design control, 133–134
 - design inputs and risk analysis, 137–143
 - development planning, 147

- 3D printed patient specific devices (*cont.*)
 testing, design verification and design validation, 151–157
- 3D printed personalized titanium plates, 7
- 3D printing, 196, 208, 211, 358, 366
- 3D printing (laser sintering) splints, 149–151
- Thresholding, 205
- Tissue engineering, 224, 226, 246, 247, 454, 497
- Tissue engineering, additive manufacturing in
 cardiovascular system, 35–40
 cartilage, 12–26
 skeletal muscle regeneration, 26–31
 tendon and ligament reconstruction, 31–35
- Tissue glue, 100
- Tissue vascularization, 37
- Toxicity test, 473
- Trachea, 80
- Tracheobronchomalacia (TBM), 135, 136
- Trademark, 489–491
- Transfer function, 208, 210
- Translation, 454, 472
- Translational applications, 454
- Transplantation, 455, 514
- Triangle mesh, 207, 212
- Triazene, 309
- Tricalcium phosphate (TCP), 163, 164, 167, 171, 174, 176
- Triple periodic minimal surfaces (TPMS), 225
 definition, 231
 elastic modulus, 238–242
 functionally gradient scaffold, 245–248
 periodic surface modelling, 232–235
 Schoen surface, 235
 Schwarz surface, 234–236
 shear modulus, 244–245
- Tweaking, 494
- Two-dimensional slices, 197
- Two-photon-absorption (2PA), 356, 360, 362
- Two-photon-initiators (2PIs), 356, 360
- Two-photon-polymerization (2PP), 357, 360, 367, 368, 387
- Two photon printing, 14
- Type I one-photon-initiators, 357
- Type II one-photon-initiators, 358
- U**
- Ultraviolet (UV) light, 385
- Urethra, 80
- uSLA, 15
- Utility patent landscape, 499
- V**
- VA-086, 358, 367
- Vascular endothelial growth factor (VEGF), 97
- Vascularized tissue, 274
- Vascular networks, 468–470
 advanced fabrication technologies, 95–97
 coaxial extrusion, 87
 extrusion of solid materials, 85–87
 in vivo integration, 99–101
 macroporous scaffolds, 81–83
 multiscale vasculature, endothelial matrix invasion, 97–99
 replica molding, 83
 sacrificial templating, 89
 stereolithography, 92–95
- Vasculogenesis, 98
- Vat photopolymerization
 digital light processing, 14
 stereolithography, 13
 two photon printing, 14
 uSLA, 15
- Vertebra (spine), 167
- W**
- Watershed, 206
- Z**
- Zirconia, 162, 163